Universidade de Lisboa

Faculdade de Ciências

Departamento de Geologia

The morphotectonics offshore Southwest Iberia and the origin and evolution of the South Portuguese submarine canyons

Vasco Loja da Silva Valadares

DOUTORAMENTO EM GEOLOGIA

Geodinâmica Interna

2012

Universidade de Lisboa

Faculdade de Ciências

Departamento de Geologia

The morphotectonics offshore Southwest Iberia and the origin and evolution of the South Portuguese submarine canyons

Vasco Loja da Silva Valadares

Tese orientada pelo Prof. Doutor Pedro António Gancedo Terrinha e Prof.ª Doutora Susana Martín Lebreiro para obtenção do grau de doutor em Geologia (Geodinâmica Interna)

2012

To my princess, Mariana ☺

In memory of my Grandfather, António

Abstract

The detailed analysis of the new bathymetric data (180.000 km^2) collected mainly in the last decade, in the Gulf of Cadiz and SW Iberia Margin allowed the identification and mapping of a wide range of morphologic seafloor features. Based on the joint inspection of the swath bathymetry, seafloor reflectivity and multichannel seismic profiles (adding up to 20.700 km), a detailed characterization of the seafloor shaping processes was carried out. This allowed a classification of the seafloor morphology into twenty two seafloor morphotectonic domains.

A detailed characterization of the processes responsible for the shaping of the seafloor is proposed based on the joint interpretation of the bathymetry, backscatter and multichannel seismic reflection profiles.

The area considered in the Gulf of Cadiz and the SW Iberia comprises part of three Abyssal Plains (Seine, Horseshoe and Tagus abyssal plains) separated by two linear submarine mountains of tectonic compressive origin, the Gorringe Bank and the Coral Patch Seamount. The Seine Abyssal Plain displays several reliefs that correspond to hangingwall thrust folds that resulted from the collision of Africa with Eurasia, whilst the Horseshoe Abyssal Plain displays isolated folds associated with the development of a possibly transpressive plate boundary in Quaternary times. The submarine mountains rise various kilometers from the seafloor and together with the i) accretionary wedge of the Gulf of Cadiz, ii) the Gibraltar Straits, iii) the Horseshoe scarp, and iv) Príncipe de Avis Spur constitute the main submarine boundaries of the Pliocene-Quaternary sedimentary systems of SW Iberia.

The sediment transport encompasses, from source to sink, an interconnected scheme of three major systems made up by submarine canyons, submarine valleys and the Mediterranean Outflow Water system (MOW). These sedimentary systems initiated in the Late Miocene-Early Pliocene associated with the major paleogeographic modifications of SW Iberia, such as, the closure and opening of the Straits of Gibraltar, uplift of part of the south Portuguese Margin, westwards roll-back of the Gulf of Cadiz oceanic slab, and subsidence of the southeast Portuguese continental slope.

On the northeastern part of the Gulf of Cadiz, the MOW system drapes the shallower parts of the accretionary wedge and the recent tectonic features of the still deforming south Portuguese Margin. However, inside the Accretionary wedge domain, several features are present like mud volcanoes, salt domes, crests and troughs, extensional fault collapses and strike-slip faults attesting for important internal tectonic and fluid escape processes activity.

This work revealed the interaction involving several processes of different origins that are responsible for the seafloor shaping, at different time and spatial scales. Particularly obvious is the diachronic interaction of tectonics, fluid injection and halokinesis in the Seine Abyssal Plain and in the accretionary wedge and also mass transport processes, uplift and deep water contourite currents.

The combined inspection of several multichannel seismic profiles and the multibeam bathymetry of the SW Iberia allowed the mapping the major tectonic structures of the area. These are grouped in three classes; the NW-SE to N-S thrusts, the long WNW-ESE strike slip faults, and the accretionary wedge.

The S. Vicente Canyon lies in the transition between the South Portuguese and the Western Portuguese margins. Its head sector starts at the edge of the continental shelf and extends for 120 km (with a mean slopes of 2.3º, locally up to 25º) until it reaches the Horseshoe Abyssal Plain at depths of 5000 meters below sea level. The geomorphology study of the submarine canyon revealed four distinct sectors. The shallower one displays a wide and poorly incised bottom (walls with less than 800m command) with low gradient flanks (<6º). The following sector displays a narrower bottom with steeper (~8º) and higher flanks (>900m), except for the areas affected by mass movement processes that show lower gradient values for the walls. The third sector displays an increase in the thalweg pitch (~14º) and the walls are also steep and highly incised by gullies and display evidences of mass wasting processes. In this sector a major kink of about 60º is present in the trend of the canyon that results from a tectonic control. The deepest sector displays a wide bottom, low gradients for both the flanks (<4º) and the thalweg, and low flanks (~550m). The canyon initiated as a subsided area at the base of Late Miocene in its present day middle sector associated to the activity of the Marquês de Pombal Thrust. However, only in Late Miocene-Pliocene times the clear morphologic and sedimentary features of the canyon are well marked as it propagated upslope along the S. Vicente Canyon Fault. The upslope retreat of the canyon's head is still an ongoing process at present as evidenced by the pattern defined by tributary channels and gullies around its head.

To the east, the Portimão Canyon displays an overall N-S trend. Its head starts incising the continental shelf at about 100 of water depth and extends for 50 km with a mean slope of 2.7º; it is sub-divided in three sectors. The first sector displays flanks with little command over the thalweg (less than 200m high) with moderate gradients. In the middle sector, the flanks are steeper and the walls are higher (about 300m high), the canyon axis displays sinuosities where the canyon captures the MOW and intersects the Alvares Cabral Moat and erodes the contourite drifts. The deeper sector displays some irregularities on the bottom, very high and steep walls that decrease

their size and gradient as the canyon merges with the Portimão Valley at 2500 meters water depth, part of the orthogonal drainage system that originates in the Gibraltar approaches. The Portimão Canyon started to form in its present day middle sector by the convergence of bottom currents caused by localized salt ascent in post base of Miocene times linked with the Portimão Fault. A more accurate dating for these events is difficult to assign, although it was probably during the Lower Pliocene when an older drainage system (now buried under the Faro contourite drift) ceased its activity and the bottom currents started to erode the seafloor generating the present day Portimão Canyon. Afterwards, the canyon migrated upslope and downslope from this area along the Portimão Fault. The Quaternary development of the canyon is not only associated with movement in the Portimão Fault but rather with the overall deformation of the continental margin (vertical movements) and source to sink drainage of sediments. These processes account for the canyon upslope retreat and development of a localized erosion at the meeting point of the canyon mouth and the Portimão Valley (part of the east to west drainage system that extends from the Gibraltar approaches to the Horseshoe Abyssal Plain).

Keywords: Multibeam swath bathymetry, Morphotectonics, Seafloor shaping processes, Submarine Canyons, Southwest Iberia.

Resumo

A análise pormenorizada dos cerca de 180.000 km^2 de dados de batimetria multifeixe adquiridos na margem continental do Golfo de Cádis e da Margem Sudoeste Ibérica, na primeira década deste século, possibilitou a identificação e mapeamento de uma grande variedade de formas de relevo do fundo marinho. Com base na interpretação conjunta da batimetria, reflectividade e de cerca de 20.700 km de perfis de sísmica de reflexão multicanal foi elaborada uma descrição detalhada dos processos modeladores das formas do fundo marinho. Este estudo resultou na identificação de vinte e dois domínios morfotectónicos distintos.

A área do Golfo de Cádis e Sudoeste Ibérico engloba parte de três Planícies Abissais (Sena, Ferradura e Tejo) separadas por duas montanhas submarinas alongadas de origem tectónica, o Banco de Gorringe e o Monte Submarino Coral Patch. A Planície Abissal do Sena contém relevos de origem tectónica (dobras a tecto de cavalgamentos) resultante da colisão entre a África e a Eurásia enquanto que a Planície Abissal da Ferradura apresenta relevos isolados que estão associados a dobras relacionadas com o possível desenvolvimento actual de uma nova fronteira de placas de natureza transpressiva. As montanhas submarinas elevam--se vários quilómetros acima do fundo marinho e, juntamente com i) o Prisma Acrecionário do Golfo de Cádis, ii) o Estreito de Gibraltar, iii) a escarpa da Ferradura e iv) o Promontório dos Príncipes de Avis constituem os limites submarinos dos sistemas sedimentares profundos do Sudoeste Ibérico durante o Plio-Quaternário.

O sistema de transporte sedimentar no Sudoeste Ibérico inclui três subsistemas constituídos pelos canhões submarinos, vales submarinos e o sistema associado à saída da àgua Mediterrânea (MOW, *Mediterranean Outflow Water*). Estes sistemas iniciaram a sua actividade no Miocénico Superior-Pliocénico Inferior ao mesmo tempo em que se deu uma reconfiguração paleogeográfica maior do Sudoeste Ibérico, envolvendo o fecho e posterior abertura do Estreito de Gibraltar, soerguimento da Margem Sul Portuguesa proximal, retro-rolamento (*rollback*) da subducção associada ao Arco Bético para oeste em direcção ao oceano Atlântico e subsidência da Margem Sudeste Portuguesa distal.

No sector nordeste do Golfo de Cádis, o sistema da MOW tem acção essencialmente deposicional e mascara as estruturas do prisma acrecionário e de deformação recente da Margem Sul Portuguesa. Contudo, longe da influência deste domínio e no interior do prisma acrecionário, é possível identificar diversas estruturas tais como vulcões de lama, domas de sal, cristas (elevações) e fossos, colapsos

extensionais e falhas de desligamento que comprovam a importante actividade actual dos processos tectónicos e de escape de fluidos.

Este trabalho mostra ainda a existência da interacção entre vários processos de diversas naturezas que são responsáveis pelas formas de relevo submarino existentes na área, a diferentes escalas temporais e espaciais. Constituem exemplos, a interacção diacrónica entre tectónica, escape de fluidos e haloquinese na Planície Abissal do Sena e no interior do prisma acrecionário e também a interacção entre os processos gravíticos de transporte de massa, o soerguimento tectónico diferencial entre blocos e as correntes contorníticas.

Foi produzido um novo mapa tectónico com recurso à análise e interpretação conjunta dos perfis de sísmica multicanal e da batimetria multifeixe do Sudoeste Ibérico, o que possibilitou o mapeamento das principais estruturas principais da área. Estas encontram-se agrupadas em três classes; os cavalgamentos NW-SE a N-S, as longas falhas de desligamento WNW-ESSE e o prisma acrecionário.

O Canhão Submarino de S. Vicente situa-se na zona de transição entre a Margem Sul e a Margem Oeste Portuguesa. A sua cabeceira situa-se no bordo da plataforma continental e prolonga-se por mais de 120 km (inclinação média de 2,3º, podendo atingir localmente 25º) até à Planície Abissal da Ferradura a profundidades de 5000 m. O seu estudo geomorfológico permitiu a individualização de quatro sectores. O primeiro, mais superficial, caracteriza-se por apresentar um amplo fundo com pouca incisão no fundo marinho e vertentes baixas (até 800m) e de baixos pendores (<6º). O sector seguinte apresenta um fundo mais estreito ladeado de vertentes mais desenvolvidas (>900m) e com maiores pendores (~8º), à excepção das áreas onde os processos de movimento de massa são ou foram mais intensos. No terceiro sector o talvegue apresenta pendores mais elevados (~14º), bem como as paredes do canhão (>900m), estas encontram-se bastante dissecadas por *gullies* e apresentam evidências de escorregamentos de massa. Neste sector, o eixo do canhão apresenta um desvio de origem tectónica de cerca de 60º em relação ao anterior. O sector mais profundo apresenta um fundo mais largo, eixo menos inclinado e flancos de menores dimensões (~550m) de baixos pendores (<4º). O canhão começou por ser uma zona deprimida no Miocénico Superior no seu actual terceiro sector associada à movimentação cavalgante na falha de Marquês de Pombal. Contudo, foi apenas no Miocénico Superior-Pliocénico Inferior que passou a ter as características morfológicas e sedimentares típicas de um canhão submarino. Foi nessa altura que se deu a sua propagação em direcção às áreas menos profundas ao longo da falha do Canhão de S. Vicente. Este recuo e a erosão remontante é um processo ainda activo evidenciado pelo actual padrão dos tributários em redor da cabeceira.

O Canhão de Portimão apresenta uma direcção geral N-S e a sua cabeceira erode actualmente a plataforma continental a cerca de 100 metros de profundidade, encontrando-se a sua desembocadura, à distância de cerca de 50 km a sul, a cerca de 2500 metros de profundidade (inclinação média de 2,7º). Este canhão foi dividido em três sectores, o primeiro (menos profundo) apresenta flancos de pendor moderado com pequeno comando sobre o talvegue (cerca de 200 metros). No sector médio, as paredes são mais inclinadas e mais altas (cerca de 300 metros), o eixo apresenta sinuosidades importantes na área onde o canhão intersecta o Fosso Alvares Cabral capturando a MOW e erodindo o *drift* contornítico. No sector mais profundo, o fundo apresenta algumas irregularidades, as paredes são mais altas e com elevados pendores, diminuindo ambos à medida que a profundidade aumenta e o canhão desemboca no Vale de Portimão (a profundidades em torno dos 2500 metros) que faz parte do sistema de drenagem submarina que se inicia à saída do Estreito de Gibraltar. A formação do Canhão de Portimão teve início no seu actual sector intermédio através da convergência e focalização das correntes de fundo devido à ascensão até à superfície do fundo marinho de um doma de sal ligado à Falha de Portimão no Neogénico. É difícil de precisar a datação destes processos, especulando-se, que deverão ter-se iniciado durante o Pliocénico Inferior, altura em que se começaram a formar os depósitos contorníticos do Algarve e que selaram um sistema de drenagem mais antigo, favorecendo a instalação de um novo sistema de drenagem submarina. Após estes primeiros eventos, o canhão desenvolveu-se ao longo da Falha de Portimão tanto para jusante como para montante. Durante o Quaternário, o seu desenvolvimento está associado aos eventos tectónicos de deformação (movimentos verticais) da área e processos sedimentares de transporte de sedimentos para maiores profundidades. Estes processos são responsáveis pelo recuo de cabeceira e erosão localizada na confluência do canhão com o Vale de Portimão (parte de um sistema de drenagem complexo que tem origem próximo do Estreito de Gibraltar e termina na Planície Abissal da Ferradura).

Palavras-chave: Batimetria multifeixe, Morfotectónica, Processos modeladores do fundo marinho, Canhões Submarinos, Sudoeste Ibérico.

Acknowledgments

This thesis is the final outcome of a long project, it would have not been possible for me to finish it without the help and support of many people and here I would like to thank them.

The first words of acknowledgments are directed to my thesis supervisors, Pedro Terrinha e Susana Lebreiro. Without them this project would have never existed and their help on this work was nothing less than unsurpassed. Their reviews of several versions of this thesis greatly improved it to what it is now. A special word to Pedro for all his help, friendship and advices in all these years.

To all my colleagues at the Marine Geology Dept. at Ineti/Lneg and especially the ones of the "Seismic Group" for all the help and friendship: Ana Branco, João Noiva, Henrique Duarte, Luis Batista, Gabriela Carrara, Rui Quartau, Sónia Silva, Marisa Loureiro, Ruben Borges, Manuel Teixeira, José Vicente, Célia Pata and Leire Iribarren. Thanks to João Duarte for all the productive talks and his friendship too. A special word to Cristina Roque for the revision of the manuscript, the endless talks and help in discussing the seismic profiles and geological interpretation. Also, a special word to Tiago Cunha for all the help, advices and reviews of several parts of this text. Henrique Duarte is thanked for his "endless" patience, nice character and seismic and computational skills.

An acknowledgment is due to Dra. Fátima Abrantes, Dr. Luis Rebelo and Dr. Pedro Terrinha as coordinators of the Marine Geology Dept. of Ineti/Lneg that provided me with all the conditions for me to work on this PhD project.

To my family and friends in general that were always supportive of me through the hard times during this PhD project and help me in several ways to achieve this goal.

Pedro Terrinha, Luis Matias, Marc-André Gutscher, Nevio Zitellini, Eulàlia Gràcia, Susana Lebreiro and Christian Hensen are thanked for allowing me to participate on their sea surveys, have access to the data collected and be able to use it; also as a personal experience it was one of the best parts of this work. A special thanks to Nevio Zitellini for welcoming me so nicely on ISMAR in Bologna and all the nice talks. An acknowledgment is due to Marc-André Gutscher for all the nice times at sea, the amazing talks and the time he took to make some suggestions on the text of Chapter 1. Eulàlia Gràcia is thanked for welcoming me in the UTM-CSIC in Barcelona; Susana Diez is thanked for the time and patience she had in teaching me how to use Caraibes.

I acknowledge a PhD scholarship from FCT (SFRH/BD/17603/2004).

It is acknowledged the support by Landmark Graphics Corporation via the Landmark University Grant Program.

A special acknowledgment to my daughter Mariana for all the wonderful times we have and the beautiful life perspective she has given me, also an apology is due for all the times that I was not available.

Figure Index

Table Index

TABLE OF CONTENTS

Chapter 1 – Introduction and objectives

This thesis is focused on the submarine canyons of the South Portuguese Margin. The project is largely based on recent multibeam swath bathymetry data acquired in the study area during marine geophysical surveys funded by national, and European projects (e.g. MATESPRO, DELILA and SWIM2005) all made available through the European funded SWIM project and after by the NEAREST project. The latter gathered and merged all previously acquired bathymetry data in the region to produce the maps presented here.

The first goal of this thesis is to identify, characterize and date the processes responsible for the origin and evolution of two of the South Portuguese Canyons, the S. Vicente Canyon and the Portimão Canyon. The second goal is to identify and characterize the different seafloor morphologic features and to understand their morphogenesis. This is the first comprehensive work on the description of the morphology of the SW Iberia margin, which straddles the slow moving and tectonically complex Nubia-Eurasia plate boundary, the Gibraltar oceanic subducted slab (its roll back and the accretionary wedge), the Morocco continental margin and portions of the Tagus, Horseshoe and Seine Abyssal Plains.

To achieve these goals the author contributed to the acquisition and processing of a large dataset (multibeam bathymetry and reflectivity data) and interpreted a large number of multichannel seismic reflection profiles in order to perform the mapping of the different morphotectonic domains of the SW Iberia. This involved the participation of the author in various oceanographic missions for the acquisition of geological and geophysical data, totalling more than 100 days of ship time (see list of missions below). Also, the author was able to develop his skills on interpreting seismic profiles using the Landmark Graphics Corporation suite of software of the Unit of Marine Geology of LNEG.

Thanks to a close collaboration with different national and international teams and researchers and to analogue modelling experiments performed at the IDL-LATTEX laboratory, the author actively participated in the publication of various peer reviewed papers, listed below and included as appendixes.

The second chapter of this thesis (*Setting of the area*) describes the study area from several different perspectives. The third chapter (*Data and methods*) describes the different types of marine geophysical data the methods used to compile, process and present these data. The fourth chapter (*Morphotectonic domains of Southwest Iberia*) focuses on the morphology and morphotectonics of the Gulf of Cadiz and SW Iberia and on the geomorphology of the S. Vicente and Portimão submarine canyons. The fifth chapter (*Origin and evolution of the south Portuguese submarine canyons*) presents and interprets the seismic profiles and the seismic structural maps for both canyons. Finally, the sixth chapter summarizes the main conclusions and scientific innovations of this study.

List of marine surveys:

TRANSFLUX – Gulf of Cadiz. Multibeam swath bathymetry, backscatter, acquisition and processing of sidescan and bathymetry from AUV. 22nd February - 18 th March 2012. P.I.: C.Hensen (GEOMAR). R/V Meteor.
LxCAN – South sector of the Estremadura Spur and the submarine canyons around the Lisbon area. Multibeam swath bathymetry and backscatter. 10 th September - 14 th September 2007. P.I.: S. Lebreiro (INETI). R/V NRP D. Carlos I.
SADOGEOROB_01 – Sado River Submarine delta and Setubal Canyon. High resolution monochannel seismic, Chirp, Sparker and sidescan sonar. 26th February – 2nd March 2007. P. I.: P. Terrinha (INETI). R/V NRP Auriga.
SWIM 2006 – Gulf of Cadiz. Multibeam swath bathymetry and backscatter, high resolution monochannel seismic, multichannel seismic TOPAS sub-bottom profiler, magnetic and gravimetry anomalies. 31st May – 14th June 2006. P. I.: E. Gràcia (UTM-CMIMA-CSIC). R/V Hesperides.
IMPULS – Mediterranean Sea, Gulf of Almeria. Multibeam swath bathymetry and backscatter, high resolution monochannel seismic, TOPAS sub-bottom profiler, magnetic and gravimetry anomalies, gravity coring, dredging. 16th May – 29th May 2006. P. I.: E. Gràcia (UTM-CMIMA-CSIC). R/V Hesperides.
SWIM 2005 – SW sector of the Gulf of Cadiz. Multibeam swath bathymetry, backscatter and Chirp sub-bottom profiler. 1st – 23rd October 2005. P.I.: N. Zitellini (ISMAR, Bologna). R/V OGS Explora.
DELILA – South sector of the Gulf of Cadiz. Multibeam swath bathymetry and backscatter, magnetic anomalies. 27th September - 8 th October 2004. P.I.: M. A. Gutscher (CNRS, UBO). R/V NRP D. Carlos I.
MATESPRO (2nd, 3rd legs) – North sector of the Gulf of Cadiz. Multibeam swath bathymetry and backscatter. 14 June- 7 July 2004. P.I.: L. Matias (FCUL) and P. Terrinha (INETI). R/V NRP D. Carlos I.

List of papers:

Terrinha, P., Matias, L., Vicente, J., Duarte, J., Luís, J., Pinheiro, L., Lourenço, N., Diez, S., Rosas, F, Magalhães, V., Valadares, V. ,Zitellini, N., Mendes Víctor, L., MATESPRO Team (2009) - Morphotectonics and Strain Partitioning at the Iberia-Africa plate boundary from multibeam and seismic reflection data. Marine Geology, Volume 267, Issues 3-4, pages 156-174.

Rosas, F.M.; J. Duarte, P. Terrinha, V. Valadares, L. Matias, (2009) Morphotectonic characterization of major bathymetric lineaments in Gulf of Cadiz (Africa-Iberia plate boundary): Insights from analogue modelling experiments. Marine Geology, Volume 261, Issues 1-4, pages 33-47.

Duarte, J.C., Valadares, V., Terrinha, P., Rosas, F., Zitellini, N., Gràcia, E. (2009). Anatomy and tectonic significance of WNW-ESE and NE-SW lineaments at a transpressive plate boundary (Nubia-Iberia). Trabajos de Geología 29, 237-241.

Duarte, J.C., P. Terrinha, F.M. Rosas, V. Valadares, L.M. Pinheiro, L. Matias, V. Magalhaes, C. Roque (2010) - Crescent-shaped morphotectonic features in the Gulf of Cadiz (offshore SW Iberia). Marine Geology, Volume 271, Issues 3-4, 15, pages 236-249.

C. Roque, H. Duarte, P. Terrinha, V. Valadares, J. Noiva, M. Cachão, J. Ferreira, P. Legoinha, N. Zitellini (2012) - Pliocene and Quaternary depositional model of the Algarve margin contourite drifts (Gulf of Cadiz, SW Iberia): Seismic architecture, tectonic control and paleoceanographic insights. Marine Geology, Volumes 303-306, pages 42-62.

Chapter 2 – Setting of the area

2.1. Spatial setting and toponomy

The area studied in this work involves the Gulf of Cadiz *s.l.* and the Southwest Iberian margin, located in the Northeastern Atlantic Ocean (Figure 2.1). From a tectonic point of view this is a structurally complex area, comprising the poorly defined eastern segment of the Azores-Gibraltar plate boundary between Nubia and Eurasia. This region was part of the northwest Africa-southwest Eurasia plate boundary from the earliest stages of the Pangea Triassic rifting, i.e. it has experienced the earliest continental rifting, the formation of the Jurassic oceanic lithosphere that separated Africa from Eurasia and its subsequent subduction and collision.

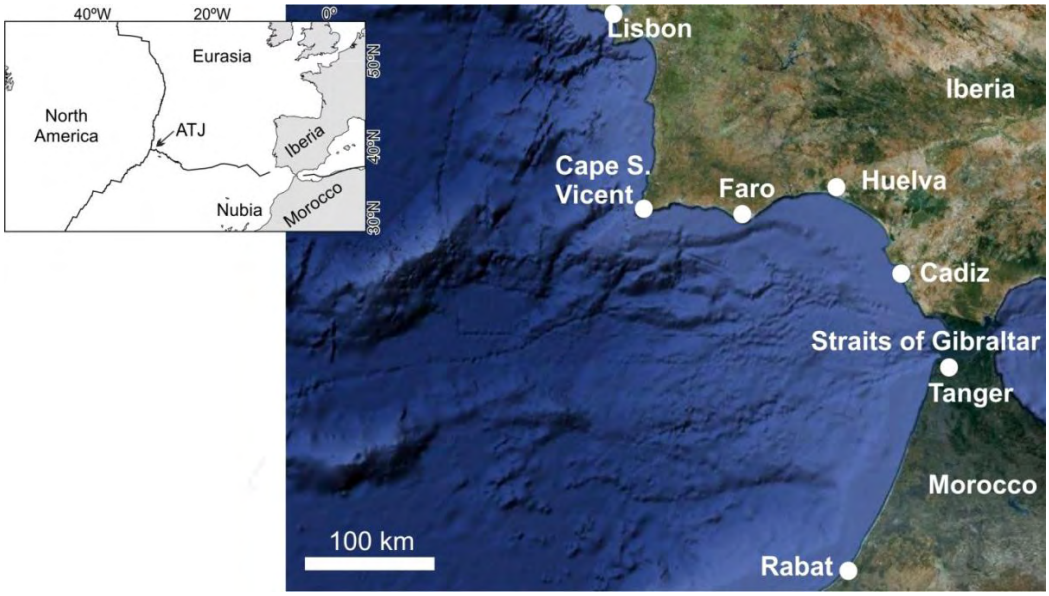

Figure 2.1 – Position of the SW Iberian margin including the Gulf of Cadiz with respect to the coast of Iberia and Morocco. Inset shows tectonic plate's framework in the Northern Atlantic Ocean, displaying the SW Iberia at the end of the Azores-Gibraltar plate boundary with Eurasia Plate to the north and Nubia Plate to the south. This plate boundary extends from SW Iberia until the ATJ (Azores Triple Junction) joining to the rift that separates the North America Plate with Eurasia and Africa. Satellite imagery and bathymetry data taken from Google Earth.

The Gulf of Cadiz (GoC) forms an arc bounded to the north, east and southeast by the Iberia and NW Africa continental blocks, with the exception of the small opening to the Mediterranean Sea, the Straits of Gibraltar (Figure 2.1). Its coastline is approximately 660 km long, from the S. Vicente Cape, passing through Faro, Huelva, Cadiz, the Straits of Gibraltar and Tanger, until near Rabat. The offshore southwest Portuguese margin is approximately 210 km long, between Lisbon and the Cape S. Vincent. The wide variety of submarine features in the GoC-SW Iberia Margin will be described in chapter 4 (see Figure 2.2 for the main features and toponyms).

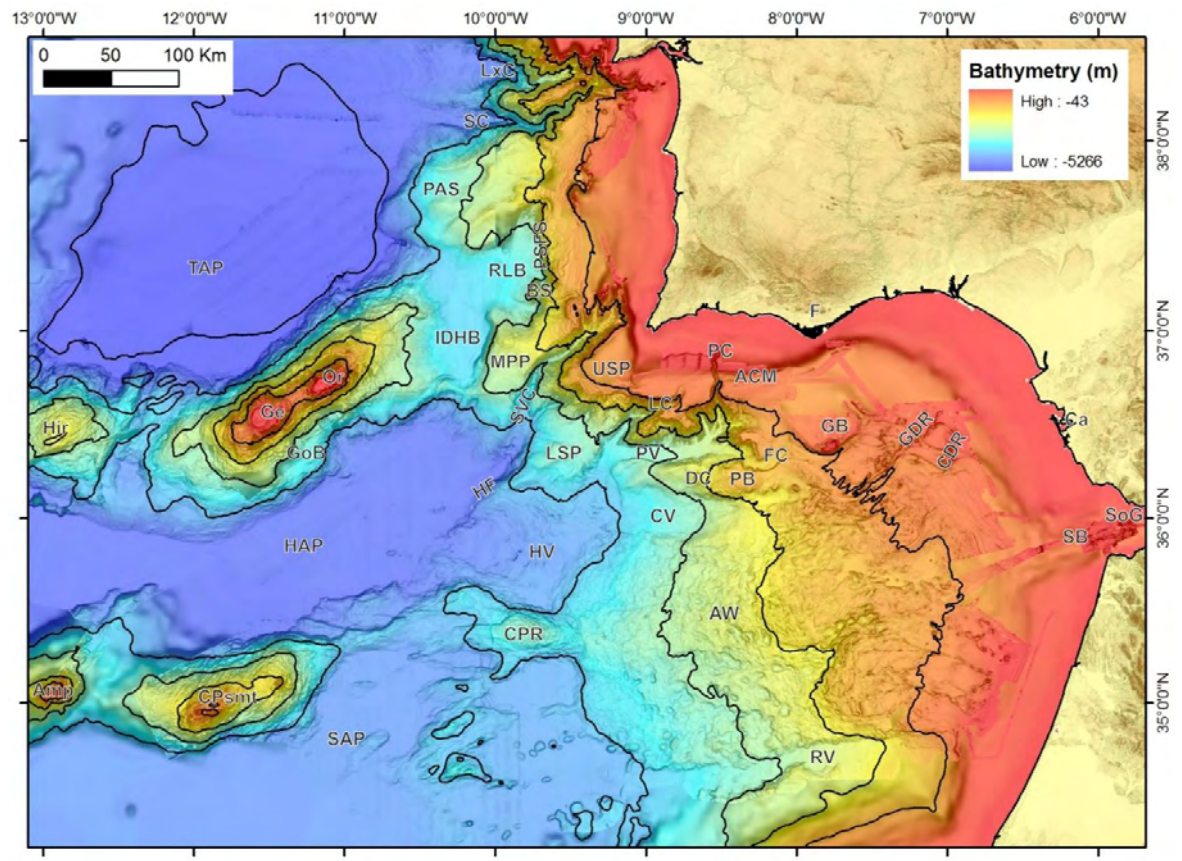

Figure 2.2 – Digital Terrain Model with topography and bathymetry of SW Iberia, locating the main morphological features and respective toponyms. In alphabetical order: ACM – Alvares Cabral Moat, Amp – Ampére seamount, AW - Accretionary Wedge, BS – Bow Spur, CPR – Coral Patch Ridge, CDR – Cadiz Diapiric Ridge, CPsmt – Coral Patch seamount , CV – Cadiz Valley, DC – D. Carlos salt dome, FC – Faro Canyon, GB – Guadalquivir Bank, GDR – Guadalquivir Diapiric Ridge, Ge – Gettysburg seamount, GoB – Gorringe Bank, HAP – Horseshoe Abyssal Plain, Hir – Hirondelle seamount , HF – Horseshoe Fault, HV – Horseshoe Valley, IDHB – Infante D. Henrique Basin, LC – Lagos Canyon, LSP – Lower Sagres Plateau, LxC- Lisbon Canyon, MPP – Marquês de Pombal Plateau, Or – Ormonde seamount, PAS – Príncipes de Avis Spur, PB – Portimão Bank, PC – Portimão Canyon, PSFS – Pereira de Sousa fault scarp, PV – Portimão Valley, RLB – Rincão do Lebre Basin, RV – Rharb Valley, SAP – Seine Abyssal Plain, SB – Spartell Bank, SC – Setubal Canyon, SoG – Straits of Gibraltar, SVC – S. Vicente Canyon, TAP – Tejo Abyssal Plain, USP – Upper Sagres Plateau.

2.2. Geomorphological setting

The SW Iberia offshore is characterized by a smoother seafloor on the shallower areas (continental shelf) and deepest domains (abyssal plains) and an irregular bathymetry on intermediate depths (continental slope) as shown on Figures 2.3 and 2.4.

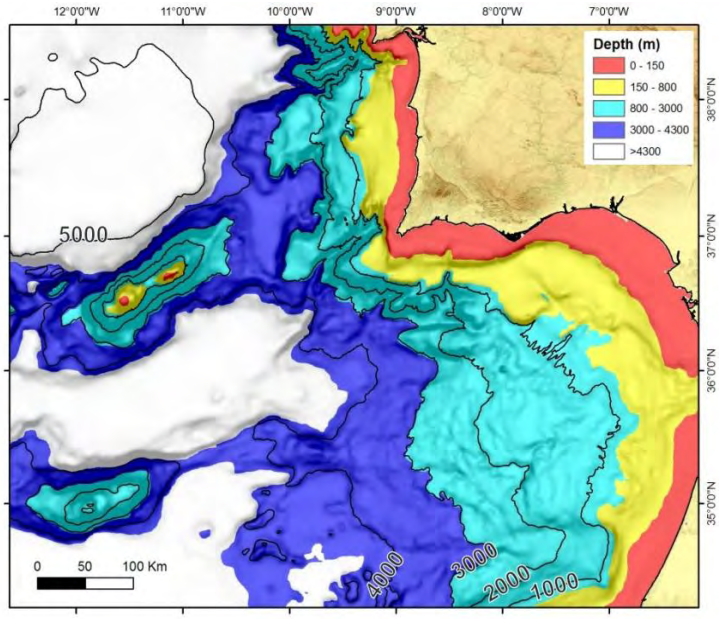

Figure 2.3 – Coloured depth map for the Gulf of Cadiz, divided into classes. The 150 meters contour corresponds to the limit of the continental shelf, the yellow/blue transition marks a major slope break that defines the beginning of the continental slope (displayed in blue tones) and the white areas represent the deep domains.

Three Abyssal Plains are identified in the deep margin, the Tagus, Horseshoe and Seine abyssal plains (Figure 2.2). The abyssal plains are separated by two elongated submarine mountains; the Gorringe Bank and Coral Patch Seamount, formed mainly by tectonic processes, and also by volcanism. The Ormonde seamount of the Gorringe Bank was intruded by alkaline volcanic rocks in the Early Paleogene (66 My, Bernard-Griffiths *et al.*, 1997). The Coral Patch Ridge (CPR) seamounts were intruded by Neogene volcanic bodies as described by Geldmacher & Hoernle (2000) and D'Oriano *et al.* (2010). The average depths in the Tagus, Horseshoe and Seine abyssal plains are 5000, 4800 and 4400 meters (white areas in Figure 2.3), respectively, thus showing progressively shallower depths towards the south. The deepest part of the Horseshoe Valley (north of CPR, Figure 2.2), although not as flat and deep as the Horseshoe Abyssal Plain, it is also included in this domain, as it displays a smooth seafloor surface below 4300 meters below sea level (mbsl) (Terrinha *et al.*, 2009; Duarte *et al.*, 2010).

Along the Western Portuguese Margin, the continental shelf (red areas in Figure 2.3) varies between 10 to 15 km in width with gradients between 0.4º to 0.5º, and a slope break located at around 150 meters (Figure 2.4). In the S. Vicente Canyon (SVC) area, the shelf is narrower and the slope break is just under 150 meters deep. In the area north of the SVC, the shelf is wider and its lower limit is just above 150 meters of water depth (mwd). The continental margin in the Gulf of Cadiz, north of the Straits of Gibraltar displays a continental shelf that ranges from 10 to more than 30 km wide, its gradient is usually below 0,3º and the slope break is located at around 150 meters water depth. In the area south and southeast of

Faro, the shelf is narrower and does not reach 10 km in width with the slope break at around 100 mbsl. In the Moroccan coast the shelf is very wide (over 30 km) and slopes are below 0.2º until the slope break located at around 200 meters deep. At the Straits of Gibraltar the continental shelf is disrupted by the ENE-WSW erosive trough that connects the Atlantic Ocean with the Mediterranean Sea.

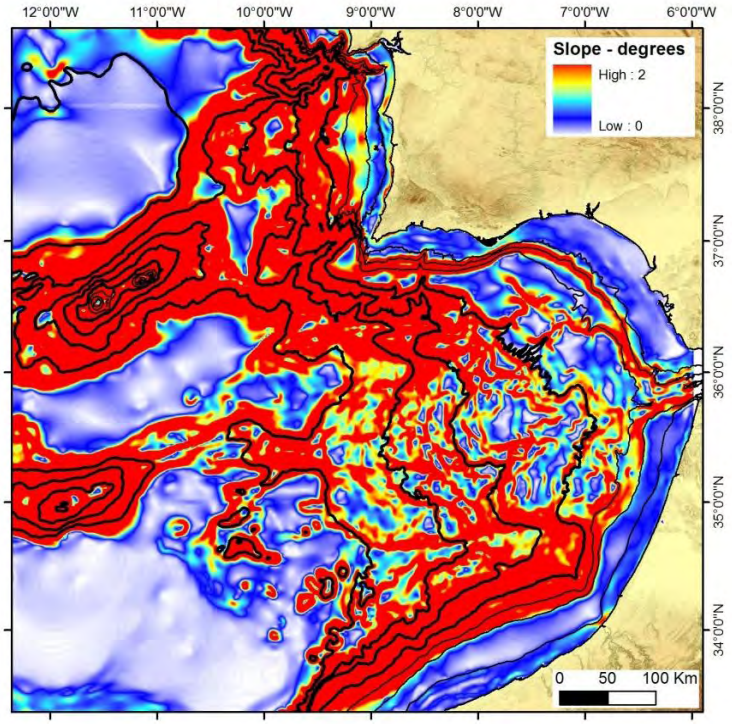

Figure 2.4 – Slope Map of the SW Iberia from Gebco dataset. Red indicates higher gradient values (≥2º), thin contour lines correspond to depths of: 100, 200 and 500 meters; thick contour lines are every 1000 meters. Note the contrast between shallower and deepest areas and the intermediate ones, where the latter displays a more undulated seafloor with higher mean gradients; also the submarine mountains are very well depicted due to the high slopes, on the other hand, abyssal plains are identified by their extent and flatness.

The continental slope is steepest in the northern part of the Gulf of Cadiz, west of the 8ºW meridian. In this area, a major slope break is located at around 800 meters deep (yellow/light blue transition on Figure 2.3), and the bathymetric drop reaches over 1500 meters, with mean gradients as high as 12º and local values higher than 25º. Slope widths in this area vary between 12 to 25 km. Between the upper slope break at around 150 m deep and the sharper one at around 800 m, there is an area with very low average gradients (<1º) where no major irregularities or features exist (Figure 2.2 and 2.4). The foot of the slope is located at depths between 3000 and 3500 meters and does not connect directly with the Horseshoe Abyssal Plain, but through the Horseshoe Valley (Figure 2.2). To the east, in the inner part of the Gulf of Cadiz, the continental slope is smoother, with mean slopes of 0.8º over an area 270 km wide, a prominent slope break with incised gullies is absent.

The continental rise lies at around 4200 meters, defined by the Horseshoe Valley to the north of Coral Patch Ridge (CPR), and by the Seine Abyssal Plain to the south (off NW Morocco; Figure 2.2). The absence of a steep continental slope is at least partially explained by the presence of a thick accretionary wedge that obliterates the original structure and features of a passive margin (Torelli *et al.*, 1997; Maldonado *et al.*, 1999; Gutscher *et al.*, 2002). Only near El Jadida (170 km SW of Rabat), a steep continental slope is observed, with mean gradients over 4º and a width of approximately 40 km, between 300 and about 4000 meters of depth.

In the SW Portuguese margin, due to the presence of important active fault scarps, the continental margin bathymetric profile is atypical, showing a stepped continental slope made up of two flat areas and two prominent scarps. The continental slope in this area is up to 150 km wide, between the continental shelf break and the Tagus Abyssal Plain.

The northern part of the GoC, the Southern Portuguese Margin, has a well-developed submarine drainage system, where canyons, minor valleys and gullies incise the steep continental slope. In the shallower areas (above the 800 meters slope break), several depositional sedimentary bodies are present. These are the contourites deposits associated to the Mediterranean Outflow Water (Hernandez-Molina *et al.*, 2006; Terrinha *et al.*, 2009; Roque *et al.*, 2012) and are responsible for most of the flat and smooth seafloor (yellow areas on Figure 2.3). Along-slope processes are also dominant towards the East, in the vicinities of the Straits of Gibraltar. In this area, the Mediterranean Outflow Water system dominates the seafloor morphology producing channels, erosive furrows, contourite channels, several types of drifts, sand waves, dunes and ribbons and sedimentary lobes (Mulder *et al.*, 2003; Somoza *et al.*, 2003; Hernandez-Molina *et al.*,2006; Hanquiez *et al.*, 2007).

The centre of the GoC is occupied by a prominent feature; the arcuate horseshoe shaped wrinkled accretionary wedge (Gutscher *et al.*, 2002), where a succession of crests and trenches, minor closed depressions, salt domes and mud volcanoes have been described (Pinheiro *et al.*, 2003; Gutscher *et al.*, 2009; see Figure 2.2). Active tectonics is well marked on the seabottom morphology, where several fault traces can be identified (some extending for several hundreds of kilometers), in places associated with steep fault scarps and several tectonic plateaus, some with uplifts up to 1km (Gràcia *et al.*, 2003; Zitellini *et al.* 2004; Rosas *et al.*, 2009; Terrinha *et al.*, 2009; Zitellini *et al.*, 2009).

2.3. Tectonic setting

The Gulf of Cadiz is a tectonically complex region, characterized by diffuse deformation over a broad area (> 200 km; Sartori *et al.*, 1994; Hayward *et al.*, 1999; Gutscher *et al.*, 2002; Terrinha *et al.* 2009; Zitellini *et al.*, 2009), where the plate boundary between Africa (Nubia)

and Eurasia (Iberia) is not clearly defined (Morel & Meghraoui, 1996; Hayward *et al.*, 1999). To the East, the plate boundary is located along the Betic-Rif/Tell Arc, and to West along the Azores-Gibraltar Fracture Zone, that includes the Terceira Rift and the dextral strike-slip Gloria Fault (Tortella *et al.* 1997; Hayward *et al.*, 1999; Figures 2.1 and 2.5). The passive margins formed during the opening of the Neotethys Ocean in Mesozoic times, and have been converging since late Cretaceous, controlling the formation and westward migration of the Gibraltar Arc from the Miocene onwards (Srivastava *et al.*, 1990; Rosenbaum *et al.*, 2002; 2004). The present day complex structure of the Gulf of Cadiz results from the oblique convergence between the SW Iberia and NW Morocco rifted margins that was preceded from frontal convergence and progression of a westwards rolling-back slab of oceanic lithosphere under the Gibraltar orogenic Arc. The tectonic extensional fabric associated with the Mesozoic rifting and oceanic break up strongly controls the present day deformation (e.g. Terrinha *et al.*, 2009; Sallarés *et al.*, 2011).

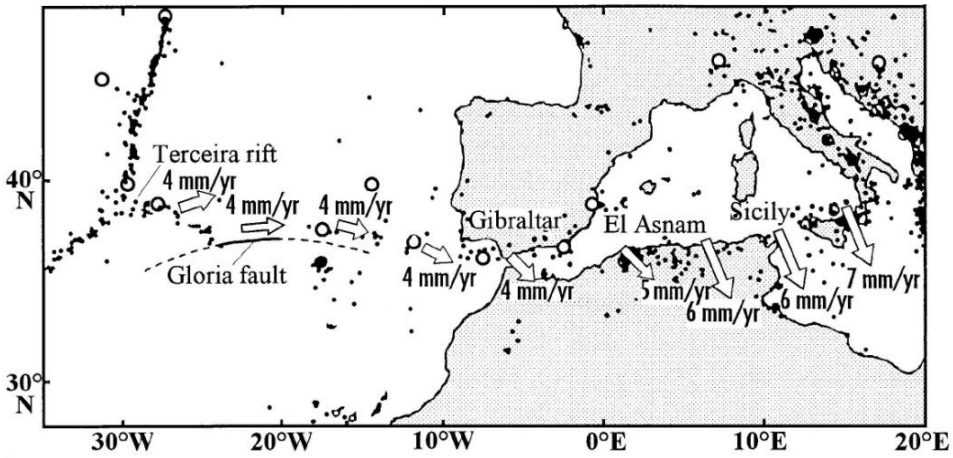

Figure 2.5 - Convergence rates along plate boundary between Africa and Eurasia from NUVEL 1 model (Argus *et al.,* 1989). Dots indicate earthquakes, arrows indicate the direction of plate movement; adapted from Morel & Meghraoui (1996).

For the Gulf of Cadiz, some authors have proposed a discrete, inherited plate boundary, either passing through the Straits of Gibraltar (McKenzie, 1972), or located along the southernmost part of the Morocco Betic Domain (Buforn *et al.,* 1988). Others, however, believe that there is not a single plate boundary, and that the deformation is distributed over a wide area, in agreement with the seismicity and the widespread evidences of recent compressional/transpressional deformation (Grimison & Chen, 1986; Westaway, 1990, Sartori *et al.* 1994; Hayward *et al.,* 1999; Cunha *et al.*, 2012). Gutscher *et al.* (2002), on the other hand, based on MCS profiles, seismic refraction and tomographic data proposed that the Gulf of Cadiz encompasses an active eastwards dipping, subducting oceanic plate under the Gibraltar Arc. More recently, Zitellini *et al.* (2009), using high resolution multibeam swath bathymetry and MCS profiles, recognized the existence of long (up to 600 km), continuous

lineaments between south of the Gorringe Bank and the eastern Gulf of Cadiz, and proposed a new, embryonic plate boundary connecting the Rif-Tell boundary with the Gloria Fault.

Located in the center of the Gulf of Cadiz there is a thick pile of deformed sediments (up to 10 km; Gutscher *et al.*, 2009), which prevents the imaging of the basement and a better constrain of the deep structure. Despite this, in recently acquired multi-channel seismic (MCS) profiles, it is observed that the sediments overly a gently east-dipping strong reflector (Gutscher *et al.*, 2002). This voluminous sediment package was originally interpreted as an olistostrome body by several authors, e.g. Maldonado *et al.* (1999). More recently, Gutscher *et al.* (2002) re-interpreted it as an accretionary wedge associated with the active descending slab of Neothetys oceanic lithosphere. The activity and formation of this large unit is also related with the formation of the Gibraltar Arc.

The amount of shortening associated with the Eurasia-Nubia convergence (Figure 2.5 and 2.6) since the Miocene has been estimated, based on recent geodetic measurements, between 3.5-6 mm/year (Figure 2.5 and 2.6; Calais *et al.*, 2003; McClusky *et al.*, 2003; Fernandes *et al.*, 2003, Stich *et al.*, 2006). Despite of such a slow convergence rate, the SW Iberian margin is the most probable source location for the November 1st, 1755 Great Lisbon earthquake and associated destructive tsunami (estimated M=8.5–8.7; Abe (1979); Mw=8.7±0.4, Johnston (1996); Mw=8.5±0.3, Solares & Arroyo (2004)). This area has generated posterior and large events like the 1969 earthquake (Ms=7.9, Fukao, 1973) or the February 12th, 2007 (Mw=6; Stich *et al.*, 2006).

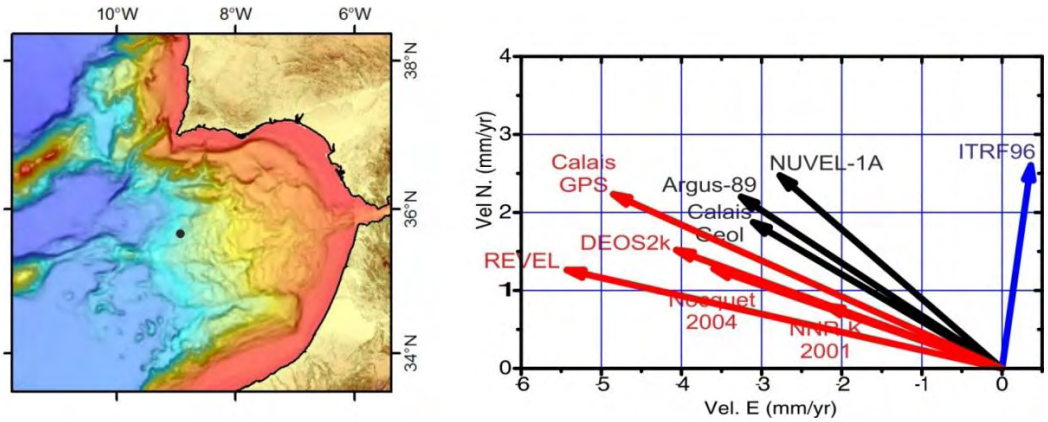

Figure 2.6 – Relative movement between Iberia and Africa calculated from several sources for the position located on the map with the black dot. Vector figure modified from Teves Costa (2005).

2.4. The seismicity and the 1755 Lisbon Earthquake

The seismicity in the Gulf of Cadiz (Figure 2.7) is characterized by disperse, mostly low magnitude earthquakes ($M_w \leq 5$) at relatively shallow depths (<50km), although a large proportion of the events occur within upper mantle depths (Geissler *et al.*, 2010). In nearby areas, some exceptions were registered, like the Granada 1954 event, important by its depth

(<600km) and magnitude (M_w~7; Udías, 1988; Buforn *et al.*, 2004;) and more recently, the M=6.3, 2010 event with hypocentre at 620 km of depth.

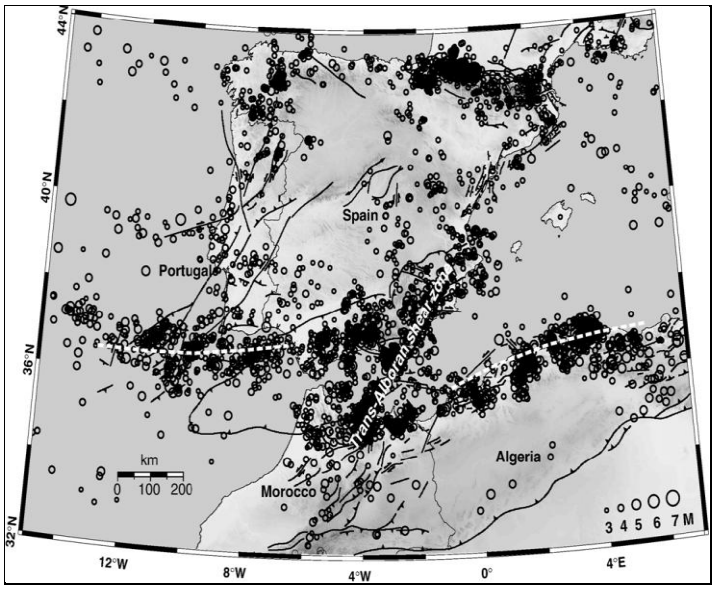

Figure 2.7 - Seismicity of the Ibero–Maghrebian region projected on the map of active and potentially active faults. From Stich *et al.* (2006).

The seismicity pattern is diffuse over a 200-300 km wide area (Figure 2.7 and 2.8). Despite this, most epicentres focus along two elongated belts striking ENE-WSW, and a third one striking NE-SW, between southern Spain and northern Morocco (the Trans-Alboran Shear Zone-TASZ; Figure 2.7), which connects the previous two, defining an overall Z-shape pattern (Stich *et al.*, 2006). The predominant focal mechanisms in the ENE-WSW oriented belts are of reverse and left strike slip faulting, whilst in the TASZ is characterized by predominantly strike-slip and frequent normal faulting events (or a combination of the 2 mechanisms - i.e. transtensional; Bufforn *et al.*, 2004; Stich *et al.*, 2006, 2007). In summary, at a large scale the structures can be defined as two transpressional belts or corridors connected through a transtensional shear zone.

As represented in Figure 2.7, the westernmost ENE-WSW seismicity corridor, located on the northern part of the Gulf of Cadiz, consists of an alignment of three areas of more focused seismicity (see also Figure 2.8): the Gorringe Bank, the S. Vicente submarine canyon and the Guadalquivir Bank (Borges *et al.*, 2001).

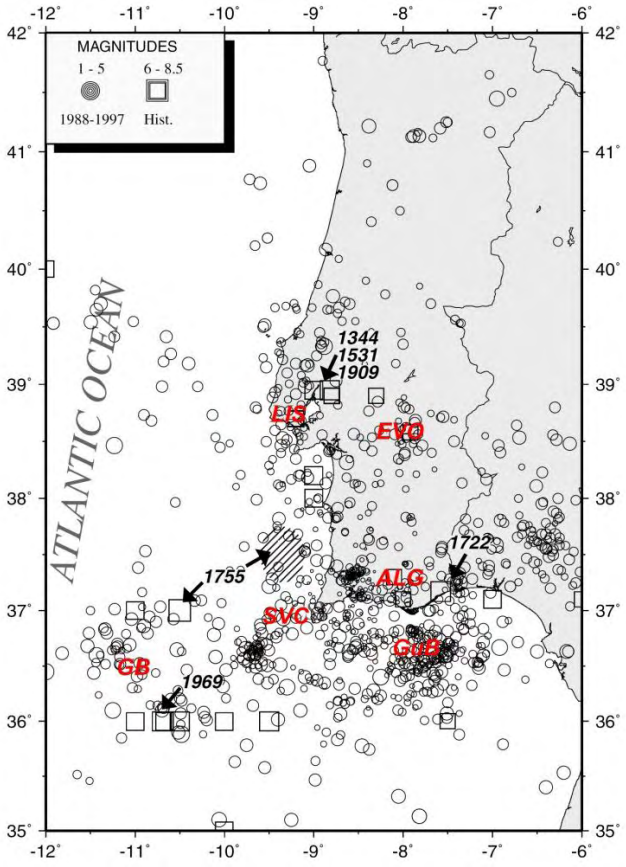

Figure 2.8 - Instrumental seismicity (1988-1997) and location of important historical earthquakes. LIS – Lisbon, ALG – Algarve, EVO – Évora, GB – Gorringe Bank, SVC – S. Vicente Canyon, GuB – Guadalquivir Bank; 1755 points to two possible source areas for the 1755 Lisbon Earthquake. Modified from Borges *et al.* (2001). See text for description.

Although the instrumental seismicity (Figure 2.8) indicates that the area is mainly characterized by moderate seismic activity (mean M < 5), there is evidence in the historical records of a number of major earthquakes and some associated tsunamis. Examples of these are: (1) the 1755 Great Lisbon earthquake (8.5<M<8.8); (2) the 1722 Tavira earthquake (M ~ 7.5), with an associated tsunami that swept half of the south Portuguese coast (Mezcua, 1982); (3) the 1531 event, that hit the SW coast; (4) the February 28th, 1969 event (M=7.9; Fukao, 1973) with epicentre in the Eastern HAP and the 60-63 A.C. tsunami that devastated the city of Cadiz (Gutscher, 2006).

The November 1st, 1755 earthquake in particular, was a major catastrophic event, which destroyed a large part of Lisbon, one of the largest European metropolis at the time. The city was devastated firstly by the very destructive earthquake, then by several tsunami waves, and finally by the fires that burnt for more than a week. It is believed that the seismic intensity (Mercali scale) in the Lisbon area was around X-XI (Figure 2.9; Baptista *et al.*, 1998a). The shakes were felt at great distances, in places like the Azores and Madeira Islands, Great Britain, Belgium, Sweden and Finland, and the tsunami waves travelled across the Atlantic and were felt in the Caribbean Sea.

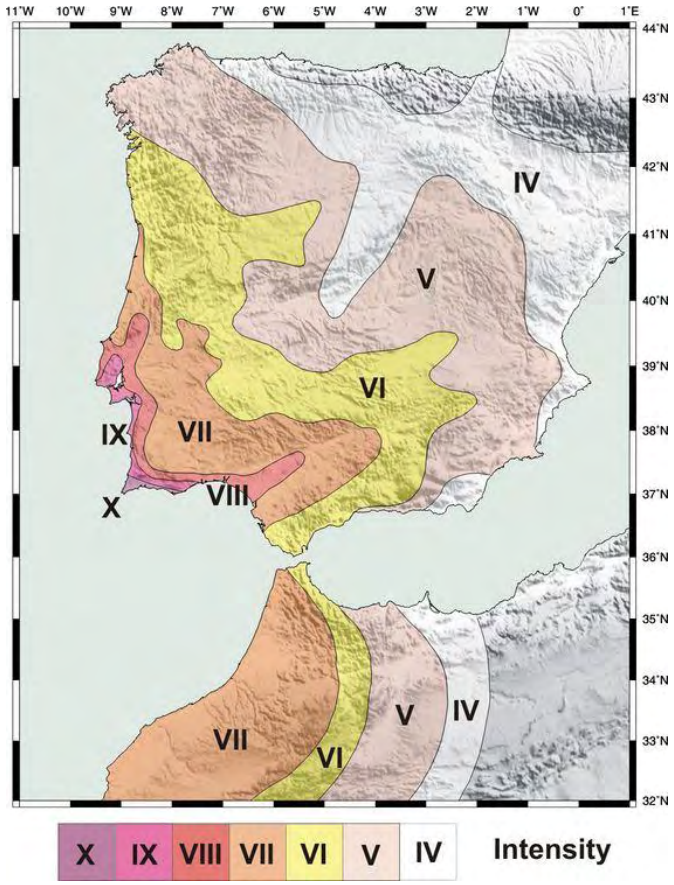

Figure 2.9 – Isoseismals calculated for the 1755 Lisbon earthquake, Adapted from Levret (1991) in Teves Costa, 2005.

The tsunami waves reached about 15 meters in S. Vicente Cape, 11 meters in Lagos and around 15 meters in the vicinity of Cadiz. In the city of Lisbon the records of the tsunami point to a wave height of about 6 meters and a land penetration of 250 meters, responsible for a death toll of around 900 people. Records of the tsunami are widely spread and found in the south of Algarve (Andrade, 2002), south Spain (Morales *et al.*, 2008), Morocco (Levret, 1991), in the seafloor of the Horseshoe Abyssal Plain (records of a turbidite, Lebreiro *et al.*, 1997) and in the Scilly Islands (Bryant, 2001).

Gutscher *et al.* (2006) computed a recurrence rate for these kind of events of about 1000-2000 years. More recently, Cunha *et al.* (2010) based on a numerical model for the Gulf of Cadiz neotectonics, which takes into account the distribution of the seismic strain and the geodetic data, suggested larger recurrence periods (>3500 years) for an earthquake of M_w 8.5-9 in the area. These authors, however, did not consider a tectonic regime dominated by an active, dipping to the east subduction zone but controlled only by the oblique convergence of Nubia and Eurasia.

Despite its magnitude, and the large amount of historical, geological and geophysical studies carried out in this region the source of the 1755 Lisbon earthquake is still matter of debate. The first studies, suggested the Gorringe Submarine Mountain as the most likely source

(e.g. Machado, 1966). Further studies and new data started to provide other more reliable and also more complex models as candidates for the source. After some seismic and bathymetry surveys the Marquês de Pombal Thrust (MPT) was proposed as a source for the event, as is displaces the seabottom around 1 km and was located in an area where it could be responsible for the tsunami (Zitellini *et al.*, 1999).

It has been shown, however, that the area of rupture associated with the MPT is insufficient to generate an earthquake the magnitude of the 1755 earthquake (Jonhston *et al.*, 1996; Stich *et al.*, 2007). These led several authors to propose compound, multiple rupture models, which involve the MPT and other mapped active structures, both in the Gulf of Cadiz and in the SW Iberia Margin (Terrinha *et al.*, 2003; Gràcia *et al.*, 2003; Zitellini *et al.*, 2004, Ribeiro *et al.*, 2006; Stich *et al.*, 2007; Terrinha *et al.*, 2009; Cunha *et al.*, 2010).

Other models were also developed that involve the MPT acting together with a back-thrust (Zitellini *et al.*, 2001), MPT in conjunction with the south thrust of the Guadalquivir Bank (Baptista *et al.*, 2003), surface rupture of the accretionary wedge associated with the East-dipping subduction beneath the Gibraltar arc (Gutscher *et al.*, 2002), the rupture of the accretionary wedge associated with another source located in the NW of the area (Gutscher *et al.*, 2006) or an unspecified source acting together with the lower Tagus valley fault (Vilanova *et al.*, 2003).

Despite this, until now no proposed model has gathered consensus concerning the 1755 Lisbon Earthquake tectonic source, when considering the tsunami travel times and heights, the recorded seismicity and fault activity.

2.5. The geologic evolution of the SW Iberian Margin

The existence of oceanic lithosphere of probable Jurassic age between southwest Iberia and northwest Nubia has apparently been confirmed by recent seismic refraction data published by Sallarés *et al.* (2010). Palinspatic reconstructions (Fourcarde *et al.*, 1991; Dewey *et al.*, 1989; Srivastava *et al.*, 1990; Stampfli & Borel, 2004) had already proposed the existence of oceanic lithosphere as part of a transtensional tectonic corridor between southwest Eurasia and northwest Africa. The western Iberia margin break up, between Iberia and Newfoundland in Canada, occurred only during Early Cretaceous times, propagating from the south to the north (e.g. Fourcarde *et al.*, 1991; Pinheiro *et al.*, 1996; Tucholke *et al.*, 2007; Sibuet *et al.*, 2007).

In order to understand the present setting and structural framework of southwest Iberia it is required to take into account the complex geodynamic history of the area: rifting and continental breakup in the Mesozoic, compression between Late Cretaceous and Late Miocene, and predominant dextral transpressive regime since the Pliocene. The first major event refers to continental rifting, followed by the continental breakup and oceanic drifting,

responsible for the formation of sedimentary basins in the south of Iberia. The compressional event is associated with the northward movement of Africa with respect to Eurasia and the consequent Africa-Eurasia plate collision, causing basin inversion and consumption of oceanic lithosphere below Iberia. In more recent times (Pliocene-Recent) the transpressional strain is caused by the oblique convergence between Africa and Iberia.

All these tectonic regimes have been associated with either the formation of large faults or their re-activation, some of them presently active, the development of diapiric structures, the uplift of large crustal blocks forming tectonic plateaus and, more recently, the emplacement of the so-called accretionary wedge, and the extrusion of fluids (gas and oil seeps and mud volcanoes).

2.5.1. The Mesozoic Rifting

During the Mesozoic Iberia drifted apart from the American and African plates due to the opening of the Atlantic and Neotethys Oceans, respectively (Figure 2.10a and 2.10b). The Neotethys in the eastern Mediterranean started to spread in the Permian, separating Eurasia and Africa, but it was only in late Jurassic times that the spreading propagated into the western segment of the Mediterranean, contemporaneous with the opening of the Central Atlantic (Figure 2.10b) (Olivet *et al.*, 1984). The rifting and oceanic crust formation in the Mediterranean was in fact a complex process comprising the formation of several minor basins, spreading centers and abandoned rift branches (Stampfli & Borel, 2004).

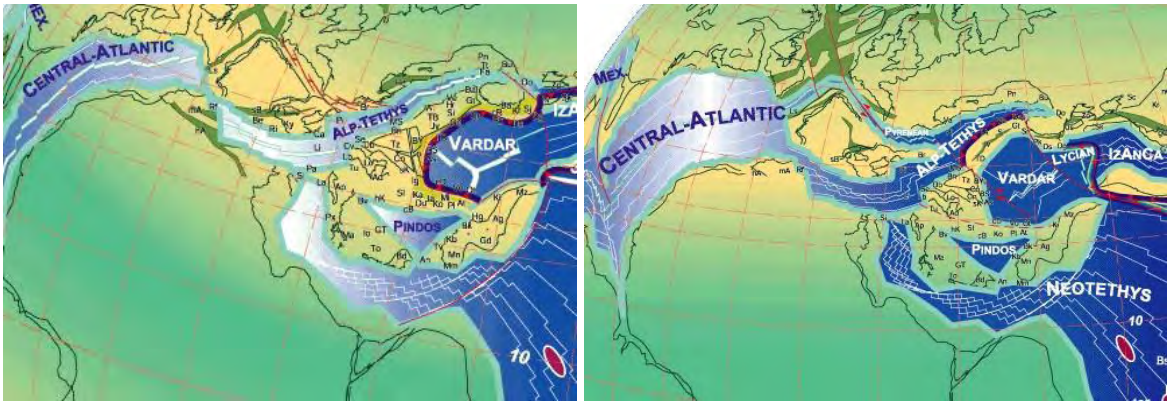

Figure 2.10 - The Mediterranean plate tectonic framework showing: a) the spreading of the Neotethys and the Central Atlantic in the Oxfordian (M25 anomaly, 155 My); b) the beginning of the oceanization in the North Atlantic in the Aptian (M0 anomaly, 112 My). From Stampfli & Borel (2004).

Due to this configuration, the local effects are that the Algarve Basin developed with more intensity when Africa was drifting away from Iberia (Figure 2.11) allowing the basement to sink and sediments to accumulate. In the same manner, the western margin basins were developing faster when Iberia was drifting away from North America, during the late Jurassic-Early Cretaceous (Rosenbaum *et al.*, 2002)

During the Triassic, the SW Iberian margin was part of the Neotethys rift systems and formed what is now the present continental margin of southern Portugal and Spain and, to the south, Morocco. During the latest Triassic-earliest Jurassic stages southern Iberia was part of the Central Atlantic Magmatic Province were rifting were accompanied by a vast episode of tholeiitic volcanism (Verati *et al.*, 2007).

During the first stages of the opening of the Central and North Atlantic Ocean (~133 My, Pinheiro *et al.*, 1996), the precursor of the Gloria Transform Fault consisted of a major transform boundary between the Iberian and African plates, pushing the latter eastwards (Figure 2.10; Dewey *et al.*, 1989; Maldonado *et al.*, 1999).

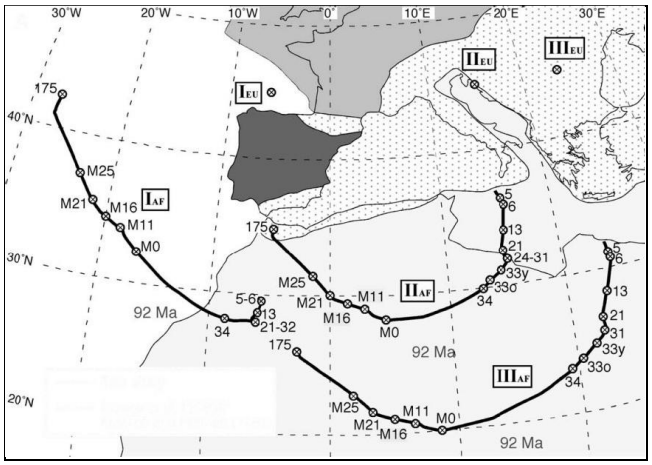

Figure 2.11 – Relative movement between Africa and Iberia since Middle Jurassic. From Rosenbaum *et al.,* 2002.

The relative motion between the two plates has been estimated in ~200 km between the Middle Jurassic (170 My) and the Early Cretaceous (Figure 2.11; 120 My, Srivastava *et al.*, 1990). Associated with this left-transtensional kinematics, the Late Variscan NE-SW trending faults were reactivated with extensional movement (Ziegler, 1988; García-Navarro *et al.*, 1994) causing progressive thinning of the continental crust in the southern Iberian continental crust and the formation of rift basins, like along the Algarve Basin in Portugal (Terrinha, 1998).

This extensional regime lasted throughout the Mesozoic, interspersed with minor tectonic inversion episodes taking place in the Lower Jurassic, Middle-Upper Jurassic boundary and Lower Cretaceous (Grafe & Wiedmann, 1993; Terrinha, 1998; Terrinha *et al.*, 2002), and was followed by a post-Upper Cretaceous compressive tectonic regime with associated inversion and uplift causing sub-aerial exposure of the sediments and erosion.

2.5.2. The Iberia-Africa-Eurasia Convergence

Due to the opening of the North Atlantic, since the Late Cretaceous, the western part of the Mediterranean, including the Africa plate and the Adria Block, rotated in a counter clockwise

sense with respect to the main Central European block (Srivastava *et al.*, 1990). This rotation forced the convergence between Africa and the European plates and led to the formation of the overthrust of the Alpine Tethys by the Adria Block and stoppage of the spreading of the Ligurian Ocean (Facenna *et al.*, 2001; Stampfli & Borel, 2004). The compressional deformation in the Gulf of Cadiz and Western Mediterranean (Neothetys) has been amplified by the contemporaneous (123 to 80 Ma), ~30º counter clockwise rotation of Iberia (and its westwards migration) associated with the opening of the Bay of Biscay (Figure 2.12; Galdeano, 2000; Sibuet *et al.*, 2004).

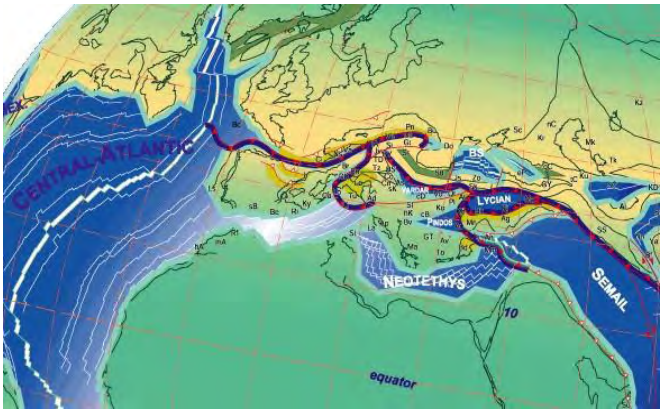

Figure 2.12 – Plate tectonic setting in the Central-North Atlantic and the western Neothetys at 70 Ma, highlighting the subduction zones around Iberia. Modified from Stampfli & Borel (2004).

During the Eocene, the northwards slow movement of Africa with respect to Iberia (Dewey *et al.*, 1989), led to the trapping of the Ligurian Ocean between Africa and Europe (Cavazza *et al.*, 2004). In Iberia, most of the deformation focused in the north, with crustal shortening and the formation of the Pyrenees, to the East, and subduction in the Bay of Biscay, to the west. In the Oligocene, the Ligurian Ocean started to be subducted beneath SE Iberia leading to the formation of back-arc basins and scattered continental terranes (Figure 2.13a). This subduction zone could have extended further west, possibly underneath SW Iberia (Terrinha, 1998).

In the Western Mediterranean, this compressive regime, which resulted in the inversion of the Mesozoic extensional structures, had its peak around Eocene-Oligocene times and lasted until the Miocene (Srivastava *et al.*, 1990; Terrinha, 1998; Maldonado *et al.*, 1999; Stampfli & Borel, 2004). According to Dewey *et al.* (1989) the N-S shortening between the Africa and Iberia amounts to about 200km from Middle Oligocene to Upper Miocene, followed by more than 50km of oblique NW-SE shortening since the Upper Miocene until the present day.

In post-Oligocene times the convergence rate between Africa and Iberia and Central Eurasia was considerably reduced, causing the roll-back of the northwards-subducting slab, which in turn induced its southward migration (Figure 2.13b). This led to the formation of several

back-arc, extensional basins and production of new oceanic crust, such as in the Valencia Trough and the Gulf of Lion Basin (Royden, 1993; Gutscher *et al.*, 2002; Rosenbaum *et al.*, 2002). Simultaneously, some terranes were transported south with the overriding plate, such as the Alboran Block, the Kabylies, the Sardinia/Calabria Block and Corsica, which eventually collided with Africa (Figure 2.13c and 2.13d).

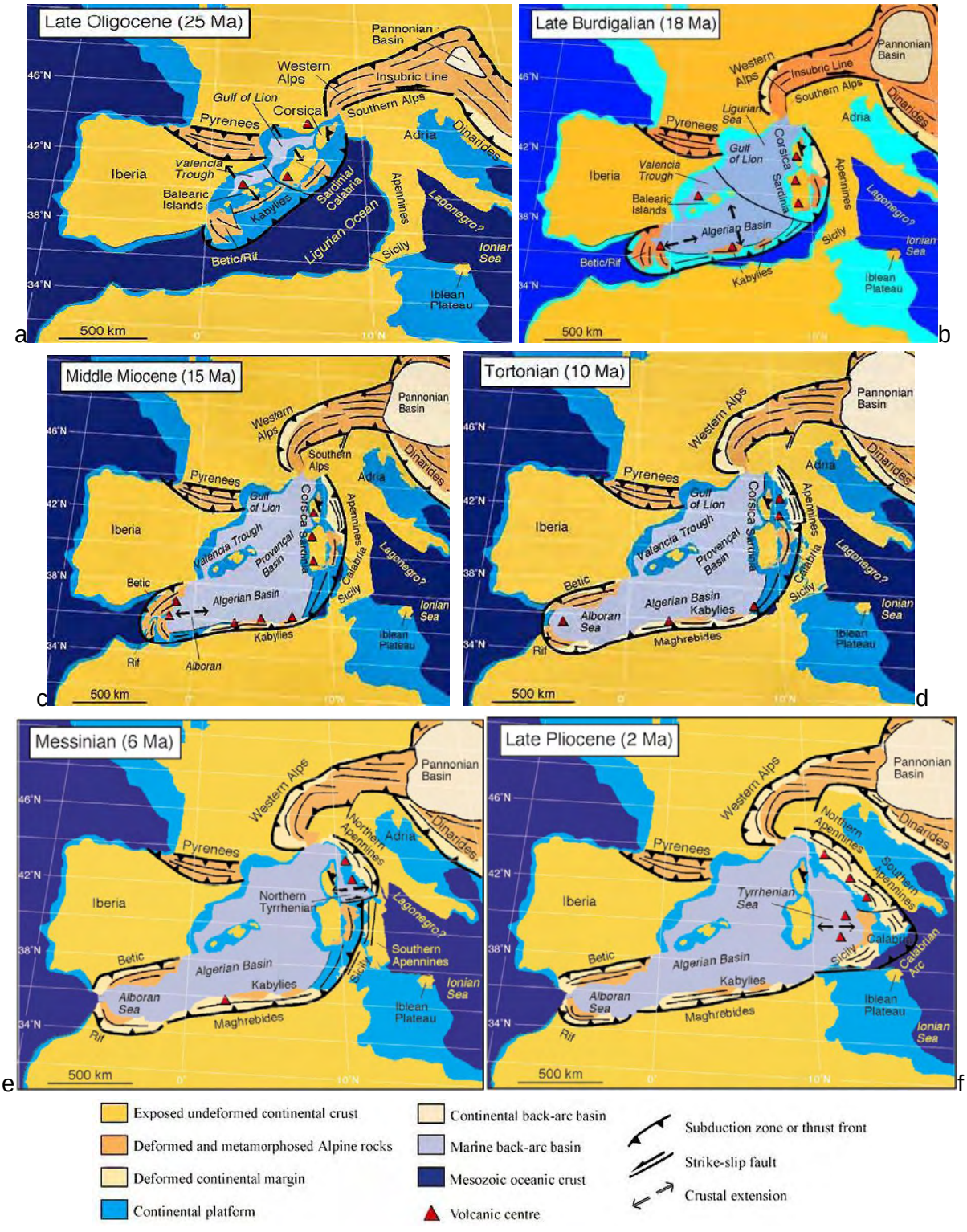

Figure 2.13 – Diagrams illustrating the tectonic plate framework evolution since the Late Oligocene. From Rosenbaum *et al.* (2002). See text for description and references.

These changes caused the subduction to become more curved and its southward migration pushed Alboran towards the SW, to a position closer to its present location (Figure 2.13d). The SW migration caused it to collide with African and SE Iberian margins generating the Betic (Iberia) and Rifian (Africa) orogens in Middle/Lower Miocene times. In the same way, the southward movement of the Kabylies and consequent collision with the African margins generated the Maghrebides and the collision of Corsica and Sardinia with the present day Italian Block generated the Apenines (Figure 2.13e and 2.13f).

The Miocene through Present westwards roll back of the oceanic slab of the Neo-Tethys (or western part of the Ligurian ocean shown in Figure 2.13e and 2.13f, dragged continental terranes that were later emplaced onto the southern Spain and northern Morocco, forming the internal domains of the Betic and Rif orogens. Continuation of the roll-back and collision of Africa and Iberia led to the formation of the Gibraltar Arc.

The Gulf of Cadiz is now undergoing a generalized transpressional tectonic regime as a result of a NW to WNW movement of Nubia (African Plate) with respect to Iberia.

2.6. Oceanographic setting

After the Messinian salinity crisis and subsequent flooding of the Mediterranean Basin, the water circulation and current paths' in the GoC have been highly controlled by the exchange of masses of water through the Straits of Gibraltar, the Mediterranean Outflow Water (MOW, circulating between 600 and 1500 mwd) and the Atlantic Inflow surface and intermediate waters. The water flowing out of the Mediterranean Sea is immiscible with the Atlantic waters since it is hotter and denser (salinity <38‰), therefore, it forms an individualized current which can reach speeds up to 2,5m/s (Hernandez-Molina *et al.* (2006) and references therein). Further to the west, it deflects towards the north, due to the Coriolis effect, and separates into two main branches (Figure 2.14a): the Mediterranean Upper Water and the Mediterranean Lower Water.

The main current is a geostrophic current (Mediterranean Upper Water), which is warmer (T>13.7ºC) and circulates along the Iberian slope (between -300m and -700m) as far as the Cape S. Vicente, carving the Alvares Cabral Moat (see Figure 2.2 for location). The other current (Mediterranean Lower Water) is ageostrophic, less saline (under 37.4‰), colder (T<13.5ºC), and is separated by the complex morphology of the seabottom into 3 minor sub-branches (Hernandez-Molina *et al.*, 2006), all flowing cross-slope towards the west/NW sector (Figure 2.14a).

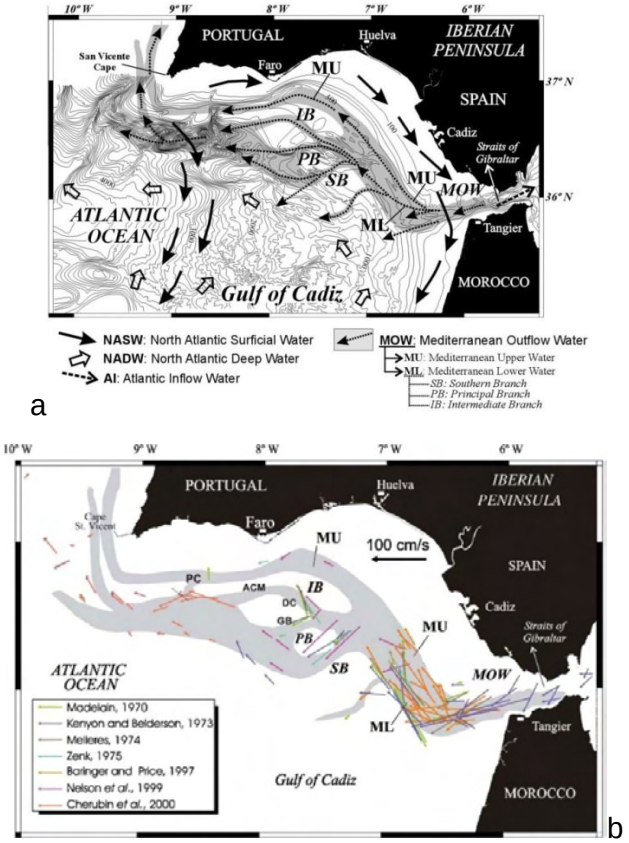

Figure 2.14 – Water circulation patterns in the Gulf of Cadiz. a) Diagram illustrating the travel path of the different currents in the Gulf of Cadiz, including the Mediterranean Outflow Water; b) Measurements of the direction and speed of the several branches of the MOW. Different length segment corresponds to measured speeds. ACM - Alvarez Cabral Moat; DC - Diogo Cao Channel; GB - Guadalquivir Bank; PC - Portimão Submarine Canyon; MU - upper core of the MOW; ML - Lower core of the MOW; SB - southern branch of the ML; PB - principal branch of the ML and IB - Intermediate branch. Images from Hernandez-Molina *et al.* (2006).

All these currents flow at the seabottom level carving more or less important channels at depths between -1200m and -1500m. Around the 7º30'/8ºW the currents loose speed (Figure 2.14b), become neutrally buoyant and detach from the seafloor, flowing between the intermediate and deep Atlantic waters. The decrease in speed also leads to sediment charge sorting, therefore generating different sedimentary bodies along its track. The coarser sediments deposit closer to the Straits of Gibraltar, while the more fine grained (like the contourite deposits south of Algarve) deposit further away from it. This sorting and changes in currents and seafloor characteristic, define three major morphosedimentary domains (Figure 2.15): (1) the proximal scours in the major channel that carries all the waters flowing out of the Mediterranean; (2) the more deeply incised channels (although smaller in size); and (3) the sedimentary lobes, where the suspended charge settles on the seafloor (Hernandez-Molina *et al.* (2006) defines more domains as it includes the submarine canyons and other features).

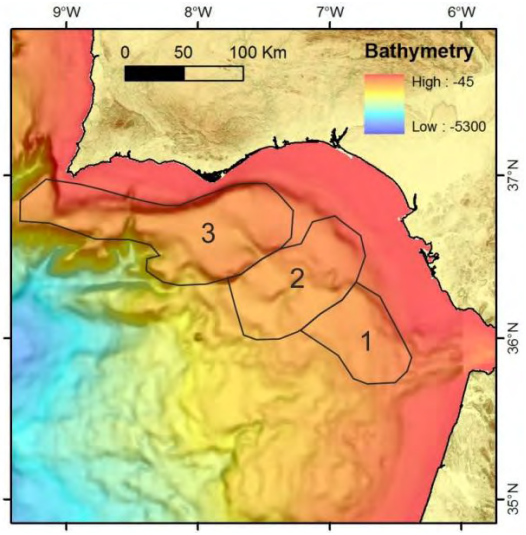

Figure 2.15 – Map of the Gulf of Cadiz displaying the three major domains regarding their features related to the MOW: 1- the proximal scours domain; 2 - the channels domain and 3 - the sedimentary lobes domain. Domains names and mapping modified from Hernandez-Molina *et al.* (2006). See text for further details.

Chapter 3 - Data and methods

In this chapter, a description of the different types of data used for this work, such as bathymetry, seafloor reflectivity and seismic profiles is presented, followed by an explanation of the methods and procedures used to prepare this data ready for interpretation, which includes processing of the bathymetric and reflectivity data and map production in GIS environment.

3.1. Bathymetry

The bathymetric maps were performed using the following three datasets: the multibeam data that belongs to the SWIM dataset (Zitellini *et al.*, 2009), the General Bathymetric Chart of the Oceans (GEBCO) bathymetry to fill the *no data* areas of the SWIM dataset, and the INGMAR dataset for shallow areas.

3.1.1. The multibeam swath bathymetry

The SWIM dataset resulted from a compilation of nineteen high resolution multibeam swath bathymetry surveys (Figure 3.1 and Table 3.1) performed in the Gulf of Cadiz and SW Iberia (Diez *et al.*, 2006; Zitellini *et al.*, 2009). It involved several research vessels from seven countries, sixteen different research teams and over 200 days of ship time. The data was acquired from 1978 to 2006, mapping an area that exceeds 180.000 km^2, from depths ranging from 30 meters to more than 5200 meters.

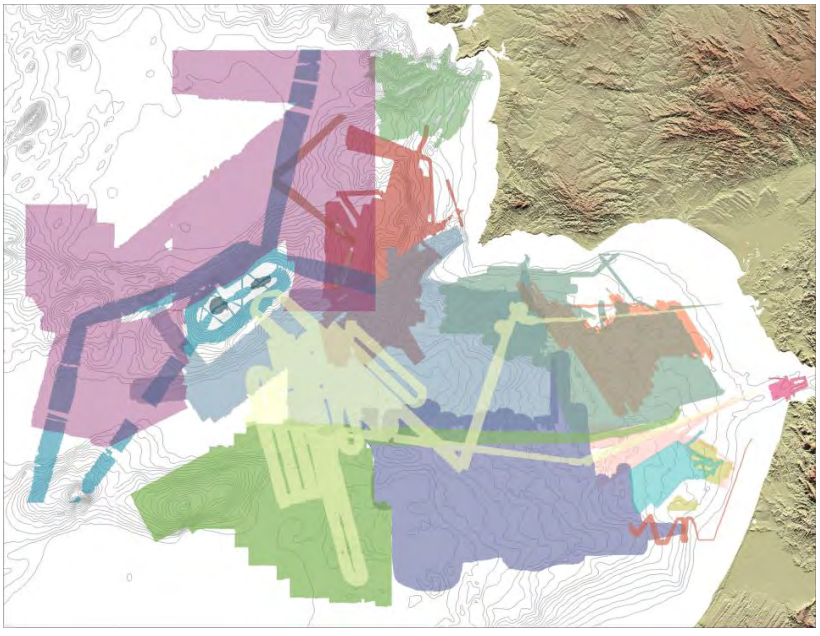

Figure 3.1 - Coverage of the different surveys that were compiled in the SWIM multibeam dataset.

Table 3.1 - Summary of the surveys of the SWIM compilation.

Survey		Year	Institution	Vessel	Data*	Echosounder
1	ESPICHEL	1991	IFREMER	R/V L'Atalante	MB	Simrad EM 12D
2	TASYO	2000	IGME	R/V Hespérides	MB	Simrad EM 12S
3	PARSIFAL	2000	CSIC-CMIMA	R/V Hespérides	MB	Simrad EM 12D
4	CADISAR 1	2001	Univ. Bordeaux	R/V Le Suroît	MB	Simrad EM 12D
5	HITS	2001	CSIC-CMIMA	R/V Hespérides	MB	Simrad EM 12D
6	CADIPOR	2002	Ghent Univ.	R/V Belgica	MB	Simrad EM 1002
7	GORRINGE	2003	IAMC – CNR	R/V Urania	MB	Reason Seabat 8101
8	TV-GIB	2003	UBO	R/V Le Suroît	MB	Simrad EM 12D
9	PICABIA	2003	CSIC-CMIMA	R/V Marion Dufresne	MB	Thompson Sea Falcon 11
10	GAP	2003	Bremen Univ.	R/V Sonne	MB	Simrad EM 120
11	MATESPRO	2004	CGUL	R/V D. Carlos I	MB, ref	Simrad EM 120
12	CADISAR 2	2004	Uviv. Bordeax	R/V Le Suroît	MB	Simrad EM 12D
13	DELILA	2004	IUEM/UBO	R/V D. Carlos I	MB, ref	Simrad EM 120
14	DELSIS	2005	IUEM/UBO	R/V Le Suroît	MB	Simrad EM 12D
15	SWIM 2005	2005	ISMAR	R/V OGS Explora	MB	Reason Seabat 8150
16	HERMES	2006	NOC	R/V Charles Darwin	MB	Simrad EM 12S
17	SWIM 2006	2006	CSIC-CMIMA	R/V Hespérides	MB	Simrad EM 120
18	EMEPC data	2005	EMEPC	R/V D. Carlos I	MB	Simrad EM 120
19	SISMER database	1978	IFREMER	R/V Jean Charcot	MB	GIC Seabeam
		1990	IFREMER	R/V L'Átalante	MB	Simrad EM 12D

*Data: MB- multibeam; ref- backscatter data.

Most of the area was surveyed to comply with an IHO order 3 hydrographic surveys (Standards for Hydrographic Surveys 4th Edition, April 1998). This implies that accurate and true sound velocity profiles had to be acquired during the survey and that all areas should be covered by verification lines crossing the main survey direction at 90 degrees, these should cover 10% of the surveyed area, thus providing a good quality control. However, some surveys did not perform true sound velocity profiles (SVP) and the bathymetric data was calibrated with XBT (Expendable Bathythermograph) sampling. The sound velocity in the water varies with several parameters (especially temperature and salt concentration) being its control in this area vital to identify the MOW currents and the effects it has on the data collected. Most of the SVP profiles were performed until a depth of 2000 meters and a global LEVITUS database was used to extrapolate to higher depths. The dataset has been improved with new data every year and merging of new surveys is done in a way to minimize artifacts and maintain a 100 m cellsize overall grid for the Gulf of Cadiz and SW Iberia.

3.1.2. The Gebco Global Bathymetry

The General Bathymetric Chart of the Oceans (GEBCO) (2008 edition, www.gebco.net/) dataset was used to fill the unsampled areas of the multibeam datasets. Since it is a global database its detail and precision is not comparable with the multibeam dataset. It is largely generated by combining quality-controlled ship depth soundings with interpolation between sounding points guided by satellite-derived gravity data. This data was imported into ArcGIS and gridded with a cellsize of 1 km; when merged with other datasets its depth scale was resampled to fit with the SWIM dataset in order to eliminate color shifts in the borders between the datasets.

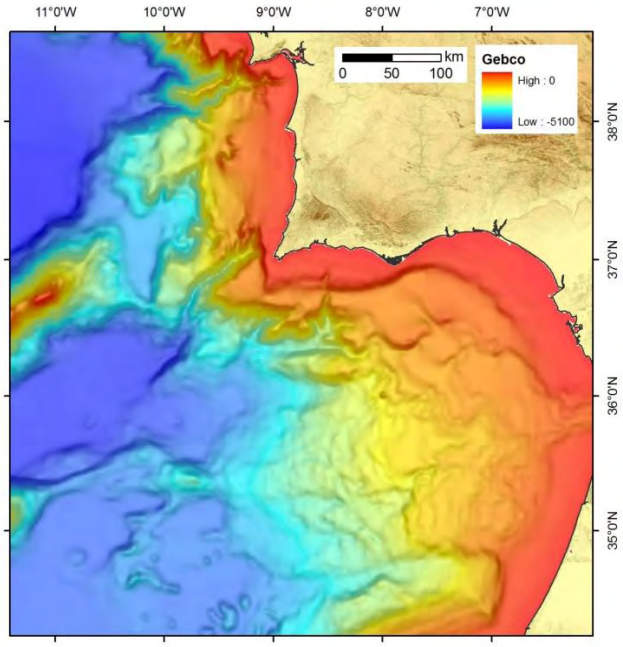

Figure 3.2 - Example of a Gebco grid for the Gulf of Cadiz and SW Iberia.

3.1.3. The Ingmar Bathymetric Model

For the shallower areas, the INGMAR dataset (acronym of INvestigação em Geologia MARinha, in English "Investigation on Marine Geology") was used because its bathymetric model is of better quality then the GEBCO dataset. This is a bathymetric model produced by the Marine Geology Dept. of LNEG from 1971 to 1999 and consists of bathymetric contours spaced every 10 meters which start at the shoreline and extends until 200 meters water depth (mwd). It resulted from the merging of data from several oceanographic cruises, depths of sampling surveys and ship track depth data.

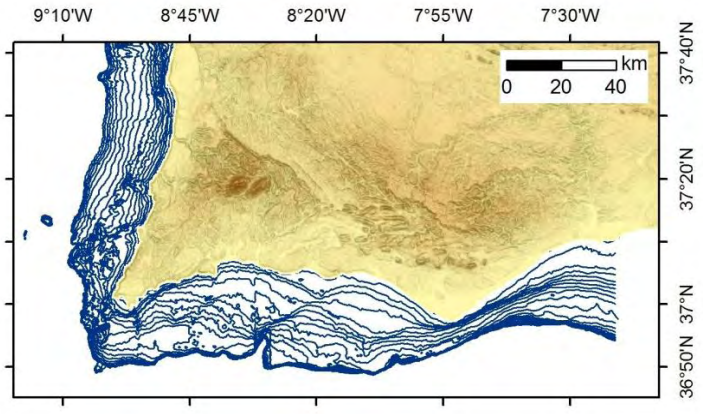

Figure 3.3 - The Ingmar bathymetric model, contours every 10 m down to 200 mwd.

3.2 Seafloor reflectivity

The reflectivity dataset used in this work for the geologic interpretation has two main sources (Figure 3.4): i) the reflectivity data from the MATESPRO and DELILA surveys and ii) data

from sidescan sonar from the Naval Research Laboratory (USA) published in Hernandez-Molina *et al.* (2006).

The reflectivity data available was acquired by the same probe of the multibeam data, the Simrad EM120 installed on the keel of the R/V D. Carlos I used for the MATESPRO and DELILA surveys.

The data from the Naval Research Laboratory (NRL), USA, covers a large area of the Gulf of Cadiz, from the vicinities of the Straits of Gibraltar to close to the Horseshoe Abyssal Plain. The two datasets were merged for the purpose of the geologic interpretation.

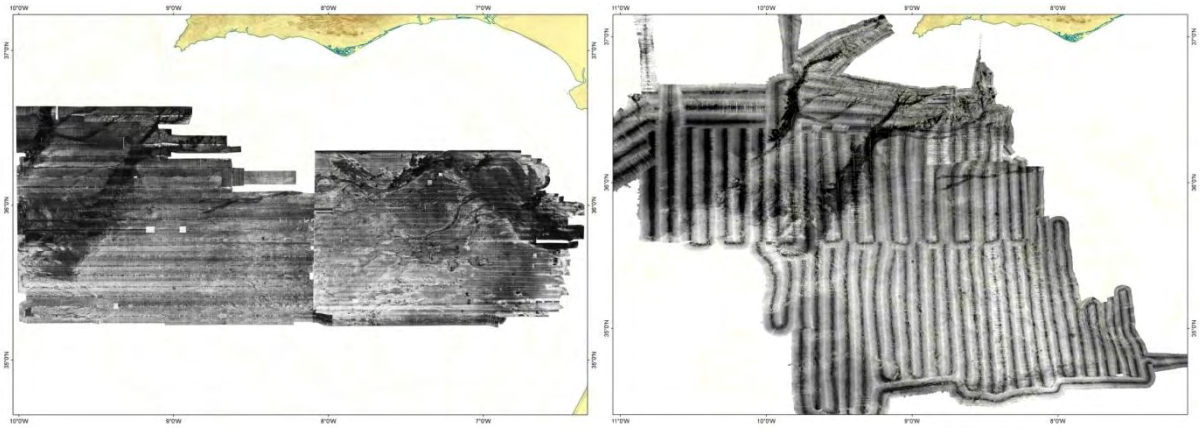

Figure 3.4 – Images of the acoustic response of the seafloor; left: sidescan sonar mosaic from the NRL, USA. Original data published in Hernandez-Molina *et al.* (2006); right: backscatter data from the multibeam probe of the Matespro and Delila surveys.

3.3 Seismic profiles

Several high resolution and multichannel seismic profiles were used to better constrain the boundaries between the morphotectonic domains, as well as to understand the subsurface dependence of these domains in what respects their nature, formation and evolution.

3.3.1. The Multi-Channel Seismic (MCS) Database

The MCS database was constructed of profiles acquired in the Gulf of Cadiz and Western Iberian margin from 1974 to 2006. These surveys were imported into a data management and interpretation software suite from Landmark Corporation (OpenWorks, SeisWorks and ZMap-plus). The database comprehends vintage seismic profiles, profiles acquired by different scientific teams, different equipment and processed with different techniques. Thus, the data had to be prepared, to allow the integrated interpretation of all the available profiles.

3.3.2. Summary of the MCS dataset

The interpreted MCS profiles were acquired during the cruises Chevron, ARRIFANO 92, BIGSETS, IAM, SISMAR, VOLTAIRE and SWIM-2006 (see Figure 3.5 for location). Below

follows a description of the acquisition systems and of the known and/or inferred processing steps of each survey.

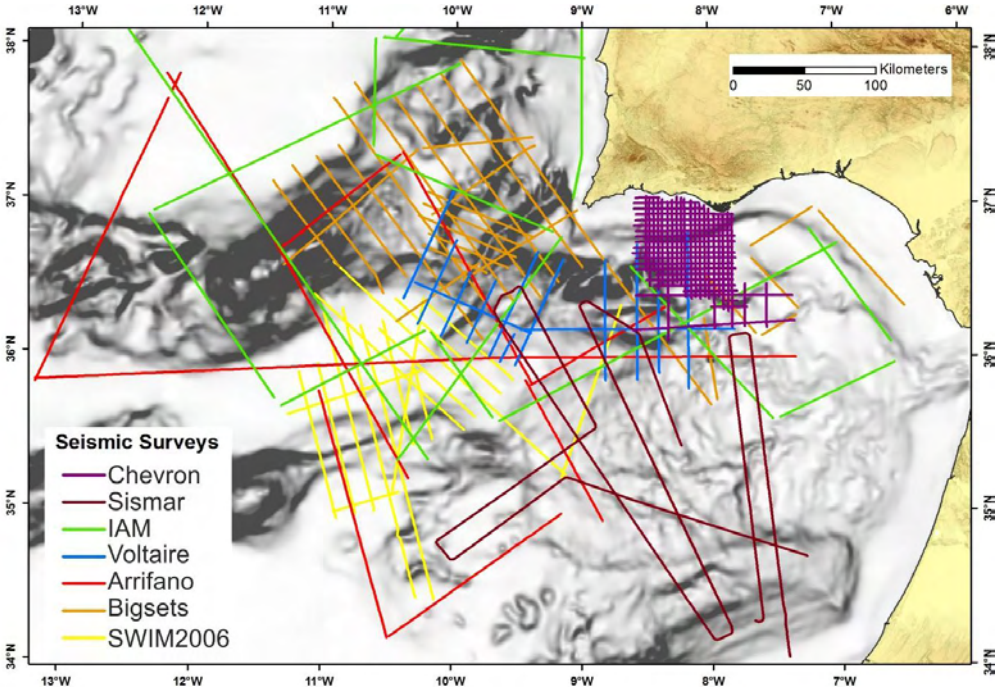

Figure 3.5 - Location of the seismic profiles loaded in the seismic workstations and used for this study.

3.3.2.1. The ARRIFANO survey

The ARRIFANO survey was carried out in 1992, onboard the R/V Explora (Figure 3.6). ARRIFANO is the acronym of Rifean Arc (Arco Rifano). According to Sartori *et al.* (1994) the ARRIFANO profiles were acquired using a seismic source of 32 air guns array, 3 km long streamer, 120 recording channels, with a sampling rate of 2 ms and a shooting interval of 50 meters.

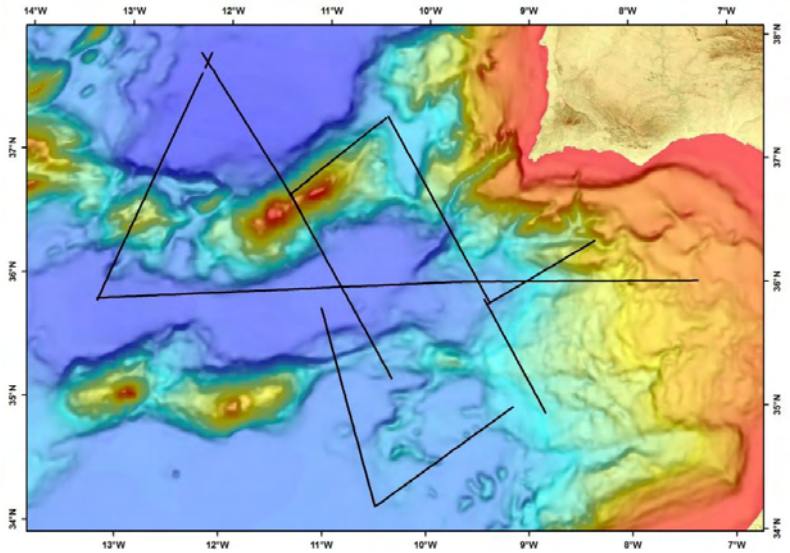

Figure 3.6 – Location of the ARRIFANO seismic profiles.

The processing stages of the ARRIFANO profiles included re-sampling to 4 ms, spiking deconvolution, NMO (normal move out) correction, spherical divergence correction, finite-difference wave-equation migration and a time variable filter.

3.3.2.2. The BIGSETS survey

The BIGSETS MCS profiles were acquired in 1998 on board the R/V Urania (Figure 3.7). The technical information regarding the BIGSETS profiles is found in the headers of the paper plots. These indicate that a 1200 m streamer and four GI guns were used, shooting at 25 meters intervals. Data was recorded from 48 channels, at 4 ms sample rate.

The processing sequence included a re-sampling to 4 ms, the NMO correction and an automatic gain control (AGC) with a 1000 ms time gate. Absence of diffractions on the water bottom suggest that the profiles were time migrated with a constant sound velocity profile (approx. 1500 m/s?). The large AGC time gate modified vertically and/or laterally the seismic facies of some seismic units.

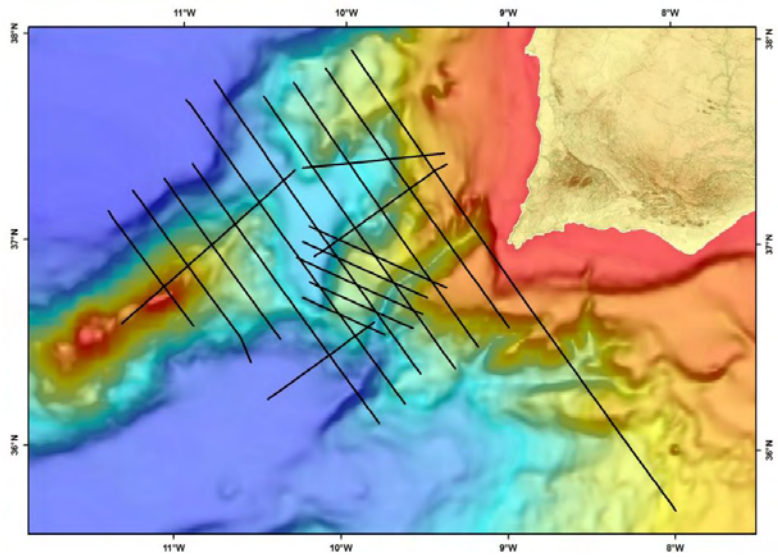

Figure 3.7 – Location of the BIGSETS seismic profiles.

3.3.2.3. The IAM survey

The Iberian Atlantic Margin (IAM, Figure 3.8) survey performed in 1992 (Banda *et al.*, 1995). The technical information of this survey was found in the headers of the paper plots. The profiles were acquired using an air gun array for seismic source, shooting at 75 meters intervals; 5 km long streamer with 192 channels were recorded with a 4 ms of sample interval.

The processing history of the IAM profiles was also inferred from the headers of the paper plots. These profiles were re-sampled to 8 ms and have a lower vertical resolution in the input SEG-Y files. Processing also included the NMO correction, a Kirchoff migration with a

constant velocity of 1700 m/s and an AGC with a 500 ms time gate. The AGC effect, like in the BIGSETS profiles, alters much the seismic facies of several units, this was due to the fact that these profiles frequently image the chaotic seismic facies units common in the Gulf of Cadiz, and these facies had sharp variations in mean amplitude. The result was the characteristic high/low amplitude bands with the AGC time gate height.

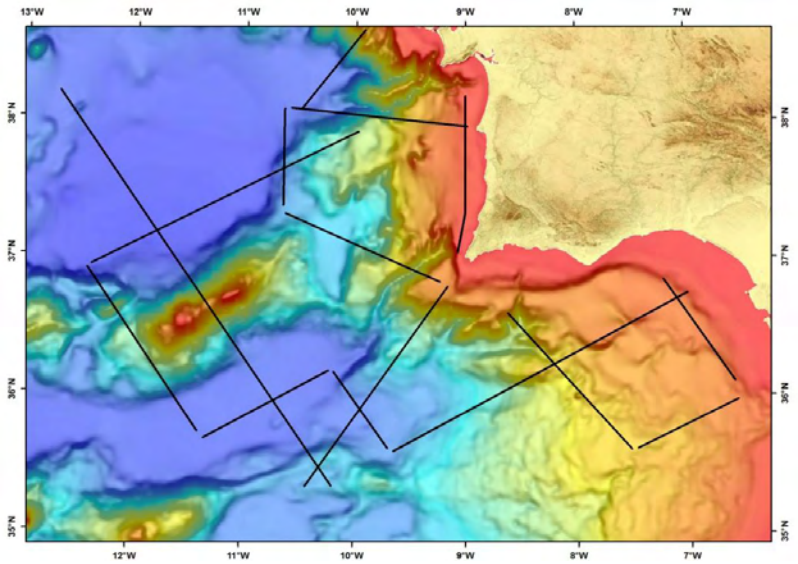

Figure 3.8 – Location of the seismic profiles of IAM survey.

3.3.2.4. The SISMAR survey

The SISMAR survey was done in 2000 onboard the R/V Nadir (Figure 3.9). According to Thiebot & Gutscher (2006), MCS acquisition was done with an air gun array shooting at 75 and 150 meters intervals (for 30 and 15 fold CDP coverage), and data was recorded from 360 channels with 4 ms sample interval. The imported SISMAR files all had abundant diffractions suggesting that these were non-time-migrated stacks (or single fold?).

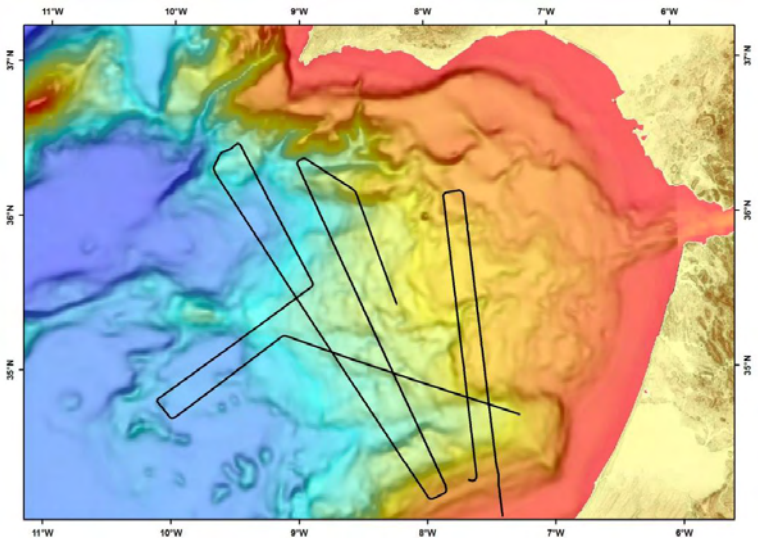

Figure 3.9 – Location of SISMAR seismic profiles.

3.3.2.5. The VOLTAIRE survey

The VOLTAIRE survey (Figure 3.10) was executed in 2002 onboard the R/V Urania. The cruise report (Zitellini & Scientific-Party, 2002) gives the technical details of the acquisition and processing. The streamer was 1.2 km long, four GI guns were used, shooting at 50 m intervals; trace data was recorded from 48 channels with 1 ms sample interval.

The processing flow of the VOLTAIRE profiles included: re-sampling to 2 ms, trace editing, shot delay removal, amplitude recovery, predictive deconvolution, velocity analysis every 200 CMPs, NMO correction, stack, band-pass frequency filtering and time-migration using stacking velocities.

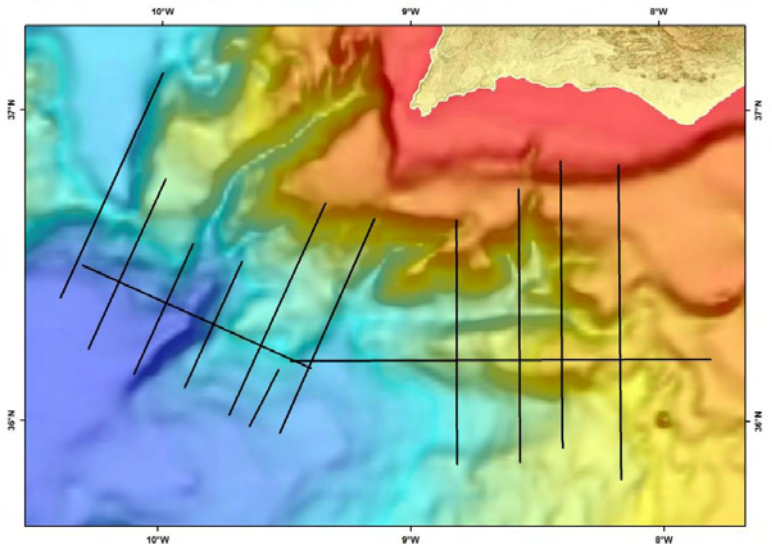

Figure 3.10 – Location of the VOLTAIRE seismic profiles.

3.3.2.6. The SWIM-2006

The SWIM-2006 survey was carried out onboard the R/V Hesperides in 2006 (Figure 3.11). The source used was an eight air guns array shooting every 25 meters; trace data was recorded from 96 channels, with a sample interval of 2ms.

The SWIM-2006 cruise report provides a detailed description of the processing flow applied during the survey (Gràcia & Scientific-party, 2006). Processing consisted of trace editing, static recording delay correction, spherical divergence correction, top mute, FK and bandpass frequency filter, predictive deconvolution (minimum phase), NMO correction (constant velocity of 1700 m/s), spiking deconvolution and Stolt FK migration (1500 m/s).

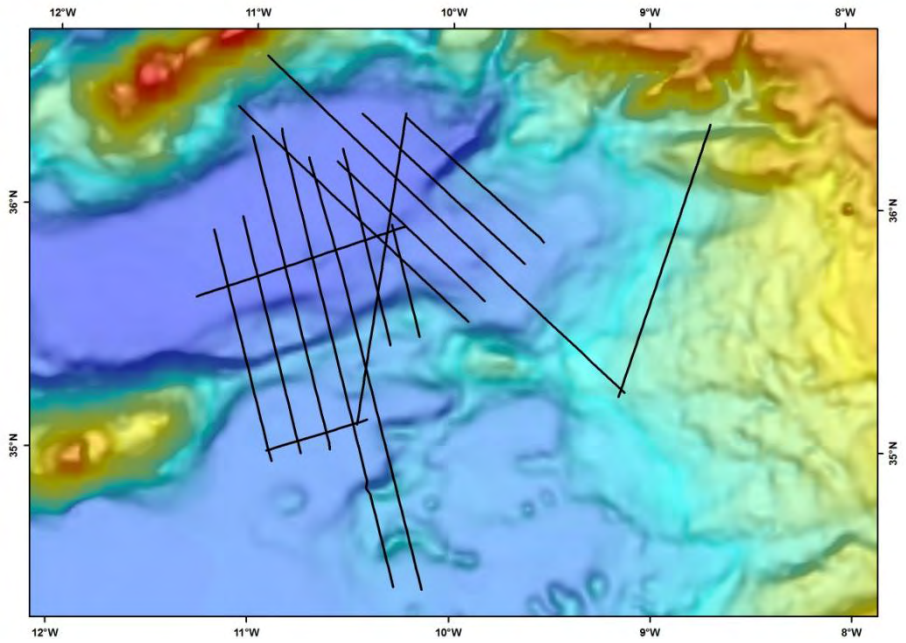

Figure 3.11 – Location of the SWIM-2006 seismic profiles.

3.3.2.7. The Chevron Survey

This survey was done by the Chevron oil-company in the 1970's and was aimed for hydrocarbon exploration in the areas closer to shore, in the Algarve Basin, east of the Portimão Canyon. The position of the MCS profiles display an orthogonal regularly spaced pattern striking N-S and E-W (Figure 3.12). These data were only available in paper format, therefore had to be scanned, undergo image treatment and then converted to SEG-Y format and finally imported into the seismic projects. By doing this, data was available for display and interpretation alongside all the others survey's profiles.

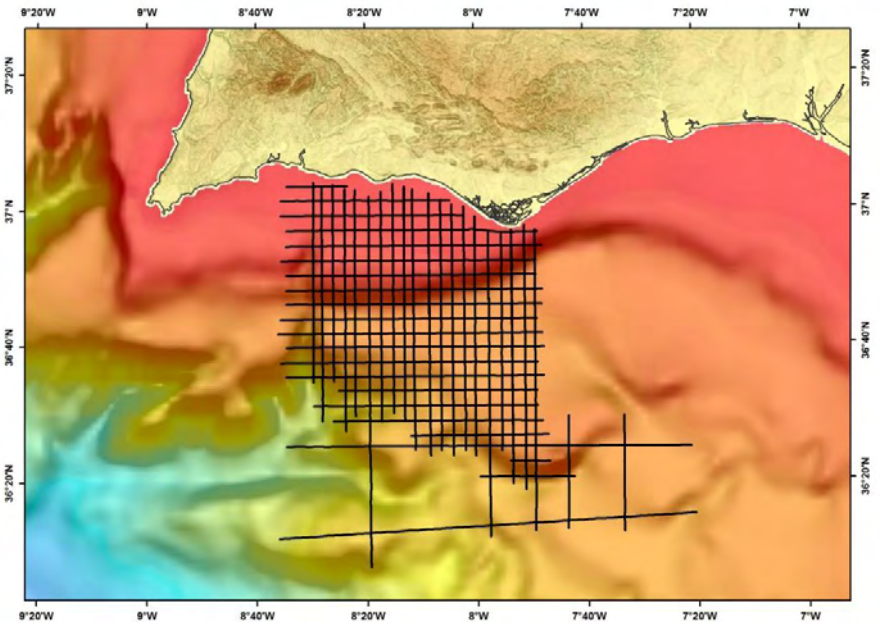

Figure 3.12 – Location of the seismic profiles of the Chevron survey.

3.3.3. Data formats

The number of MCS from each survey is listed in Table 3.2. The profiles imported into the MCS database were originally in SEG-Y format, these were imported, both non-migrated and migrated, maintaining their respective sampling intervals. The Chevron survey SEG-Y's were not original as they were created from paper profiles. All imported profiles had at least one 4 ms sample interval version (when the original was not available a resampled version was created). This was done in order to allow consistent visual ties between different seismic surveys.

Table 3.2 – Number of seismic profiles available from each survey.

Surveys	Year	Number of profiles
Chevron	1974	44
IAM	1992	15
Arrifano	1992	11
Bigsets	1998	23
Sismar	2000	9
Voltaire	2002	14
SWIM	2006	16

3.3.4. Trace positioning

Trace positioning was done preferably through the coordinate fields in the SEG-Y trace headers. ASCII files with shot point navigation were used in the cases where coordinate data was absent in the SEG-Y trace headers; shot point numbers were matched to the values of the FFID field in the SEG-Y trace headers to determine shotpoint-trace relationships. There were no perceived horizontal misties between the digital profiles with the exception of the profile VOL03 (VOLTAIRE cruise) that had inconsistent FFID values. The position of the imported profile VOL03 respects roughly its navigation trackline but has perceived horizontal misties around 500 meters with respect to the bathymetry grid and other MCS profiles (this problem was latter manually corrected).

3.4. Data Processing

Both bathymetry and sonar data, after acquisition, needed to undergo several editing and filtering processes. An overview of the multibeam echo-sounders is given followed by a brief description of the bathymetry and sonar data processing.

3.4.1. The multibeam echo-sounders

3.4.1.1. Introduction

In the last 30 years, acoustic mapping of the seafloor has seen major improvements: from single beam echo-sounders to multibeam swath bathymetry echo-sounders with reflectivity probes.

The development and improvement of multibeam bathymetry was a major turning point in the seafloor related studies as it can rapidly sample large areas with great detail and accuracy which are essential for the study of geomorphology and seafloor facies. The advantage of such systems is enhanced when combined with accurate positioning systems (such as Global Positioning System), GIS software and advanced computer graphics output (such as live 3D models).

3.4.1.2. Multibeam echo-sounders: Overview

At first, seafloor mapping was done using single beam technology. Although accurate, this method was time consuming as the area covered was reduced and depth data was only acquired directly below the ship's position. Multibeam systems brought a major improvement with its instant acquisition over a large area and not only along the ship's track (Figure 3.13) greatly reducing the amount of ship time required to survey.

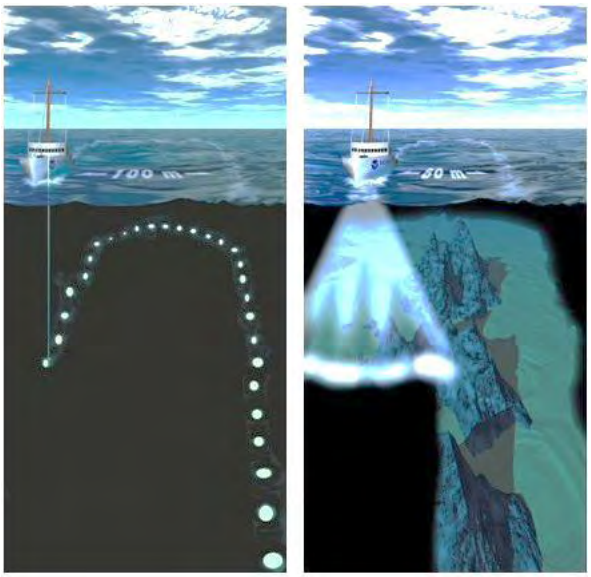

Figure 3.13 - Schematic representation of the difference between single beam and multibeam swath seafloor surveying.

The new deep water systems allows to sample areas up to 6 times the water depth, for example in an abyssal plain 4000 meters deep, data is acquired up to 24 kilometers in one sweep.

The multibeam systems work by sending an acoustic impulse from a transducer (located at the bottom of the ship) that travels through the water column, reaches the seafloor and gets

bounced back to the receiver in the ship. The time taken is calibrated with the sound travel speed in the water and a distance is calculated by the following formula:

$$\text{Depth} = \text{speed} \times \text{time}/2$$

Another advantage of the multibeam systems is that it can retrieve the acoustic intensity (backscatter) providing not only bathymetry data but also a rough sonar imagery, both acquired at the same time. The first provides information of morphology of the seafloor and is measured in meters; the latter provides data related to the reflectivity of the seafloor surface and is measured in decibels (dB). It is dependent on the incidence angle, local topography and substratum nature. Thus, in an area of no major morphological variations, different values of acoustic backscatter must be related to different seabed facies, i.e., hard acoustic responses are indicative of hard rock or coarse grainsizes (gravel, sands) while softer returns are indicative of loose materials or thinner grainsizes (silts or clays).

3.4.1.3. The main characteristics of the multibeam probe

A multibeam echo-sounder is composed by several elements: transmission and reception parts (at 90º at the bottom of the ship), transmission electronics, reception unit and ancillary systems, such as a positioning system, attitude sensor unit (giving roll, pitch, heave and the heading values) and sound velocity profiles sensor (SVP).

Its main characteristics are acoustic frequency, maximum angular aperture, number of beams, beam spacing, length of emission and cadence of the emission (Figure 3.14).

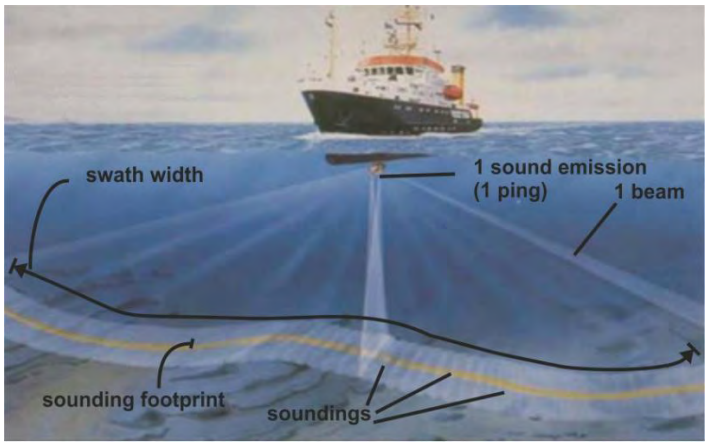

Figure 3.14 - Diagram of some elements related to a multibeam echo-sounder. For each sound impulse (known as ping) several beams (make up a swath) are emitted and reach the seafloor in one point (footprint), each value is named as sounding.

The resolution of systems increases with frequency, but so does the attenuation in the water column, in this way higher frequency systems can only operate at smaller depths than low frequency ones. The maximum angular aperture determines the swath width with typical values between 90º to 150º. The total number of beams changes depending on the echo-

sounder. The time interval between two successive emissions (pings) of the sounder has to be longer than the duration of the return trajectory of the more external beams.

3.4.2. Multibeam data processing

The multibeam swath bathymetry data has to undergo a process of data cleaning in order to be ready for map production. All the surveys underwent such a process before being merged onto the SWIM compilation. This involved various tasks that were carried out mainly using Ifremer's Caraibes, Caris HIPS and SIPS and PDS2000 software.

3.4.2.1. The original data

For the software to use the data, the original data provided had to have two types of information: the navigation and the soundings data, the first was the position of the vessel at all times and the latter had information for each ping: time and ship's attitude (heading, roll, pitch and heave) and also values attached to every beam (vertical depth and relative position to the ship).

3.4.2.2. Import

The first task was to import the raw data onto the software; this import process had different modules for the different probes from the various ships used. Each one had different attributes related with the properties of the equipment, like the number of beams or the angles between each beam. The purpose of this first step was to have the data available and ready to be edited on the program. The data imported in this step was related to the navigation, bathymetry (ping data) and sound velocity measurements. The data associated with each ping was: time (1/1000 second resolution), heading of ship at the moment and a validity status (at the import stage all the soundings are valid). Concerning the beams per ping (number depends on sounder) the following data was imported: vertical depth, across distance (distance perpendicular to ship's axis) and along distance (gap in the direction of ship's axis).

3.4.2.3. The project

A project was created in order to have a workspace available to access the data. Associated with it, was the Geodesic system, where geographic coordinates referred to the WGS84 ellipsoid. This was an important setting as it influenced map production. Other data such as information regarding the area, vessel and project were defined. Merging several navigation and bathymetric files were also done before any editing. Corrections for shifts in the

navigation, if needed, were done either manually or automated and were applied before editing.

Attitude corrections, such as heading, roll, pitch and heave, done to correctly place the soundings were also done at this stage and before editing.

3.4.2.4. XY creation

Data were imported as pairs of XY positions of the ship and relative position of the soundings with respect to the vessel, thus the bathymetry information did not have a geographical data associated with it. This step merged the sounding depths and the geographical information, creating a XYZ database with all the imported information that was then available and ready for editing.

3.4.2.5. Filtering/data cleaning

The first step was to invalidate (no data was erased, but neglected for any action taken) the outer beams as these are the ones less accurate and the overlap between contiguous track lines was enough to produce a 100% coverage without using these beams. Following that, an automated filtering was applied; this filtering of soundings from the bathymetry files was done by comparison to an estimated value on a Digital Terrain Model (DTM). This general DTM was built (using only the validated pings) by interpolating the true soundings and generate a regularly spaced XYZ grid. There were many variables that controlled this process such as the algorithms used and the weight of the original data in the creation of this grid. The weight of the neighbouring data refers to the relative importance of the adjacent cells of the grid in the value of one cell, i. e., the produced DTM presented a more smooth or sharper surface if the more distant values had higher or lower significance in the central value of a cell, respectively. The generated DTM has to be made in order to represent all the bathymetric features surveyed and was used as a first reference in an automated quality control of the data. This was done in a way that every sounding that differed more than a percentage value (usually 1%) from the grid was considered invalid (Figure 3.15). There had to be a balance between flagging a sounding as invalid and allow many soundings to be valid so that this automatic filtering was useful and saved time in the future.

After the automated filtering, a manual one was applied (Figure 3.16) where the reviewer invalidated more values (that passed the automated filtering and would only add noise to the final grid) or validated soundings previously considered invalid. This was done one line at a time but was best performed with several rows simultaneously as this allowed better removing of artifacts between adjacent rows and better understanding of the bathymetric features.

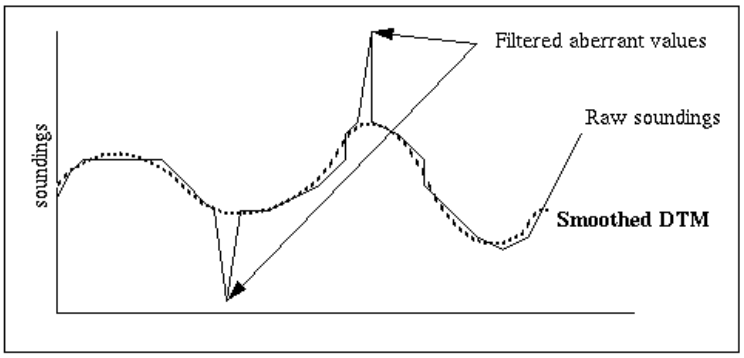

Figure 3.15 - Schematic representation of the relation between the reference DTM (dotted) and the raw true soundings (line) and the values invalidated.

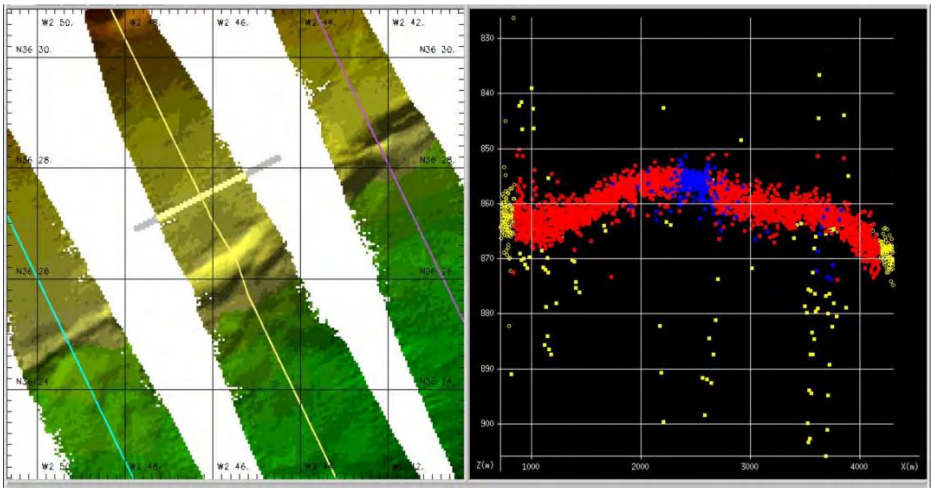

Figure 3.16 - Example of the bathymetric manual filtering module. On the left: plan view of three rows; right: vertical section of the middle row (highlighted band over the data). Open yellow circles (on the borders) are outer beams invalidated at the import stage, filled yellow squares are soundings invalidated by the automated filtering using the reference DTM, blue and red are valid soundings (colors indicate if depth was calculated using amplitude or phase). In this graphical interface soundings are selected and manually classified as valid or invalid.

3.4.2.6. SVP corrections

The SVP corrections were applied only to the validated soundings dataset. In the case of the south Portuguese margin this correction was particularly important to compensate for the different sound travel velocities of the Mediterranean Outflow Water (Figure 3.17). This was done by applying the correction of the sound travel velocity in the water to the last SVP performed.

At the end, with all the validated and corrected soundings, two kinds of files were extracted and imported into other software or used in map production; these were either a grid (regularly spaced DTM) or a file with all the validated soundings of the survey (irregularly spaced).

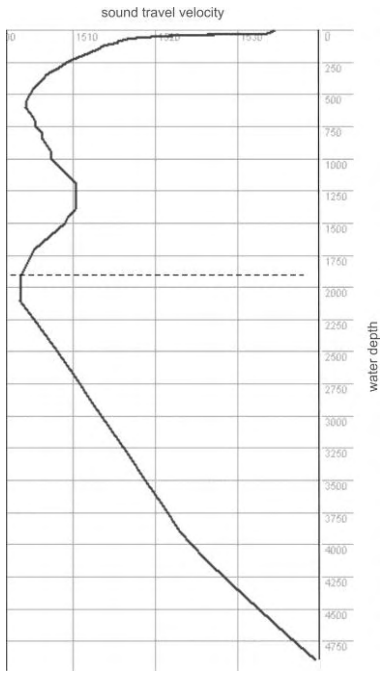

Figure 3.17 - Example of a SVP data collected in the Delila survey. On the top profile the inflection is due to the presence of the MOW; the dotted line at around 2000 mwd is the limit between real data measured (above the line) and data from Levitus global database of sound travel velocities (under the line).

3.4.3. Seafloor Reflectivity Processing/Filtering

Reflectivity data was processed using Ifremer's Caraibes software suite. When reflectivity data is handled and edited it results in a mosaic. Processing of data acquired by multibeam echosounders followed these steps: data importation, mosaic preparation and creation, mosaic editing and modification.

3.4.3.1. Original data

The data required for Caraibes to process reflectivity was mainly composed of three types of information: navigation, bathymetry containing soundings, and the seafloor reflectivity values. The first gave the ship positions at any time, it is a chronological time series of points including time, latitude and longitude; the bathymetry data were organized as a series of pings containing the time, ship's attitude (heading, roll, pitch, heave) and bathymetry data (vertical depth and position relative to the ship); the reflectivity data is measured in dB. The reflectivity mosaic created is defined by a cartographic projection (in this case the Mercator projection was used) and a cell size (contains a set of lines and columns with a constant spacing).

3.4.3.2. Data import and mosaic creation

In the import step, the software had to identify the data regarding the navigation, bathymetry and reflectivity values. The navigation data was given in order to place the soundings but also to have the ship tracks to minimize artifacts related to central beams. The bathymetric data was imported to have a more accurate placement for the soundings (plotted using a 3D surface instead of a flat surface) and also to correct some values for the reflectivity related to the incidence angle between the beams and the seafloor (perpendicular angles tend to give a higher “false” response).

3.4.3.3. Operations on mosaic

After the mosaic creation some operations was made to improve the quality of the maps. One of them was interpolation, used to fill in gaps of the record. This was done taking into account that there is more information along beams of one ping (perpendicular to the ship’s track) than across pings (along ship’s track). Therefore, the interpolation had a higher search window along navigation than in the perpendicular direction (7x3 was used in most maps). Histograms modification, stretching and shrinking in some sectors and range editing did visually improve maps. Image smoothing and contrast enhancements also did help to clean or fade out some artifacts. The DTM was also provided in order to better place the soundings and improve the data (Figure 3.18).

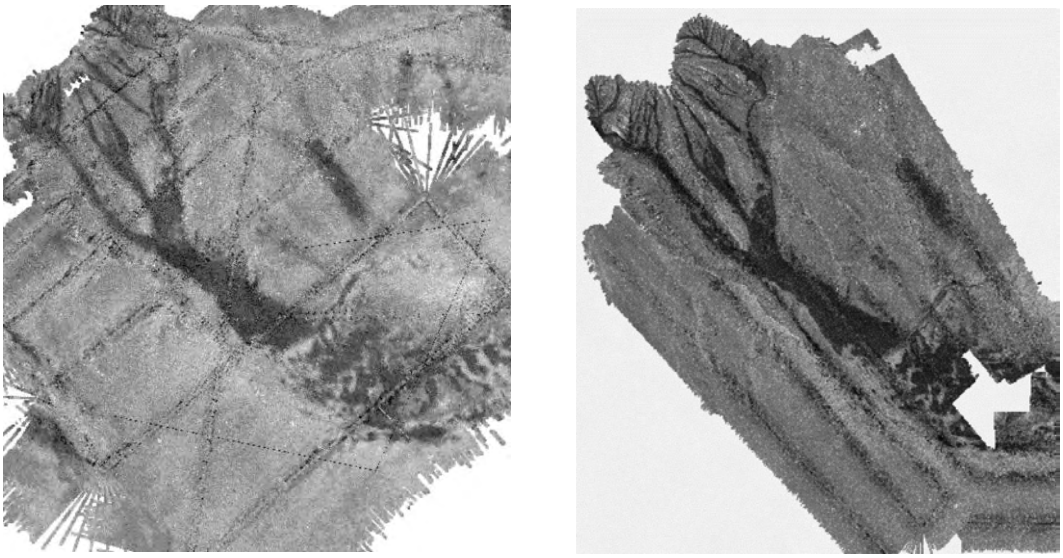

Figure 3.18 – Backscatter data. Left: raw data; right: after the DTM correction, data interpolation and histogram enhancements.

3.4.4. Bathymetry operations on the GIS

In recent times, the study of the ocean floor features has greatly improved especially due to the development of the multibeam echosounders since the 1970’s and to the more widely

spread and more friendly usable GIS applications that constitute a better, more integrated and more upgradable solution than the older paper maps with isobaths (Figure 3.19).

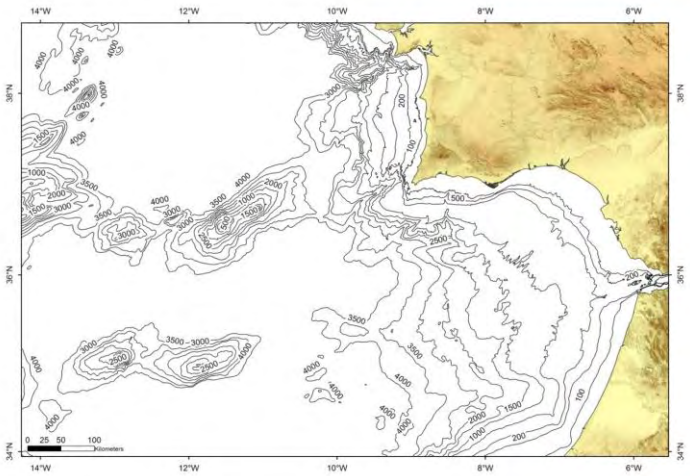

Figure 3.19 – Bathymetric map of the Gulf of Cadiz, contours every 500 m, data derived from Gebco database.

The morphological bathymetric studies are much alike their onland counterparts and several parameters are calculated relatively ease with the new GIS applications. The following parameters were determined in order to perform these studies: bathymetry, bathymetric profiles, contours, slope, aspect, profile and planar curvature and terrain variability (rugosity and fractal dimension) and are now described.

3.4.4.1 - DTM generation and interpolation methods

The bathymetric studies and seafloor morphologic analysis were carried out based on the constructed digital terrain model. Its surface according to Evans (1980) is described as a second order equation (Equation 3.1) and a function of planar coordinates (x and y) and their depth (z).

$$Z = aX^2 + bY^2 + cXY + dX + eY + f \qquad \text{Equation 3.1}$$

The remaining parameters are solved by the floating sampling window of 9 points, 3x3 centred in the pixel in question and its neighbours as exemplified in the picture below (Figure 3.20).

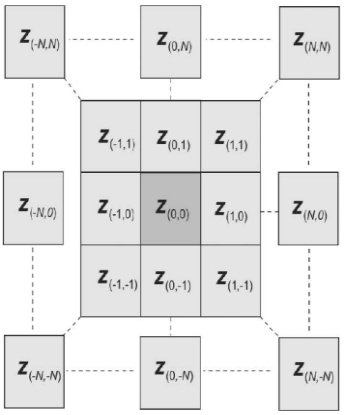

Figure 3.20 – Example of a floating window (3x3 cells) of the sampled points used in the interpolation to generate a surface.

In order to obtain a surface (DTM) that corresponds to the seafloor, the 100 m cellsize grid that Caraibes produced was imported into the ArcGis Application Suite 9.3 as points in the WGS 84 geographical projection. Those points (digital elevation model, DEM) were then interpolated to produce a surface (Figure 3.21) and projected using the Mercator projection with the central meridian 36ºN as the most adequate for this region of the globe.

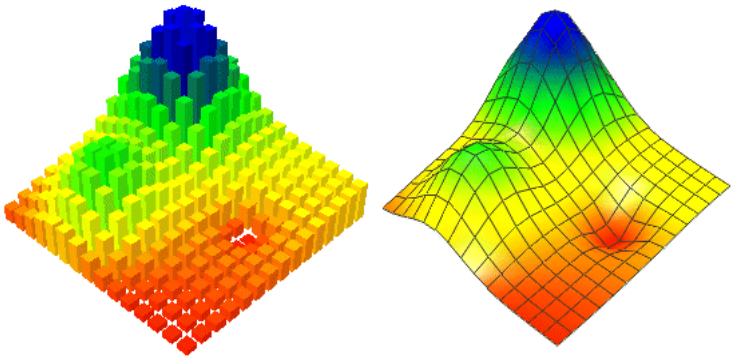

Figure 3.21 – Example of interpolation of the points of a DEM (left) in order to generate a surface, the DTM (right).

This method allowed to have a parameter (depth) for every (x,y) coordinate and not only for the sampled points (multibeam soundings). This interpolation was done according to various methods as: Inverse Distance Weighted (IDW), Spline, Kriging and Natural Neighbours.

The simplest interpolation tools are IDW (Figure 3.22a) and Natural Neighbours' interpolation. These methods estimate surface values for each cell using the value and distance of nearby points. The interpolated values for IDW surfaces are a weighted average of the values of a set of nearby points, weighted so that the influence of nearby points is greater than that of distant points.

Natural Neighbours' (Figure 3.22b) interpolation is like IDW interpolation, except that the data points used to interpolate the surface values for each cell were identified and weighted using a Delauney triangulation, as in a triangulated irregular network (TIN). Natural

Neighbours' interpolation reliably works with much larger datasets than the other interpolation methods.

Spline and Trend interpolation interpolate best-fit surfaces to the sample points using polynomial and least-squares methods, respectively. Spline interpolation (Figure 3.22c) fits a mathematical surface through the points that minimizes sharp bending; it is useful for surfaces that vary smoothly.

The final interpolation method used was IDW as it showed better results, capability to work with a large dataset, less artifacts and seemed to better reproduce the seabottom features.

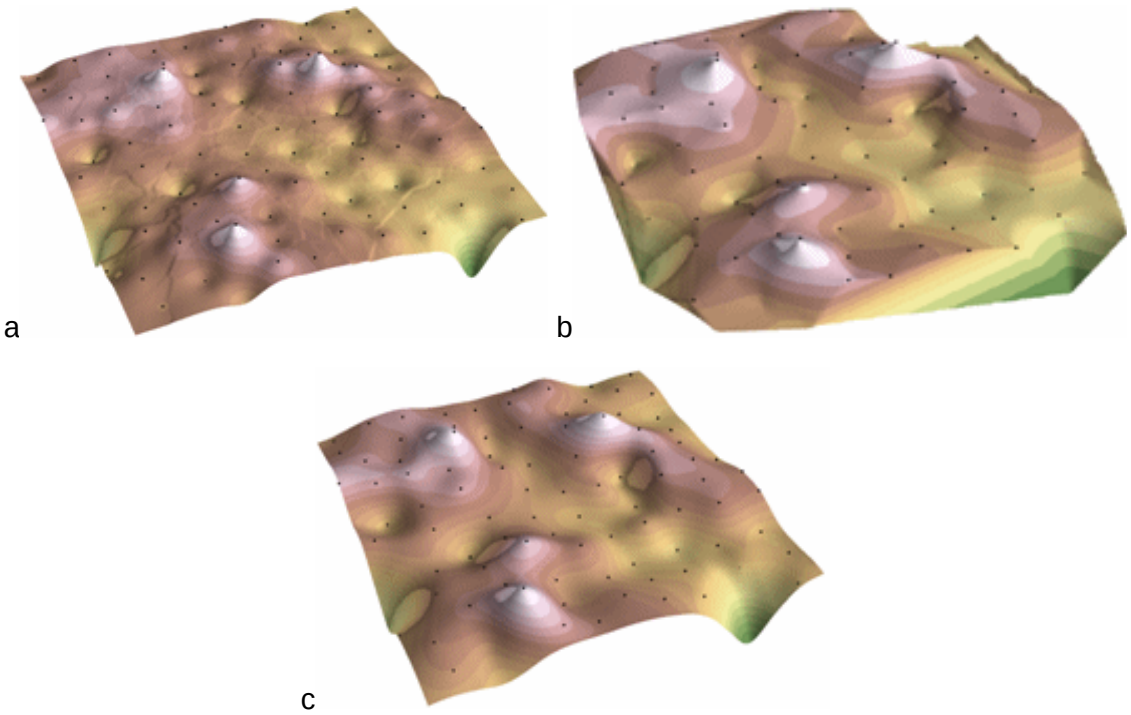

Figure 3.22 – Interpolation using the same grid and different methods: a - IDW interpolation, b - Natural Neighbors, c - Spline. Note that IDW interpolation is the method that best represents the features without creating artifacts or enhancing small details or smoothing out some features.

In what regards the maps produced in this work, the scale reports to the parallel 36ºN. The legend when in the continuous/stretched format was not linear, i.e., the color in the middle of the scale was not the value in the middle of the minimum and maximum values. Instead, the standard deviation n=2 display was used in order to enhance the majority of the features and not to give too much weight to the outliers.

3.4.4.2. The maps of the SWIM dataset

After the import and interpolation, the seafloor surface was generated and available for the GIS application. This surface was the base for all the bathymetric studies and other parameters further calculated.

This surface was presented in several ways: as isobaths maps (like the old bathymetric maps, Figure 3.23), as shaded single colour maps (Figure 3.24), as colour depth-dependent maps (Figure 3.25) or as a combination of the two as shaded depth-colour maps (Figure 3.26).

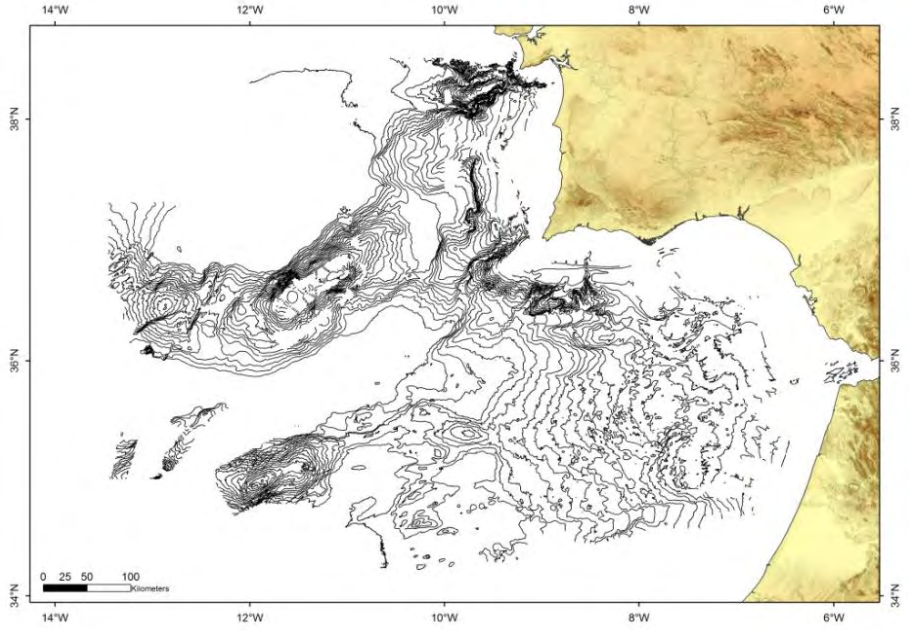

Figure 3.23 – Bathymetric contours of the SWIM multibeam dataset in the Gulf of Cadiz, contours every 200 m.

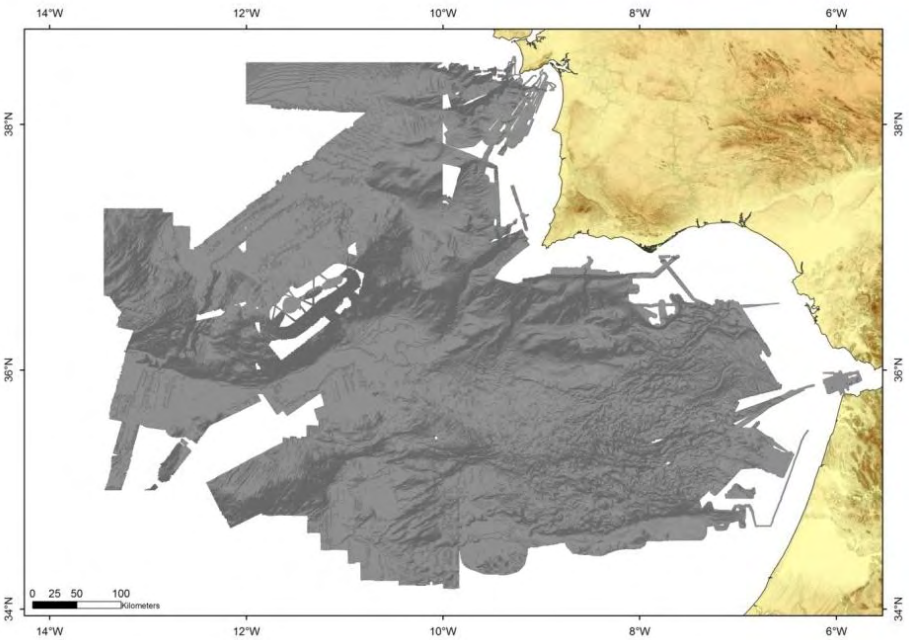

Figure 3.24 – Bathymetric map of the Gulf of Cadiz, shaded single color with illumination source from the NW. Note the shadows of the Gorringe and Coral Patch submarine mountains.

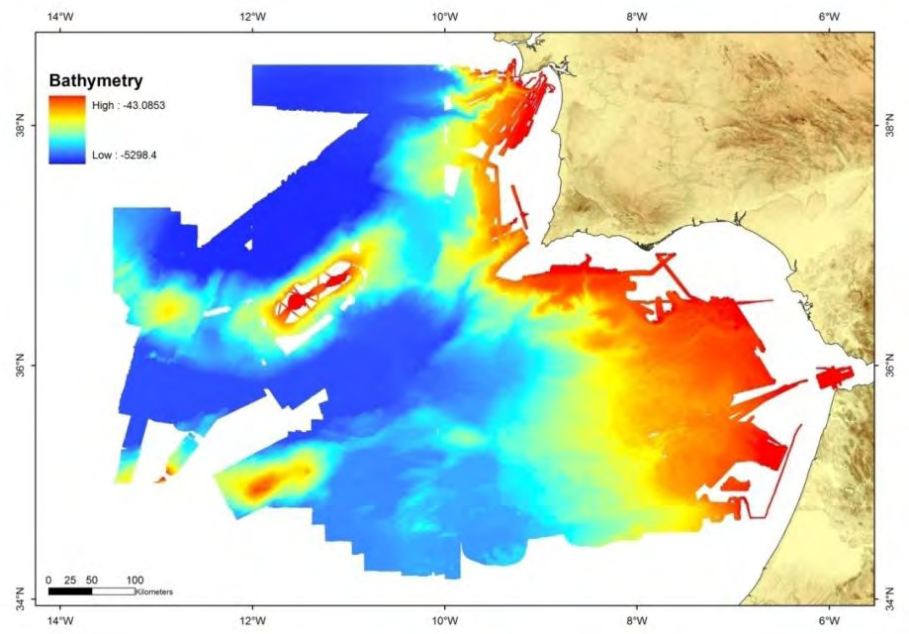

Figure 3.25 – Colorscale depth dependant map of the SWIM multibeam dataset.

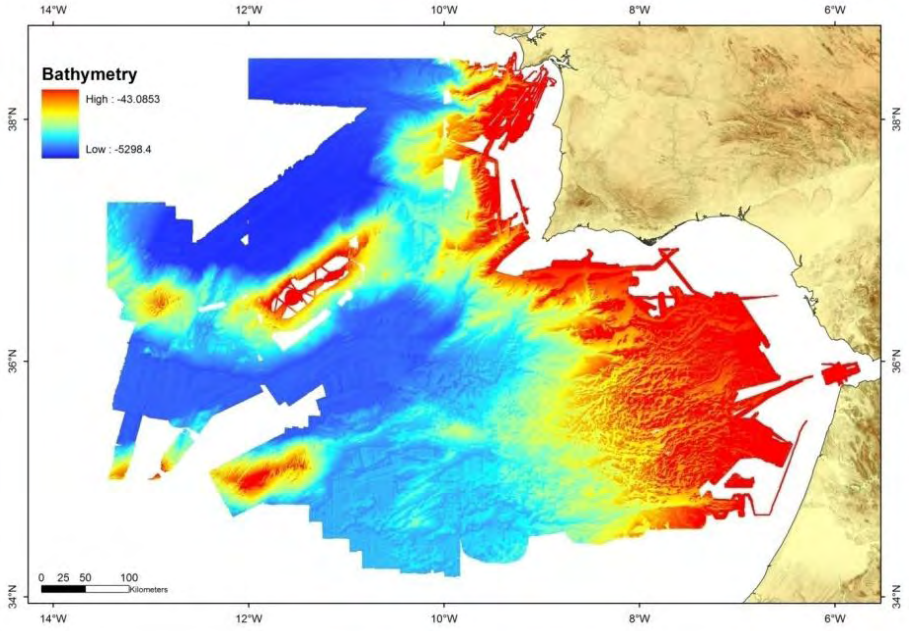

Figure 3.26 – Shaded colorscale depth dependent map, lighting source from NW; the network of the drainage system in the East is highlighted by the shading applied.

3.4.4.2.1. Aspect

Aspect is the direction that an inclined surface faces. This tool identifies the steepest downslope direction at a location on a surface. It is thought as slope direction and is calculated for each cell of the DTM. Aspect (A in Equation 3.2) is calculated according to the following formula and its value is found for each of the cells of the moving window.

$$A = \tan^{-1}\left(e/d\right)$$

Equation 3.2

The produced raster (Figure 3.27) has an azimuthal value for each cell and the maps produced usually have 8 classes of 45º each that are centred in the 8 main cardinal directions.

Aspect is a very useful parameter to detect lineaments that generate some marginal reliefs or to detect small hillsides that face in a different direction than the main flank where they are situated: it also proved useful in the analysis of the drainage system or to check if a certain area was more or less affected by directional processes (like bottom currents).

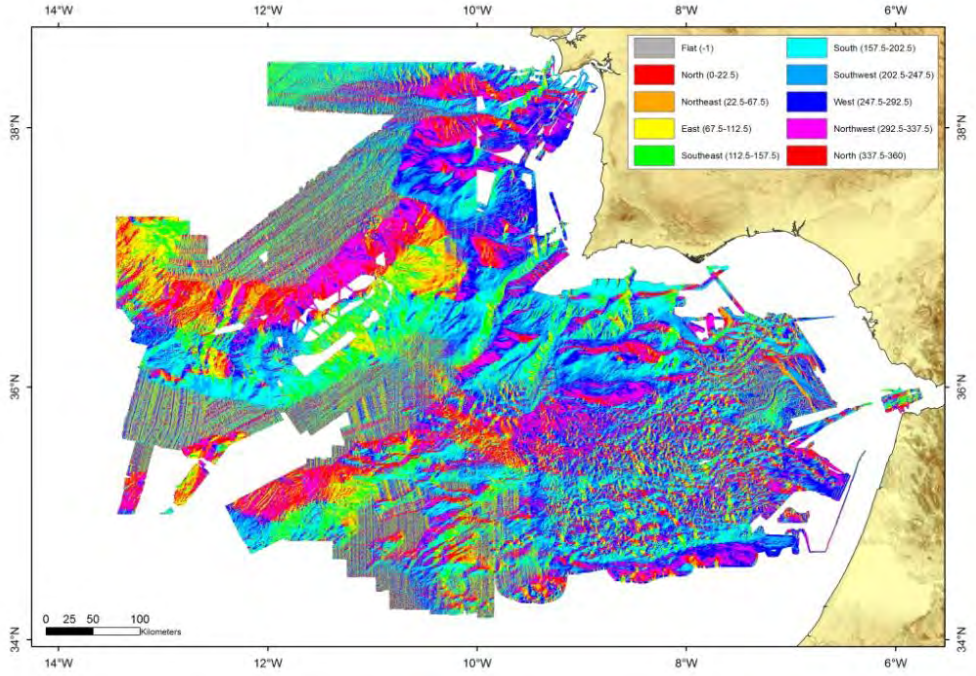

Figure 3.27 –Aspect map for the SWIM dataset, 8 classes of dipping directions. The Abyssal Plains do not appear as flats because of minor artifacts of the bathymetry processing.

By the inspection of the aspect map it is seen that both the Gorringe Bank (GoB) and Coral Patch Seamount (Figure 3.28) have all-directions' facing hills, in the latter there are some parallel and regular crests and troughs that are nicely seen in this aspect map, similar to the ones also present in the Hirondelle Seamount. Concerning the submarine mountains (GoB and CPR) and the Seine Plain Abyssal Hills it is seen that their sides face all the 360º in a way that the NE and SW facing sides are fewer compared to the NW and SE facing ones, due to the NE-SW elongation they present. Regarding the accretionary wedge, there are few east facing slopes and in the deepest areas in the north there are more NW facing sides whilst in the south there are more SW facing sides.

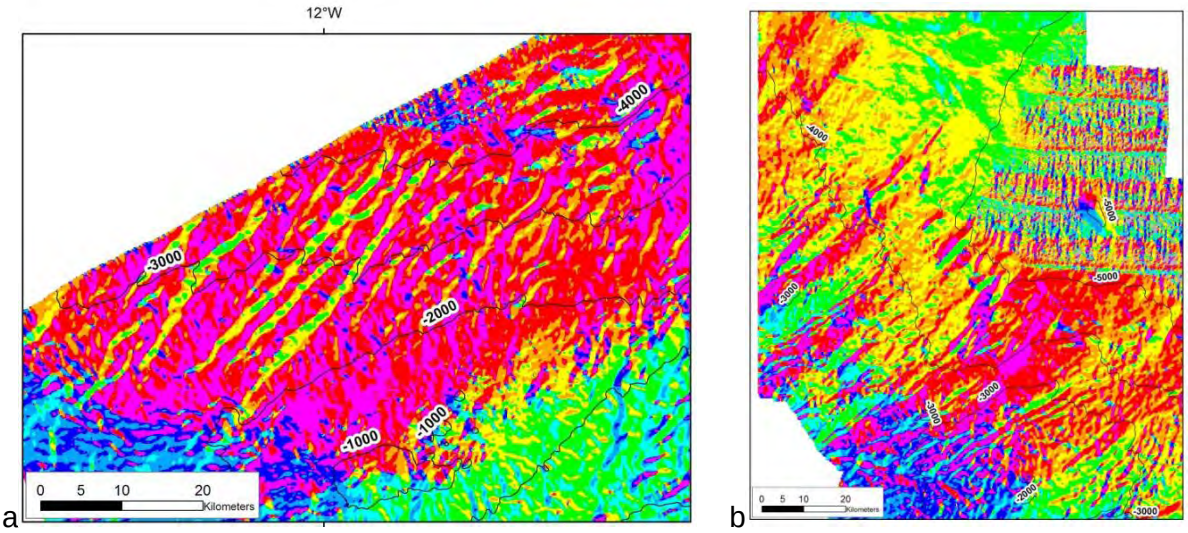

a b

Figure 3.28 – Magnifications of Figure 3.27 on the CP Smt. (left) and Hirondelle Smt (right). Aspect map of this area greatly enhances the directionality of the features present.

3.4.4.2.2. Slope

The slope of a physical feature (seafloor in this case) refers to the amount of dip of that surface, where the lower the slope value, the flatter the terrain; the higher the slope value, the steeper the terrain and zero indicates flats. It is calculated as the maximum rate of change between each cell and its neighbours (Equation 3.4), i.e. the maximum change in elevation over the distance between the cell and its eight neighbours (3x3 sampling window). Like the original bathymetric raster, every cell in the output raster has a slope value. The output DTM of the slope was calculated as percent of slope or degree of slope (degrees were used for this work after the projection was set to Mercator).

Slope is deduced from the Evans (1980) equation (Equation 3.1):

$$\frac{\partial Z}{\partial X} = S_X = 2aX + cY + d \qquad \frac{\partial Z}{\partial Y} = S_Y = 2aY + cX + e$$

Equation 3.3

If a local coordinate system is taken, for example for the center cell of a sampling window where x and y are both zero, Slope (*S*) is calculated as follows:

$$S = \tan^{-1}(\sqrt{d^2 + e^2})$$

Equation 3.4

The slope (Figure 3.29 and 3.30) as well as its derivatives are key parameters to describe the seafloor morphology, as well as its modifications and hence also very important to understand the near-seabottom processes. Abrupt changes in the bathymetry correspond to areas of high slope values that have a geomorphologic origin, such as fault scarps, canyons or gullies walls, or simply a geological boundary between different rock types.

The slope is displayed in two ways, as a grayscale map or as a color map; both give a sense of perception of the gradient values.

The greyscale slope map can also be used in another way: with a transparency layer together with bathymetric data, this is done in order to produce a better looking and more intuitive maps as the color gives the depth information and the slope layer enhances the shapes (Figure 3.31). This display has an advantage when compared to the hill-shaded map because the latter only enhances a set of shapes with one specific direction whilst using a slope layer enhances all the shapes regardless of their orientation (Figure 3.32 and 3.33).

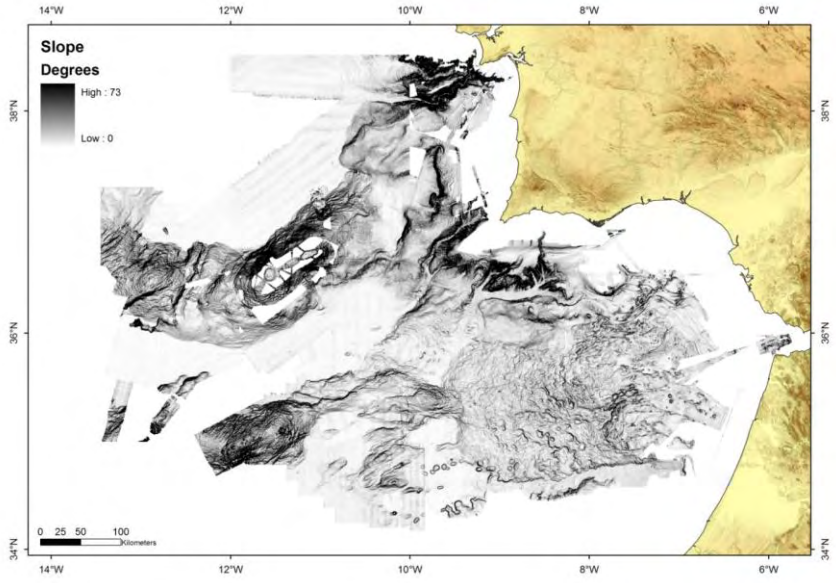

Figure 3.29 - Grayscale slope map.

The slope map is fundamental for geomorphologic studies. As an example, in the work area it highlights the flatness of the abyssal plains in the West in contrast with the steepness of the submarine mountains, of the canyons and of active fault scarps (Figure 3.29 and 3.30).

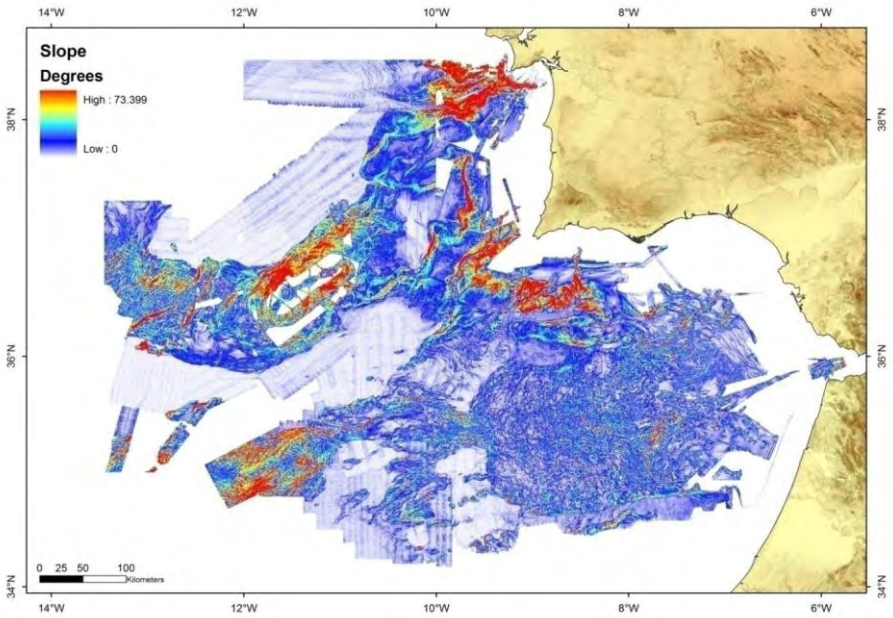

Figure 3.30 – Colour-scaled slope map.

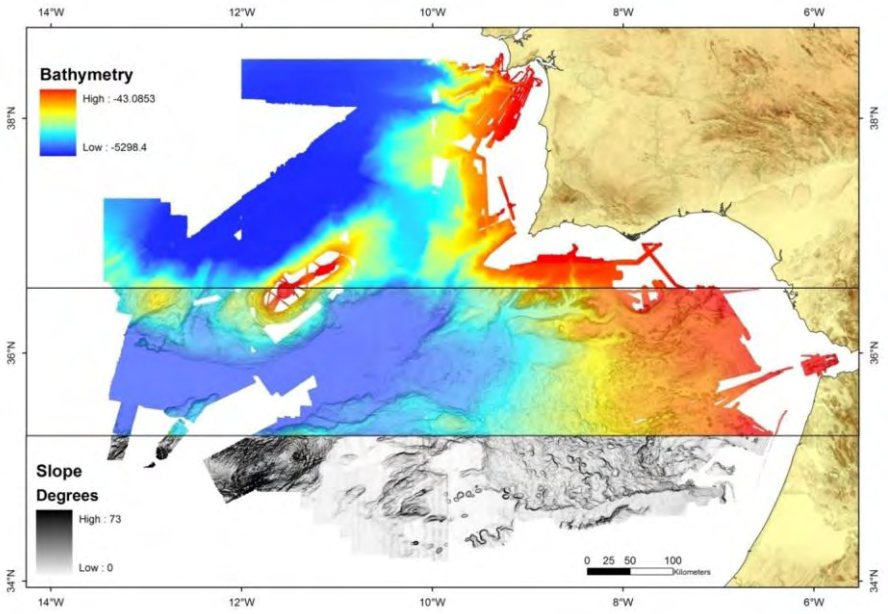

Figure 3.31 - Composite map of the Gulf of Cadiz: the top part displays the bathymetric data, the lower one displays the slope in grayscale, and the middle section is the slope overlain with the transparent colours of the depth. Note the definition of the features in the middle section, where the added value is having both the definition of the slope in all directions and the coloured bathymetric information.

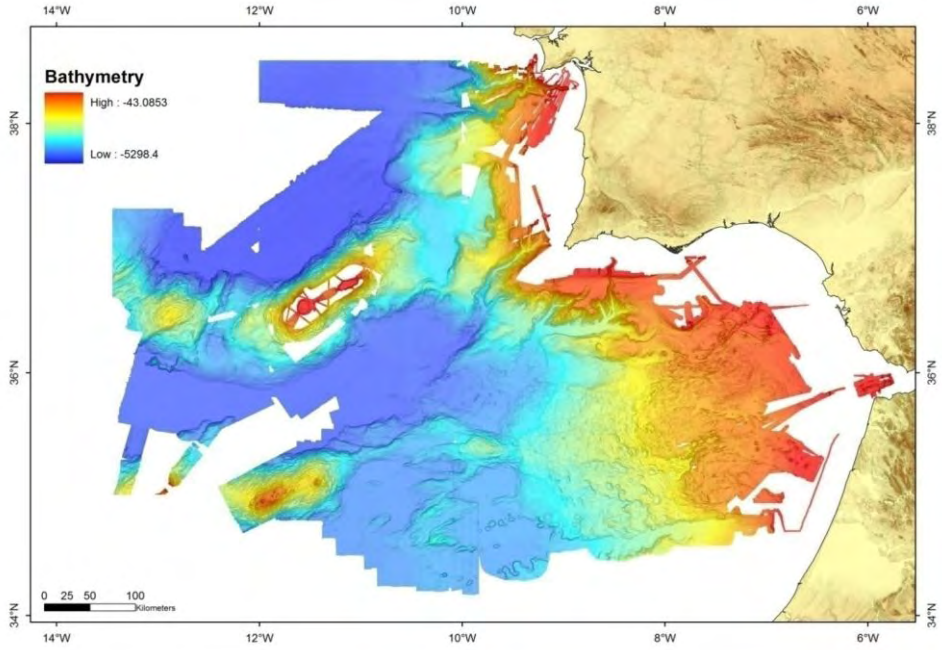

Figure 3.32 – Map of the Gulf of Cadiz, where colours represent depth, with a transparency layer over a grayscale map that represents gradients.

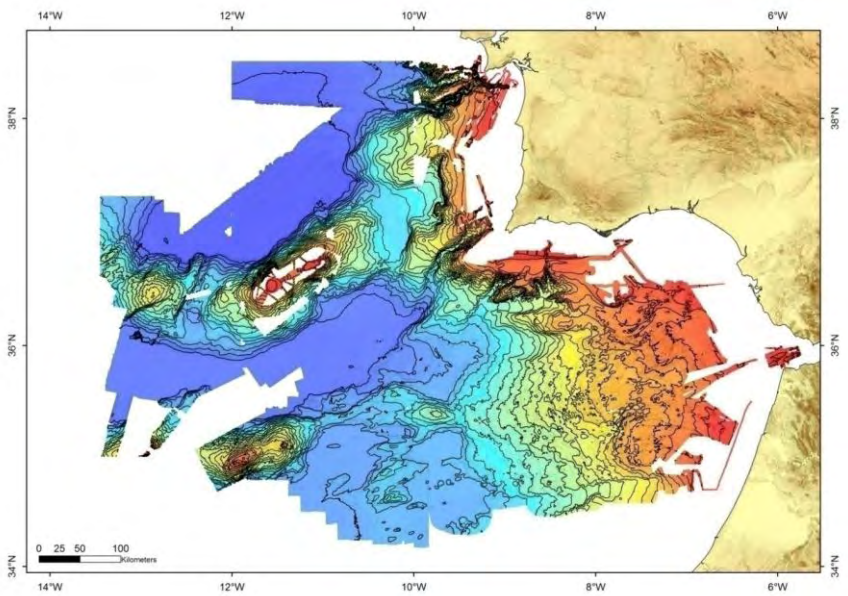

Figure 3.33 – Bathymetric map of the SWIM dataset. It is the Figure 3.32 overlain with bathymetric contours.

3.4.4.2.3. Curvature

Several types of curvature are described, here presented are the planar and profile curvatures (see Figure 3.34).

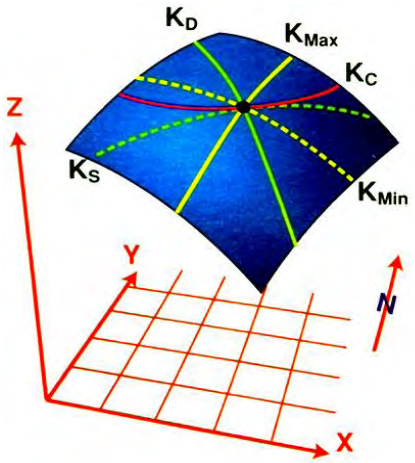

Figure 3.34 - Surface and types of curvature, Kd – dip (profile) curvature, Kc – contour (planar) curvature, Ks – strike curvature.

The curvature of a surface is calculated on a cell-by-cell basis. For each cell, a fourth-order polynomial of its form is a fit to a surface composed of a 3 x 3 window.

$$Z = Ax^2y^2 + Bx^2y + Cxy^2 + Dx^2 + Ey^2 + Fxy + Gx + Hy + I \qquad \text{Equation 3.5}$$

The coefficients A, B, C, D, E, F, G, H and I are calculated from the surface in Figure 3.35. The relation between the coefficients and the nine values of elevation for every numbered cell is shown in Figure 3.35.

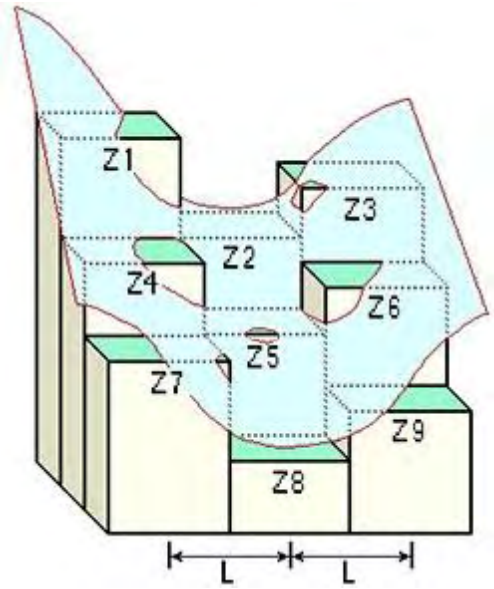

$A = [(Z1 + Z3 + Z7 + Z9) / 4 - (Z2 + Z4 + Z6 + Z8) /2 + Z5] / L^4$

$B = [(Z1 + Z3 - Z7 - Z9) /4 - (Z2 - Z8) /2] / L^3$

$C = [(-Z1 + Z3 - Z7 + Z9) /4 + (Z4 - Z6)] /2] / L^3$

$D = [(Z4 + Z6) /2 - Z5] / L^2$

$E = [(Z2 + Z8) /2 - Z5] / L^2$

$F = (-Z1 + Z3 + Z7 - Z9) / 4L^2$

$G = (-Z4 + Z6) / 2L$

$H = (Z2 - Z8) / 2L$

$I = Z5$

Figure 3.35 – Diagram illustrating the parameters used to calculate the A to I values in the curvature formula and their relation with the depth values.

The output of the Curvature tool is the second derivative of the surface in a way that:

Curvature = -2(D + E) * 100 Equation 3.6

ArcGis uses Wood (1995) formulas (Equations 3.7 and 3.8) to calculate the curvature:

Profile curvature

$$\frac{-200\left(ad^2 + be^2 + cde\right)}{\left(e^2 + d^2\right)\left(1 + e^2 + d^2\right)^{1.5}}$$ Equation 3.7

Planar curvature

$$\frac{200\left(bd^2 + ae^2 + cde\right)}{\left(e^2 + d^2\right)^{1.5}}$$ Equation 3.8

From an applied perspective, the curvature is used to describe the physical characteristics of a drainage basin and to understand erosion and runoff processes. The profile curvature (Figure 3.36) displays the variation of the slope along the direction of the maximum dip. These variations induce acceleration or deceleration of near bottom currents, and so there is a relation between profile curvature and erosive or sedimentary processes.

The planar curvature (Figures 3.37 and 3.38) is related to the variation of the bathymetry in a direction perpendicular to the maximum dip and displays the convergence and divergence of

flow, it converges on the convex planar forms and diverges on the concave ones, thus this is a very useful tool to identify and characterize the drainage system.

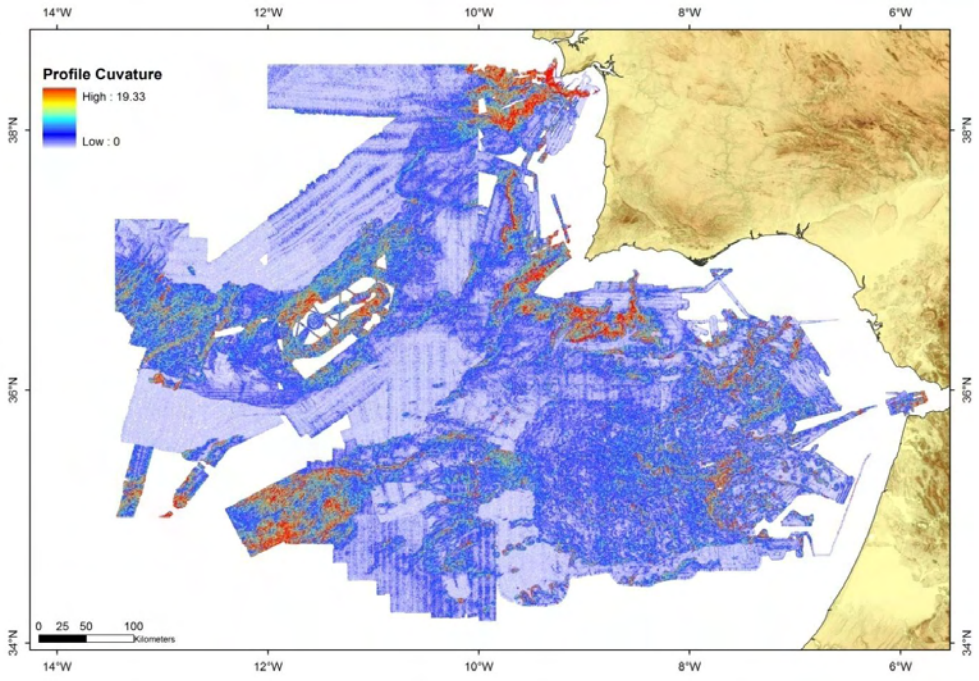

Figure 3.36 – Coloured profile curvature map for the SWM dataset.

The profile curvature map shows high values in the same places where there are high values in the slope map, i.e., in the work area there are not large areas where the slope is high and there is no variability in it. These high slope areas are: the canyons drainage system, the Gorringe Bank and Coral Patch submarine mountains, the upper south lobe of the accretionary wedge, the salt ridges (west of Cadiz City) and the Pereira de Sousa fault scarp.

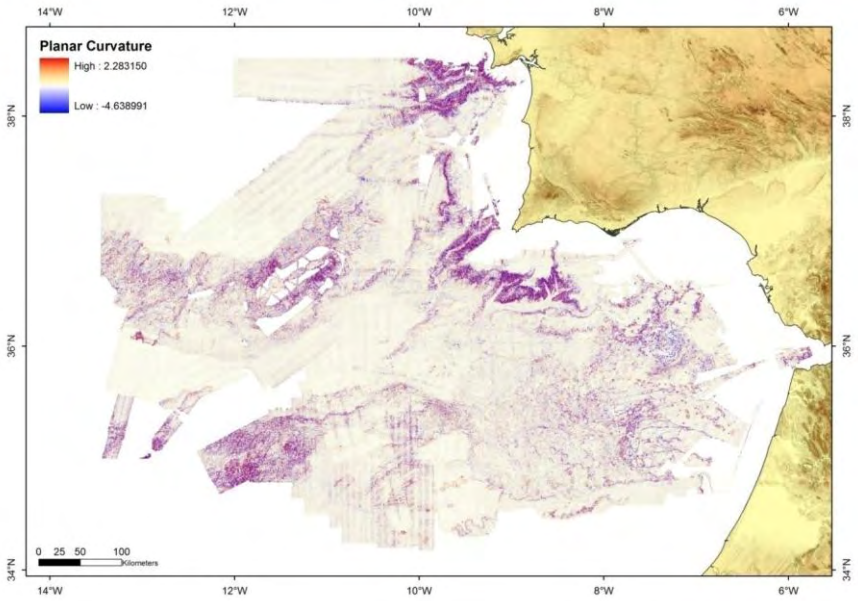

Figure 3.37 – Planar curvature map, red colour indicates divergence of flow and blue indicates convergence of flow.

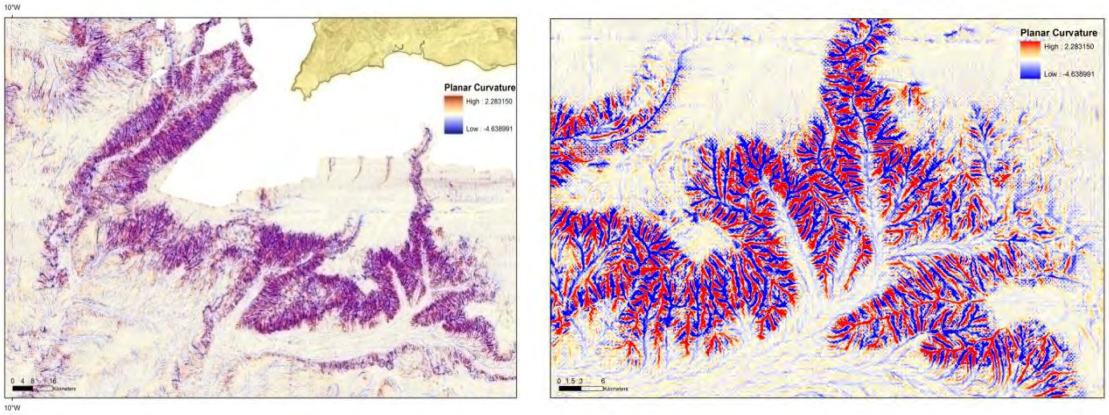

Figure 3.38 – Details of Figure 3.37 in the south Portuguese canyons area (left), and in the Portimão canyon (right). Red indicates divergence of flow and blue indicates convergence of flow.

The planar curvature map does not reveal a lot of information a large scale (Figure 3.37), however a magnification of the same map (Figure 3.38) displays its usefulness in terrain analysis as it defines nicely the incised submarine drainage system.

3.4.4.2.4. Terrain variability

These parameters (like rugosity and fractal dimension) and their application to submarine environments have been given some emphasis along the last decade (Thompson *et al.*, 2001), especially with the development of very shallow working multibeam probes.

The rugosity parameter describes the difference between the surface of an area (Figure 3.39) and its equivalent planimetric area. A case that exemplifies this concept is that of a steep submarine mountain where a square kilometer of horizontal area is much different than the same area but in the real wavy and steep seabed.

The first and most used tool, called the Benthic Terrain Modeller, is designed for the use of 1 to 5 meters cellsize, and therefore, not suitable for the dataset used in this work with a 100 meter cellsize. Instead, the Vector Ruggedness Measure (VRM), a similar parameter to rugosity, developed by Sappington *et al.* (2007) after the definition of Hobson (1972) was calculated. An additional tool, the Surface Tools for Points, Lines and Polygons (Jenness, 2004) was used to evaluate the rugosity, and the results were very similar to the VRM output.

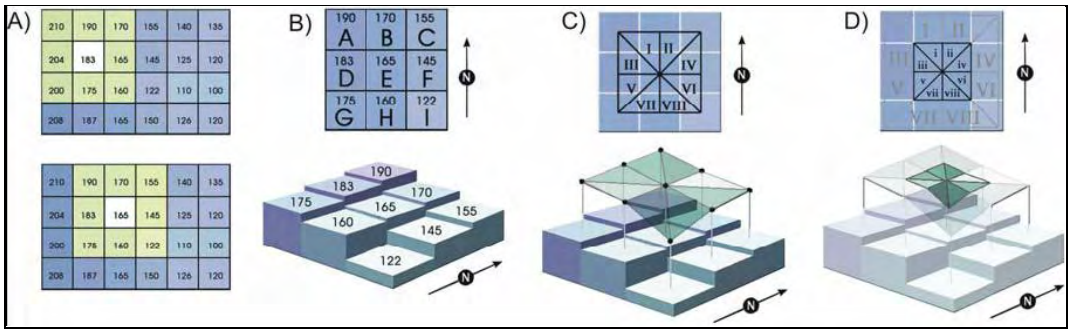

Figure 3.39- How the surface area is calculated from a grid: A – the grid (blue) and the floating window (green); B- a DEM representation of the grid; C – definition of the 8 triangles that connect the center cell with the center of the other 8 cells in the 3x3 window; D – adjustment of the calculated triangles to the planimetric projection taking in account the cellsize value of the grid (in A). It is the ratio between these two surfaces that is the concept of rugosity. From Jenness (2004).

This tool expresses the amount of elevation difference between adjacent cells of a digital elevation grid. The process essentially calculates the difference in elevation values from a centre cell and the eight cells immediately surrounding it. The ruggedness index (Figure 3.40) measures terrain ruggedness as the variation in three-dimensional orientation of grid cells within a neighbourhood. This method effectively captures variability of slope and aspect into a single measure.

In the VRM map (Figure 3.40A) the areas with higher values are the canyons drainage system, the two submarine mountains, the Pereira de Sousa scarp and the salt ridges area (Figure 3.40B). These areas have appeared before as areas of high values in the slope map (Figure 3.29 and 3.30) and profile curvature map (Figure 3.36). These are areas of high values of gradient variability, indicating substantial bathymetric changes to which corresponds high values of the rugosity (or the calculated VRM parameter).

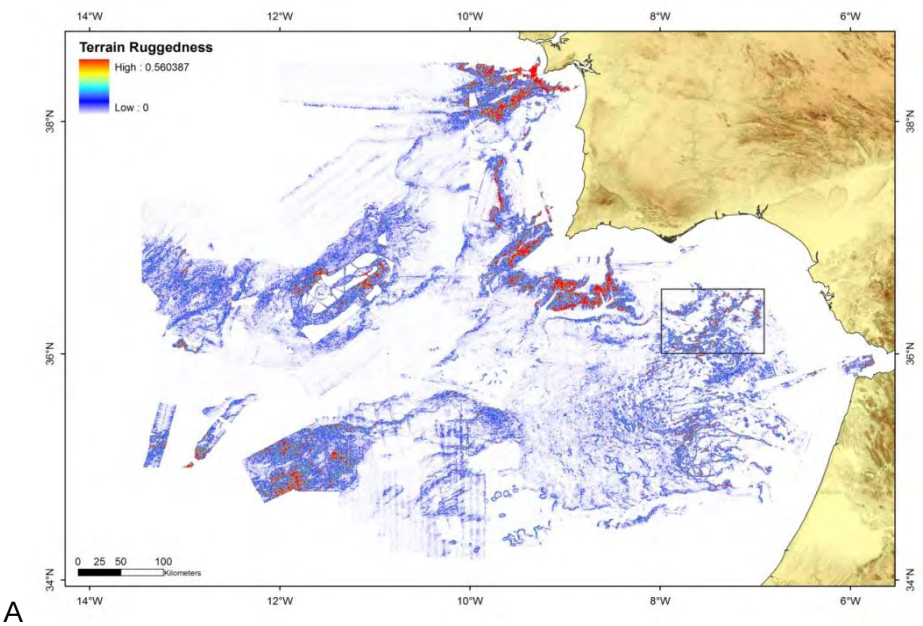

A

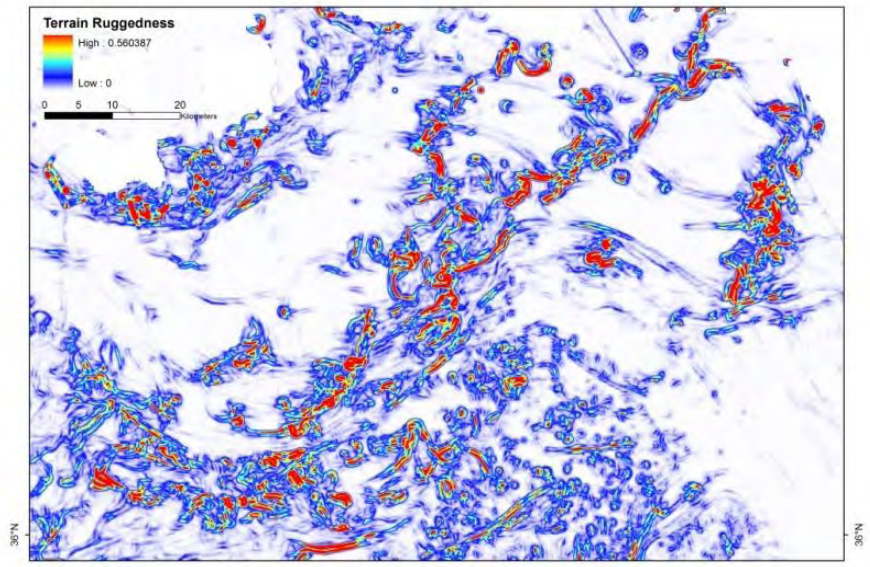

B

Figure 3.40 - Vector Ruggedness Measure map: A – for the Gulf of Cadiz; B – for the area delimitated in A.

Chapter 4 – The Morphotectonic Domains of Southwest Iberia

4.1. Introduction

In this chapter the interpretation of the morphology of Southwest Iberia is presented based on various types of maps of the seafloor and on seismic reflection profiles (see Chapter 3 for the date used) with the focus on the influence of tectonics on the shaping of the seafloor.

The morphotectonic interpretation is divided in two parts. Firstly, an interpretation of areal features, i.e. two dimensional features on the seafloor surface that allowed the definition of morphotectonic domains; secondly, the interpretation of linear features that were found to correspond to major tectonic elements. This sub-division of the morphologic elements was done only for the sake of organization of the information and interpretation and is followed by its integration into a final unified model. Following that, a detailed description of the geomorphology of the S. Vicente and Portimão submarine canyons is given.

A morphotectonic map of the Southwest Iberia is presented, accompanied by a detailed description of each one of the morphotectonic domains and of the morphotectonic lineaments. These morphologic features where identified and mapped using the bathymetry maps with a 100 meters cellsize Digital Terrain Model (Figure 4.1a), the slope and profile curvature maps (Figure 4.1b and 4.1c), and the reflectivity maps of the seafloor. Other maps, such as contour maps and orientation of the hillsides were also used as support for the interpretation (all these maps and how they were produced are presented in Chapter 3). In a first stage, a morphological analysis was performed and the morphological features were thoroughly mapped (Figure 4.2a). All the features were identified and mapped regardless of their size. This was followed by a second stage of identification and mapping of the morphotectonic domains and lineaments (Figure 4.2b). Inspection of the seafloor reflectivity and MCS lines were also helpful to establish a more precise location for the placement of boundaries between the morphologic domains and some were used to understand the active and past processes responsible for the seafloor shaping. The scrutiny of the literature relative to the geology of the southwest Iberia and Gulf of Cadiz was essential to classify some of the analysed morphologic features and was used to decide on the classification of the mapped domains.

The domains were mapped using ESRI's ArcGIS v.9.3 taking advantage of its powerful 3D spatial analysis and using IVS' Fledermaus for flyby, excellent 3D display and cross-sections.

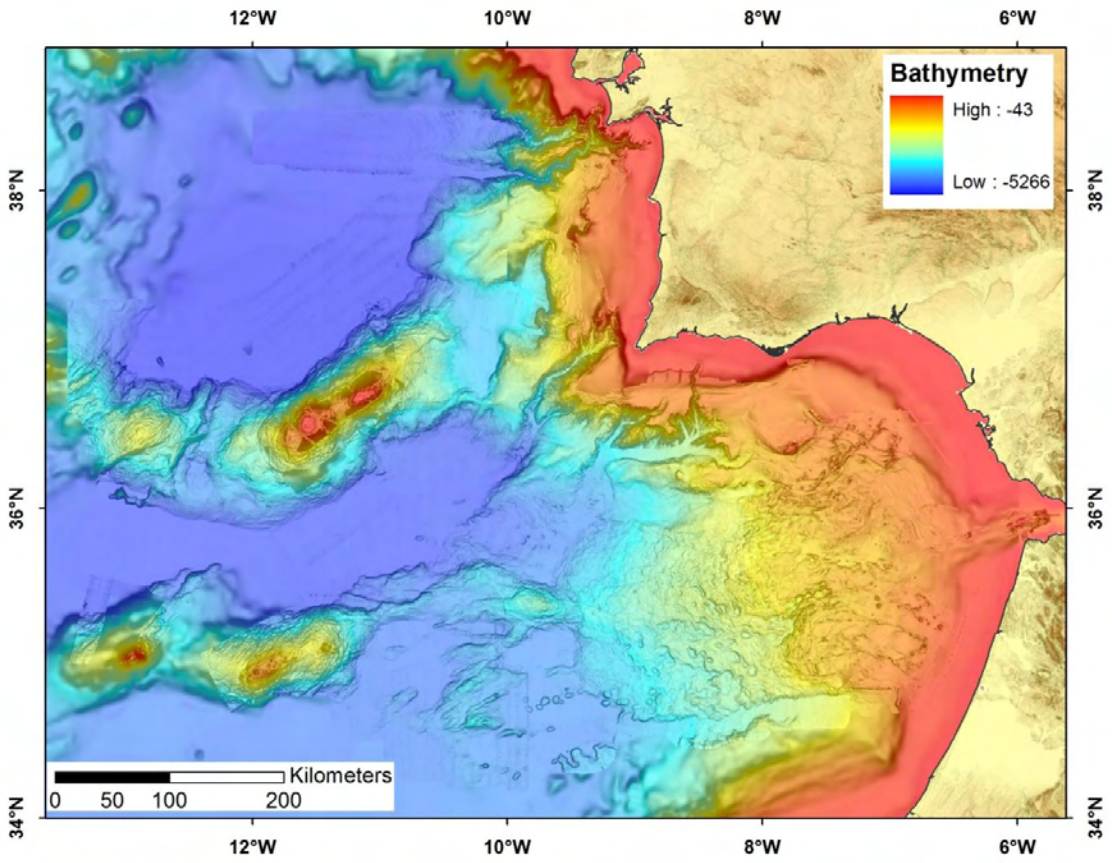

Figure 4.1a – The bathymetric map of the Gulf of Cadiz and SW Iberia using the SWIM multibeam dataset and the global Gebco data. The GEBCO bathymetry was used to fill in the gaps of the SWIM dataset and to envelop the study area. For toponyms and other detailed maps see chapters 2 and 3.

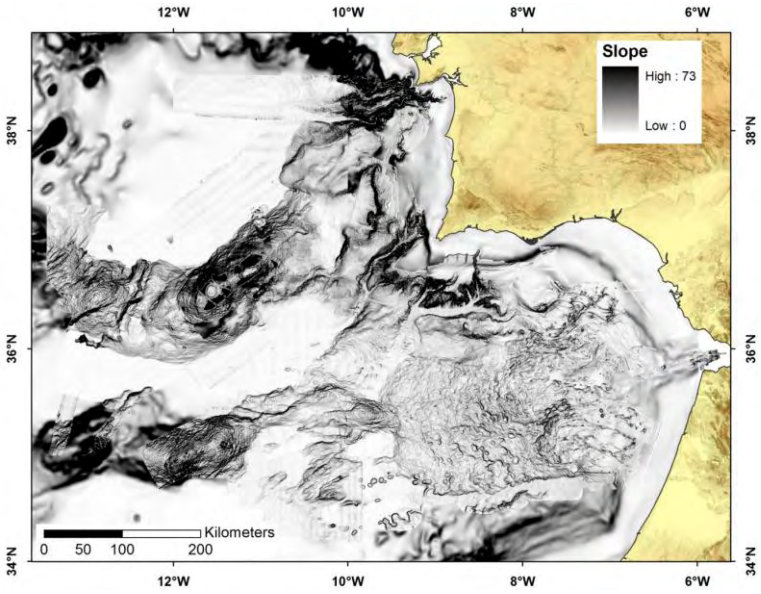

Figure 4.1b – The slope map of the Gulf of Cadiz using the SWIM multibeam dataset and the Gebco dataset. The slope unit is degrees. This map was used to identify areas where the bathymetry changes: like scarps and different patterns of seabottom features.

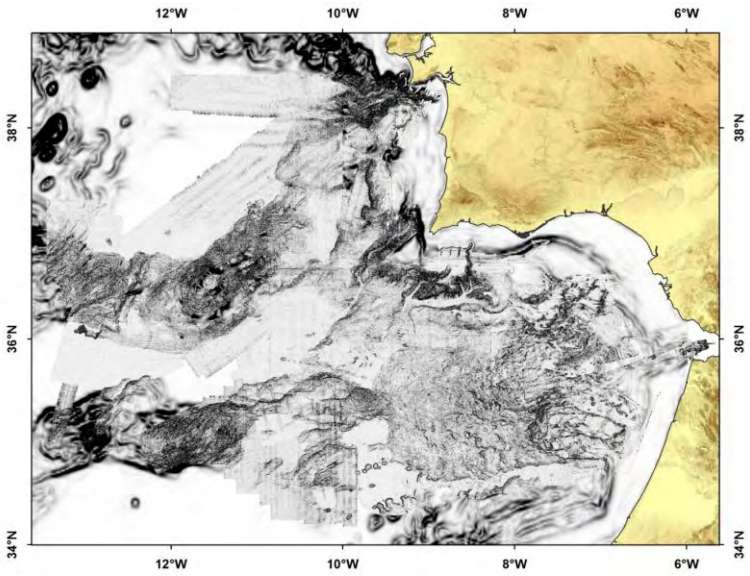

Figure 4.1c - Profile curvature map of the Gulf of Cadiz using the SWIM and Gebco datasets. This map was helpful in detecting gradient variations and to better map some areas that were not possible to be mapped with the bathymetric and gradient maps alone.

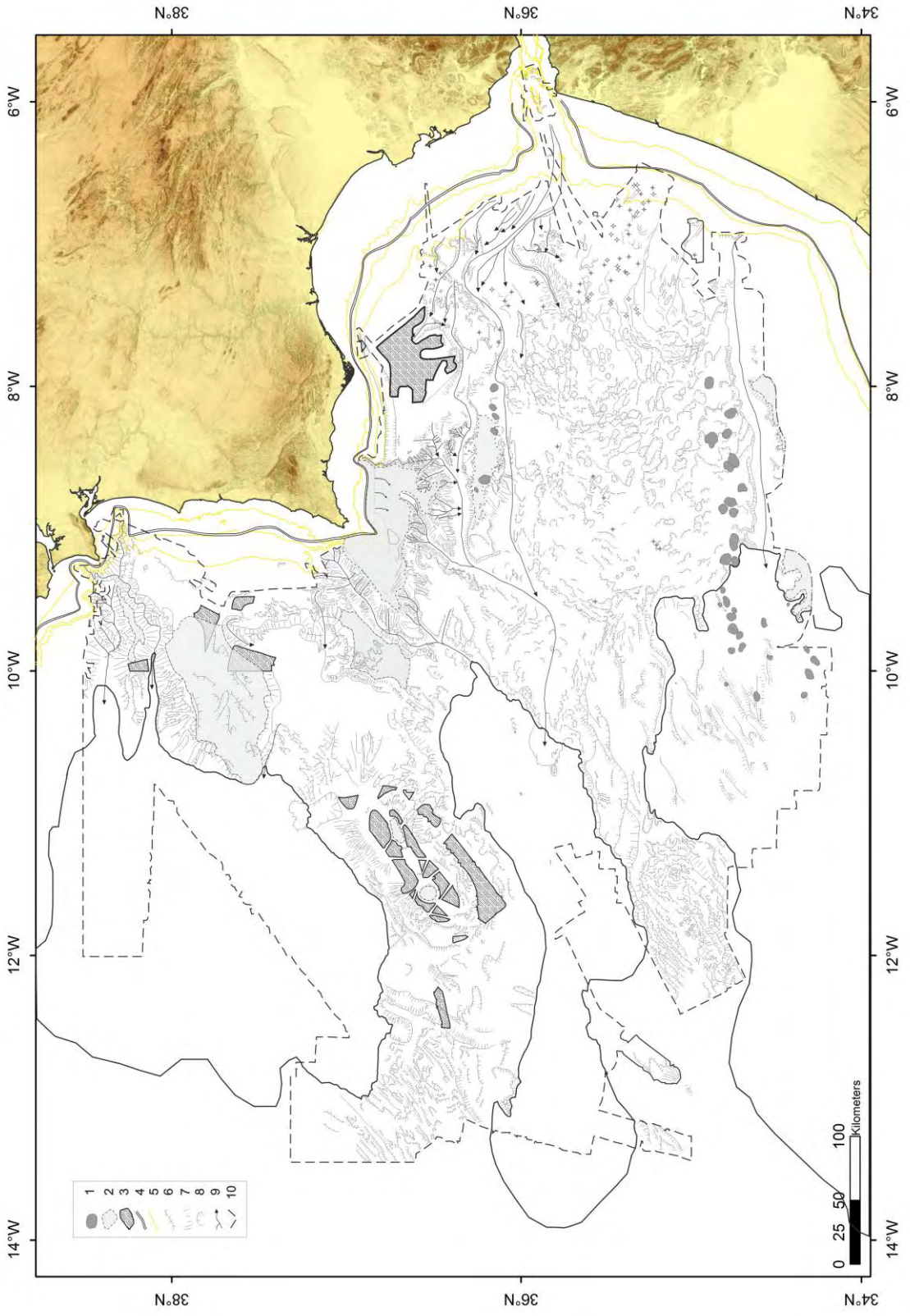

Figure 4.2a – The morphologic map of the study area from interpretation of the multibeam dataset. 1- salt domes; 2- plateaus; 3- *no data*; 4- limit of the continental shelf; 5- bathymetric contours (100, 200, 500 m); 6- ridges; 7- dip direction; 8- slope failure; 9- submarine drainage axis; 10- outer limits of the SWIM multibeam dataset; crosses indicate mud volcanoes and single solid lines limit of abyssal plains.

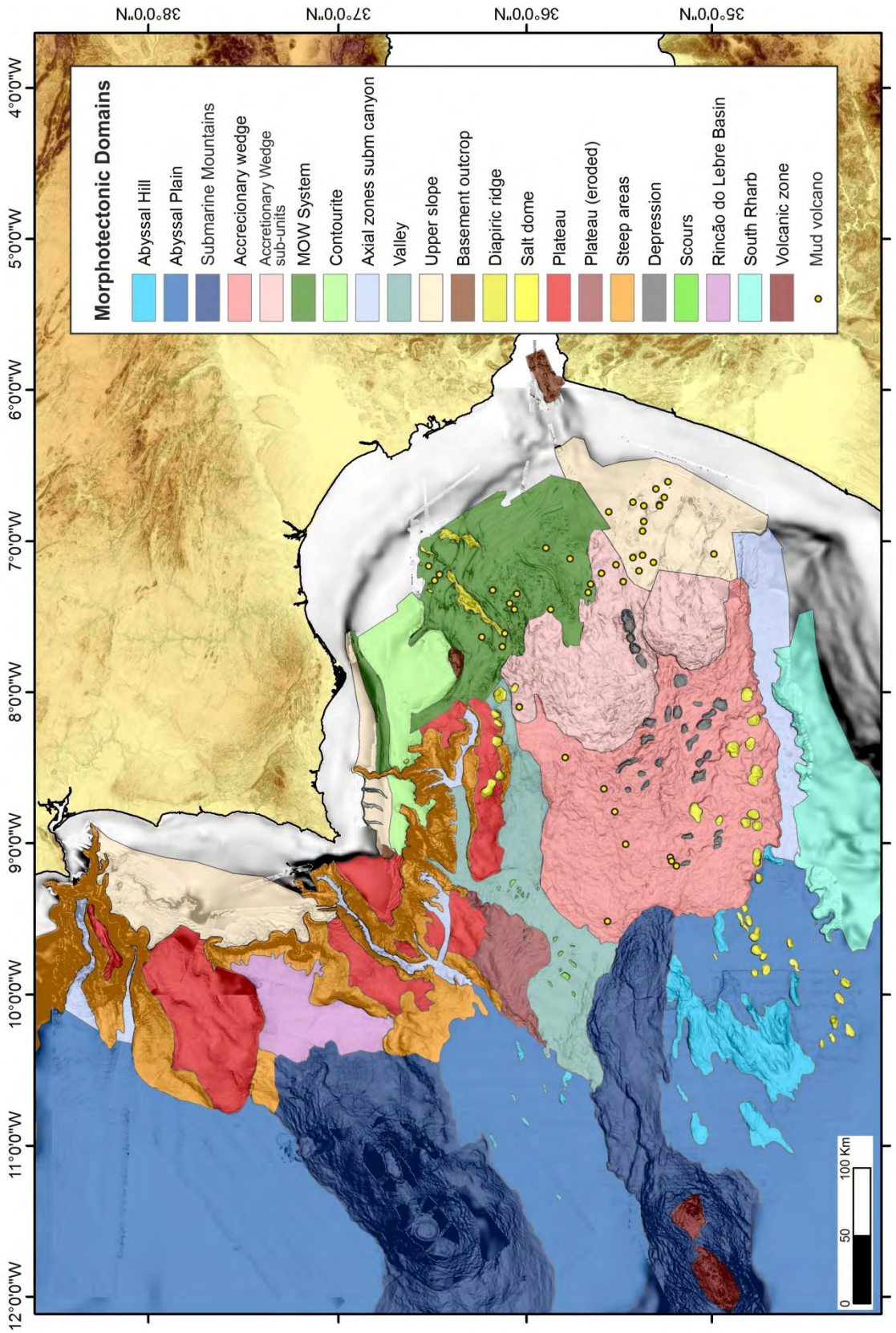

Figure 4.2b – The map of the morphotectonic domains of the Southwest Iberia. Basemap is the slope map similar to Figure 4.1b.

The morphotectonic map here presented is a result of an integrated analysis and interpretation of the several active and past seafloor shaping processes. It aims to provide a mapping of the different morphotectonic domains that exist in the Gulf of Cadiz as a result of distinct shaping processes. These processes vary from erosive to depositional, fluid escape and volcanism, among others.

4.2. Abyssal Domains

The Abyssal Domains are areas generally located below the foot of the continental rise or located oceanwards with respect to this. Positive reliefs (with the exception of submarine mountains) such as submarine ridges are included in this item when surrounded by abyssal plains.

Two different sub-domains are described, the Abyssal Plains and the Abyssal Hills.

4.2.1. The Abyssal Plains

Generally, an abyssal plain is a submarine domain located deep in the ocean floor, usually between 3000 and 6000 meters, located between the foot of the continental rise and the mid ocean ridge and are one of the flattest, undisturbed and smoothest geomorphological units of the Earth. The AP constitute oceanic basins whose sedimentary fill (mainly silt and clay; Weaver & Thomson, 1987) can be terrigenous (from continents of oceanic islands or ridges) or pelagic. The first can be deposited by mass transport processes (e.g. turbidites or landslides; Lebreiro *et al*., 1997) and the second end member result from deposition of oozes. The basement of these basins consists of oceanic crust or transitional crust.

In the study area three regions of flat to very gently dipping seafloor were identified in the deep ocean: the Tagus Abyssal Plain (TAP), the Horseshoe Abyssal Plain (HAP) and the Seine Abyssal Plain (SAP), from North to South respectively (Figure 4.2b). They are separated from each other by elongated submarine mountains, the Gorringe Bank and the Coral Patch Ridge and Seamount. The seafloor on these domains is not completely flat and some range of depths can be found, however these variations occur over very long distances and the slope values are very close to zero (practically inside the analytical error interval). So, the depths within the abyssal plains vary from -4280m to -5100m in the TAP, from -4860m to -4905m in the HAP and from -4220m to -4450m in the SAP (Figure 4.3). At a wider scale, the depths display a staircase-like pattern deepening towards the North.

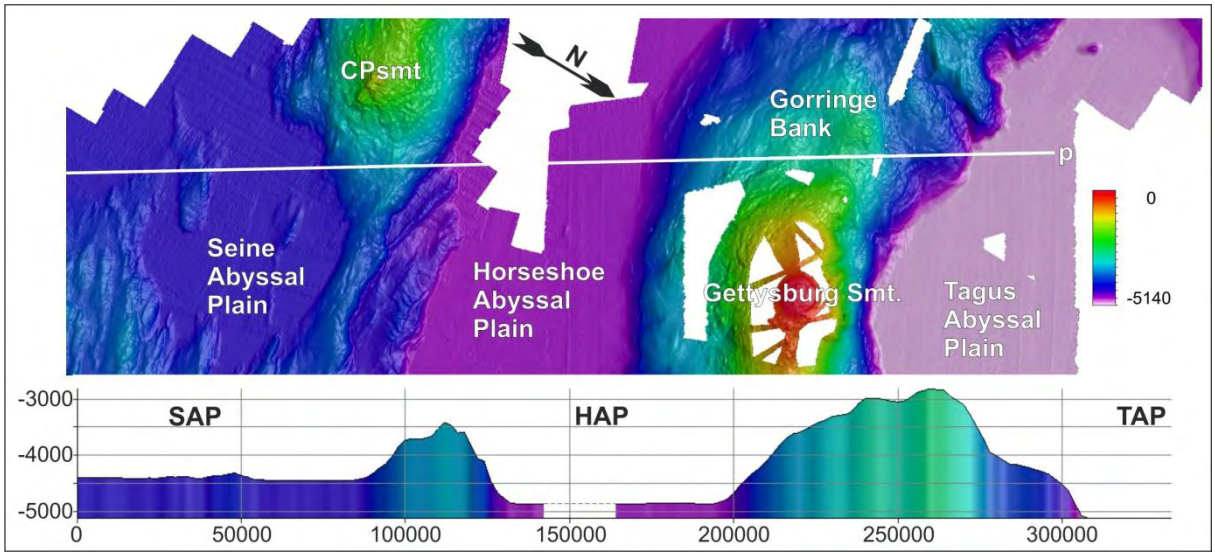

Figure 4.3 – Map view and bathymetric profile (p) across the three Abyssal Plains present in the area. White line is the profile trace, with NW-SE direction and extending for more than 300 kilometers. In the cross-section it is visible that the three abyssal plains display a staircase-like pattern deepening towards the north. Colors indicate depth (red is shallower and purple is deeper); the horizontal and vertical axes are in metres. To be noted the small hill in the TAP on the upper right corner of the image.

None of the three plains is fully imaged by the multibeam coverage but the Gebco database can be used to have a large scale view of their shape (Figure 4.1a and 4.2a). Thus, using the available data the TAP displays a NE-SW elongated ellipsoidal area. It is bounded to the east by the continental slope (Figure 4.1a), to the south by the Gorringe Bank and Hirondelle Seamount, to the west by the Tore-Madeira Rise and to the north by the Estremadura Spur and the Egas Moniz Ridges (these two features are present at the northern edge of Figure 4.1a).

The HAP, as shown in Figure 4.1a, is a more than 300 km long narrow basin separated by a constriction between the west part of Gorringe Bank and the Coral Patch Smt., where it's width is reduced from more than 60 kilometers (south of Ormonde Seamount) to about 20 kilometers. The HAP is bounded by the Horseshoe Fault to the east, by the CP Smt. in the south, the Gorringe Bank and the Hirondelle and Ampere seamounts to the north and the Tore-Madeira Rise to the west.

The Seine Abyssal Plain extends much to the south than the available coverage and is elongated along a E-W direction, bounded to the north by the CPR and CPSmt., to the east by the Moroccan continental slope and to the west merges with the Agadir Basin.

The backscatter map shows areas of high response for the seafloor of the HAP (Figure 4.4). The difference of the acoustic response between the HAP and the surrounding areas is clear and only the SVC axis displays higher values for the backscatter. The high reflectivity displayed in these deeper areas is probably due to presence of turbidites in the abyssal plain. The coarser material is carried from places near the continent mainly by the SVC and

the Horseshoe Valley (HV) to the deepest parts where it rests. The presence of turbidites in the Horseshoe Abyssal Plain is well known (Lebreiro *et al.*, 1997) and accounts for the high backscatter observed. The backscatter signature for this area also indicates that the sediment transport dynamics on the canyon and deposition on the abyssal plain is active since the penetration of the beams of the multibeam/backscatter probe is not very deep and samples only the more recent deposits.

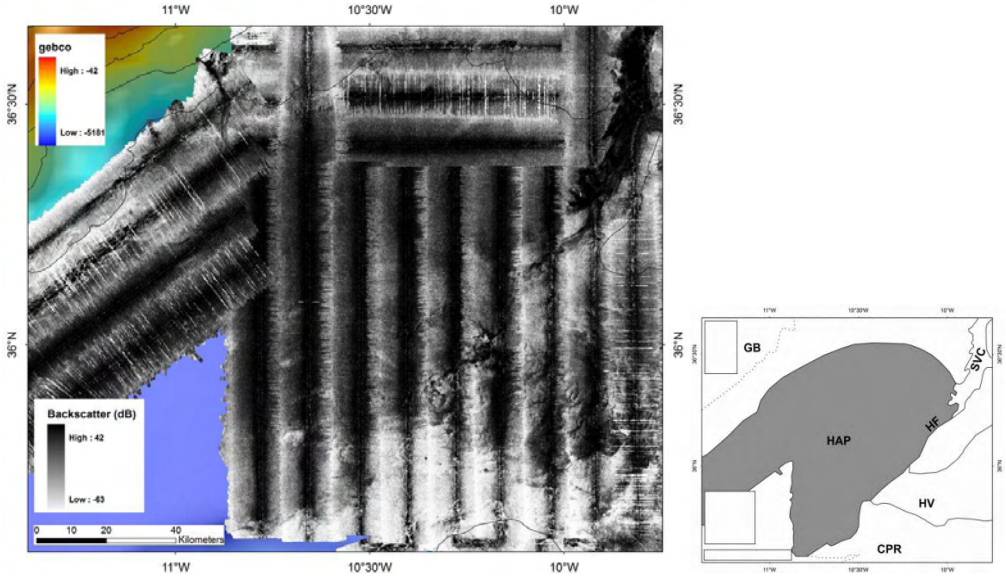

Figure 4.4 – Backscatter mosaic of the eastern part of the HAP (left). The HAP is in the center of the image, in the NW corner the flank of the Gorringe Bank can be seen, to the NE is the S. Vicente submarine canyon and the SE corner is the side of the Coral Patch Smt. The dark colors (HAP and SVC) indicate high response that corresponds to coarser or more competent material. Schematic interpretation of the backscatter mosaic (right); grey area represents higher backscatter response that corresponds to the HAP; GB – Gorringe Bank, SVC – S. Vicente Canyon, HF – Horseshoe Fault, HV – Horseshoe Valley, CPR – Coral Patch Ridge.

Despite the fact that the seabottom of the HAP is relatively flat the inspection of MCS profiles shows that the sub-seafloor structure is rather complex. Underneath the smooth seafloor, a chaotic body and several faults and folds affecting the sediments can be identified in the HAP (Figure 4.5). Although most of the tectonic structures are covered and sealed by the Pliocene-Quaternary sediments, thus forming the flat seafloor that can be seen in the bathymetry, some faults breach out the seafloor of the HAP. The TAP is punctuated by the occurrence of peaks of oceanic crust close to the Tore-Madeira Rise (see example in Figure 4.3).

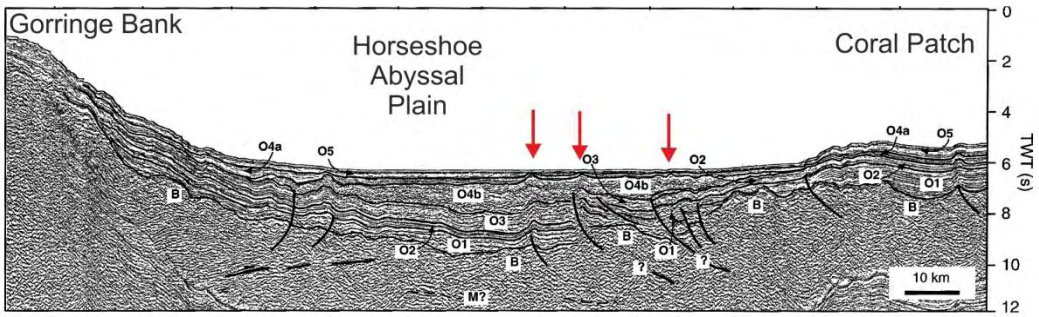

Figure 4.5 – IAM4 Multichannel seismic profile, showing the underlying structure of the HAP. Whilst the seafloor is flat and monotonous (except for the minor disturbances pointed by the red arrows), the structure beneath it can be quite complex and isn't only more perceptible on the bathymetry due to covering of the sediments on top of it. B: Basement; M: Moho; O1 to O5: Stratigraphic units. Modified from Tortella *et al.*(1997).

4.2.2. Abyssal Hills

The Abyssal Hills are elevations on the seafloor located within the abyssal plains. They are much smaller in scale when compared with the submarine mountains or seamounts (described ahead) that separate the Abyssal Plains. The Abyssal Hills are present in all the three abyssal plains in SW Iberia, larger in size (more elongated) in the SAP; smaller and more scattered in the HAP and only two present in the TAP.

4.2.2.1. The Abyssal Hills in the SAP

The most important abyssal hills appear in a cluster in the northwestern part of the SAP where they are subparallel and display two major trends: NE-SW and E-W. They are linear features; the larger ones can reach over 70 km in length, almost 20 km across and about 700 meters in height (Table 3.1 and Figure 4.6). The bathymetric profiles shown in Figure 4.6 across this cluster of the abyssal hills shows a staircase-like pattern with higher depths in the northern side; similar with the profile on Figure 3.3 and with the same trend.

Table 4.1 – Dimensions (in meters) of the Abyssal Hills in the SAP and their location.

Feature	Length	Max. Height	Location
1	13900	400	
2	37500	500	
3	24200	620	
4	34000	380	
5	15700	200	
6	36000	320	
7	72500	720	
8	40000	360	
9	38000	320	
10	37000	100	
11	13000	50	
12	15000	130	
13	44000	180	

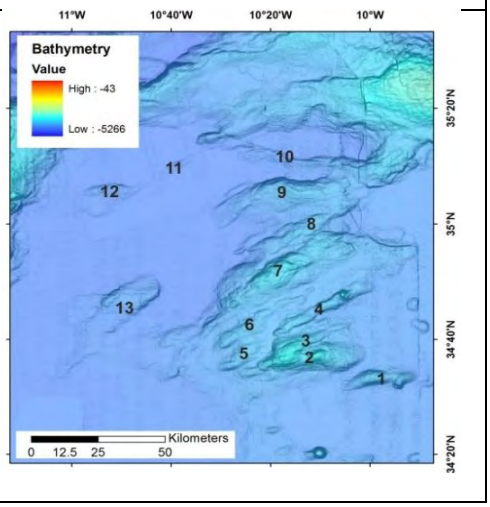

These elevations present more irregularities on the flanks than the ones on the other abyssal plains and sometimes also display a flat top (Figure 4.6). The slopes of their flanks are usually around 2º to 4º, however values over 10º can be found in the steepest areas.

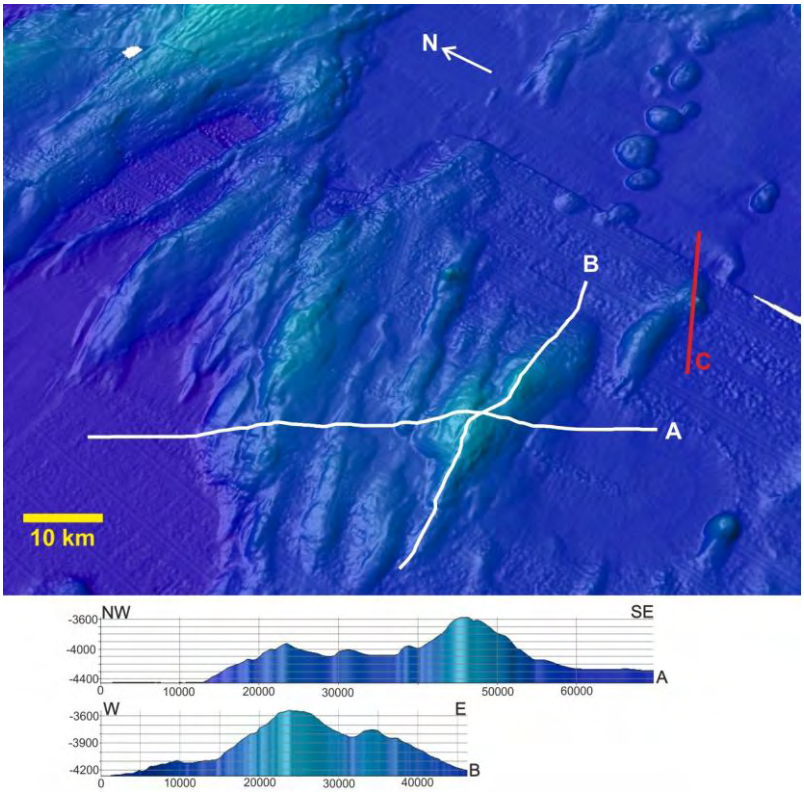

Figure 4.6 – 3D view (from SW) of the abyssal hills in the Seine Abyssal Plain. White lines A and B represent the bathymetric profiles shown on the bottom; red line C is the location for the section of Arrifano06 shown on Figure 4.8.

The very elongated shape of these reliefs together with their parallel strike suggested a tectonic origin for these features (Figure 4.7), in agreement with the sub-surface structure imaged on the Arrifano06 MCS (Figure 4.8). This MCS profile reveals that these reliefs correspond to folds affecting the seafloor that seat on top of underlying thrusts, corroborating the interpretation drawn from the analysis of the Chirp profile on Figure 4.9. This multichannel profile shows that the reliefs are tectonically controlled, displaying a NW-verging thrust.

The analysis of a chirp profile (Figure 4.9) that crosses one of the features (number 12 in table 4.1) does not supply any undoubtfull evidence but suggests that the fold associated with this relief is related to the north-verging underlying thrust. Its geometry is also indicative of a presence of such a structure since its general bathymetric expression is also northwards vergent with a steeper North side and a shallower dipping south flank.

Other abyssal hills also display a bathymetric asymmetry, like those numbered 4, 7, 9 and 10 in Table 4.1 that are north-verging and numbers 5 and 13 that verge to the South. This fact is indicative that the other reliefs are also tectonic related with the structures dipping

both towards the North and South. The preliminary interpretation of other Chirp profiles onboard during the SWIM2005 cruise also led to the same conclusion (Figure 4.7).

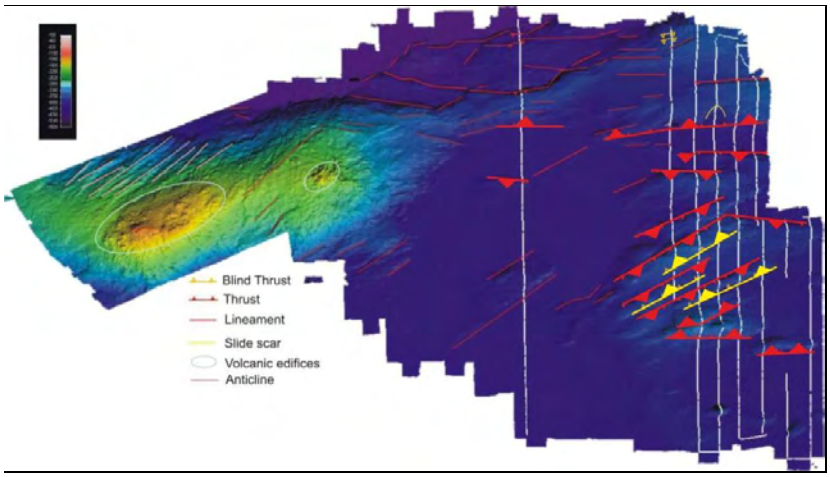

Figure 4.7 - Preliminary map of structures in the SWIM2005 survey area based on interpretation of Chirp profiles showing the presence of thrusts on the base of all the reliefs. Modified from Zitellini *et al.*, 2005. This interpretation was confirmed by acquisition of MCS lines during the MCS survey SWIM 2006 (Bartolomé *et al.*, 2008).

The slope values of 20º to 22º (much higher than the 2º to 4º average) are present in some cases (features 1 and 4 in Table 4.1) where on top of the elongated reliefs some smaller elevations of around 2 kilometers are present. These elevations are believed to be salt domes due to their conspicuous round shape and to the presence of other salt domes in a nearby area. Inspection of seismic profile Arrifano06 (Figure 4.8) corroborates this information as it crosses one of these reliefs exactly on top of one of these rounded elevations. The section of this seismic profile shows the interference between tectonics and diapirism also as suggested by the analysis of the bathymetry where the salt domes protrude the central part of the elongated abyssal hills.

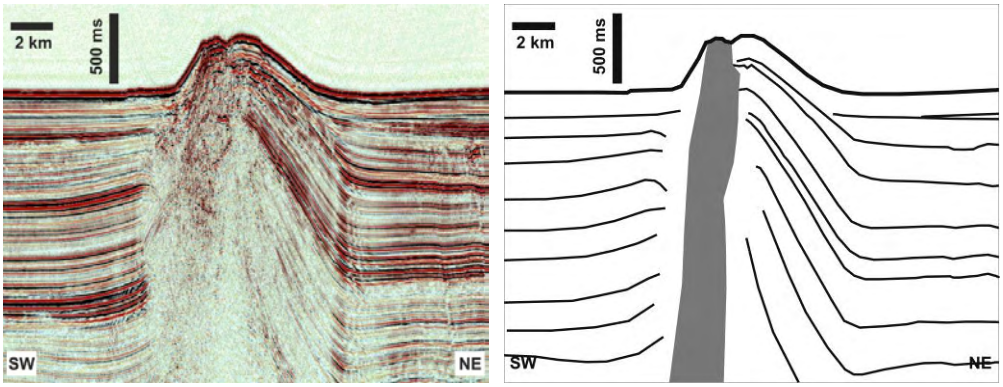

Figure 4.8 – Section of Arrifano06 seismic profile (for location see Figure 4.6) showing the interference of an ascending diapir with the thrust related hanging-wall anticline, abyssal hill imaged is feature number 1 on Table 4.1. On the right, a schematic interpretation where the evaporites are shown as the grey body.

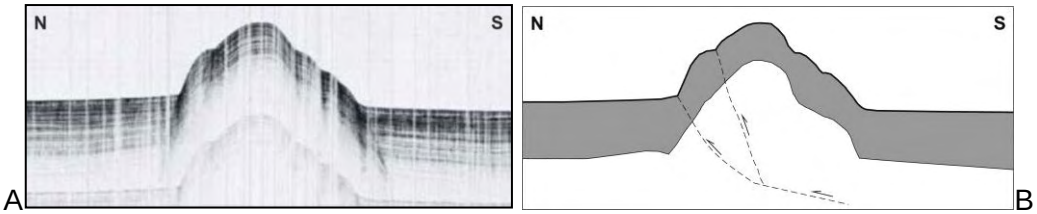

A B

Figure 4.9 – A - Chirp profile SWIM2_62 crossing an abyssal hill (number 12 in Table 4.1). Elevation on the seafloor in the profile is 3,5 km across and 50 meters high. The relief is the bathymetric expression of a fold affecting recent sediments and its asymmetry suggests the presence of a North-verging thrust underneath. Image taken from the SWIM2005 survey report. B – Schematic interpretation of A. Grey area corresponds to the layered sediments package observed in A.

4.2.2.2. The Abyssal Hills in the HAP

Smaller and much less elongated abyssal hills are found in the HAP when compared to the ones present in the SAP. The flat morphology of the HAP is locally disturbed by 10 minor reliefs (Figure 4.10), the largest and tallest of which does not reach 10 km in length and is approximately 60 meters high.

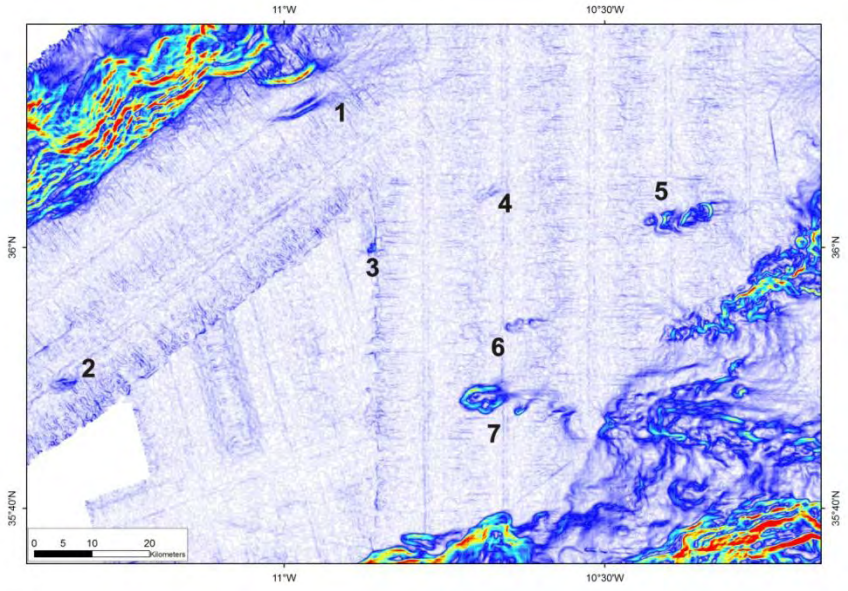

Figure 4.10 – Slope map of the HAP where some abyssal hills form clusters or exist as scattered reliefs on the seafloor (white and blue colors are low slope values, yellow and red stand for higher slope values). Numbers correspond to features on Table 4.2.

Some of these reliefs appear in groups, like elevations 5 and 7 that form linear clusters of three and two elevations each, respectively (Figure 4.11). These elevations seat on top of lineaments that correspond to sub-vertical dextral strike-slip faults that crosscut the abyssal plain known as the SWIM lineaments/faults (Rosas *et al.*, 2009; Zitellini *et al.*, 2009; Duarte *et al.*, 2010). Elevations 2 and 7; 4 and 5 are elongated and aligned on top of two different lineaments. On Table 4.2 are shown the sizes and geometry of the Abyssal Hills in the HAP, in the cases where the relief is asymmetric the different height values are presented.

Table 4.2 – Characteristics of the Abyssal Hills in the HAP.

Feature		Length (m)	Width (m)	Height (m)*	Slope (º)	Elongation	Symmetry
1		8670	1800	25(N)/40(S)	3.1	NE-SW	symmetrical
2		4400	2240	20(N)/35(S)	2	E-W	symmetrical
3		1400	1050	15(N)/25	4	ENE-WSW	South verg
4		2500	1100	10(N)/15(S)	1	NE-SW	symmetrical
5	West	1900	1700	30	2.7	NE-SW	symmetrical
	center	3055	2000	30/50	4.3	NE-SW	NW verg
	East	3500	2000	45/30	5.5	NE-SW	NW verg
6		6200	2000	20/10	2	ENE-WSW	N verg
7	West	7260	3600	90	4	E - W	symmetrical
	East	2200	950	30	5	NE - SW	Symmetrical

* - when the flanks of the same relief have different heights, both values are presented.

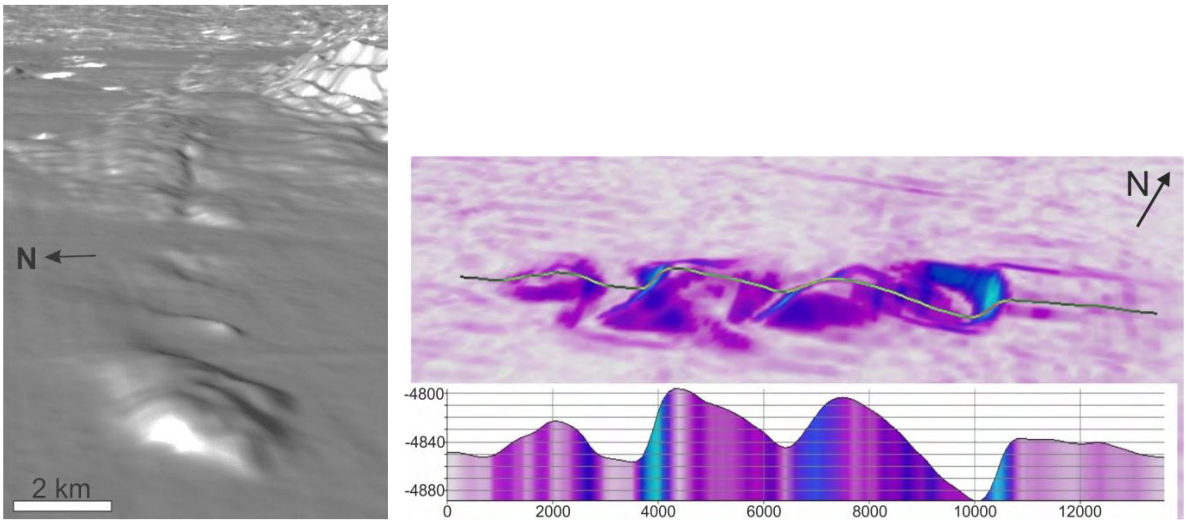

Figure 4.11 – Abyssal hills on the HAP, on the left: two elevations of the cluster 7 located over a lineament with a very important superficial expression; on the right: cluster 5 made up by three reliefs, 3D display (colours indicate gradients) on top; cross-section on the bottom. Numbers on the profile axes are in metres.

The repetitive elongation, parallelism and asymmetry of the elevations suggest, like in the similar counterparts of the SAP, a tectonic origin for these features. Whilst this assumption is quite understandable when related to the clusters that lie on top of the large wrench faults, the use of seismic profiles is indispensable to associate tectonics with the other abyssal hills. Inspection of multichannel seismic profiles as well as high resolution seismic lines showed that these reliefs correspond to folds affecting the sea bottom associated with transpressive dextral WNW-ESE wrench or reverse faults (red arrows in Figure 4.5 and Figure 4.12).

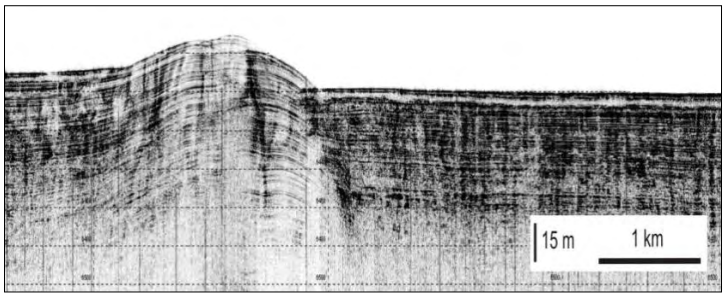

Figure 4.12 - Segment of a high resolution sub-bottom profile on abyssal hill number 6 (Table 4.2) on the HAP, NNW towards the right. It is clear that the elevation on the seafloor corresponds to a fold affecting the uppermost sediments related to the Northwards directed thrust lying underneath.

4.2.2.3. Abyssal Hills in the TAP

In the TAP only two minor elevations were found (Figure 4.13): one NE of Hirondelle Smt (8.5x4km with a 250m height, slopes up to 10º, Figure 4.14b) and another located west of Príncipes de Avis Spur (4x1,5km and 25m high, slopes up to 2º, Figure 4.14a).

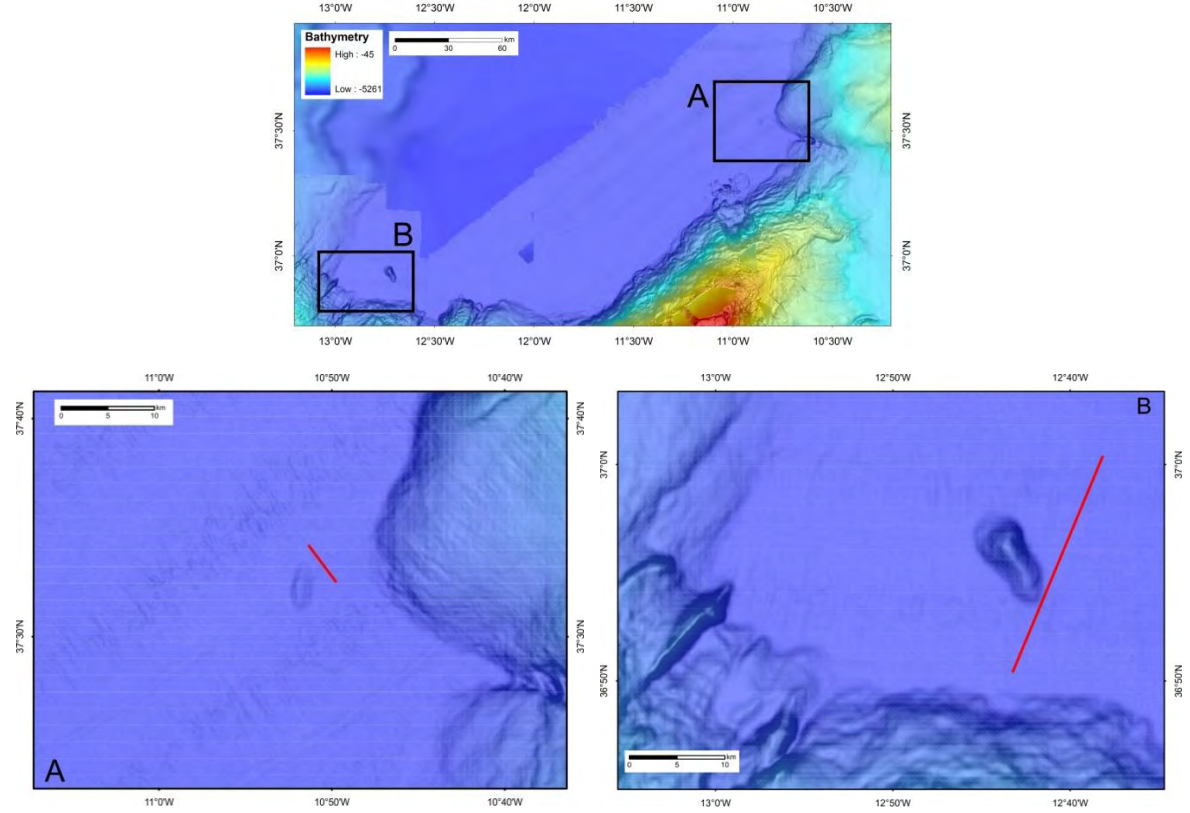

Figure 4.13 – Bathymetric map showing the location of the Abyssal Hills in the TAP; black boxes correspond to the zoomed areas bellow. Red lines are position of multichannel seismic profiles of Figure 4.14.

The sub-surface structure associated to these two features is imaged by the two seismic profiles that are located very close to both. Concerning the one closer to the Hirondelle Smt, it is possible to relate its genesis to a basement high and to the fault that bounds that high (Figure 4.14a). The other minor elevation is in the vicinity of a thrust vergent to the South and its genesis can be possibly related with this structure (Figure 4.14b).

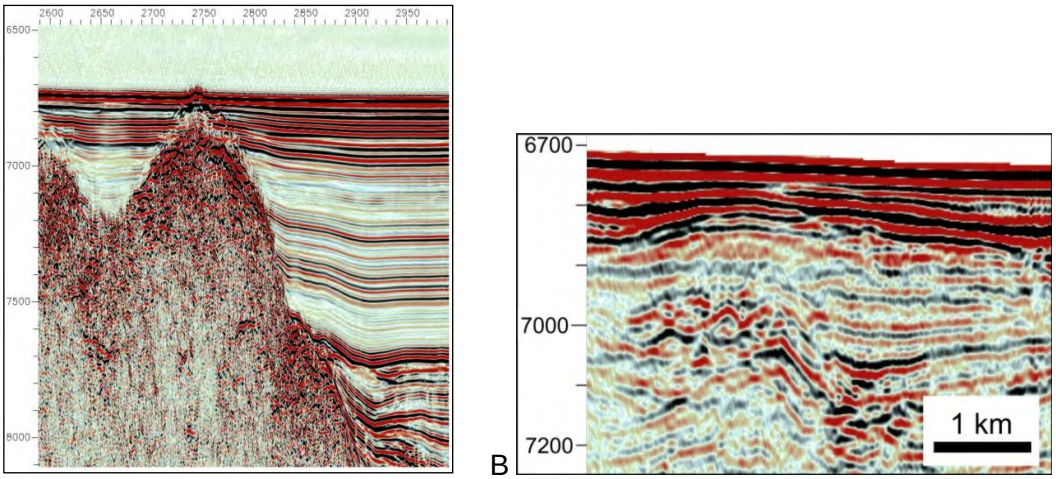

Figure 4.14 – Multichannel seismic profiles Arrifano02 (left) and BS12 (right), the first shows a fault bounded basement high and the second a thrust affecting sediments very close to the seafloor. For location see Figure 4.13, see text for description.

4.3. The Submarine Drainage System

This domain consists of 3 systems of drainage of currents and sediments that in specific places interact with each other.

4.3.1. The Submarine canyons

Submarine canyons are deep and long incised valleys in the seafloor that expose the older underlying rocks, their morphology resembles their onland equivalents with an amphitheatre like head with several tributaries, more or less sinuous axis (thalweg) and steep sides. Generally, the gradient values along the valley's axes can reach up to 15º in near shore zones and it decreases to less than 1º in distal parts.

It is common for submarine canyons to incise all the continental slope and connect to onshore valleys or rivers; however, some canyons have their headscarps at the edge of the shelf or even beneath that area.

Their origin is still in debate and the following three main hypothesis are discussed: i) at first it was supposed that submarine canyons were formed during low sea level by the carving of the seafloor by major rivers on the subaerially exposed continental shelf; ii) a second theory, relates their formation with the erosive action on the seafloor by downslope turbidity currents; iii) a last hypothesis tries to establish a link between their origin and evolution with the occurrence of gravity driven failures (mass wasting, slumps and submarine landslides) as they can contribute to the remobilization of large masses of rock and sediments on the seafloor. It is possible that submarine canyons can have different processes responsible for their formation, possibly acting with different intensities at different evolution stages and/or locations. The South Portuguese Margin is incised by a series of canyons and other erosive features as shown in Figure 4.15: the Faro canyon (FC), the Portimão canyon (PC), the Lagos canyon (LC) and S. Vicente canyon (SVC). The submarine canyons incise the upper

continental slope (FC and LC) and can reach onto the continental shelf (the PC and SVC). These last two have their headscarps shallower than the other, however, onshore no major river are connected to them, as seen on Figure 4.15 where rivers are shown (Ar: Arade River and major tributaries are highlighted).

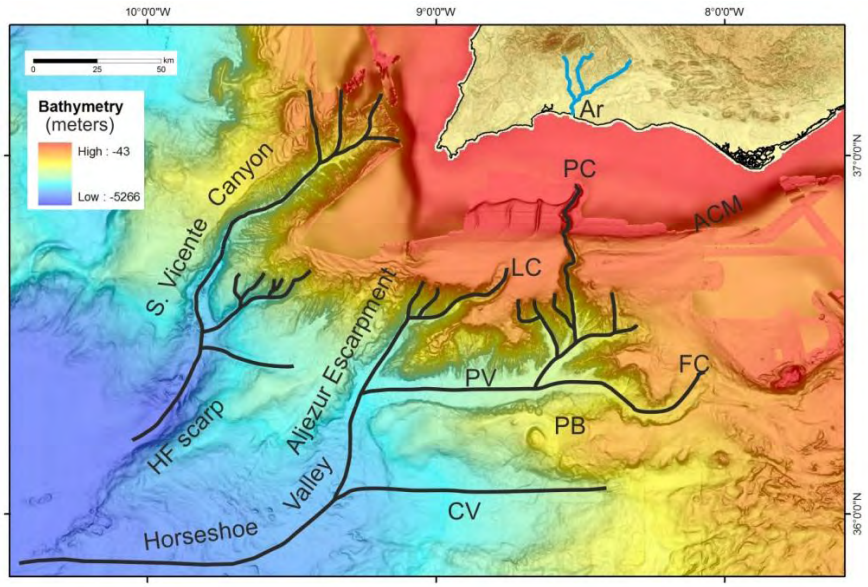

Figure 4.15 – The South Portuguese Margin displays a well-developed incision at the edge of the continental shelf and slope. Note the incision by the numerous gullies and the more important submarine canyons. In the deeper areas, wider and flat bottom valleys are present. Ar: Arade River and major tributaries; PC: Portimão Canyon; ACM: Alvares Cabral Moat; LC: Lagos Canyon; FC: Faro Canyon; PB: Portimão Bank; PV: Portimão Valley; CV: Cadiz Valley; HF: Horseshoe Fault.

The Faro canyon has an arcuate shape, varying its dip from N-S at the foot of the continental shelf edge to E-W as it merges into the Portimão valley. The Faro canyon is, about 30 km in length, with a 5 km wide flat bottom, up to 800 metres high walls with slopes up to 10º.

The Portimão canyon with a length over 50 km, striking in a N-S direction, is the one that reaches shallower depths (around 100 m below sea level), presents a V-shaped cross-section with steep walls affected by several slide scars (slope reaches more than 30º in several places) and a sinuous path till its bottom reaches 1400 m deep. Its morphology is somewhat conditioned the Mediterranean Outflow Water system since on both side of the canyon drifts are present (Albufeira and Portimão Drifts located east and west with respect to the canyon, respectively) and also due to the interference with the Alvares Cabral Moat carved by the MOW.

The Lagos canyon extends over 60 km, drains towards the SW and its morphology changes from the upper to the lower parts. In its upper part the canyon displays a wider thalweg with a smaller inner channel carved close to the SE wall. The heights of the flanks vary from 200 m (incising the contourites deposits) to 800 m (closer to the continental slope). The lower segment is separated from the upper by a major constriction point and there the incision

reaches 1 km with slopes of more than 10º on the flanks that display an asymmetrical V-shaped transverse profile.

These three canyons (the Faro canyon, the Portimão canyon and Lagos canyon) and their minor contributory valleys play a major role in the present submarine drainage of the south Portuguese margin since large part of the sediment transport to the deep basins (HAP) is processed through them.

The São Vicente canyon (transl. Saint Vincent canyon) is located in the connection point between the South and West Portuguese margins, extending from very close to the shore (less than 10 km, depths of 200 mbsl) to the HAP at around 4900 m depth. It measures more than 120 km in length (it is the largest of the South Portuguese canyons) and reach up to 20 km in width. The walls are steep and frequently display mass-wasting scars and are also strongly incised by minor contributory valleys. A major kink is present where the canyon diverts to the east about 60º from its upper course (Figure 4.15), several minor kinks can be identified as well as some knickpoints identifiable across its track. Across its length the morphology changes: the SE side is the steepest in the upper and deepest parts whilst for the intermediate sector the NW wall is steeper. Its head has an amphitheatre shape due to the pattern defined by its minor contributories as a result of slumps and slides and therefore it appears to be retreating upslope in the direction of the shore. Due to their size and importance the S. Vicente and Portimão canyons will be further characterized ahead in this chapter.

As stated before, submarine canyons play a major role concerning sediment distribution and transport to deep ocean basins and eventually to the abyssal plains. Since their head is located not far from shore they capture currents and their sediment load and transport them to deeper parts of the ocean or even directly to the abyssal plains. The backscatter of the seafloor is very helpful when studying this. The produced backscatter map (Figure 4.16) displays the seabottom response to acoustic waves and is a variable of the physical properties of the material that constitutes the seafloor. Although it is not possible to identify the exact lithology, it is possible to infer if the material present is loose or consolidated (compact) and whether fine or coarse grained.

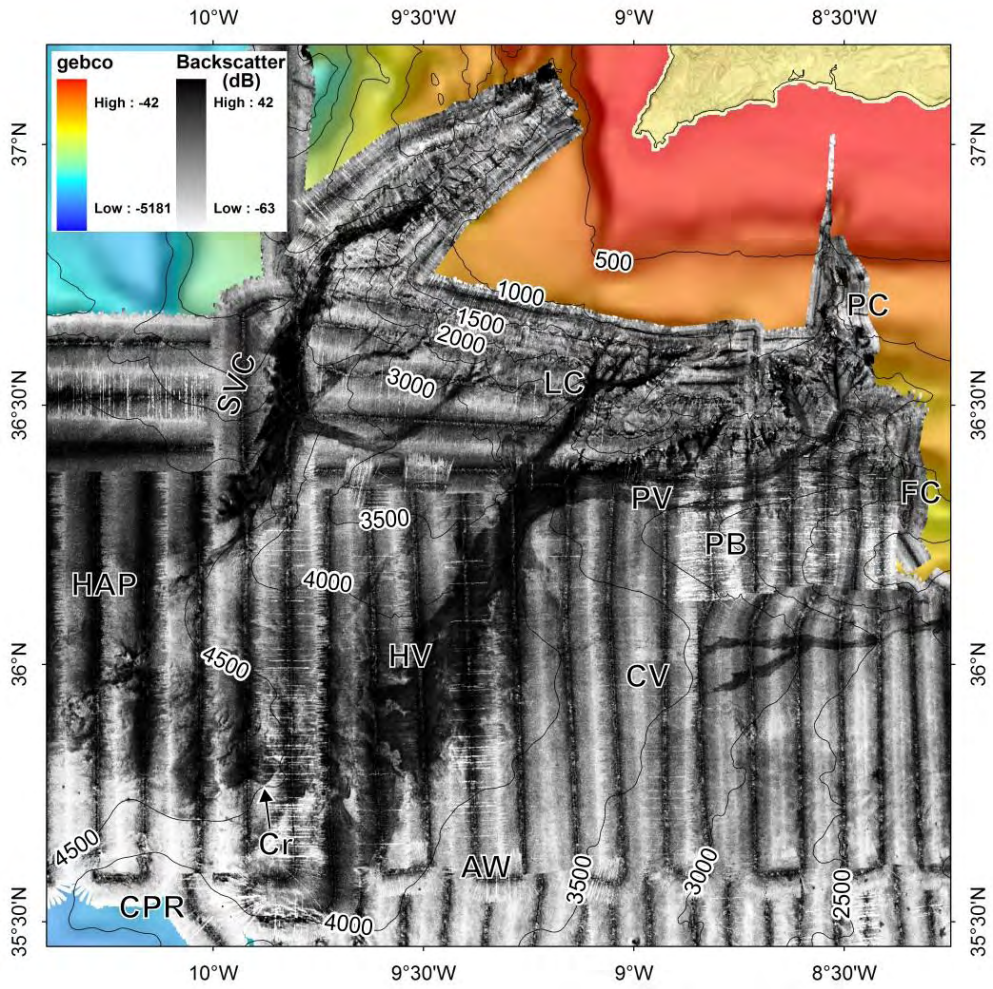

Figure 4.16 – Mosaic of the backscatter (derived from the multibeam probe) response of the seafloor. Darker colors correspond to higher responses and correspond to coarser or more compact materials. Noticeable north-south pattern corresponds to acquisition artifacts; due to bad weather, artifacts are also abundant in the PB area. SVC – S. Vicente canyon, HAP – Horseshoe Abyssal Plain, LC – Lagos Canyon, PC – Portimão Canyon, FC – Faro Canyon, PB – Portimão Bank, PV – Portimão Valley, CV – Cadiz Valley, AW – Accretionary Wedge, CPR – Coral Patch Ridge, Cr – Crescent shaped features.

By the analysis of the backscatter map the first thing that stands out is that all the canyons described are displayed with a dark color. This indicates that the material there present is either consolidated (like rock outcrop) or of coarse grain, being the last the more probable option and confirmed by inspection of MCS profiles. The presence of coarse material in the canyon axis rules out the possibility of pelagic sedimentation taking place there, therefore, its presence there suggests that this material is coming either from the walls of the canyons or that it is being captured in the areas close to the canyon's head and carried to higher depths by the currents that flow downslope along the thalweg. Both of the hypotheses seem to occur as the flanks of the canyons are steep, several slide scars can be identified and also display dark colors indicating that mass-wasting processes may be taking place, thus exposing more compact materials. Also, it is likely that the canyons' drainage system is active, since the margin is experiencing uplift and in shallow areas there is sediment

available that can be remobilized and captured by the canyons. Darker areas along the canyons walls are also present and correspond to slide scars that expose older and more consolidated rocks that give a higher acoustic response.

4.3.2. The Valleys

Besides the canyons, also involved in the drainage processes and sediment transport there are three more features that by their dimension stand out (Figure 4.15): the Portimão Valley (PV), the Cadiz Valley (CV) and the Horseshoe Valley (HV). The first two trend in an east-west direction, draining towards the west, whilst the latter has two segments: an upper NNE-SSW and a lower E-W sector.

The Cadiz Valley (Figure 4.15) is located south of Portimão Bank, is about 110 km long and can be as wide as 20 km in its western sector or as narrow as 3 km in the eastern part. Inspection of multichannel seismic profiles reveal that the flat and wide westernmost part of this valley is due to the olistostrome that originates in the Portimão Bank and from another relief to the south, where numerous slope failures can be observed on both of them (described further ahead). These erosive and depositional processes re-shaped the northwestern part of the accretionary wedge of the Gulf of Cadiz erasing its wrinkly appearance, giving the seafloor a smooth and flat appearance. This smoothly dipping seabottom is only disturbed by two shallow channels that flow towards the West and although their bathymetric expression is not very relevant (none of them is more than 20 meters deep) they display an important role in sediment transport that can be seen by their well-marked signature in the backscatter map (Y-shaped feature on Figure 4.16).

The Portimão Valley (Figure 4.15) lies between the Portimão Bank and the deeply incised upper continental slope of the South Portuguese margin. The Portimão Valley extends for about 100 km, with widths from 5 to 9 km collecting the downslope currents and sediments from the upper continental slope of the south Portuguese margin and from the approaches of the Guadalquivir Basin and External Betics in the northern part of the Gibraltar Arc. This valley displays a strong acoustic response in the backscatter map (Figure 4.16) (the noisy appearance of the record is mostly due to the bad weather during the acquisition when the area was surveyed). It is interpreted as the response of a hard ground that results from active sediment transport processes; draining the sediments that come from the north (through the Portimão Canyon) and the west (sediments transported by the MOW and along the Faro canyon).

The Horseshoe Valley (HV) (Figure 4.15) is an L-shaped feature, in its upper segment the head rests at about -3800m and the lower segment (close to the HAP) is about 1000 m deeper. In the north, where the HV connects with the Portimão and the Cadiz valleys, the valley is 60 km long dips towards the SSW and its width varies from 6 to over 20 km. In this

sector the HV is bounded by a NNE-SSW striking escarpment (the Aljezur escarpment, Figure 4.15), which is taller in the North (400 m) than in the South (90 m to nil), and shows several slide scars dipping towards the valley. The valley has a mean slope value of 0.5º and displays a smooth bottom. The lower sector of the HV is wider (values can reach 40 km) and flows westwards towards the Horseshoe Abyssal Plain. Its seafloor is flatter than in the upper sector (mean slope of 0.3º) and its southern limit (CPR) is much higher than the northern limit (an eroded plateau that corresponds to the hanging wall of the Horseshoe Thrust). The wide seafloor of the valley displays several features that disturb the bottom, like several crescent-shaped depressions (Cr in Figure 4.16), a small 80 meters high elevation (that might be related with the extrusion of fluids) and an alignment of crests and troughs that can be traced along the whole valley (Rosas *et al.*, 2009; Terrinha *et al.*, 2009; Duarte *et al.*, 2010). This valley acts as a bypass for the sediments drained by the canyons south of Algarve and the two east-west valleys until they reach the HAP, which is in agreement with the strong acoustic response of the seafloor (Figure 4.16) that indicates the presence of coarse materials in the bottom of the valley.

4.3.3. The Mediterranean Outflow Water Sedimentary System

This is a complex domain by its spatial extend and by the diversity of features it presents. It stretches from the Straits of Gibraltar and can be mapped till the S. Vicente Canyon. This domain is formed by the features resulting from the interaction of the Mediterranean Outflow Water (MOW) currents with the seafloor. The MOW is a thermohaline current that flows out from the Mediterranean Sea through the Straits of Gibraltar. These currents extend much further than the Gulf of Cadiz and carry on into the open North Atlantic Ocean, where they can be traced up to Greenland or the Azores Islands (Reid, 1979; Jia, 2000). Several authors (Hernandez-Molina *et al.*, 2003, 2006; Mulder *et al.*, 2003) have already reported on the morphologic and sedimentary features associated with the MOW with great detail (multibeam bathymetry, sonar, sediment cores, high resolution seismic, water column sampling, underwater TV cam). The warmer and saltier MOW flows out of the Straits of Gibraltar (SoG) and stretches west, northwestwards and also to the southwest. The features generated by the MOW, vary from place to place, and are related with the speed of the currents, their interaction with the seafloor and the Coriolis effect. Part of the MOW currents after crossing the SoG are deviated towards the right (north) due to the Coriolis effect; clearly visible in the drag marks and carved channels in the seabottom. The speed of the currents is also a major factor taken in account when studying the features generated by the MOW as it systematically decreases away from the SoG. Thus, the numerous channels excavated by the MOW are found east of 8ºW meridian (with the exception of the Álvares Cabral Moat that extends as far as the Portimão Canyon) because as it flows westwards it

loses speed and therefore its erosive capacity; the fact that it becomes neutrally buoyant (and detaches from the seabottom at depths ranging from 1000 m to 1400 m) also contributes to this fact. These facts lead to the formation and interaction between erosive features (closer to the SoG) and sedimentary/constructive features (more to the west). The MOW pathway is divided into two major branches (Ambar *et al.*, 2002, 2008; Hernandez-Molina *et al.*, 2003): the Mediterranean Upper (MUW) and Lower Water (MLW). However, a third smaller branch is present which is responsible for the carving of a smaller channel (Gil Eanes Channel) flowing towards the SW and is not mentioned by the referred authors.

The MUW separates itself from the remaining currents just after the SoG and is responsible for the carving of the Alvares Cabral Moat (Figure 4.17A), whilst the MLW is itself divided into three branches: the southern, principal and intermediate branches (Figure 4.17 A).

A

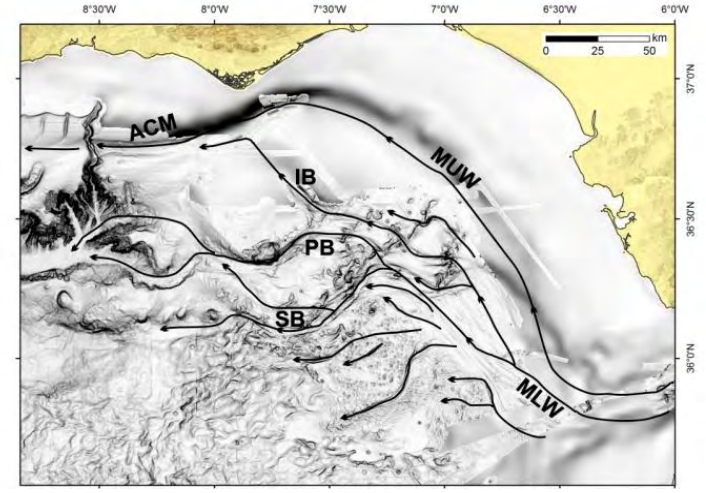

B

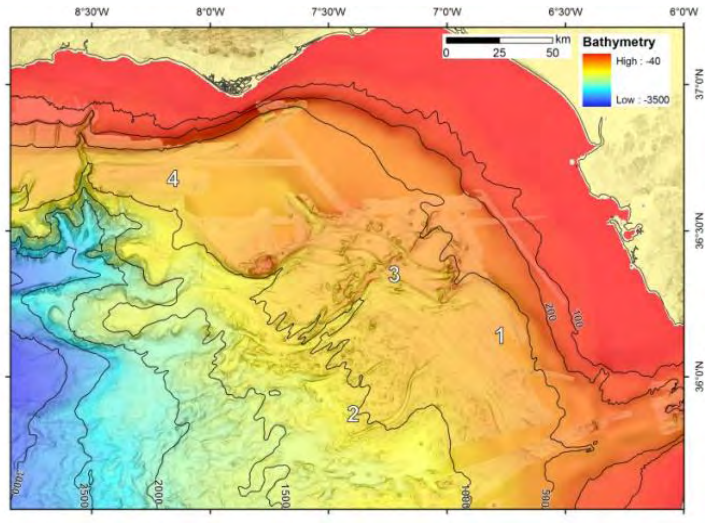

Figure 4.17 – **A**: Paths of the several branches of the Mediterranean Outflow Water system; MUW- Mediterranean Upper Water, MLW- Mediterranean Lower Water, IB- intermediate branch, PB- principal branch, SB- southern branch. **B**: Bathymetric map of the northeastern part of the Gulf of Cadiz. It is in this area that the MOW system is installed and several features can be identified. The numbers refer to the four sectors of the MOW system: 1 – Scour and sand waves sector; 2 – Sedimentary lobe sector; 3 – Channel and Ridges sector and 4 – Drift sector. Name of the MOW currents and sectors modified from Hernandez-Molina *et al.* (2003).

The features generated by the MOW differ from place to place and 4 different sectors can be mapped inside the MOW system (Figure 4.17B). The different morphologies found are a function of the speed of the currents and the interaction between them and the seafloor. The four sectors are (Figure 3.18): 1 – Scour and sand waves sector; 2 – Sedimentary lobe sector; 3 – Channel and Ridges sector and 4 – Drift sector.

Figure 4.18 (next page) – Backscatter map of Northeast of the Gulf of Cadiz, imaging the MOW system and the interpretation of the various morpho-sedimentary sectors: sector 1, Scour and Sand waves (yellow), sector 2, Sedimentary Lobe (red), sector 3, Channels and Ridges (green) and sector 4, the Drifts (orange). Labelled features: 1-rock outcrop; 2-scours and elongated sand dunes; 3-Gil Eanes Channel and sand mud waves; 4-gravitational mud lobe; 5-sand lobe with slide scars and scours; 6-sand wave field; 7-minor channel; 8-mud patch (?); 9-mud volcano (?); 10-Cadiz Ridge; 11-Guadalquivir Ridge; 12-Doñana Ridge; 13-IAM-GC3 seismic profile location; 14-Gusano Channel; 15-Cadiz Channel; 16-Guadalquivir Channel; 17-Huelva Channel; 18-Diogo Cão Channel; 19-Faro Drift; 20-Albufeira Drift; 21-Portimão Drift; 22-Lagos Drift; 23-Sagres Drift; 24-Alvares Cabral Moat; 25-Portimão Canyon; 26- P81-21 seismic profile location. Backscatter dataset is composed by sidescan sonar on the East part (E-W marked artifacts, Hernandez-Molina *et al.*, 2006) and by the SWIM backscatter dataset on the West (N-S artifacts).

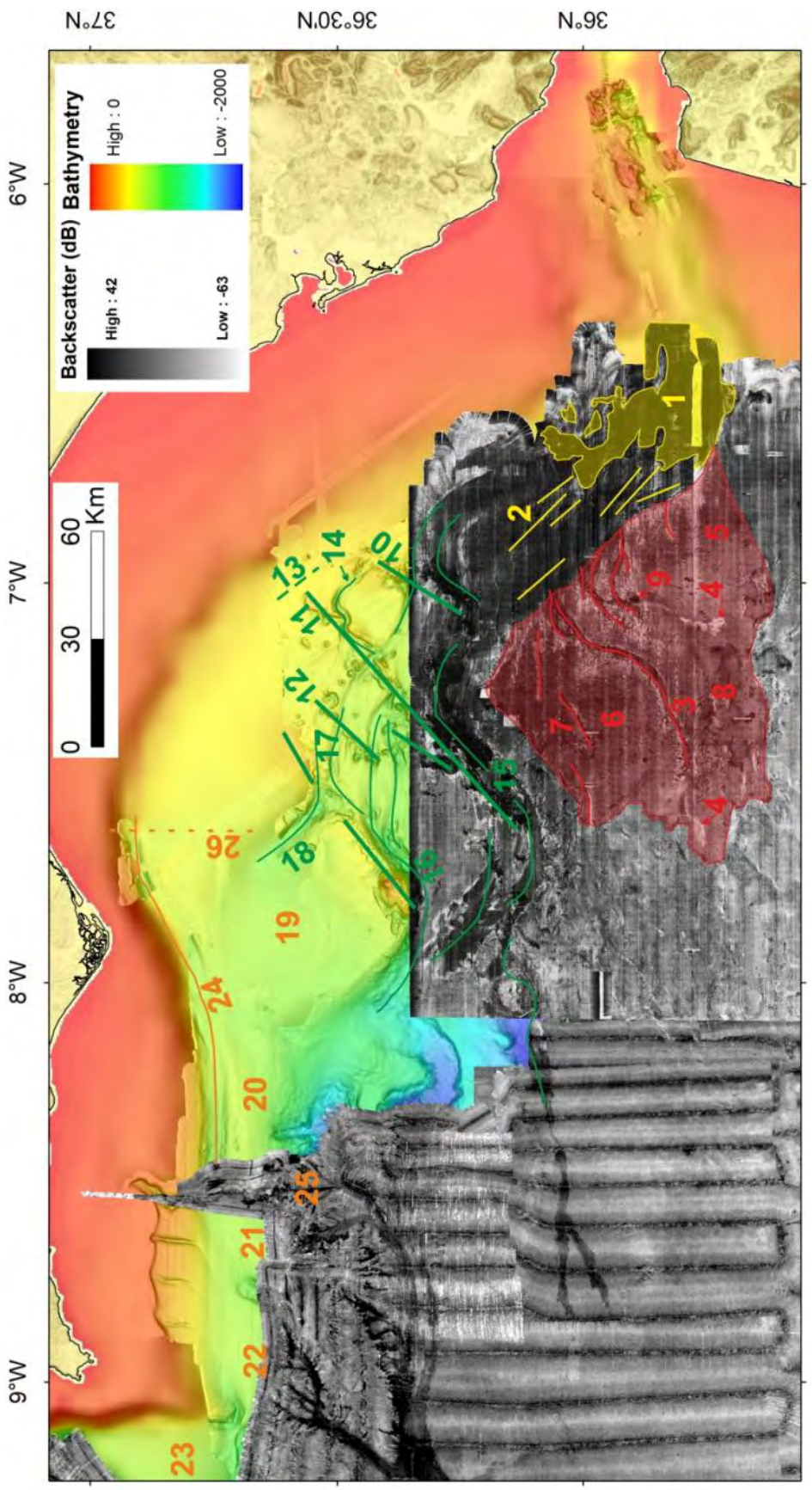
37°N
36°30'N
36°N
6°W
7°W
8°W
9°W
Backscatter (dB)
High : 42
Low : -63
Bathymetry
High : 0
Low : -2000
0
30
60
Km
1
2
3
4
5
6
7
8
9
10
11
12
13
14
15
16
17
18
19
20
21
22
23
24
25
26

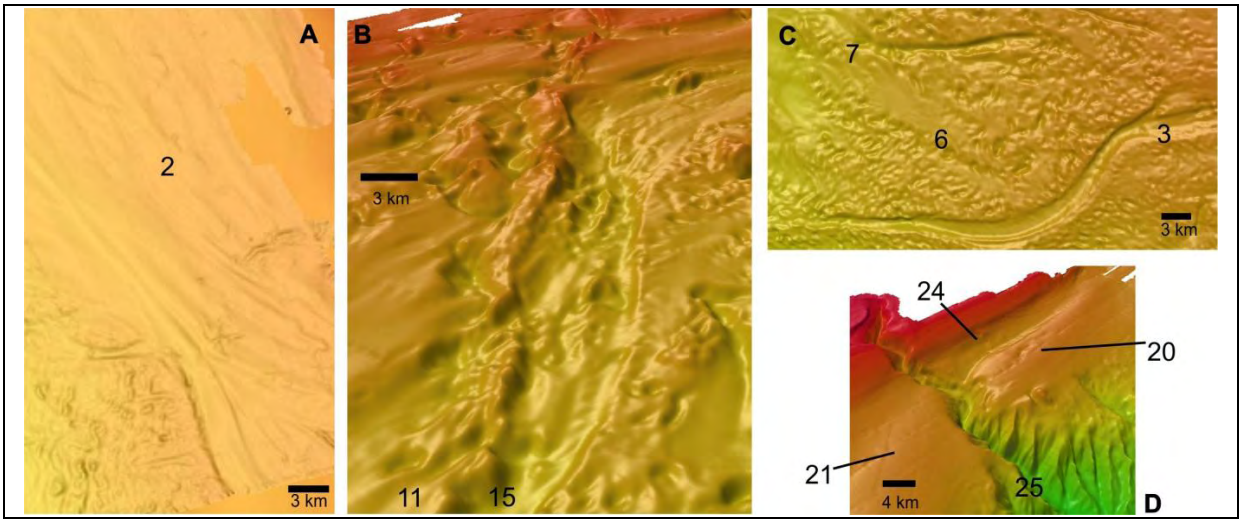

Figure 4.19 – Some particular aspects of the MOW system generated features in 3D view. Numbers correspond to the features of Figure 4.18. A- Scour marks and elongated sand dunes in the main channel of the MOW, just outside the Straits of Gibraltar; B- Down slope deflection of the Cadiz Channel (15) as it meets the Guadalquivir Diapiric Ridge (11); C- Gil Eanes Channel (3) and another carved channel (7), in the middle there is a large sand wave field with some scouring (6); D- Interaction between the Alvares Cabral Moat (24) and the Portimão Canyon (25), the Albufeira (20) and Lagos (21) contourite drifts are present on both sides of the canyon. The scale varies across the images and the scale bar is indicative for the place where it is located.

4.3.3.1. Scour and Sand waves – sector 1

This sector is the one closest to the SoG and is therefore the one where the MOW has the more significant erosive capability and highest speed (up to 2.5 m/s, Hernandez-Molina *et al.*, 2006). Accordingly, erosive features are dominant, like the prominent abrasive surface carved on a large rock outcrop (probably Miocene flysch from the Betics Domain, high backscatter response, number 1 in Figure 4.18) and the numerous plough and scour marks on the seafloor (Figure 4.19A). Despite the strong erosive capacity of the currents in this sector, depositional features are also found, like very elongated sand dunes that mark distinctively the currents SE-NW path (ridges on number 2 of Figure 4.18 and Figure 4.19A).

4.3.3.2. Sedimentary Lobe – sector 2

The Sedimentary Lobe sector is a domain located westwards of the previous one, outside the path of the strong MOW currents that shaped sector 1, it lies between depths of 750 and 1400 meters. It is a sector where the depositional features outnumber the erosional ones. The latter are essentially scours and erosive channels (number 7 in Figure 4.18), where the Gil Eanes Channel (number 3 in Figure 4.18 and Figure 4.19C) stand out by its dimensions: more than 50 km long and more than 1 km wide. The depositional features are related to overbanking processes that occur in the dependency/vicinity of the minor channels or westwards of the MLW channel (Figure 4.17A). Several sand and mud deposits result from the overflow of the MLW current (number 8 in Figure 4.18). Also, on both sides of the Gil Eanes Channel (number 3 on Figure 4.18 and 4.19C), sand deposits can be found with an

undulated seafloor that corresponds to a sand waves field (number 6 in Figure 4.18). The deposits of this sector exhibit some gravitational slides and erosion scours. Some gravitational/debris flow deposits, with a fan like shape (number 4 in Figure 4.18), can also be found at the end of some channels, like at the tip of the Gil Eanes Channel.

4.3.3.3. Channels and Ridges - sector 3

This sector is located just after the scours and sand waves sector in the direction of the flow of the MOW. As shown in Figure 4.17A and 4.17B, the uniform flow of the northwestwards directed MOW, splits into various branches in this sector, forming several channels that swing around elevations and ridges (Figure 4.19B). This causes one larger current to separate into various minor ones that carve smaller channels like the Cadiz, Guadalquivir, Gusano, Diogo Cão and Huelva Channels (Figure 4.18). Although sinuous, channels have two main trends: the NW-SE are sectors where the channel flows along slope, whilst its NE-SW sectors flow downslope towards the SW. Their dimensions can vary from a few kilometers (just over 10 km for the Diogo Cão Channel) to almost 100 km (Cadiz Channel), are 2 to 10 km wide and their incision has values ranging from a few meters up to 300 meters. In these channels due to the high hydrodynamism only the coarser materials can settle as it is displayed in the reflectivity maps (Figure 4.18).

The ridges are the result of either diapirism or the interaction between tectonics and diapirism (Hernandez-Molina *et al.*, 2006), i.e., some ridges like the Doñana or Cadiz ridges (numbers 10 and 12 in Figure 4.18) seem to result from the sole action of evaporites ascent to the surface or near it causing it to bulge. The Guadalquivir Diapiric Ridge (number 11 in Figure 4.18) stands out from the remaining ones as a 70 km long lineament of very elongated intermittent diapirs that border the Cadiz valley on the edge of the Guadalquivir allochthonous body. This interaction of ascending evaporites and fault zones can be observed on the seismic profile presented in Figure 4.20 that crosses the Guadalquivir Ridge in an area where it does not outcrop (location is feature 13 in Figure 4.18), but where the interference between tectonic structures and diapirism is clear.

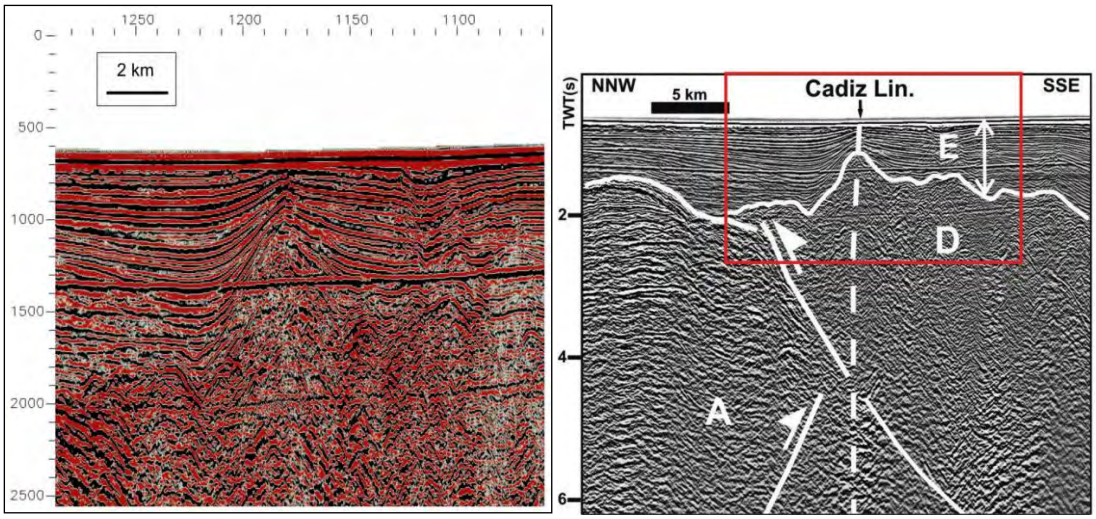

Figure 4.20 – Section of multichannel profile IAM-GC3, just NW where the Guadalquivir Ridge is identifiable on the bathymetry. Although the seafloor is flat, deeper down a diapir is present and it is ascending through a fault zone, identifiable by the different sedimentary packages on each side of the fault/diapir. Profile direction is NW-SE, NW is towards the left and location of profile is feature 13 of Figure 4.18. On the right side, a wider perspective of the same mcs profile and its relation with the deeper structure; red box is the section shown on the left (adapted from Duarte *et al.*, 2009).

4.3.3.4. The Contourite Drifts - sector 4

This sector is located in the Northern part of the Gulf of Cadiz, further away from the Straits of Gibraltar with respect to the previous ones, i.e. where the MOW system starts. It extends over a large area South of Portugal, west of 7ºW, depths between 500 and 800 meters deep and is mainly a depositional sector as it is the one where the currents have a lower speed and therefore lose their transport capacity and drop the sedimentary load. Also the fact that the MOW becomes neutrally buoyant and detaches from the seafloor inhibits the erosion action of the currents. The seafloor morphology in this sector is much smoother than in any other due to the presence of several contourite drifts and is only disturbed by some incisions like the Alvares Cabral Moat (more than 80 km long, about 8 km wide and command up to 300m, number 24 in Figure 4.18 and Figure 4.19D) and the head of the Portimão and Lagos canyons (number 25 in Figure 4.18 and Figure 4.19D).

There are several distinct contouritic bodies, from east to west (Roque *et al.*, 2012): Faro, Albufeira, Portimão, Lagos and Sagres (numbers 19 to 23 in Figure 4.18). All together they extend for around 200 km and have widths ranging from 10 to 40 km, are limited to the north by the Alvares Cabral Moat in the central and eastern part or by the slope break at around -600 m in the western sector.

These deposits are formed by the MOW where it deposits the materials eroded along its path generating two kinds of contourite deposits: sheeted drifts (southeastern part of Faro-Albufeira Drift and the Portimão, Lagos and Sagres drifts) and the elongated (E-W) separated (from the upper slope by the ACM) mounded drifts (northern part of Faro-Albufeira Drift, Figure 4.21). The first displays a very regular pattern of parallel reflectors of medium to

high amplitude, whilst the latter shows a basal unit with a strong aggradant geometry that becomes progressively prograding towards the north where the moat is located.

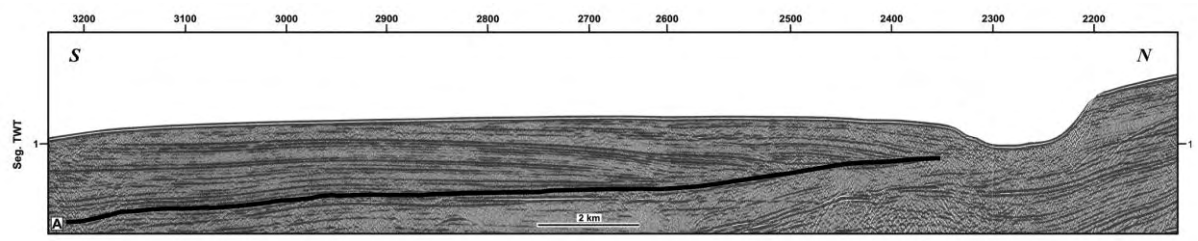

Figure 4.21 – Section of MCS profile P81-21 displaying the Faro Drift (in the south) and the Alvares Cabral Moat (in the north), black line represents the base of the contourite deposit (modified from Roque, 2007).

4.4. The Submarine Mountains

The Submarine mountains are major elevations that rise above the seafloor and do not reach the water level. In the Southwest Iberia region two of these features, the Gorringe Bank (GoB) and Coral Patch (CP) are the most prominent bathymetric submarine mountains that rise from the seafloor at abyssal depths and separate the three abyssal plains (Figure 4.1a). The GoB is located 120 kilometers WSW of Cape S. Vicente, strikes in a NE-SW trend, is very large in size (200 km long by 70 km wide) and separates the HAP, in the south with depths of 4800 meters, from the TAP in the north, with a depth of -5100 meters. It is topped by the two flat peaks of Ormonde (-33 to -46m) and Gettysburg Smts. (-20 to 28m) separated by a 30 km wide and 850 m deep saddle (Figure 4.22A). The overall elongation ratio is 1:2.8 but for shallower parts higher values (up to 1:4.5) can be found.

The Gettysburg Smt. is very smooth and circular shaped from the top to 300m water depth, the Ormonde Smt. is slightly elongated (with a ENE-WSW trend) and presents a more irregular seafloor surface. In general, the slope values vary between 5º and 10º (Figure 4. 22B), with one flank steeper than the other. In the southwest sector (Gettysburg Smt.) the NW flank displays higher slope values (close to 30º); on the NE sector of the GoB (Ormonde Smt.) the SE flank is the steeper flank (slopes up to 20º; Figure 4.22B).

A 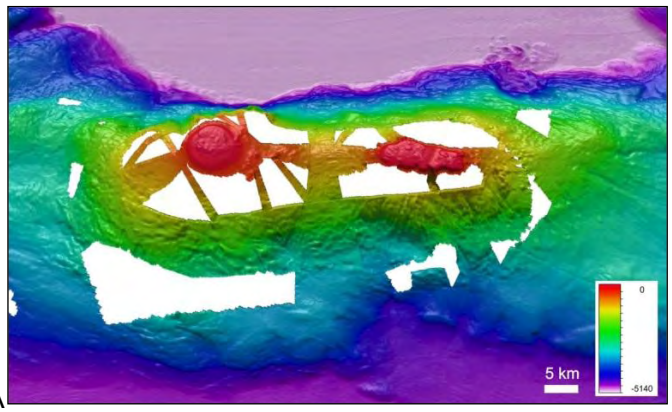

B 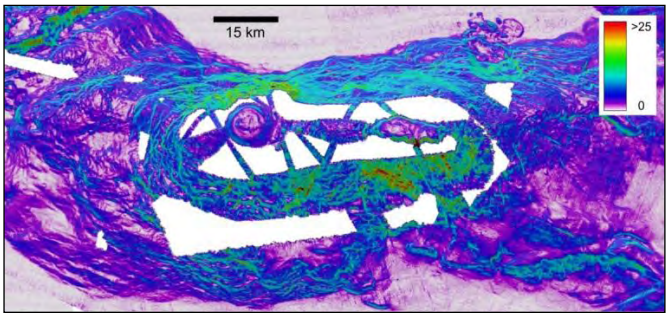

Figure 4.22 – **A**: 3D bathymetric view from the SE of The Gorringe Bank, comprising the Ormonde and Gettysburg seamounts, east and west, respectively. It is clear the undulated and irregular seafloor of the flanks as well as the flat tops on both seamounts. Another feature that stands out is the slide scar and debris on the north side of the Gorringe Bank. **B**: 3D slope model, showing the two distinct areas of higher slope values: south of Ormonde and north of Gettysburg. Scales are approximate values for closer areas and white colors are *no data* areas.

Such high slope values and steepness of the seafloor is favourable to the genesis of mass-wasting processes as the materials do not withstand these gradients, especially in such a tectonically active area as this one. Thus, several slumps, slide scars and mass movements can be identified on the Gorringe Bank, some of them with large dimensions (Figure 4. 23).

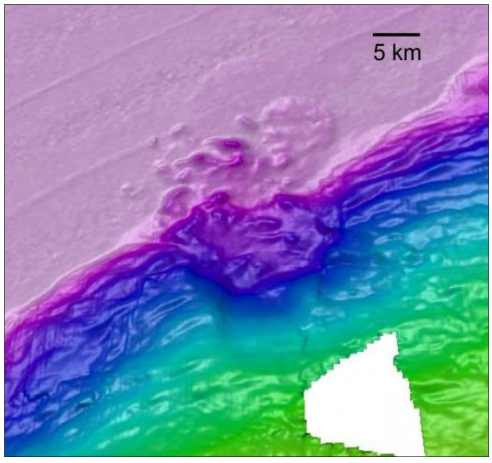

a b 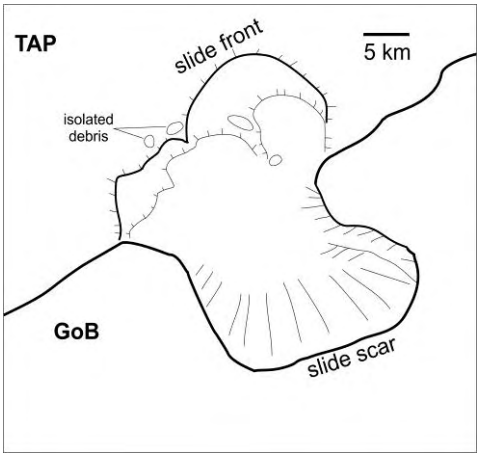

Figure 4. 23 - Detail (a) and schematic interpretation (b) of a part of the Northern flank of the Gorringe Bank (GoB) displaying a major slide scar affecting the seafloor and the debris deposits seating on the base of the slope over the Tagus Abyssal Plain (TAP). North is up.

The Coral Patch is made up by the Coral Patch Seamount and the Coral Patch Ridge (CPR) (Figure 4.24). The first arises from two abyssal plains: the HAP (in the north) and the SAP (in the south) and is connected by a continuous minor elevation to the last. The CPR is located to the east and seats between the Horseshoe Valley (to the north), the accretionary wedge (to the east) and the SAP (to the south).

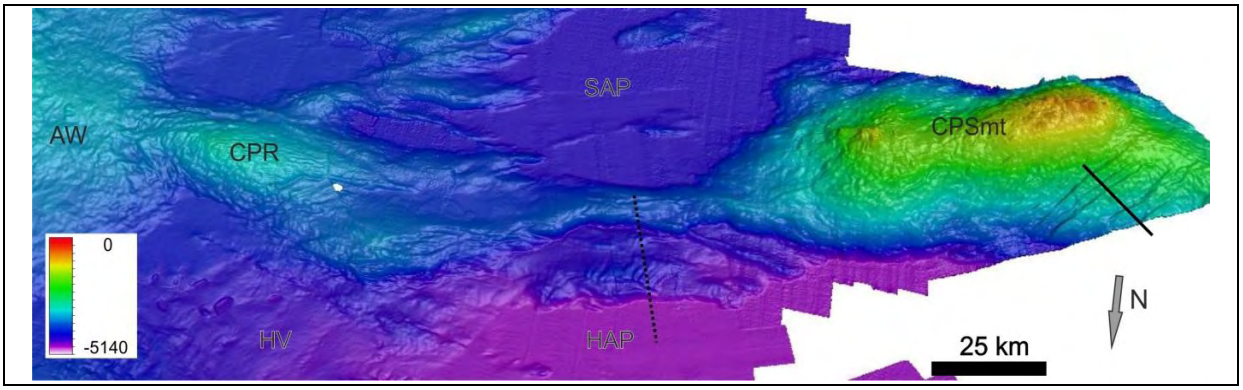

Figure 4.24 – 3D bathymetric model of the Coral Patch Smt. (CPSmt) and the Coral Patch Ridge (CPR), view from the North. To be noted the irregularities on the seafloor on both the CPR and CP Smt. as well as the linear features on the north flank of the CPSmt. In the close plane the Horseshoe Abyssal Plain (HAP) can be seen, the far plane displays the Seine Abyssal Plain (SAP) and the abyssal hills, on the left is the accretionary wedge (AW) and the Horseshoe Valley (HV). Black solid line is location of seismic profile in Figure 4.26, stippled line corresponds to bathymetric profile on Figure 4.25; white areas are *no data* areas.

The Coral Patch Seamount, when compared to the GoB is smaller in size (120x60 km), is topped by two peaks at -650m and -1300m. It is an elongated relief (ratios of 1:2.2 to 1:2.5) and has an ENE-WSW direction. The CPR is also elongated (70kmx25km), strikes WNW-ESE with a similar elongation ratio of the CP Smt. (value of 1:2.35). The angle between the CPR and the CP Smt is of 30º. The connection between the CPR and the CP Smt. is through an elongated 400 meters high crest. Between this elevation and the HAP (to the North) there is an intermediate bathymetric step (Figure 4.24 and 4.25), of 20 km in width and 50 km long, located 400 meters below it and also 400 meters above the HAP.

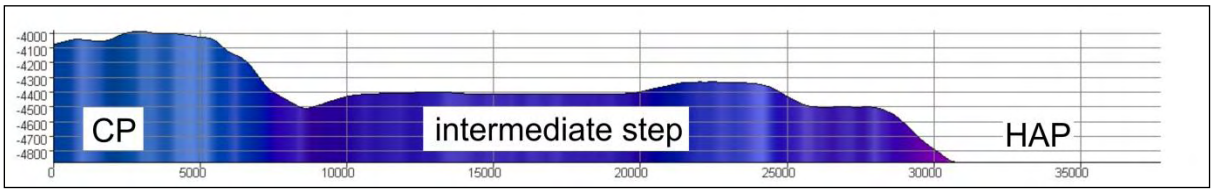

Figure 4.25 - Bathymetric profile SSE-NNW (left to right) across the Coral Patch (CP) until the abyssal plain (HAP), passing through the intermediate plateau, see text for description.

The submarine mountains of the SW Iberia (GoB, CP Smt. and CPR) display steep walls with an undulated and rough seafloor. This is generally due to mass-wasting gravity-related processes and incision of a submarine drainage network of minor valleys. However, the northern flank of the CP Smt. displays a different morphology: a set of persistent crests and troughs (Figure 4.24) of about 100 meters high spaced from 1.5 to 4 km and reaching more than 50 km in length. These features correspond to folds affecting the uppermost sediments and the seafloor as seen in a section of the seismic profile on Figure 4.26.

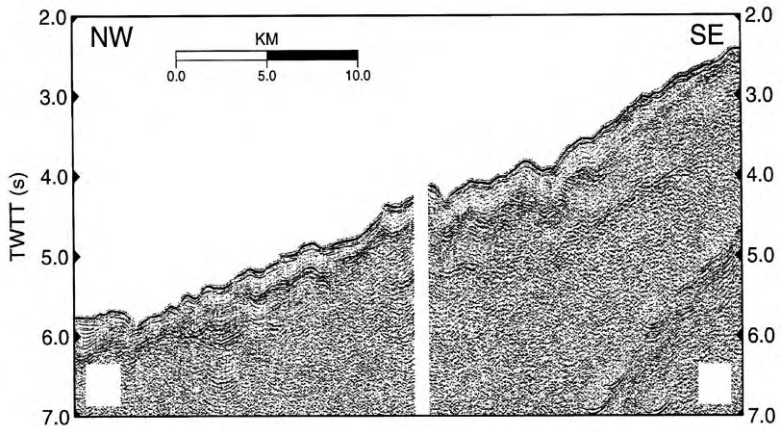

Figure 4.26 - Multichannel seismic profile on the north flank of the Coral Patch Seamount over the crests and troughs well marked on the bathymetry, these correspond to folds affecting the sediments and the seafloor. Location of seismic profile is in Figure 4.24. Modified from Hayward *et al.* (1999).

On the top of the CP Smt., near the two peaks, a different kind of morphology is present, less wrinkled and irregular than the surroundings. This can be a result of the presence of several basaltic lava flows (Geldmacher & Hoernle, 2000) generated from the nearby volcanic edifices that correspond to the peaks on top of CP Smt. described further ahead.

Using DSDP drill cores (Ryan *et al.*, 1973), submersible dives (Auzende *et al.*, 1978; Girardeau *et al.*, 1998) and dredged samples it was possible to discover a portion of the structure of the Gorringe Bank. The Gettysburg Smt. seems to correspond to a section of oceanic lithosphere where serpentinized peridotites, gabbros, tholeiitic dykes and pillow-lavas were drilled. The Ormonde Smt. does not appear to be of the same nature and might be a part of the continental lithosphere displaying several alkaline rocks such as alkali basalts, nephelinites, nepheline syenites, tinguaites, phonolites and monchiquites (Bernard-Grifiths *et al.*, 1997). Along with its very large size, the GoB also displays a large geoid anomaly, one of the largest in the globe (Souriau, 1984).

In what respects the relief of these two prominent highs they have a common origin. Both submarine mountains correspond to major anticlines (Figure 4. 27) located on the hanging-wall of northwards directed thrusts over the abyssal plains located north of the structures: the TAP is overthrusted by the Gorringe Bank and the HAP is overthrusted by the CP Smt. The sense of thrusting is in accordance with the staircase-like pattern of the seafloor depths of the abyssal plains, with the Seine Abyssal Plain overthrusting the Horseshoe Abyssal Plain which is overthrusting the Tagus Abyssal Plain. Due to the size of these structures it is believed that they extend through all the crust and affect the Moho generating the gravity anomalies that are recorded over both seamounts. For the Gorringe Bank (Figure 3. 27A) some authors recognise a major role and importance for the structure there present and propose that it was a plate boundary responsible for the consumption of lithosphere from 10 to 50 kilometers (Srivastava *et al.*, 1990; Sartori *et al.*, 1994; Terrinha, 1998; Hayward *et al.*,

1999). In the case of the CP Smt. such a similar hypothesis was not presented (it was even denied by Hayward *et al.*, 1999) although the observed gravity anomaly (Figure 4. 27B) points to a crustal magnitude for such structure and displacement of the Moho of about 2 kilometers between the HAP and the CP Smt. (Hayward *et al.* 1999; Sartori, 1994). The CP Smt. overthrusts the HAP (to the North), in the east the structure is complex and two major tectonic features can be identified (Figure 3.27B) with an intermediate plateau (Figure 4.25).

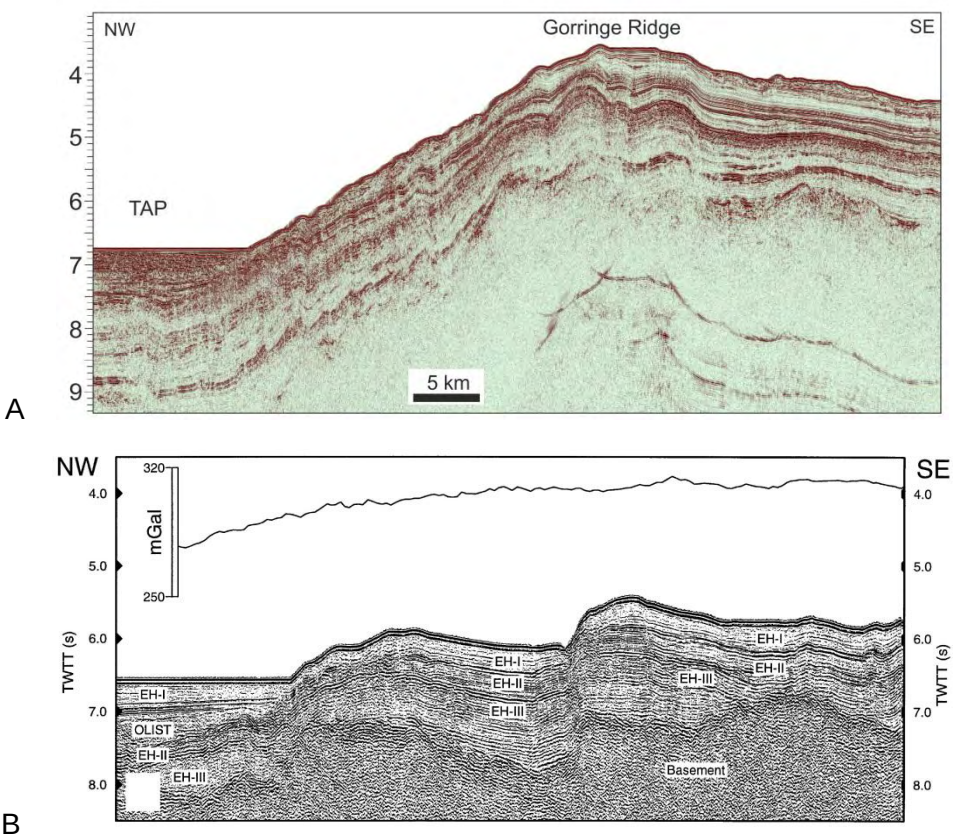

Figure 4.27 – **A**: section of seismic profile BS13 displaying the structure of the Gorringe Bank just east of the Ormonde Smt. imaging the anticline where the sediments are folded; to be noted the numerous gravity slides that affect the sedimentary package on the northern flank of the seamount. **B**: seismic profile east of the CP Smt. imaging two northward vergent thrusts that cut through the sedimentary package and also displace the basement. Graph on top displays gravity anomalies that points to a crustal scale structure. Modified from Hayward *et al.* (1999).

4.5. The Accretionary Wedge

The Accretionary Wedge morphologic feature refers to the shape of the seafloor that tops a series of westward directed stacked thrusts. There has been a lot of discussion on the origin of this feature that lies approximately in the centre of the Gulf of Cadiz and represents a horseshoe-shaped domain with a remarkable wrinkled seafloor (Figure 4.28). The initial works classified this body as the result of the accumulation of a giant olistostrome (Bonnin *et al.*, 1975, Lajat *et al*., 1975, Torelli *et al*., 1997), whilst later works considered it as a stack of thrusts associated with the westward thrust of the Betic-Rif or Gibraltar Arc (e.g. Maldonado

et al., 1999, Medialdea *et al.*, 2004, Iribarren *et al.*,2007). Gutscher *et al.* (2002) considered this body as an accretionary wedge associated to active subduction roll-back of an oceanic slab under the Gibraltar Arc.

The Accretionary Wedge is large in size (240x130km), extends from about 1000 meters (near the MOW sedimentary system) to more than 4000 meters water depth (in the SAP or the Horseshoe Valley) and dips gently (<1º) to the West. The south border corresponds to the North side of the E-W trending Rharb Valley (with a drop that varies from 200 m to 300 m) and the north border (Cadiz Valley) is irregular with a main ENE-WSW trend. At higher depths, the AW curved front is asymmetrically indented by the CPR (Figure 4.28).

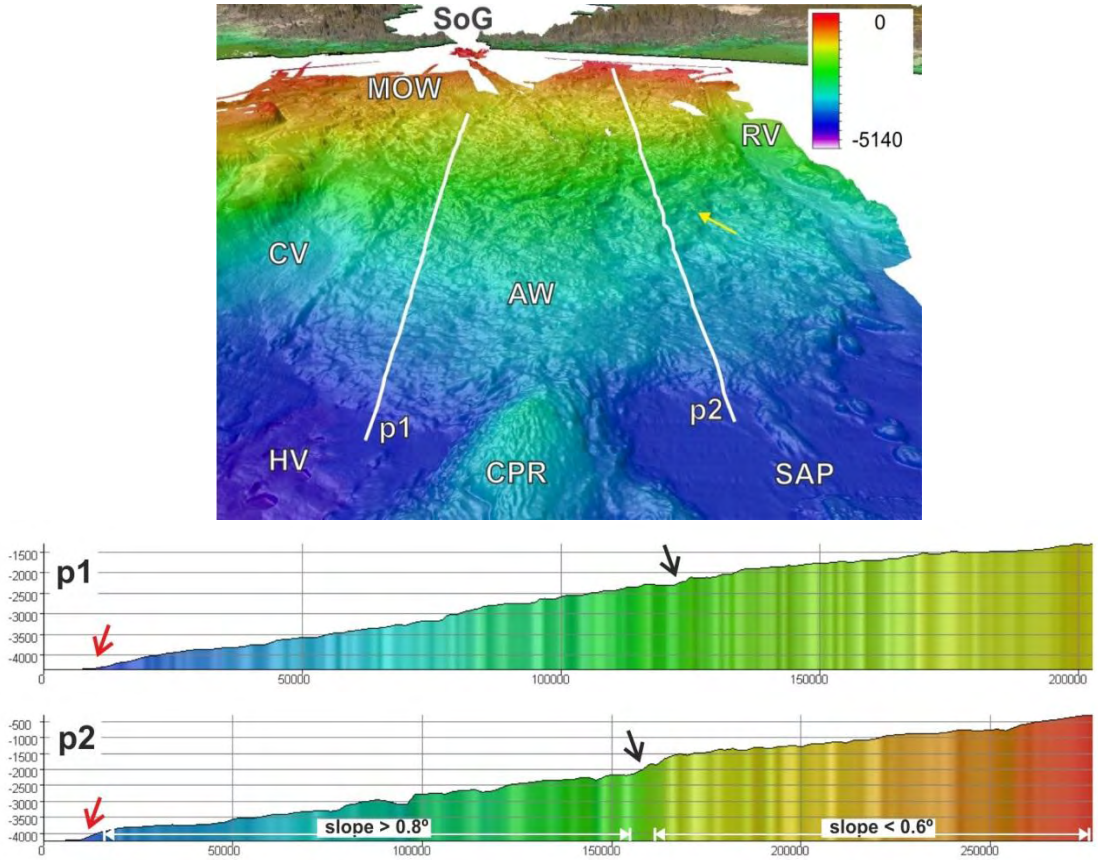

Figure 4.28 – 3D bathymetric view looking east (towards the Straits of Gibraltar - SoG) of the central Gulf of Cadiz, displaying the accretionary wedge (AW). The limits of the AW are the Horseshoe Valley (HV) and the Seine Abyssal Plain (SAP) at depth, the Cadiz Valley (CV) and the Rharb Valley (RV) to the north and south, the MOW domain to the NE. To be noted the indentation imprinted on the AW by the Coral Patch Ridge (CPR). Yellow arrow points to location of closed depressions of Figure 4.29. White lines, p1 and p2 correspond to the bathymetric profiles on the bottom. Black arrows point the lower limit of the upper lobes of the AW; red arrows indicate the lower limit of the AW. On the bathymetric profiles it is clear the differences between the seafloor pattern below and above the lobe limit, see text for description.

On its deeper part the seafloor is more undulated with short wavelengths (<5km) and these irregularities on the seafloor are parallel to the main arcuate trend of its border (Figure 4.28). The middle and upper sectors are dominated by a succession of crests and troughs (several kilometres wide and up to 25 km long) displaying elongated closed depressions (some more

than 200 m deep, Figure 4.29), these features all trend parallel to the borders of the two smaller, shallower and crescent-shaped domains.

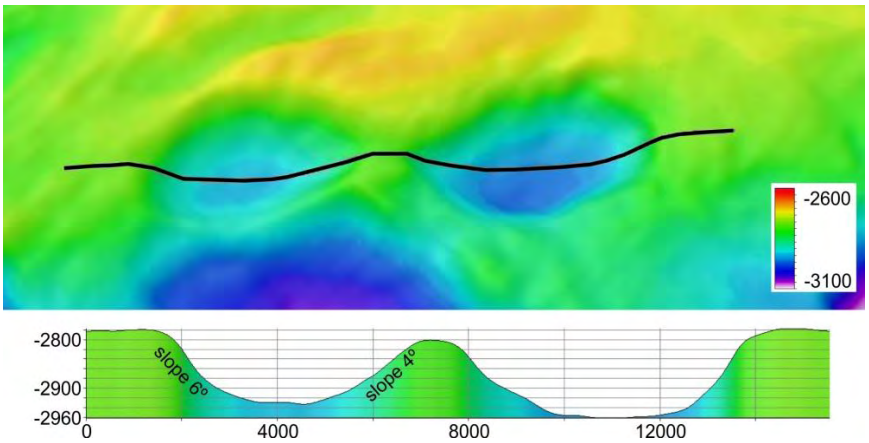

Figure 4.29 - 3D bathymetric view and profile of two adjacent closed depressions located on the accretionary wedge (for location see Figure 4.28).

The two smaller lobes are located in the uppermost part of the accretionary wedge, above -2000 m and present a less steep seafloor with slopes under 0.6º whilst for the lower part values are above 0.8º (profiles on Figure 4.28). The border between the southern lobe and the lower parts of the accretionary wedge is marked by a steep wall of up to 10º, whilst for the northern one is more discrete.

The southern sub-domain has a smoother seafloor and displays several alignments of small ridges and troughs, sometimes with a downthrown side. These striking WNW to WSW linear features crosscut from one side to the other this small domain and extend beyond it reaching several hundreds of kilometres in total. The Northern sub-domain presents a more wrinkled and irregular seafloor than the southern one and these lineaments are not so conspicuous. Throughout the domain, several single elevations can be found, these correspond to either mud volcanoes or salt domes, the first are scattered through the whole domain but most of them lie above -1200 m deep (although they can be found until depths around -4000 m), whilst the latter are present mainly in the South part forming a discrete lineament (Figure 4.28).

The origin of the accretionary wedge domain is tectonically related as it is formed on top of a major décollement (Figure 4.30) from where multiple smaller structures detach. The wrinkled seafloor observed in this domain is due to the action of these structures, either by the deformation they imprint on the sediments or by the direct deformation of the seafloor in the places where they reach the surface (arrows in Figure 4.30). The very undulated, irregular and rough seafloor of the accretionary wedge together with the deformation that reaches the seafloor suggests that this domain is tectonically active (Gutscher *et al.*, 2002). The irregular surface is thus associated to thrust deformation and/or fluid exhalation on mud volcanoes and salt diapirs.

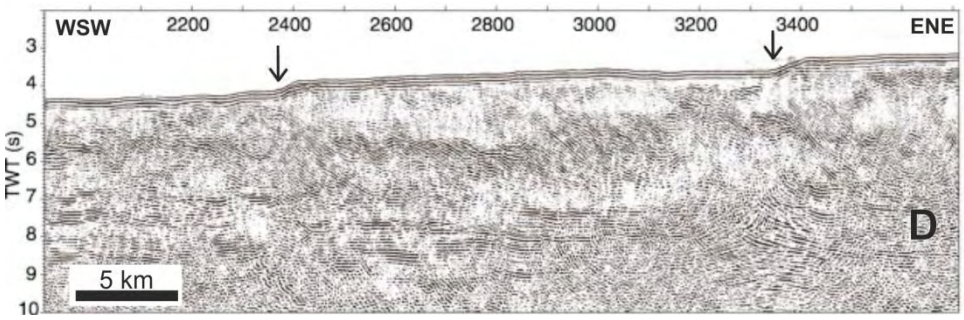

Figure 4.30 – Section of Sismar16 multichannel seismic profile across the central part of the accretionary wedge imaging the décollement (D) slightly dipping to the east and the more deformed overlying sedimentary package affected by several west directed thrusts. Arrows indicate places where these thrusts reach the seafloor. Modified from Gutscher *et al.* (2002).

4.6. The Plateaus

These are relatively flat areas that are more elevated than their surroundings and bordered by steep sides. The following are identified, the Sagres Lower and Upper Plateau, the Portimão Bank and the Marquês de Pombal Plateau (shaded areas on Figure 4.2a).

The Sagres Lower Plateau is a roughly square block (30x30 km) hanging above the surrounding seafloor of the SVC and Horseshoe Valley and its height progressively decreases towards the south meeting the lower Horseshoe Valley.

The Portimão Bank is an E-W elevated plateau over the Portimão Valley (to the north) and the Cadiz Valley (to the south). It extends for more than 120 km and measures up to 20 km in width. The Eastern part is shallower with top lying at -1360 meters whilst the opposite end is at -3800 meters. This plateau is an asymmetric relief tilted to the South, with a steep wall towards the North and a smoother hill towards the Cadiz Valley in the south (see the bathymetric profiles in Figure 4.31). With slope values of 7º and 8º in the north wall whilst towards the opposite side are between 4º and 5º. The limits lie at different depths: the Portimão Valley goes from -1500 meters (in the east) to -3500 meters (west) and the Cadiz Valley from -2000 meters to about -4000 meters. In the higher areas of the plateau, the command can reach 500 meters towards the north and 1000 meters towards the south.

The Portimão Bank top is not a flat and smooth surface. Instead, it corresponds to a structural anticline surface (Figure 4.32) that is incised by linear drainage and mass-wasting processes related features and has also been protruded by intrusion of salt domes that have left their circular imprints on the surface (Figure 4.31).

The Marquês de Pombal Plateau is located 80 km WSW off Cape S. Vicente (Figure 4.1). It is bounded by the S. Vicente Submarine Canyon to the east, the HAP to the south, the Infante D. Henrique Basin to the west and the Rincão do Lebre Basin to the north. The plateau has a uniform seabottom that dips just less than 2º to the SSE and from depths of 2200 meters to 3600 meters water depths. It is bordered by escarpments: to the north has a

command of more than 1400 meters and to the west presents a drop of 1400 m in the northern sector that is only of 800 m in the south.

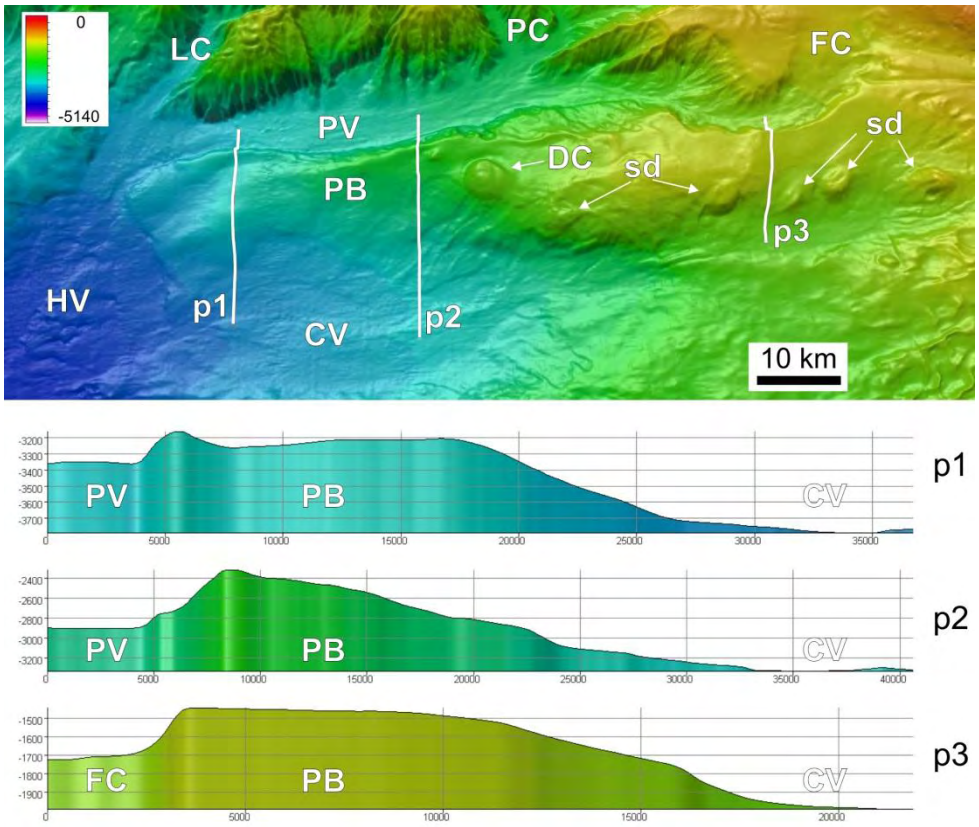

Figure 4.31 – On top: Bathymetric map of the Portimão Bank, showing the canyons (Lagos and Portimão) to the north of the Portimão Valley (PV) and the upper Horseshoe Valley (HV) and the Cadiz Valley (CV) can be seen bordering the PB. To be noted the presence of several salt domes (sd) including the D. Carlos salt dome (DC) that stands out by its dimensions and shape. White lines (p1, p2 and p3) correspond to bathymetric profiles. On the bottom: three bathymetric profiles across the PB showing the marked asymmetry of the relief tilted to the south, a steep northern flank and more smooth slope to the south.

Although the seafloor appears smooth and undisturbed, Terrinha *et al.* (2003) using sidescan sonar images managed to identify several fractures and irregularities that are below the multibeam swath bathymetry dataset resolution. The deformation and active tectonics is also testified by the large volume landslides identified in the area (Gràcia *et al.*, 2003; Terrinha *et al.*, 2003); their erosive action as they flow is marked in the MPP scarp also mapped in the referred publications.

The three plateaus are tectonically controlled, as the Portimão Bank is a E-W pop-up between two north and south-verging thrusts (Figure 4. 32) and the Marquês de Pombal and low Sagres Plateau are on the hanging wall of the Marquês de Pombal Thrust (Figure 4. 33) and the Horseshoe Fault (Figure 4.34), respectively. Some of these features exhibit some signs of erosion with more or less well developed slide scars and mass wasting processes, fractures and incision of submarine drainage system by gullies and valleys.

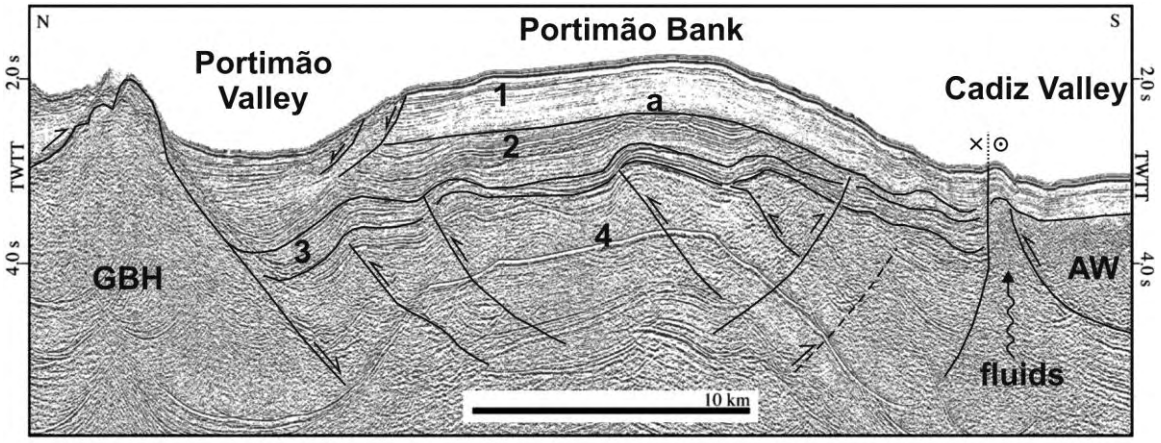

Figure 4.32 - Section of the MCS profile Voltaire03 across the Portimão Bank and interpretation. GBH- Guadalquivir basement high; AW- accretionary wedge; 1- top Lower Pliocene and Quaternary; 2- mid Lower Miocene and Lower Pliocene; 3- Paleogene; 4- Mesozoic; a- major unconformity (end of northwards thrusting). Modified from Terrinha *et al.* (2009).

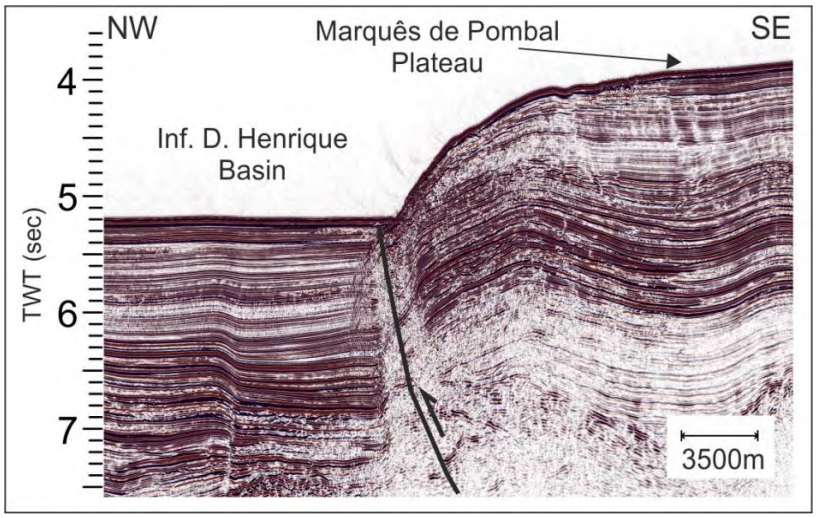

Figure 4.33 – Segment of seismic profile AR10 across the Marquês de Pombal Fault (traced in black), to be noted that the Marquês de Pombal Plateau is located in the hanging wall of this structure. The profile also displays the steep 1 kilometer high wall that links the plateau to the basin at the foot of the fault.

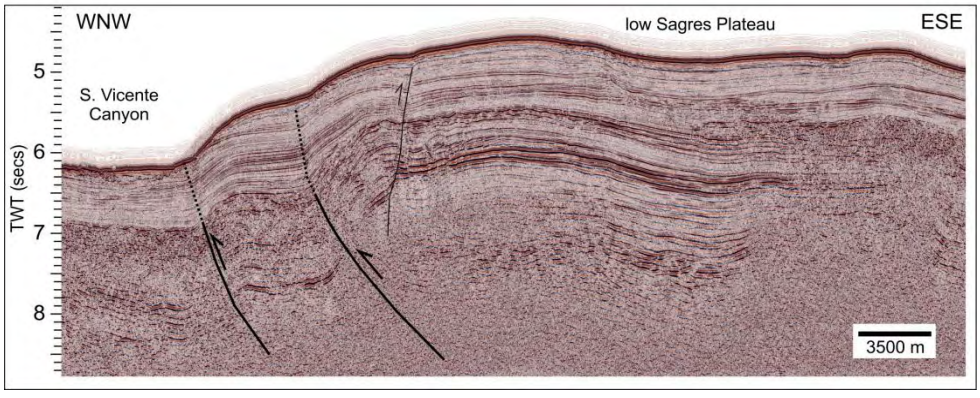

Figure 4.34 – Section of the MCS profile Voltaire20 imaging the low Sagres Plateau located on the hanging wall of the Horseshoe Fault (black lines) that has two segments that probably connect at depth.

4.7. The escarpments

This domain is made up of the several areas of SW Iberia and of the Gulf of Cadiz that display high slope gradients (> 30º). The escarpments are found bordering the thalweg of the submarine canyons, the elevated areas of tectonic plateaus, on the continental slope or associated with fault scarps. Some areas with similar characteristics also exist on the flanks of submarine mountains but where there included and previously described. Due to their steepness, the escarpments are often cut by gullies and slope failures scars and affected by slumping and mass wasting processes.

One of the most prominent escarpments is the Pereira de Sousa scarp, located on the Western Portuguese margin about 70 km offshore. It extends for about 70 km parallel to the N-S direction. It has a drop of almost 2000 meters connecting the continental slope to the Rincão do Lebre Basin (p2 on Figure 4.35). Closer to its southern end, the fairly linear scarp is disturbed by the Bow Spur (p3 on Figure 4.35), a relief separated in part from the scarp and more advanced towards the West (about 10km) but somewhat still morphologically bounded to it. In the north and south tips this scarp merges with the escarpments that border the Príncipes de Avis Spur and the Marquês de Pombal Plateau, respectively (p1 and p4 of Figure 4.35 and 4.37). The scarp is very steep, forming the steepest area of the bathymetry dataset with gradient values between 15º and 40º. The steepness of the scarp and incision therein is favourable to the development of gravity processes that generate some deposits just at the foot of the slope (Figure 4.36).

a 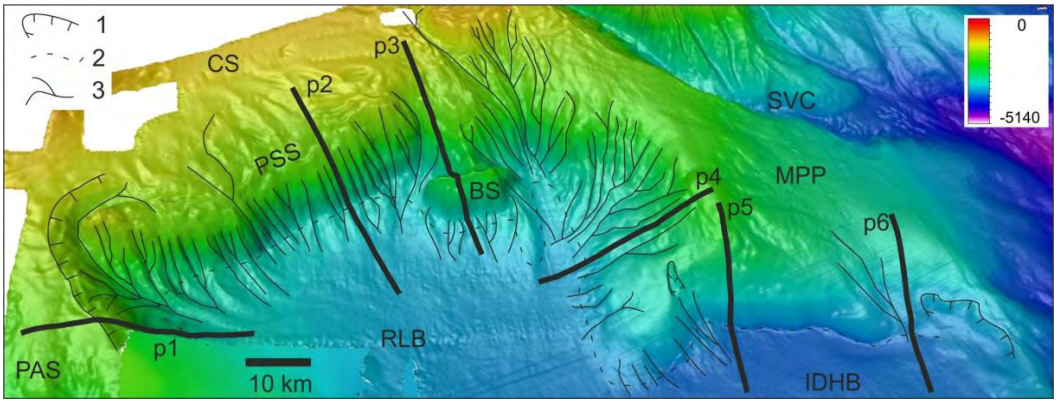

b

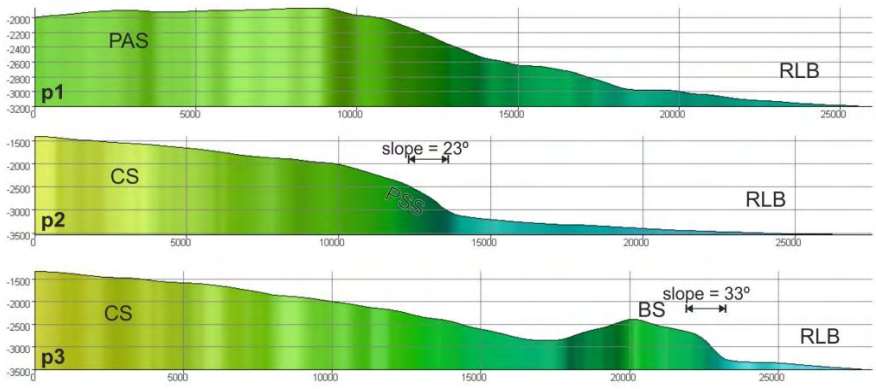

Figure 4.35 – a) 3D bathymetric view towards the east of the Pereira de Sousa scarp (PSS) and the Marquês de Pombal Plateau (MPP) with an overlay of the interpretation of the incision of the scarps. To be noticed the heavy incision on the steep walls of the PSS and on the north side of the MPP. CS- continental slope; RLB- Rincão do Lebre Basin; BS- Bow Spur; SVC- S. Vicente Canyon; IDHB- Infante D. Henrique Basin; p1 to p5 are location of bathymetric profiles; 1- slope failure scars; 2- foot of the slope of the escarpments; 3- paths of the incised drainage network. b) p1, p2 and p3 bathymetric profiles across the PSS. The foot of the slopes of the Pereira de Sousa scarp and of the Marquês de Pombal plateau correspond approximately to the traces of a Mesozoic rift fault and of an active reverse fault, respectively (see text for details and references).

The origin of this steep scarp is related to the Mesozoic rifting tectonics. The Pereira de Sousa normal fault (Figure 4.36) is responsible for marked drop in the bathymetry. The Bow Spur is also of tectonic origin as it corresponds to a structurally controlled basement high. Some authors have shown that this fault is cross cut by strike-slip faults and the whole area is undergoing uplift to which are associated the more than 20 km long turbidite levees at the foot of the Pereira de Sousa scarp (Gràcia *et al.*, 2003; Terrinha *et al.*, 2003).

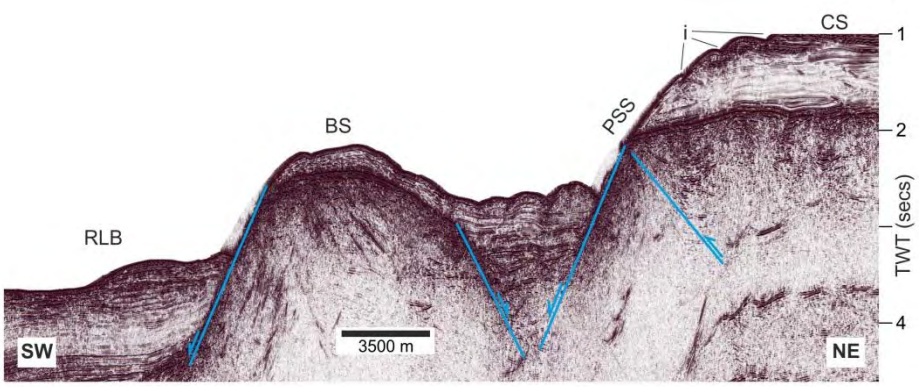

Figure 4.36 – Section of MCS profile BS19 (interpretation in blue) across the Bow Spur (BS) and the Pereira de Sousa scarp (PSS) showing the tectonic control on both the main scarp and the Bow Spur relief. The heavy incision by the multiple gullies is also imaged on the seismic (i). In the SW side of the Bow Spur (left side of the profile), in the Rincão do Lebre Basin (RLB) some gravitational deposits can be identified at the base of the scarp.

Escarpments are also found bordering the Marquês de Pombal Plateau, located south of the area previously described. There are two distinct areas of higher gradients (Figure 4.35), one towards the north (to the Rincão do Lebre Basin) and another towards the west (to the Infante D. Henrique Basin). The north facing slope is deeply incised in all its length by gullies

that start from the top and reach down to the base of the slope. Gradient values are between 3º and 7º for the western sector, associated to the thrust fault (Figure 4.33), whilst for the eastern sector (closer to the PSS) higher values of up to 15º are present. The top of the scarp rests at around -2200 meters and the base at -3600 meters (p4 on Figure 4.37). The N-S elongated scarp dipping towards the west has remarkably less erosion than the previous one and can be divided into two segments. The south part has a top at around 3000 meters water deep and the foot of the slope is at -3800 meters (p6 on Figure 4.37). The slope values are around 5º and can reach up to 9º. The North sector has a promontory on its northern tip with a command of about 600 meters regarding the IDHB with slope values from 5º to 10º. For the rest of the northern sector the slopes are above 10º and can reach up to 20º in some places. The command is higher in the north than in the south with scarp heights ranging from 1500 m to 1000 m (p5 on Figure 4.37).

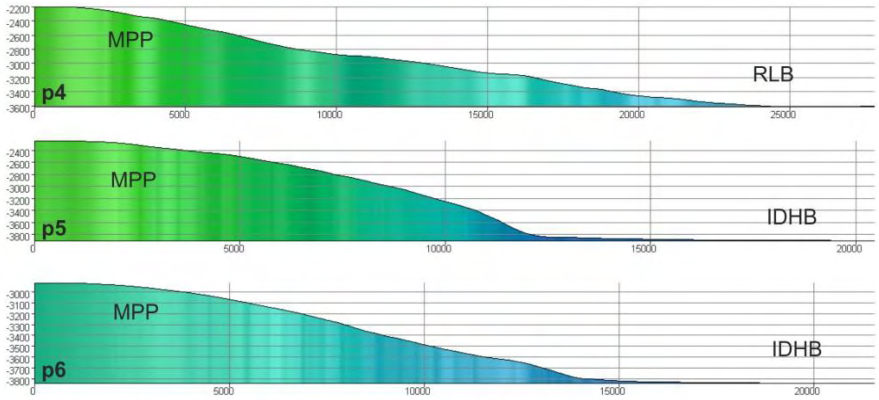

Figure 4.37 – Bathymetric profiles across the escarpments bordering the Marques de Pombal Plateau (MPP) leading towards the Rincão do Lebre Basin (RLB) and to the Infante D. Henrique Basin (IDHB), for location of profiles see Figure 4.35. Note the higher steepness of the seafloor on profile p5 when compared to the other two.

Another area with high slope gradient values is a sector of the South Portuguese margin that separates two parts of the continental slope, the inner and the outer continental slope. It extends for about 100 km, from the S. Vicente Canyon to the Portimão Canyon. Slopes can reach up to 35º in the steeper areas and are generally above 8º (Figure 4.38). The flat part of the inner continental slope lies at depths between 800 m and 1000 m and the foot of the slope break is at -2500 m near the Portimão Canyon, at -3000 m in the low Sagres Plateau and reaches depths of -3500 m near the Lagos Canyon.

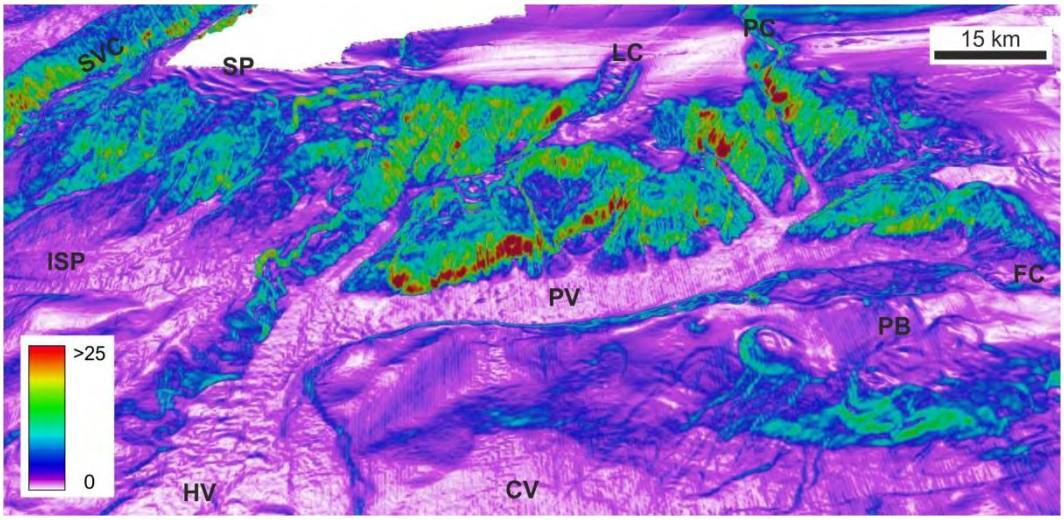

Figure 4.38 – 3D bathymetric model with a gradient draped grid. In this view towards the North, the continental slope stands out by the high slope values and heavy incision. The PB despite the less gradient values also displays several erosive features. Submarine canyons: SVC- S. Vicente, LC- Lagos, PC- Portimão, FC- Faro; Valleys: PV- Portimão, CV- Cadiz, HV- Horseshoe; Plateaus: ISP- low Sagres; SP-Sagres, PB- Portimão Bank. See text for description.

In all its extent, the inner to outer continental slope break is highly incised by the submarine canyons but also by the numerous gullies that dissect the entire area due to it steepness. The intense mass-wasting processes are common and repetitive as can be seen by minor slope failures inside larger slide scars. These events expose, in the scarps, the older and harder sediments that have high coherency displaying high reflectivity response visible in the backscatter map on Figure 4.16 and 4.18.

The E-W elongated Portimão Bank also displays on both the north and south sides, scarps with relatively high gradients, generally between 2º and 4º, but values of 10º are also found and very locally slopes can go high as 25º. The description of this area was already made in the section of the plateaus and here will only be focused on the escarpments. Although the slope is not so high as in other areas mentioned before, the flanks of the plateau are experiencing active mass-wasting shaping processes as the incision by gullies and slope failures that often develop inside older scars. It is common for these features to cut the entire wall from near the top to the base of the relief transporting large quantities of material and giving the seafloor the irregular texture it displays (Figure 4.39).

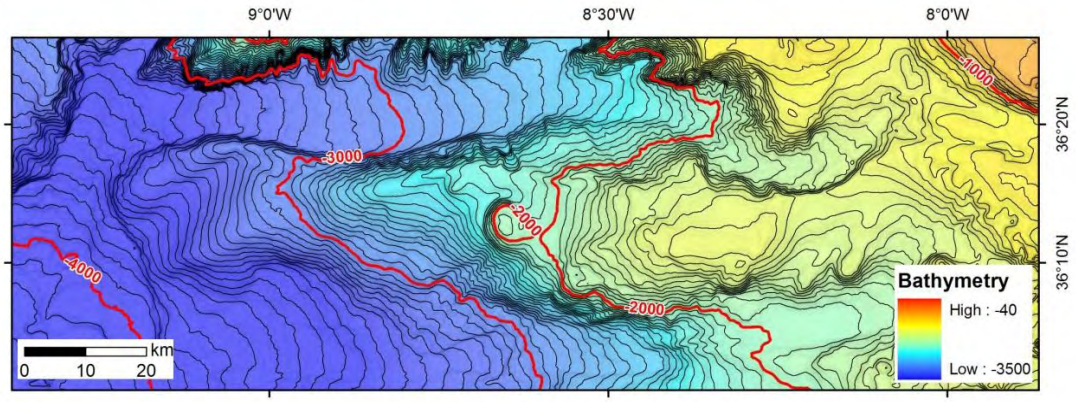

Figure 4.39 – Bathymetric map of the Portimão Bank, red contours every 1000 meters, black contours every 50 meters. Note the irregular pattern of the contours due to seafloor features caused by gravity driven processes. On the north side the retrogressive failure scars are well imprinted on the bathymetric contours, evidence of intense erosion of the slope.

Another area belonging to this domain is located to the south and SW of the MPP, south of Gorringe Bank and west of the SVC (Figure 4.40). It is about 60x20 km and is the slope that sits between the elevated Infante D. Henrique Basin and the lower Horseshoe Abyssal Plain. Gradient is generally around values of 4º and 5º reaching locally up to 10º in the west sector. In the east sector (South of the MPP) slope values are smaller and around 2º or 3º.

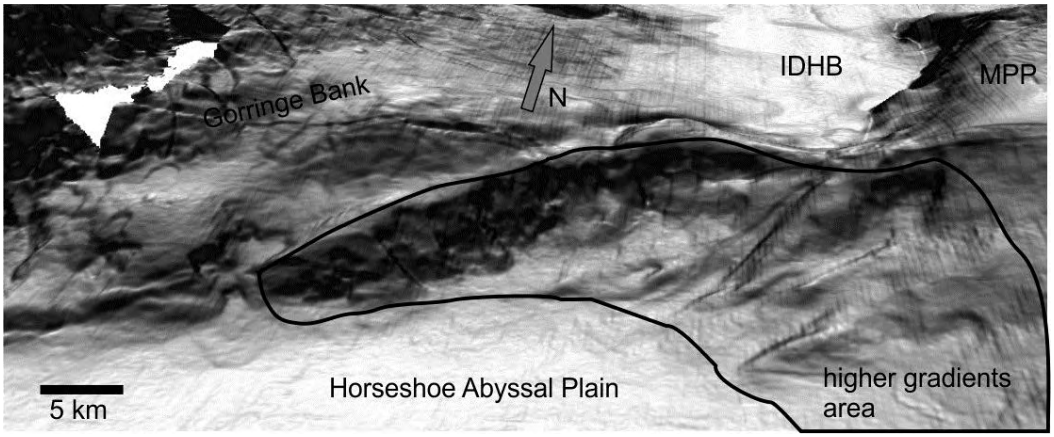

Figure 4.40 – 3D model of the slope (darker colours correspond to higher slope values) imaging the higher gradient area east of Gorringe Bank, SW of the Marquês de Pombal Plateau (MPP) and south of Inf. D. Henrique Basin (IDHB). See text for further details.

4.8. The Upper slope

This domain corresponds to the area located upslope of the slope break; in some areas this slope break can correspond to the continental shelf slope break (Figure 4.41), marking the upper border of the upper continental slope. This domain is poorly imaged as is located on the edge of the multibeam dataset and is mapped where there are no individual geomorphological features between a domain mapped at higher depths and the limit of the dataset. Thus, the seafloor is characterized as relatively smooth, shallow and gently dipping towards the open sea. It is present in the shallower parts of the dataset in the Western

Portuguese margin where it spreads over a considerable area with several kilometers in length and width: from the Setubal Canyon to the S. Vicente Canyon and upslope from the Pereira de Sousa scarp and the Príncipes de Avis Spur. The seafloor in this area presents as relatively smooth with a dip of 1.5º towards the west. Other areas of this domain are found upslope of the Alvares Cabral Moat (starts to erode at depths of 300 m and 400 m), one part is located south of Faro and the other stretches from Portimão to Albufeira. West of the last, there is also another patch of this domain (Figure 4.41) which includes a slope break in the bathymetry that correspond to limit of the continental shelf that rests at around 150 meters water deep. Deeper than this, at around -800 meters is another slope break that marks the border between the Upper slope and the contourite (Portimão Drift) flat seabottom. The domain characterized here as Upper Slope encompasses the area shallower above this last slope break.

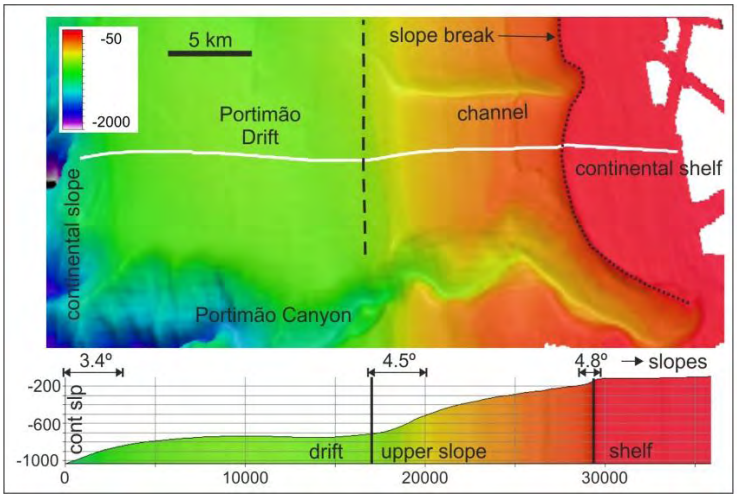

Figure 4.41 – 3D bathymetric profile of the area west of the Portimão Canyon (north is to the right). White line is the location of the bathymetric profile, dotted line is the lower limit of the continental shelf, dashed line is the lower limit of the Upper slope domain. Bathymetric profile displays two areas of flat seafloor (continental shelf and the Portimão Drift), the lower part of the profile displays higher gradients and a convex seabottom at the beginning of the continental slope.

4.9. Suspended Basins (Rincão do Lebre / Infante D Henrique)

This domain is a submarine confined basin and there is no geomorphological limit between the Rincão do Lebre Basin and the Infante D. Henrique Basin, the first refers to the area in front of the PSS and the last is the area in front of the Marquês de Pombal Plateau. This domain is to east and NE of the Gorringe Bank, to the south of the Príncipes de Avis Spur and to the north a small ridge (200 meters high) that connects the GB and the south part of the MPP. Since it is physically constrained by other morphological features its shape is not regular, and extends about 80 km in a N-S direction and almost 70 km in an E-W direction. Its depth varies a little from -3500 m near the PSS, -4000 m to the west and in front of the MPP. The seafloor is smooth (except for the sedimentary/erosive features located at the

base of the scarps) and almost flat, dipping less than 1º towards the West (p1 on Figure 4.42). This basin can be considered to be in an intermediary basin as it is located below the continental slope and 1200 meters above the TAP (Figure 4.42) and 1000 meters above the HAP.

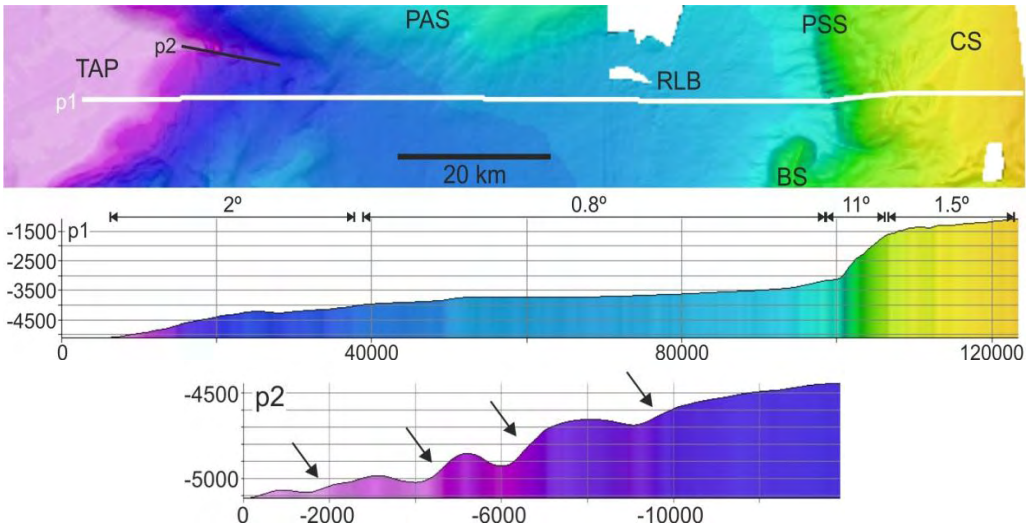

Figure 4.42 – E-W bathymetric profile across the Rincão do Lebre Basin (p1) and WNW-ESE profile across the channel to the west (p2) and their location. The p1 profile displays the almost flat seafloor of the RLB, the elevated continental slope (CS) and the high scarp (PSS) between the two. The along track (p2 profile) displays several knickpoints (arrows) present in the thalweg of the channel responsible for the drainage of the basin.

This basin in surrounded by reliefs in all directions and the drainage to the TAP is done by a small valley (20 km long and 3 km wide). This small channel displays some knickpoints (p2 on Figure 4.42) in its path and in some cases depressions probably due to over-excavation resulting from the excess erosion in such a narrow channel.

It lies more than 1000 m higher than the TAP and just a little less regarding the HAP. The drainage is performed trough a small valley in the NW sector towards the TAP. The general dip it is to the NW but the gradients are small: to the west (0.3º) and north (0.1º). In the centre of the basin some inner depressions can be found, they are large in size but their deepest parts are not more than 15/20 m deeper than the basin itself.

4.10. Hard Rock outcrop

This domain is made up of outcrops of hard rocks in four restricted and confined areas. Just on the limit of the multibeam bathymetry dataset, on the upper Sagres Plateau there is a 5x2km and 50 meters high relief that arises from the flat seafloor (Sagres drift) and is made up by Cretaceous and Jurassic rocks (Mougenot, 1989). The presence of this older rocks outcrop in the middle of the plateau is related to the presence of a normal fault.

Another area of rock outcrop is located just outside the Straits of Gibraltar, on the Spartel Bank a 16x6 km relief. The top of the relief seats at a depth of -52 m and the high resolution

bathymetry acquired displays a set of well-marked ridges that correspond to outcropping strata of a sedimentary flysch of the outer Betic and Rif allochthonous units (Gutscher, 2005).

On the south tip of the Guadalquivir Bank there is an area that rises 300 meters above from the smooth seabottom of the bank that lies at depths of 600 meters. This 10x5 km patch of irregular seafloor is located near and on the south slope of the Guadalquivir Bank (Figure 4.43) where the MOW related Cadiz Channel has a curved path to get around the bank. This area is also not very well imaged as it is located just on the limit of the multibeam bathymetry dataset. Dredges performed in this area recovered some Paleozoic slates. The whole of the Guadalquivir Bank is a basement high and is covered by more recent sediments, however this area is exposed probably by the erosive action of the MOW and its currents.

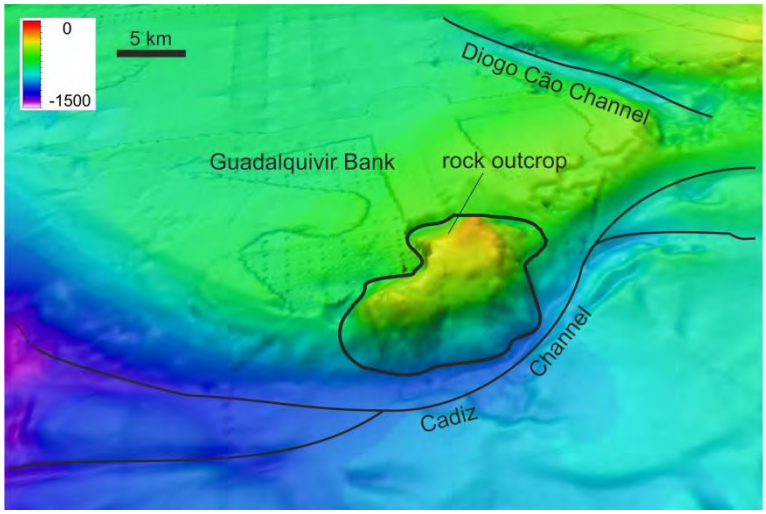

Figure 4.43 – 3D bathymetric model, looking north to the Guadalquivir Bank. It is clear the curved path of the Cadiz Channel around the Guadalquivir Bank and the different seafloor texture of the rock outcrop when compared to the smooth top of the bank (textures on top are artifacts) covered by the contourite drifts. Bathymetric model created from three merged datasets: SWIM, Ingmar and seismic profiles depths (Roque *et al*., 2012).

One other area that is made up by rock outcrop is on the limit of the dataset close to the Straits of Gibraltar and was previously described and included in the MOW domain in the scour sector (sector 1, feature 1 on Figure 4.18).

4.11. Volcanic edifices

On top of the Coral Patch Seamount two distinct areas were mapped because of their seafloor pattern that differs from the surroundings. The seafloor of these areas has a "stippled" like texture and their extent has very clear and well-marked limits (Figure 3.44a). Besides this particular pattern inside these areas several minor reliefs are found, these can be more than 300 meters high and the smaller ones are about 30 meters high. Their size varies from 500 meters to more than 3 kilometers. In these areas, the seabottom reflectivity

is very different than the one in the surroundings, which is probably due to the presence of lava flows or other extrusive volcanic related formations. This is agreement with the fact that the depicted areas of distinct bathymetric texture correspond to high acoustic response of the seafloor (Figure 4.44b). In fact, basaltic pillow-lavas were dragged from this area. Taking these facts into account, the areas with different seafloor texture are also of high backscatter could represent areas of volcanic formations and the reliefs that are found inside them could be interpreted as volcanic edifices.

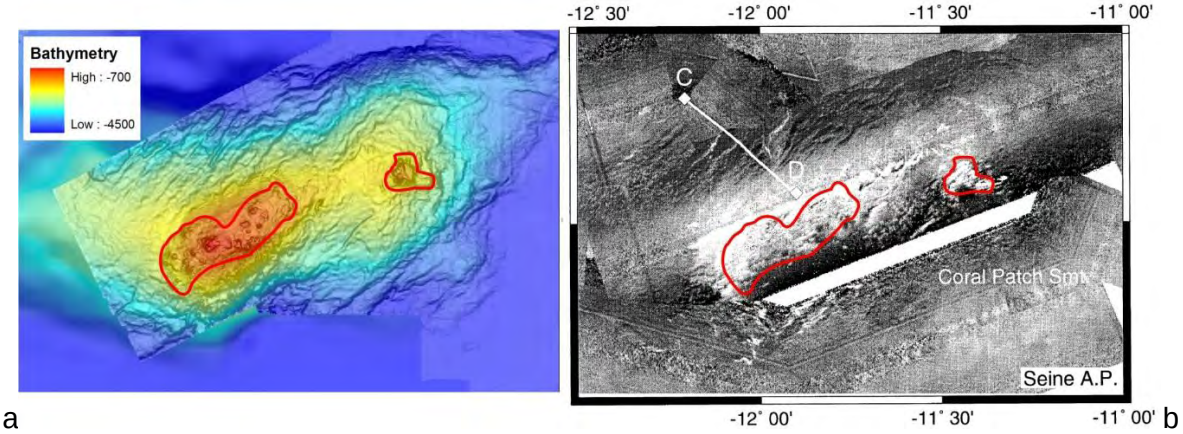

Figure 4.44 – **a**) Bathymetric map of the Coral Patch Seamounts. **b**) GLORIA mosaic of the same area (modified from Hayward *et al.*; 1999). Areas of distinct seafloor texture are delimited in the bathymetry and they perfectly match with the GLORIA mosaic to areas of high acoustic seafloor reflectivity (white patches). Also to be noted the well-marked lineaments on the north side of the CP Smt. on the GLORIA mosaic mentioned before. C-D white line corresponds to the seismic profile on Figure 4.26.

4.12. Fluid escape structures: Mud volcanoes, salt domes and diapiric ridges

Salt diapirs and mud volcanoes form individual positive reliefs with an approximate circular shape in map view. This morphology results from impingement and/or extrusion of fluidized sediments into the seafloor. Their distribution is believed to be conditioned by tectonic mechanisms, such as, transpressive deformation along the WNW-ESE dextral strike-slip faults that cut across the Horseshoe Abyssal Plain and Accretionary Wedge, active thrusting in the accretionary wedge, other regional structures associated with the present day compressive stress field that reactivate Mesozoic rifting faults.

Mud volcanoes are geological features that result from the escape of fluids and can be small as a few meters high or several kilometres in width. Their flows are mainly made up of clay materials (with several degrees of compaction) and clasts of other rocks. More than 1100 of these features have been identified worldwide (from the 10000 that is believed to exist) both onland and underwater on tectonically active areas. In the Gulf of Cadiz the first mud volcanoes were discovered in 1999 in the Morocco offshore (Gardner, 2001) and several others were discovered since then throughout the rest of the area (Figure 3.45). Almost all

the confirmed mud volcanoes (by sampling) are located inside the accretionary wedge and occur at very different water depths, ranging from only a few hundred meters deep to more than 4 kilometers meters of water depth. Very recently 3 new mud volcanoes were discovered north of the coral Patch Ridge close to the Horseshoe Abysssal Plain. The mud volcanoes can be found associated with carbonate chimneys, pockmarks, hydrocarbon-rich fluid venting, methane hydrates (e.g. Pinheiro *et al.*, 2003; Somoza *et al.*, 2003) and they host specific chemosynthetic ecosystems (Hensen *et al.*,2007). Due to the extrusion of clay mixed with clasts from the underlying rocks, the mud volcanoes are characterized to display very high reflectivity on the backscatter maps (Figure 4.45).

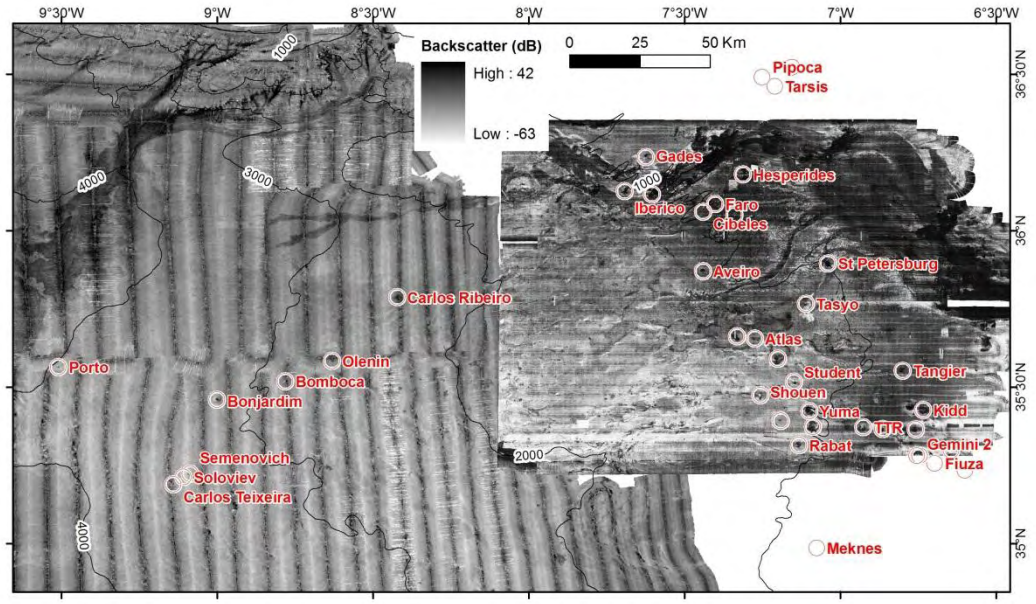

Figure 4.45 – Reflectivity map of the Gulf of Cadiz with the location of the confirmed mud volcanoes, to be noted the alignment of several mud volcanoes and their high reflectivity. See text for description.

The mud volcanoes are circular or sub circular (slightly elliptic) elevations that have steep sides (up to 10º) and may display a flat top, or the opposite with an irregular seabottom top. Usually, the mud volcanoes appear as single features but can produce an alignment (Figure 4.45) which can be related to deep seated faults.

The mud volcanoes present a wide variety regarding their sizes, ranging from less than 500 m across and 60 m high to more than 4 km across and 300 m high. In some cases a concentric moat may be present around the relief, as well as an outer peripheral ridge as in the case of Bonjardim mud volcano (Figure 4.46).

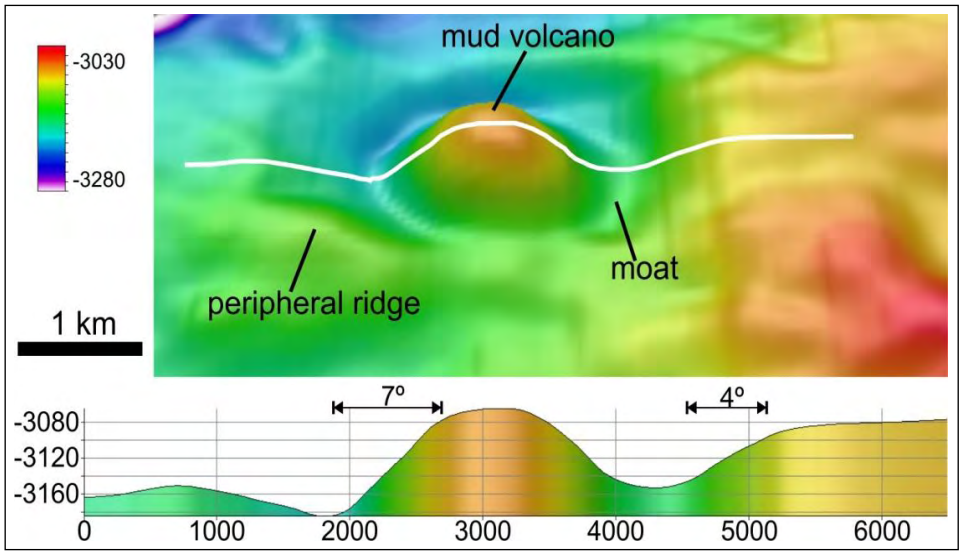

Figure 4.46 – 3D bathymetric model of the Bonjardim mud volcano displaying a surrounding moat and also a concentric external ridge; north is up.

The salt domes also form reliefs well marked in the bathymetry and are present in the Portimão Bank, near the Portimão canyon, on the south part of the accretionary wedge and the Seine Abyssal Plain.

In the NE sector of the Gulf of Cadiz, evaporites also form reliefs but as ridges and not as individual dome (Figure 4.47). These are the features that deflect the MOW currents as previously described before. These ridges extend over large distances, and although discontinuously can reach 70 km long and rise about 300 m from the seafloor.

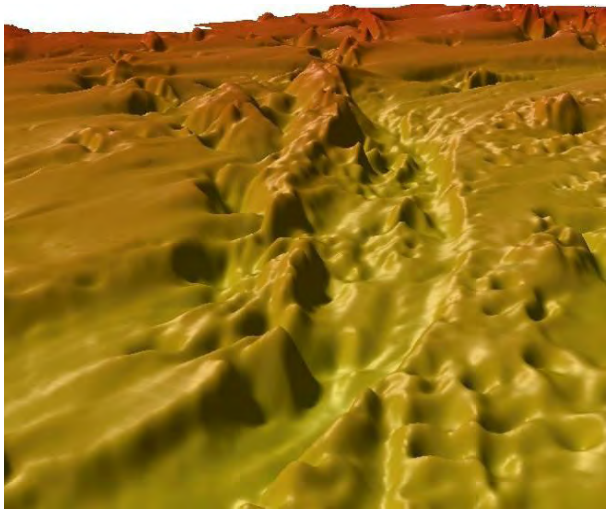

Figure 4.47 – Guadalquivir diapiric ridge (70 km in length), SE of the Guadalquivir Bank. The ridge elevates with very steep walls about 300 meters from the seafloor and deflects the MOW currents.

The salt domes can measure from some hundreds of meters in size to several kilometers and up to 400 meters height. The ones present in the SAP form a WSW-ENE alignment over 40 km involving more than 10 reliefs. To the east, inside the accretionary wedge, more salt

domes are present although they are not so evident due to the irregularity of the seafloor (Figure 4.48).

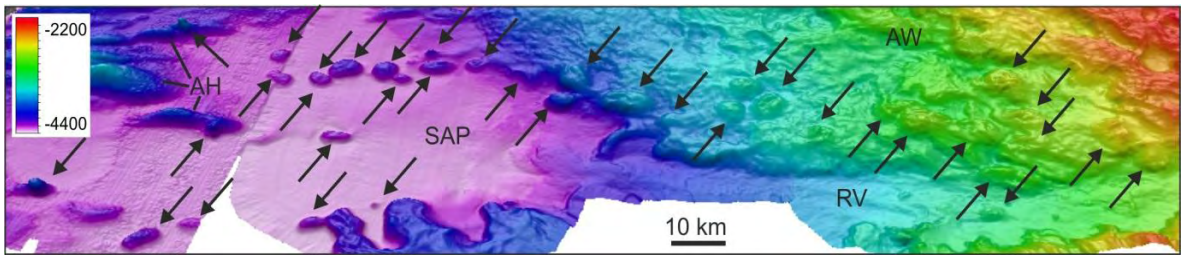

Figure 4.48 – 3D bathymetric view of the south part of the Gulf of Cadiz showing the alignment of several individual salt domes in the Seine Abyssal Plain, arising 200 meters above the seafloor at depths of 4300 meters and another alignment of salt domes inside the accretionary wedge. In the upper left corner can be seen an example of the interaction between the anticlines of the Abyssal Hills (AH) and a salt dome on top of one. Arrows indicate salt domes with morphological expression; NW is up.

To the north, the D. Carlos salt dome, in the Portimão Bank stands out by its perfect round shape and considerable size (5km in diameter and 400m high). Towards the east, another five salt domes can be identified in the bathymetry.

On the South part of the accretionary wedge, near the Rharb Valley, a relief related to a salt dome displays a high acoustic response in the reflectivity map (Figure 4.49) suggesting that the irregularities and small peaks on its top might correspond to mud volcanoes.

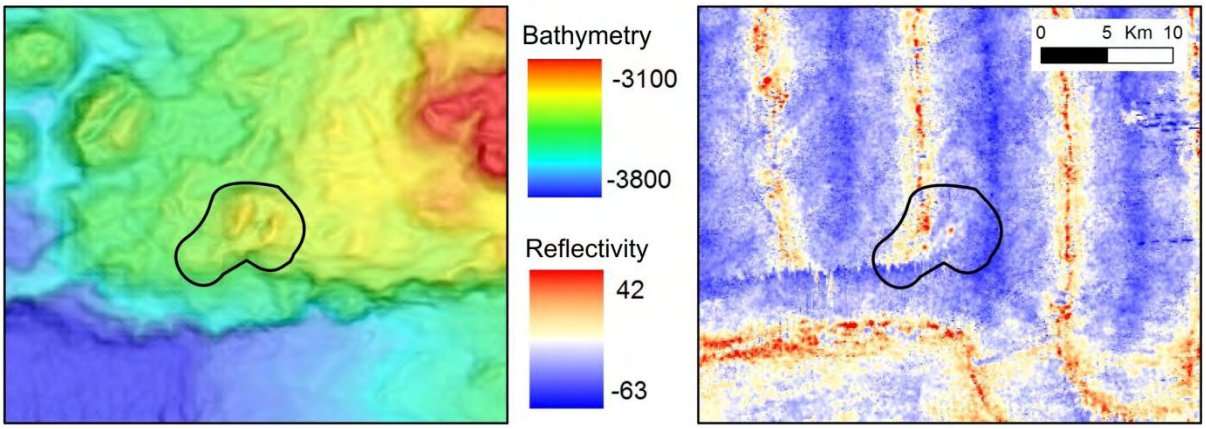

Figure 4.49 – Bathymetric and reflectivity map for the same area located in the South of the accretionary wedge, the circled area corresponds to a salt dome elevation that unlike the others (NW corner) has high reflectivity suggesting the presence of small mud volcanoes on its top.

4.13 ESE-WNW Linear features

After the multibeam swath bathymetry surveys of large areas and their compilation (Diez *et al.*, 2006; Zitellini *et al.*, 2009), a detailed map of the SW Iberia offshore was produced that enabled for the first time to have a detailed morphologic view over large distances and better relate some features seen before on MCS profiles. From the inspection of Figure 4.50 it is seen that several linear features striking WNW-ESE have been mapped extending over large distances across the Gulf of Cadiz. These features were firstly identified in 2004 during a multibeam bathymetry survey carried out onboard the research vessel N.R.P. D. Carlos I, sponsored by the project MATESPRO and the results were firstly presented and published by Duarte *et al.* (2006) at the EGU Assembly. The kinematic interpretation as dextral strike-slip faults of these lineaments led Rosas *et al.* (2009) (Figures 4.50a and 4.50b) to carry out analogue modelling experiments with scaled sand boxes analogues to explain their formation, calculating their age as 1.8 Ma. Some sectors of the same features are mapped by Medialdea *et al.* (2004) in the tectonic map and show a relation between them and the occurrence of some mud volcanoes (Figure 4.50c). The following works of Zitellini *et al.* (2009) and Terrinha *et al.* (2009) integrated these features in wider scale (Figure 4.50d and 4.50e), the former proposing them as the "missing link in the plate boundary between Eurasia and Africa" and the latter revealing their previous kinematics as Mesozoic normal faults. Later, Duarte *et al.* (2010) presented a tectonic map where these features are also mapped but focuses more on the nearby crescent-shaped features. All these authors map the referred structures in a different way (Figure 4.50).

There are several of these linear features, they extend over very large distances and are made up by alignments of different smaller features (figure 4.50). Some have a more pronounced bathymetric expression than others and their spatial continuity is sometimes interrupted. This is the reason why these features were mapped in a different way by different researchers.

A new map of the WNW-ESE is presented (Figure 4.51) based on the morphological expression of these features.

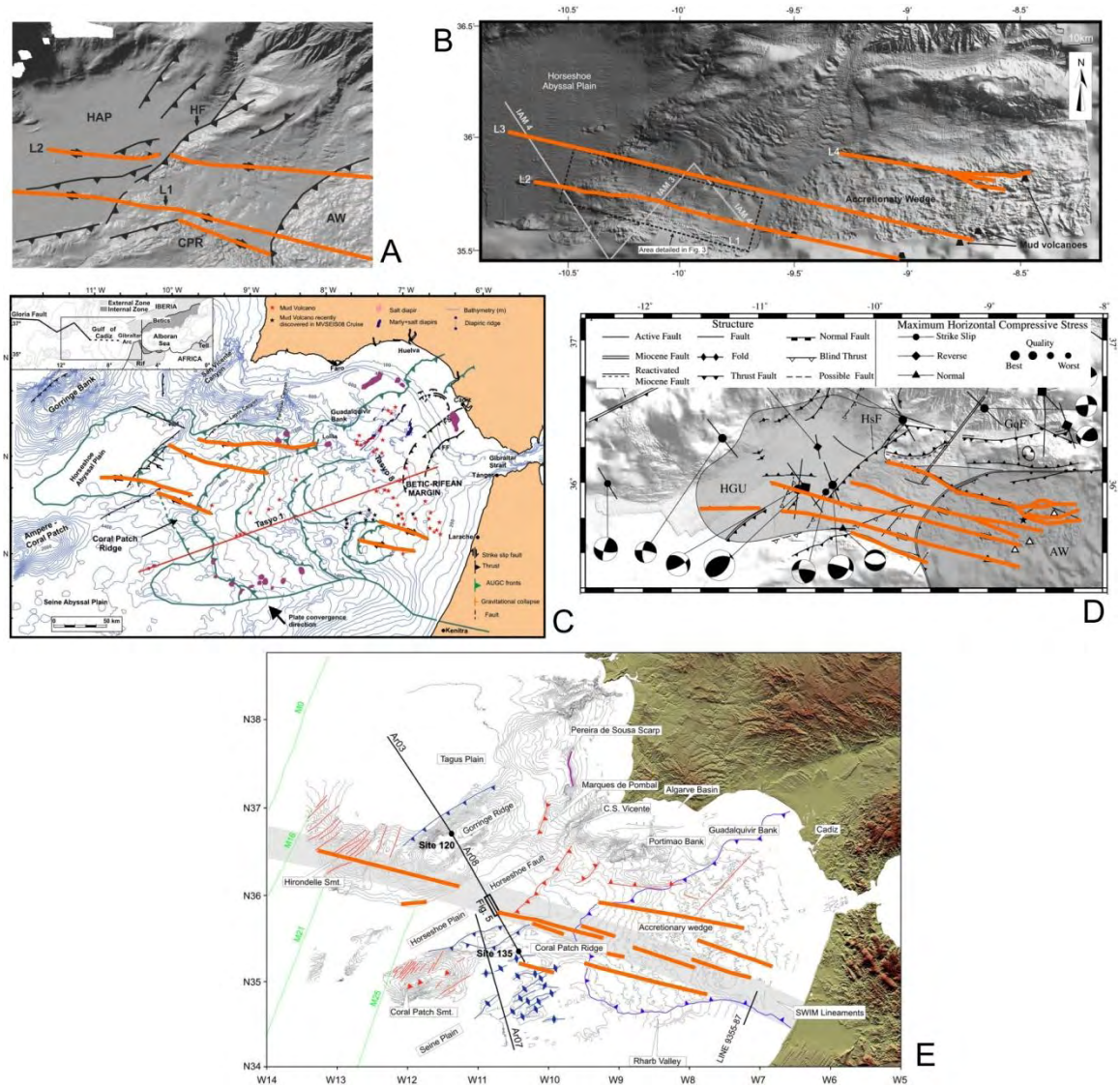

Figure 4.50 – Tectonic maps off SW Iberia with emphasis on the WNW-ESE lineaments. A – Rosas *et al.* (2008); B – Rosas *et al.* (2009); C – Medialdea *et al.* (2004); D – Terrinha *et al.* (2009); E – Zitellini *et al.* (2009).

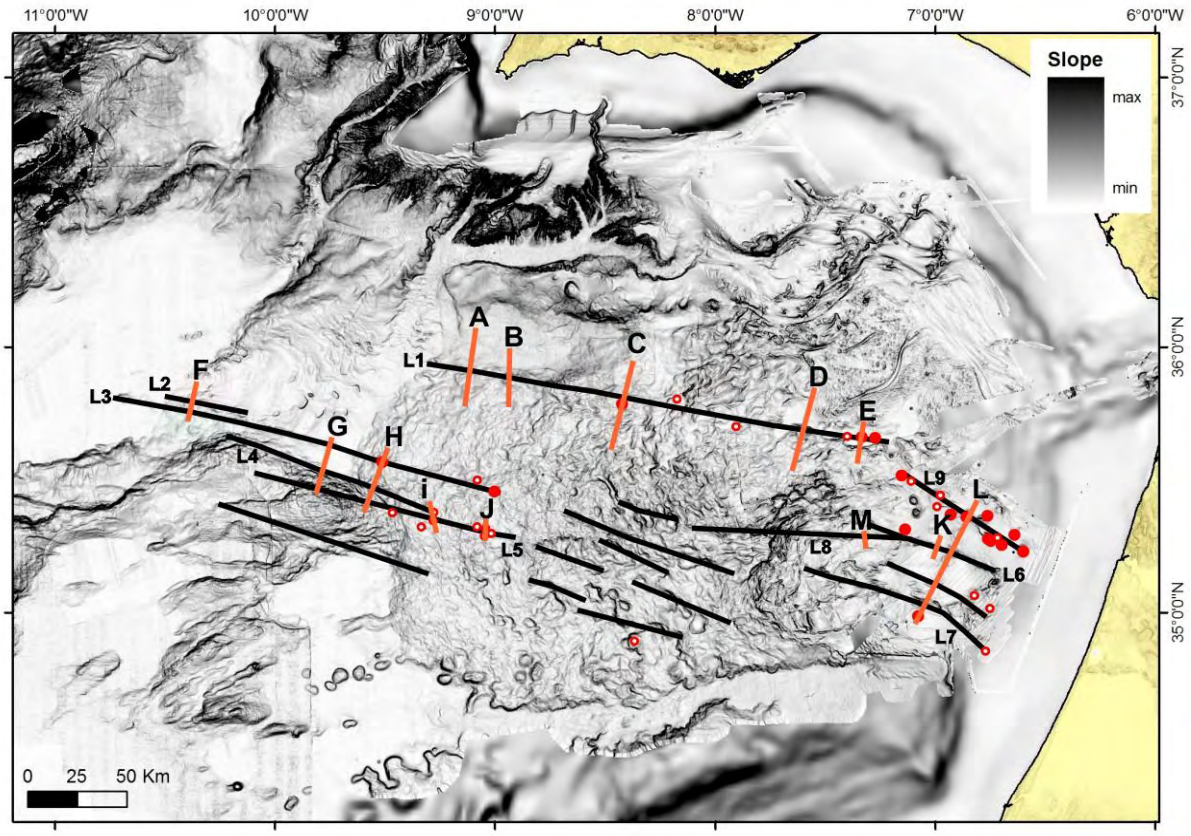

Figure 4.51 – Map of the WNW-ESE striking lineaments in the Gulf of Cadiz (black lines and L1 to L9). The figure shows several of these features have great spatial continuity (L1, L3). Coloured lines are bathymetric profiles identified by letters, closed red circles are mud volcanoes and open red circles are probable mud volcanoes. Base map is a gradient map.

A detailed characterization of the most relevant of these structures is now presented. The principal lineaments and their length are summarized in Table 4.3.

Table 4.3 – WNW-ESE bathymetric lineaments, their length and bathymetric profiles associated.

Lineament	Length (km)	Bathymetric Profiles
L1	190	A, B C, D, E
L2	32	F
L3	160	F, G, H
L4	94	G, H, I
L5	109	G, H, I, J
L6	59	K, L
L7	85	L
L8	94	M
L9	60	L

Lineament 1 (L1) is the largest one mapped, it reaches 190 kilometers and its western tip is located at -4200 meters and the eastern one at -1300 meters. To the west it coincides with the border between two morphotectonic domains, the accretionary wedge to the south and the Cadiz Valley to the north. It is in that area that its bathymetric expression is more noticeable as it lies in the border between the higher and wrinkled seafloor domain of the

accretionary wedge and the flat and smooth seafloor of the Cadiz Valley, as can be seen in profiles A and B on Figure 4.52. In the west, the lineament L1 is marked in the seafloor by different features, as a 22 km long and 3 km wide depression (Figure 4.52A), passing laterally to the east to a 21 km long and about 6 km across ridge (Figure 4.52B). Eastwards, the lineament L1 lies within the domain of the wrinkled morphology of the accretionary wedge of the Gulf of Cadiz. To the east of the ridge shown in figure 4.52B, lineament L1 materializes as an alignment of three small aligned depressions and intersects the Carlos Ribeiro mud volcano (Figure 4.52C). To the East of this mud volcano, lineament L1 cuts through the limit of the northern lobe of the accretionary wedge described by Gutscher *et al.* (2009). Closer to the lineament L1, near the place where it crosscuts this limit another probable mud volcano is present. Although this submarine feature has not been sampled, the analysis of the morphology shows it constitutes a conical sub-circular hill, 70 m high with a basal radius of 350 m, and slopes up to 7º, which are very much alike other mud volcanoes of the Gulf of Cadiz. In the area inside the AW sub-unit (upper lobes described in Chapter 3), L1 is characterized by the alignment of a series of troughs and crests. A larger crest (Figure 4.52D), elongated (9x2,2 km) along L1, presents a 150m bathymetric drop from top to bottom and slopes up to 13º. Further East, two probable mud volcano are close to its path and near its western tip, two mud volcanoes are present (Capt. Arutyunov and Atlas, Figure 4.52E) and a probable third one.

Lineament 2, is located to the southwest of L1, much smaller in length, only 32 km long, lying between 4550 and 4700 mbsl, from east to west (Figure 4.51). Its bathymetric expression is characterized by a 40 m drop with gradients of 4 to 5º (Figure 4.53), this scarp extends for 13 kilometers. Further to the east, L2 is also characterized by some smaller scarps facing north.

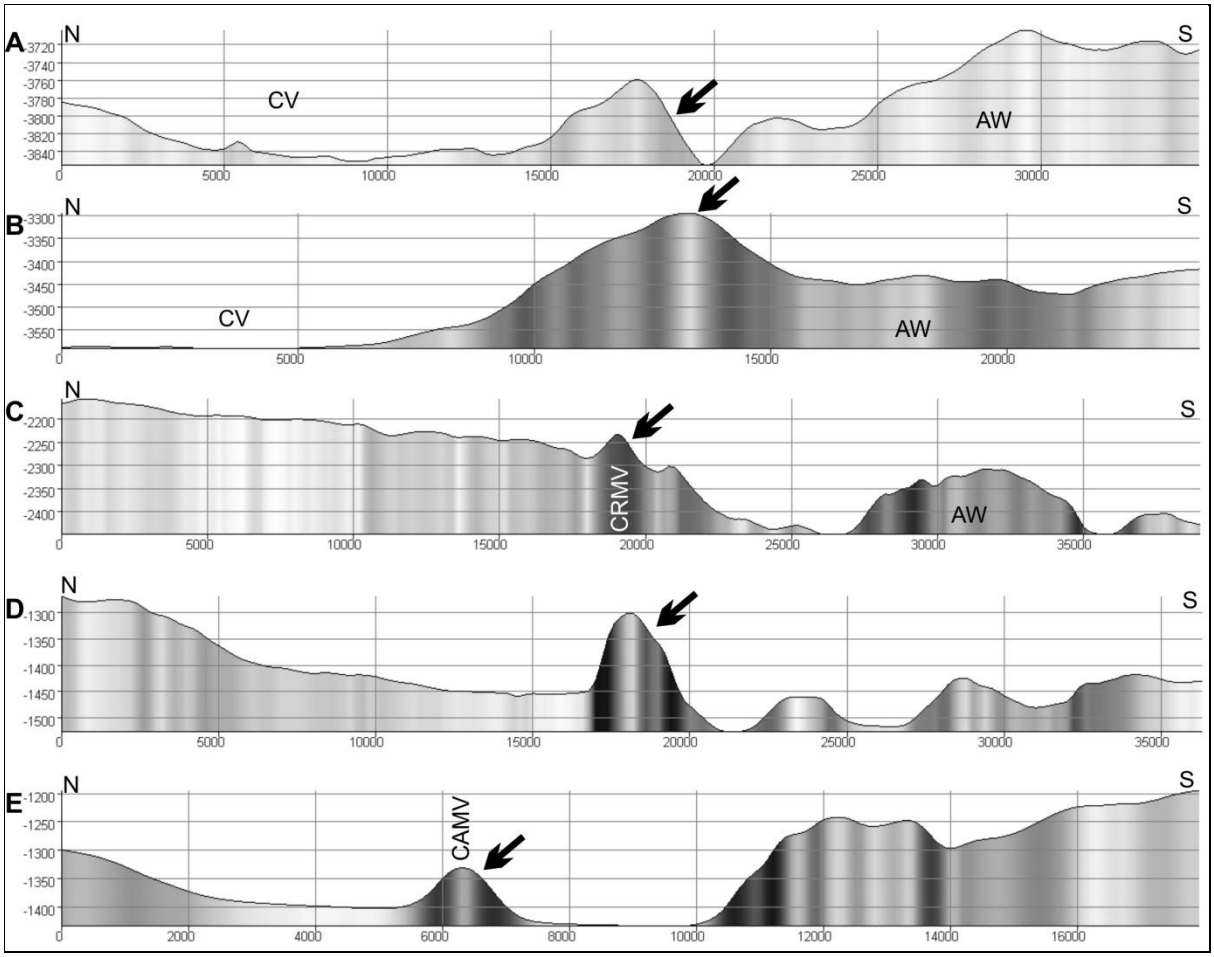

Figure 4.52– Five N-S bathymetric profiles (A to E, from West to East) crossing L1, identified by the arrows. Profiles A and B shows the L1 on the limit between the undulated seafloor of the AW and the lower flat seafloor of the HV. Profiles C and E show the mud volcanoes associated with the lineaments and profile D shows the crest with 150 or more than 200 meters command over the seafloor to the North and South, correspondingly. CV – Cadiz Valley, AW – accretionary wedge, mud volcanoes: CRMV – Carlos Ribeiro, CAMV - Capt. Arutyunov. Location of the bathymetric profiles is in Figure 4.51.

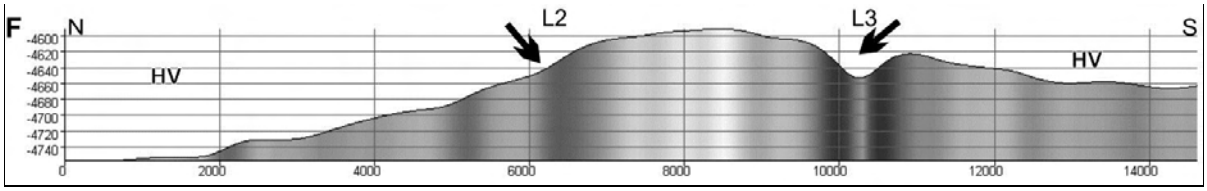

Figure 4.53 – Bathymetric profile crossing L2 and L3, located on each side of an elevation in the Horseshoe Valley. Here, L2 is marked in the bathymetry as a scarp whilst L3 as an elongated depression. Location of the bathymetric profile is in Figure 4.51.

Lineament 3 is just south of L2 (Figure 4.53) and both are subparallel (Figure 4.51). It reaches 160 km in length, extending from the HAP (in the west), across the Horseshoe Valley and through the middle of the accretionary wedge (in the east). Its bathymetric expression is variable, consisting of an alignment of several features. In its western tip, in the Horseshoe Abyssal Plain, at depths of 4870 m, L3 is identifiable by an alignment of abyssal hills that have several kilometers in length and heights up to 100 meters (described in Chapter 3). Its segment in the HAP is 20 km long. In the Horseshoe Valley, from west to east

it starts as a WNW-ESE elongated depression (Figure 4.53), changing into a 12 km long south-facing scarp and to the east it is a north-facing 80 m scarp (Figure 4.54). Eastwards, in an overall flatter area of the Horseshoe Valley, L3 is marked as an alignment of several minor crests and a 70 meters elevation of about 4 km long (Figure 4.54 and 4.56G). Further East, this lineament enters the accretionary wedge morphotectonic domain and is materialized by an alignment of a series of small crests, and passes through two mud volcanoes (Porto and Bonjardim, Figure 4.56H) and a probable third one is also located very close to L3.

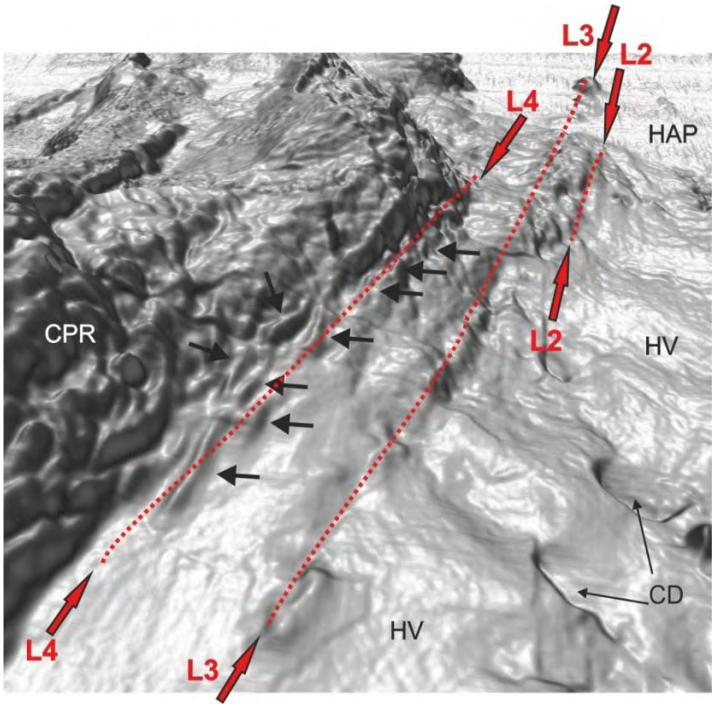

Figure 4.54 – 3D bathymetric model, view towards the west (north is to the right), greyscale color corresponds to gradient values (darker colors correspond to higher values). It is possible to identify L2, L3 and L4, the first appears north of a small elevation in the HV; L3 as an alignment of abyssal hills in the HAP, depression south of L2, north-facing scarp and a small ridge in the near plane; L4 is marked in the bathymetry as the northern linear boundary of the CPR (scarps with high gradients) and along its trace the black arrows point to the en-échelon morphologic crests that have been interpreted as folds. CD – crescent depressions, CPR – Coral Patch Ridge, HAP – Horseshoe Abyssal Plain, HV – Horseshoe Valley; red dotted lines connect the features that constitute the several alignments.

On February and March 2012, the TRANSFLUX marine survey (PI - C. Hensen, GEOMAR, Germany) was conducted aboard the R/V Meteor with the aim of inspecting several pre-selected targets related to fluid escape processes. One type of data collected was sidescan sonar from an autonomous underwater vehicle (AUV). Among other discoveries, this yielded outstanding results as three new mud volcanoes were discovered with the particularity that these are located outside the accretionary wedge unlike all the others in the Gulf of Cadiz. These new mud volcanoes (named Tiamat, Abzu and Ivanov; Figure 4.55a) are located in between L2 and L3, north of the Coral Patch Ridge and south of the Horseshoe Valley. They are active structures with associated gas hydrates, methane emissions and a wide variety of

morphological features that could be identified in the sidescan sonar imagery (Figure 4.55b and 4.55c).

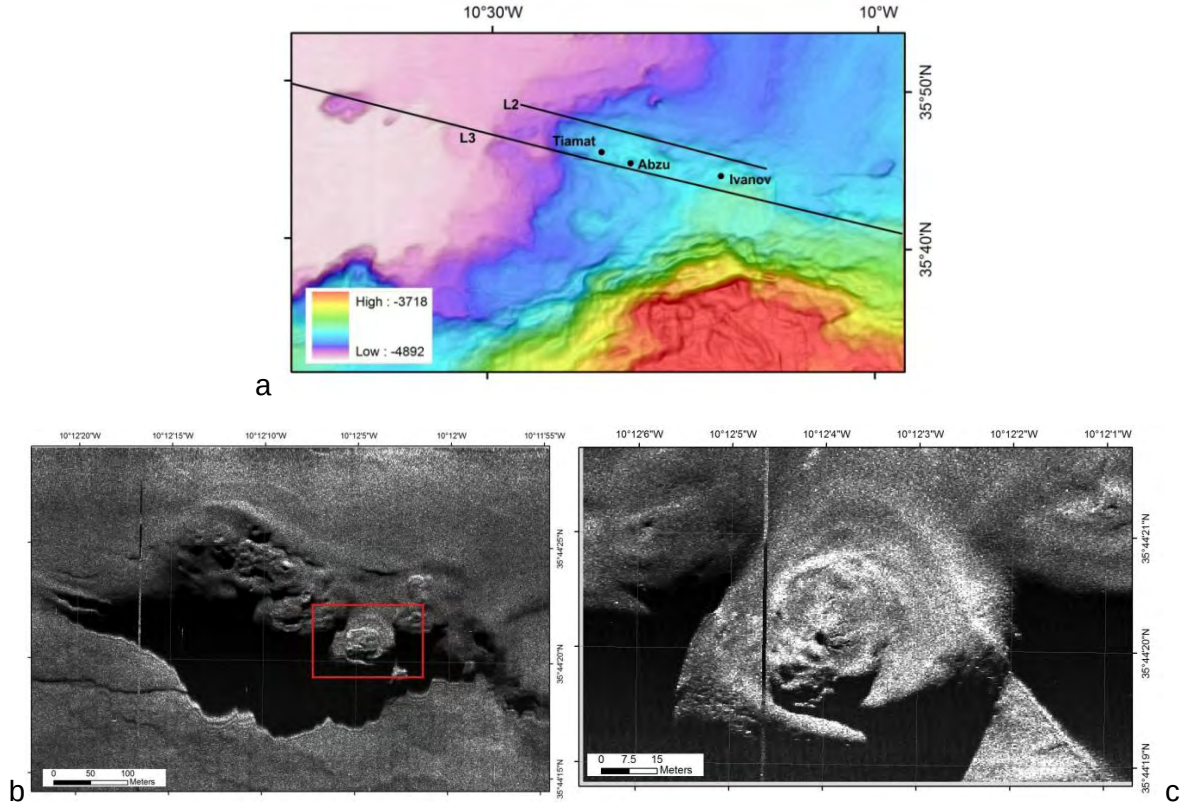

Figure 4.55 - New mud volcanoes discovered during the Transflux marine survey. A) Map of location of the three new mud volcanoes and trace of L2 and L3. b) Sidescan processed mosaic of Ivanov mud volcano, acquisition was run at 120 kHz. Black colors are low reflectivity areas or shadow areas. The image presented was collected with the AUV to the North of the mud volcano. It is noticed that the seafloor texture is different from the two edifices in the east and the major elevation to the west. Red box depicts the area imaged on c); c) AUV sidescan sonar processed data acquired at high resolution (410 kHz). In this area (imaged from the north) is displayed one of the singular heights in the east with the high reflective patches (white) near the top that displays a central small depression.

The western part of lineament 4 is the trace of the NE limit of the CPR (Figure 4.51). L4 extends for almost 100 km and its eastern sector is located inside the accretionary wedge. On its western tip, the lineament is marked on the bathymetry by a linear scarp with a bathymetric drop of about 200 meters and high gradients reaching 15º. To the east, the height of the scarp diminishes to 100 meters and gradients lower to values of 5 to 7º, further to the east the scarp gains height (back to around 200 meters) and the gradients also rise to values of 15 to 17º (Figure 4.54). Here, L4 is very well marked on the bathymetry as it constitutes the limit between the rugged and elevated seafloor of CPR to the south, and the lower, flat seafloor of the Horseshoe Valley to the north (Figure 4.56G). It is in this part of the L4 that some small crests are identified in the seafloor at the base of the scarp that limits the CPR, these are up to 6 km long and less than 70 meters high. The particularity of these features is that they are displayed in a staircase-like pattern (Figure 4.54) and could correspond to *en echelon* folds of recent sediments (Rosas *et al.*, 2009).

Further east, in the accretionary wedge, L4 is marked as a 12 km NW-SE elongated depression (Figure 4.56H) that is about 80 meters deep with steep walls with gradients of more than 10º. Near its tip it materializes as a small ridge and it ends in an isolated elevation 60 meters high, that might correspond to a mud volcano (Figure 4.56i).

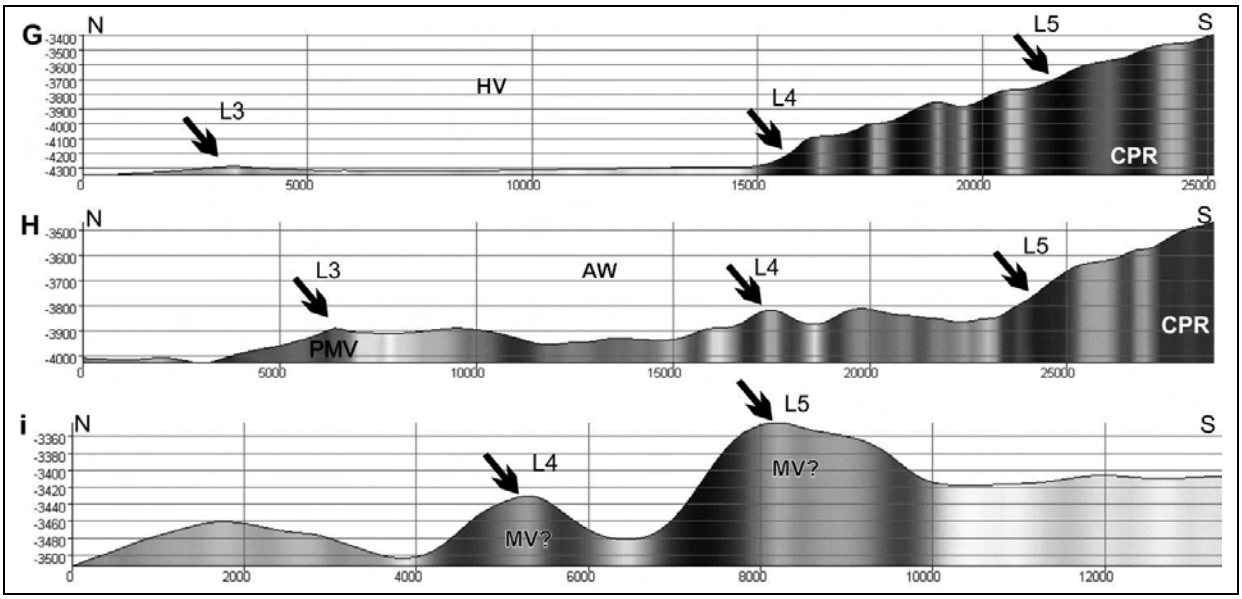

Figure 4.56– Bathymetric profiles imaging L3, L4 and L5. On profiles G and H, the CPR stands out from the deeper sea bottom to the north. L3 appears as a small elevation on the Horseshoe Valley on profile G, where L4 marks the limit between the CPR and the HV, whilst L5 does not have a significant bathymetric expression as opposed to L5 expression in profile H. In this last profile, L3 is tracked as the Porto mud volcano and L4 as a flank of a pronounced depression. Profile i shows two elevations that may correspond to probable mud volcanoes each lie on the path of L4 and L5. Location of the bathymetric profiles is in Figure 4.51.

Lineament 5 is located south of L4, extends for 109 km and is marked as a linear north-facing scarp, both inside the CPR and in the accretionary wedge (Figure 4.56G). In the CPR this scarp can reach 300 meters high, associated with up to 10º slope values (Figure 4.56H). Inside the accretionary wedge it is marked by a smaller scarp, 50 meters high and a possible mud volcano, 100 meters high (Figure 4.56i). Near its eastern tip, L5 passes through a cluster of four probable mud volcanoes (Figure 4.57), the largest of which is 50 meters high. The eastern tip of L5 consists of a WNW-ENE oriented small crest, 7.5 kilometers in length.

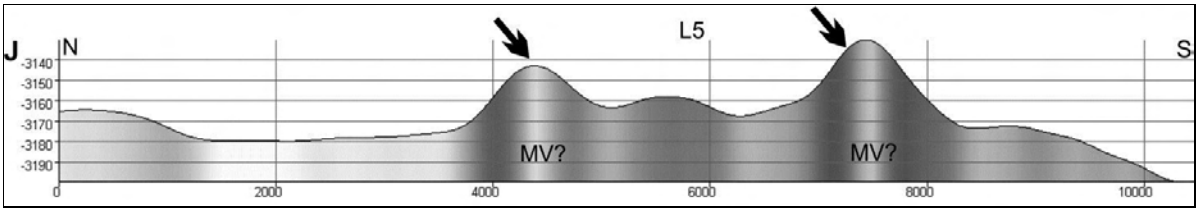

Figure 4.57 – Bathymetric profile J crossing L5 showing two of the four mud volcanoes that make up a small cluster near the eastern tip of the lineament, inside the accretionary wedge. Location of the bathymetric profile is in Figure 4.51.

Lineament 6 (N70ºW) is located on the inner and shallower parts of the Gulf of Cadiz, offshore Morocco (Figure 4.51). It extends for just less than 60 kilometers and is identifiable

on the seafloor by an alignment of several troughs (Figure 4.58). On the SE end, these depressions are 1.5 km wide with 100 meters high walls with slopes up to 10º. Towards the NW, along L6, the troughs become narrower, down to 500 m across and less incised, only 40 meters deep. In the middle, a small disturbance is present on the linear path of L6 (although it is still clearly identifiable on the bathymetry) cause by the interference with another lineament (L8). SE of this interference, there is a 40 meters depth difference (Figure 4.58K) between the NE and the SW blocks, the first higher with respect to the last.

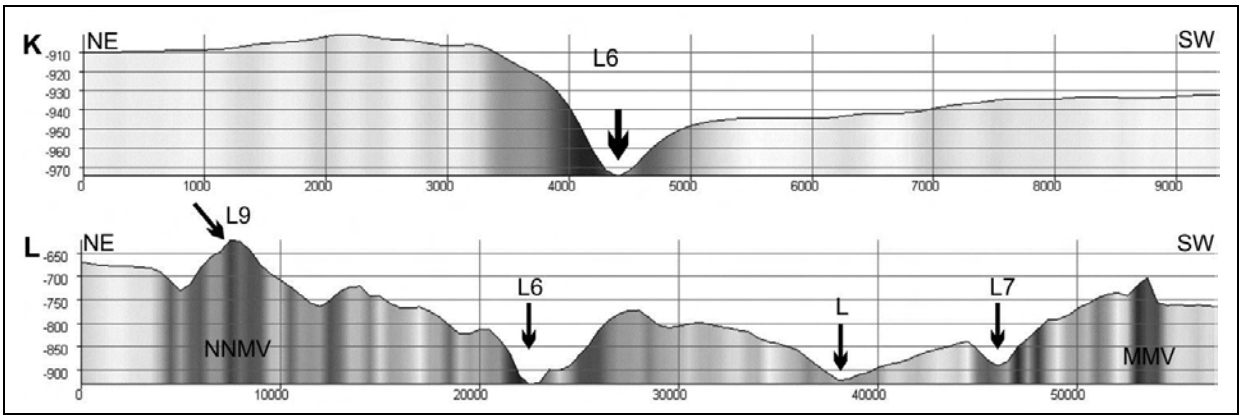

Figure 4.58 – Bathymetric profiles in the SE Gulf of Cadiz crossing L6, L7 and L9. Profile K shows L6 as a trough between two blocks with a 40 meters depth variance. Profile L displays the NNMV (No Name mud volcano) as the bathymetric expression of L9, a crest as L6, L7 also as a depression with the MMV (Meknes mud volcano) close by and another lineament between L6 and L7 also marked on the seafloor as a small trough. Location of the bathymetric profiles is in Figure 4.51.

Lineament 7 is located south of L6 and is made up of two linear segments with a small kink; the northern sector is 55 km long, strikes N70ºW, like L6, and the southern, 30 km of length, striking N50ºW. In the SE tip, it is marked in the bathymetry by a possible mud volcano, followed by a 8 km long, 100 meters high NE-facing scarp with slope values up to 8º. To the North a depression follows, of 5.5 km in length and up to 150 meters deep, although due to its asymmetry the NE wall is only 30 m deep. Further to the NW, near the kink, a 5x1.5 km elevation is present, 120 meters high with steep walls up to 9º. The north segment is made up by an alignment of several crests, troughs (Figure 4.58L) and scarps. These features can be more than 100 meters high or deep, up to 1 km across and have associated gradient values up to 15º.

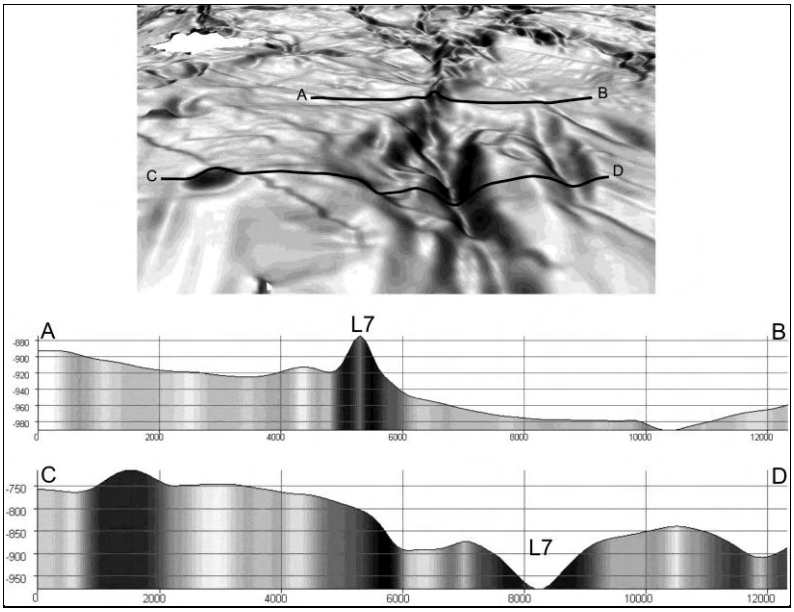

Figure 4.59 – 3D view towards the WNW along L7 the black lines correspond to the location of the two bathymetric profiles below. The two profiles are 7 km apart along L7 and as seen in the 3D and in the profiles, the morphological expression of L7 is completely different in the two areas. Profile A-B displays L7 as an elevation, section of a crest whilst profile C-D shows L7 as a depression, section of a trough, like profile L on Figure 4.58. The relief near C is the Meknes mud volcano. Greyscale colors correspond to gradient values (darker=steeper).

Lineament 8 extends for 94 km, strikes N87W and to the east merges with L6 (Figure 4.51). Its eastern segment of about 40 km, sits in the upper sub-unit of the accretionary wedge. In this part, near L6, its bathymetric expression is well noticed as the seafloor is very smooth and the aligned depressions, crests and scarps are easily depicted (Figure 4.51). Near L6, L8 starts as an elongated crest, 4 km long, 70 meters high with slopes of 5 to 6º, westwards L8 is marked as an alignment of several troughs, up to 5 km long, 1 km across and 70 meters deep (Figure 4.60). Its western part is located on the accretionary wedge main domain and is characterized by the alignment of two large South-facing scarps, adding up to 27 km in length, more than a 200 meters drop of the seafloor and associated slope values of 10º.

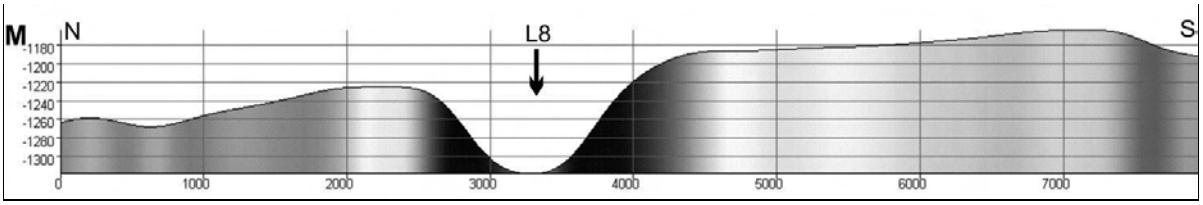

Figure 4.60 – Bathymetric profile across L8, displaying it as a 1.5 km wide depression (section of a trough) with steep flanks. Location of the bathymetric profile is in Figure 4.51.

Lineament 9, striking N60W is the one that differs the most in terms of strike from the other lineaments (Figure 4.51). It is present in the inner and shallower parts of the Gulf of Cadiz where an alignment of several mud volcanoes disturb the smooth seafloor in that area. In total there are nine mud volcanoes and possibly nine other constitute this alignment or are in

its closest vicinities. From the SE, these are: Al Idrisi, Mercator, Fiuza, Gemini1, Gemini2, Adamastor, No Name (Figure 4.58), TTR and Student. Heights range from 50 to 150 meters and diameters vary from less than 1 km to more than 3.5 km. Slope values are up to 10º and often a surrounding depression is identified. In the central sector of L9 an elongated 14x3.5 km elevation is present, with a relatively flat top, heights are up to 100 meters and gradients up to 9º.

4.14. Morphology of the submarine canyons of the south of Portugal

As described before, the South Portuguese Margin is heavily incised by minor valleys, numerous gullies and several submarine canyons. From the last ones, two stand out by their size: to the west is the S. Vicente submarine canyon and more to the east lies the Portimão submarine canyon. A more detailed description of these two features follows.

Although there is no full coverage of multibeam swath bathymetry for the shallowest parts of both canyons, it appears that only the Portimão Canyon incises the continental shelf whilst the S. Vicente Canyon does not.

4.14.1. The S. Vicente Submarine Canyon

The S. Vicente submarine canyon starts very close to the shore although its head only cuts through the continental slope and not the shelf and extends over more than 120 km where it reaches the HAP at depths of around 4900 meters (Figure 4.61a). The seafloor incision starts at depths between 600 and 200 meters, somewhere between the Ingmar bathymetric dataset (0 - 200 meters) and the swath bathymetry dataset (in this area starts around -800 meters and extends to deeper areas; Figure 4.61b).

The canyon lies in a key point, at the junction between the south and west Portuguese margins separating the Marquês de Pombal block (to the west) and the upper and lower Sagres Plateau (to the east). The first domain results from the uplift due to the westward directed thrust on the N-S striking Marquês de Pombal Thrust Fault (Zitellini *et al.*, 1999). The upper Sagres Plateau is a basement high block covered by sediments of the Algarve Meso-Cenozoic Basin; the lower Sagres Plateau is a result of the upthrust of the Horseshoe Thrust Fault (Gràcia *et al., 2003*) located to the west that also controls the lower sectors of the SVC.

In places, the SVC has more than 1km of incision into the seafloor and several knickpoints, kinks and scours are identified along its path that consists of several linear segments identifiable at different scales.

By inspection of the gradients map it stands out that the canyon wall presents the highest values in the area together with the tectonic scarps of the MPF and the PSF, as well as the South Portuguese continental slope. The backscatter map clearly highlights the canyon's

path with respect to the surrounding areas. Together, the slopes and acoustic imagery data are discussed in each of the canyon's sectors further ahead.

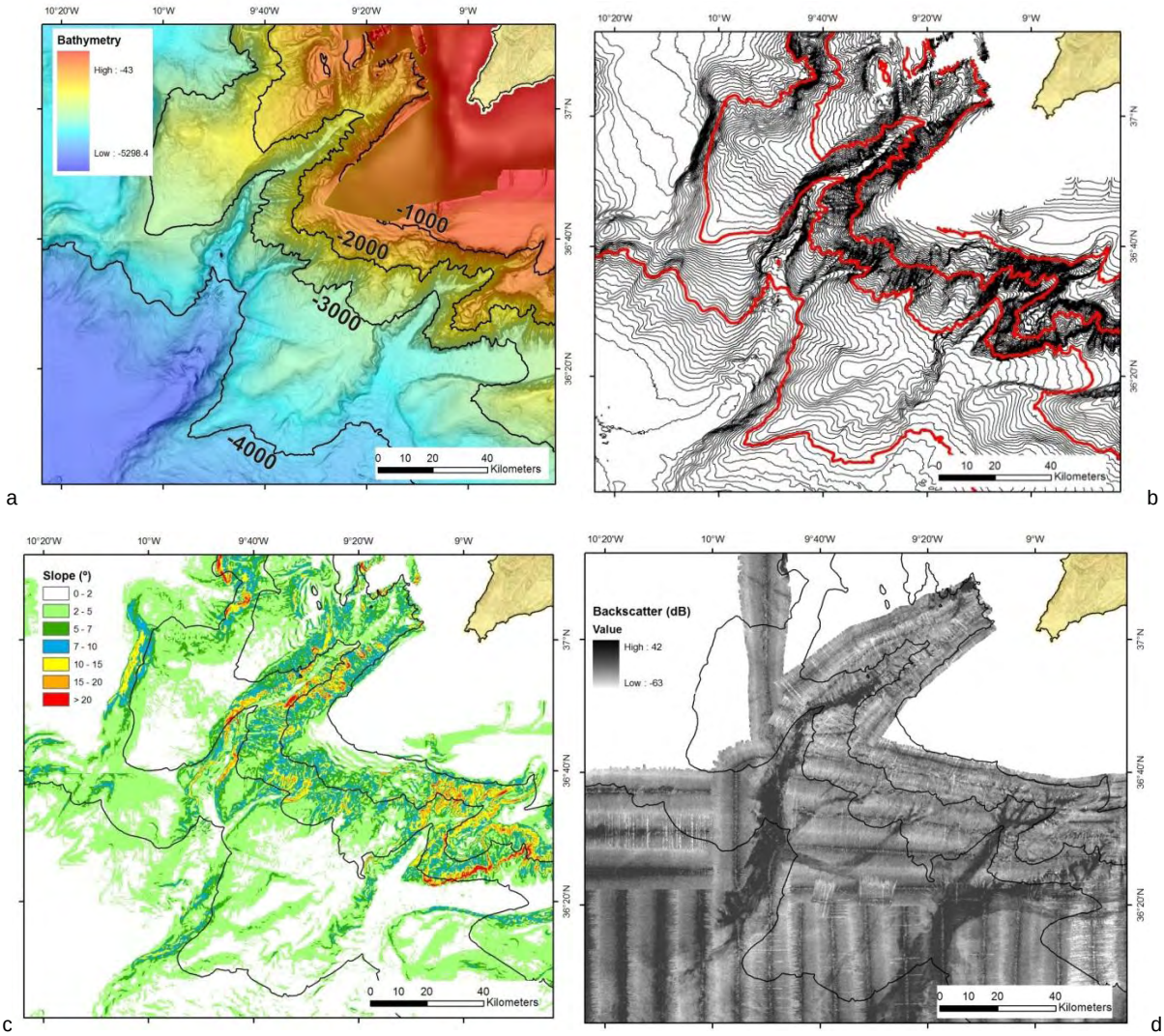

Figure 4.61 – Maps of the S. Vicente Submarine Canyon area: a) Bathymetric map of the SVC area, data derived from the SWIM multibeam dataset (Zitellini *et al.*, 2009) on top of Gebco dataset, contours from MB dataset every 1000 meters; b) Bathymetric contours for the SVC derived from multibeam swath bathymetry, red contours every 1000 meters, black contours every 50 meters; c) Gradient classified map (derived from SWIM bathymetry dataset), note the existence of localized high values for some sectors, especially in the flanks. Also clearly visible are the scarps of tectonic origin of the Marquês de Pombal, south tip of Pereira de Sousa scarp, Horseshoe and Portimão Bank faults as well as the heavily dissected and incised south Portuguese continental slope. Black lines correspond to bathymetric contours every 1000 meters; d) Backscatter seafloor map, darker colours indicate higher reflectivity index, these areas are located in the thalweg of the SVC and, the strong N-S bands in the south sector and the E-W bands in the north sector correspond to ship tracks and are artifacts. Toponyms located in Figure 2.2.

The canyon can be divided into 4 major sectors (Figure 4.62): the head, the upper, middle and lower courses. This division was made according to the morphology and dimension of the bottom and walls of the canyon and other criteria such as trend of the path as well as wall and axis slopes (Figure 4.63 and 4.64).

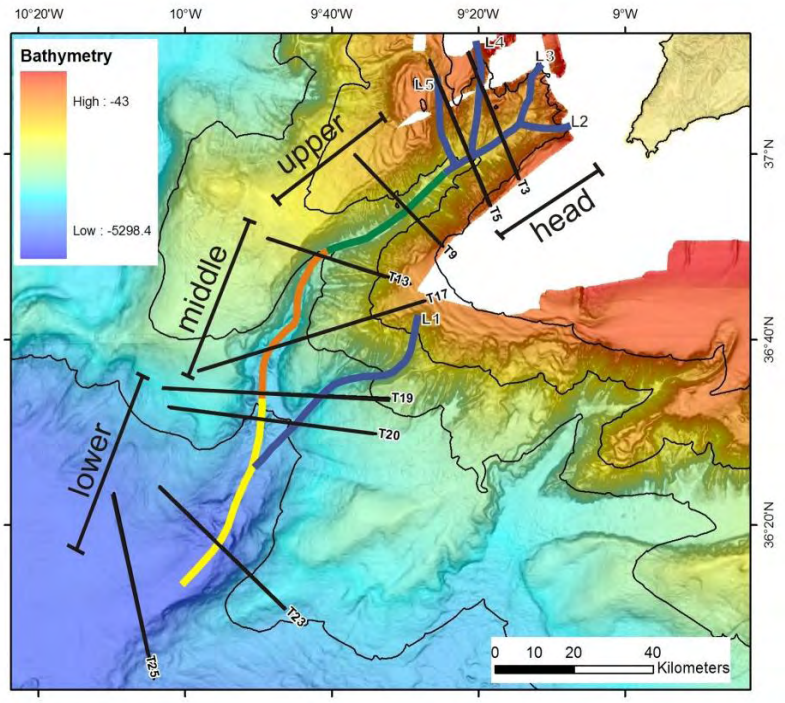

Figure 4.62 – Bathymetric map (SWIM multibeam dataset), Gebco contours every 1000 meters, displaying the four different sectors of the SVC: blue is the head; green the upper sector; orange is middle sector and yellow is the lower sector. Location of profiles: L – longitudinal profiles are along the main course of the canyon and the 5 tributaries L1 to L5; T – transverse profiles are T3 to T25; profiles are displayed in figures 4.63 and 4.64.

The longitudinal and transversal profiles shown on Figures 4.63 and 4.64 are discussed in each of the sector's description further ahead.

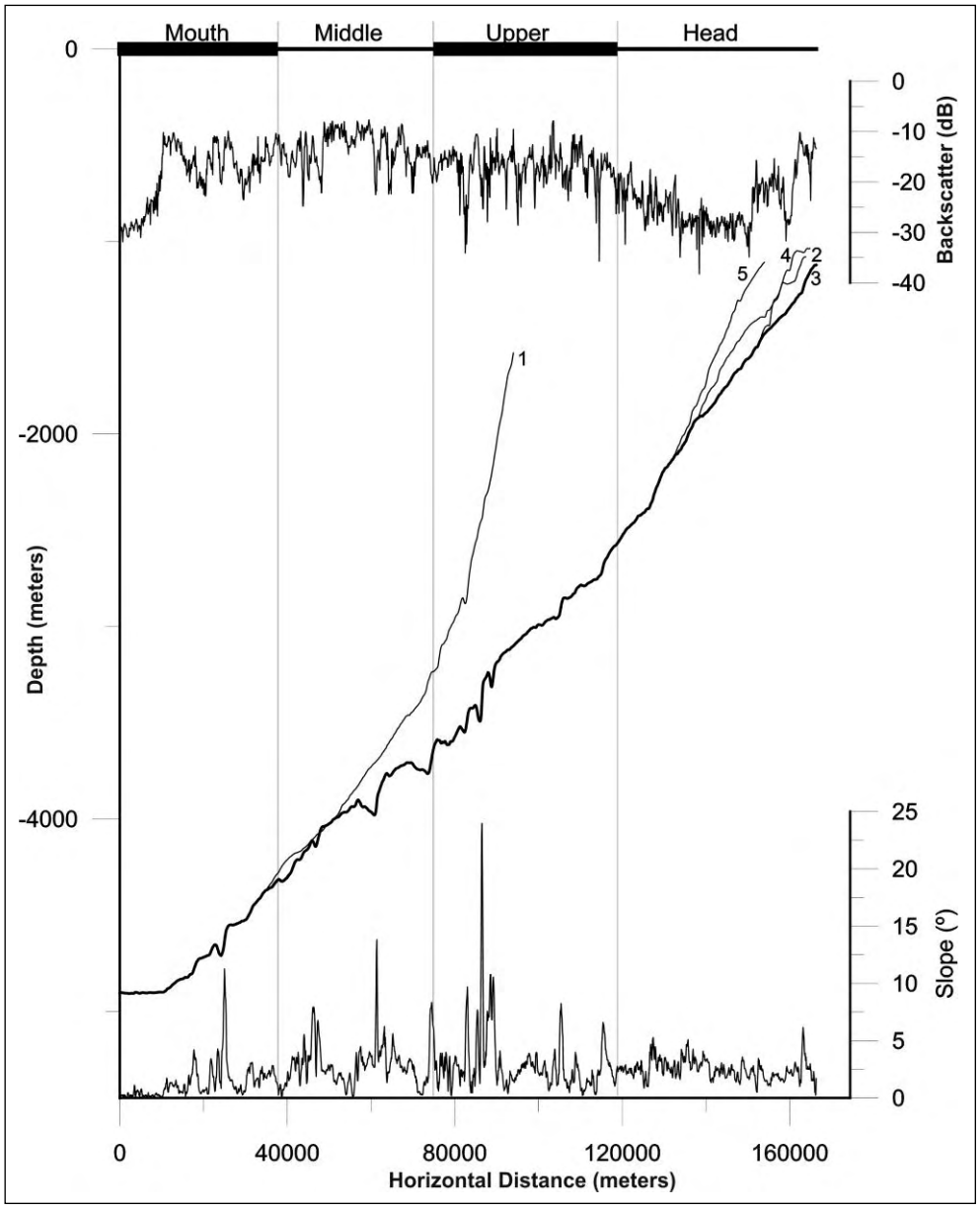

Figure 4.63 – Longitudinal profiles across the SVC, backscatter and slope profiles (upper and lower parts of the figure) were performed along bathymetric profile number 3 (thicker line); for location of profiles see Figure 4.62.

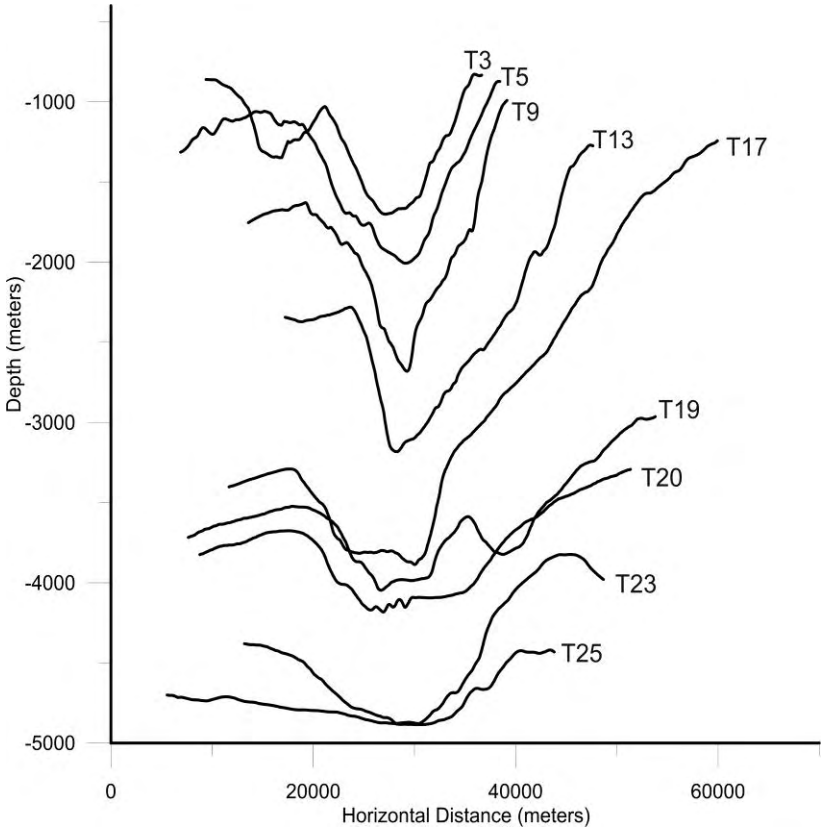

Figure 4.64 – Transverse profiles along the SVC, location of profiles is displayed on Figure 4.62. Profiles were displaced horizontally so that the axis is aligned in all of them but the horizontal and vertical scales are the same in all profiles.

4.14.1.1. The canyon head

The canyon head displays an amphitheatre shape made up from several gullies and channels poorly incised in the seafloor (Figure 4.65). It incises the uppermost continental slope of the Western Portuguese Margin. This sector is the shallowest one and is not fully imaged by the multibeam bathymetry; the smallest depth value for the dataset is around 600 meters deep, so the canyon starts at shallower depths. The head starts around 37º10'N and 9º10'W, where the axis is at 1 kilometer of water depth and extends for more than 30 km in length as the canyon thalweg reaches depths of about 2300 meters (Figure 4.63).

The along slope values are below 5º and there are no major irregularities on the seafloor of the thalweg as shown by the linear and non-disturbed longitudinal bathymetric profiles (Figure 4.63).

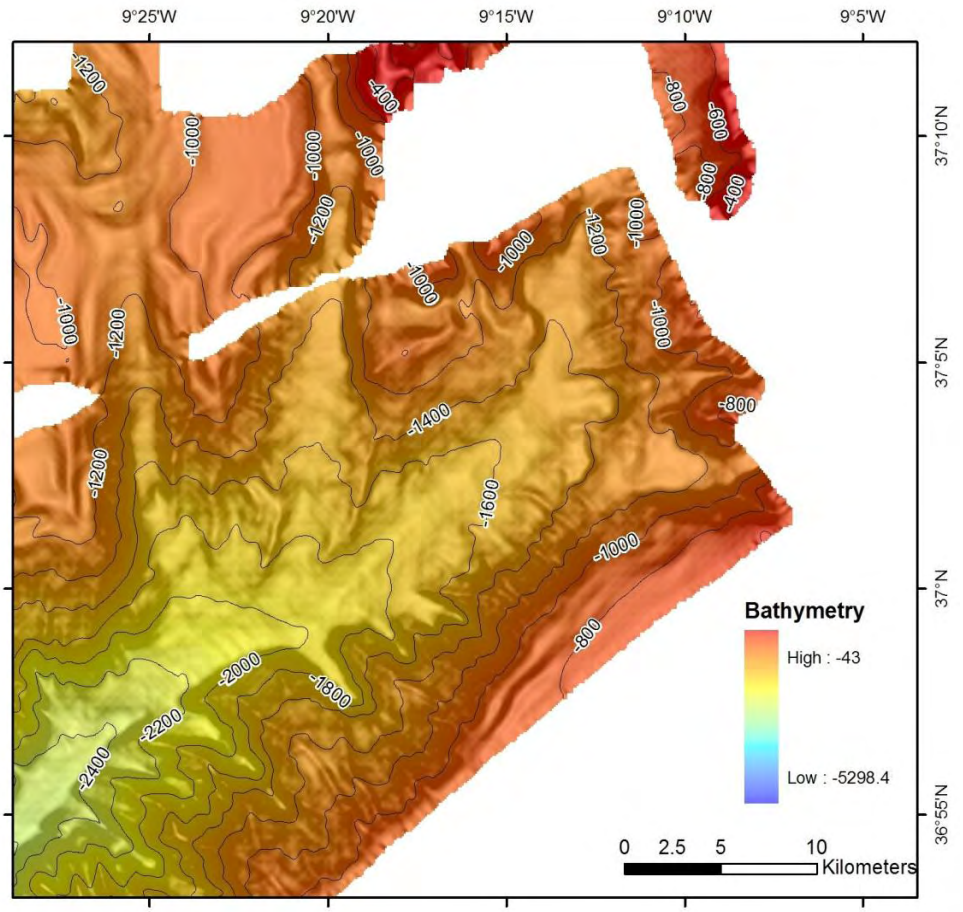

Figure 4.65 – Multibeam swath bathymetry of the head sector of the SVC; contours every 200 meters. See text for description.

The comparison of the NW and SE walls of the head sector of the SVC shows a sharp asymmetry. The NW wall displays 3 well developed channels (tributary 5 extends for about 16 kilometers and tributary 4 for more than 21 kilometers) against the more numerous but far less incised gullies (Figure 4.65). Inspection of the gradient values shows that the SE flank has a mean slope of 5 to 10º (locally can be high as 20º) while the NW flank displays values between 5 and 10º. The SE wall of the canyon has a command from 800 meters in the shallower parts and can go up to 1200 m more to the SW (Figure 4.66).

The contributories all merge to form a flat thalweg (Figure 4.65 and 4.66) reaching up to 2 km in width. This is displayed on the cross-sections T3 and T5 (Figure 4.64) as opposite of the sections more downslope where the seafloor is much more eroded and incised by the canyon. These profiles also show the slightly steeper wall on the SE flank and profile T3 images the tributary channel 4 (Figure 4.64) on the NW side of the SVC. This sector is the one that presents the lowest backscatter values (Figure 4.61), suggesting the presence of loose unconsolidated material and/or fine grained material. Gradient values are more constant without the sharp bathymetric drops that occur on the other sectors (Figure 4.63).

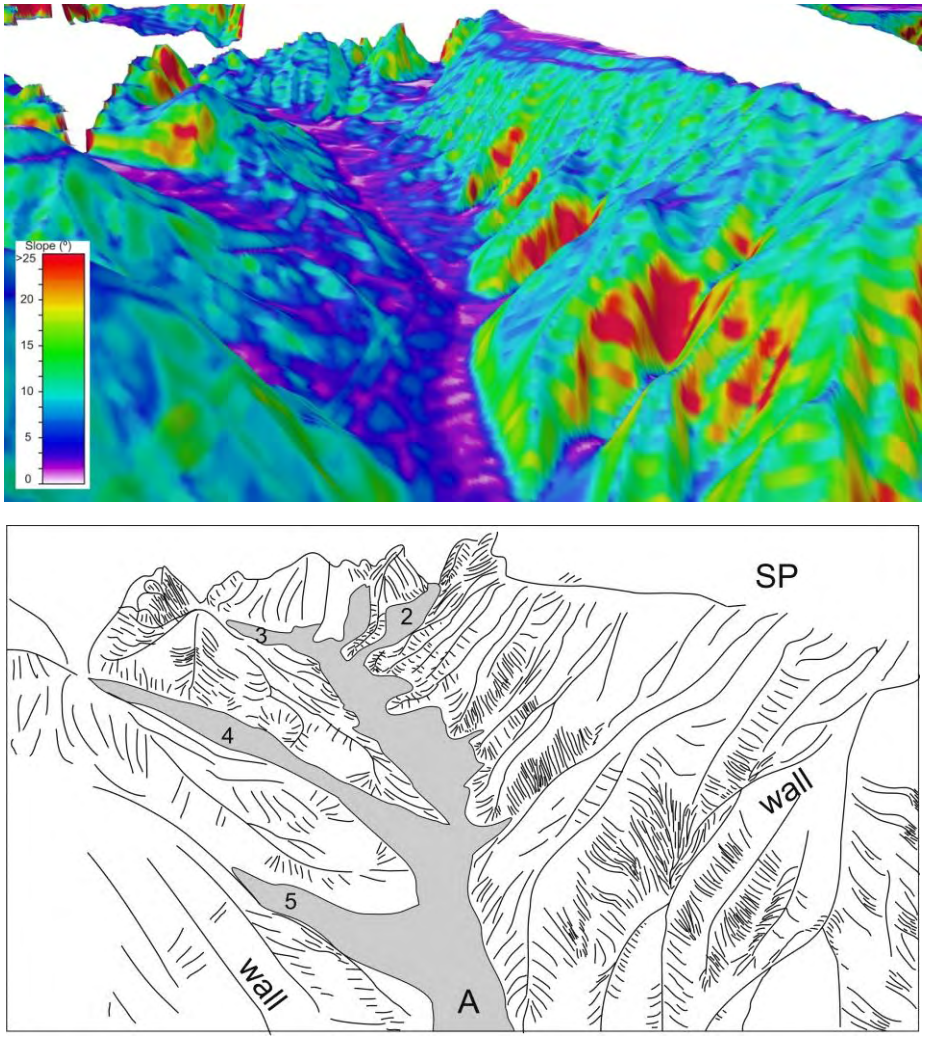

Figure 4.66 – 3D view from SW to upslope of the SVC head sector and line drawing interpretation, colours correspond to slope values. Note the higher slopes and incision in the eastern wall and the wide and flat thalweg on the bottom of the canyon. To the east there is the upper Sagres Plateau (SP). A – canyon axis; numbers refer to the various tributary channels as in Figure 4.62. Canyon's thalweg in near plane is 1 km wide.

The tributaries, although not completely imaged by the dataset, all have minor irregularities, they display similar slope values and with the exception of a small flat in profile 2 (Figure 4.63) are much like each other. The tributaries have distinct orientations from E-W to a N-S trend, from profile 2 to 5 (Figure 4.62 and 4.65) as shown by the stereograms that were made using 200 meters segments of the canyon's and tributaries' path. For the head sector they show that the tributaries are fairly linear and the trend is not very scattered (Figure 4.67).

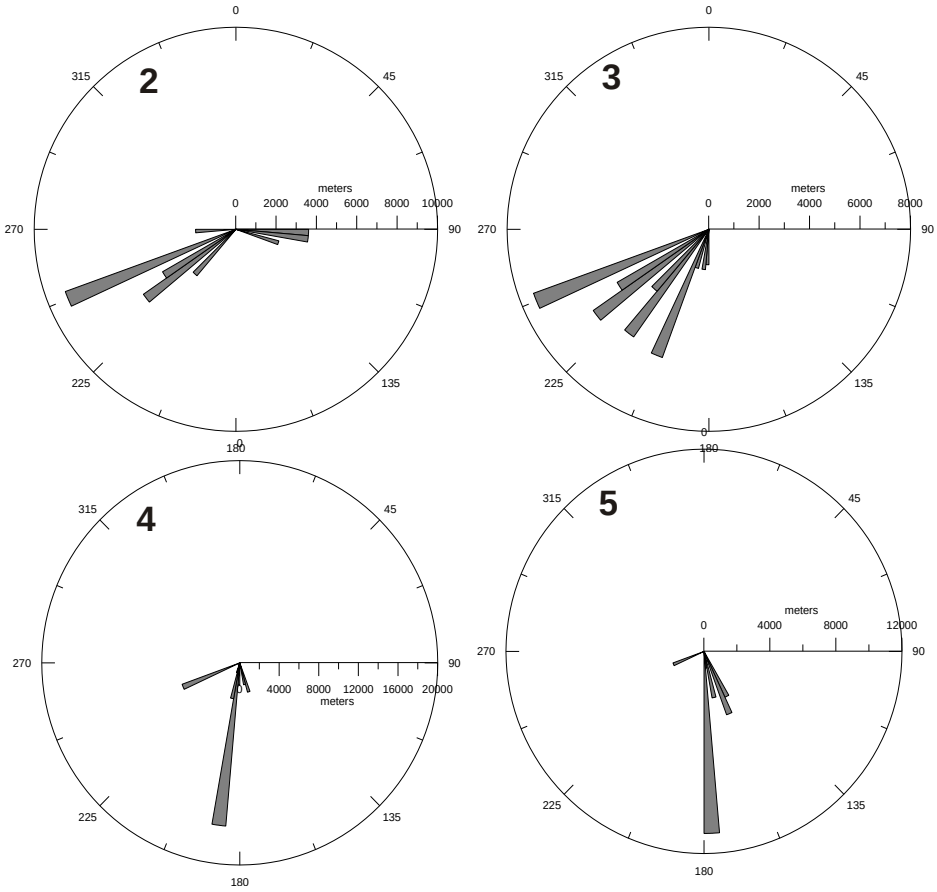

Figure 4.67 – Rose diagrams for the strike of the 4 tributaries of the SVC head section, calculated using 200 meters segments, numbers in upper left area correspond to tributary number as in Figure 4.62.

4.14.1.2. The upper course

This sector is located downwards from the previous one, its length is about 30 km long, trends in a NE-SW direction and the bottom of the canyon descends from 2300 to 3200 meters water depth. The bottom varies in width from near 2 km to 0.5 km and the width from top to top as wide as 20 kilometers (Figure 4.64 and 4.68).

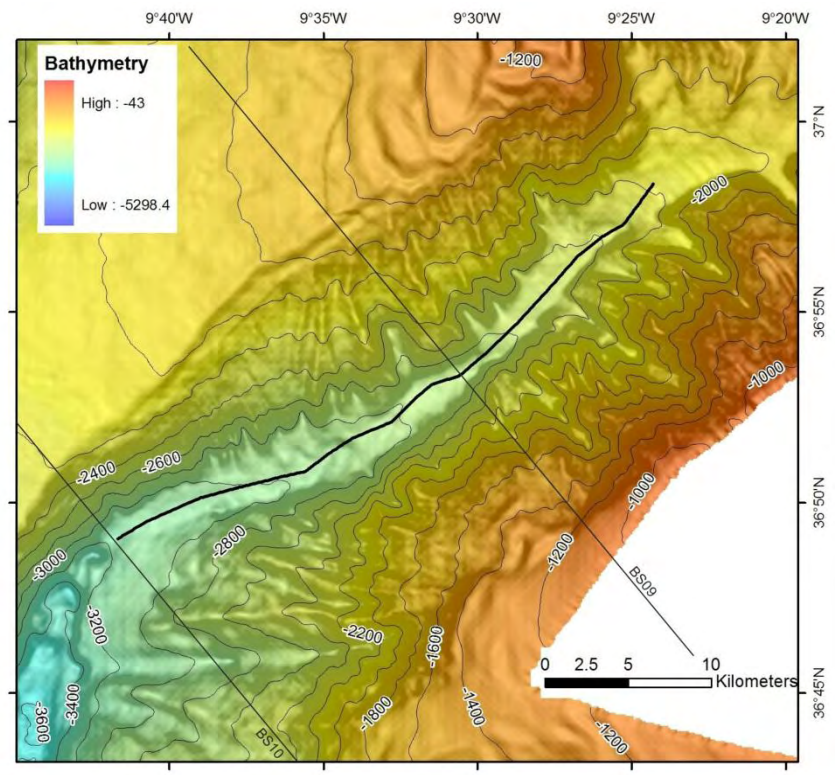

Figure 4.68 – Bathymetry of the upper sector of the SVC, black line along the axis marks the extend of the sector and corresponds to the longitudinal profile of Figure 4.62, contours every 200 meters.

This sector trends generally in an NE-SW direction (Figure 4.69) and although the canyon's path is fairly straight, in more detail it is possible to see that it is made up of minor linear segments (Figure 4.70). Throughout the entire length of the canyon, these linear segments display different lengths (from 5 to more than 30 km) and the angles between them also display a wide range of values (between 5 and 40º). For this sector, the two main classes of trends: WSW-ENE and SW-NE (Figure 4.69) correspond to the lower and upper segments of this sector, respectively.

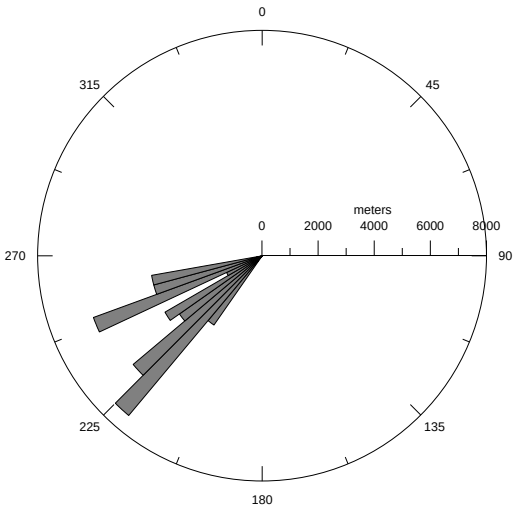

Figure 4.69 – Stereographic plot of 200 meters thalweg segments for the upper course of the SVC, see profile on Figure 4.62.

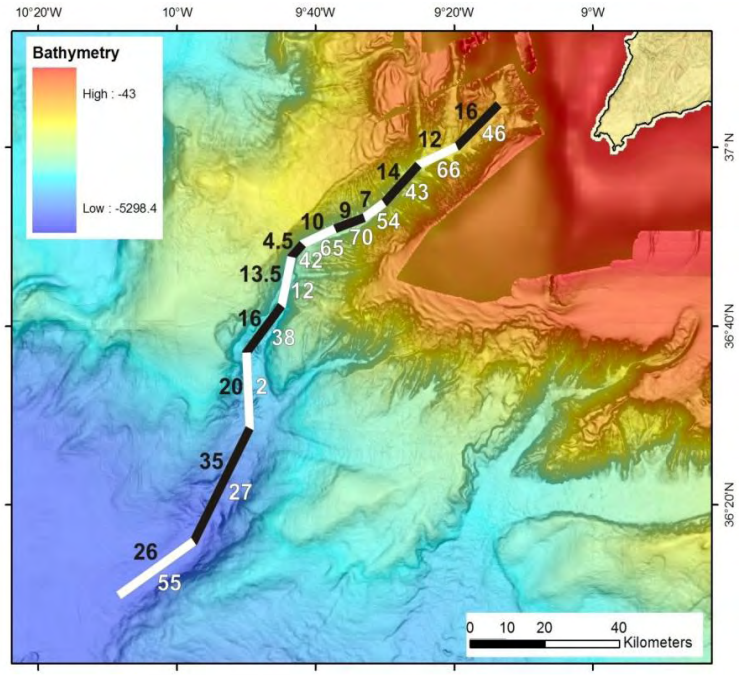

Figure 4.70 – Linear segments of the SVC path; white numbers on the right are angle between each segment and the north, black numbers on the left are the length of each sector in kilometers.

The slope along the canyon's path is higher than in the head sector (Figure 4.61) and unlike the previous sector, it displays several irregularities, known as knickpoints (Mitchell, 2006). Some of these are quite large where the seafloor drops more than 100 meters and slopes can reach more than 20º locally (Figure 4.61c, 4.63 and 4.71). Commonly these features are associated with active tectonics but that does not seem to be the case here. Furthermore, their genesis cannot be attributed to differential erosion by outcropping strata as throughout the canyon the thalweg's seafloor is made up by recent deposits that are not hard enough to produce these features. It is possible that in some sectors of the canyon the bottom currents can be accelerated increasing their eroding and carving capability generating the referred knickpoints. This phenomenon can also accentuate a slope failure generated by gravity processes, also resulting in the formation of a knickpoint.

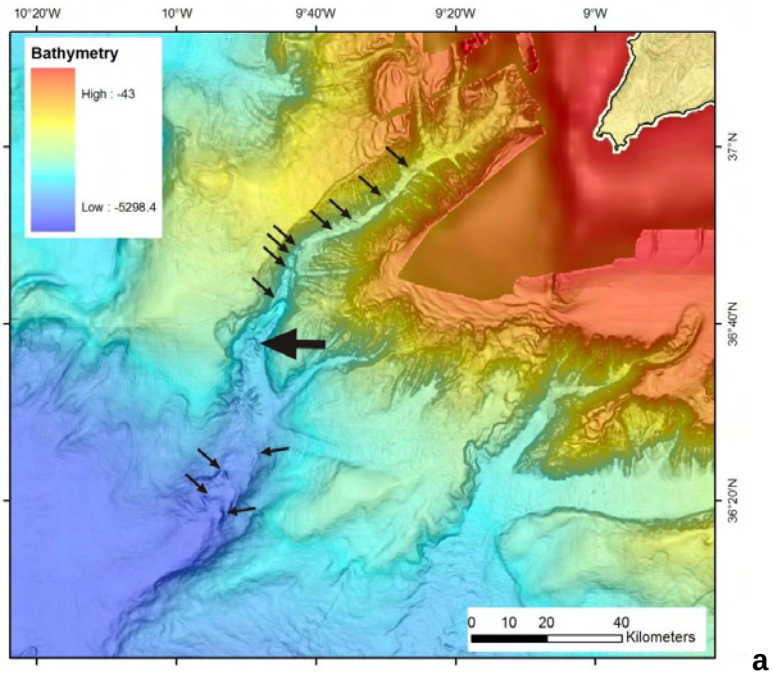

a

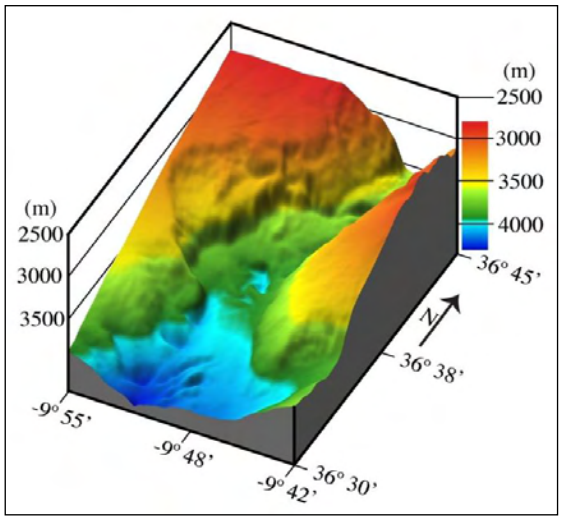

b

Figure 4.71 – **a**: Bathymetric map of the SVC, arrows indicate location of knickpoints, large arrow points to knickpoint imaged in b; **b**: 3D bathymetric DTM of a portion of the canyon's thalweg showing a knickpoint in the middle sector of the SVC. Modified from Terrinha *et al.* (2009).

Both flanks of the upper sector merge with the top of two plateaus (profile T9, Figure 4.64): to the east, the upper Sagres plateau (-2200m to -1200 m and the Marquês de Pombal Block to the west (-1000 m to -1300 m). Despite their height difference the walls are close to symmetrical with similar gradients (profile T9, Figure 4.68). The gradient values for both walls are higher closer to the thalweg (above 10º) than on the top of the wall closer to the plateaus (around 5º). On the SE flank there is an area that presents very high slopes (up to 30º). It is about 3 kilometers in length and has a bathymetric drop of about 800 m (HSA in Figure 4.72); it is here that the highest command between the thalweg and the top of the canyon's wall can be found.

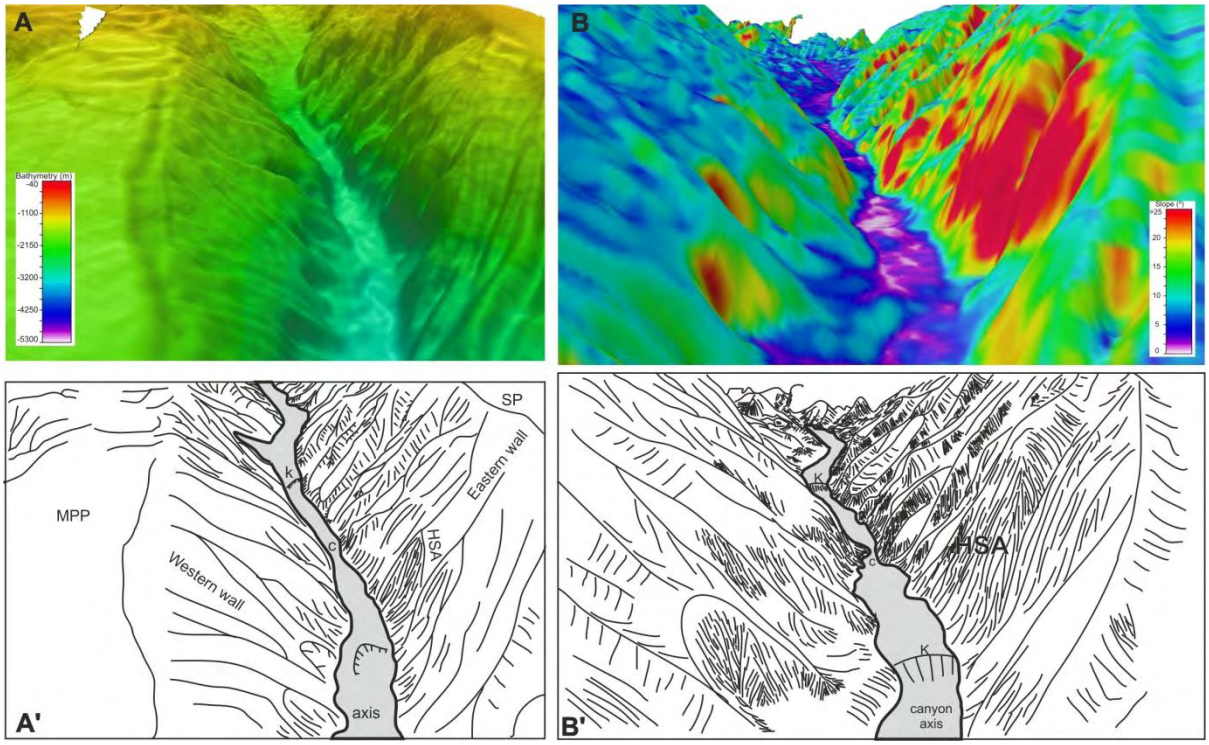

Figure 4.72 – **A** - 3D upslope view from the centre of the middle sector. Eastern wall is deeply incised by gullies, this is the area where the highest command can be found. In the canyon's thalweg two major kinickpoints (k) can be seen as well as a minor constriction point (c) where the thalweg is narrower than in the rest of the sector not reaching 1 km in width. Note the narrower thalweg when compared to the head sector (Figure 4.66). **B** - 3D view of the head and upper sectors, colours according to slope values. Head sector starts upslope of the first knickpoint. It is clear that the slopes of the east wall are higher and it is very easy to identify the HSA (high slope area). MPP – Marquês de Pombal Block, SP – Sagres Plateau. A' and B´are schematic drawing interpretations of A and B.

It is in this sector of the SVC that the walls are more affected by the incision of gullies (Figure 4.73) and due to its height and higher slopes the east wall is slightly more affected (profile T9 in Figure 4.64). Some of these gullies can cut across the entire wall from it top to the thalweg, exceeding 9 kilometers in length and about 300 meters of incision into the walls.

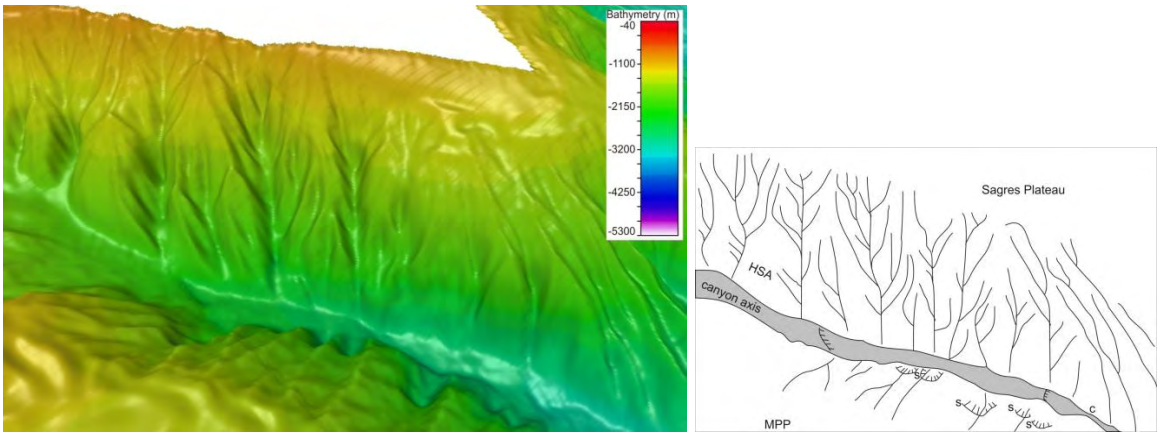

Figure 4.73 – Lower part of the upper sector. Drawing enhances the incision pattern carved in the seafloor of the canyon walls. c – constriction point, s – slide scar, HSA – high slope area (same as in Figure 4.72)

This sector can be separated from the one upwards by the characteristics of the thalweg: narrower in this sector and with a much stronger acoustic response (high values on Figure 4.61d suggest the presence of coarse materials on the bottom of the canyon). In detail, this sector (like the one before) consists of several minor segments (Figure 4.70) generally with small angles between them (however values can reach up to 30º).

The steep walls (where the gradient has values over 20º) display several slide scars that testify older mass movements (Figure 4.74).

Inspection of MCS profiles (Figure 4.74) shows that the difference between the two flanks is not only morphological (bathymetric) but is also present in the seismic facies of the sedimentary packages. The NW flank cuts through a well bedded Pliocene/Quaternary package of more than 800 meters thick. In contrast, the SE flank displays the same sedimentary package (less thick), very disturbed by the tributaries incision and mass wasting processes and shows more transparent facies with lower amplitude contrasts.

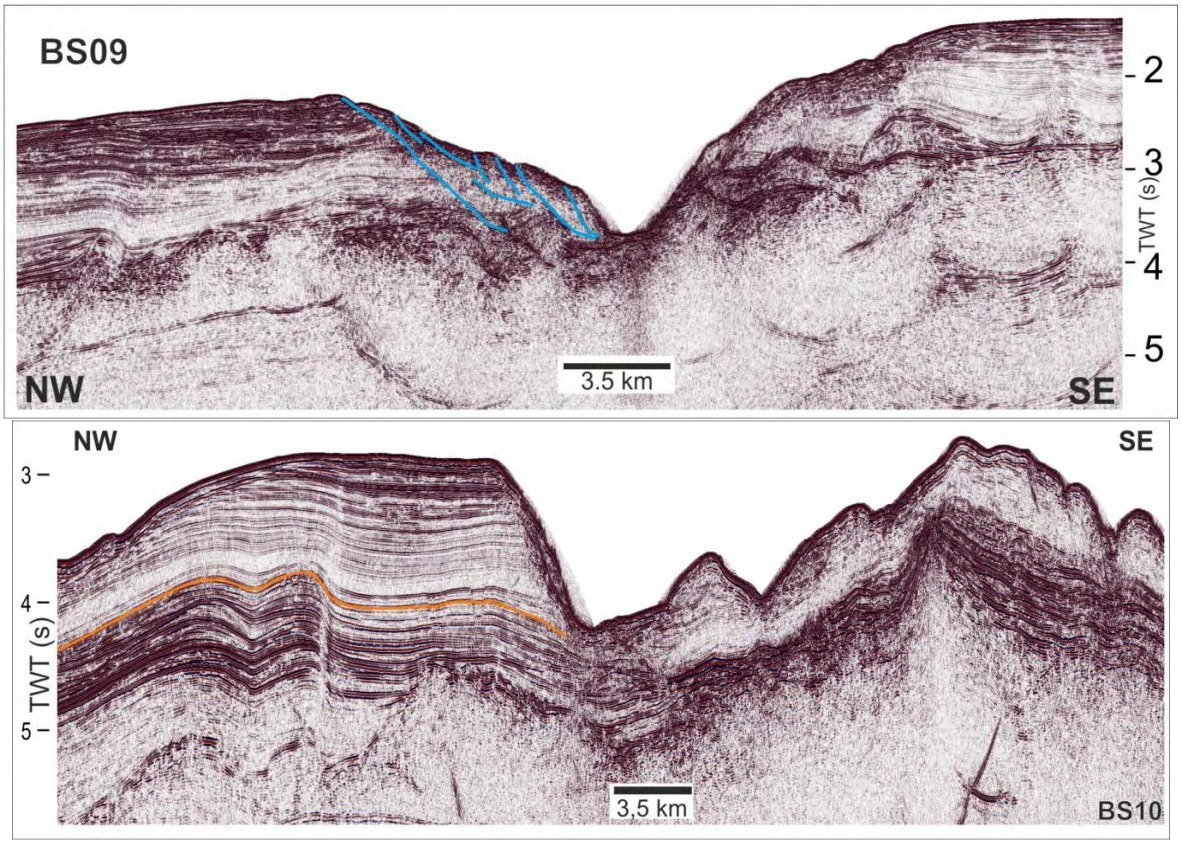

Figure 4.74 – Section of two multichannel seismic profiles, for location see Figure 4.68. Profiles show the difference between the flanks is not only morphological but the inner structure and sedimentary architecture is also very distinct. Blue line outlines slope failures and orange line highlights the base of Pliocene.

With respect to the gradients, in the shallower parts of this upper sector, the horizontal distance between the top of the northwestern flank (near MPP) and the base of the flank (thalweg) is 8.5 km, whilst for the deeper parts of this sector is around 3.6 km. Inspection of the MCS profiles on Figure 4.74 helps to explain this difference in width of the flank since the

wall in the shallower parts of the sector (imaged by the profile BS09) is made up of a very large gravity slide (with minor slope failures inside) and for the deeper parts (profile BS10) there is little loose material and the sedimentary package is nearly outcropping. The presence of this gravity slide induces the retreat of the top of the wall (away from the axis of the canyon onto the plateau) and also the advance of the base of the wall (in the direction of the canyon) due to the deposition of the fallen material. Therefore, the gravitational slide can account for the longer horizontal distance of the wall as well as for the lower gradient values that in the slide area are between 5º and 10º and for the lowermost part of the sector are above 10º (Figure 4.61d).

4.14.1.3. The middle course

At around 36º45' N and 9º45' W there is a major kink (of about 60º) in the canyons track that separates the middle course from the upper course (Figure 4.75). Like the previous sectors it also displays minor linear segments (Figure 4.70); although it strikes mainly in an NNE-SSW direction (Figure 4.76). It extends slightly over 40 km in length and its bottom drops from 3200 to 4000 meters deep (Figure 4.75).

Near the start of this sector the canyon's bottom is not wider than 500 meters whilst for the areas near the end of the sector it is over 5 kilometers. Along the track in this sector, the position of the thalweg inside the bottom also changes (Figure 4.75): in the beginning it is in the centre (since it is so narrow), in the middle part it is near the east wall (profile T17 on figure 4.64) whilst in the last kilometers it shifts closer to the west wall (profile T19 on Figure 4.64). It is in the transition between these two settings that a large knickpoint is found (Figure 4.71b).

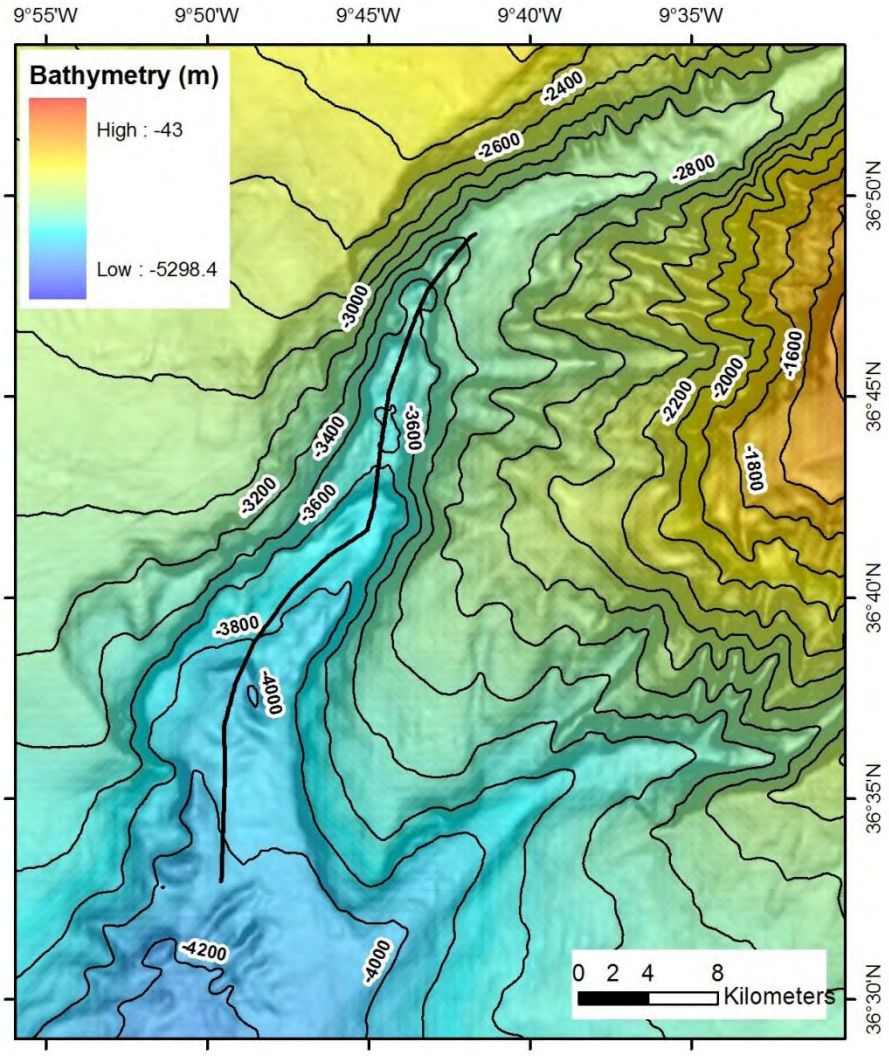

Figure 4.75 – Bathymetric map of the middle sector of the SVC, black line along the thalweg corresponds to path of longitudinal profile on Figure 4.63. Contours every 200 meters.

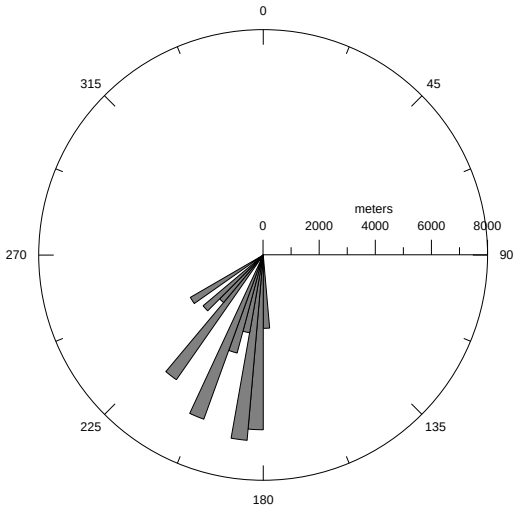

Figure 4.76 – Stereographic projection of 200 meters segments from the SVC middle sector. The SSW class corresponds to the uppermost and lowermost segments of this sector, while the WSW to SW class corresponds to the center part of this sector.

Unlike the previous sector, the higher slope values can be found in the western wall that presents an overall slope value of 15º with a 1000 meters command over the thalweg (Figure 4.77). These values are from near the kink in the canyon's path at the start of this sector. This gradient value is the highest one found for the canyon's walls, although the highest local slope values found are located in the HSA in the previous sector (illustrated in Figure 4.72).

It is in this sector that there is more asymmetry between the two flanks: the eastern wall is higher with its top at -1600 m (western wall top is 1km deeper), much more incised by gullies and with smaller gradient values (generally bellow 10º with the exception of a small area near the thalweg).

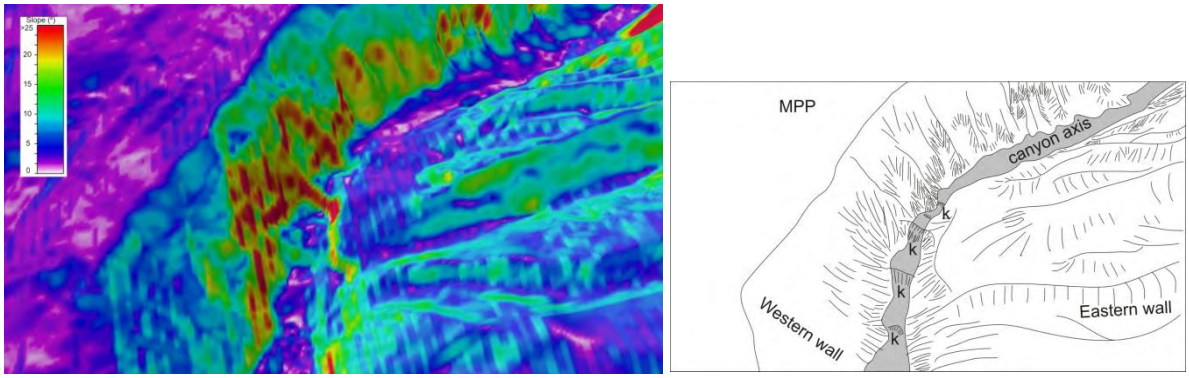

Figure 4.77 – 3D view of the canyon, colours indicate slopes. Note the high gradient values in the western wall near the kink and in the thalweg in the knickpoint, as opposite to the ones found on the other wall.

The canyon's bottom becomes progressively wider, from around 500 meters in its upper part (profile T13) to about 5 km in its deeper part (profile T17 on Figure 4.64) as the walls also become smaller and less incised by gullies. It is in this sector (low command and less steep wall with slopes under 5º) that a major slide scar (10 km in length and 800 meters from the top to the thalweg) is present (Figure 4.78). This feature has a strong acoustic signature (Figure 4.61d), displaying high reflectivity values, which indicate that the mass movements are not very old and the exposed material is consolidated and is not covered by the pelagic sedimentation.

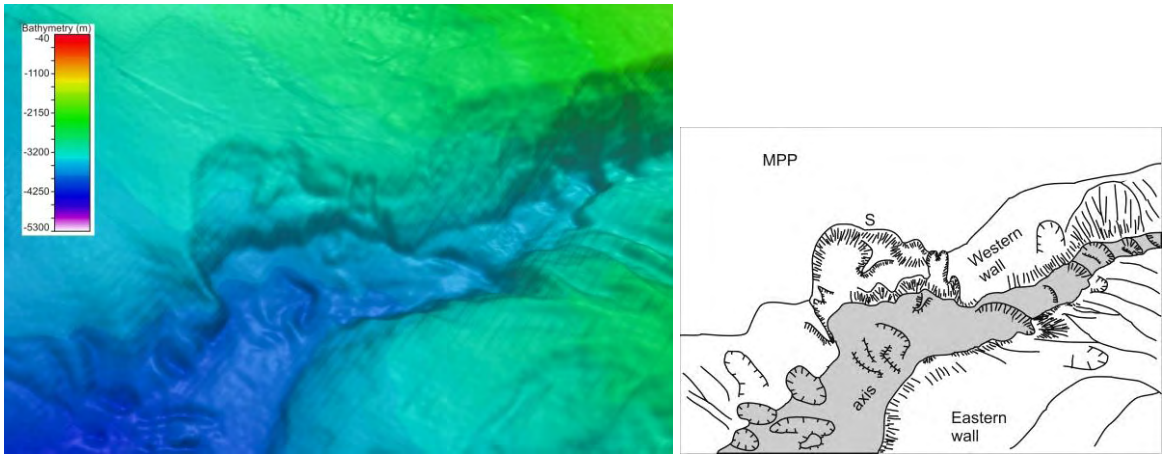

Figure 4.78 – 3D view of the slide scar (10 km in width) on the western wall topped by the Marquês de Pombal Plateau (MPP), also displayed are other slide scars and the knickpoints (k) on the canyon's thalweg.

In this sector several knickpoints were identified (5 major ones, Figure 4.71), there the slope reaches more than 15º and the seafloor can drop up to 200 meters. The along path slope values for this sector are the highest ones found for the canyon, displaying a rough staircase-like profile, where multiple knickpoints can be observed (Figure 4.63 and 4.79).

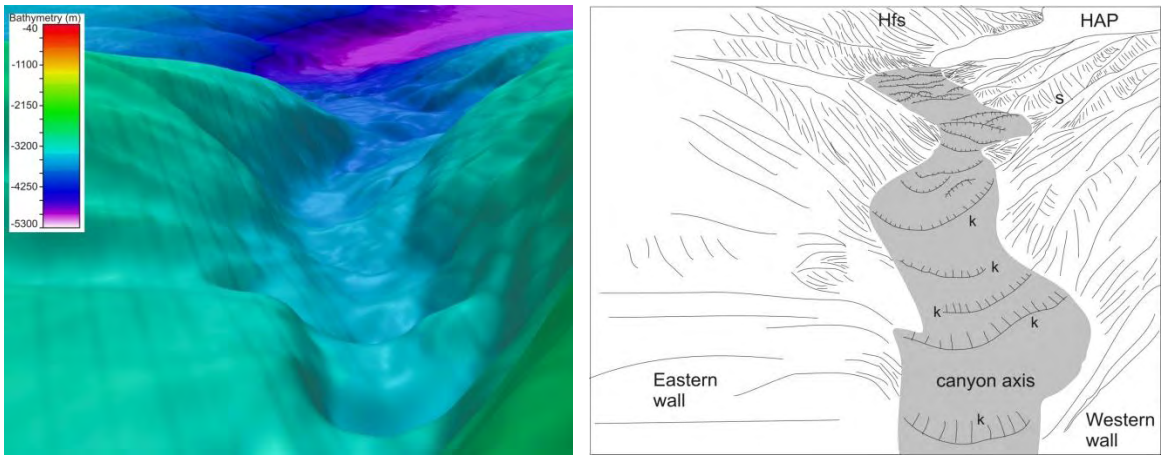

Figure 4.79 – 3D downslope view of the canyon's bottom (about 500m in width in the near plane) and walls, where is clear the numerous features that are present and affect the seafloor in the thalweg like the numerous knickpoints (k); Hfs – Horseshoe fault scarp, HAP – Horseshoe Abyssal Plain, s – slide scar (same as Figure 4.71b and 4.78).

Since there is no major deposit accumulation on the canyon's bottom near the slide scars (that affect the walls) it is possible to conclude that the downslope currents along the canyon are active and are transporting these deposits to the HAP where they are redistributed. Another supporting evidence for this is the reflectivity mosaic for this area: it is in this sector that the seafloor acoustic response has the higher values in the canyon (Figure 4.61d). This indicates that there is no presence of loose material in the bottom.

Inspection of MCS profiles (presented on the next chapter) shows fewer differences for the well stratified Pliocene/Quaternary unit on both sides on the canyon as well fewer evidences for gravity instabilities on the canyon walls when compared to the upper sector.

4.14.1.4. The mouth – lower sector

This sector starts at around 36º33'N and 9º50W, extends for about 30 km depicting a general smooth curvature (from N-E to NE-SW) as the bottom drops from 4000 to 4900 mbsl where it reaches the HAP (Figure 4.80 and 4.81).

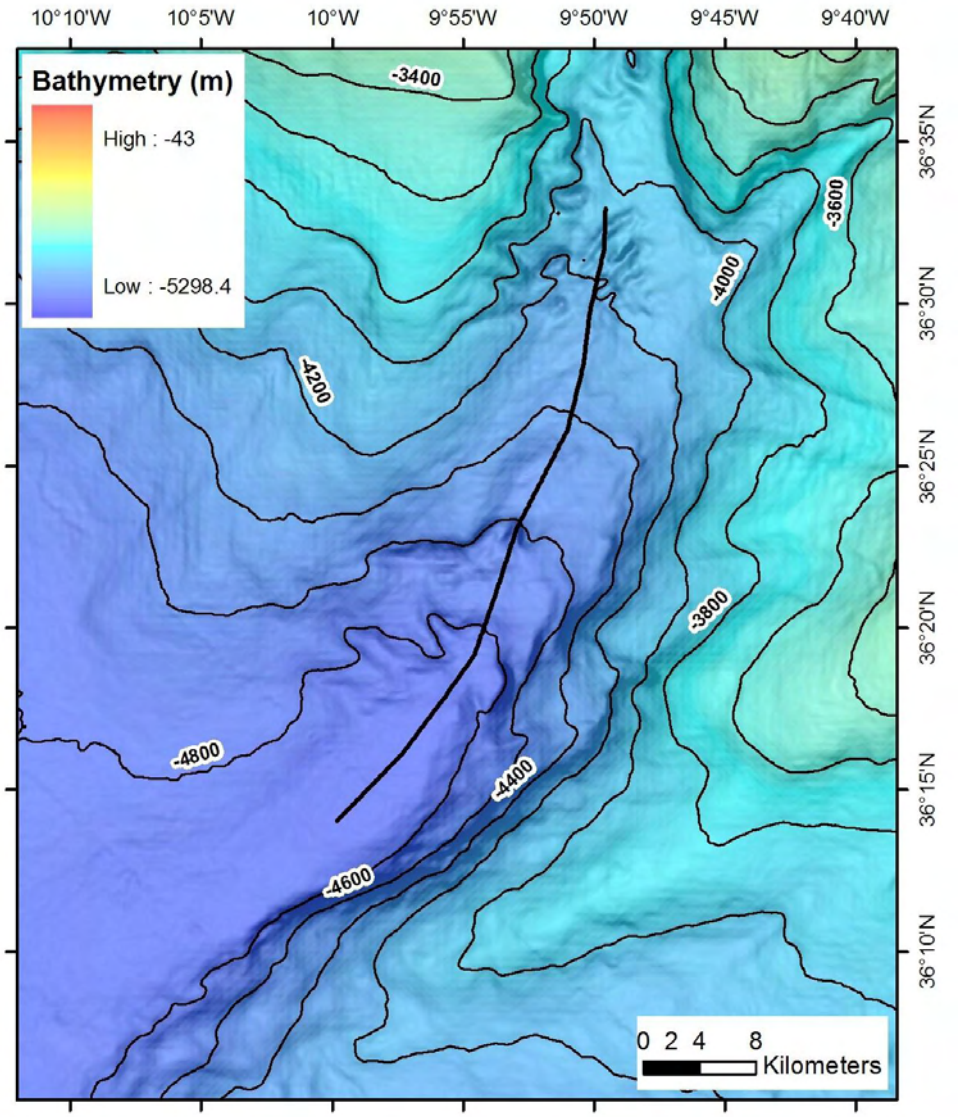

Figure 4.80 – Bathymetry map for the lower and last sector of the SVC, black line indicates location of longitudinal profile for this sector (Figure 4.62).

The stereographic plot for this sector (Figure 4.81) shows only one class with minor scattering as the trend of the canyon is a wide and gentle curve.

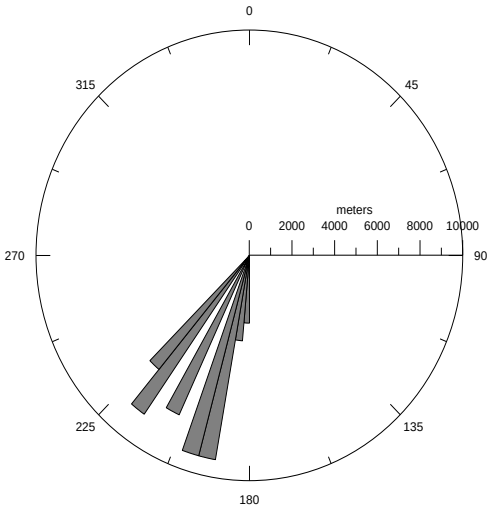

Figure 4.81 – Stereographic plot of 200 meters segments that make up the last sector of the canyon, profile in Figure 4.80.

This sector of the SVC shows the following characteristics when compared to the previous ones: i) its flanks have the least command (until eventually becomes inexistent as the canyon enters the HAP, T25 on Figure 4.64); ii) has fewer gullies and mild incision affecting the flanks; iii) wider bottom (up to 8 km) and smaller slope values both for the walls and along path (both under 5º, Figure 4.61c). At the start of this sector, the seafloor is slightly rough but becomes smoother and flat towards the end, several irregularities can be identified (profile T20, Figure 4.64), although in smaller sizes than the ones present in the previous sector. Among these there are small elongated depressions separated by minor elevations (Figure 4.82) that can reach 4x1 km and up to 80 meters deep. These features are similar to the ones described in Lastras *et al.* (2007), there named as thalweg ponds.

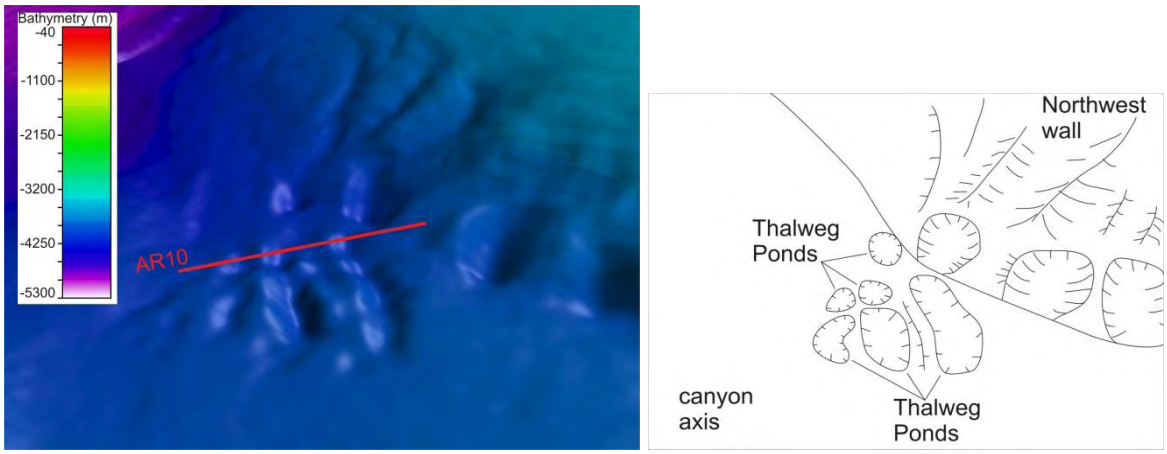

Figure 4.82 – 3D view of the irregularities on the thalweg, downslope view towards the SW. Red line is location of the section of seismic profile in Figure 4.83.

These elongated and aligned depressions seem to result from the remobilization of material from the canyon's bottom. They seem to be the result of erosion and carving on the relatively loose deposits of the canyon's seafloor that seat on top of the hard stratigraphic package.

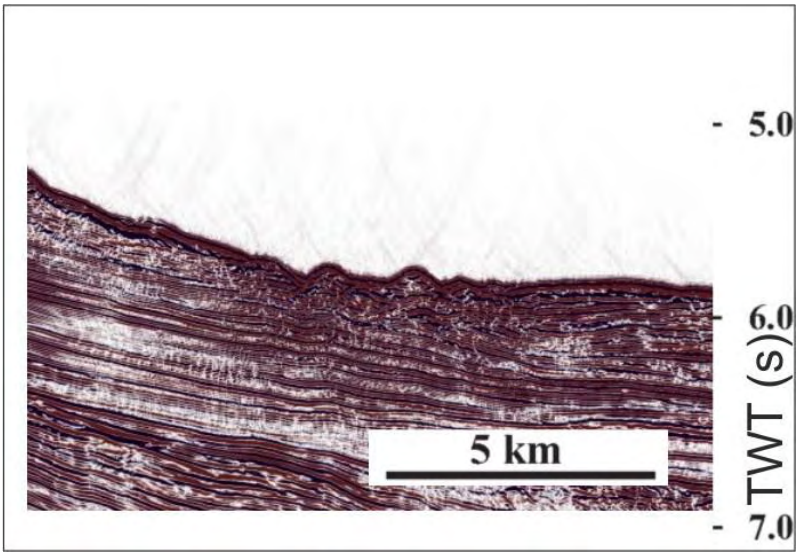

Figure 4.83 – Section of seismic profile AR10 (NW is to the left) across the elongated depressions on the canyon's thalweg, location in Figure 4.82.

In this area it is possible to identify a major contributory (Figure 4.62) that cuts across the eastern flank and is much longer than any others on the other sectors (profile 1 on Figure 4.63). Tributary 1 has its head at the edge of the upper Sagres Plateau (Figure 4.84). Near the SVC it displays a 1 km wide flat bottom that carves 800 meters onto the seafloor. Further upslope on this tributary, the bottom becomes progressively narrower until it reaches about 300 meters in width as the seafloor it is carved into becomes steeper (Figure 4.62 and 4.84) reaching values over 20º. In the middle part it also displays one knickpoint (profile 1 on Figure 4.63) where slopes of over 10º can be found along track. One other tributary incises the top of the lower Sagres Plateau (walls up to 150 meters high) and flows to the WNW towards the main course of the SVC.

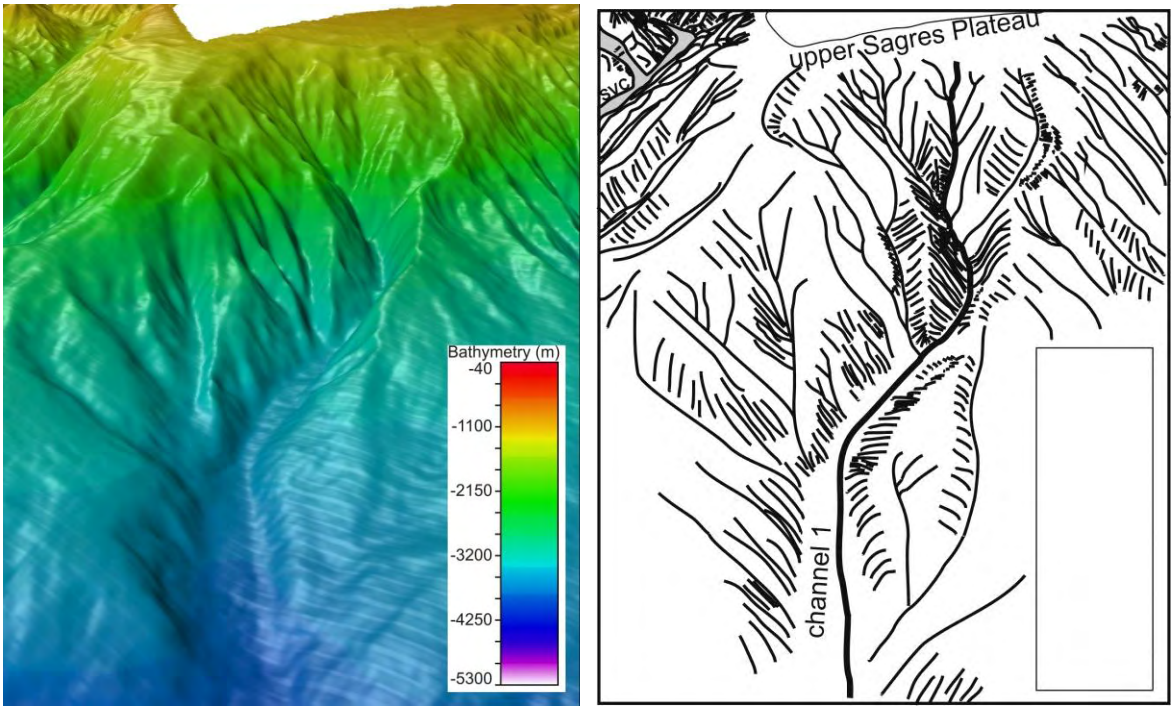

Figure 4.84 – 3D upslope view of tributary 1 (see location in Figure 4.62) starting in the upper Sagres Plateau, in the upper left corner a portion of the SVC main course is seen.

On the deeper segments (profiles T23 and T25 on Figure 4.64); as the west flank progressively fades out into the HAP, the eastern flank displays the opposite: it grows in height displaying an increasingly high wall, this is due to the fact that it corresponds to the scarp of the Horseshoe active thrust fault.

As it reaches the HAP the canyon still has some degree of erosive capacity as it carves a small depression on the seafloor of around 10 km in length and 30 meters deep (Figure 4.85).

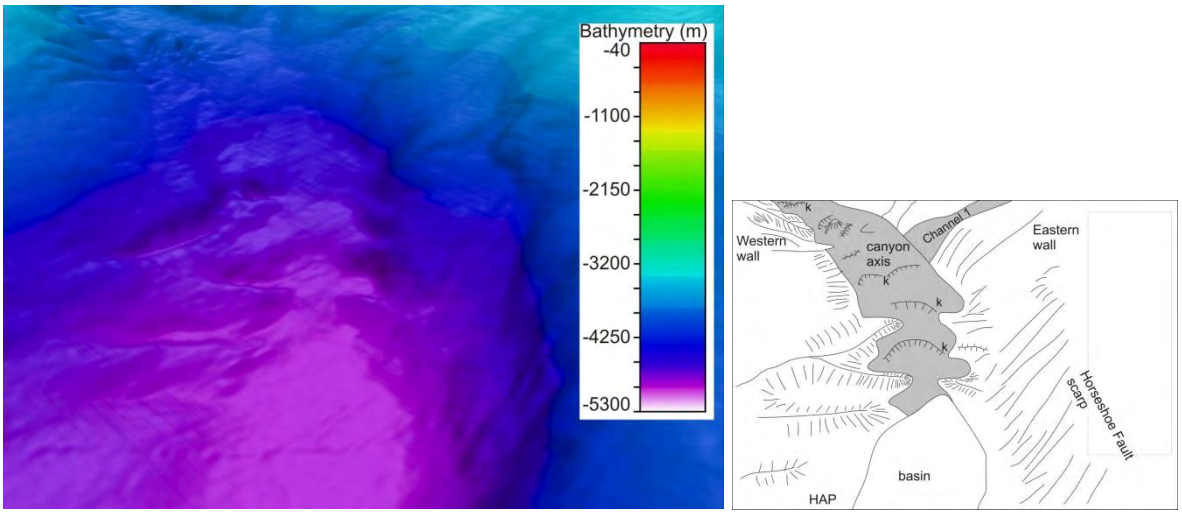

Figure 4.85– 3D view of the end of the SVC, where it meets the Horseshoe Abyssal Plain (HAP) and carves a minor depression (basin), channel 1 is the same as in Figure 4.84; k – knickpoints.

The acoustic response of the seafloor (backscatter) is lower than in the middle and upper sectors and in its deepest part (before fading away into the abyssal plain's values) it displays a pattern with alternating bands of higher and lower values. This pattern is probably related to rock outcrops that correspond to the high reflectivity values (Figure 4.86).

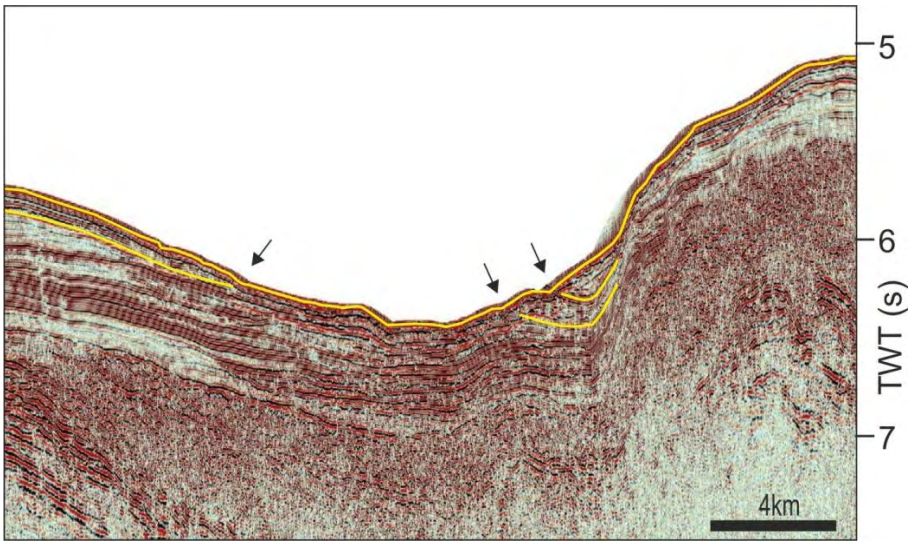

Figure 4.86 - Section of multichannel seismic BS13 (NW-SE) across the SVC thalweg in its deeper sector. Yellow lines are interpretation of the seafloor and selected horizons (paleoseafloor) that are truncated by the present day erosion and probably outcrop at the seabottom where the black arrows point. In these areas a portion of the consolidated sedimentary package also outcrops, thus accounting for the reflectivity pattern of the backscatter of this area. NW is to the left.

4.14.2. The Portimão Submarine Canyon

Located east of the S. Vicente Canyon, south of the homonymous town in Algarve, the Portimão submarine canyon (PC) extends for more than 50 kilometers starting at 36º55' N, 8º30' W and depths around 100 m to 2500 mbsl (Figure 4.87) connecting the Portuguese continental shelf to the E-W trending Portimão Valley (located north of Portimão Bank). Unlike the S. Vicente Canyon, the Portimão Canyon displays a fairly linear trend, sitting on top of the offshore prolongation of the Portimão Fault. According to Terrinha *et al.* (1999), this fault has been active as a sinistral fault from Miocene times through the present. From Late Cretaceous through Paleogene it played an important role as a transfer fault between southwards directed thrusts and before this it was a boundary fault between different sub-basins. Field evidences indicate that the Portimão Fault was inherited from the Late Variscan fracturing event.

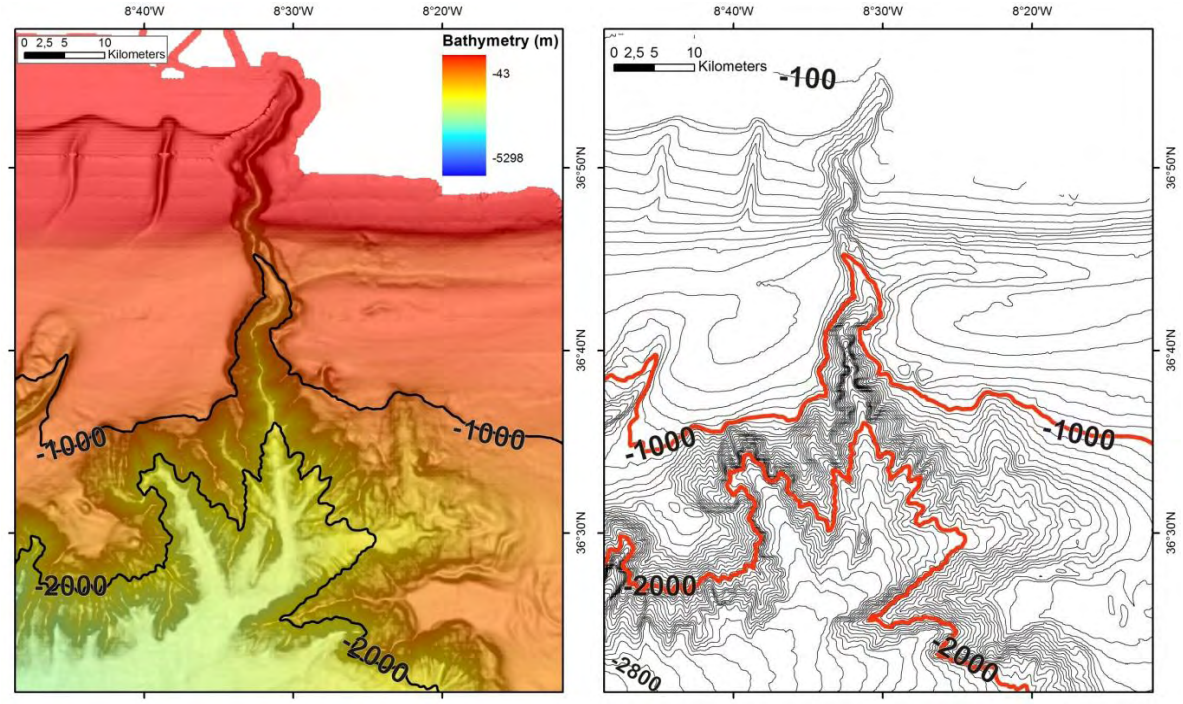

Figure 4.87 – Bathymetric map of the Portimão Canyon derived from multibeam swath bathymetry data; colours indicate depth, contours every 1000 meters (left); Bathymetric contour lines for the Portimão Canyon derived from multibeam swath bathymetry, contours every 50 meters, numbers refer to depth in meters (right).

This canyon is divided in three sectors (Figure 4.88), the upper part is short in length, has only one sinuosity in the path followed by a straight with an NE-SW trend; the middle part is longer and displays a more sinuous path (but with an overall N-S direction) for the canyon's thalweg and the last sector is very linear striking is a NNW-SSE direction (Figure 4.88 and 4.89).

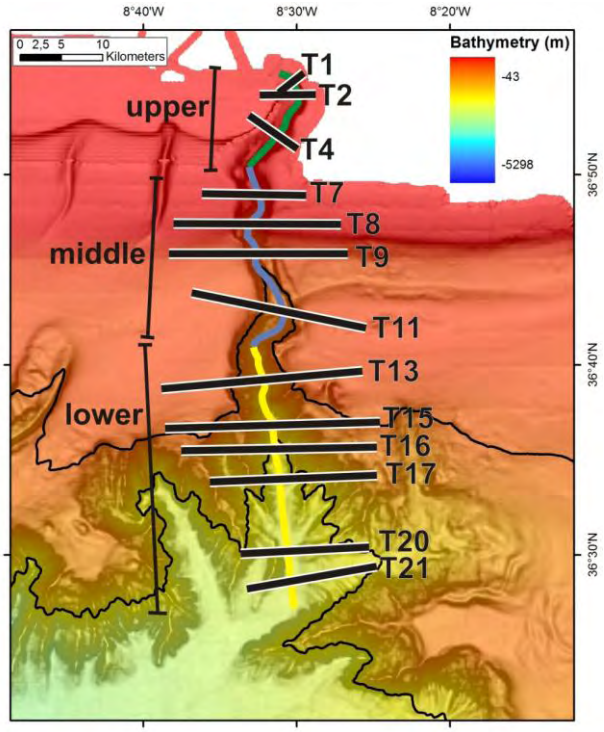

Figure 4.88 – Location of transverse profiles for the Portimão Canyon and the three sectors of the Portimão Canyon on top of bathymetric map, contours every 1000 meters. The coloured segments over the thalweg represent the track of the longitudinal profile on Figure 4.90.

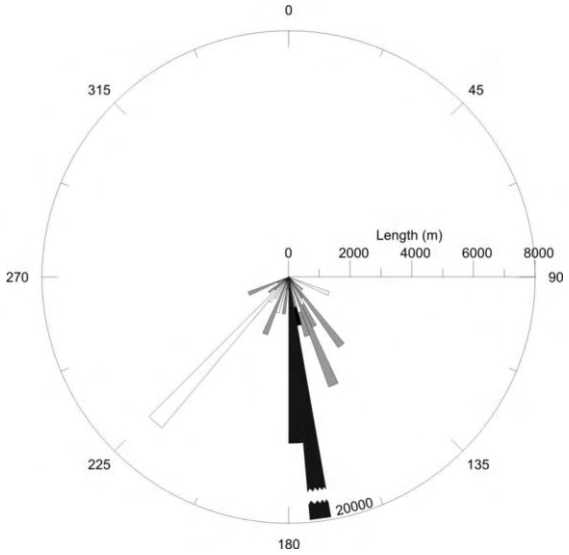

Figure 4.89 – Stereographic plot of the track of the Portimão Canyon of individual 200 meters segments, profile on Figure 4.88. Colours indicate the sectors: white – upper sector; grey – middle sector; black – lower sector.

4.14.2.1 - The upper sector

This sector extends for about 15 km, where the canyon's floor descends from depths of around -100 meters to about -500 meters (Figure 4.90).

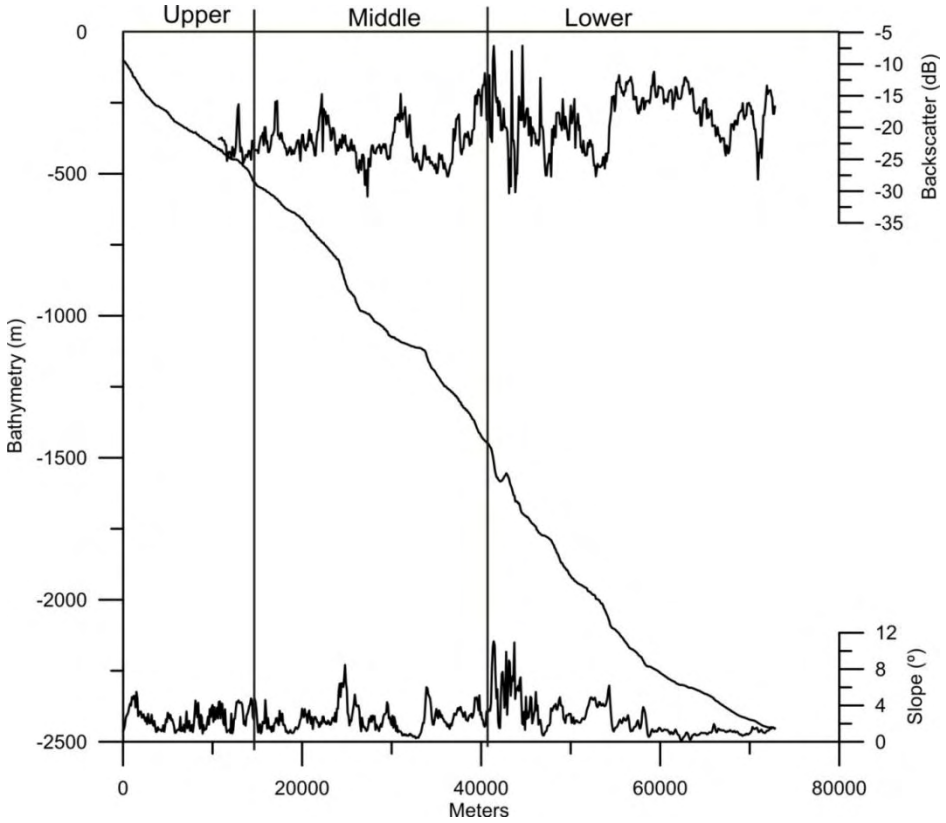

Figure 4.90 – Longitudinal profiles along track of the Portimão Canyon, lower profile corresponds to slope values, upper profile is reflectivity data, middle profile corresponds to depths. Location of profile is in Figure 4.88.

Except for the initial curvilinear shape associated with the headscarp this segment is linear and trends NE-SE. This linear segment extends for more than 7 km which constitutes the second largest straight segment of the canyon (Figure 4.89). The along path slope values are around 3 to 4º, presenting values around of 5 to 6º for the shallower parts and the seafloor is smooth with no major irregularities (Figure 4.90 and 4.92). The transverse profile displays an asymmetric V-shaped valley as the eastern wall is steeper than the western one as shown on profiles T1 and T2 on Figure 4.91; mean wall slopes can reach values over 10º and further downslope are around 7º (Figure 4.92).

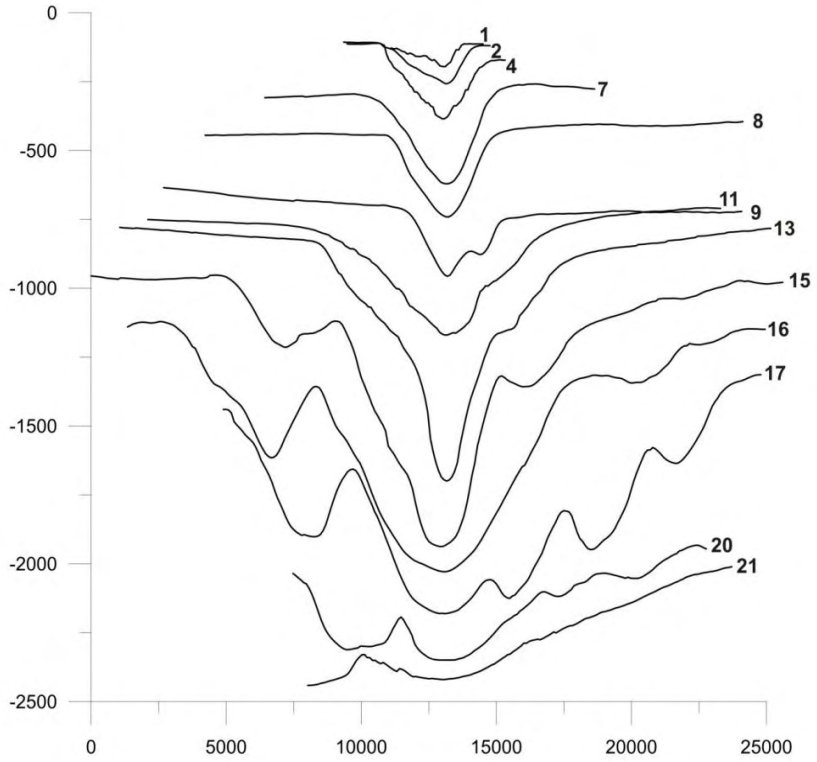

Figure 4.91 – Transverse profiles across the Portimão Canyon, for location see Figure 4.88.

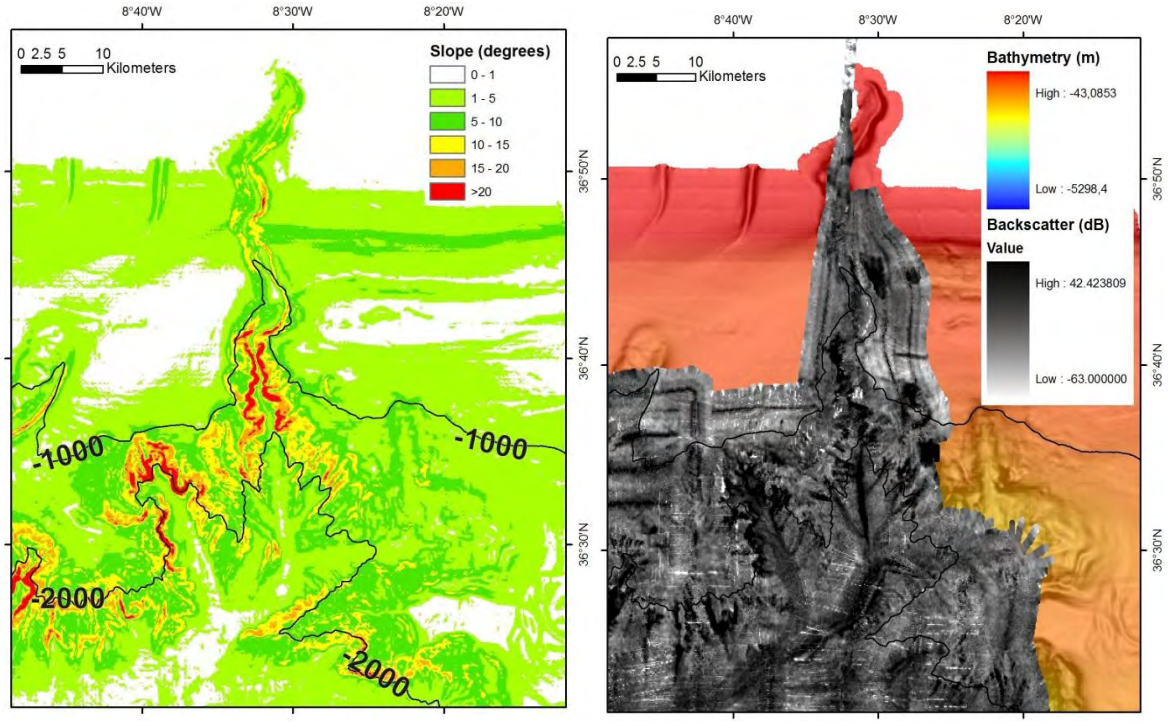

Figure 4.92 – Classified slope map for the Portimão Canyon, lines are bathymetric contours (left); seafloor imagery derived from the multibeam probe, on top of bathymetric data to give a better sense of location since this area is at the end of the coverage (right).

The western wall is slightly higher and the command over the thalweg can be up to 250 meters high, near the top presents a slope break (profile T4 on Figure 4.91 and Figure 4.93)

that has slope values up to 17º and is related to the edge of the continental shelf (incised by the canyon), the middle of the wall displays slopes around 5º and then close to the thalweg the slopes increase to reach values of up to 9º.

Close to the end of the sector there is a small (about 10 meters high) irregularity on the canyon's thalweg (Figure 4.90), probably related with the instability and falling of the flanks' material onto the canyon's bottom that causes a narrowing of the bottom (point c on Figure 4.93). This constriction corresponds to a toe deposit of a landslide on the western flank of the canyon.

The backscatter data for this sector has a poor coverage and no results can be extracted (Figure 4.92).

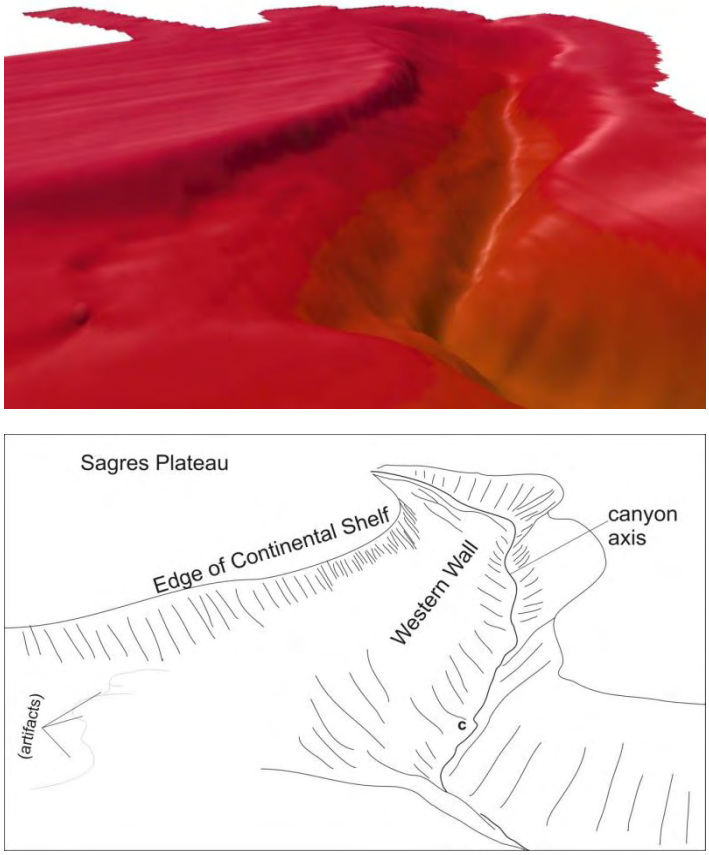

Figure 4.93 – 3D bathymetric upslope view of the upper sector of the Portimão Canyon. To the west is clear the edge of the continental shelf as the top of the western flank of the canyon and to the east the steep flank. c indicates the constriction point as the tip of the material fallen from the western flank.

4.14.2.2. The Middle sector

This sector has a more sinuous path when compared to the previous one (Figure 4.88 and 4.89), displays a relatively high sinuosity index reaching values just over 1.2, calculated over 25 km from depths of 530 meters to 1400 meters deep.

Transversal profiles across the canyon T7 and T8 (Figure 4.91) are very similar as they display the same degree of incision of the canyon and the same steepness of the flanks. The

similarity they show is probably due to the fact that the places where these profiles where made are located in the same area of non-disturbed continuous and south-dipping seafloor. Profile T9 (Figure 4.91), however presents several differences from these two: the walls are asymmetric and display different slope values and depths. The eastern side top is 50 meters deeper than the other one because the profile runs along the Alvares Cabral Moat (part of the MOW system, can be tracked in the MB dataset for over 80 km), thus accounting for the difference in height of the flanks.

The eastern flank also exhibits another difference when compared to the western flank, while the latter is a continuous and flat dipping surface towards the canyon's axis, the first has a "step" in the middle of the wall, i.e., for about 4 km in length (along the axis) the wall does not descend directly to the bottom having an intermediate flat (profile T9 on Figure 4.91 and Figure 4.94.

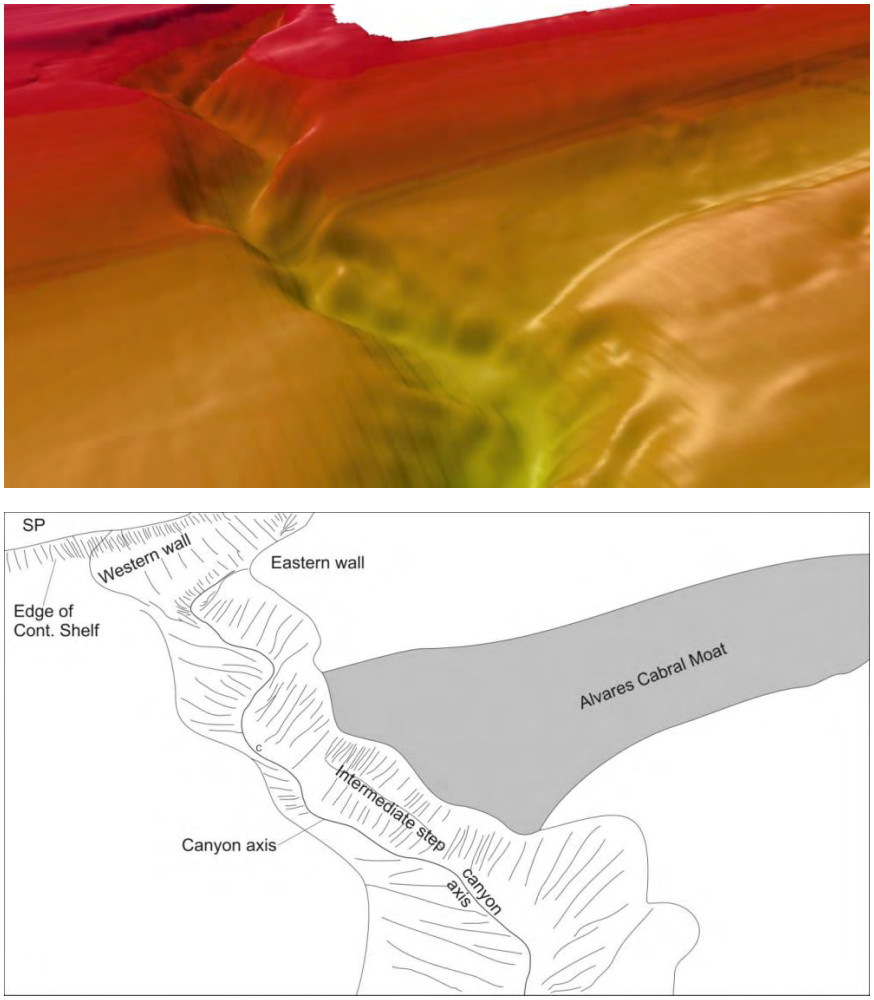

Figure 4.94 – 3D view of the middle sector of the Portimão Canyon where the Alvares Cabral Moat is intercepted by the canyon, to be noted the intermediate step in the eastern wall as well as the sinuosity this sector displays; c – constriction point.

It is in this area of this sector that the thalweg displays a slightly steeper path reaching locally values of about 10º. Transverse profile T11 (Figure 4.91) presents a more irregular and steeper western side, due to the fact that this flank is located in the concave side of a turn in a sinuous part of the path (bottom part of Figure 4.94).

Inspection of the reflectivity mosaic (Figure 4.92) shows that the higher values are not along the thalweg but are located on the upper wall of the intermediate step (Figure 4.92) and in the concave side of the last curve of this sector; this is probably due to the fact that both sites display relatively high gradients and therefore subjected to mass-movement processes that can expose harder rocks responsible for the high intensity backscatter.

4.14.2.3. The Lower sector

This sectors starts with a 4km linear segment NNW-SSE oriented (Figure 4.89), it is here that the highest slope values are found, both for the walls and the canyon axis (Figures 4. 90, 4.91 and 4.92). The walls are about the same height, with a 900 meters command over the thalweg (profile T13 on Figure 4.91), with slopes just slightly higher on the western flank where it reaches locally 30º. It is also here that the thalweg is narrower for the whole extent of the canyon not exceeding 100 meters in opposite of about 500 meters of width or more in the areas just upslope of this one. In the along-path profile it is seen that the first kilometer of this sector, that corresponds to this narrower bottom, has the higher slope values (up to 12º) for the entire canyon are present (Figure 4.90). There, a small (1 km) thalweg pond is identified (TP on Figure 4.95 and 4.96). This feature (like the ones similar to it on the SVC, Figure 4.82) could have resulted from erosion and over excavation on the bottom since it is narrower and currents accelerate as they are channelized. These first kilometers of a steep and narrow thalweg sided by also steep and high walls (Figure 4.95), are the ones that have the highest acoustic response, although not a continuous one, for the along thalweg sampling (Figure 4.90 and 4.92).

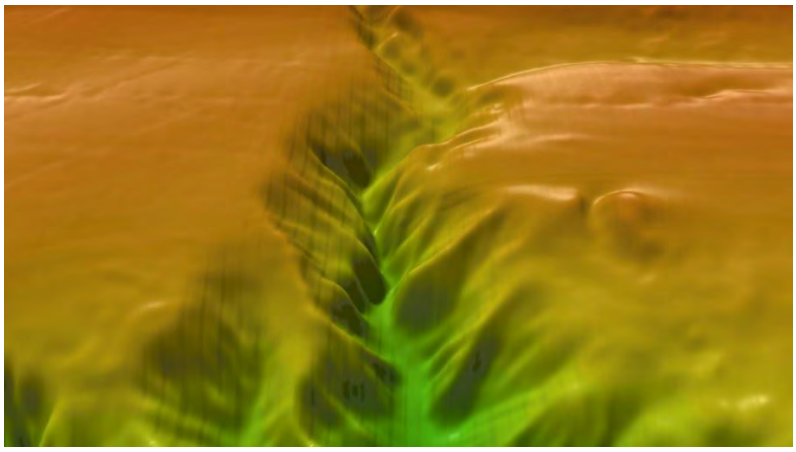

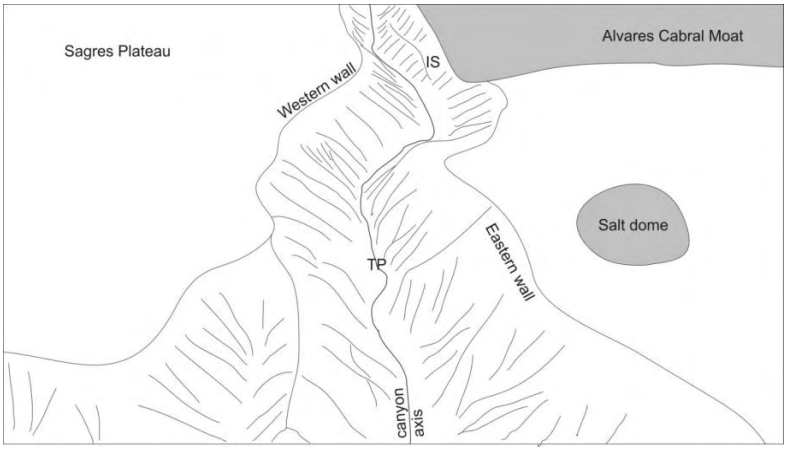

Figure 4.95 – 3D upslope view for the last part of the middle sector and first kilometers of the lower sector and its interpretation. Note the steep walls and narrow thalweg and the salt dome near the top of the east wall, on both sides of the canyon the smooth seafloor is a result of the presence of drifts; IS depicts Intermediate step as in Figure 4.94.

The remaining of the canyon is a linear segment of more than 20 kilometers where the thalweg goes from depths of 1700 meters to about 2500 meters deep, along this path the bathymetric longitudinal profile becomes progressively less steep until the PC merges with the E-W oriented, wide and flat bottom Portimão Valley (Figure 4.90). As the profile becomes less steep the canyon also becomes less incised and the walls less steep, as can be seen from profile T15 to profile T20 (Figure 4.91). Concerning the seafloor acoustic characterization, this linear segment starts with a low response followed by high values of backscatter that with the exception of a small patch (about 3.5 kilometers) extends until the end of the canyon (Figure 4.92).

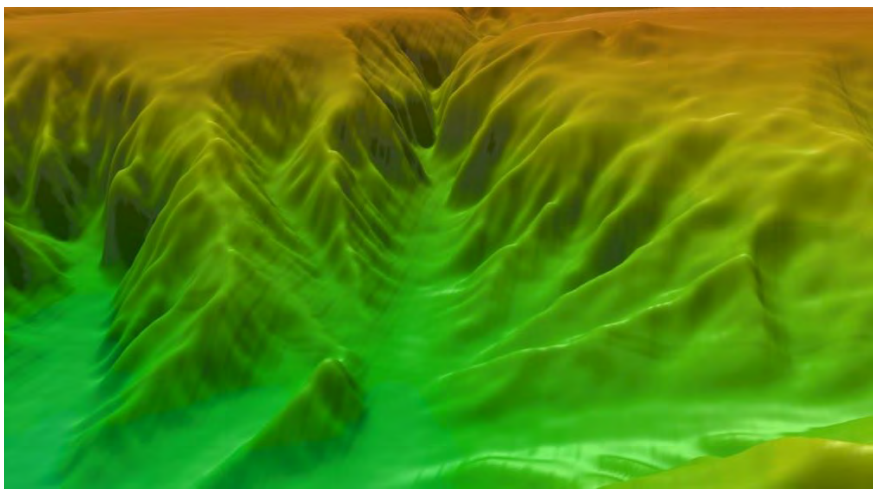

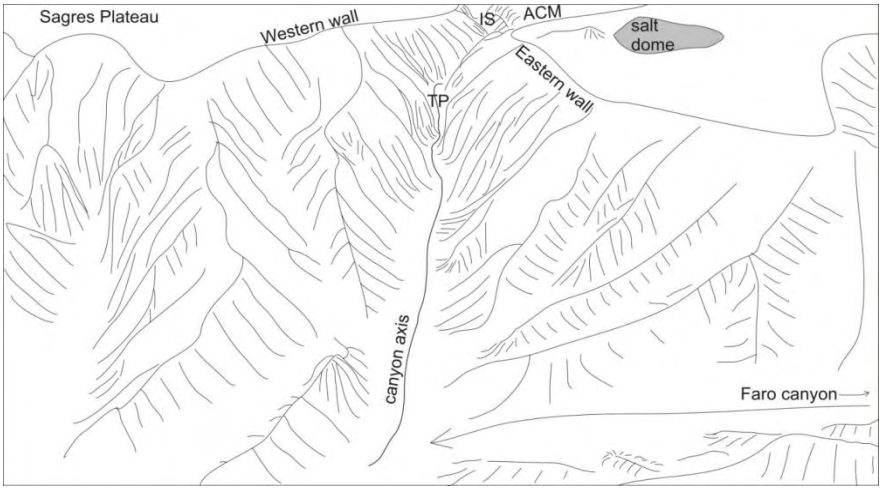

Figure 4.96 – 3D upslope view from the end of the canyon near the Portimão Valley. It is clear the wideness of the canyon in this last sector; in upslope areas the incision increases as well as the steepness of the walls and the thalweg becomes narrower.

4.15 – Synthesis

The Morphotectonics of the Gulf of Cadiz and SW Iberian Margin

The Gulf of Cadiz and the Southwest Iberian Margin display a wide variety of seafloor features (Figure 4.2a) that were formed by the action of a sole process or by the combined action of several of them. The detailed study and interpretation of high resolution bathymetry and derived maps, sidescan sonar and backscatter imagery and several seismic profiles allowed the mapping of morphotectonic domains where these features could be grouped in classes of morphologic elements. The classification of the morphologic groups took in account the origin of each element of some specific kind of processes or driving mechanism. For example, the Abyssal Hills found in the Seine Abyssal Plain refer only to the positive isolated elongated reliefs located in this abyssal plain, whilst the salt domes group (also mapped in the SAP) includes in their designation the lithology that is essential for the physical process of the development of these reliefs. The mapping of these domains was carried out taking in account the processes responsible for the shaping of the seafloor and was done also to better detail these shaping processes.

In a broad scale, the SW Iberian margin incorporates part of three abyssal plains separated by two submarine linear mountains (Tagus, Horseshoe and Seine abyssal plains and the Gorringe-Hirondelle and the Coral Patch seamounts); to the east, at the center of the Gulf of Cadiz a major arcuate horseshoe shaped and wrinkled seafloor domain is present (the accretionary wedge). The drainage arrangement and submarine sediment transport that accommodates the source to sink sediment transport is processed by three major systems: the MOW system starts on the approaches of the Straits of Gibraltar and extends on the NE and North sectors of the Gulf of Cadiz; the submarine canyons that cut across the continental slope and a system of several E-W trending submarine valleys that connect the

surroundings of the Gibraltar Straits and Guadalquivir Basin to the Horseshoe Abyssal Plain. Besides these major domains several others are present and were thoroughly mapped in this work (Figure 4.2b).

The Abyssal Plains act as large deep basins and receive the sediments brought downslope by the drainage system. The Abyssal Plains display some features that stand out from the overall flatness of these domains and were also mapped and grouped under Abyssal Hills. In the SAP, these elongated features can exceed 70 km and up to 700 meters in height and are all tectonically related as they usually correspond to hanging-wall anticline folds affecting the entire sedimentary cover, including the uppermost sediments, therefore well marked on the seafloor. Some of these hills also contain a core of deformed salt diapir depicting once more the role of the interaction between different shaping processes (Figure 4.8). Inspection of seismic profiles revealed that the majority of these hills found on the Horseshoe Abyssal Plain, lie on top of active thrusts or on top and on the prolongation of ESE-WNW wrench faults of the SWIM fault system (Terrinha *et al*., 2009; Zitellini *et al*., 2009).

The submarine mountains (the Gorringe and the Coral Patch) that separate the abyssal plains are large scale folds that seat on top of thrusts verging to the north giving the abyssal plains behind the mountains a staircase like pattern because of the depth difference (Figure 4.3). These thrusts are hundreds of kilometers in length and they are also important at a lithospheric level since both are believed to cut through to the Moho because there are important gravity anomalies associated with both structures. Besides the tectonic nature of the Coral Patch Seamount relief, volcanism also plays a role since its top is punctuated with minor extrusive edifices and some lava flows were also mapped. Furthermore, these reliefs are strongly affected by mass wasting and mass movement processes testified by the abundant slide scars, slumps and gravity instabilities on their flanks; once again demonstrating the interaction between active shaping processes on the same domain.

One of the most interesting domains is the one generated by the Mediterranean Outflow Water (MOW) currents. It is immiscible with the Northern Atlantic waters due to its higher temperature and salinity. The MOW flows out the Straits of Gibraltar bordering the SW coasts of Spain and Portugal. Due to its high speed and because it flows at the seafloor parallel to the edge of the continental slope it has a strong erosive behavior carving erosive features on the seabottom. As it heads towards the northern sector of the Gulf of Cadiz it becomes neutrally buoyant (detaches from the seafloor) and loses speed therefore reducing its erosive capability. Thus, as it gets further away from the Straits of Gibraltar it starts to drop its suspended sedimentary load but still has enough strength to redistribute the local sediments. These two processes combined are responsible for the formation of the large contourite drifts south of Portugal. In between the two scenarios (erosive near the Straits of

Gibraltar and predominantly depositional south of Portugal) there is an area where both the erosive and depositional features coexist.

The S. Vicente and Portimão canyons are the major submarine canyons present on the South Portuguese Margin, while on the Western Atlantic Margin the Lisbon, Cascais and Setúbal Canyons connect the shelf to the Tagus Abyssal Plain. All these canyons present steep walls and a well-developed incision on the seafloor. The S. Vicente Canyon captures sediments from near the continental shelf break and transports them directly to the Horseshoe Abyssal Plain. On the other hand, the Portimão Canyon has a head that cuts into the continental shelf and captures currents and sediments and transports them downslope to the base of the continental slope. There, it meets the Portimão Valley that together with the Cadiz Valley transports the sediment load through the Horseshoe Valley onto the Horseshoe Abyssal Plain, acting as a large scale bypass conduit. These two valleys have both their heads connected to MOW carved channels and also carry some sediments derived from this system. The two valleys, as well as the two south Portuguese submarine canyons are very active concerning the sediment transport to the deep as evidenced by the strong acoustic signature revealed by the seafloor acoustic reflectivity (sonar and backscatter, see Figure 4.16).

Occupying a central position in the Gulf of Cadiz lies a major domain, the accretionary wedge. This domain is related to the east dipping oceanic slab subducting beneath the Betic Orogen. It displays a typical pattern of undulated and wrinkled seafloor that is tectonically controlled by several folds that form on top west vergent thrusts that are active and reach and shape the seafloor (e.g. Gutscher *et al*., 2002; Iribarren *et al*., 2007). In addition to the seafloor undulation that results from the hanging-wall thrusts and associated gravitational collapses (e.g. Gutscher *et al*., 2009), several minor features like mud volcanoes and salt domes are also present inside this domain (Figure 4.45 and 4.48). The frontal part of the accretionary wedge displays another example of interaction between processes as it is offset by its indentation onto the rigid block of the Coral Patch Ridge (Gutsher *et al.*, 2009). The NE sector of the accretionary wedge is essentially flat due to the high sedimentary effect of the MOW masking the underlying tectonic features. Interaction between tectonic processes is also well evidenced by the bulges and landslides at the edge of the Horseshoe Valley and result from the interaction between the SWIM Faults and the Horseshoe Fault (Duarte *et al*., 2011).

Another domain that is also tectonically controlled is the one made up by the Plateaus. These have a more or less flat top and are associated with tectonic structures; most of them are uplifted hanging-wall block of active thrusts like in the cases of the Sagres Lower Plateau, the Portimão Bank and the Marquês de Pombal Plateau. These bathymetric highs

are usually bordered by high gradient walls that commonly display evidences of erosion, incision by gullies and mass wasting scars.

Throughout the study area, several features associated with fluid escape processes can be depicted on the bathymetry. These are of three types: salt domes, salt ridges and mud volcanoes. The mud volcanoes are all (but three of them) found inside the accretionary wedge domain and they are more abundant in the shallower part of this domain. The three newly discovered ones lie between the front of the accretionary wedge and the Horseshoe Fault along one of the SWIM Faults, north of Coral Patch Ridge (Figure 4.55a). Inside the accretionary wedge, several mud volcanoes form E-W to ESE-WNW trending lineaments containing several of these features. The salt ridges are present in the NE sector of the Gulf of Cadiz and they are easily depicted in the bathymetry also because part of these elevations are accentuated by the interaction with these features and the MOW and carved channels. The salt domes are present in all areas of the Gulf of Cadiz but are more abundant in the Portimão Bank and in the alignment that is present in the south part of the accretionary wedge where it overthrusts the Seine Abyssal Plain and is traced onto the Seine Abyssal Plain. Some of these salt domes have their top pierced by minor features that could correspond to mud volcanoes.

From all said it is unmistakable that there are several processes that are responsible for the shapes found on the seafloor of the SW Iberian Margin. These processes are varied in nature ranging from erosional to depositional, encompassing also others as volcanism, evaporites ascent and mud volcanism, tectonic and oceanographic. These act separately or in conjunction, throughout time to produce the wide variability of features observed and studied here.

The WNW-ESE Lineaments

The multibeam swath bathymetry mapping of large areas of the Gulf of Cadiz revealed the presence of large, partially discontinuous lineaments on the bathymetry maps that allowed the correlation between structures observable on seismic profiles that were interpreted as different structures. The so called SWIM Lineaments are made up of an alignment of several types of features like: crests, troughs, salt diapirs, mud volcanoes, steep scarps and single elevations. Inspection of several multichannel seismic profiles, as well as high resolution seismic profiles that image the subsurface structure of these features allowed to conclude that these lineaments are the morphological expression of strike-slip faults (Duarte *et al*., 2006, Rosas *et al*., 2009, Zitellini *et al*., 2009, Terrinha *et al*., 2009). It was also possible to infer its activity at present times based on the chronology of the affected sediments, the freshness of the bathymetric features involved, and by the presence of active mud volcanoes that lie on top of the faults/lineaments. Some faults that are associated with these lineaments

are reactivated structures originally formed as extensional faults during the Mesozoic. These extensional faults are experiencing reactivation as wrench faults, thus generating the lineaments at the seafloor level. The lineaments cross some active thrusts (like the Horseshoe Fault), defining a particular interaction tectonic pattern.

Some authors, taking in account their present day activity and their favorable orientation regarding the present day stress field, have proposed that these faults could be related to the establishment of a new plate boundary between Europe and Africa in the Gulf of Cadiz area.

The Geomorphology of the South Portuguese Canyons

The most prominent submarine canyons in the south of Portugal are the S. Vicente and the Portimão canyons. The first seats in the meeting edge of the South Portuguese Margin and the West Portuguese Atlantic Margin. Its headscarp starts at the edge of the shelf break and it cuts through the continental slope for about 120 km until it reaches the Horseshoe Abyssal Plain at around 5000 meters of water depth. By the detailed analysis of the bathymetry and slope maps, seafloor reflectivity and multichannel seismic profiles it was possible to establish four sectors for this canyon: the head, upper, middle and lower sectors. The individual sectors were defined based on several parameters like, trend of the course of the thalweg, wideness of the bottom and steepness of the thalweg and walls.

The head sector is the shallowest one, trends in a NE-SW direction and it displays a poorly incised canyon with a wide and flat bottom, the flanks are relatively tall (less than 1km in its deeper parts and less on the shallower parts) and the incision is processed differently on both flanks (fewer and more incised channels on the NE side and more numerous and less incised gullies on the SE side). This sector displays several tributary channels displaying an amphitheater-like shape for its shallowest areas (Figure 4.65). The position of the canyon is tectonically controlled by the S. Vicente Canyon Fault, a NW verging thrust that is located underneath the bottom. The next sector - upper sector - is aligned with the previous one, and displays a steeper canyon axis and higher walls highly incised by gullies. The flanks are steeper than in the head sector with the particularity that for the NW wall its deeper part is steeper than its shallower one as opposed to the SE wall. This is attributed to the action of mass wasting processes since the parts of both walls that display lower gradients correspond to slumped sediments, carpeted by fallen material from the walls and from the available materials at the top of the flanks (Figure 4.74). On the bottom of the canyon some irregularities are present; corresponding to knickpoints, and have slopes of more than 20º and a bathymetric drop of more than 100 meters. These knickpoints are probably related to over-excavation of the bottom since no relation was found either with tectonics or lithological

differences. In this sector, the tectonic control is still important as the S. Vicente Canyon Fault is present on the canyon bottom, uplifting its eastern flank.

The middle sector trends in a different direction than the two previous; there is a major kink of about 60º that shifts the canyon from the NE-SW direction to the NNE-SSW. The bottom of the canyon starts very narrow (around 500 meters) and becomes wider as it gets deeper, and by the end of the sector it is around 5 kilometers wide. The highest gradients on the walls throughout the entire canyon are found at the start of the sector in the western flank with gradients of 15º for the whole wall. It is also here that the largest asymmetry in the flanks is present; the top of the eastern flank (Sagres Plateau) is about 1km shallower than the top of the western flank (Marquês de Pombal Plateau). One factor that could account for part of this difference is the high sedimentation rate, generating a considerable amount of thickness of contourite deposits that make up the top of the eastern flank. In the deeper half of this section, the canyon's path displays a curvature towards the SE and at the same time the thalweg incision shifts from the center of the bottom to the base of the western flank.

The lower sector is the one that displays the less features related with mass wasting processes, the lowest command of the walls with respect to the bottom, the less incision by gullies on the flanks, the smaller gradient values for both the walls and the thalweg, and the widest bottom.

The Portimão Canyon is located south of the Portimão town on the prolongation of the Portimão Fault and Arade River and like the S. Vicente canyon it is divided into sectors according to its morphologic and structural characteristics. The three sectors reveal differences in trend of the canyon, steepness of the walls and canyon axis among other characteristics. The first sector starts incising the continental shelf at around 100 meters of water depth. The uppermost part is slightly curved to the west followed by a straight segment towards the SW, although displaying some scattering the axis slope values appear to be higher in the shallower sector. The walls are asymmetric with the western wall being slightly higher and the eastern wall displaying higher gradient values. The middle sector is more sinuous than the previous one and displays the particularity of the interaction of the canyon with the MOW carved Alvares Cabral Moat. The walls display a symmetric cross section, except in the area where it meets the moat where there is a large slide scar at halfway of the eastern flank (Figure 4.94, exposing compact deposits with high reflectivity) and the top of the eastern wall is deeper than the western one because of the erosion caused by the MOW. The sector ends in another curvature of the axis and displays several evidences of mass wasting processes on the concave flank (eastern wall). The end sector is fairly linear and it is in this area that the higher gradient values are found both for the walls and the axis of the canyon as well as the narrowest bottom. The bottom also displays some features that could be attributed to over excavation by the currents, similar to the ones found in the S. Vicente

Canyon. In its deeper parts, the along axis slope values become smaller, the bottom widens and the command of the walls also diminishes as the canyon merges with the flat E-W trending Portimão Valley. This valley is responsible for sediment transport derived from the Portimão Canyon and the dense network of gullies (on the deeper parts) remobilizing it through the Horseshoe Valley that connects to the Abyssal Plain.

Chapter 5 – Evolution of the South Portuguese submarine canyons

5.1 – Introduction and general concepts

Seismic stratigraphy and its concepts were set in the seventies by R. M. Mitchum and P. R. Vail and published in Payton (1977). This new method of basin analysis is based on the interpretation of seismic profiles and the geometry of the reflectors therein providing new insightful geological information related with paleoenvironments, sea level changes, tectonics as well as several other processes. As an overall view, seismic stratigraphy can be described as interpretation of the seismic record and the reflections there present, giving particular emphasis on their geometric relations (especially their termination styles) and their study in sequences that are bounded by unconformities; it then attempts to establish the depositional environment and geological evolution.

5.2 – Theory and seismic stratigraphy concepts

The basics of seismic stratigraphy lie on the principles that: i) sedimentation is a cyclic process; ii) primary seismic reflections are produced by abrupt contrasts in acoustic impedance (material's resistance to the propagation of sound waves) and are parallel to the stratigraphic surfaces and unconformities; iii) the reflectors have a chronostratigraphic sense. The importance of the association between reflectors and stratigraphic surfaces is crucial since it gives the reflectors a chronostratigraphic meaning and can be used to correlate strata and units between different areas. However reflectors such as "bottom simulating reflectors" (usually associated with fluids and/or gas trapped inside sediments) and other resulting from lateral echoes or seismic processing cannot be used for these matters as they are deprived of a chronological sense.

5.2.1– Concept of Depositional Sequence

The concept of depositional sequence was first established by Sloss (1963) based on the repetitive occurrence of depositional and erosional events on the records of cratonic basins. At this time the concern was to identify unconformity bounded major stratigraphic units so that correlation could be made across large areas. The definition for a **stratigraphic sequence** is "a stratigraphic unit composed of unconformable succession of genetically related strata and bounded at its top and base by unconformities or their correlative conformities" (Figure 5.1). Afterwards, Mitchum *et al.* (1977a) applied this concept on the interpretation of seismic reflection sections and turned it into the basis of seismic stratigraphy. The new perspective of the seismic stratigraphy focused the works more on seismic geometry and termination styles to delineate unconformity-bound seismic sequences (Mitchum *et al.* 1977a, b), derivation of eustatic curves using coastal onlap, and

global sequence correlation based on biostratigraphic control (Vail *et al.,* 1977). However this matter is questioned by several authors regarding the definition of the depositional sequences, their lateral variations, selection of which surfaces to better date the strata and other matters (Miall, 1986; Sloss, 1988; Galloway, 1989; Walker, 1990).

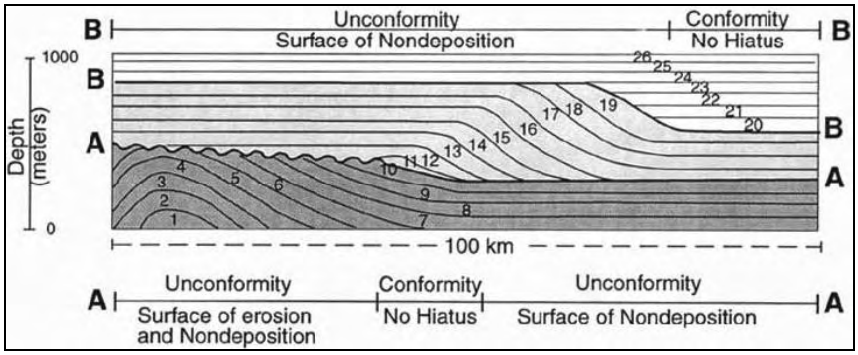

Figure 5.1 – Basic concept of depositional sequence as introduced by the Exxon group in AAPG Memoir 26, focusing on the bounding unconformities, their relative conformities (surfaces A and B) and termination of reflectors.

A **seismic sequence** is a depositional sequence identifiable on the seismic record; it is made up by seismic units (numbers in Figure 5.1) and bounded by discontinuities. **Seismic units** are tri-dimensional bodies made up by sets of reflectors (interpreted as genetically related strata) whose parameters and configuration differ from the ones in the adjacent units. Also according to Mitchum *et al.* (1977b) a sequence has to be bounded by unconformities, associated with erosion or nondeposition, which can, however, laterally pass onto conformities.

5.2.2 – Chronostratigraphic significance of a Depositional Sequence

According to Mitchum *et al.* (1977b) the chronostratigraphic sense of a depositional sequence can be establish since it was deposited during a time period limited by the ages of the boundaries where these are conformities although the range of ages of the strata can vary where these are unconformities.

5.2.3– Boundaries of depositional sequences

In order to define and to correlate a depositional sequence its boundaries must be well defined, these are defined at unconformities where the strata lay discordantly with respect to them. Dating the rocks below and above an unconformity is also helpful to have a notion of the hiatus associated with it. Laterally an unconformity can become concordant and still have an associated hiatus (paraconformity) or this hiatus can also be undetected (conformity).

An **unconformity** (Figure 5.2) has an associated hiatus and is itself a surface generated by erosion or non deposition that separates rocks of different ages.

A **conformity** (Figure 5.2.) is a surface that separates strata of different ages but where no physical evidence of erosion or non-deposition can be identified and no significant hiatus is identifiable.

A **hiatus** (Figure 5.2.) is a time interval that is not represented in a geological record, if the time interval is significant at a geological scale then the surface it originates is defined as an unconformity. Its genesis can be attributed to erosion, non-deposition or both.

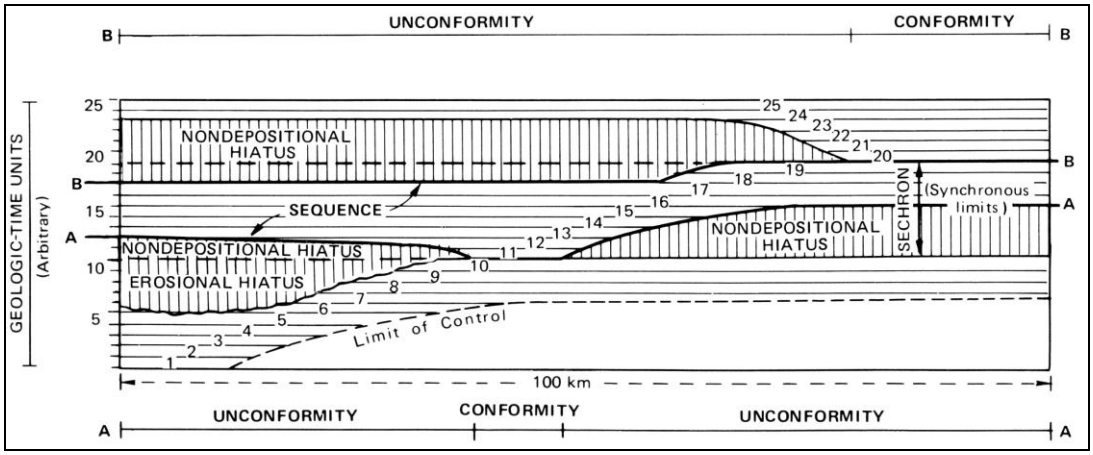

Figure 5.2 – Diagram of general chronostratigraphic section of a seismic sequence (in Figure 5.1). The seismic sequence is defined by the bounding surfaces A and B and is represented from strata 11 to 19. The diagram has the geological time in the ordinates axis and the two profiles (A-A and B-B, in the bottom and top of the diagram) display the type of surfaces generated. From Mitchum *et al.* (1977a)

5.3 – Seismic facies analysis

Seismic facies can be defined as a set of seismic and geometric parameters that allow to characterize a seismic unit and to differentiate it from others. The parameters include configuration, continuity, amplitude, frequency and interval velocity. These parameters allow to characterize the gross stratification pattern and give a way to access the depositional processes, erosion and paleotopography that were responsible for the formation of the seismic unit.

Seismic facies analysis is a key process in seismic interpretation and can be divided into four stages: i) identification of the kind of terminations of the reflectors; ii) identification of the characteristics of the reflectors; iii) identification of the geometry of the internal reflectors for each seismic unit and iv) identification of the external form of each seismic unit.

The detailed analysis of the seismic facies can then be used to extract geological information from the seismic record, such as depositional environments and lithology (Mitchum *et al.*, 1977b) or occurrence of tectonic events (Winter, 1984).

5.3.1 – Geometry and termination of the reflectors

According to the geometric relations between reflections five types of terminations are defined: truncation, toplap, concordance, onlap and downlap (Figure 5.3); these allow the identification of the discontinuities that bound the seismic sequence. The first two apply to terminations regarding the top of the sequence, whilst the last two refer to the base of the sequence. These four types of discordant terminations are the ones that are used to define a seismic sequence as stated before according to the criteria of Mitchum *et al.* (1977a). In the case where a termination cannot be exactly determined as onlap or downlap, the term baselap is applied.

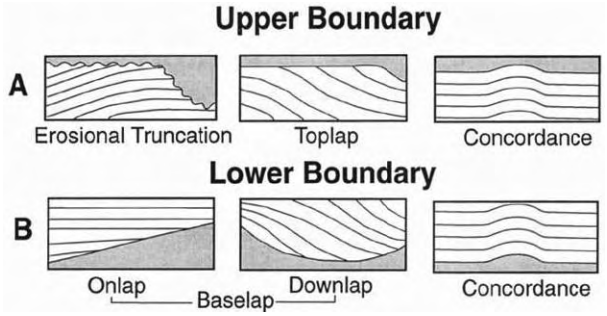

Figure 5.3 – Schematic drawing illustrating possible configuration of the types of termination of internal reflectors with respect to the seismic sequence boundaries; adapted from Mitchum *et al.* (1977a).

Concordant relations can be used both in relation to the upper and lower sequence boundaries and are characterized by the parallelism of reflectors (Figure 5.4a).

The different types of terminations (Figure 5.3), against both top and bottom boundaries, has itself a stratigraphic meaning as it owes its formation to the occurrence of depositional hiatuses resulting from erosion or nondeposition (see also Figure 5.2.).

Other concepts are also associated with these terminations, such as lapout which refers to the lateral termination of a reflector (strata) and can be further classified as toplap or baselap.

Baselap is a lapout related with a lower sequence limit and two terms can be defined: onlap and downlap (Figure 5.3).

Onlap is a baselap in which an originally horizontal reflector ends against a more incline surface, or an inclined reflector laps out on an even more inclined surface (Figure 5.4 b). Onlap terminations can be associated with seabottom irregularities and constitutes one of the more reliable indicators to define a lower boundary for a seismic sequence.

Downlap is baselap in which a more inclined reflector dies out downdip against a less inclined (or horizontal) surface (Figure 5.4c). Both onlap and downlap reflect cases of non-deposition instead of erosional hiatuses. There are several types of onlap and downlap: a proximal onlap is when the onlap is towards the sediment supply origin; a distal onlap is

when the onlap is in the opposite direction of the sediment source; distal downlap can be applied when the downlap is made in the opposite direction of the source of sediments.

Toplap is the lapout of more inclined reflectors on an upper boundary of a seismic sequence or unit (Figure 5.3 and 5. 4e). This type of termination is typical of a non-depositional hiatus, it is usually associated with a low base level that does not allow the strata to extend updip, during its formation sediment bypass and minor erosion can take place.

Two types of **truncation** (Figure 5.3 and 5.4d) can be identified: erosional and structural. Both are characterized by the abrupt lateral ending of the reflectors against a discordant surface (of erosive or structural origin) that bounds an underlying sequence. It can be generated by tectonic tilting of a sequence followed by erosion and extended over large areas or be confined to the flanks of submarine drainage channels. Structural truncation results from the disruption of the reflectors in direct result of fault activity.

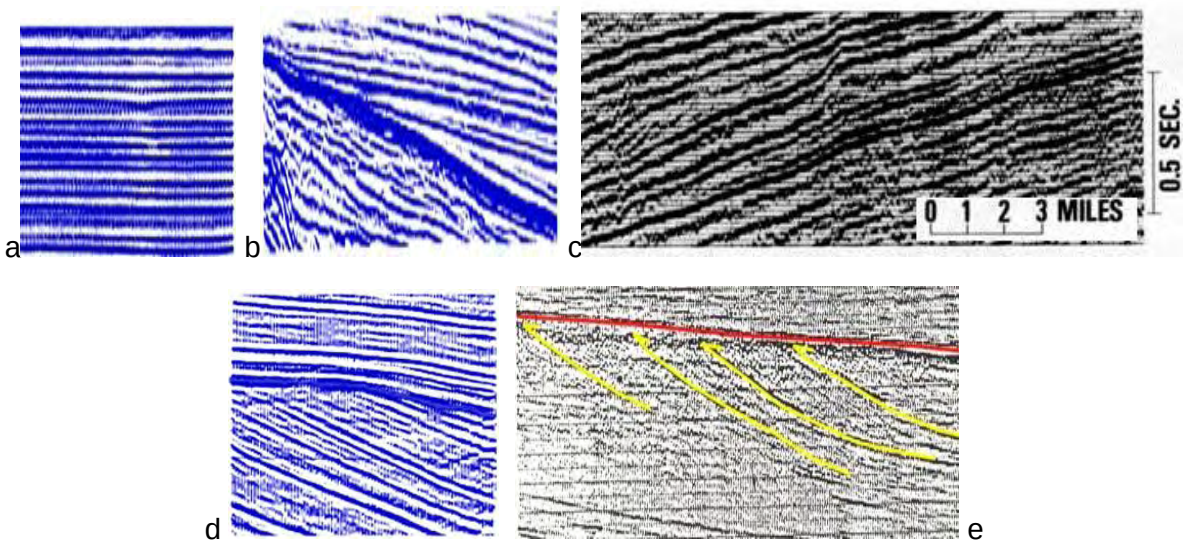

Figure 5.4 – Sections of seismic profiles with examples of terminations: a - concordance, b - onlap, c – downlap, d - erosive truncature, e - toplap (a, b, d from Prakia Seismos; c from Mitchum *et al.* (1977b); e adapted from Alonso *et al.*, 1989).

5.3.2. – Characteristics of the reflections

Changes in the geological properties of the sedimentary sequences can be identifiable in outcrops, well-log sections, cores and, with more importance regarding this work, also in seismic profiles. Seismic sections reveal most of the geology of the sequences maintaining large of the geological characteristics, including their chronological sense. Thus, several seismic parameters are studied, namely: reflection configuration, continuity, amplitude and frequency. Each of these seismic parameters provides different geological information about the rocks imaged on the seismic profiles.

Reflection configuration of a seismic sequence can give useful information about the gross stratification patterns and therefore more information regarding depositional processes,

erosion, paleotopography and fluid presence are extracted. This is one of the most studied parameter as is the one that gives out more geological information about the rocks.

Reflection continuity corresponds to lateral juxtaposition of successive reflections of a same horizon and is closely associated with physical strata continuity in such a direct manner that continuous reflections suggest widespread, uniformly stratified deposits. Continuity of a given horizon is interpreted as maintenance of the depositional conditions with no major changes in the energy of the environment, as well as, minor continuity of a horizon indicates more changes in depositional energy at the time of formation of the deposit.

Reflection amplitude refers to the maximum amplitude of the reflected wave which is dependent on the velocity and density contrasts of each individual interface and their spacing. Fluid content in the sediments can also have an influence in this matter. High amplitudes reflect high acoustic impedance which is reflected in the seismic record as an important reflection. If laterally this high reflection diminishes rapidly it is an indicator of a high energy depositional environment, the opposite suggests a large continuity of the formations and a stable depositional environment. Generally high amplitude reflections are typical of detritic platforms environments where intercalations between high and low energy deposits can be found, whilst low amplitude reflections are typical of more stable and constant energy deposits.

Reflection frequency is the time (depth) between two reflections; it reflects the instrumental seismic characteristics but is also influenced by other factors such as the presence of fluids and especially by the natural thickness of the layer deposits. Regarding the last case there is an inverse relation between natural thickness and frequency, thus, high frequencies correspond to thin strata.

5.3.3. – Configuration of internal reflections

Depositional processes, erosion, paleotopography as well as the presence of fluids can influence the geometric relations between the internal reflections of a seismic sequence. Several types of these (Mitchum *et al.*, 1977b) are now presented (Figure 5.5).

Parallel and **Subparallel** types refer to the direct sense of the word, where reflections are parallel and continuous (Figure 5.6) and display high amplitude, additional terms can be used to more particular cases, such as even or wavy (Figure 5.5). Parallel type reflections are typical of sheet, sheet drape and fill unit's external forms of the sequence. For this simple configuration minor divisions are used based upon variations of other seismic parameters such as amplitude or continuity. Parallel and subparallel patterns suggest uniform rates of deposition on an environment like a steady subsiding shelf or a stable basin.

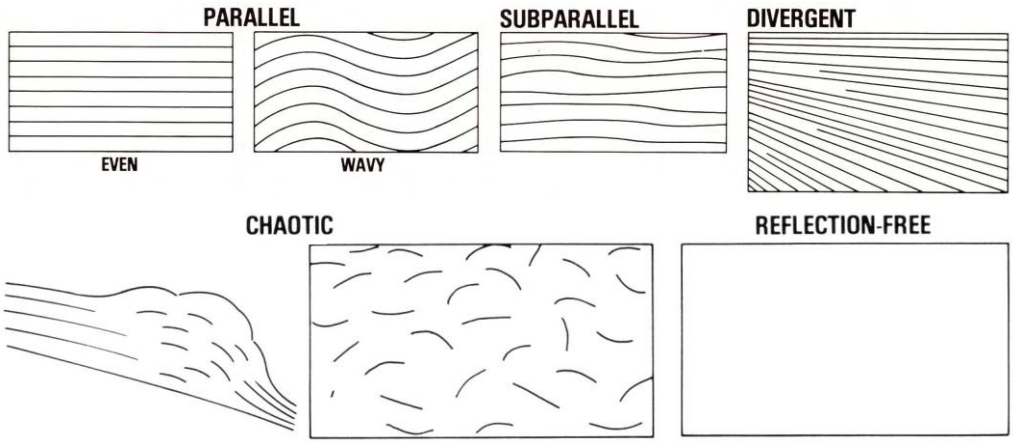

Figure 5.5 – Seismic reflection patterns, modified from Mitchum *et al.* (1977b).

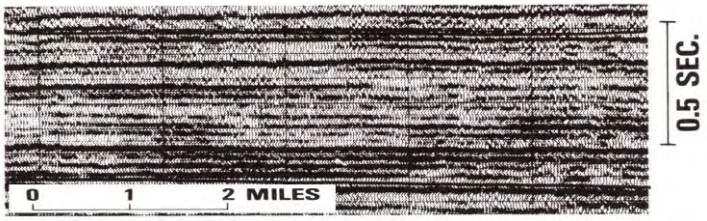

Figure 5.6 – Section of a seismic profile displaying a parallel reflection type configuration (from Mitchum *et al.*, 1977b).

Divergent pattern is characterized by a wedge-shaped sequence (Figure 5.7) in which the thickening is accomplished by the thickening of the reflection's cycle rather than by onlap, toplap or erosion at the bottom or the top of the sequence. This pattern is associated with lateral variations of the deposition rate or to the progressive tilting of the depositional surface. The term convergent or divergent are applied when referred to the sediment source.

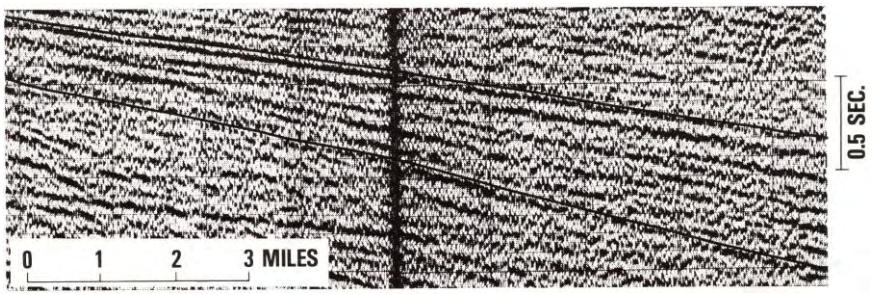

Figure 5.7 – Divergent configuration on a seismic profile, seismic unit boundaries are outlined, from Mitchum *et al.* (1977b).

Chaotic type refers to discontinuous, disconcordant and disordered reflections (Figure 5.5), suggesting a total disarrangement of the reflections, characterized by high frequencies. This kind of internal reflections is associated with an high energy environment with large variability of the depositional conditions and it is commonly found in slumps, erosion derived deposits, cut-and-fill channel bodies and on high energy zones affected by faults or folds.

Transparent pattern is characterized by the total or partial absence of reflections or by its small lateral continuity. It is related to homogeneous rocks (with low acoustic impedance contrasts), highly deformed or metamorphosed rocks, evaporites or igneous masses. Rapidly deposited large deposits of pelitic rocks can also give an acoustic response such as this.

Prograding configurations are more complex and several sub-types can be identified (Figure 5.8). These are characterized by strata with significant deposition, due to prograding or lateral outbuilding generating several different patterns called clinoforms. These largely result from variations of deposition rate and water depth and are formed in a wide variety of environments. The subdivisions are: sigmoid, oblique (tangential, parallel), sigmoid-oblique, shingled and hummocky.

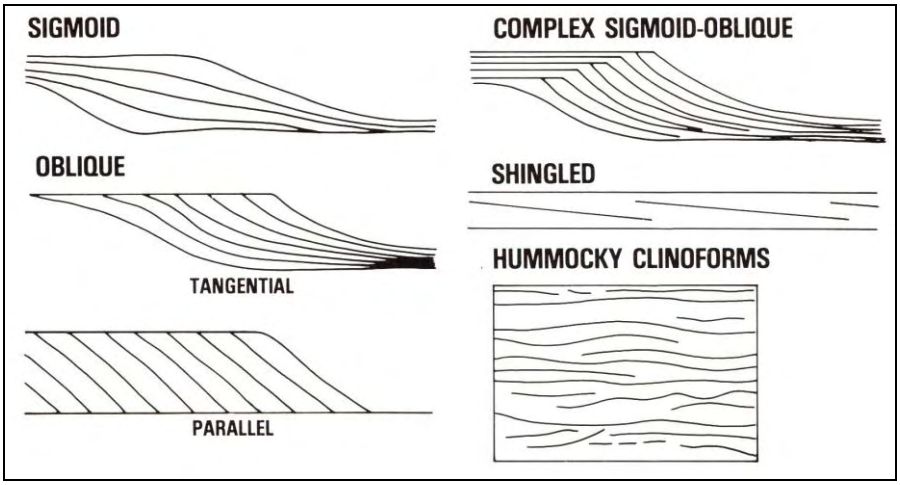

Figure 5.8 – Types of seismic reflection patterns of prograding clinoforms (from Mitchum *et al.,* 1977b).

Sigmoid progradational configuration is an S-shaped clinoform with thin and less inclined strata at the top and base and a thicker and steeper intermediate sector (Figure 5.9). The upper segments (topset) are horizontal or gently dipping reflections that are concordant with the top boundary of the sequence. The middle segments (foreset) are lens-shaped and superimposed on another to allow younger foresets to be displaced downdip in the depositional direction and generate a prograding pattern. The lower segments (bottomset) have very low angles near the bottom boundary, may display downlap terminations and are commonly parallel and concordant with the boundary. The most distinctive feature of the sigmoid configuration is the parallelism and concordance of the topset, thus suggesting an upbuilding (aggradation) of the deposit coincident with the prograding foreset. These features are characteristic of a low energy environment with a relatively low sediment supply (Sangree and Widmer, 1977), rapid basin subsidence and/or rapid sea level rise (in order to preserve the topset).

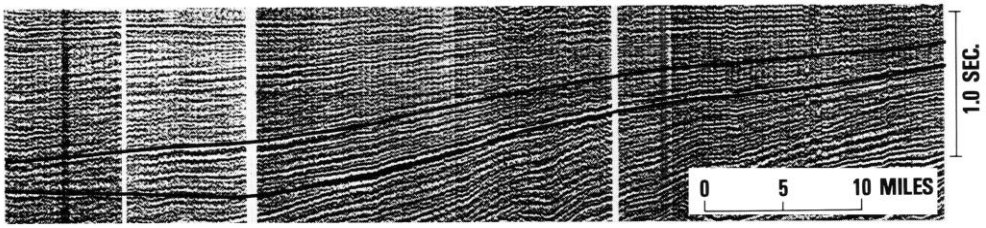

Figure 5.9 – Seismic example of a sigmoid reflection configuration. From Mitchum *et al.* (1977b).

Oblique configuration is interpreted as a prograding clinoform pattern of steep dipping strata with a toplap termination at a horizontal or subhorizontal upper boundary and a downlap termination at the bottom boundary. Due to the foreset steepness, the new strata builds almost laterally. They start to form from a constant upper surface without a topset segment and have pronounced toplap terminations of the foreset strata. Unlike the sigmoid configuration where the foreset has a small dip of around 1°, the foreset for this configuration can reach up to 10°. In the **tangential oblique** pattern the dip diminishes gradually in the foreset generating a concave-upward architecture that passes onto a gently dipping bottomset (Figure 5.10). Towards the bottom the strata becomes thinner and has downlap termination. In the **parallel oblique** configuration the foreset maintain its high dip from the top to the bottom where it has a downlap termination at a high angle with the lower boundary. The oblique progradational configuration owes its formation to a high energy sedimentary regime characterized by a high sediment supply (Sangree & Widmer, 1977), slow to none basin subsidence or a stillstand of sea level to allow sediment bypass and scouring of the upper depositional surface.

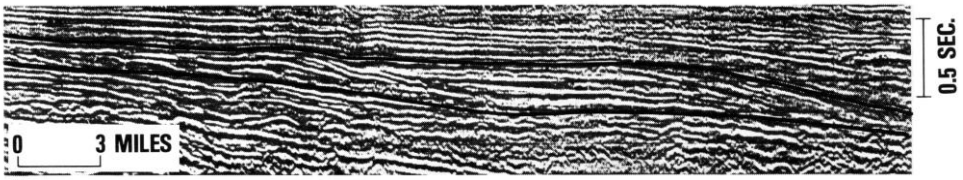

Figure 5.10 – Seismic profile displaying mostly tangential oblique configuration, with some sigmoid (from Mitchum *et al.*, 1977b).

The **complex sigmoid-oblique** configuration is a complex prograding clinoform made up of a combination of variably alternating sigmoid and oblique progradational configurations within the same seismic unit (Figure 5.11). The top sector is characterized by a complex alternation of horizontal sigmoid topset reflections and segments of oblique patterns with toplap terminations. This architecture suggests an alternate history of upbuilding and depositional bypass on a high energy environment. As for the rest this configuration resembles the sigmoid configuration. With the exception where the toplap termination is prominent, the topset has small segments of toplap termination that are usually bellow seismic resolution, these small scale units are interpreted as discrete lobes of a prograding depositional unit.

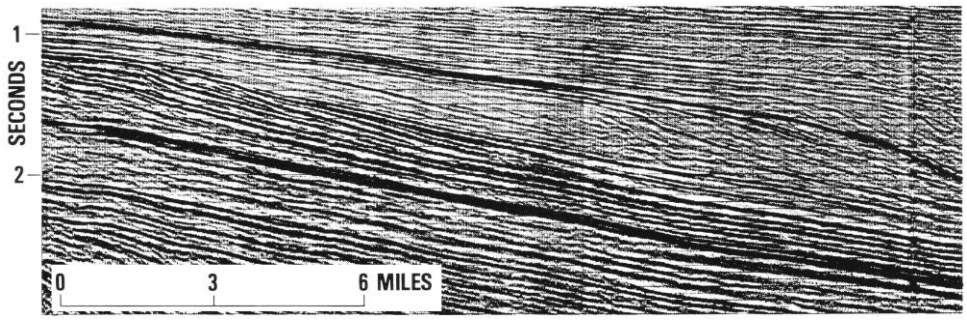

Figure 5.11 – Complex sigmoid-oblique reflection pattern on seismic profile (Mitchum *et al.,* 1977b).

Shingled configuration (Figure 5.12) is a thin prograding pattern, commonly with parallel top and bottom boundaries and with gently dipping parallel internal reflectors oblique to these boundaries that terminate with apparent toplap and downlap. The few internal reflectors show little to none overlap. The overall pattern of this configuration resembles much the parallel oblique configuration, except that of the thickness of the unit that in this case is much thinner just above the seismic resolution for the gently dipping internal reflectors. This configuration is generally interpreted as prograding seismic units formed in shallow water.

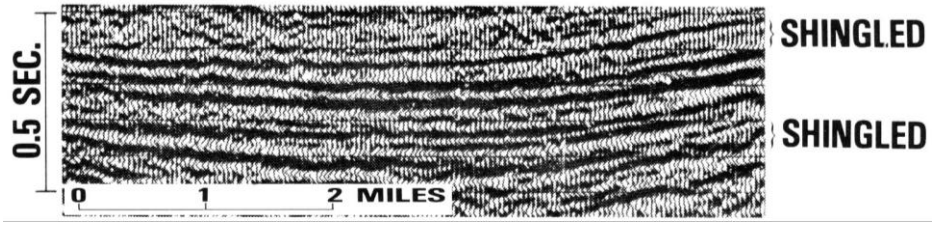

Figure 5.12 – Shingled patterns on strata from section of a seismic profile, from Mitchum *et al.* (1977b).

The **hummocky** clinoform consists of irregular discontinuous and subparallel reflection segments forming a somewhat irregular pattern marked by non-systematic termination and splits (Figure 5.13). The undulation of the reflections is small and just above seismic resolution. Usually this pattern laterally passes onto another type of better defined larger clinoforms and upwards to parallel reflections. This pattern is interpreted as the strata forming small, interfingering clinoforms lobes forming in a shallow water prodelta or interdeltaic environment.

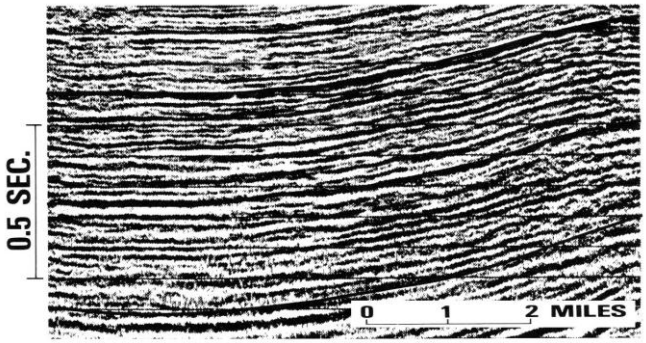

Figure 5.13 – Example of hummocky clinoforms from seismic profile, from Mitchum *et al.* (1977b).

5.3.4. – External form of seismic units

This classification is used to identify and distinguish one seismic unit from the adjacent ones and is also useful to infer a unit's depositional environment. A seismic unit's form is dependent, among other factors, from the form of the surface on which it lies. However, some caution must be taken when addressing this matter if there is a poor seismic coverage and the studied object is poorly imaged. Also, the lateral extent of seismic sequences can exceed the seismic coverage so this is why lateral terminations only play a minor role in this kind of analysis. With respect to this matter, the seismic units can be classified as (Mitchum *et al.*, 1977b, Figure 5.14): sheet, sheet drape, wedge, bank, lens, mound and fill; latter subdivision may apply as these terms can occur in a variety of minor shapes. Their depositional environment is briefly outlined bellow.

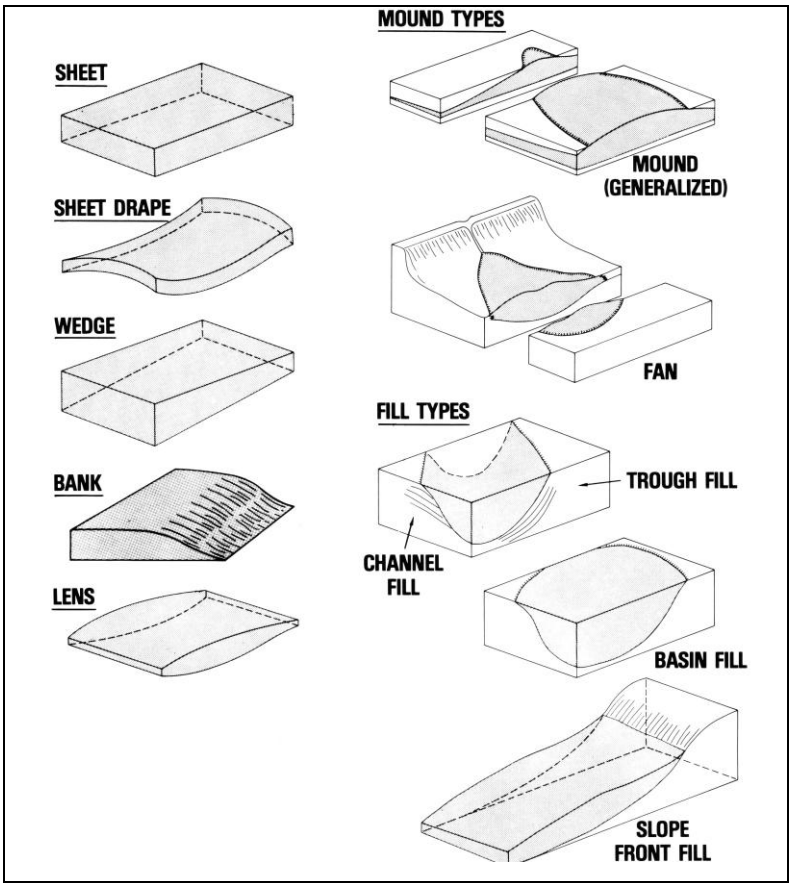

Figure 5.14 – External forms of seismic facies units (from Mitchum *et al.*, 1977b).

External forms as **sheet**, **wedge** and **bank** can reach over large areas, are commonly associated with platform deposits and can display internal configurations as parallel, divergent or prograding. **Sheet drape** forms are usually associated with pelagic or hemipelagic sediments deposited in a low energy environment or in deep domains. **Lobular** forms are common in a slope environment. **Mound** forms type can be of different origins (mound s.l., fan, carbonate edifications and diapirs) and their dimensions are usually small,

the internal reflection's configuration is varied and when associated with detritic deposits it reflects a high energy event. **Fill** type deposits like the mound type ones can have different configurations (onlap, chaotic, prograding, divergent, ...), however these deposits may reach over larger areas when is a basin context or can be smaller when in a dependency of a channel.

5.4 – Summary of the concepts

The study of seismic parameters and seismic facies analysis is an important task as a wide range of geological information can be extracted from the study of seismic profiles. These are summarized below.

Table 5.1 – Types of geological information that can be drawn from the seismic facies.

Seismic facies parameters	**Geological information given**
Continuity	Strata continuity, depositional environment
Amplitude	Acoustic impedance contrast, strata spacing
Frequency	Strata thickness
Reflection configuration	Bedding type, depositional processes, erosion events, paleotopography
External form	Depositional environments, sediment source

Table 5.2 – Inventory of the parameters to identify for the seismic analysis and interpretation.

Seismic facies analysis	
Termination of reflections:	Onlap Downlap Toplap Truncation
Characteristics of reflections:	Configuration Continuity Amplitude Frequency
Configuration of internal reflections:	Parallel Subparallel Divergent Chaotic Transparent Semitransparent Prograding: Sigmoid Oblique Sigmoid-oblique Shingled Hummocky

External form of seismic units:	Sheet Sheet drape Wedge Bank Lens Mound Fan Fill

5.5 – Interpretation procedure

As stated before, seismic stratigraphy interpretation aims to determine the geological meaning of the information contained in the seismic profiles, allowing the identification and correlation of depositional units, infer their depositional environment and the tectonic deformation imprinted on them.

The first step consists on defining which seismic units/sequences are going to be defined based on the reflections facies, termination and the unit's internal configuration. The following stages of the interpretation include the determination of the lithologies, depositional environments and tectonic history.

By definition, and following the work flow adopted in this task, it involved: 1 – recognition of the unconformities; 2 – definition of the seismic sequences; 3 – seismic facies analysis; 4 – stratigraphic calibration of the seismic record with cores and/or samples; 5 – determination of the lithologies by the seismic record facies (in the absence of cores); and 6 – try to establish connections between seismic facies, lithology type, depositional environment and tectonics. However, this is a complex task and several constrains existed and a description follows.

5.5.1 – Restrictions/Constraints

One of the main tasks was to establish a tectonostratigraphic model, this was done with some selected horizons, and several constrains were present during this task. One of the first constrains was related with the data itself: the dataset included mcs profiles from several surveys, dating from 1974 to 2006, acquired with different equipment, horizontal and vertical resolution, spacing between the profiles and different processing and filters were applied on different surveys. Furthermore, part of the mcs dataset was old and only available on paper; profiles were rasterized, converted to seg-y, georreferenced and imported onto the workstation running the Landmark software. Also, different surveys had distinct objectives: some were scientifically focused whilst others were aimed for hydrocarbon surveying. Altogether, the mcs dataset is composed by a wide array of profiles that vary much from each other. These were important restrictions to the work to be carried out. Regarding the

older mcs profiles, the process of converting paper profiles into digital format has errors associated with the scanning of the images, which had to be corrected by an image editing software and then converted to a seg-y file type through a script by the MacRae (2001). After this step, the seg-y format had to be spatially georreferenced using the coordinates for the CDP or shotpoints of the profiles. At the end, each seg-y file is available in the Landmark application suite and positioned together along with the other profiles. Different goals for the surveys also interfere with the seismic analysis, as some have a regular spatial distribution and profiles are parallel and orthogonal to each other with several points of intersection, whilst other surveys have very few intersection points between the profiles (and with other profiles from other surveys) and lines are of different orientations and lengths and no regular spacing exists (Figure 5.15). Thus, it is clear that the resolution and quality of the interpretation based on the distinct surveys is very different.

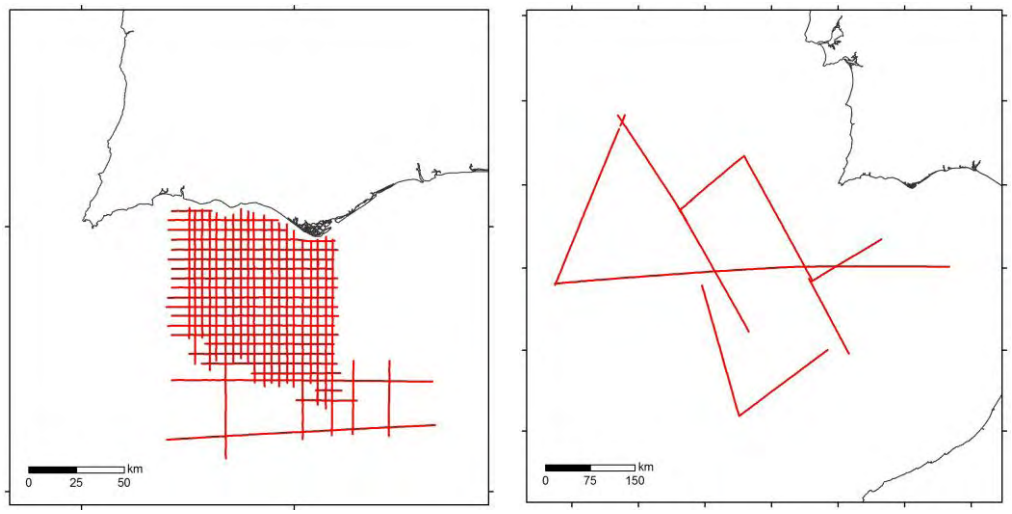

Figure 5.15 – Example of two different surveys: Chevron (left) and Arrifano (right). It is clear that the spatial distribution, orientation and intersection points is very unlike on the two surveys.

In the Algarve basin (vicinities of the Portimão canyon) and the rest of the Gulf of Cadiz the surveys are very inconsistent, in the first case the surveys present a dense and regular pattern with many intersection points whilst for the last several surveys the profiles have different orientations and do not have many tie lines. Another factor, also present is a strong limitation to the interpretation: the profiles do not present a dense network and to some extent may not sample all of the features in the area and the interpretation may leave out some features that may be important to the understanding of the geology of the area.

5.5.1.1 – Positioning

The positioning of the seismic profiles may also present some limitations (at different levels) to the seismic interpretation. Firstly, old surveys are likely to have more errors in the position of the profiles as the technology used is not compared to surveys performed 30 years later.

Another level of uncertainty may be present when working with mcs profiles from different surveys, as different methods (with different precision) and equipment were used to position each one. This may be especially relevant when dealing with intersections of profiles.

5.5.1.2 – Data quality

Given the wide variety of ages for the surveys, another factor that may also interfere with the interpretation is the quality of the data itself. Besides the already mentioned fact that some of the profiles were only available in paper format, the acquired seismic data have different degrees of quality as the technology available to record this data has greatly evolved throughout time. This involves not only the acquisition equipment, but also, the apparatus related with the recording (amount of data that can be recorded, overall and during a time interval). Another factor that can influence data quality is the weather, because bad conditions can cause artifacts to be present in the profiles or give different facies to the units when compared to adjacent profiles collected with better conditions. Regarding the penetration/resolution compromise, the profiles used have similar parameters with good horizontal and vertical resolution and a medium, yet adequate penetration. The IAM survey profiles are the only exception as they have more penetration. Although similar, different surveys were acquired with different spatial resolutions and distinct vertical sampling.

5.5.1.3 – Post-processing

Seismic signal processing also influences the interpretation; despite all the profiles are time migrated (not stacked) differences are present and detectable at the intersections. This is due to different parameters used and the post processing procedures carried out. Also different filters, on different surveys, were applied and some change the seismic facies of the units and this represents sometimes a limitation to the stratigraphic correlation between sedimentary packages.

5.5.2 – Tectonostratigraphic Model

In order to study the genesis and evolution of the south Portuguese margin submarine canyons, several mcs profiles were analysed, from this analysis and its interpretation several horizons were selected for this work. The importance and geological meaning of each reflector is different and these were selected because are the ones that correspond to major regional events with a meaningful geological sense, crucial to understand the genesis and evolution of the submarine canyons in particular and the SW Iberia in general.

For both the South and Southwestern Portuguese Margins, Roque (2007) identified and selected major discontinuities in the seismic records in order to define seismic sequences then performed seismic facies analysis. This led to the establishment of a

seismostratigraphic model (Figure 5.16), age-calibrated by 5 oil industry drills and 3 piston cores in the Algarve Basin, and in 2 DSDP drills in the Western margin.

The reflectors selected for this work where identified in Roque (2007) seismic stratigraphic model and their ages determined according with the ones of that model. The calibration was carried out using the multichannel seismic reflection profile AR-10 in the Marquês de Pombal Plateau. The five reflectors chosen for this work correspond in Roque's model to the M unconformity, base of MW3, base of MW4, top of MW5 and base of MW7 (Figure 5.17).

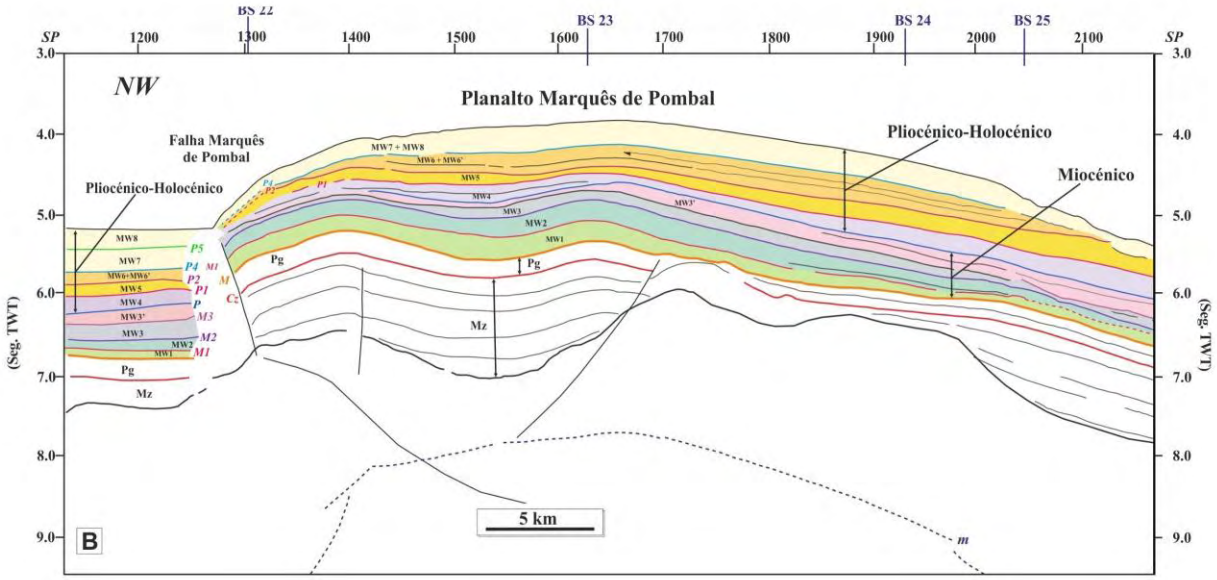

Figure 5.16 – Stratigraphic model of Roque (2007) on seismic profile AR-10.

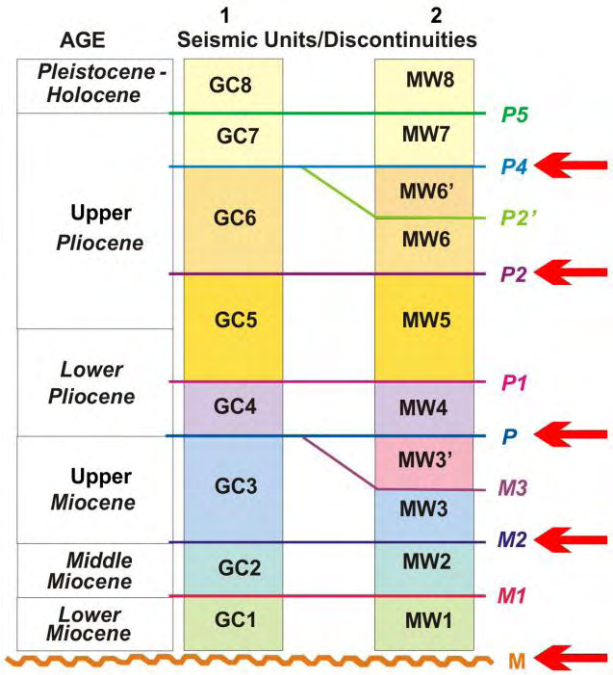

Figure 5.17 – Chronology and seismostratigraphic correlation between the Gulf of Cadiz (column 1) and the Marquês de Pombal/SVC/Upper Sagres Plateau according to Roque (2007). Red arrows indicate the selected horizons for this work.

The selected reflectors were chosen due to their relation with particular geological events that took place in this area.

Using the referred selected horizons, the work carried out consisted on: 1- to characterize each of the selected discontinuities (and the seismic parameters of the units they bound), 2- to perform the tectonostratigraphic correlation between the different areas (identify the horizons in all the available mcs profiles in order to produce the thickness maps and understand the variability of the sedimentary packages throughout the area), 3- to identify the various tectonic structures (classified by their geometry, kinematics and activity period), 4- to produce a tectonic map, and 5- to analyse the horizons from the chronostratigraphic point of view in order to date the processes they are associated with. These tasks are of extreme importance in order to understand when the major tectonic and sedimentary/erosive processes took place, when they were most active and which features can be identified on the stratigraphic record to characterize these processes. This is done in order to determine when canyon formation took place, when in time and space their evolution took place and which processes throughout the geological time were the most relevant.

5.5.3 – Seismostratigraphic correlation criteria

Besides the constraints previously stated, there are others more related to the geology itself that limit the establishment of a seismostratigraphic model, correlation and interpretation, such as: basement highs, salt diapirs and fault zones that interrupt and/or displace the sedimentary cover, major erosive features like canyons and valleys that disrupt the stratigraphic continuity of the horizons, and presence of units that are not present at a regional scale and cannot be correlated to other places.

Several tectonostratigraphic domains were defined by several criteria: geological, morphological, sedimentary and tectonic. The selected horizons were marked throughout the area starting in the Marquês de Pombal Block where they were chronologically calibrated with Roque (2007) seismostratigraphic model. The reflectors where then marked onto the other domains in all the available mcs profiles in a way to cover all the domains and entire area. This procedure was first carried out between different mcs profiles at the intersection points and between different domains by identifying marker horizons or marker units. These have a wide spatial distribution, distinct seismic facies and are easily identified, therefore are of great importance when attempting correlation between sedimentary packages.

5.6 – Seismostratigraphy overview

The interpretation of the vast available seismic reflection profiles of the south and southwest Portuguese Margin by Roque (2007) allowed the establishment of three seismic mega-sequences that correspond to major tectonostratigraphic mega-sequences calibrated using the stratigraphic information of the oil industry wells (Figure 5.16 and 5.17). Although previous works (Terrinha, 1998; Lopes, 2002; Lopes *et al.*, 2006) had already published stratigraphic correlations for the Algarve Margin, the more recent work of Roque (2007) extended the correlation from the south to the southwest Portuguese Margins, and revised the biostratigraphy of the wells reports.

The seismic mega-sequence 1 is the oldest and corresponds to the Mesozoic sediments. It lies on top of the Paleozoic basement or the acoustic basement; its upper limit is either the unconformity at base of Paleogene deposits or the Miocene basal unconformity. The deposits that constitute this lower mega-sequence display internal reflections with variable amplitudes with low lateral continuity. This mega-sequence is made up of two sedimentary sequences, the Triassic-Jurassic and the Cretaceous, separated by a major discontinuity. Their seismic facies is similar in the Algarve Basin and in the S. Vicente submarine canyon area.

The seismic mega-sequence 2 corresponds to the Paleogene deposits and is bounded by the Paleogene basal unconformity (P) at the base and the M unconformity at the top. The lower unconformity is widely recognized in the Algarve Basin by its strong amplitude and large spatial continuity; it also corresponds to a hiatus between the Lower Cretaceous (Upper Cretaceous was not found in any of the drillings) and Upper Paleocene. It denotes a clear erosive behaviour as it truncates the Mesozoic sediments of the lower seismic mega-sequence.

The seismic mega-sequence 3 consists of Neogene sediments and its lower limit is the Miocene basal unconformity (M) and the top is the most recent deposit at the seafloor; the first is a major feature in the seismic record throughout the whole area as it is easily recognised by its high amplitude, relatively irregular geometry and erosive behaviour cutting into any older materials. This mega-sequence is made up of ten seismic sequences after Roque (2007) and some of the inner discontinuities were mapped in this work because this mega-sequence is the one that records the major events regarding the genesis and evolution of the studied submarine canyons.

5.7 – The Multichannel Seismic Profiles

The interpretation of the available seismic profiles together with the mapping of the selected horizons and production of depth and thickness maps was made in order to try to understand the geological processes and timing of the formation and evolution of the S. Vicente canyon.

This section displays selected MCS profiles (their positioning is presented on Figure 5.18, at the end of section 5.7), its interpretation and the main conclusions drawn. The two main discontinuities of the base of Paleogene (P) and Miocene (M) were identified in almost all the extent of the profiles and wherever possible other reflectors were also mapped. In all the profiles the red reflector is the Paleogene unconformity, the green is the Miocene unconformity, the dark blue is the base of MW4 unit (Lower Pliocene), the light blue is the top of MW5 unit (near base Upper Pliocene), the orange is the base of MW7 unit (Upper Pliocene) and the yellow reflector is the surface that corresponds to the start of the uplift of the Marquês de Pombal Block.

5.7.1 – MCS profile BS07

The BS07 multichannel profile images a time section across the S. Vicente canyon in its head sector at relatively shallow water depths (Figure 5.19, at the end of section 5.7).

With the exception of the northwestern tip where a more than 1.0 sec TWT thick sedimentary basin is imaged, the sediment package is very thin, reaching less than 0.2 sec TWT. In the southeastern tip of the profile, in the upper Sagres Plateau, although the seismic architecture is not perceived due to the strong interference with the multiple, it is not probable that a thick sedimentary package is present since it corresponds to a structural high and the Meso-Cenozoic sedimentary cover onshore is strongly condensed when compared with the equivalent record in the Lusitanian and Algarve Basin (Manuppella, 1988; Terrinha, 1998; Kullberg *et al.*, 2000). The area between SP 1520 and 1630 also corresponds to a basement high with none to very thin Cenozoic sedimentary cover.

To the northwest, the two depressions correspond to tributaries of the S. Vicente canyon, imaged in the central sector of the profile (see location on Figure 5.18). The strong amplitudes displayed in the bottom of these two tributaries suggests on-going erosion, in agreement with the thin sedimentary cover in those areas.

In the canyon area (SP 1400-1520), the Paleogene and Miocene basal unconformities are present and easily identified by their strong acoustic signature. On top of these unconformities some deposits are present, the sedimentary package is thin and of chaotic facies. Some undulated reflections are present and together with the many truncations identified, they suggest the presence of erosion and gravity instability on these deposits. The

steepness of the flanks also favours these processes and altogether they can be responsible for the diminute thickness of the Neogene package.

In the northwest, the Miocene unconformity truncates the whole underlying sedimentary package and to the southeast the Paleogene deposits are very thin emphasizing the erosive behaviour of the basal Miocene unconformity.

5.7.2 – MCS profile BS08

This seismic profile (Figure 5.20, at the end of section 5.7) images, from NW to SE, the Alentejo Basin and a small channel that drains towards it, a structural high, the S. Vicente canyon and its flanks and the upper Sagres Plateau.

The Alentejo Basin (2 sec TWT thick) and the Upper Sagres Plateau are the areas where the sedimentary thickness is greater, as opposed to the canyon's floor and flanks which are heavily eroded and therefore the sedimentary thickness is much thinner.

In the Alentejo Basin, the Cenozoic reflectors are slightly tilted towards the northwest and are located much deeper than in the basement high (SP4000) due to a normal fault with downthrow of the western block. In this block, the lower units display onlaps on top of the Miocene unconformity, which truncates the whole Paleogene sedimentary package and its basal unconformity. This fault outcrops at the seafloor (around SP 3840) underneath a small channel that flows to the west. East of this channel, a thin amount of Neogene deposits seat on top of the planar westward dipping Miocene basal unconformity (SP3850-4100). In the canyon's bottom and flanks, the sedimentary cover is highly affected by the bottom process and displays signs of gravity instability and slumping. This fact suggests that throughout time, the sediments were not able to settle and accumulate as they were strongly affected by erosion and mass movement processes (Figure 5.21).

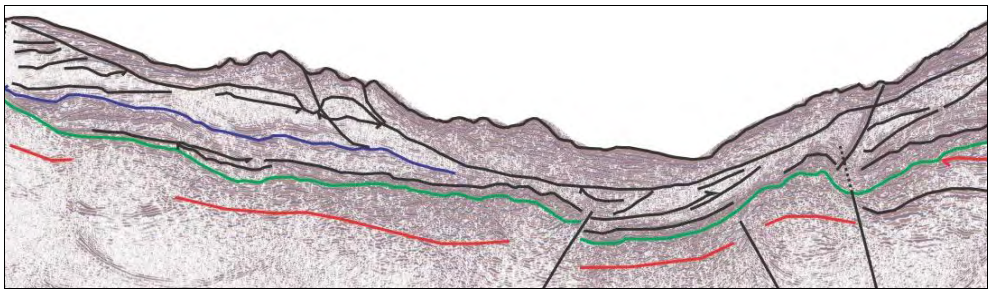

Figure 5.21 – Section of BS08 MCS profile (SP4200-5150) in the canyon area displaying the thin sedimentary package affected by erosional processes.

To the east, the Miocene basal unconformity cuts deep into the sedimentary sequence along the main canyon channel, where a maximum of around 1 sec TWT sediments thickness have been deposited. The Miocene unconformity is picked on top of acoustic basement that possibly corresponds to Mesozoic strata (SP3700-3820). The reflectors are frequently

disrupted, display low amplitudes and their undulated geometry also point to gravity driven processes, namely slumping. Although a seismic stratigraphic model is difficult to establish here due to the instability of the sedimentary package and seismic facies variations, it seems that a significant portion of the materials found in the canyon axis derive from the materials that collapsed from the walls and also from upslope material dragged to this area. Near the canyon axis several faults can be identified, these structures are not outcropping and are post-Paleogene as they affect the Miocene basal unconformity but no more accurate age can be provided because the sediments are not easy to correlate.

To the east of SP 5200, the sedimentary thickness reaches over 2 sec TWT for the Cenozoic alone. Like in the western tip, the Miocene unconformity obliterates almost the whole Paleogene unit and with the exception of the lowermost materials and those closer to the seafloor in the flank, the reflectors are continuous and parallel forming a package of alternating high and low amplitudes.

5.7.3 – MCS profile BS09

This MCS profile (Figure 5.22, at the end of section 5.7) is a time section across the north sector of the Marquês de Pombal Plateau (MPP), the S. Vicente canyon and the SW tip of the upper Sagres Plateau.

The profile is parallel to BS08 and one important differing factor is that in this one the sedimentary record is thicker when compared to the previous one where only a thin and very disturbed sedimentary cover was present above the Miocene unconformity.

The Miocene unconformity is well identifiable by its strong amplitude and truncation of the underlying reflectors and by the onlaps of the overlying Neogene units. On the MPP, some faults affect the Miocene unconformity and the lower units. In one case (SP1920), a dating for the fault's activity can be ascribed to the Late Miocene due to the presence of onlaps on top of the associated drag fold (Figure 5.23) that was undergoing local subsidence.

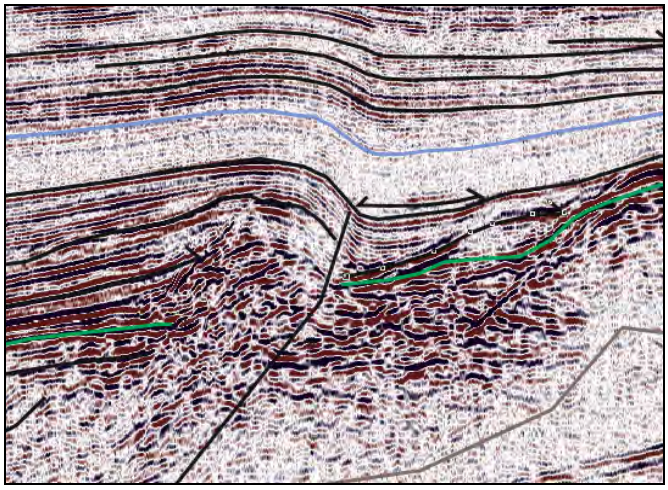

Figure 5.23 - Section of BS09 (SP2000-1850) imaging the reverse fault on the MPP.

Within the Neogene package, several internal discontinuities can be identified defining several units (MW1 trough MW8, after Roque 2007) that have different seismic facies. Unit MW5 is semi-transparent whilst units MW7 and MW8 display parallel reflectors with high amplitude. Units MW7 and MW8 display an overall wedge shape thickening towards the canyon, thus suggesting that the process responsible for its formation is related with the SVC and the processes taking place there. Given the pattern defined by its seismic facies (alternating high and low amplitude reflectors), together with the overall geometry of the unit and the geological setting, it is probable that this sedimentary package corresponds to overbanking deposits generated by the SVC, and thus levee deposits.

On the MPB, reflectors of unit MW4 and upwards, are continuous and parallel, gently folded and slightly tilted towards the west. Unit MW5 and MW6 display consistent onlaps towards the east suggesting that the present day canyon area was higher than the MPP, also consistent with the westwards dip of the units. This was probably the result of the uplift caused by the thrusts in the SVC area.

Near the submarine canyon, the lower units (lower Miocene and older) display evidences of deformation (affected by folds and faults) and the reflectors are frequently disrupted due to this deformation. The younger sedimentary units are greatly disturbed by the mass wasting processes taking place in the flanks of the canyon (Figure 5.24). Whilst in the western flank slumping takes place affecting the whole flank (above the marked surface), in the eastern flank besides slumping it also seems that gravity is triggering movement and rotation of large gravitational slides.

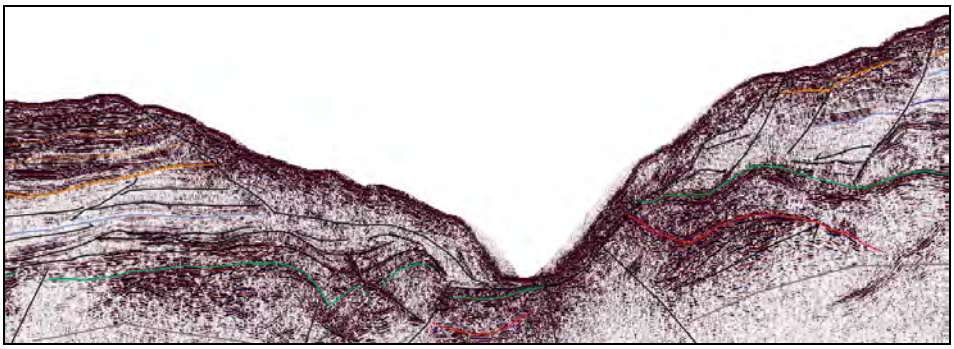

Figure 5.24 - Section of BS09 (SP1800-1200) displaying the mass wasting processes on both flanks of the canyon: slumping on the western side and rotational slides on the eastern side. Also to be noted the thrust that uplifts the entire eastern flank of the SVC.

The very high amplitude of seafloor in the bottom of the canyon suggests that erosion is taking place on that area; the chaotic facies of the sediments near the bottom also corroborates this idea since they might have resulted from older erosive events and are now being eroded and transported downslope along the canyon path.

The canyon's flanks are also experiencing erosion, testified by the presence of a thin package of debris that make up the uppermost deposits and display chaotic seismic facies

(often with high amplitudes) where the reflectors are frequently disrupted, therefore with small lateral continuity; all these are evidences of erosive and mass transport processes.
Near the base of the eastern flank, a westwards verging thrust outcrops (the S. Vicente Canyon Thrust), uplifting the eastern sector. The eastern flank of the canyon displays some preserved Paleogene deposits, on the remaining of the profile these were interpreted with some doubts. The Paleogene basal discontinuity truncates the underlying reflectors and the units above it display reflectors with low lateral continuity some of high amplitudes and evidences of deformation as they are affected by faulting and folding. These structures are also responsible for the undulated geometry and segmentation of the Miocene unconformity.
Still on the western side, the Neogene units are disrupted by large slides that dip towards the lower parts of the SVC. The associated gravity instability disrupts the reflectors and is responsible for their undulated geometry, only the easternmost part of the profile is not affected by slumping and gravity instabilities, displaying continuous, parallel reflectors of alternating medium to high amplitudes.

5.7.4 – MCS profile BS10

BS10 MCS (Figure 5.25, at the end of section 5.7) is a section across, from the NW to SE, the Rincão do Lebre Basin (RLB), the elevated Marquês de Pombal Block (MPB), the S. Vicente submarine canyon and flanks and part of the south Portuguese continental slope.
The Mesozoic units display a more transparent seismic facies with few reflectors of low amplitudes that are often folded. The Paleogene and Miocene basal unconformities display high amplitudes and are subparallel, therefore important truncatures are not observed. The Paleogene package is around 200 msec TWT and displays continuous reflectors with high amplitudes; however the Paleogene package was not identified in the canyon area. The Neogene package displays several internal units with different seismic facies separated by discontinuities that can be identified by the geometry of reflectors terminations.
Beneath the flat seafloor of the RLB, a basement high is present (SP1850) that is onlapped by the sedimentary units older than the Lower Miocene. These units are also thicker in the small basin eastwards of the basement high than in the monoclinal that connects to the MPB. The onlaps on the Neogene package are present on both sides of the basin or towards the east in a way that reflects the thickening of the sedimentary package in the referred basin especially in the MW4-5 units where an increase of about 20% in thickness is observable.
To the SE, in the monocline that connects to the MPB, the Mesozoic units display gentle folds and some internal truncations (SP2600) and Cenozoic units are gently folded with the more recent sediments affected by slumping due to the high gradients of the seafloor.

Near the top of the Marquês de Pombal Plateau, a southeastwards directed reverse fault is observed (SP3050), with major activity in Lower Pliocene times as most of the onlaps are found in the footwall on the MW4 and MW5 units (Figure 5.26). This fault is probably related with another one with the same geometry and activity period that is imaged in profile BS09 (Figure 5.23), furthermore both structures are found nearby and on the same geological setting.

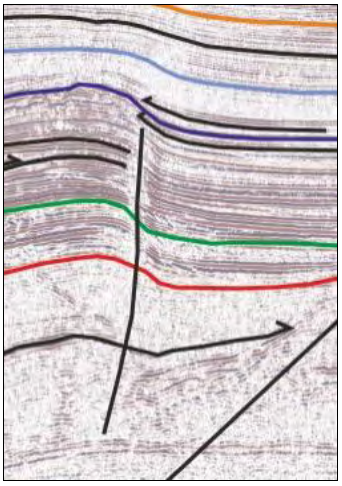

Figure 5.26 – Section of MCS profile BS10 (SP2000-1850); onlaps on fault zone near the top of the MPP, in the deeper areas the reflectors are displaced and in the areas towards the top the reflectors define onlaps on the downthrown side of the fault, dating its activity.

Eastwards of this fault, a basement high is present (SP3200) and the units older than the Miocene display onlaps on top of this high. Towards the SVC area a slight thickening of units MW4 and MW5 is observed.

In the canyon area, the older sediments are affected by two faults, however these do not seem to affect the Miocene package.

The sedimentary sequence of the Marquês de Pombal Plateau is not present on the canyon area, where the erosive valley cut down to close to the M unconformity, nor on its eastern flank, where the Cenozoic seismostratigraphic record although present displays a different facies. Both flanks of the canyons display slumping and mass movements in the deposits closer to the seafloor and in the canyon axis area some deposits accumulate above an erosive surface.

Near the axis and towards the east, a high amplitude surface is present (dotted line on the profile). Due to its unusual high amplitude and geometry it is interpreted as a multiple erosive surface, the presence onlaps on its top (that could correspond to the first deposits after the last erosive event) is also in agreement with this.

Beneath the present day canyon axis, a particular sedimentary package with a distinct lobular architecture is present (grey shaded body). This unit is probably related with the erosive surface to the east and could constitute a deposit resulting from the erosion on the

referred surface as they appear to have the same age and are closely spatially related (Figure 5.27).

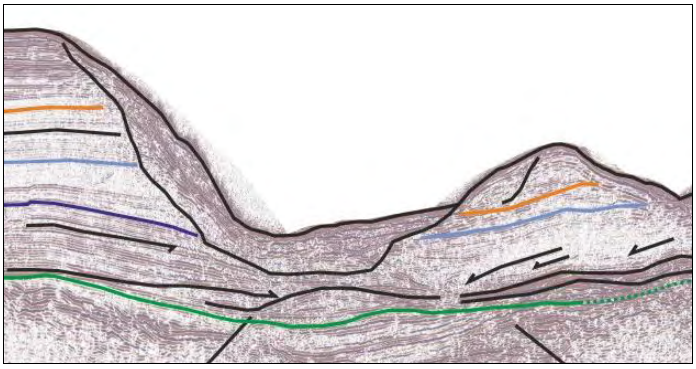

Figure 5.27 - Section of BS 10 (SP3250-3600) in the SVC area displaying the accumulated sediments (debris) above one paleo-erosive surface and beneath the canyon's axis the lobular-shaped sedimentary body at the tip of the high amplitude erosive surface just above the Miocene unconformity.

The eastern flank displays several slumps and slide scars, some buried and preserved in the seismic record and others that cut through to the present day seafloor. The slumping processes are well depicted in the low amplitudes of the seismic record as well as by the numerous onlaps towards downslope (west) on top of the lower surfaces (near base of Miocene). These mass movements affecting the deposits, together with the fact that the western side of the canyon was an elevated block (the unconformities are also higher towards the west) account for the minute thickness of the sedimentary package on the western flank.

Eastwards, near the top of the canyon's wall a major disturbance on the older seismic units is present (SP 3800). It can be related to a basement high although its geometry is not typical, or can be associated with a magmatic intrusion (Figure 5.28). This feature also separates two domains; the one to the east has a thicker sedimentary column, dips in a different direction and due to its location appears to be more related to Meso-Cenozoic Algarve Basin than with the Western Atlantic Margin.

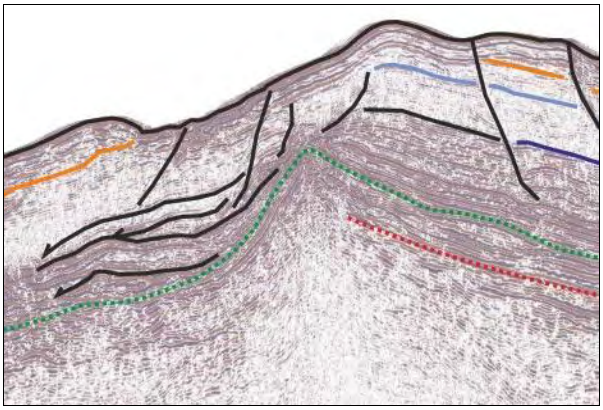

Figure 5.28 - Section of BS10 (SP3650-3850) displaying the basement high with sharp boundaries and the different seismic facies of the sedimentary package on both sides.

In this area the mass wasting processes do not seem to be as much important (affecting only the more recent sediments closer to the seafloor), and the original seismic architecture and facies of the sedimentary units are better preserved.

5.7.5 – MCS profile BS20

This multichannel seismic profile (Figure 5.29, at the end of section 5.7) images the sub-surface structure, from west to east, of the Infante D. Henrique Basin (IDHB), the Marquês de Pombal scarp and Plateau, the S. Vicente Canyon and the western tip of the Upper Sagres Plateau. Although the Marquês de Pombal Thrust is not imaged in this profile, the mapped yellow reflector that marks the beginning of its activity and the uplift in the area is mapped.

In the western sector (IDHB), the sedimentary package is sub-horizontal, while to the east in the MP scarp it is gently tilted and folded, and in the central sector of the MPB it is again sub-horizontal, with the exception of some minor folds; more to the east, the sediments are deformed and affected by slumping in the canyon area and subhorizontal in the Sagres Plateau.

The Mesozoic sedimentary package is just over 1 sec TWT thick in the western tip of the profile (west of the basement high). Here, several Mesozoic reflectors are truncated by the Paleogene basal unconformity that is itself truncated by the erosive basal Miocene unconformity, evidences for strong erosion on Early Miocene times. Thus, the Paleogene deposits are thin, not exceeding 200 msec TWT in general and even less east of the basement high near the western tip. Above the basal Miocene unconformity, the first units do not display a well-defined inner structure as only some reflectors are identified in the middle of a relatively transparent facies unit. Unit MW1 displays onlaps on the Miocene unconformity (above the structural high). Unit MW3 and the ones above it display chaotic facies bodies and onlaps towards the MPF. Units MW3, MW7 and MW8 display higher contrasting acoustic facies, whilst units MW4 and MW6 have some well-defined reflectors but with not so high contrasts; unit MW5 has seismic transparent facies.

At the Marquês de Pombal scarp, units MW3 and above are affected by slumping. The material that flowed downslope is likely related to the chaotic bodies found in the western sector. This is probably related with the activity of the MPT, located very close to this area. In the western part of the MPB, although the top of the basement is not imaged, the Mesozoic units are quite thick, probably around 1.5 sec TWT. The Paleogene sequence is thin due to truncation of these materials by the basal Miocene unconformity. More to the east, the Neogene units are no longer affected by mass-wasting processes (are away from the scarp with its high gradients, eastwards of SP 900) and are gently tilted to the west. In the lower units some onlaps towards the east are observed and are responsible for the higher

thickness of these units in the west. To the east, some truncations are observed (between SP1500-1700) inside MW2 and MW3 units and as result these reflectors are interrupted and not observed to the west.

More to the east, the same structure observed in profiles BS09 and BS10 (Figure 5.23 and 5.26) is again identified and the onlaps on the drag fold can be used to date its activity; the onlaps found in the MW1 unit (hanging-wall) show activity in Lower Miocene times and some onlaps found in MW4 unit (footwall) suggest a reactivation phase in the Lower Pliocene.

Above the structural high (just west of the SVC, SP2200), the Mesozoic series are condensed and eroded, attesting for the existence of a structural high during the Mesozoic that was subject of important erosion and uplift during the Paleogene.

The Neogene package is more than 1.5 sec TWT thick, one third made up by MW7 and MW8 units displaying subparallel reflectors with high amplitude contrasts that define a general triangular shaped unit thinning towards the west (Figure 5.30). Units MW4 and MW5 are thicker in the vicinities of the canyon (from the referred basement high to the east).

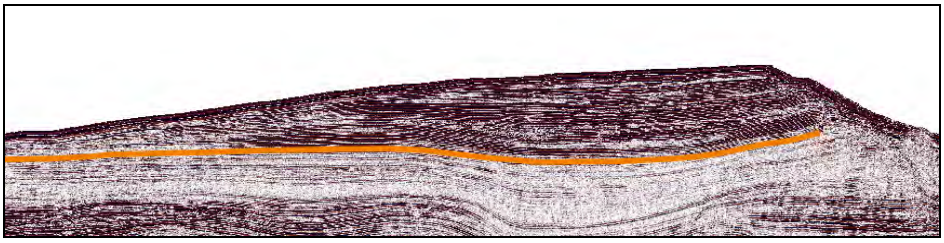

Figure 5.30 - Section of BS20 (SP1600-2400) west of SVC displaying the uppermost sediments where the levee deposits (units MW7 and MW8 above orange horizon) have a general triangular shape with thickening towards the canyon and high seismic amplitudes.

The western flank of the canyon is made up by a large body of material dragged/fallen from the wall with chaotic/transparent facies with few disrupted reflectors. These deposits seat on top of a surface that cuts down across most of the whole Neogene series, more than 1 sec TWT. However, just beneath the present-day submarine canyon, the thickness of these materials is much less than in the flank indicating that there is active downslope transport along the thalweg of the materials from the flanks when these reach the bottom of the canyon.

Below the SVC, the Mesozoic and Paleogene sedimentary packages are deformed, folded and truncated by Miocene unconformity.

In the middle of unit MW2, a lense-shaped unit is present, displaying chaotic seismic facies, probably as the result of the accumulation of debris at the tip (base) of an erosional surface that is identifiable to the west and displays very high amplitude (Figure 5.31). A similar setting was observed on BS10 seismic profile where an erosive surface with high amplitude

was present above the Miocene basal unconformity and to the west of this feature near its base a lense chaotic facies body was present.

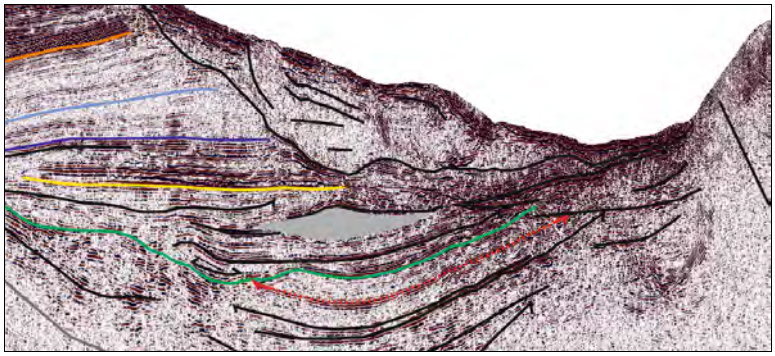

Figure 5.31 – Section of MCS BS20 (SP2250-2750); detail of the SVC area, displaying the truncatures of the Mesozoic reflectors, the thickening of the MW4 and MW5 units in this area, the slumped materials of the western flank, the lenticular body at the end of the high amplitude erosive surface and the tip of the thrust that uplifts the eastern body.

At the foot of the slope of the eastern flank there is a major reverse fault (the S. Vicente Thrust Fault) that is responsible for the uplift of the units on the eastern flank of about 1 sec TWT for the lower reflectors and about 1.5 sec TWT for the upper units (Figure 5.32). On the flank the sedimentary package is affected by the thrust and mass movements, only at the top of the upper Sagres Plateau it is possible to identify the well-structured upper sedimentary units underlain by more transparent seismic facies units and the Miocene and Paleogene unconformities.

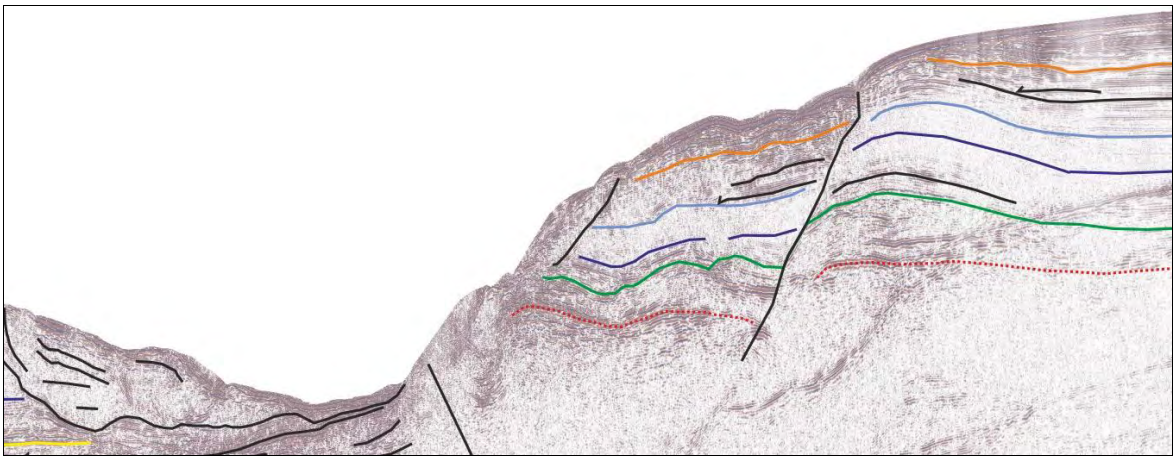

Figure 5.32 - Eastern section of the MCS BS20 (eastwards of SP2400) profile imaging the SVC axis and areas eastwards. The images nicely depicts the thrust at the base of the eastern flank that uplifts the entire flank and the gravity instabilities and associated disturbances on the deposits close to the seafloor. More to the east of the thrust, a structure is present that defines a collapsed block with is probably related with gravity instability that is also responsible for the slumping.

The onset of the uplift of the Marquês de Pombal Thrust (yellow reflector) was depicted by its truncations of underlying reflectors and onlaps from the ones above it in the Marquês de Pombal scarp area. In that area it also marks the appearances of chaotic bodies on the lower parts that corresponds to debris fallen from the uplifted block. It also marks the start of

the signs of gravity instability in the more elevated areas of the scarp, thus generating the chaotic facies bodies in the lower areas. All these evidences combined point to the start of the uplift of the Marquês de Pombal Block.

5.7.6 – MCS profile BS21

The BS21 MCS profile (Figure 5.33, at the end of section 5.7) strikes NW-SE and cuts across the Infante D. Henrique Basin, the Marquês de Pombal Plateau, the S. Vicente submarine canyon, the south Portuguese continental slope and the SW tip of the Upper Sagres Plateau.

The top of the basement can be relatively well constrained in the western sector of the profile as well as in the easternmost part of the MPB, as these areas are structural basement highs.

In the footwall of the MPT, the Mesozoic unit has a thickness up to 1.5 sec TWT, however only some reflectors are identifiable between the acoustic basement and the Paleogene unconformity. These onlap on top of the basement high in the east and the uppermost ones are truncated by the Paleogene unconformity at the top. On the hanging wall of the MPT, the geometry is similar with 1.3 sec TWT of thickness (Figure 5.34). Only a few reflectors are distinguishable, some top reflectors are truncated and several onlap towards the basement high on the east (close to the SVC). Eastwards of this basement high, the Mesozoic reflectors are few and the seismic architecture is not well perceived.

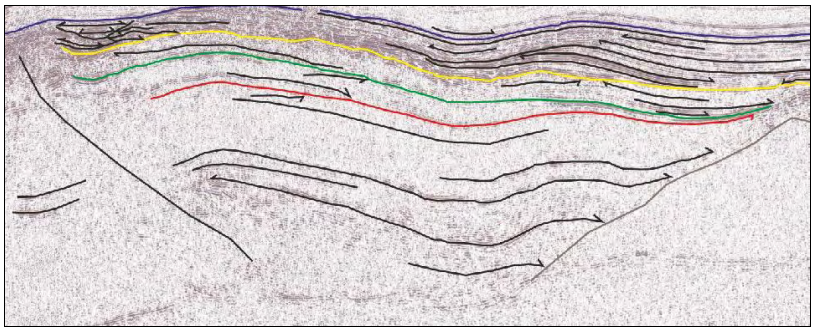

Figure 5.34 - Section of profile BS21 (SP2150-1200) imaging the central part of the elevated Marquês de Pombal Block where a thick Mesozoic package is present (below the red reflector, the base of the Paleogene) bounded to the east by a basement high.

The Paleogene package in the western part has a constant thickness of 200 msec TWT until the eastern tip of the footwall where it appears to be eroded in full by the Miocene basal unconformity at the top. In the uplifted MPB, the Paleogene sediments display a semi-transparent seismic facies with few and discontinuous reflectors. To the east, its thickness diminishes and it also appears to be truncated by the Miocene unconformity near the basement high (SP1200). Eastwards of the S. Vicente canyon, the seismic facies for the

Paleogene are different, the reflectors display high amplitudes with large acoustic contrasts (Figure 5.35).

Figure 5.35 - Section of the BS 21 (SP1500-500) in the SVC area, to be noted the distinct facies of the Paleogene sedimentary package on both sides of the canyon signaled by the two arrows; very high reflective on the eastern side with irregular reflectors and continuous of medium amplitude on the western side. The red horizon is the base of the Paleogene sequence.

This acoustic facies variation suggests that the present-day SVC area was a paleogeographical boundary between distinct depositional environments. The Paleogene package is affected by some faults and folds and therefore the precise identification of the base is more difficult than in the other sectors of the profile. However, like in the other sectors, it maintains its erosive behaviour as several truncations of the underlying Mesozoic reflectors are identified.

The Neogene package seats on top of the Miocene basal unconformity, easily depicted in most of the profile by its high amplitude and associated truncations of older reflectors and onlaps of the Lower Miocene sediments. Several units are present and separated by discontinuities, some of them easily identified. On the footwall of the MPT, the Neogene base obliterates the total Paleogene sequence. Upwards, in the Neogene mega-sequence, the base of the MW3 unit is also easily identified, because of the truncation of the MW2 reflectors and some onlaps on its top. The base of this unit marks the presence of several sedimentary wedges of chaotic facies (Figure 5.36) that might correspond to deposits at the base of the relief caused by the initiation of the uplift of the MPB and localized subsidence in this area (footwall).

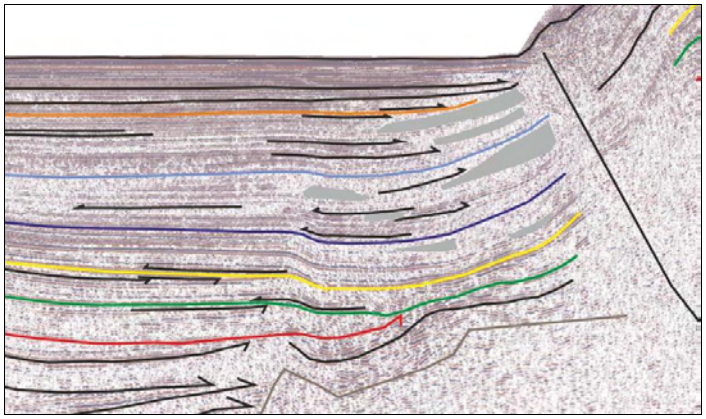

Figure 5.36 – Section of BS21 (SP2700-2200); the Marquês de Pombal Thrust (eastern side of the figure that cuts through the entire sedimentary package and reaches the seafloor) and its footwall displaying the truncation of the Mesozoic sediments by the Paleogene unconformity that is itself eroded by the Miocene basal unconformity. Several bodies of chaotic facies that correspond to debris originated from the uplifted block are present (grey). Yellow reflector marks the onset of these bodies and is therefore associated with the uplift of the MPB and the beginning of the activity in the MPF.

Unit MW5 has a transparent seismic facies that is not present in more recent units that display parallel high amplitude reflectors, especially MW7 and MW8 units. Units MW4 and MW5 display a thickening towards the fault, and some onlaps are found within these units, the same direction of onlaps can also be found in the upper units.

In the western sector of the MPB, close to the Marquês de Pombal Thrust, the Neogene units are deformed and strongly affected by slumps and another thrust (SP2000) located to the east of the MPT. The latter cuts through the entire sedimentary sequence and affects the seafloor carrying a folded hanging-wall anticline that affects the uppermost sediments, thus, suggesting it is active. The other thrust is also westwards verging and deforms the sedimentary package but its activity ceases before the deposition of the MW4 units, i.e. the dark blue reflector is not displaced by the fault. Eastwards of this thrust (SP 1950) there is a small upward concave structure that truncates the underlying strata of MW4 and MW3. Inside the concave erosional feature there are some reflectors that display onlaps on both sides (Figure 5.37). This feature could correspond to a slide scar that flowed off the profile's section since no deposits are found on the seismic profile.

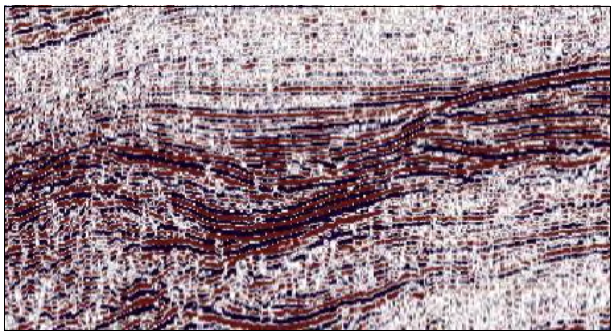

Figure 5.37 – Section of BS21 (SP2000-1850) displaying a detail of the erosional feature on the MPB, this may correspond to a gully or a slide scar since it truncates the underlying reflectors and is filled with deposits that display onlaps on top of the concave surface.

In the central part of the MPB area, the reflectors of units MW1, MW2 and MW3 show evidences of gravity instability and deformation as they are frequently disrupted and display wavy facies. More to the east, a major truncation of a large section of the MW2 unit is observed. A west dipping reflector (from unit MW3) obliterates several others from the previous unit (between SP 1400 and 1600) reducing this package thickness by half to west. Closer to the S. Vicente Canyon, the Mesozoic reflectors and the more recent ones, like the basal Miocene unconformity, display onlaps on top of the structural high. Units MW4 and MW5 display a thickening towards the canyon. The uppermost units, MW7 and MW8, are made up of a continuous succession of parallel reflectors of high acoustic contrasts with some transparent bodies in some areas. These units are present in the MPB and much thicker closer to the canyon than in its western sector, as observed in profiles BS09, BS10 and BS20. Underneath the S. Vicente Canyon, a paleo valley is found; it truncates the sedimentary units MW3 and MW2 and is filled with chaotic facies materials probably originated from gravity slides from the canyon walls and from material channelled from areas upslope. To the east of the canyon, the classification of the Neogene sedimentary units that are correlative with the ones in the west is not possible to make because the acoustic facies are totally different. The Neogene units on the eastern flank of the canyon are affected by folding, thrusting and downslope gravitational transport.

The beginning of the activity of the Marquês de Pombal Thrust is well depicted in this profile. On the footwall, the yellow marker (base of MW3) marks the appearance of debris that are originated by the uplift of the MPB. It also displays onlaps towards the west from the upper units which is a sign of localized subsidence to the east; compatible with the thrust movement since the footwall might undergo subsidence during its activity. Also the erosional feature located at SP1950 is directly above the base of MW3 which can be another indicator of its activity since the uplifted block is more exposed to erosional features. In the segment between SP 1400 and 1600 the geometry of the reflectors and the thickness variation of the MW3 unit indicates depositional instability and existence of bottom currents and the resulting deposits are also associated with the uplift of the MPB. The activity of the MPT and uplift of this area can also be responsible for the erosion taking place recorded as some truncations of some reflectors under the base of MW3.

5.7.7 – MCS profile BS23

The BS23 multichannel profile (Figure 5.38, at the end of section 5.7) follows a NE-SW direction across the Infante D. Henrique Basin, the Marquês de Pombal Block, the S. Vicente submarine canyon and the lowermost part of the SW Portuguese continental slope.

In an overall perspective from NW to SE, the MCS profile images the MPF, its footwall where the reflectors are subhorizontal, the hanging-wall with the associated drag fold, the MP

plateau with a thick Mesozoic basin, a basement high, the canyon erosion, the units that make up the lower continental slope and another basement high at the SE end of the profile.
The Paleogene and basal Miocene unconformities are well depicted as they truncate several underlying reflectors. The Paleogene basal unconformity truncates the Mesozoic strata at the footwall of the MPT, near the drag fold in the hanging-wall and close to the basement high located west of the canyon. The basal Miocene unconformity also obliterates several underlying reflectors throughout the profile.
The Mesozoic sediments located just beneath the Paleogene unconformity display weak and discontinuous reflections in the footwall of the MPT while to the west of the central basement high the reflectors display higher amplitudes and they can be traced in the full extent of the MP block. Beneath the SVC and to the east, just a few Mesozoic reflectors are present display low amplitudes.
The Paleogene sedimentary sequence is up to 200 msec TWT thick and displays different seismic facies. The footwall of the MPT displays few very discontinuous reflectors of low amplitude, the facies are similar in the MP block although some reflectors display higher amplitudes. To the east of the basement high (SP1150-1350), the reflectors maintain the same seismic characteristics whilst they are subhorizontal, more to the east as they become steeper their amplitude becomes higher and they are more continuous and can be traced over larger distances.
The Neogene package displays several internal discontinuities; the more important ones are the base of the MW3 unit (yellow reflector) and the top of the MW5 (light blue) as these are the ones that truncate more reflectors and therefore are more noticeable. The MW1 and MW2 sedimentary units together with MW7 and MW8 units are the ones that display reflectors of higher amplitudes and more spatial continuity. For the lower units this is especially evident between the basement high (SP1150) and the eastern tip of the profile, for the remaining of the profile the two packages are easily depicted from the rest of the sedimentary units by their higher amplitudes and more spatial continuity of their reflectors. Unit MW5 exhibits a more transparent facies, especially in the vicinities of the canyon (Figure 5.39).

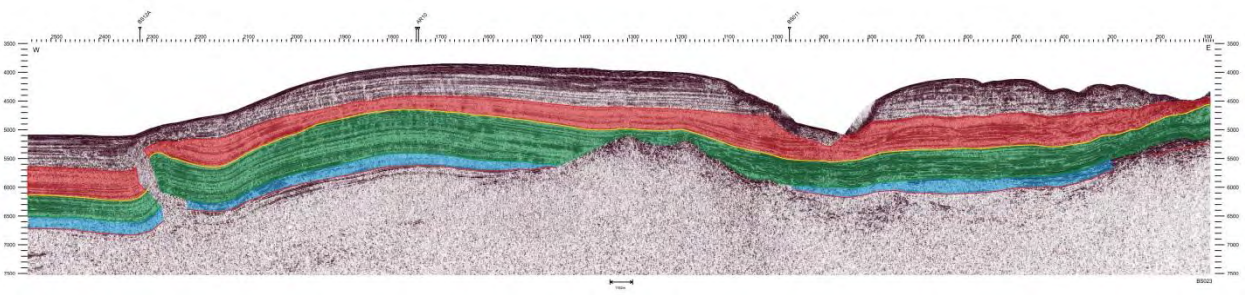

Figure 5.39 - BS23 MCS profile. Highlighted sedimentary packages: blue package corresponds to Paleogene deposits, green package corresponds to deposits from the M unconformity to the base of MW3, red package corresponds to sediments from the base of MW3 to top of MW5.

The main structural high constituted a paleogeographical relief on the seafloor as shown by the onlaps on both sides for the Mesozoic, the Paleogene and Lower/Middle Miocene units. The seismic facies shift from one side to the other of the basement high (especially for the Early and Middle Miocene deposits) is also indicative that the depositional environment was not the same. For the basement high at the eastern tip of the profile it seems that it was of a smaller expression because in Paleogene times it no longer constituted a relief in the seafloor as evidenced by sediments draped over the high. Onlaps are only depicted in the lower deposits, of Cretaceous (?) age.

The Marquês de Pombal Fault deforms and displaces the units; on the footwall they are flat and have a small drag towards the structure; on the hanging-wall a small drag is also present defining a small anticline a larger and wide syncline further away from the fault (SP 2150; Figure 5.40). The Paleogene (blue) and the Lower through Late Miocene (green) sedimentary packages do not display any thickness variation across the fault (Figure 5.39). The MPT activity probably begun at the base of the MW3 seismic unit (yellow reflector), where the first sedimentary wedges can be identified in the footwall; these wedges are eventually debris originated from the uplifted MP block. Also, the base of MW3 shows signs of erosive events, truncating some underlying reflectors of the MW3 unit, suggesting that the MPB was being lifted by the action of the fault. The onlaps on top of the same reflector can be ascribed to the onset of the compression, which also led to folding in the hanging-wall of the MPF, with sediments depositing in the lower parts of the syncline. All evidence combined, same packages across the fault until the base of the MW3 unit, presence of sedimentary wedges (that resulted from erosion from the uplifted area) truncation of lower reflectors and onlap of reflectors above and in the lower part of the fold suggest that the base of the MW3 seismic unit can mark the beginning of the activity of the MPT.

At the time that the MPB was experiencing uplift due to the activity of the MPF, the present day S. Vicente canyon area was undergoing subsidence, marked by the geometry of the base of MW3 reflector and by the onlaps towards both sides of several reflectors throughout the entire MW4 and MW5 overlying seismic units.

On the east part of the profile, the base of the MW4 unit (dark blue) shows signs of erosion as opposite to the area underneath the present day submarine canyon where signs of subsidence were described. The erosive events are testified by the truncation of several reflectors of the top of the MW3 unit and are identified throughout the MW4, MW5 and MW6 units. Several truncations are observed and the units display wavy seismic facies with numerous lateral truncations and therefore their lateral continuity is small. These closely spaced truncations display an upward concave shape with several onlaps on its top, probably as a result of, i) base of gravity slides, or ii) base of erosive submarine channels or gullies; both of the processes would run off section of the profile towards the southwest. Due to the location of the seismic profile at the base of the continental slope, the first hypothesis is more probable to correspond to the features observed as several slide scars are observed in the multibeam bathymetry in this area (Figure 5.18).

The top of the MW5 unit marks the end of the subsidence in the submarine canyon area since it is at that time that the infill reflectors began to be conformable. Further to the west, this reflector is well identifiable as it truncates numerous underlying reflectors and also truncates the drag fold and the syncline close to it. These truncations testify a new uplift event with continuation of folding with tightening of the hanging-wall syncline and thinning of the hanging-wall anticline crest responsible for the thickness variations for the MW5 unit across the MPB.

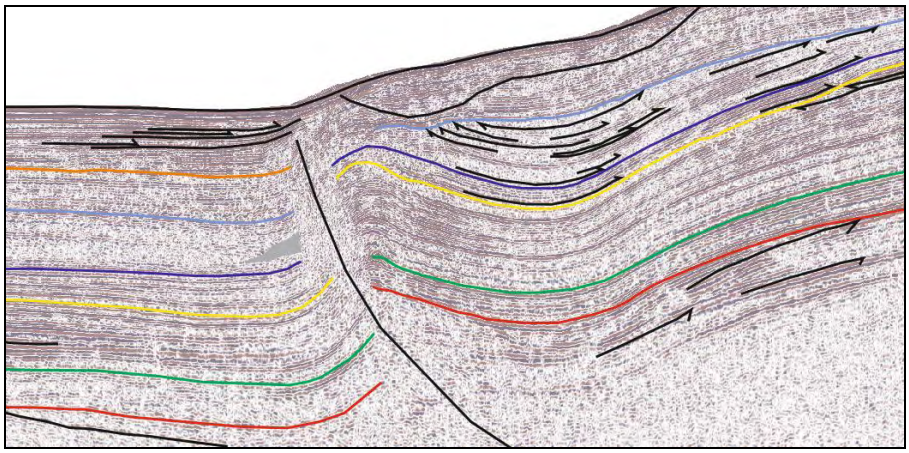

Figure 5.40 - Section of BS23 (SP2500-1950) across the Marquês de Pombal Thrust, displaying the infilling of the syncline (onlaps on both flanks) and the drag fold, both truncated by the top of MW5 unit (light blue).

In the more recent units (MW7 and MW8), facies are different with parallel and high amplitude reflectors that are slightly affected by mass wasting processes in the MPF scarp and display some onlaps in its footwall. These onlaps are caused by the activity of the MPT providing another evidence for its activity in more recent times.

5.7.8 – MCS profile BS24

The seismic profile BS24 (Figure 5.41, at the end of section 5.7) trends NNW-SSE direction cutting across the southern tip of the Marquês de Pombal Thrust Fault and the S. Vicente Canyon at the end of its middle sector (see chapter 4). To the West, it displays a 800 meters high scarp (slope of about 4º) separating the top of the MP plateau and the Infante D. Henrique Basin. The plateau is slightly tilted to the east towards the S. Vicente canyon. The canyon displays a relatively smooth seabottom and a 700 meters wall to the west and a smaller one to the east although it is not fully imaged in the profile.

The profile displays a good record of the Cenozoic sedimentary units; these are easily depicted and mapped as they are only disrupted in the MP thrust fault zone. In the footwall the sedimentary sequences are gently folded, in the hanging-wall they depict a broad asymmetric anticline.

The Mesozoic reflectors are poorly imaged on this profile. The top of the basement is also poorly imaged and its mapping is difficult. Nevertheless, this profile appears to display two basement highs: one close to the MPF and the other eastern part of the plateau (SP 700 and 1400, respectively). To the west of the MPF, the top of the basement appears to be deeper and therefore sedimentary thickness is higher.

The Paleogene package is not very thick (from 0.1 sec TWT at the eastern tip of the profile to 0.5 sec TWT at the hinge on the MPP) with some high amplitude reflectors with lateral continuity alternating with some weak reflectors with little spatial importance.

The Neogene deposits display discontinuities separating several minor seismic units. The seismic facies of these units can change laterally; however they are generally described as displaying reflectors of moderate to high amplitude, which become more faded and with less contrasts laterally as these are commonly discontinuous reflectors. Nevertheless, some seismic units display a more transparent facies (like MW5) or other (MW7 and MW8) display parallel reflectors of very high amplitude in the entire profile (with the exception of the area east of the canyon). East of the SVC, all units bellow MW6 display different seismic facies (compared to the rest of the profile) as they all have high to very high amplitude reflectors internally.

Despite the activity of the MPF during the Neogene times, the correlation of the stratigraphic units on both sides of this fault was attempted. The footwall of the MPF displays a sedimentary package with reflectors displaying higher amplitude contrasts when compared to the same sedimentary units present elsewhere, these high contrasts are only comparable to eastern tip of the profile for the units below MW6.

The Paleogene unconformity truncates the underlying strata of probable Cretaceous age as it is seen in the canyon area and in the footwall of the MPT. In the same way, the Miocene

unconformity cuts the underlying Paleogene deposits in the same areas and in the hinge of the anticline on the footwall of the MPF.

The onset of the uplift of the MPT hanging-wall is marked by truncation of some reflectors by the base of MW3 unit that also corresponds to the shift of the thicknesses of the units above it between the two sides of the fault. The base of MW6 unit truncates the underlying reflectors (SP2200) in the drag fold of the MPT (like in MCS BS23) corresponding to another big event of uplift of the MPB.

In a broad scale, inspecting the entire profile, the sedimentary units define a peculiar pattern as the sequence between the Paleogene unconformity and the base of the MW3 unit thickens towards the west whilst the overlying sequence (starting at the base of MW3 till the top of MW5 unit) thickens towards the east as it is seen in Figure 5.42; displaying a similar pattern as in BS23 (Figure 5.39). In the first case the thickening in the west is shown by consistent and repetitive onlaps towards the east throughout the sequence; in the sequence above it, the opposite happens with thickening in the east shown by onlaps towards the west. This suggests that the area near the present-day MPF was firstly a subsided area and afterwards an uplifted area, with the opposite taking place in the present-day SVC area. The tectonic inversion between the two settings is due to the beginning of the uplift of the MPB by thrusting in the MPB that occurred at the base of the MW3 unit.

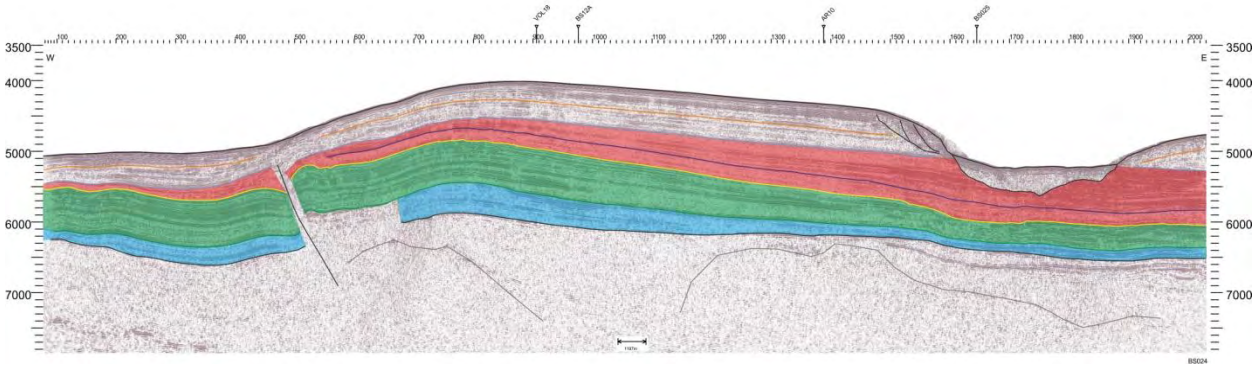

Figure 5.42 - BS24 MCS profile. The lower blue package corresponds to Paleogene deposits, intermediate green package corresponds to deposits from the M unconformity to the base of MW3, and the red package corresponds to sediments from the base of MW3 to top of MW5.

5.7.9 – MCS profile AR10

The multichannel seismic profile AR10 (Figure 5.43, at the end of section 5.7) cuts across the Infante D. Henrique Basin, the Marquês de Pombal scarp and plateau related to the Marquês de Pombal Fault, the S. Vicente submarine canyon and its eastern wall uplifted by the Horseshoe Fault.

In the western tip of the profile, the top of the basement is imaged underneath a sedimentary basin of about 4 sec TWT. The lowermost sedimentary units above the top of the basement are not very well imaged and their inner structure is hard to perceive. However, in the Mesozoic units some reflectors are identified and towards the top, several onlaps are identified towards both sides of this basin. Upwards, in the sedimentary column, it is possible to see the record of well stratified Mesozoic deposits, the high amplitude basal Paleogene and Miocene unconformities truncating the underlying reflectors.

In MW3 and MW4 units, several onlaps towards the west are present. These features can be related to the activity of one or both of the faults in the area, the MPT and a smaller reverse fault located to the west (SP1100). This reverse fault cuts across the units till MW5 whilst the MPT breaches the seafloor cutting across all units (Figure 5.44), thus extending its activity till the present. Both structures probably became active at the same time, when the MW3 units was started to be deposited, causing the onlaps towards the more elevated areas. On the east side of the MPF, the uppermost units are affected by slumping related with the scarp steep gradients. This can be related with some deposits found on the MPT footwall that might correspond to deposits made up of debris, due to their seismic chaotic facies and disturbed reflectors (signalled on the seismic profile as partially transparent grey bodies).

The western sector of the Marquês de Pombal Block, east of the MPT is made up of two anticlines separated by a syncline and more to the east a structural high is present. The folding of the beds is concordant until the top of the MW2 unit, i.e. the reflectors are parallel until this horizon and above it some onlaps are found in the syncline and some disturbances in the hinge of the anticlines. This is related with the activity of the MPT, responsible for the origin of this folding and for the onlaps on the footwall that are also present from the base of the MW3 unit and upwards. The faulting is accompanied by folding and as the anticlines build up, the sediments become unstable and experience slumping accounting for the referred disturbances and at the same time the syncline between them acts as a small subsiding basin accounting for the identified onlaps.

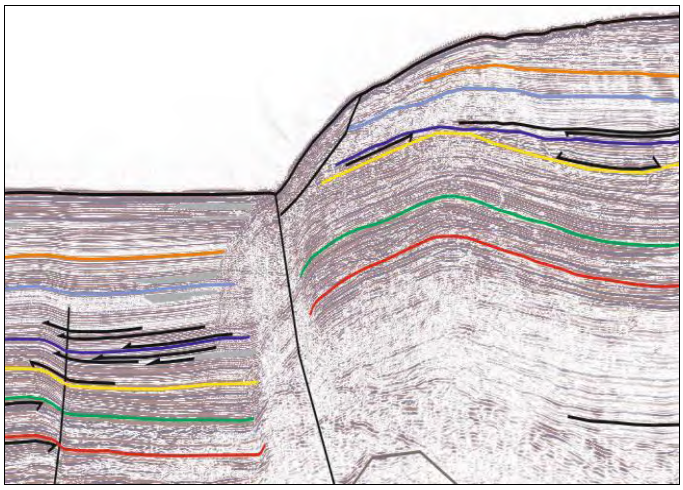

Figure 5.44 - Section of AR10 (SP1100-1500) across the MPT cutting through the whole sedimentary package reaching the seafloor, to the west the yellow reflector (base MW3) marks the onset of onlaps towards the west. On the hanging wall of the MPT the image displays the drag anticline fold with the reflectors above the base of MW3 displaying signs of erosion and deformation due to the uplift of the referred structure.

The basement high located more to east (SP1700) was a seafloor feature that controlled the deposition possibly from early Mesozoic syn-rifting deposition through Miocene. The base of the Miocene is one of the earliest horizons to cover the structural high, whilst the reflectors below are interrupted and display onlaps towards on top of the basement high (Figure 5.45).

The uppermost units (MW6 to MW8) are thicker in the vicinities of the canyon when compared to the area closer to the MPF, partially due to the slumping that affects the sediments near the scarp. These upper units (MW6-8) display their characteristic seismic facies with spatially continuous and low/moderate amplitude alternating reflectors.

Towards the S. Vicente canyon area it is observed that the sedimentary package from the base of Miocene till the top of MW2 becomes thinner whilst an upper package (from base of MW4 to the top of MW5) becomes thicker, the intermediate MW3 unit does not vary its thickness much. This feature is also depicted in profiles BS23 and BS24.

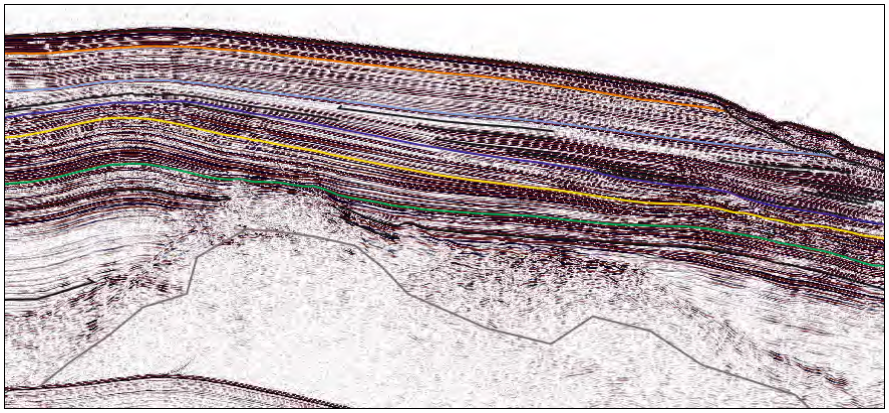

Figure 5.45 - Section of AR10 MCS profile (SP1550-2150) in the eastern MPB area displaying the basement high and the thickening of the units MW4 and MW5 (between the dark and light blue) towards the east.

The thickening of the lower Miocene package (MW1 and MW2) in the west can be accounted as a result from two factors: downlaps are towards the east and truncation of the top reflectors in the eastern area. The first suggests subsidence and larger sediment accumulation in the west, the last one points to erosion of some reflectors and so the unit thins towards the east, therefore these two facts combined can be responsible for the thickness variations. The top package (MW4 and MW5) thickens towards the east as a direct result of time lasting subsidence in the canyon area recorded by onlaps towards the west present during the deposition of both units.

On the SVC area, the Mesozoic sequence is thick and reaches at least 2 sec TWT. Towards the east, in the canyon's flank, folding of the units is observed and is accompanied by faulting: two thrusts are west-verging (two branches of the Horseshoe Fault) and a back-thrust towards the east is also present. The lowermost reflectors are displaced by the fault planes whilst the upper units are folded on top of the fault (Figure 5.46), thus providing a dating for the uplift. The abundant onlaps on the flanks of the synclines (drag folds associated with the Horseshoe Fault) are present above the top of the chaotic body (above the yellow reflector) were formed towards more elevated areas. These areas were higher because of the uplift and this event is synchronous with the onlaps, therefore it started at the same time the last deposits of MW3 unit were being deposited (terminal stages of the Miocene). This age is approximately the same given for the start of the uplift of the Marquês de Pombal Block (and activity of the Marquês de Pombal Thrust).

Underneath the present-day submarine canyon and towards the east, a different seismic unit is present that is not identified anywhere else on this seismic profile and in none of the previously described ones. It has an overall lenticular shape (slightly distorted by the later deformation) with pinch-outs on both sides, a well-defined top (yellow marker, corresponds to the base of MW3 unit) and a more irregular base. It displays a characteristic chaotic facies with some irregular reflectors that have not a large spatial continuity. This unit was firstly described as a gravitational unit (olistostrome like) by Torelli *et al*. (1997) and many others that followed (e.g. Maldonado *et al*., 1999; Iribarren *et al*., 2007).

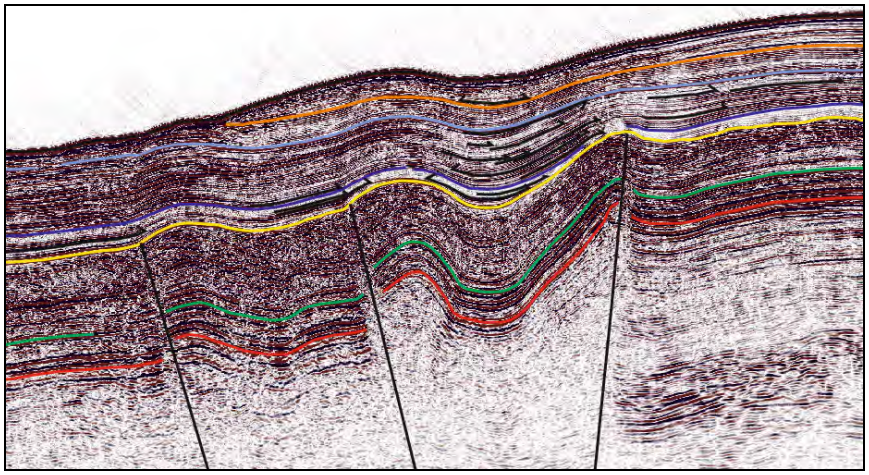

Figure 5.46 – Section of AR10 profile (SP2400-2750) imaging the eastern flank of the SVC displaying the chaotic body affected by faulting (Horseshoe Fault) and folding and numerous onlaps present on the units above it. See text for more details.

By the absence of thickness variations of the chaotic body between the two sides of the fault and the presence of onlaps in the units above it (and above the yellow reflector), the fault activity and associated folding was post-chaotic body deposition. Thus, it suggests that the MPF and the HF were active at the same time after the deposition of the chaotic unit, i.e., yellow marker onwards. The back-thrust (verging towards the east, SP2680) also displays rupture of the lower units and folding of the upper ones that also display some onlaps, pointing to having the same activity time interval of the HF and the MPF. To the east of this thrust fault the sedimentary package is well observed, especially the lower units displaying numerous, continuous reflectors alternating with moderate amplitude reflectors.

Figure 5.18

Position and Shotpoint map for the MCS profiles

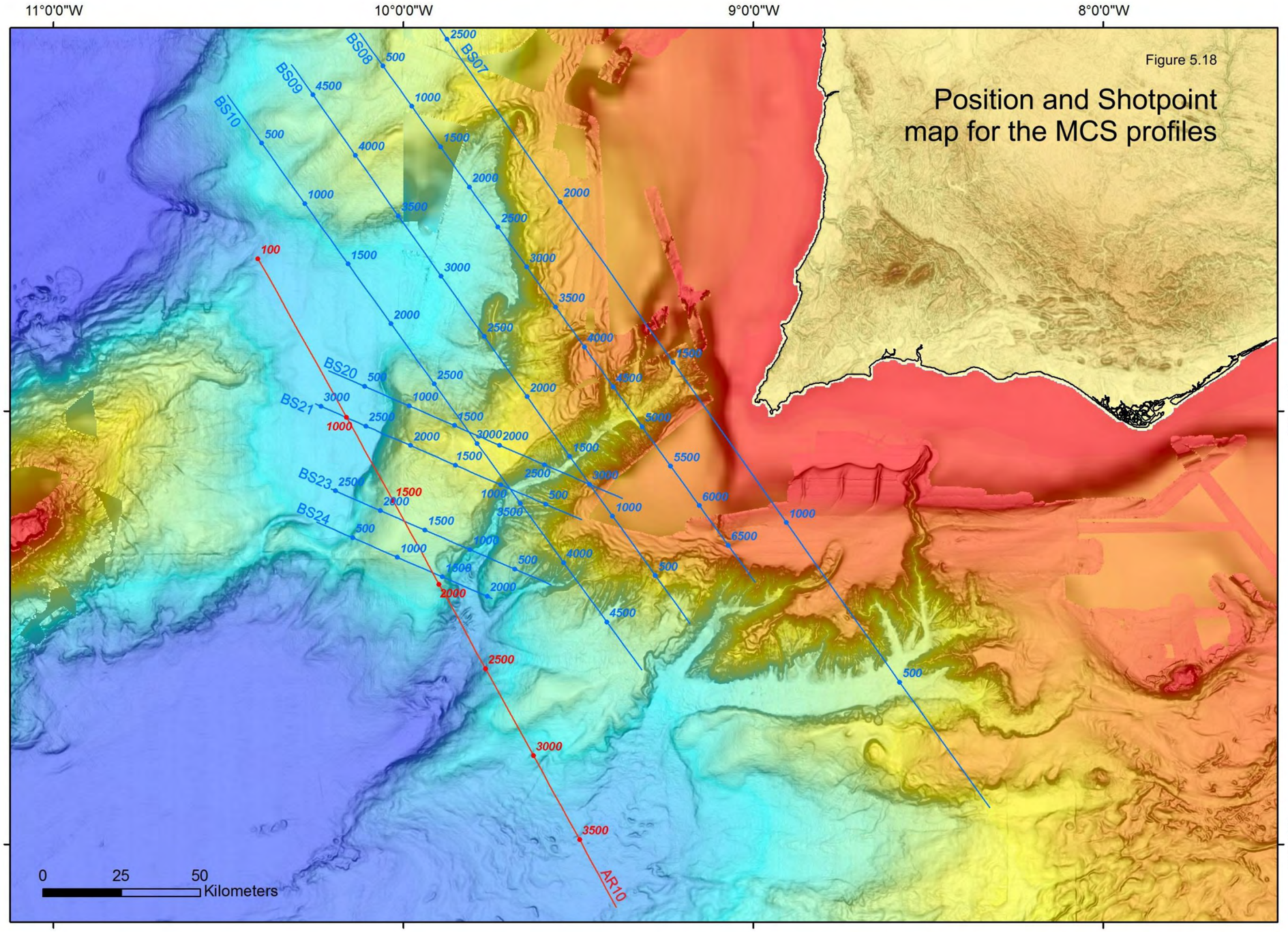

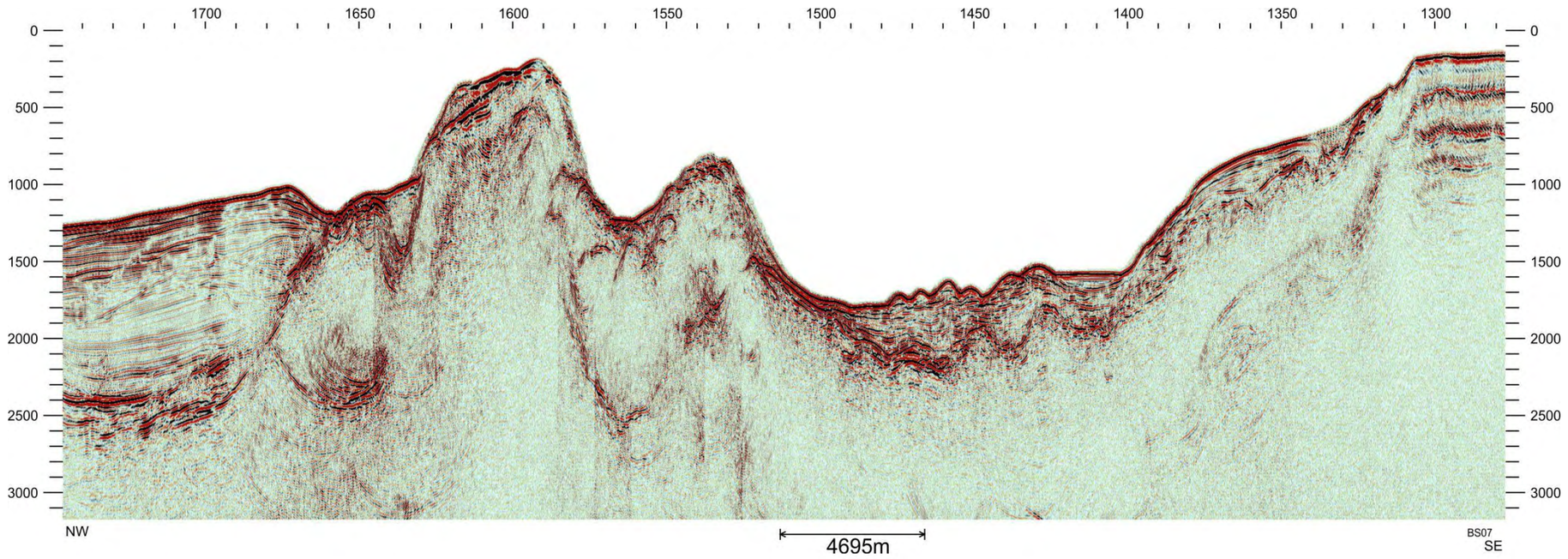

Figure 5.19 - MCS BS07 and its interpretation

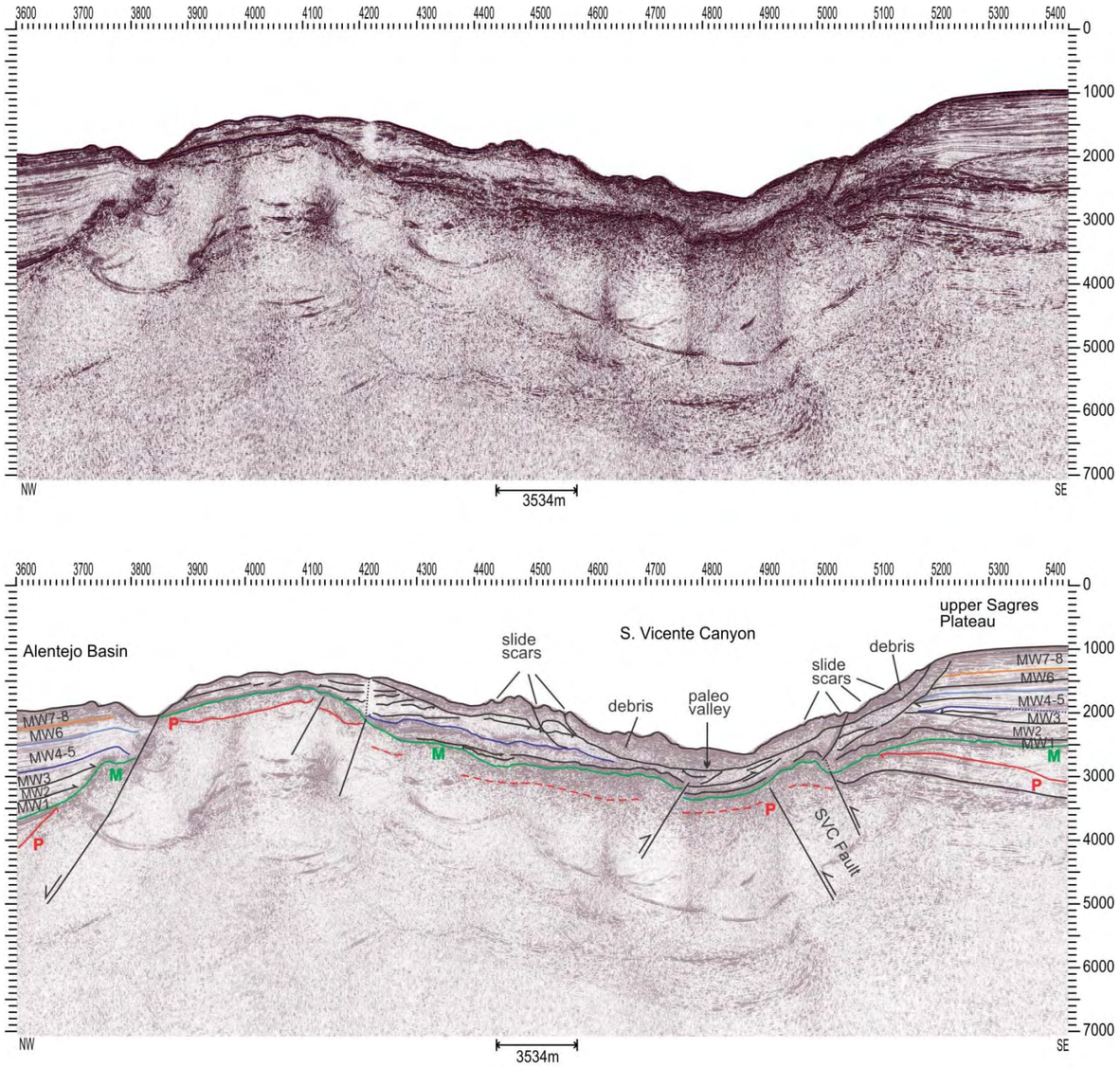

Figure 5.20 - MCS BS08 and its interpretation

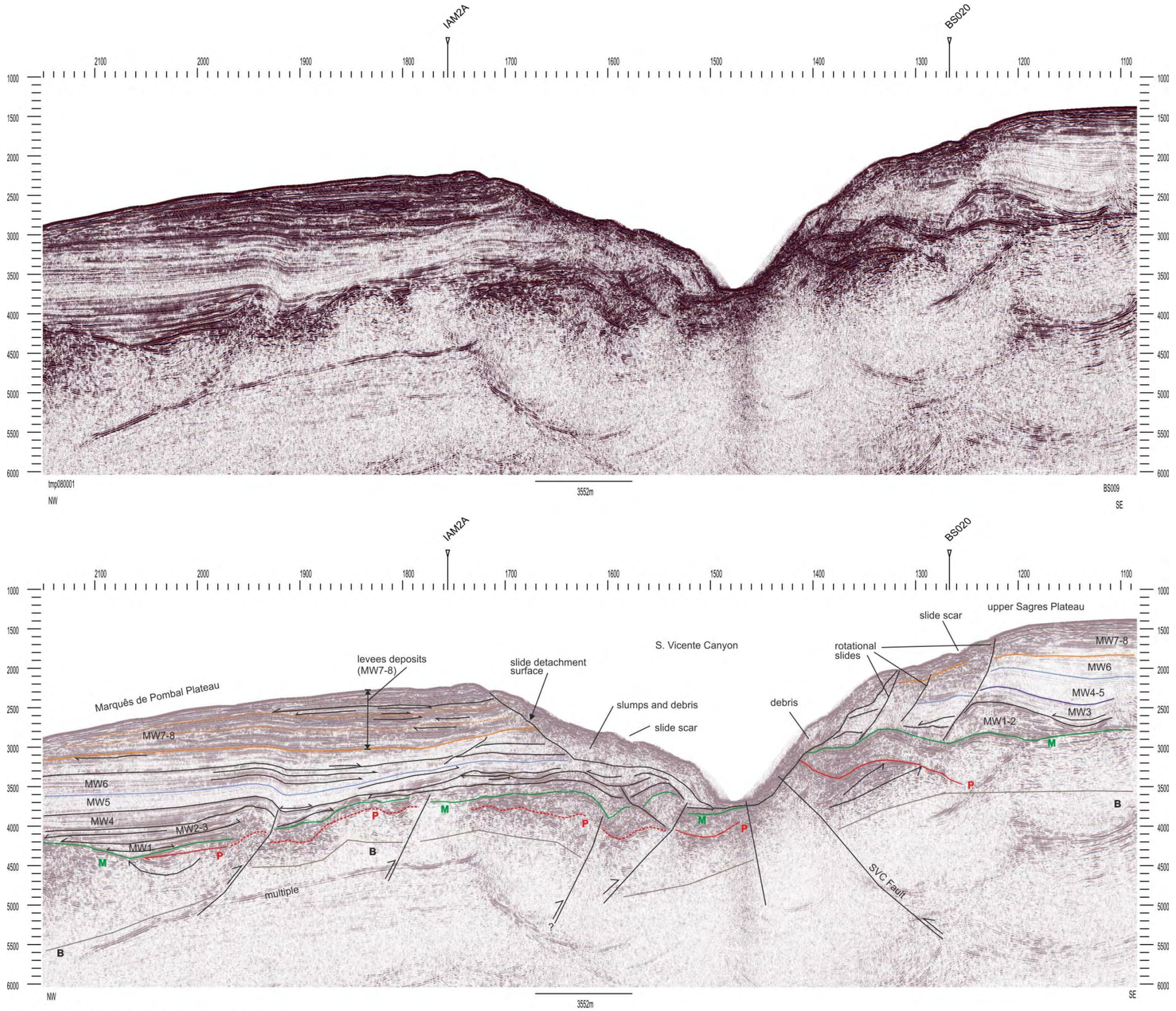

Figure 5.22 - MCS BS09 and its interpretation

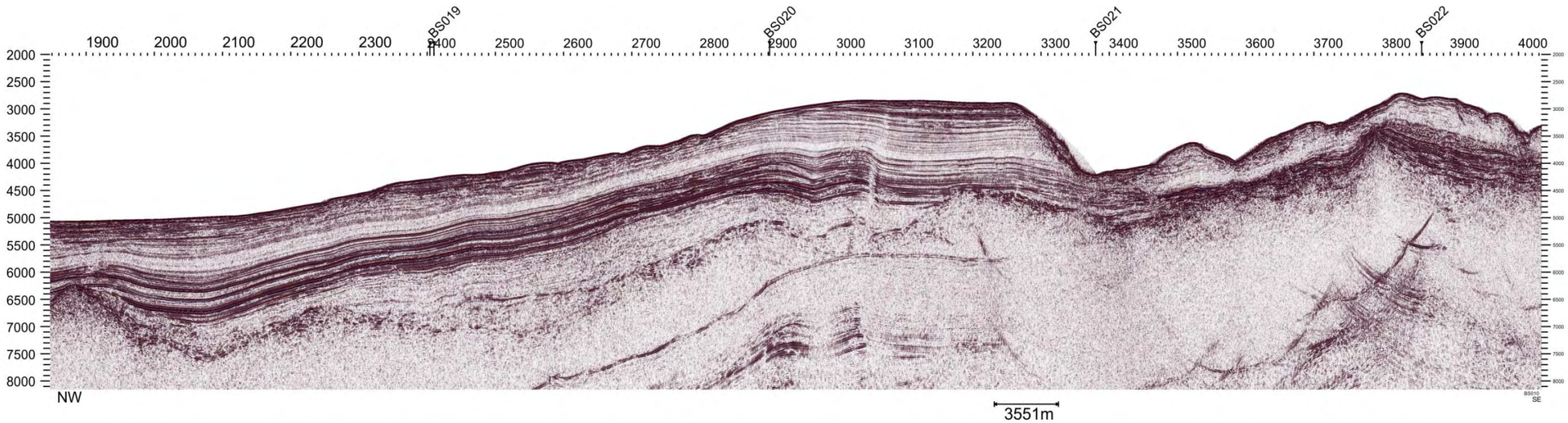

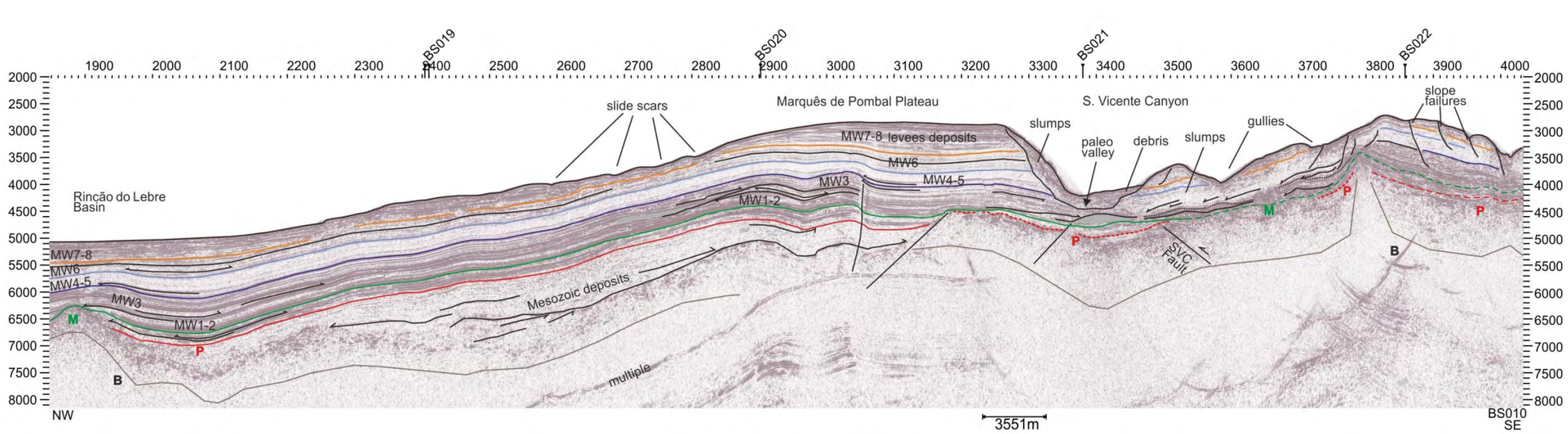

Figure 5.25 - MCS BS10 and its interpretation

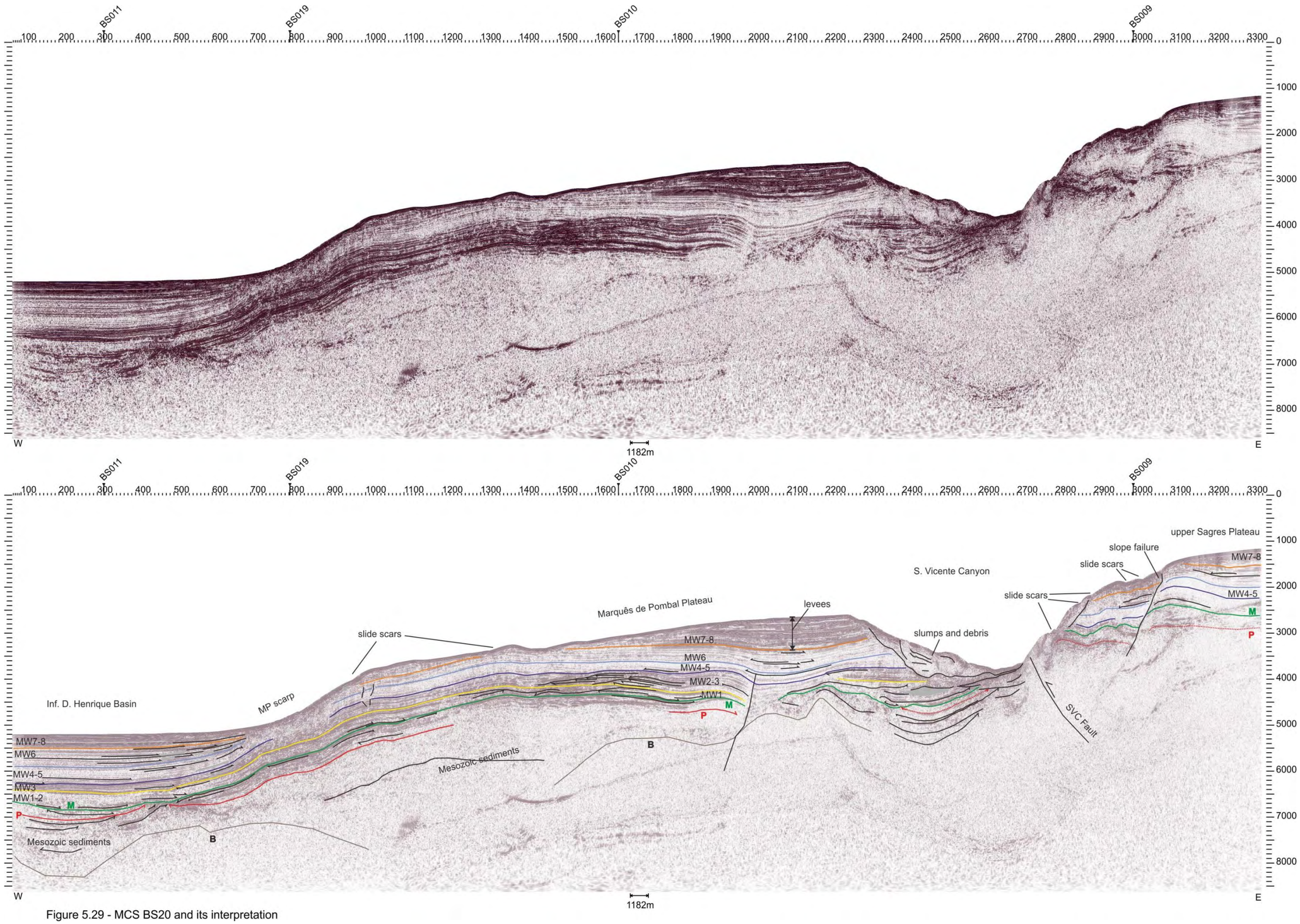

Figure 5.29 - MCS BS20 and its interpretation

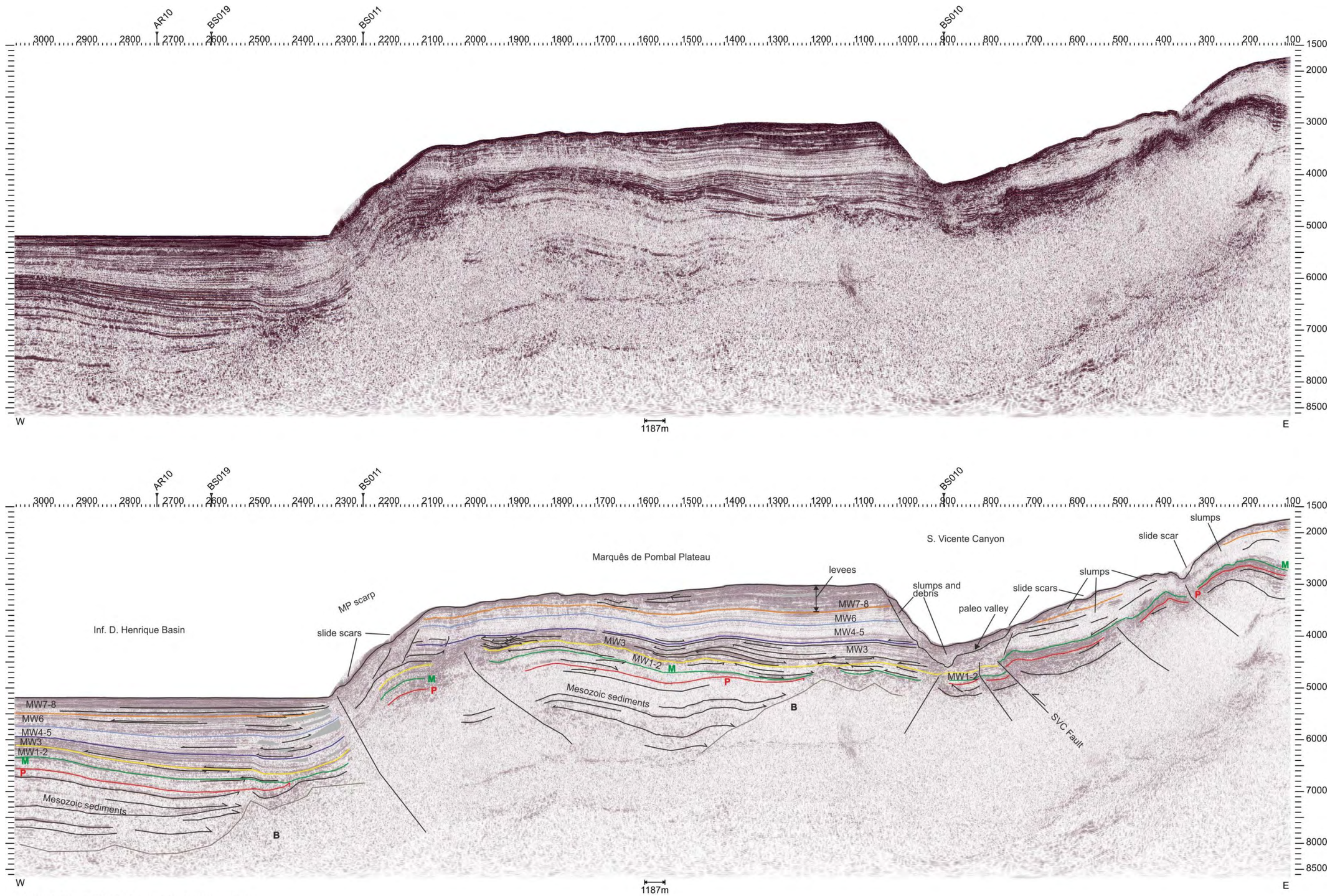

Figure 5.33 - MCS BS21 and its interpretation

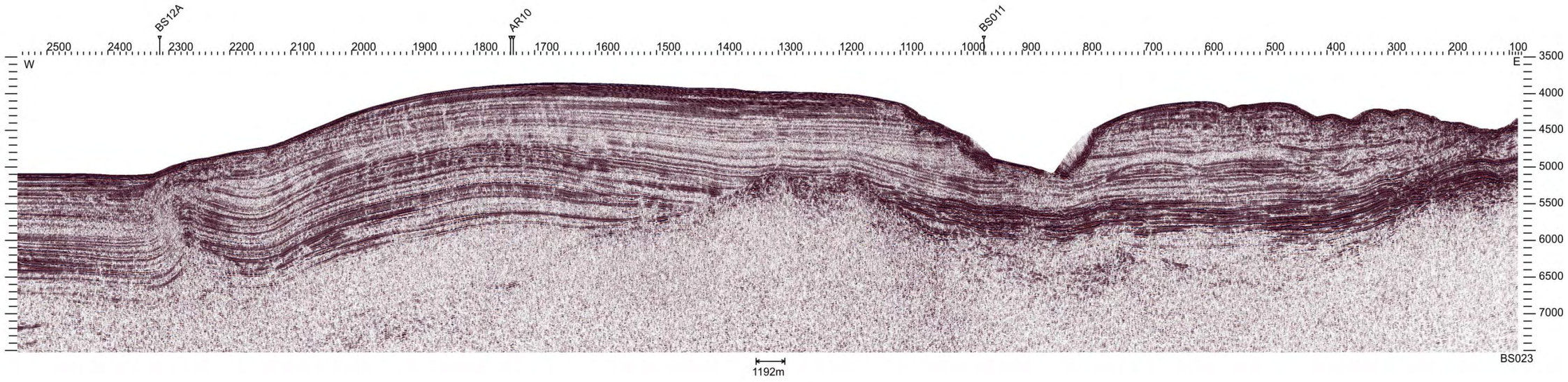

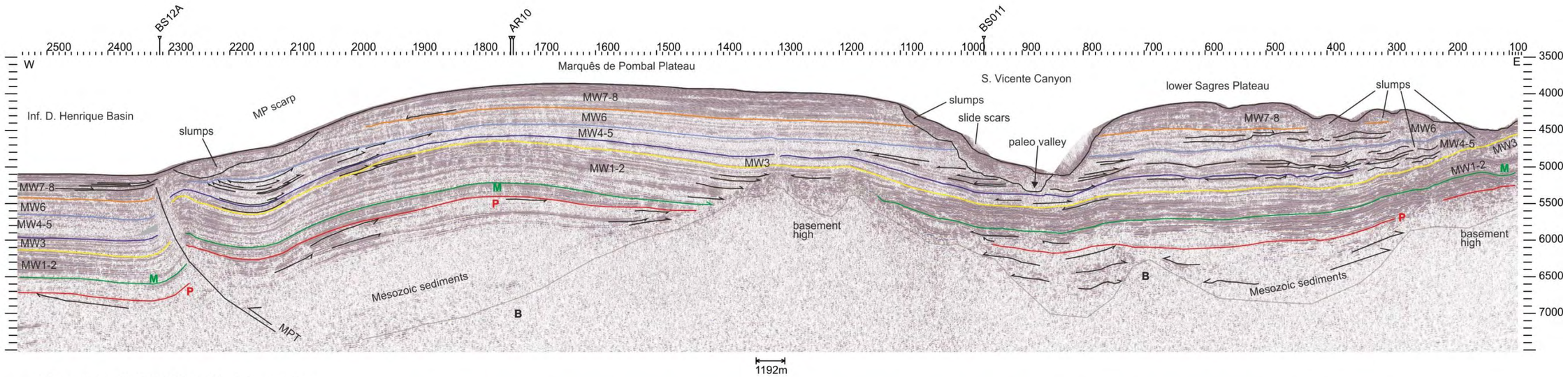

Figure 5.38 - MCS BS23 and its interpretation

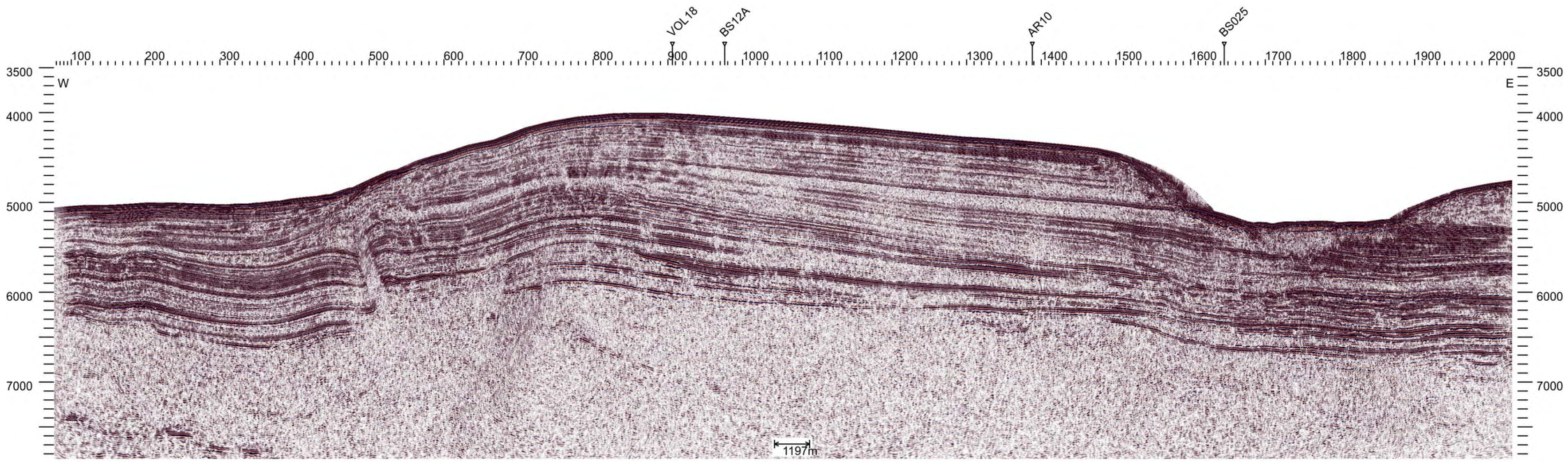

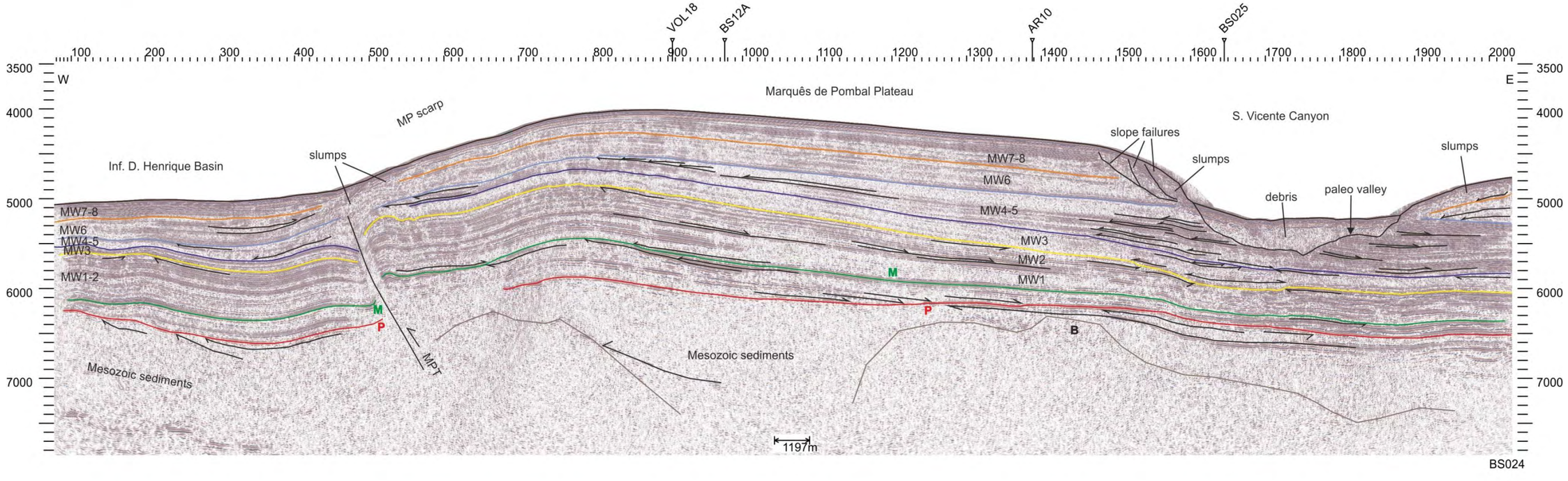

Figure 5.43 - MCS BS24 and its interpretation

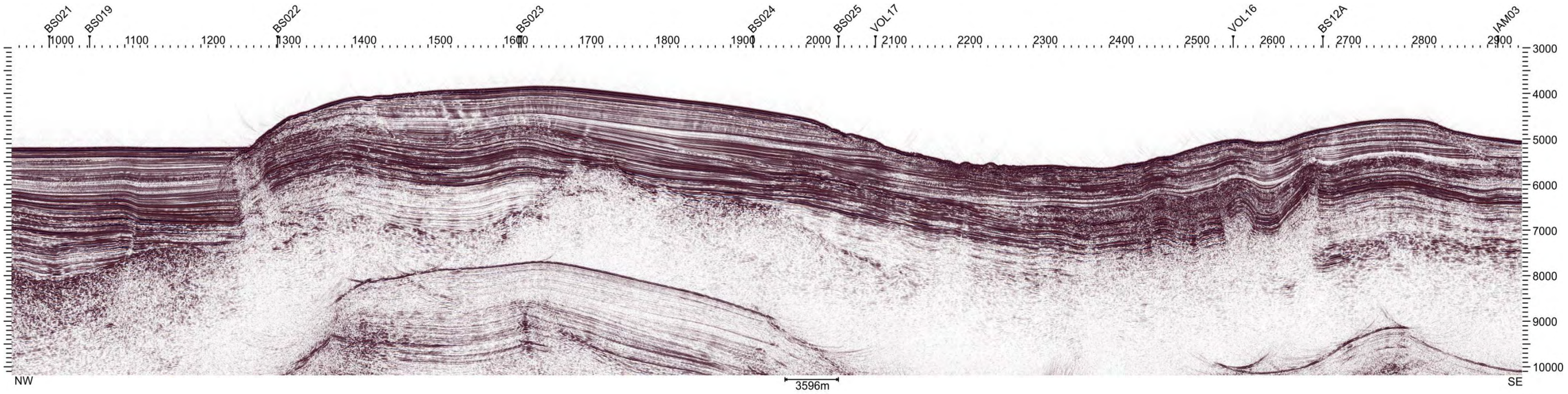

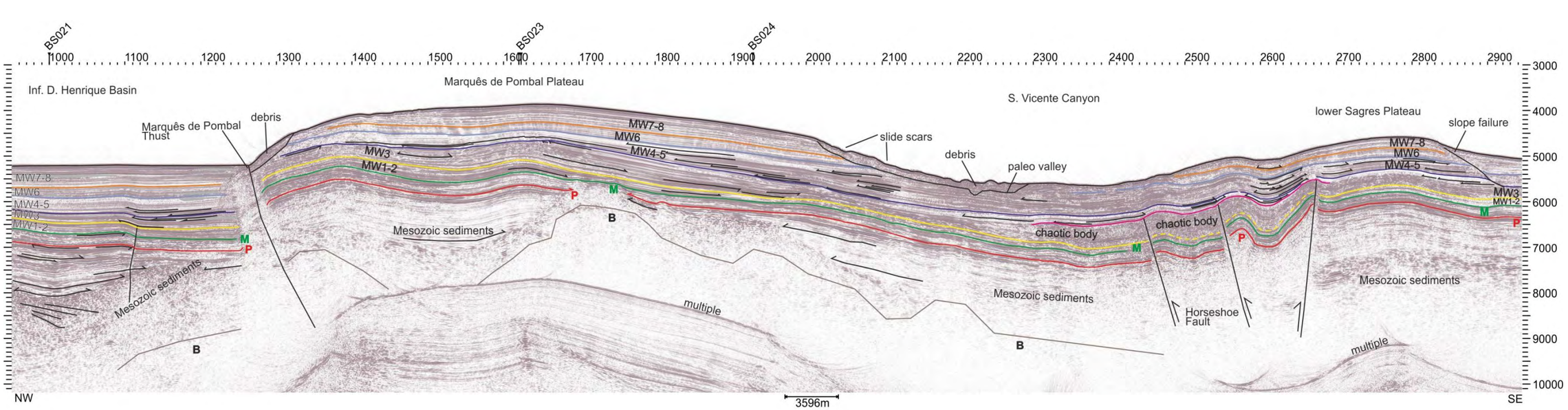

Figure 5.43 - MCS AR10 and its interpretation

5.8 –Depth and thickness maps in the São Vicente Canyon area

In this section, several maps with depth and thickness grids generated in the Landmark seismic workstation using the Z-Map plus application, and the seismostratigraphic interpretation of the seismic profiles described above, and several others that were studied, will be presented.

There are two types of grids: one refers to depths and the other to thicknesses, for both the units are in milliseconds TWT. Contour lines were plotted in order to give a more quantitative assessment of the values. Each colour grid was plotted on top of the bathymetry of the area with a 20% transparency degree, in order to link the structural horizon with the present physiography and to the study area. The contour interval for the isopachs and isobaths varies from map to map and the color pallete is the same for both depths and thicknesses grids, however the colors are inverted. The cell size in all the grids is of 1000 meters.

The grids presented and described are the following: depth map of the top of the basement, thickness map of the sediments, base of the Neogene depth map, Neogene sedimentary thickness map, Thickness map of units MW4 and MW5, Thickness map for the units MW7 and MW8.

5.8.1 – The top of the basement map

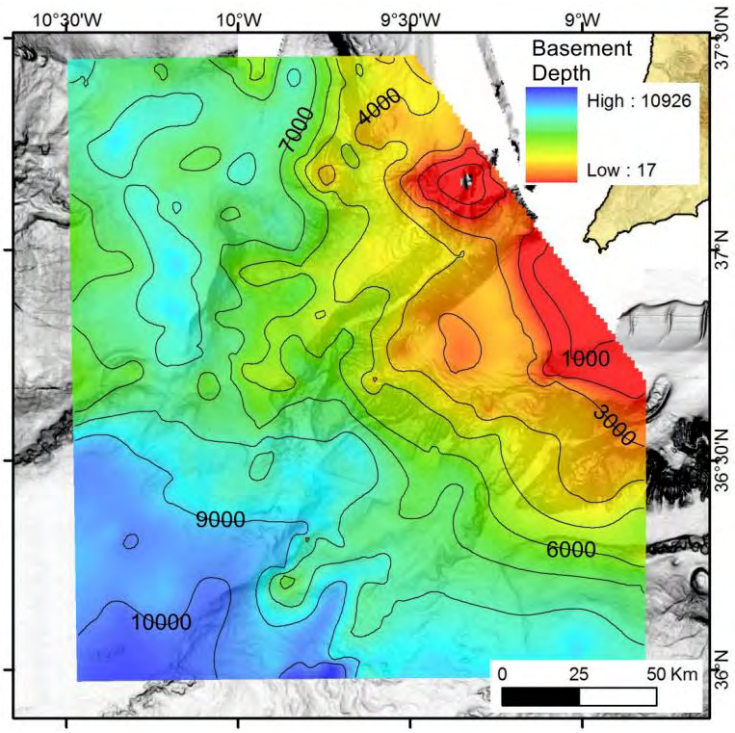

Figure 5.47- Depth to the top of the basement, isochron interval of 1000 ms.

The depth map for the top of the basement shows a close correspondence of the variation of the sea floor depth and basement depth. The top basement is much shallower closer to the shore and deeper in the deep abyssal plain. The basement structural highs also have a close correspondence with bathymetric positive features.

The areas where the top of the basement is shallower are the Sagres Plateau and the shelf of the Western Portuguese Margin. The area in the foot-wall of the MPT (the Infante D. Henrique Basin), displays the top of the basement a little deeper than in the surrounding areas and there is also a slight difference of the top of the basement between the two sides of the thrust; thus revealing its importance since it affects not only the upper section of the sediments but also the basement, i.e. this is a thick skinned thrust.

The basement high just west of the SVC seen in several MCS profiles is also depicted in the map and constitutes a NE-SW elongated basement high ridge. The depth variation pattern of the top of the basement and the sea floor along the canyon is the same, indicating that the basement is generally depressed underneath this valley.

The Horseshoe fault and the associated backthrust are also identifiable in this map, highlighting their importance.

The Pereira de Sousa normal fault is also very noticeable in the map since it has a large displacement between the two sides. To the west, in the Rincão do Lebre Basin some areas also display a slightly deeper basement top.

All the main faults, both extensional and thrusts, are thick skinned faults as the bathymetry of the sea floor and that of the top of the basement vary in the same way across these faults, as described by other authors (e.g. Zitellini et al., 1999, 2004; Gràcia et al., 2003; Terrinha et al., 2003).

5.8.2 – The sedimentary thickness map

The comparison of this map (Figure 5.48) and the isobaths map of the top of the basement show the following: i) firstly, a shorter wave length between troughs and highs giving the map a different “spotty” appearance; secondly, the lesser values (thinner sedimentary cover) correspond to the continental slope and shelf areas and to the SVC; thirdly, the higher values (thicker sedimentary cover) are located on the deeper areas where sediments are more easily accumulated, including the Horseshoe Abyssal Plain (southwest of the Portuguese continental slope just east of the SVC) and the Infante D. Henrique Basin, some areas of the Marquês de Pombal Block.

It is interesting to note that constant thick values spread across the Neogene thick skinned thrusts (Marquês de Pombal and Horseshoe thrusts) attesting for an important sedimentary filling before the shortening occurred. This is consistent with observations of previous

authors based seismic profile interpretation only, who suggested that these faults were syn-rift faults during the Mesozoic rifting (e.g. Terrinha *et al*., 2003).

The SVC displays lower values because of the erosion taking place on its axis. This is more noticeable in the shallow areas where the basement is closer to the seabottom and not so evident on its deeper segments because the basement is deeper and the erosion does not cut into the sedimentary cover with the same magnitude. The erosion and gravity-driven mass movements also account for the lower values on the Pereira de Sousa scarp; just west of the fault, the basement high of the Bow Spur is also noticeable by the diminute sedimentary thickness.

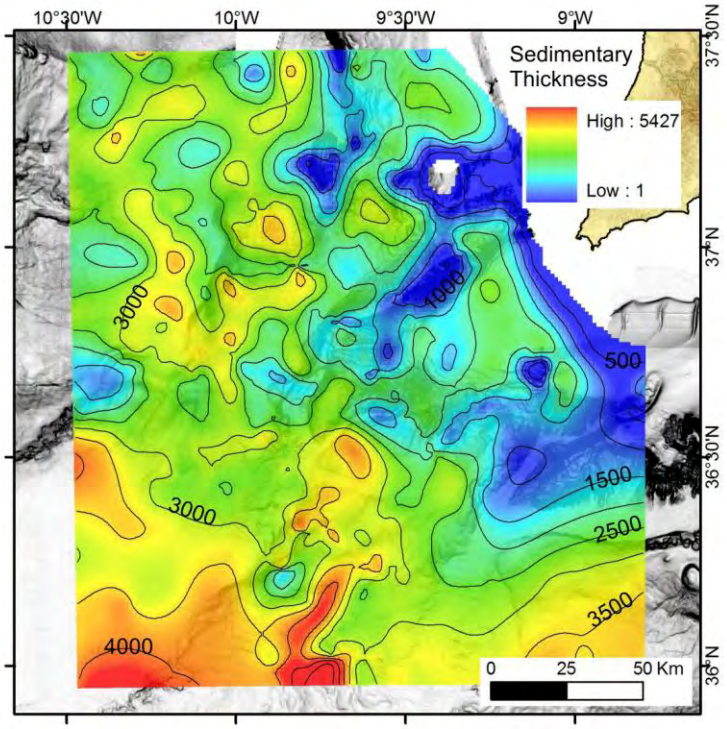

Figure 5.48 - Thickness of the sedimentary cover above the basement, isopachs every 500 ms TWT.

The upper Sagres Plateau displays a relatively constant thickness as well as the western Portuguese shelf in the areas North of the Montanhas dos Descobridores where the thickness is diminute (Mesozoic rocks outcrop on the seafloor). These structural highs correspond to inversion tectonic uplifted structures as described by Zitellini *et al*. (2004).

5.8.3 – The base of the Neogene isobaths map and the Neogene isopach map

The depth of the Base of the Neogene map (Figure 5.49) and the Neogene thickness map (Figure 5.50) were both produced using the mapping of the basal Miocene unconformity on the MCS profiles. The first one displays an overall increasing depth from the continental

shelf to the deep sea, parallel to the present day bathymetry, approximately, with some irregularities on the MPB, the SVC and the Sagres Plateau.

The thickness of the Neogene sedimentary package increases towards the deep sea indicating a strong relationship between accommodation space and deposition. However, the isopach map in Figure 5.50 shows a number of highs and lows of sediment thickness. The SVC is well depicted as a low whilst the flanks constitute highs. Of particular interest is the high on top of the Marques de Pombal plateau. This shows an increase of thickness from higher depths to the top of the plateau, which raises two alternative explanations: i) either the main thickness was obtained prior to uplift of the MP plateau on top of the MP Thrust or ii) there are local depositional processes that control sediment deposition on the western flank of the canyon. The latter is the correct alternative, since the activity of the thrust and uplift of the plateau controlled the inception of the canyon and the depositional processes on the canyon western flank. Adding to this, the existence of a localized depocentre at the front of the MP Thrust is a strong indication of filling a small foreland basin of this thrust.

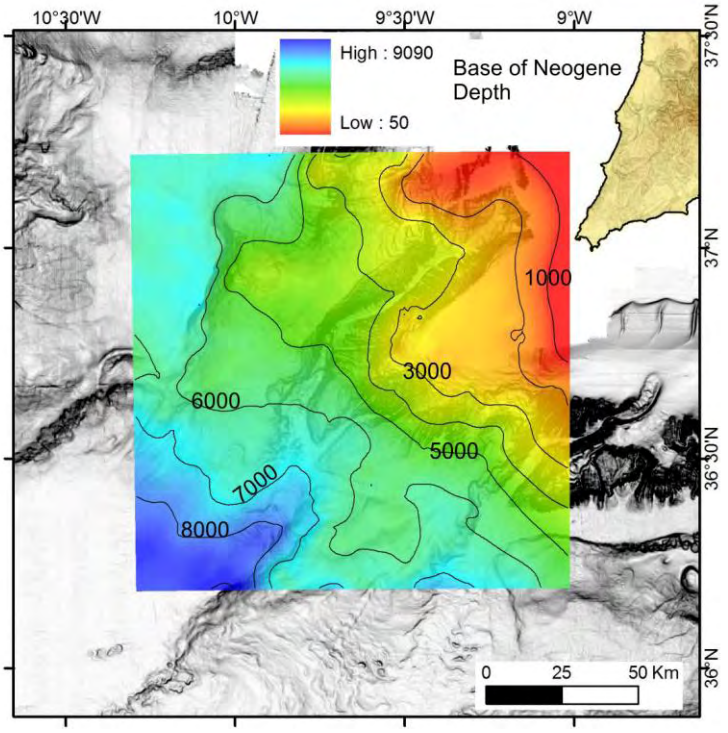

Figure 5.49 - Map for the depth of the Miocene basal unconformity, isochrons every 1000 ms. See text for details.

The thickness of the Neogene also increases from the hanging-wall of the Horseshoe Thrust to its foot-wall. In this case this is an expression of syn-tectonic deposition. The thickness across the Pereira de Sousa fault increases from east to west, i.e. from the foot-wall to the hanging-wall, because this is a normal fault dipping to the west (Terrinha *et al.,* 2003).

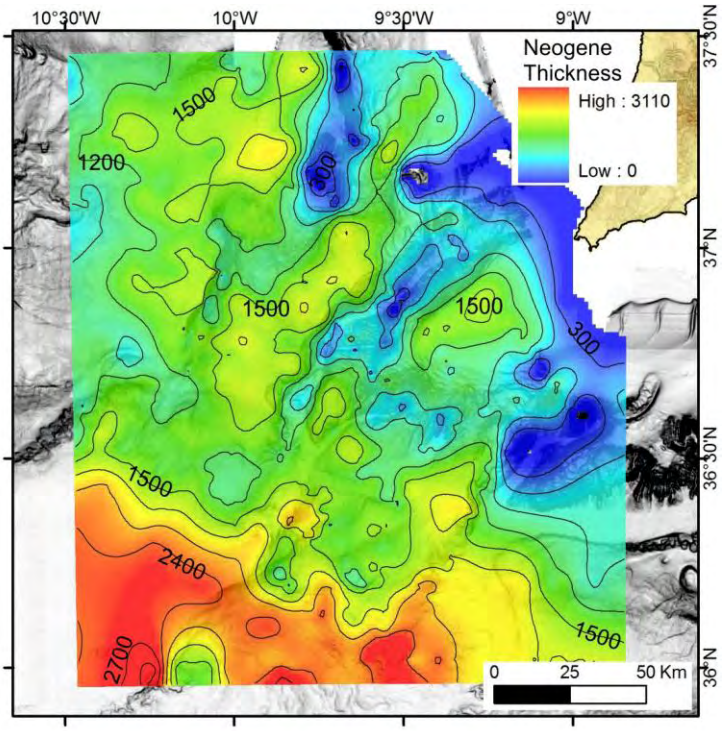

Figure 5.50 - Thickness of the Neogene sedimentary package, isopachs every 300 ms TWT.

5.8.4 – Thickness map for units MW4 and MW5

The TWT thickness map of units MW4 and MW5 (Figure 5.51) was made because on several of the MCS profiles a thickening of these units was observed. As depicted in the map this thickening takes place at the deeper segment of the SVC. This corroborates the interpretation of the MCS profiles where the onlaps and thickening of these units suggested a relatively long time lasting subsidence on the deeper areas of the SVC. On the northern sector of the footwall of the MPT a thickening of these units is observable due to the localized subsidence related to the active thrusting on the MPF. In the slope that connects the Inf. D. Henrique Basin to the HAP there is also a thickening of the units MW4 and MW5. This is explained because an intermediate sedimentary unit is present and part of it is made up of debris that is probably originated from the elevated areas to the north (where signs of erosion are present). The areas where these units are thinner are the base of the Gorringe Bank, the Horseshoe Abyssal Plain and the central sector of the Marquês de Pombal Block.

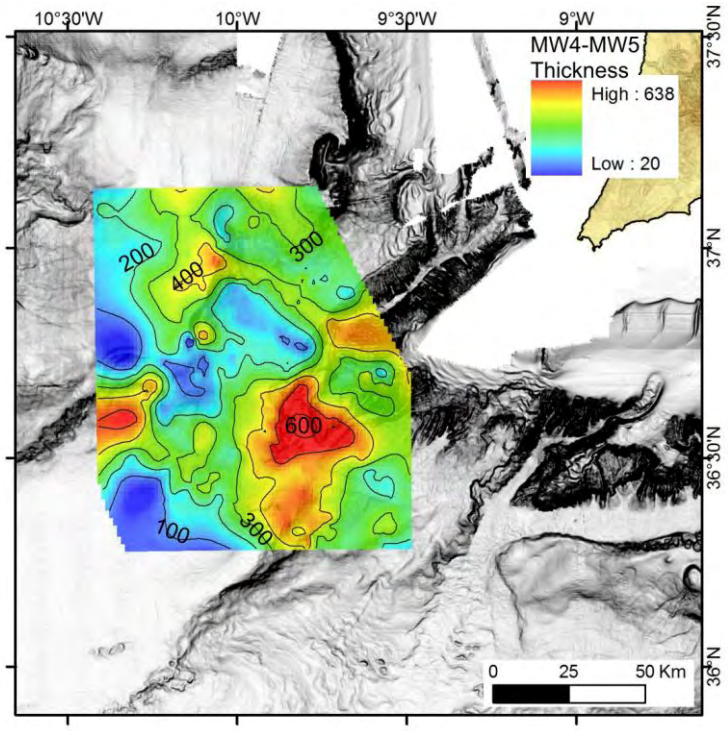

Figure 5.51 - Thickness map of units MW4 and MW5, isopachs every 100 ms; see text for description.

5.8.4 – Thickness map for units MW7 and MW8

The map of the thickness of units MW7 and MW8 displays a peculiar pattern, in most areas these units are not present in the canyon's axis area (interpolation for the gridding algorithm attributes a small value) however it displays some relatively high thickness values for the Marquês de Pombal Block (especially its northern sector) close to the S. Vicente Submarine Canyon. This suggests that the genesis of these deposits is related to the canyon's ongoing processes. In fact these two units correspond to levee deposits and their origin is related to overbanking processes. For the remaining area of the map, the base of these units was also mapped but it is only a stratigraphic correlative and the unit is not genetically the same. In the SW corner of the upper Sagres Plateau, there is also a thickening of these units which can correspond to the buildup of levee deposits associated with the South Portuguese Margin contourite deposits (Roque et al., 2012).

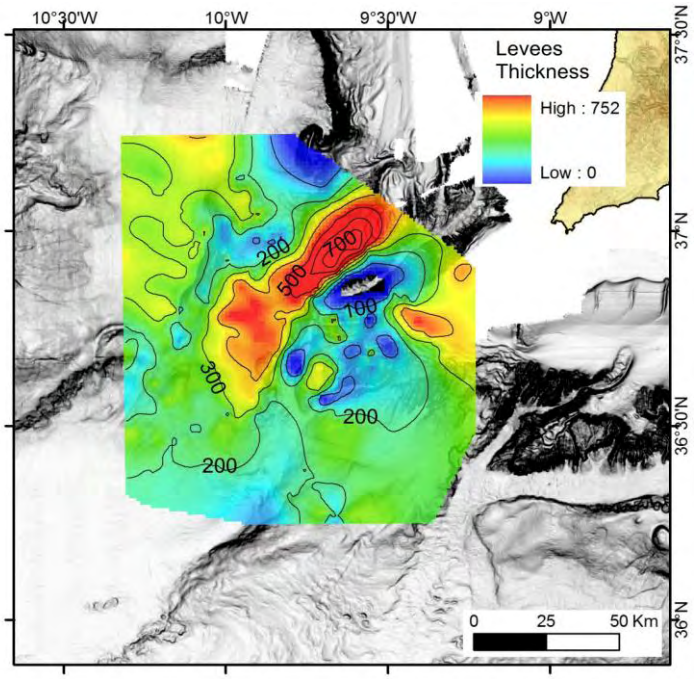

Figure 5.52 - TWT thickness map of units MW7 and MW8, isopachs every 100 ms; see text for description.

5.9 - Genesis and evolution of the Portimão Submarine Canyon

For the genesis and evolution of the Portimão Canyon several MCS were selected and interpreted (Figure 5.53). Presented in Figure 5.54 are a series of E-W trending seismic reflection profiles that cut across the canyon in all of its sectors. The seismic profiles are from the Chevron survey performed in 1974 and were available in paper format. They were scanned and transformed in digital format to be imported into the general database of the seismic laboratory of the UGM/LNEG interpretation using the Landmark Graphics Corporation software. Therefore, these MCS do not have the same detail and quality as the ones presented here for the SVC area, i.e. their resolution is lesser and so the interpretation is more constrained.

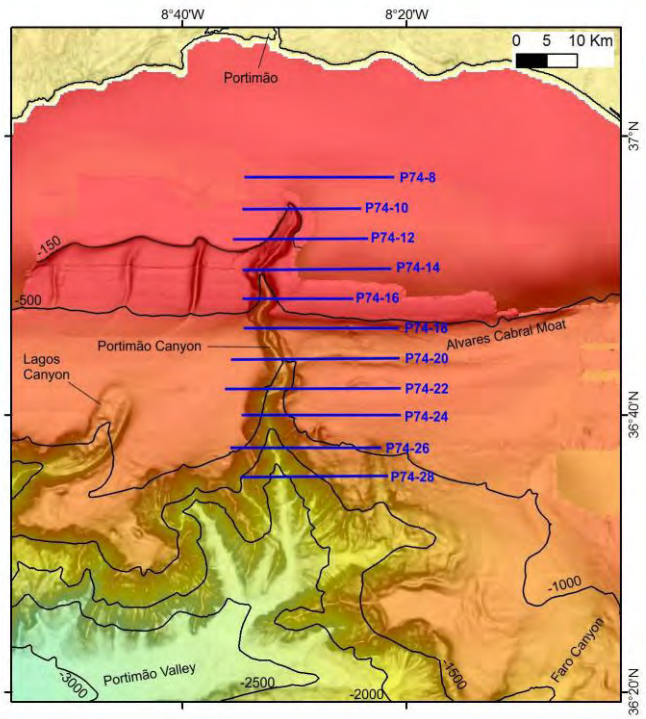

Figure 5.53 - Location of the selected MCS for the study of the Portimão Canyon. Blue colors are related to seismic profiles and black numbers are labels for the bathymetric contours.

On these profiles the basement is not identifiable. The Mesozoic sedimentary package displays continuous reflectors with high amplitude contrasts often displaying evidences of deformation like folding and faulting. In some areas, near a Mesozoic extensional fault it is possible to identify some growth strata towards these faults, thus corresponding to syn-rift deposits. Near the top of this package some reflectors with distinct seismic facies are present. These deposits are present only in some areas and are truncated by the Miocene basal unconformity and can either correspond to some different lithologies of Upper Cretaceous deposits or to Paleogene deposits. The basal Miocene unconformity is identified in all of the seismic profiles and is easily depicted by its strong acoustic signal and frequent truncations on the deformed underlying stratigraphic record. The Neogene package rests on top of the Miocene unconformity and its uppermost section is often masked by the ringing effect of the seafloor and by the multiple of the seabottom. It is difficult to map reflectors inside this package; nevertheless a tentative mapping of the base of the Quaternary was performed using the seismostratigraphic model proposed by Roque *et al.* (2012), based on the analysis of the five boreholes drilled in the seventies of the last century and on their reports and three piston cores. No more horizons were mapped as the quality and resolution of the MCS profiles did not allowed for it. The interpretation of the selected profiles is divided into three areas based on the features and processes there identified, the upper, middle and lower sectors of the canyon, as follows.

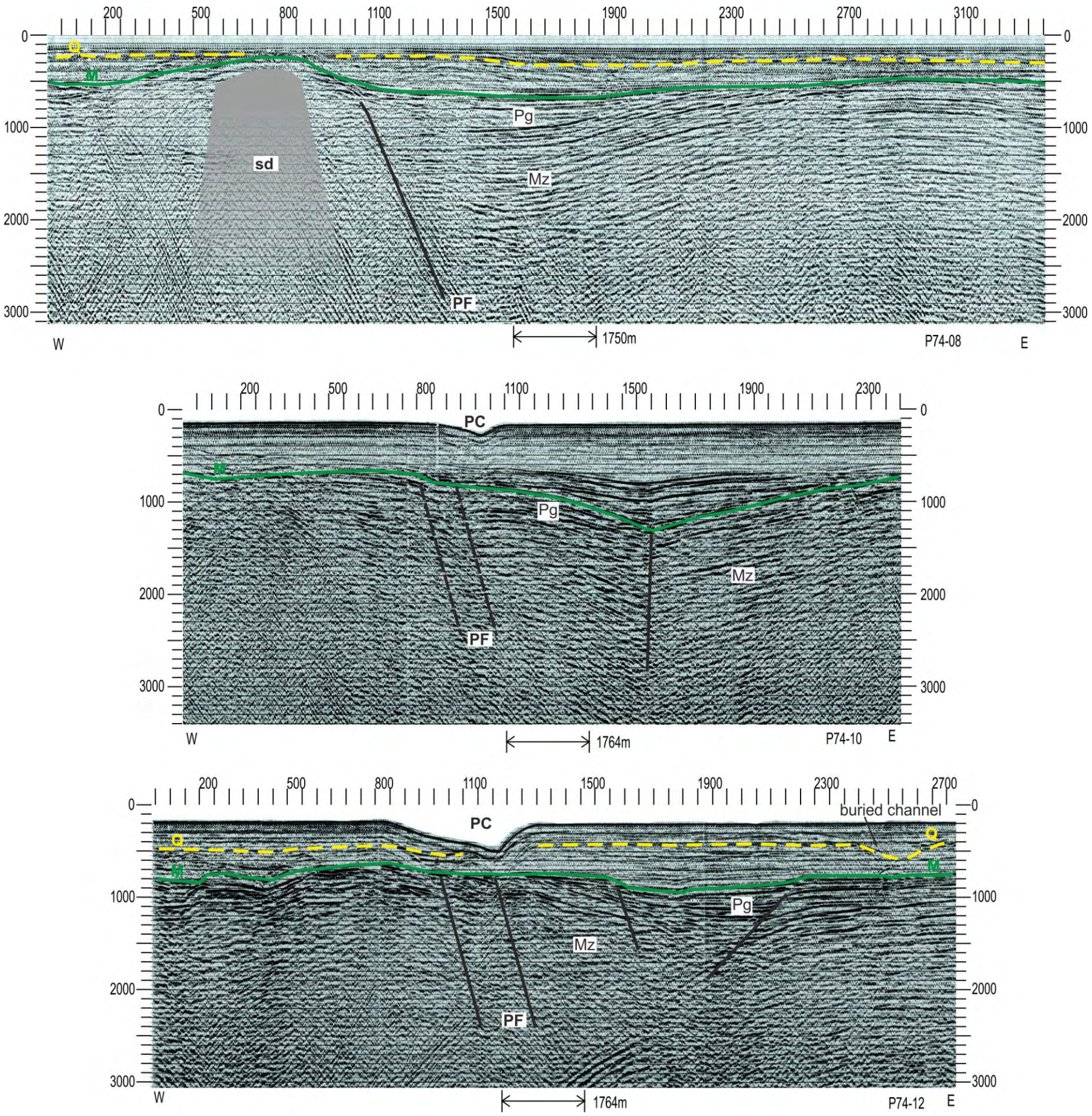

Figure 5.54 - MCS profiles across the Portimão Canyon

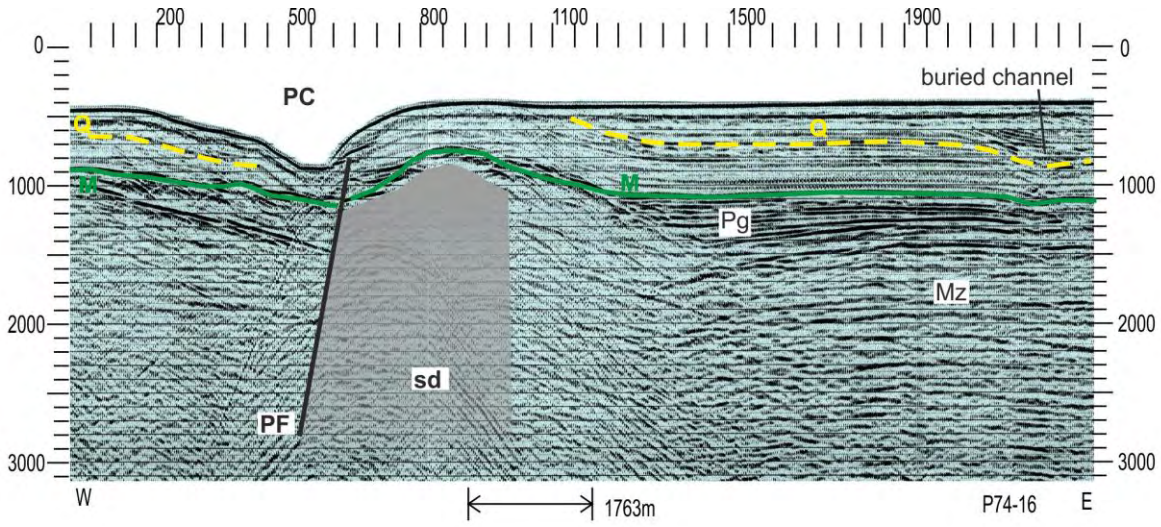

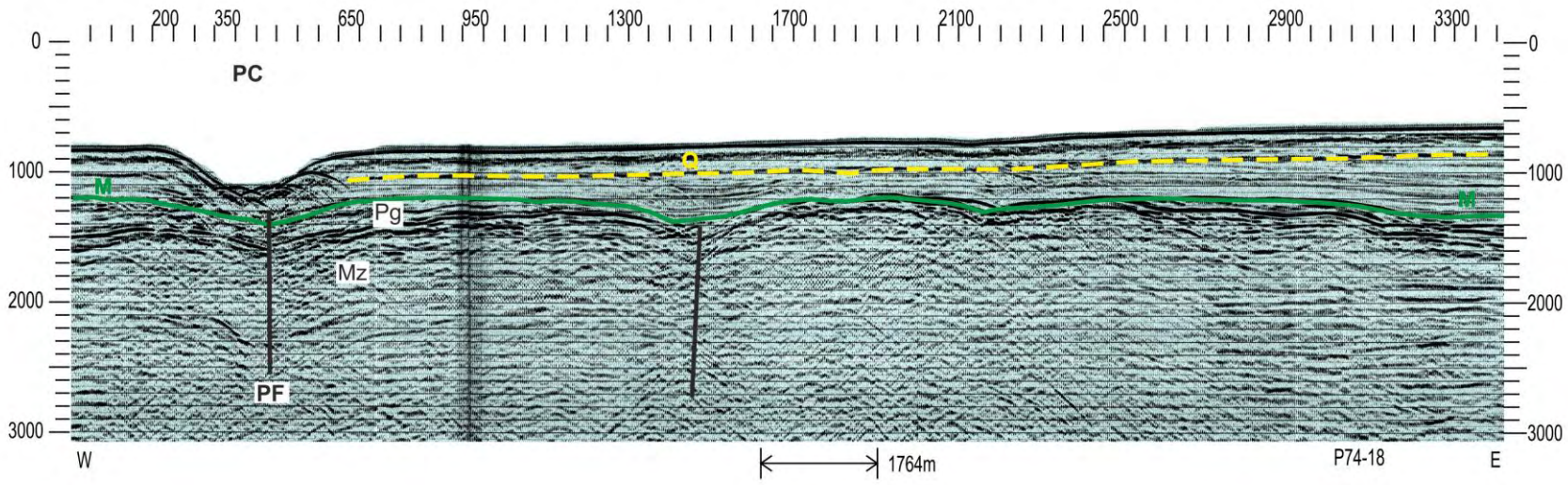

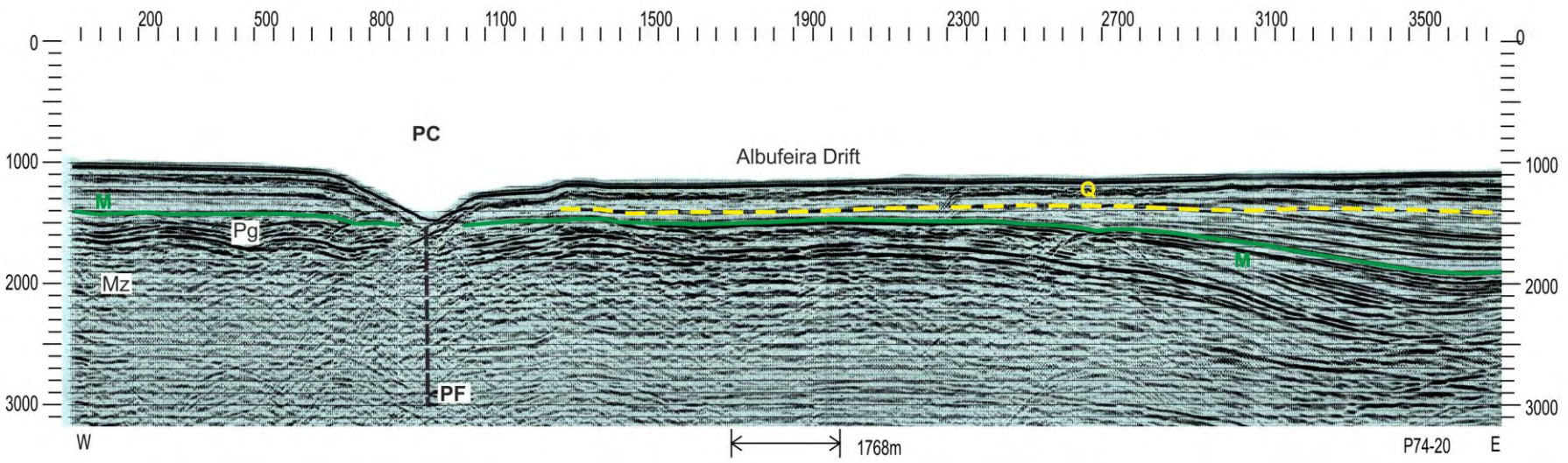

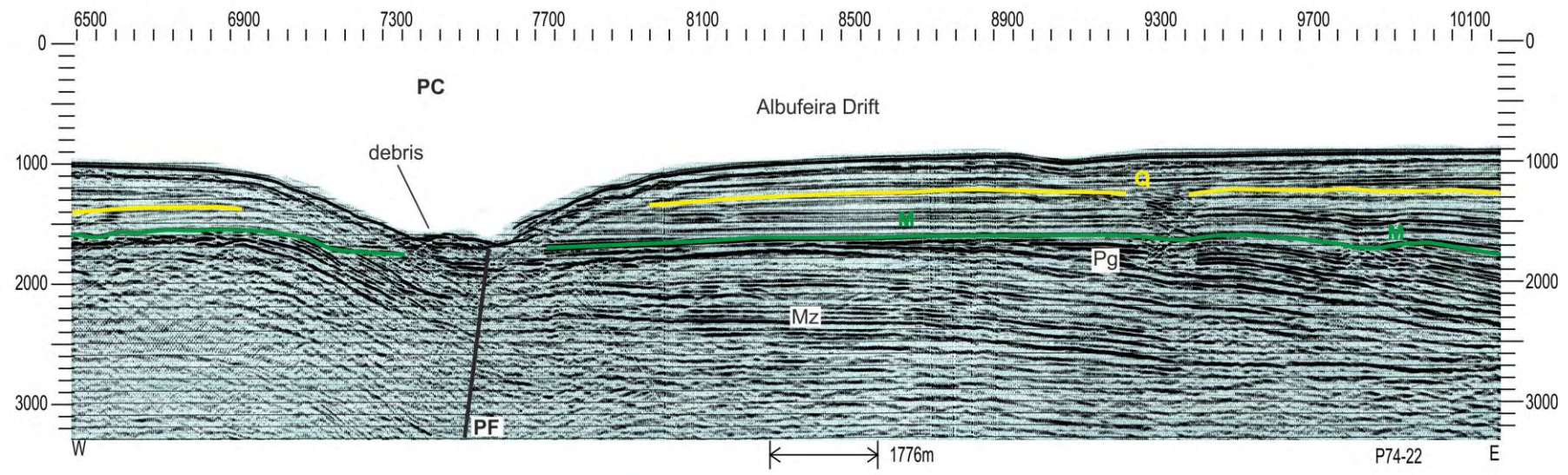

Figure 5.54 (cont.) - MCS profiles across the Portimão Canyon

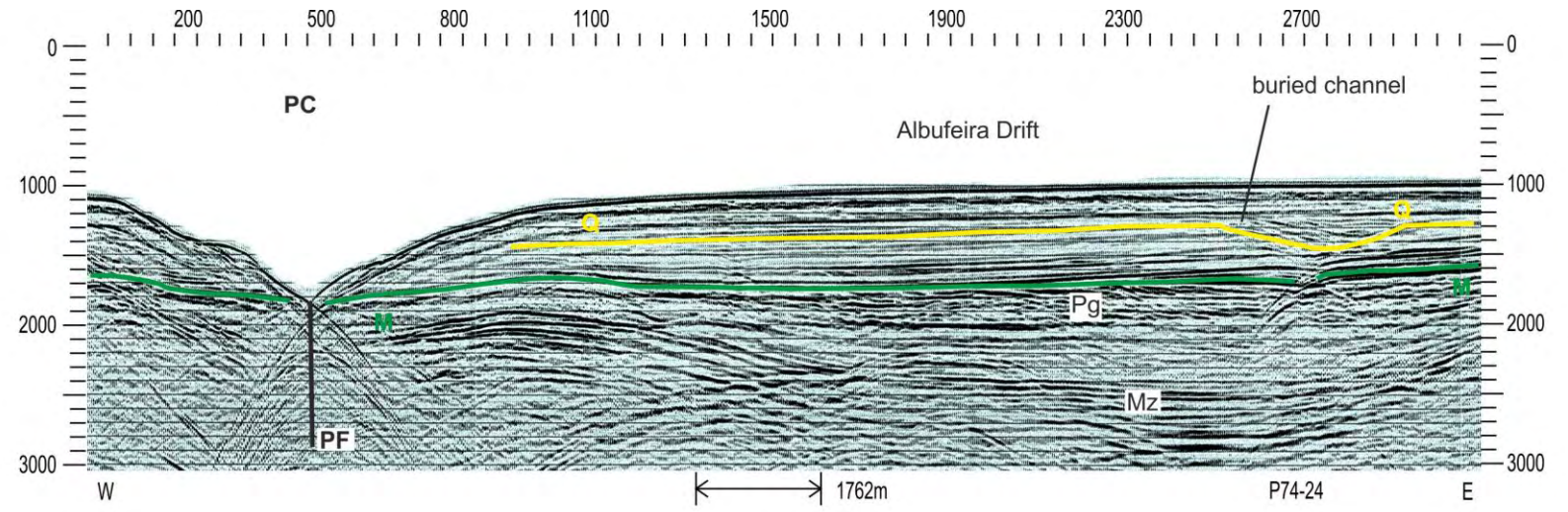

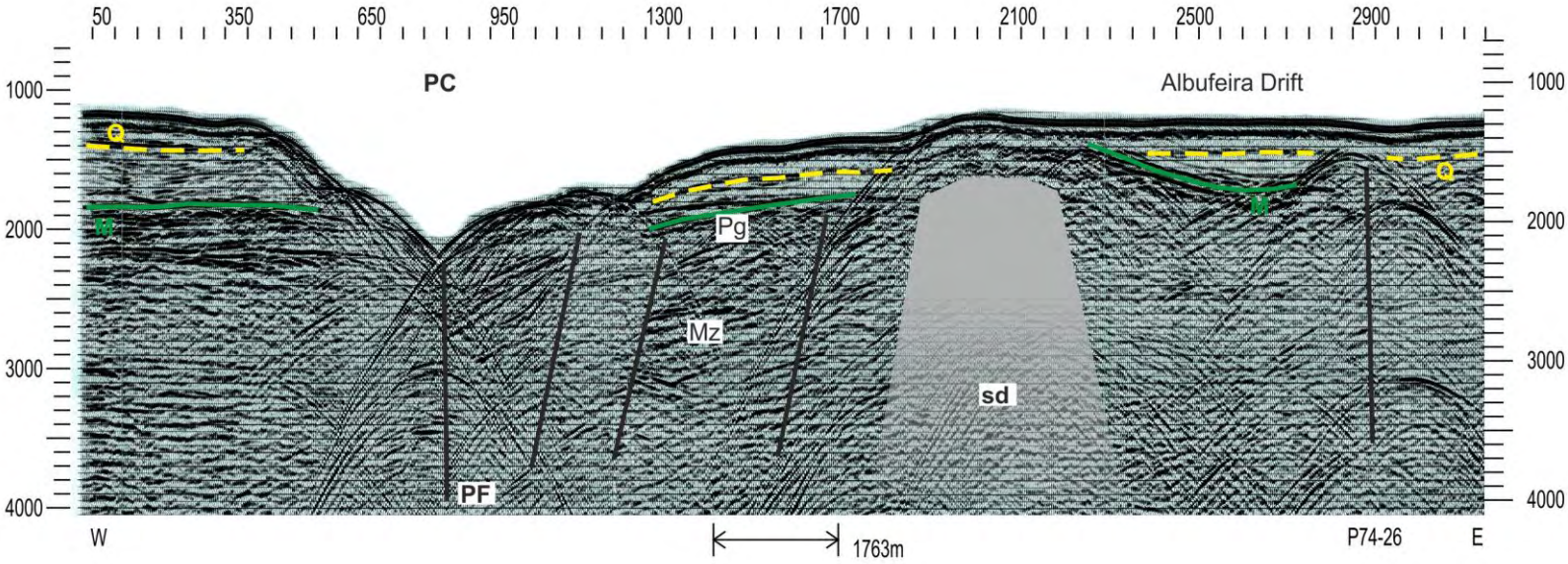

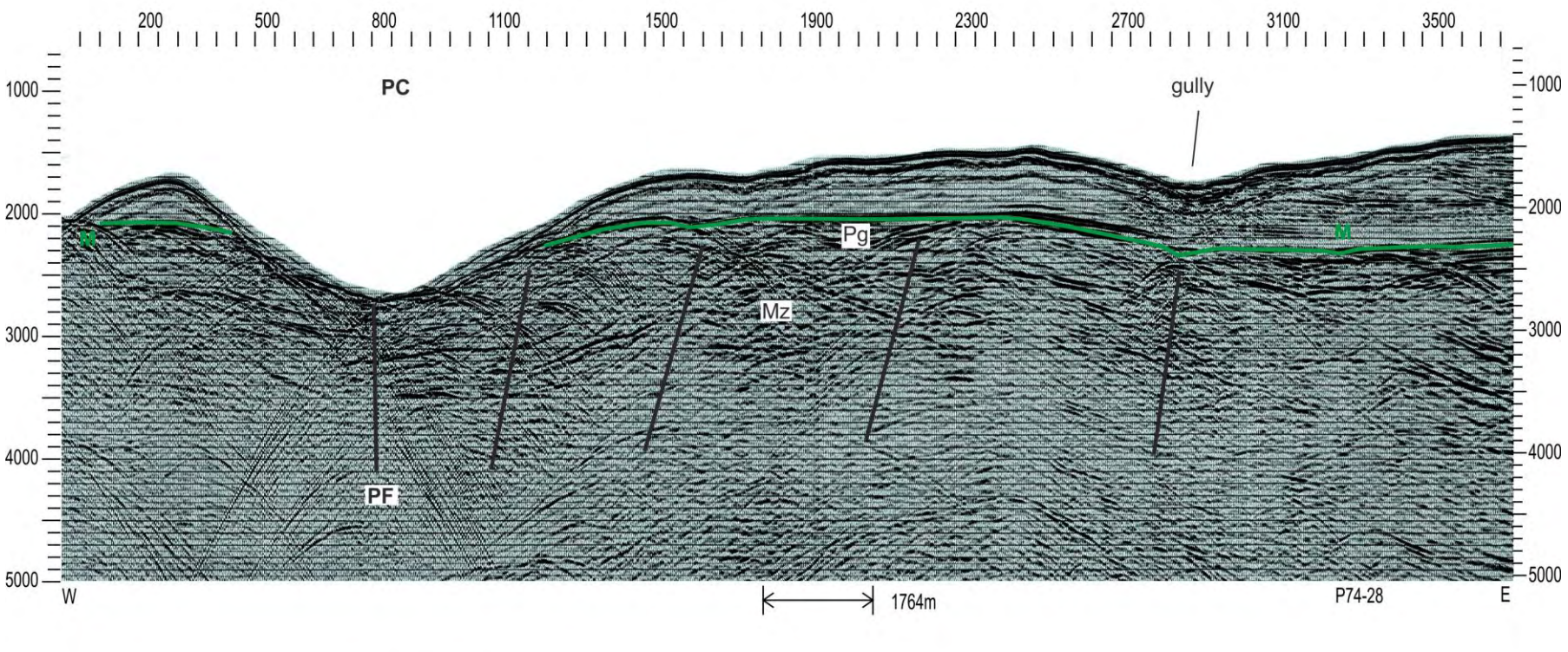

Figure 5.54 (cont.) - MCS profiles across the Portimão Canyon

Upper Sector (profiles P74-8, P74-10 and P74-12)

The MCS profile P74-08 cuts across the area upslope of the canyon head. Apart from a salt dome that does not have any bathymetric expression and a Mesozoic extensional fault with growth strata there is no feature or evidence of any process that might favor the location of a submarine canyon here.

Profiles P74-10 and P74-12 image the canyon in its uppermost sector. On MCS profile P74-10, the Miocene unconformity located at SP 1500 constitutes a subsided area that probably was a submarine channel that was rapidly covered up by the first Miocene deposits that display onlaps on both sides of this feature. This feature maybe connected with a graben that affects the Miocene unconformity located between SP 1600 and 2300 as both display a similar setting: the Miocene unconformity seems to have been in a bathymetric low at the time it was generated and was covered by the sediments that were deposit immediately after. This feature together with another disturbance that affects the Miocene unconformity at the western tip of profile P74-12, are the only places where the referred unconformity is not planar and subhorizontal. On the western sector of profile P74-12 there are evidences of deformation with folded strata. The disturbed sedimentary package and the deformation are truncated by the basal Miocene unconformity. This unconformity also truncates several other faults present on profiles P74-10 and P74-12 and the overlying Neogene sedimentary package appears as undisturbed in almost the whole area. The only exceptions, both on profile P74-12, where the Neogene deposits exhibit some features are a paleo-channel at SP 2600 and some paleo-slope failures beneath the western flank of the present day submarine canyon.

Middle Sector (profiles P74-14 and P74-16)

Like in the previous profiles the Miocene unconformity displays little to no deformation with the exception of a salt dome and the Portimão Fault that bounds it, located in the vicinities of the canyon. On both profiles, the Miocene unconformity and the Neogene package display folding on top of the dome and some recent horizons are also truncated by the seafloor. This suggests that the dome is active and is still rising. The dome initiated its rise in/or after Miocene times as the Miocene unconformity is folded. In the area above the dome the sedimentary package from the Miocene unconformity to the base of the Quaternary is evenly folded, whilst some reflectors above the base of the Quaternary seem to display onlaps on top of it. Therefore it seems that part of the deformation, or at least its most recent events, took place during the Quaternary. The onlaps testify that the dome was a bathymetric feature that rose above the smooth and relatively flat seafloor at the time.

Lower sector (profiles P74-18 through P74-28)

Here, like in the majority of places on the previously presented profiles, the Miocene unconformity and the overlying Neogene sedimentary package appear as almost undeformed despite the underlying reflectors display signs of deformation. Exceptions to this are: 1) the Portimão Fault that is found in all the profiles beneath the axis of the Portimão Canyon and vertically displaces the unconformity; 2) some paleo- channels infilled (SP 1550 on profile P74-18, SP 9350 on profile P74-22 and SP2750 on profile P74-24); 3) near the Albufeira Fault (not imaged but close to the easternmost tip of profile P74-20) where the Miocene unconformity is tilted and the Neogene package becomes progressively thicker towards the fault; and 4) in the vicinities of a salt dome on profile P74-26 (SP 2100). The filled up channel identified on profiles P74-22 and P-74-24 is part of an older drainage channel that became inactive and covered by the contourite drifts in the Lower Pliocene (Roque *et al*., 2012)

In almost all the studied profiles, the Miocene unconformity appears displaying its strong seismic amplitude, and is relatively undeformed, apart from some vertical displacement. This points to the fact that the major Alpine tectonic events that took place in the area occurred in Paleogene or even in Late Cretaceous times (Terrinha, 1998). An example of this is found on the western sector of profile P74-20 where the Miocene is flat and undeformed whilst the underlying truncated reflectors are tightly folded. Therefore, the Neogene package is also relatively undisturbed with some minor localized tectonic deformation.

The only places where a profuse Neogene deformation is found is on profiles P74-14 and P74-16 associated with the Portimão Fault and the salt dome. These features generally interfere with the bottom currents causing them to accelerate. One hypothesis for the origin of the Portimão Canyon is that this acceleration could have nucleated the erosion on the seafloor thus triggering the origin of the canyon. This could have been favored when these erosive currents reached the Portimão Fault as the rocks there may be weakened by the fracturation associated with the tectonic deformation. By these means, this process allowed the currents to continue to erode downslope from that area along the fault path thus accounting for the lower sector of the canyon to be fairly linear. This may have not been a passive process as the Portimão Fault has a cluster of seismicity associated with it. The Portimão Fault is still active at present and its activity may have breached the seafloor and together with the weakened and softer rocks in the fault zone could have favored the canyon's incision and further propagation.

The profiles that cut across the canyon in the areas upslope of where the salt dome is identified (profiles P74-8, P74-10 and P74-12) do not display any obvious evidence of any disturbances of tectonic or sedimentary origin that can allow the dating of the inception of the canyon in the upper sector. The canyon inception is possibly the result of upslope erosion,

parallel to the dip of the continental shelf. The upslope erosion probably initiated after the canyon started to erode the seafloor in the areas surveyed on profiles 14 and 16 and its continuation downslope until the canyon met the Cadiz Valley.

5.9 - Tectonic map and active structures

The tectonic structures in the Gulf of Cadiz, particularly the active ones at Present, were mapped and studied (Figure 5.55) by a large number of authors mainly after 1998, within national and European sponsored projects, using almost exclusively academic seismic profiles acquired with the particular goal of understanding the earthquake and tsunamigenic structures and the tectonics of the Eurasia-Africa plate boundary west of the Gibraltar Arc. Therefore, the profiles were not performed in a way that the area was totally covered, and their spacing, orientation and length were designed to study a specific target. These academic studies profited from: i) the previously existent geological mapping, ii) other studies of the onshore of the Gulf of Cadiz (Portugal, Spain and Morocco), such as published papers and PhD thesis, iii) the DSDP-120 and ODP-135 sites drilled on top of the Gorringe and Coral Patch Seamounts, respectively, iv) the oil industry boreholes on the continental shelf offshore south Portugal and southwest of Spain, and v) the dense MCS dataset acquired by the oil industry in the seventies of the last century and 2000.

The map presented in this work was obtained by the re-interpretation of multichannel seismic profiles from six academic surveys and one oil industry survey (see chapter 3 for the data used), all combined with a detailed study of the seafloor using the SWIM multibeam swath bathymetry dataset. The structures were mapped and classified after their kinematics (thrust, normal, strike-slip), age (pre-Miocene, Miocene, Pliocene and Miocene/Pliocene undifferentiated) and their cross-cutting relation with the seafloor (blind, outcropping). All the profiles investigated were stratigraphically calibrated using the seismostratigraphic model defined by Roque (2007) and Roque *et al*. (2012).

The criterion for “active tectonic structures” is the one proposed by Cabral (1995) and Ribeiro *et al*. (1996), who established that the remote tectonic field considerably changed from Late Miocene times to Pliocene-Quaternary. According to these authors, the main compression direction rotated from a NW-SE orientation to WNW-ESE, which in the Present is the orientation of the movement of Africa with respect to Iberia in the Gulf of Cadiz.

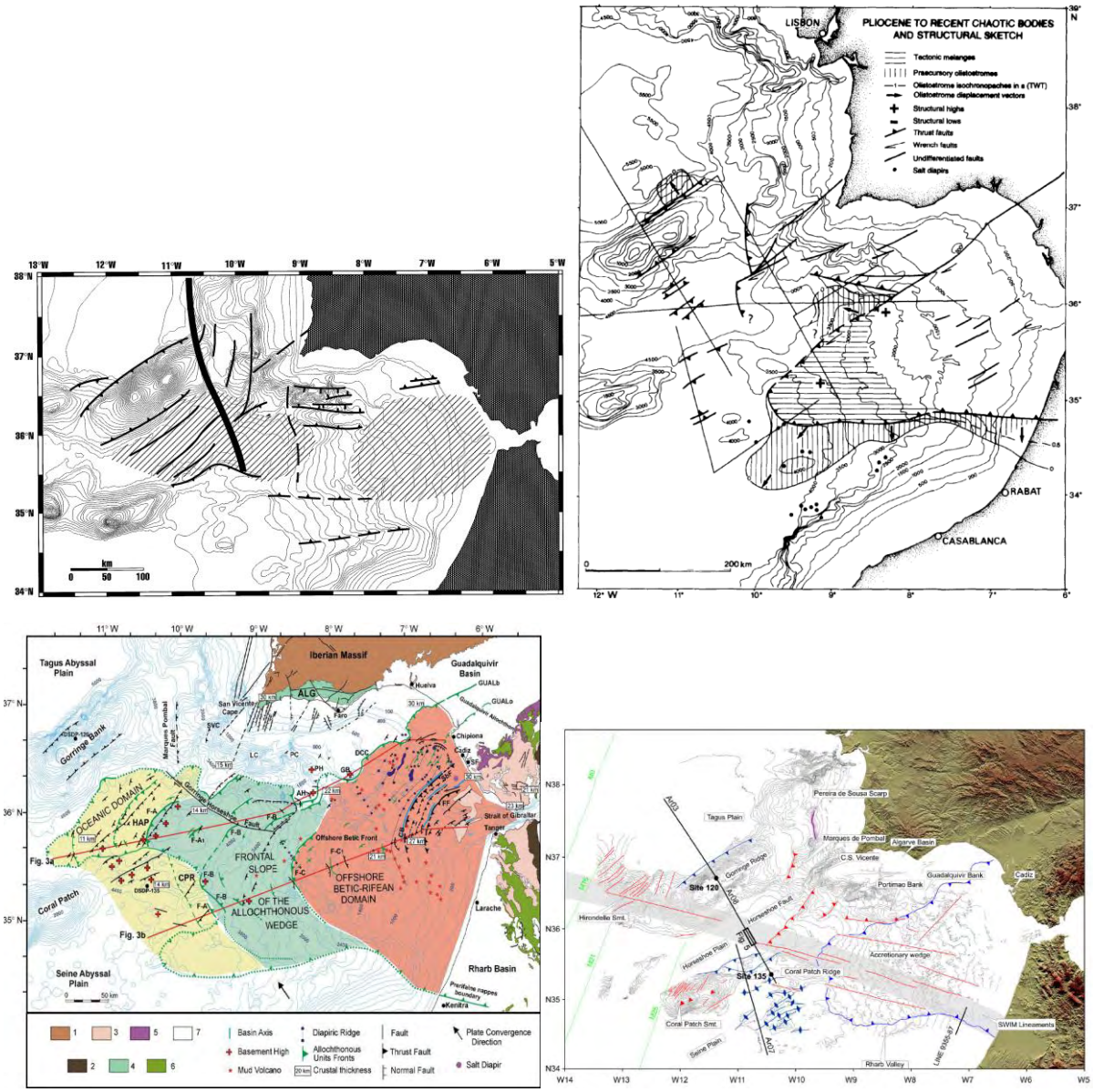

Figure 5.55 - Some structural maps of the SW Iberia by Tortela *et al*. (1997); Torelli *et al*. (1997); Medialdea *et al*. (2004); and Zitellini *et al*. (2009).

The Miocene was the climax of the formation of the inversion tectonics of the Mesozoic rift basin of the Portuguese continental margin and formation of the Alpine orogens in Portugal. At Present the main deformation concentrates in the deep offshore as revealed by continuously monitored instrumental seismicity and the published scientific papers. Hence, active tectonic structures are those that were active from Early Pliocene times in the study area.

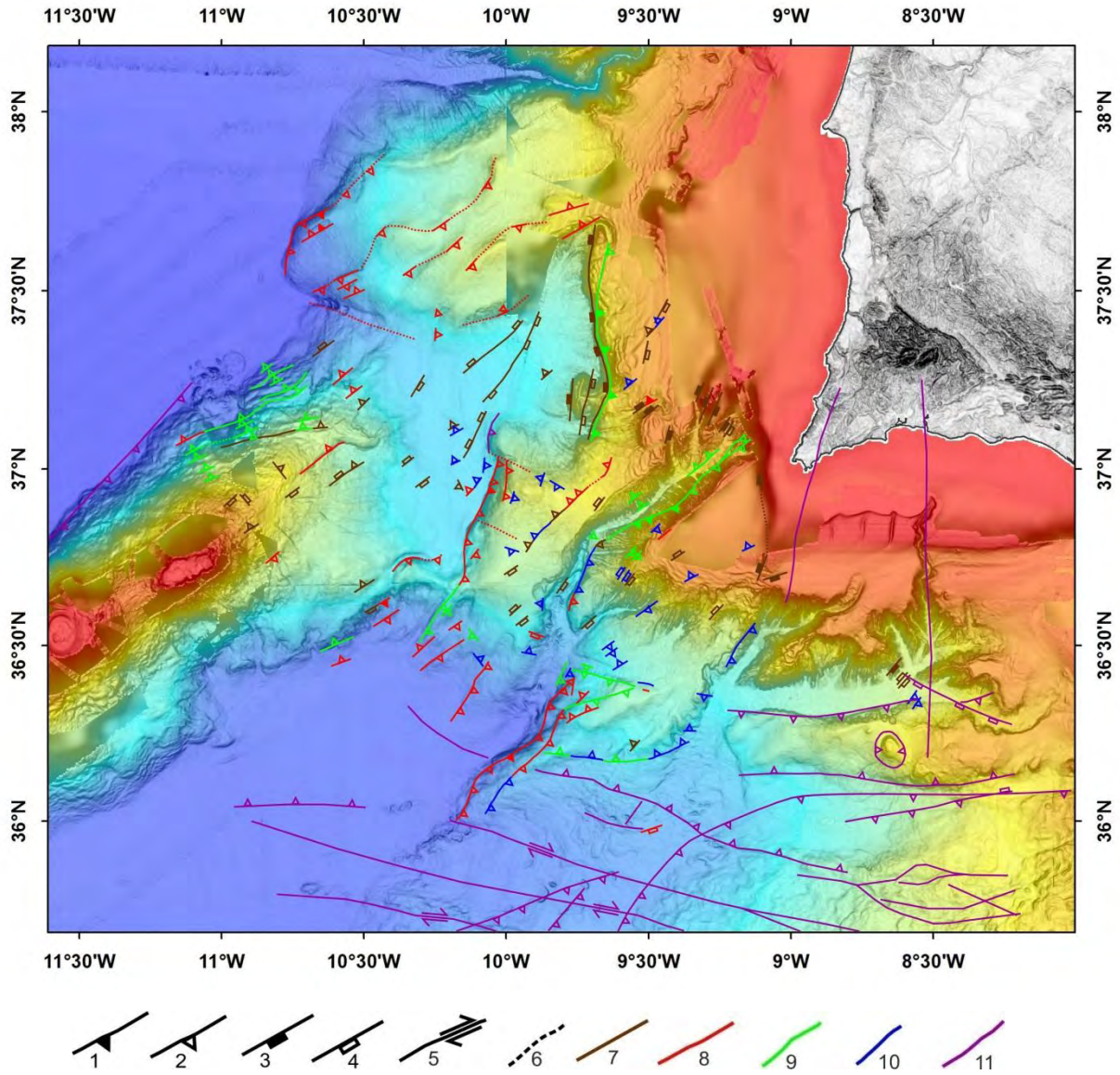

Figure 5.56 - Structural map for SW Iberia. Legend: 1- reverse fault outcropping; 2- blind reverse fault; 3- normal fault outcropping; 4 – blind normal fault; 5- strike-slip fault; 6- probable fault; 7- pre-Miocene structure; 8- post-Pliocene structure (active), 9- Miocene/post-Pliocene undefined structure (possibly active); 10- Miocene structure (not active); 11- structures from Terrinha *et al*. (2009) and references therein.

From the analysis of the map shown on Figure 5.56, the active tectonic structures in the area are grouped in three classes: i) the N-S to NE-SW trending thrusts directed to the west to NW; ii) the WNW-ESE trending dextral strike-slip faults; and iii) the Gulf of Cadiz accretionary wedge. The first class encompasses the Tagus Abyssal Plain Fault, the Gorringe Thrust, the Marquês de Pombal Thrust, the Horseshoe Fault and the S. Vicente Canyon Thrust. The second one comprehends the SWIM dextral strike-slip faults present in the central part of the Gulf of Cadiz, the Horseshoe Abyssal Plain and go as far as to the base of the Gorringe Bank. The last class is made up by the subduction-related accretionary wedge (Gutscher *et al*., 2002), which by other authors was considered barely active at Present (e.g. Zitellini *et al*., 2009) or under other type of tectonic classification (Sartori *et al*.,

1994; Torelli *et al*., 1997; Maldonado *et al*., 1999; Iribarren *et al*., 2007). Other tectonic structures were mapped and they will be addressed separately later. Besides the mapping and interpretation of the seismic profiles, the seismicity of the area (Figure 5.57) brings an insight to the importance of the structures regarding their activity.

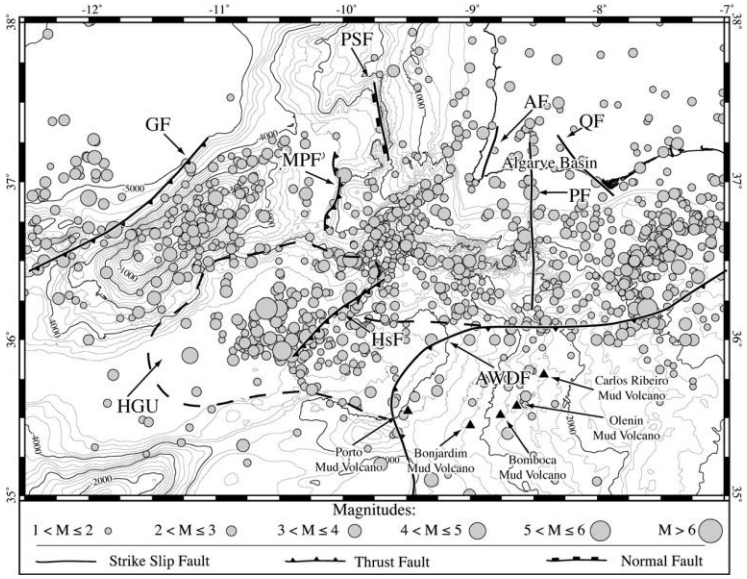

Figure 5.57 - Active seismicity in the SW Iberia with traces of the more important structures; after Terrinha *et al*. (2009).

5.9.1 – N-S to NE-SW Thrusts

The four more important structures of this group are present in the central to the western part of the Gulf of Cadiz and in the Western Portuguese Margin encompassing several hundreds of kilometers from the Coral Patch Ridge to the Príncipes de Avis Spur (see Figure 2.2). They all have an important bathymetric expression and associated seismicity (Sitch *et al*., 2007; Terrinha *et al*. 2009; Silva *et al*., 2010) suggesting, therefore, that they are active at the Present (Figure 5.57).

5.9.1.1 - The Tagus Abyssal Plain Fault

This structure extends for about 70 km and displays a continuous but not always prominent scarp that can reach up to about 1.5 km. The scarp is steeper on the south sector of the fault and gradually becomes gentler to the north where it is affected by mass wasting processes with smaller gradient values. It constitutes the eastern limit of the Tagus Abyssal Plain that is underthrusted by the Príncipes de Avis Spur. There is not much seismic activity associated with this structure but from the inspection of MCS profiles it is seen that the fault cuts through all the sedimentary package (even the more recent deposits) and reaches the seafloor (Figure 5.58). To the east of the fault, there is a backthrust that connects with the main structure towards the deep and is present between the two anticlines. It is possible to

trace the fault deep in the seismic record and it displays a listric profile and cuts deep onto the subsurface displacing the basement (Cunha *et al*., 2010).

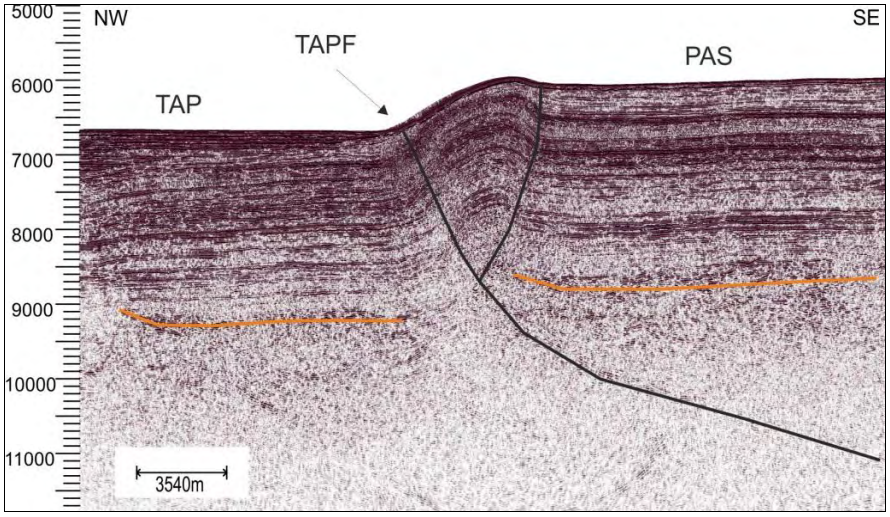

Figure 5.58 - Section of MCS BS11 across the Tagus Abyssal Plain Fault (TAPF), that thrusts the Príncipes de Avis Spur (PAS) over the Tagus Abyssal Plain (TAP); the orange line marks the top of the basement. See text for details.

5.9.1.2 – The Gorringe Thrust

The Gorringe Bank is the most prominent bathymetric high on the SW Iberian Margin, rising from near 5 km depths of the Horseshoe and Tagus Abyssal Plains to close to 20 mbsl. It displays a wide array of unusual rocks that probably correspond to exhumed serpentinized peridotites from the mantle (Girardeau *et al*., 1998). The Gorringe Thrust (Figure 5.59) roots very deep onto the basement, probably displacing the Moho (Sartori *et al*., 1994) and has a large-amplitude gravity (Purdy, 1975) and geoid (Souriau, 1984) anomalies. The flanks are affected by mass-wasting processes, and in the Tagus Abyssal Plain a chaotic body that thins away from the elevation probably corresponds to a major debris deposit. The structure is associated with an important cluster of seismic activity.

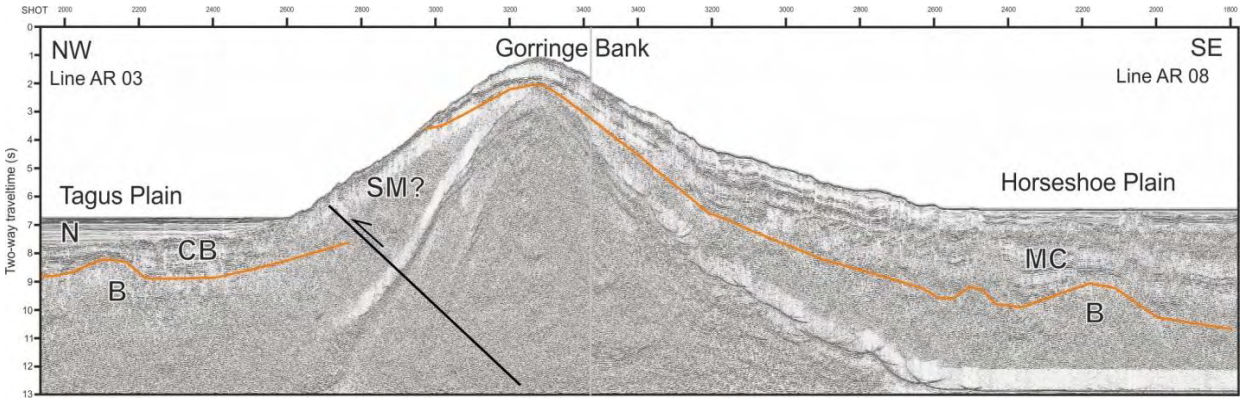

Figure 5.59 - The Gorringe Bank and adjacent areas imaged by MCS profiles AR03 and AR08. To be noted is the steep wall of the seamount and the magnitude of the thrust strongly displacing the basement. Orange line depicts the top of the basement (B); CB – chaotic body; MC – Meso-Cenozoic sediments; N – Neogene sediments; and SM – serpentinized mantle.

5.9.1.3 – The Marquês de Pombal Thrust

This structure (Figure 5.60) has been described in detail but its general features are that it extends for more than 60 km, bounds the homonymous plateau to the west, and its scarp is steeper and higher (more than 1km) in its northern sector.

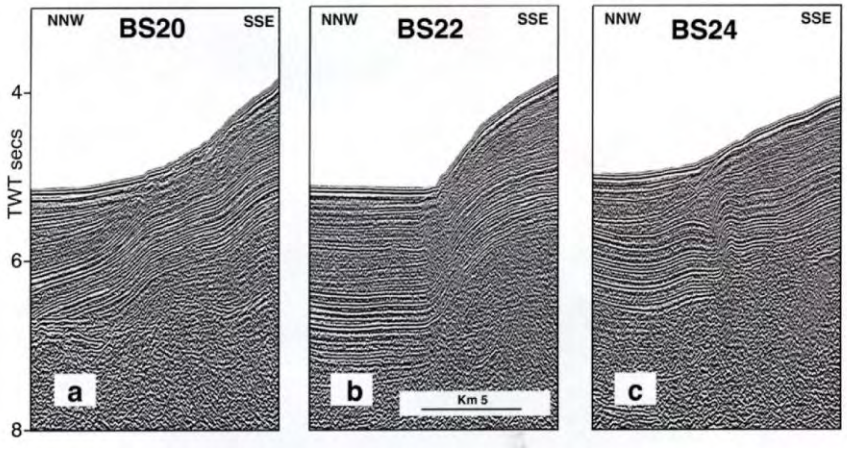

Figure 5.60 - Details of the Marquês de Pombal Thrust and associated scarp in three MCS on different sectors on the fault. To be noted that in the cases where the fault does not reach the seafloor there is still signs of major deformation in the recent sediments. After Zitellini *et al*. (2001).

The fault trace appears to have 2 inflections: one near the northern tip and the other in the middle part. It roots deep in the basement and might displace the Moho. Has a record of present day seismic activity that reinforces the seismic interpretation that already pointed out for its activity in modern times.

The fault scarp reaches heights of over 1 km and the fault trace is covered by deposits that slid from the scarp and plateau. Gràcia *et al*., 2003 and Terrinha *et al*., 2003 reported scars of mass transported deposits that extend approximately 20 km from the top of the plateau to the Infante D. Henrique Basin, the foreland basin of the thrust.

5.9.1.4 – The Horseshoe Fault

This thrust fault extends for over 100 km from the Coral Patch Ridge to the base of the South Portuguese Continental Slope. It bounds the Horseshoe Abyssal Plain to the east and has a scarp that can reach about 1km (Figure 5.61). In the northern sector, the fault has two branches and it is possible to identify a backthrust. In this area, the fault has a steeper scarp that fades out progressively to the south where it is disrupted by the end sector of the south Portuguese submarine canyon's drainage system. In this area the thrust interferes with the SWIM lineaments and further to the south interferes again with the Coral Patch Ridge block merging with some other structures. The fault roots to the east and cuts down through the basement testifying its importance at a crustal scale. It has an associated cluster of seismic activity that together with the deformation of the uppermost and recent sediments, and the fact that it reaches the seafloor, confirm its activity in present day times.

The sites of interference of this thrust with the SWIM faults have a complex fault pattern buried under the Horseshoe Abyssal Plain only revealed by MCS interpretation and studied by analog and numerical modeling (Rosas *et al*., 2012). However, on the hanging-wall, this fault interference has clear morphologic manifestations, such as localized landslides and positive flower structure deformation (like in the area where the new mud volcanoes were discovered and displayed in Figure 4.55).

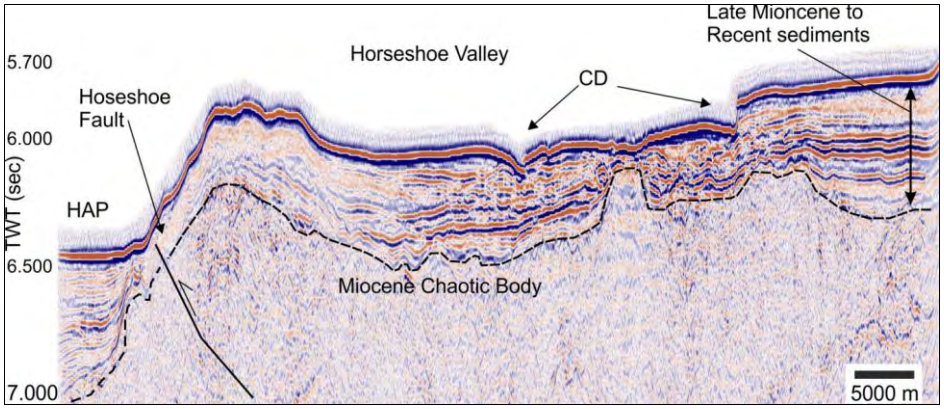

Figure 5.61 - Section of the IAM4e MCS profile imaging the Horseshoe Fault; dashed marker corresponds to the top of the chaotic body; CD stands for crescentic depressions like the ones depicted on Figure 4.54.

5.9.1.5 – The S. Vicente Canyon Fault

This fault extends from the shallow parts of the canyon until about 4000 mbsl over a distance of about 80 km presenting a slightly sinuous map trace. It is located near the axis of the canyon slightly closer to its eastern wall, in the cases where it is outcropping it constitutes the base of the slope of that flank (Figure 5.62). It is associated with a cluster of seismicity suggesting its Present day activity, however due to the active slumping and erosion in the canyon area the sediments that could provide a better dating for its activity are very disturbed or heavily eroded, thus not allowing for proper age deduction. However, in some of the MCS profiles it was possible to identify this structure as an active structure. Its activity started in the Neogene but no accurate date can be given, however by the seismic facies of the units affected and by the absence of thicknesses variations across the fault, it is likely that this structure started its activity at the same time as the major structures in the area did (Marquês de Pombal Thrust and Horseshoe Fault).

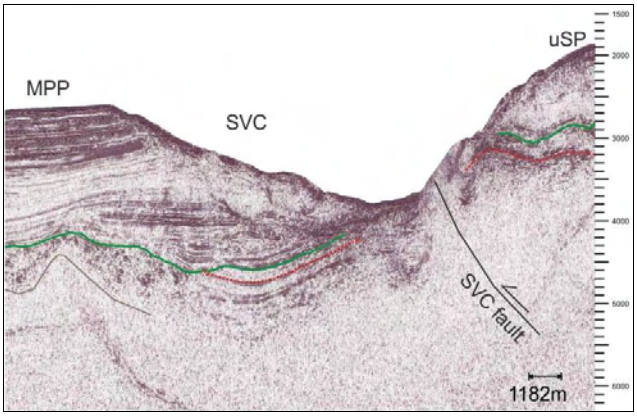

Figure 5.62 - Section of the BS20 seismic profile imaging the S. Vicente Canyon (SVC) area, the profile depicts the SVC thrust at the base of the eastern flank of the canyon that uplifts the eastern block (topped by the upper Sagres Plateau).

5.9.2 – WNW-ESE dextral strike-slip faults

The WNW-ESE strike slip fault system (also known as the SWIM lineaments, Duarte *et al*., 2009, Terrinha *et al*., 2009, Zitellini *et al*., 2009) is mapped over large distances, from the near-shore Moroccan area to the vicinities of the Gorringe Bank, over 500 km in length crossing several different morphotectonic domains (Figure 5.63). These structures interfere with other tectonic structures like the accretionary wedge, the Horseshoe Fault and the Coral Patch Ridge.

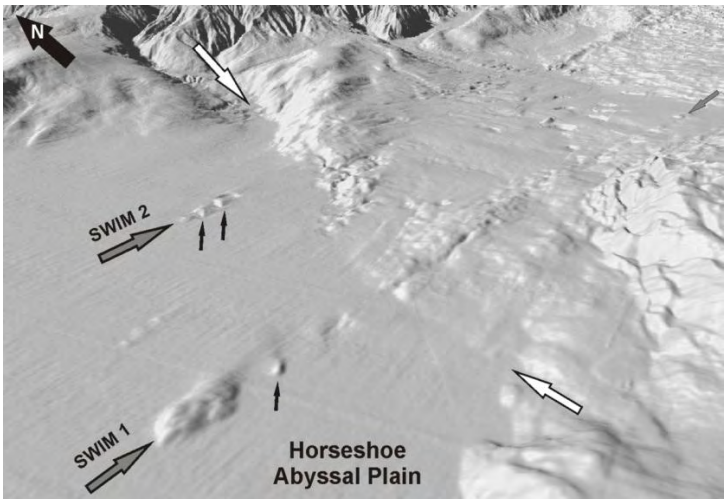

Figure 5.63 - 3D bathymetric view of two of the SWIM lineaments as they enter the Horseshoe Abyssal Plain. Small black arrows point to folds on the seafloor that materialize the lineaments, white arrows point to the Horseshoe Fault trace. After Duarte *et al*. (2009).

The morphological expression of these structures is varied and was addressed in a previous section of this thesis but in general it is made up of an aligned succession of crests and troughs. Some of these features correspond to en-echelon folding of the most recent sediments, i.e. of Late Pliocene-Quaternary age. It is also common for active mud volcanoes to be located on top of these lineaments, several of them inside the accretionary wedge and

three new ones (Figure 4.55) discovered on top of one of these structures north of the Coral Patch Ridge. Although some of these structures are traced over large distances with strong bathymetric features their morphological expression is minute in some sectors. This fact leads to different interpretations on the mapping of these lineaments by the different authors (Terrinha *et al*., 2009, Rosas *et al*., 2009 and Zitellini *et al*., 2009). Nevertheless, these lineaments are the morphological expression of strike-slip faults that result from the reactivation of older faults that are deep rooted into the basement (Rosas *et al*., 2009; Terrinha *et al*., 2009) and important at the crustal-scale level. These faults are Mesozoic extensional faults that cut through the basement, some show signs of reactivation as reverse faults and the seismic profiles depict deformation of the uppermost sediments defining the lineaments (Figure 5.64). Some of these structures seem to play an important role in fluid migration as displayed in some seismic profiles.

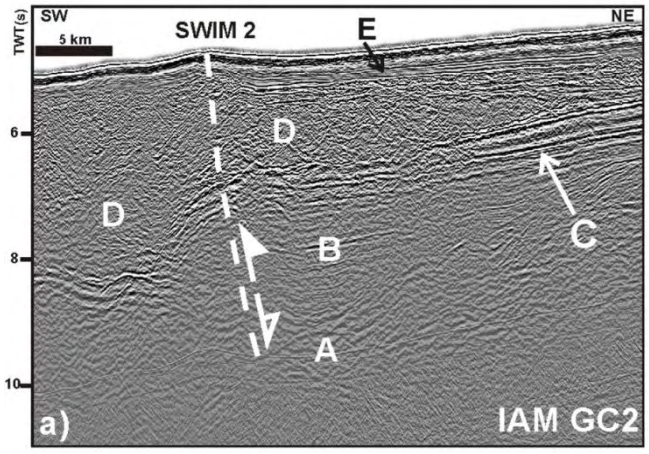

Figure 5.64 - IAM GC2 seismic profile across one of these structures. The white dashed line corresponds to the fault zone related with the bathymetric lineament with its previous kinematics (white arrows). A- Basement; B- Sin-rift wedge (Mesozoic age); C- Post-rift unit; D- Accretionary Wedge unit (Miocene age); E- Cover unit (Plio-Quaternary age). After Duarte *et al*. (2009).

Rosas *et al*. (2009) using the angular relationship of the folds with the major lineament trend concluded that the observed en echelon folding on the sea floor associated to the SWIM faults formed 1.8 Ma ago.

5.9.3 – Gulf of Cadiz accretionary wedge

This feature was described in a previous chapter of this work and is the most prominent feature in the Gulf of Cadiz, occupying a large area and standing out by its pattern in the bathymetry. It is a concave feature with opening to the east that extends from the near-shore area to depths of more than 4000 mbsl located more than 250 km to the west and with about 150 km in width. In the vicinities of the Straits of Gibraltar, its upper part is masked by the MOW system that deposits some materials on its top. It is bounded to the NE by the Cadiz

Fault in the salt domes and ridges domain, to the north by the Cadiz Valley, to the NW by the Horseshoe Valley, to west it is indented by the Coral Patch Ridge, to the SE by the Seine Abyssal Plain and to the south by the Rharb Valley. It displays a rough bathymetry that is the result of many active processes like thrusting, folding, fluid escape, salt tectonics, wrenching and raft tectonics and active mud volcanism (Mulder *et al*., 2003; Pinheiro *et al*., 2003; Gutscher *et al*., 2002; Terrinha *et al*., 2009, Zitellini *et al*., 2009). Structurally, it is a westward thrusted pile of deformed sediments (Figure 5.65) that reaches almost 15 km over an eastward dipping base (Thiebot and Gutscher, 2006). This overall geometry coincides with the subducting slab under the Gibraltar Arc.

The accretionary wedge appears to be active and propagating to the west as new thrusts are being formed under the flat seabed of the Horseshoe Valley westwards of the deformation front.

From a sheer structural point of view this is a roughly N-S striking thrust detachment and for this reason it could be included in the above described group of N-S to NE-SW Thrusts. However, it stands for a separate group because of its unique seafloor morphology, the internal structure, and the fact that this is the only important westwards directed shortening structure in the Gulf of Cadiz region s.s.. Although it does not show significant instrumental seismicity it has been argued that it is the only capable of producing a M>8 earthquake in the area (Gutscher *et al*., 2002) and its extension in depth has recently generated earthquakes at more than 600 km in southern Spain (epicenter in the Granada region).

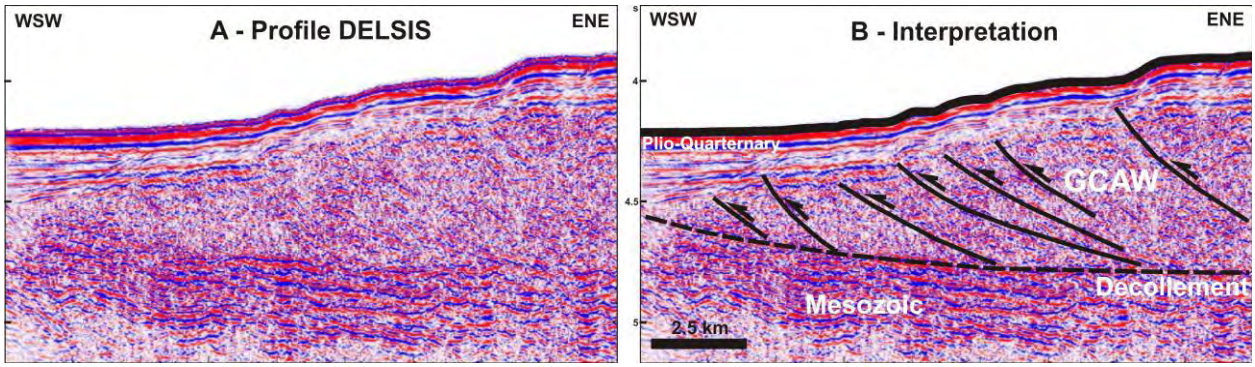

Figure 5.65 – Delsis MCS profile (A) and interpretation (B) across the deformation front of the accretionary wedge displaying the recent thrusts formed outside the bathymetric expression of the accretionary wedge. After Duarte *et al*. (2011).

5.10 – Synthesis

The S. Vicente Canyon

The inspection and interpretation of several multichannel seismic profiles (Figure 5.18), the description of some of which was presented in this chapter, allowed the analysis of the subsurface structure of the area and the establishment of a chronological succession of the main geological events that took place and controlled the evolution of the SW Portuguese

area, in particular how and when the S. Vicente Canyon was formed and how its evolution was processed.

In its shallower parts, the SVC displays a thin sedimentary cover on the axis area. The Miocene and Paleogene unconformities are very irregular, defining an overall syncline form, between two basement highs. The Neogene sediments display disrupted reflectors with many truncations, little horizontal continuity and high amplitude contrasts evidencing the effects of erosion and mass wasting processes (Figure 5.21). The flanks show almost no sediments, probably they became unstable and have fallen and flushed and been redistributed downslope through the canyon. The few sediments found on the eastern flank display abundant signs of gravity driven processes like slumping. Towards deeper areas of the upper sector, the structure underneath the canyon bottom is similar to the one described now; the Miocene and Paleogene define a wide and gentle syncline form and the Neogene sedimentary package is still minute although slightly thicker than upslope. The sedimentary cover found in the canyon bottom display abundant truncations and evidences of mass wasting processes, as well as the ones found on its flanks. On the central part of the canyon's bottom a paleo-valley is perceptible and the filling sediments found display high amplitude contrasts, probably corresponding to debrites. This provides evidences that the canyon had a previous strong erosive event and later the carved bottom was filled with more recent deposits (debris). This upper sector displays a tectonic control supported by the presence of the S. Vicente Canyon Thrust, located on the canyon bottom affecting the lower units.

Deeper downslope, in the canyon's upper sector, with the increasing incision and the steepness of the flanks, the mass wasting processes are also common in the seismic record like slumping, slide scars and gravity-driven rotational blocks. As in the previous sector, the bottom of the canyon coincides with the westwards-vergent thrust (S. Vicente Canyon Thrust), and it is possible to identify a paleo-valley underneath the present day submarine canyon that is filled with chaotic facies deposits corresponding to debris-flows. As the depth increases and there is more space to accommodate the sediments, the sedimentary thickness also increases. On the western wall, the uppermost sediments define a triangular shaped unit with continuous reflectors and high amplitude contrasts (compatible with levee deposits) that result from the overbanking processes associated with the canyon. The Neogene deposits on the eastern wall are affected by slumping causing their seismic facies to be very different from the same deposits on the opposite side (Figure 5.24). Another major seismic facies shift takes place beneath the canyon axis area (slightly eastwards of the thalweg); the Paleogene and Lower Miocene deposits display major differences from both sides of the canyon. The same deposits on the eastern side have much higher amplitude than the ones found beneath the canyon and towards the west.

The Marquês de Pombal Block displays a well-structured sedimentary package of Mesozoic and Cenozoic strata and only the uppermost deposits are affected by mass wasting processes in the Marquês de Pombal area. The Mesozoic and Paleogene reflectors display onlap terminations against the basement highs; these define alignments found westwards of the SVC and near the MPF and some scattered highs throughout the area (Figure 5.47). The Paleogene and Miocene basal unconformities are very well identifiable throughout the whole study area by their strong amplitude, large spatial continuity and frequent truncations of the underlying reflectors. They mark important and widespread geological events of uplift and erosion.

For the larger part of the MPB, the Neogene sedimentary package is sub-horizontal and only locally disturbed by some sedimentary features, a reverse fault in the center of the Plateau and deformed in the vicinities of the Marquês de Pombal Thrust. The activity of the Marquês de Pombal Thrust accompanied by the uplift of the area on its hanging-wall is well recognizable in the seismic record, by several evidences: i) subsidence and presence of chaotic facies' bodies on the footwall of the MPF, ii) signs of gravity instability and slide scars in the Marquês de Pombal scarp area, iii) truncations of reflectors in the western and central part of the MPB (that corresponds to the area that experienced more uplift), iv) onlaps on the syncline drag fold associated with the MPT, and v) onlaps as sign of subsidence in the present day submarine canyon and eastern part of the MPB (as a compensation for the uplift near the fault). All these features are found at the same time throughout the Marquês de Pombal Plateau and S. Vicente Canyon area.

As the thrust fault initiated its activity, the uplift of the hanging wall caused relative subsidence of the footwall, resulting in the formation of onlaps near onto the fault and hanging-wall drag fold. The presence of the chaotic bodies that are found in the footwall of the MPT and thicken towards the fault probably correspond to debris of material that fall down from the uplifted block, mainly from its scarp, due to its steepness and instability. Therefore, it is proposed that the presence of the first bodies with these characteristics is a good indicator of the start of the activity of the MPT. The debris-flows on the footwall are present in unit MW3 and units above. Unit MW3 also features the onset of onlap terminations, identified in the same area of the footwall. These are associated with the localized subsidence of the footwall when the thrust is active and represent another evidence for its activity. Another feature that helps to determine the start of the uplift of the area, is the presence of onlaps on the syncline (between two anticlines) of the MP Thrust drag fold. When the thrust is active the closest sediments near the fault undergo some folding; the major fold is an anticline and is in direct contact with the thrust, eastwards of this anticline there is a syncline. As the fault moves, the drag folds increase in size and as this occurs the syncline becomes deeper and so sedimentation takes place preferably on the

more subsided areas and form onlaps on the flanks of the syncline. The identification of these terminations will allow the dating of the activity of the fault, also pointing to the start of the activity in the Late Miocene (unit MW3). Along with the uplift in areas near the fault plane, the hanging-wall distal areas further east undergo relative subsidence and/or tilting to the east, which is shown by the presence of onlaps in the sedimentary units near the present-day submarine canyon area (Figure 5.51). However, this thickening is registered latter than the previous cited evidences, only during unit MW4 (Early Pliocene) and onwards.

The Portimão Canyon

The selected MCS profiles (Figure 5.53) image the continental shelf and slope in the submarine canyon area. The area upslope of the canyon is also surveyed and it showed no relevant features which could be related with the canyon emplacement in the area where it is, thus the processes and features responsible for its formation had to be found downslope.

The uppermost sector of the canyon incises the South Portuguese continental shelf and the seismic profiles reveal that in the vicinities of the canyon several faults are present. None of these features have played an important role on the canyon formation and evolution since the faults seem to be inactive since the Miocene.

Further downslope, the seismic profiles depict several features that are located near the canyon and are of high importance regarding its origin and evolution. These features are the Portimão Fault and a salt dome. The Portimão Fault seems to control the location of the submarine canyon since it is located beneath the canyon and on profile P74-16 it appears to cut through the entire sedimentary package and outcrops on the seafloor on the bottom of the canyon. The salt dome present in the area is also located close to the canyon and is related to the Portimão Fault constituting its western boundary. There are also evidences of deformation of the Neogene package in the vicinities of the canyon where some reflectors are tilted and folded. All these evidences combined, suggest that the canyon's location and emplacement was related to the tectonic events that took place in the canyon area in Neogene times, and are not so widespread in the South Portuguese offshore area.

Apart from the Portimão Fault, the lower sector of the Portimão canyon does not display any major features that could have been important in the evolution of the canyon.

Important active tectonic structures

The Gulf of Cadiz displays important seismic activity and from the studies carried out in this work it was possible to identify three major classes of active tectonic structures: the N-S to NE-SW trending thrusts (directed to the west or NW); ii) the WNW-ESE dextral strike-slip faults, and iii) the Gulf of Cadiz accretionary wedge. The first includes the Tagus Abyssal Plain Fault, the Gorringe Thrust, the Marquês de Pombal Thrust, the Horseshoe Fault and

the S. Vicente Canyon Thrust; the second comprises the SWIM faults present in the central sector of the Gulf of Cadiz; and the latter is made up by the central feature of the Gulf of Cadiz, the accretionary wedge.

Regarding the thrusts, with the exception of the Tagus Abyssal Plain Fault, all the others display a close relation with the present day recorded seismicity. From the inspection of the MCS profiles, the Marquês de Pombal Thrust started its activity at the base of the Late Miocene and the Horseshoe Thrust was formed after that time, near the base of the Early Pliocene. The SWIM Faults, according to Rosas *et al.* (2009) are older than 1.8 Ma.

Chapter 6 – Conclusions

Morphotectonics and seafloor shaping processes in the Gulf of Cadiz and SW Iberia

A new map of the morphologic features of the seafloor and a map of the morphotectonic domains of the Gulf of Cadiz and SW Iberia offshore were produced using the new multibeam swath bathymetry, seafloor reflectivity mosaics and multichannel seismic profiles. The first highlights the individual seafloor morphologic features of the study area and the second depicts several mapped domains that were defined based on the features there present. One of the results of this work is the recognition of the past and present seafloor shaping processes acting on the several domains and the way different processes act in a combined action in order to generate the wide variety of the seafloor features identified. This combined action of several processes is present at several scales, from the scale of the entire margin to the scale of a small bathymetric feature. In this way, the northern-east and northern sector of the Gulf of Cadiz displays the MOW system which near the Straits of Gibraltar generates some erosive features, as it continues to flow northwards, interacts with the north-east striking salt ridges that have a pronounced bathymetric expression and further to the north and north-west it is responsible for the deposition of large contourite drifts that drape a vigorous morphology inherited from Miocene and Paleogene times and confers the seafloor its present day smoothness. This is particularly obvious in the Portimão canyon mouth where the paleo-drainage system is still observable at the seafloor because it has not been completely covered by the contourite drifts. The MOW domain greatly expresses the referred interaction between processes: it is generated by oceanographic processes (the MOW currents), produces erosive and depositional features and in some areas interacts with the fluid ascent related features (salt ridges) that are tectonically controlled (they ascend through fault zones, namely the Cadiz Fault).

The interaction between processes is observable in the abyssal hills. These are tectonically controlled but also display fluid ascent processes accommodated by the salt domes that are well depicted in the bathymetry. Likewise, in the several plateaus present in the area the overall shape of the domain is tectonically controlled but in these cases there are evidences of interaction between these main processes and the gravity driven processes marked by abundant mass wasting processes scars evident in the bathymetry. Some features even display evidences of interaction of the similar processes, like in the south part of the accretionary wedge where some mud volcanoes pierce through the surface of some salt domes where fluid ascent processes interact with each other. On the front of the accretionary wedge there are also evidences for the interaction of tectonic processes between the deformation front thrusting and the SWIM strike-slip faults, as well as between the Horseshoe Fault and one of the SWIM faults. The submarine canyons are also the result

of the balance between depositional, erosive and mass wasting processes; the first is a constructive one when sediments accumulate in the canyons floor and the others remobilize materials found in the flanks, near the top of the walls and/or also the materials that accumulated in the bottom and are transported downslope.

It is concluded that from a geomorphical point of view, the uniqueness of the study area results not only from its geologic-geodynamic characteristics but also from its oceanographic and climate settings, since all these constituted forcing mechanisms that interacted in the formation of the morphologic features with different weights, both in what respects time of duration and modeling capacity.

The S. Vicente Canyon

The study of the bathymetry and seismic reflection profiles of the S. Vicente Canyon that extends for 120 km from near the continental shelf break to the Horseshoe Abyssal Plain allowed its sub-division in 4 sectors. The first and shallowest sector displays a relatively wide bottom, an amphitheater-like head scarp and a network of tributaries that gather and discharge materials downslope as indicated by the canyon walls that are affected by mass movements. These features associated to the fact that the sedimentary cover is thin relative to the deeper areas is a strong indication that this sector of the canyon i) acts mainly as a trap for subsequent discharge of the shelf sediments, and ii) the canyon head is, at present, expanding laterally by means of gravity sliding, probably as a consequence of the slowdown of the Holocene sea level rise.

As the depth increases, the bottom becomes narrower and steeper and the walls also become steeper and highly incised by gullies. In the areas where the flanks have smaller gradients this is due to the accumulation of near source slumps and debris. An important cause for these is the rapid accumulation of sediment at the edge of the eastern flank due to the along slope deposition of the contourite deposits carried by the MOW from the Sagres Plateau.

A major detour in the canyon's path of about 60º is found half-way. Further downslope the canyon's bottom becomes wider, the flanks less steep and their command over the bottom also decreases. In the last sector there are several irregularities in the canyon bottom like knickpoints and over excavation features.

The S. Vicente Canyon is tectonically controlled in the three first sectors by the S. Vicente Canyon Fault and on the last sector by the Horseshoe Fault.

Regarding its origin and evolution, the S. Vicente Canyon has a complex history. The first evidences for the establishment of a depressed area that evolved to a canyon are from the base of the Lower Pliocene. This is seen on the seismic profiles of the bottom sectors of the canyon where unit MW4 is thicker beneath the present day canyon area. However, although

it was a subsided area it was not a submarine canyon because the same seismic facies are present on the axis and on the sides, thus suggesting that there were no downslope currents passing through that depressed area. This subsided area formed as a consequence of the backward tilting of the hanging-wall of the Marquês de Pombal reverse fault that started its activity in early Late Miocene times.

This depressed area continued to subside and it was during the deposition of unit MW4 that it became a submarine canyon where the bottom currents flowed, initiating axial erosion instead of deposition. Unit MW5 shows an increase of the localized subsidence and the deposits along the canyon axis display a seismic facies different than the ones on the sides. After the canyon was established it started to propagate upslope along the S. Vicente Canyon Fault.

Within the Upper Pliocene (at the base of MW6 unit) the Marquês de Pombal Thrust experienced a burst of activity with major uplift of the Marquês de Pombal Block registered by the truncature that cuts the top part of the drag fold anticline associated with the thrust. Afterwards, still in the Upper Pliocene (start of unit MW7), probably due to the increase of the uplift, the activity of the S. Vicente Canyon also increased as marked by the intense buildup of overbanking deposits, the levee deposits. These deposits are found on the western side of the canyon, in the central and northern sector of the Marquês de Pombal Block. This increase in activity of the canyon regarding its sediment transport capacity continued throughout the Pleistocene and Holocene as MW8 unit is made up of levee deposits. The present day activity of the canyon is also well noticeable by the inspection of the reflectivity data of the canyon's floor that reveals the presence of coarser materials on the canyon's bottom.

The Portimão Canyon

This submarine canyon starts its incision in the continental shelf and finishes in the Portimão Valley at depths of 2500 meters over a total length of 50 kilometers. It displays an overall N-S trend strongly controlled by the Portimão Fault that is also mapped onshore. It was divided into three sectors taking in account its geomorphology. The uppermost one displays a small incision on the seafloor with relatively steep walls, the middle sector displays higher walls, some undulations on the canyon's path and it interacts and captures the MOW excavated Alvares Cabral Moat. The last sector is again straighter, and displays steep and high walls and the thalweg also display high gradients on some areas, fading down towards the end.

Its geological evolution from what it was deduced, from the available low resolution multichannel seismic profiles dataset, was not very complex unlike the S. Vicente Canyon. The canyon probably formed initially in its present-day middle sector due to the convergence of bottom currents because of the ascent of a salt dome (causing a seafloor rise) that was

likely linked with the activity of the Portimão Fault. It is in this sector of the canyon that evidences for recent deformation are found, as opposite in almost all the areas near the canyon where the deformation is sealed by the basal Miocene unconformity. After the localized incision on the seafloor it propagated both upslope and downslope along the Portimão Fault.

The active tectonics in the Gulf of Cadiz

The new tectonic map presented in this work results from the re-interpretation of several MCS profiles from different surveys together with the bathymetric multibeam swath bathymetry dataset. This new mapping of the tectonic structures coupled with the seismostratigraphic model allowed the dating of the activity of these structures. From the tectonic interpretation of the area it was possible to identify 3 main classes of structures that play an important role on the seismic activity of the area as well as their importance on the morphotectonics of the SW Iberia. These classes are: the NE-SW to N-S thrusts, the WNW-ESE strike-slip SWIM Faults and the accretionary wedge. The first encompasses several structures like the S. Vicente Canyon Fault, the Marquês de Pombal Thrust and the Horseshoe Fault that strongly influence the past history and present day shape of the S. Vicente Canyon. The WNW-ESE lineaments are important because of their size (although in a more detailed scale of observation they can be considered segmented) and by the wide array of bathymetric features that are associated with these structures. Also, from a geodynamic point of view these features may play an important role on the establishment of the present day plate boundary between Iberia and Africa. The accretionary wedge is a major tectonic structure that is responsible for the homonymous morphotectonic domain that incorporates several interesting morphological features.

Chapter 7 – References

Alonso, B.; Farrán, M.; Maldonado, A. 1989. Estratigrafía sísmica de alta resolución en márgens continentales passivos: factores de control durante el Cuaternário. Re. Soc. Geol. España, 2, (3-4), 199-289.

Ambar, I., Serra, N., Brogueira, M. J., Cabeçadas, G., Abrantes, F., Freitas, P., Gonçalves, C., Gonzalez, N., 2002. Physical, chemical and sedimentological aspects of the Mediterranean Outflow off Iberia. Deep-Sea Research 49, 4163–4177.

Ambar, I., Serra, N., Neves, F., Ferreira, T., 2008. Observations of the Mediterranean Undercurrent and eddies in the Gulf of Cadiz during 2001. Journal of Marine Systems 71, 195-220.

Andrade, C., 1992. Tsunami generated forms in the Algarve Barrier Islands (South Portugal). Sc. Tsunami Hazards, 10(1), p. 21-34.

Argus, D. F.; Gordon, R. G.; DeMets, C.; Stein, S. 1989. Closure of the Africa-Eurasia-North America plate motion circuit and tectonics of the Gloria Fault. J. Geophys. Res., 94, p. 5585-5602.

Auzende, J-M.; Charvetz, J.; Le Lann, A.; Le Pichon, X.; Monteiro, J. H.; Nicolas, A.; Ribeiro, A. 1978. Sampling and observations of mantle and crust on Gorringe Bank. Nature, 273, p. 45-49.

Banda, E., Torné, M. & IAM group (1995). IAM group investigates deep structure of ocean margins. EOS, v.76, pp. 25-29.

Baptista, M. A.; Heitor, S.; Miranda, J. M.; Miranda, P.; Mendes-Victor, L. 1998. The Lisbon tsunami; Evaluation of the tsunami parameters. J. Geodyn., 25, 2, p. 143-157.

Baptista, M. A.; Miranda, J. M.; Chierici, F.; N. Zitellini. 2003. New study of the 1755 earthquake source based on multi-channel seismic survey data and tsunami modeling. Nat. Hazards Earth Syst. Sci., 3, p. 333-340.

Bartolome, R., E. Gràcia, D. Stich, D. Klaeschen, S. Martínez, P. Terrinha, JJ. Dañobeitia, N. Zitellini and the SWIM working group, 2008. Seismic evidence of active strike-slip faulting in the Horseshoe Abyssal Plain (SW Iberian Margin), Geophysical Research Abstracts, Vol. 10, EGU2008-A-08636.

Bernard-Giffiths, J. B.; Gruau, J.; Cornen, J.; Azambre, B. & Macé, J. (1997) – Continental Lithospheric Contribution to Alkaline Magmatism: Isotopic (Nd, Sr, Pb) and Geochemical (REE) Evidence from Serra de Monchique and Mount Ormonde Complexes. Journal of Petrology, 38, n 1, pp. 115-132.

Bonnin, J.; Olivet, J. L.; Auzende, J. M. 1975. Struture en nappe a l'ouest de Gibraltar. C. R. Acad. Sci. Paris, 280 (5), p. 559-5562.

Borges, J. F.; Fitas, A. J. S.; Bezzeghoud, M.; Teves-Costa, P. 2001. Seismotectonics of Portugal and its adjacent Atlantic area. Tectonophysics, 337, p. 373-387.

Bronner, A., D. Sauter, G. Manatschal, G.. Péron-Pinvidic, M. Munschy (2011) Magmatic breakup as an explanation for magnetic anomalies at magma-poor rifted margins. Nature Geoscience.

Bryant, E. 2001. Tsunami – the underrated hazard. Cambridge University press, 320 p.

Buforn, E.; Udías, A.; Colombas, M.A. 1988. Seismicity and focal mechanisms in south Spain. Bull. Seismol. Soc. Am., 78, p. 208-2024.

Buforn, E; Bezzeghoud, M.; Udías, A.; Pro, E. 2004. Seismic sources on the Iberia- African plate boundary and their tectonic implications. Pure Appl. Geophys., 161, p. 623-646.

Cabral, J. 1995. Neotectónica em Portugal Continental. Mem. Inst. Geol. Min., 31, 265 p.

Calais, E., DeMets, C., Nocquet J.-M., 2003. Evidence for a post-3.16-Ma change in Nubia-Eurasia-North America plate motions? Earth and Planetary Science Letters 216, 81-92.

Cavazza, W.; Roure, F. M.; Ziegler, P. A. 2004. The Mediterranean area and the surrounding regions: Active processes, remnants of former Tethyan Oceans and related thrustbelts. In: Cavazza, W.; Roure, F. M.; Spakman, W.; Stampfli, G. M.; Ziegler, P. A. (Eds.). The Transmed Atlas – The Mediterranean Region from Crust to Mantle. Springer, p. 1-29.

Cunha, T.A., Watts, A.B., Pinheiro, L.M., Myklebust, R., 2010. Seismic and gravity anomaly evidence of large-scale compressional deformation off SW Portugal. Earth Planetary Science Letters 293, 171-179.

Cunha, T., A., Matias, L. M.,Terrinha, P., Negredo, A. M., Rosas, F., Fernandes, R. M. S., Pinheiro, L. M.. 2012. Neotectonics of the SW Iberia margin, Gulf of Cadiz and Alboran Sea: a reassessment including recent structural, seismic and geodetic data. Geophy. J. Int. 188, 850-872.

Dewey, J. F.; Helman, M. L.; Turco, E.; Hutton, D. H. W.; Knott, S. D. 1989. Kinematics of the western Mediterranean. Geol. Soc. Spec. Publ., 45, p. 265-283.

Diez, S.; Gràcia, E.; Gutscher, M-A.; Matias, L.; Mulder, T.; Terrinha, P.; Somoza, L.; Zitellini, N.; De Alteriis, G.; Henriet, J-P.; Dañobeitia, J. J. 2006. The SWIM bathymetric compilation of the Gulf of Cadiz. 5th Symposium on the Iberian Atlantic Margin, Aveiro, Portugal, p. 55-56.

D'Oriano, F., Angeletti, L., Capotondi, L., Laurenzi, M. A., López Correa, M., Taviani, M., Torelli, L., Trua, T., Vigliotti, L. and Zitellini, N. (2010), Coral Patch and Ormonde seamounts as a product of the Madeira hotspot, Eastern Atlantic Ocean. Terra Nova, 22: 494–500.

Duarte, J.C., Valadares, V., Terrinha, P., Rosas, F., Zitellini, N., Gràcia, E., 2009. Anatomy and tectonic significance of WNW-ESE and NE-SW lineaments at a transpressive plate boundary (Nubia-Iberia). Trabajos de Geología 29, 237-241.

Duarte, J.C., Terrinha, P., Rosas, F.M., Valadares, V., Pinheiro, L.M., Matias, L., Magalhães, V., Roque, C., 2010. Crescent-shaped morphotectonic features in the Gulf of Cadiz (offshore SW Iberia). Marine Geology 271, 236–249.

Duarte, J.C., F.M. Rosas, P. Terrinha, M-A Gutscher, J. Malavieille, Sónia Silva, L. Matias, 2011. Thrust - wrench interference tectonics in the Gulf of Cadiz (Africa - Iberia plate boundary): insights from (sand-box) analog models. Marine Geology 289, 135–149.

Evans, I. S. 1980. An integrated system of terrain analysis and slope mapping. Zeitschrift für Geomorphologie, N.F., Supplement Band, 36: 274–295.

Faccena, C.; Becker, T. W.; Lucente, F. P.; Jolivet, L.; Rosseti, F. 2001. History of subduction and back-arc extension in the Central Mediterranean. Geophys. J. Int., 145, p. 809-820.

Fernandes, R.M.S., Ambrosius, B.A.C., Noomen, R., Bastos, L.,Wortel, M.J.R., Spakman,W., Govers, R., 2003. The relative motion between Africa and Eurasia as derived from ITRF 2000 and GPS data. Geophysical Research Letters 30 (16), 1828.

Fourcarde, E., J. Azéma, F. Cecca, M. Bonneau, B. Peybernés and J. Dercourt, 1991. - Essai de reconstitution cartographique de la paléogéographie et des paléoenvironnements de la Téthys au Tithonique supérieur (138 à 135 Ma), Bull.Soc.Geol.France,162,6,pp.1197-1208,

Fukao, Y., 1973. Thrust faulting at a lithospheric plate boundary, The Portugal earthquake of 1969. Earth and Planetary Science Letters 18: 205-216.

Galdeano, C. 2000. Evolution of Iberia during the Cenozoic with special emphasis on the formation of the Betic Cordillera and its relation with the western Mediterranean. Ciências da Terra, UNL,14, p. 9-24.

Galloway, W. E. 1989. Genetic Stratigraphic sequences in basin analysis I: Architecture and genesis of flooding-surface bounded depositional units. Amer. Assoc. Petrol. Geol. Bull., 73, p. 125-142.

García-Navarro, E., Fernandez Rodriguez, C., Castro, A., 1994. The volcanics of Ayamonte at the Atlantic margin of Huelva. GAIA Spec. Vol. 9, 99–102.

Gardner, J., 2001. Mud volcanoes revealed and sampled on the Western Moroccan continental Margin. Geophys. Res. Lett., 28, pp. 339–342.

Gebco, 2003. GEBCO Digital Atlas, British Oceanographic Data Centre on behalf of IOC and IHO.

Geissler, W. H., Matias, L., Stich, D., Carrilho, F., Jokat, W., Monna, S.,. IbenBrahim, A , Mancilla, F., Gutscher, M.-A., Sallarès, V., Zitellini, N.. 2010. Focal mechanisms for sub-crustal earthquakes in the Gulf of Cadiz from a dense OBS deployment. Geophysical Research Letters, VOL. 37, L18309.

Geldmacher J. & Hoernle K., 2000 - The 72 Ma geochemical evolution of the Madeira hotspot (eastern North Atlantic): recycling of Paleozoic (≤500 Ma) oceanic lithosphere. Earth Planet. Sci. Lett., 183 (1-2): 73-92.

Girardeau, J.; Cornen, G.; Agrinier, P.; Beslier, M.-O.; Dubuisson, G.; Gall, B.; Monnier, C.; Pinheiro, L.; Ribeiro, A.; Whitechurch, H.;1998. Premiers résultats des plongées du Nautile sur le banc de Gorringe (Ouest Portugal). C. R. Acad. Sci. Paris, 326, p. 247-254.

Gràcia, E.; Dañobeitia, J.; Verges, J.; PARSIFAL team. 2003. Mapping Active Faults offshore Portugal (38ºN-36ºN): Implications of seismic hazard assessenent along the southwest Iberian margin. Geology, 31(1), p. 83-86.

Gràcia, E. and SWIM 2006 scientific party. 2006 – SWIM 2006 Cruise Report. Unpublished.

Gräfe, K.-U., Wiedmann, J., 1993. Sequence stratigraphy in the Upper Cretaceous of the Basco-Cantabrian Basin (Northern Spain). Geol. Rundsch., 82, pp. 327–361.

Grimison, N.L. and Chen, W.P. (1986), The Azores Gibraltar Plate Boundary: Focal Mechanisms, Depth of Earthquakes and their Tectonic Implications, Journal of Geophyical Research, 91, 2029-2047. Jonhston, A.C., Kanter, L.R., (1990), Earthquakes in Stable Continental Crust, Scientific American, v.262, n. 3, pp 42-49.

Gutscher, M-A, 2006. The great Lisbon earthquake and tsunami of 1755: lessons from the recent Sumatra earthquakes and possible link to Plato's Atlantis. European Review 14, Issue 2, 181-191.

Gutscher, M.-A., Malod, J., Rehault, J.-P., Contrucci, I., Klingelhoefer, F., Spakman, W., Mendes-Victor, L., 2002. Evidence for active subduction beneath Gibraltar. Geology 30 (12), 1071–1074.

Gutscher, M.A., 2005. Destruction of Atlantis by a great earthquake and tsunami? A geological analysis of the Spartel Bank hypothesis. Geology, 33, pp. 685–688.

Gutscher, M.-A.; Baptista, M. A.; Miranda, J. M. 2006. The Gibraltar Arc seismogenic zone (part 2): Constrains on a shallow east dipping fualt plane source for the 1755 Lisbon

earthquake provided by tsunami modeling and seismic intensity. Tectonophysics, 426 (1-2), p. 153-166.

Gutscher, M-A., Dominguez, S., Westbrook, G.K., Gente, P., Babonneau, N., Mulder, T., Gonthier, E., Bartolome, R., Luis, J., Rosas, F., Pedro T., and the Delila and DelSis Scientific Teams, 2009. Tectonic shortening and gravitational spreading in the Gulf of Cadiz accretionary wedge: observations from multi-beam bathymetry and seismic profiling. Marine and Petroleum Geology 26, 647-659.

Hanquiez, V., Mulder, T., Lecroat, P., Gonthier, E., Marchès, E., Voisset, M., 2007. High resolution seafloor images in the Gulf of Cadiz, Iberian Margin. Marine Geology 246, 42-59.

Hayward, N., Watts, A.B., Westbrook, G.K., Collier, J.S., 1999. A seismic reflection and GLORIA study of compressional deformation in the Gorringe Bank region, eastern North Atlantic. Geophysical Journal International 138, 831–850.

Hensen, C.; Nuzzo, M.; Hornibrook, E.; Pinheiro, L.M.; Bock, B.; Magalhães, V.; Brückmann. 2007. Sources of mud volcano fluids in the Gulf of Cadiz – indications for hydrothermal imprint. Geoch. Cosmo. Acta, 71, p. 1232-1248.

Hérnandez-Molina, J.; Llave, E. ; Somoza, L.; Fernández-Puga, M. C.; Maestro, A. ; Léon, R. ; Medialdea, T. ; Barnolas, A. ; García, M. ; Díaz del Río, V. ; Fernández-Salas, L. M. ; Vázquez, J. T. ; Lobo, F. ; Alveirinho Dias, J. M. ; Rodero, J. ; Gardner, J. 2003. Looking for clues to paleoceanographic imprints : a diagnosis of the Gulf of Cadiz contourite depositional system. Geology, 31, p.19-22.

Hérnandez-Molina, J.; Llave, E. ; Stow, D. A. V. ; García, M. ; Somoza, L.; Vázquez, J. T. ; Lobo, F. J. ; Maestro, A. ; Díaz del Río, V. ; Léon, R. ; Medialdea, T. ; Gardner, J. 2006. The contourite depositional system of the Gulf of Cadiz : a sedimentary model related to the bottom current activity of the Mediterranean outflow water and its interaction with the continental margin. Deep-Sea Res. II, 53, p. 1420-1463.

Hobson, R.D. 1972. Surface roughness in topography: quantitative approach. Pages 221–245 in R. J. Chorley, editor. Spatial analysis in geomorphology. Harper and Row, New York, New York, USA.

Iribarren, L., Vergés, J., Camurri, F., Fullea, J., Fernàndez, M., 2007. The structure of the Atlantic–Mediterranean transition zone from the Alboran Sea to the Horseshoe Abyssal Plain (Iberia–Africa plate boundary). Marine Geology 243, 97–119.

Jenness, J. S. (2004) - Calculating landscape surface area from digital elevation models. Wildlife Society Bulletin, 32 (3): 829–839.

Jia, Y. (2000) Formation of an Azores Current due to Mediterranean overflow in a modeling study of the North Atlantic. Journal of Physical Oceanography, 30, (9), 2342-2358.

Johnston, A., 1996. Seismic moment assessment of earthquakes in stable continental regions: III. New Madrid, 1811–1812, Charleston 1886 and Lisbon 1755. Geophysical Journal International 126, 314–344.

Kullberg, M.C., Kullberg, J.C., Terrinha, P. 2000. Tectónica da cadeia da Arrábida. Mem. Mus. Nac. Hist. Nat., nº2.

Lajat, D.; Biju-Duval, B.; Gonnard, R., Letouzey, J.; Winnock, E. 1975. Prolongement dans l'Atlantique de la partie externe de l'Arc bético-rifian. Bull. Soc. Geol. Fr., 17, p. 481-485.

Lebreiro, S. M.; McCave, I. N.; Weaver, P. P. E. 1997. Late Quaternarty turbidite emplacement on the Horseshoe Abyssal Plain (Iberian Margin). J. Sediment. Res., 67 (5), p. 856-870.

Levret, A. 1991. The effects of the November 1, 1755 “Lisbon” earthquake in Morocco. Tectonophysics, 193, p. 83-94.

Lopes, C. 2002. Análise e modelação da Bacia do Algarve. Dissertação de doutoramento, Univ. Nova de Lisboa, 173 p.

Lopes, F. C.; Cunha, P. P.; Le Gall, B. 2006. Cenozoic seismic stratigraphy and tectonic evolution of the Algarve margin (offshore Portugal, southwestern Iberian Peninsula). Mar. Geol., 231, p. 1-36.

Machado, F. 1966. Contribuição para o estudo do terramoto de 1 de Novembro de 1755. Rev. Fac. Ciências, Lisboa, C14, p. 19-31.

MacRae, A., 2001. The Unixshell script Tif2segy. http://seismic.ocean.dal.ca/pwpwiki/static/Tif2segy.html

Maldonado, A.; Somoza, L.; Pallarés, L. 1999. The Betic orogen and the Iberian-African boundary in the Gulf of Cadiz: geological evolution (central North Atlantic). Mar. Geol., 155, p. 9-43.

Manuppella, G. 1988. Litoestratigrafia e tectónica da Bacia Algarvia. Geonovas, 10, p. 67-71.

McClusky, S. ; Reilinger, R. ; Mahmoud, S.; Ben Sari, D.; Tealeb, A. 2003. GPS constrains on Africa (Nubia) and Arabia plate motion. Geophy. J. Int. 155, 126-138.

McKenzie, D.P. (1972), Active Tectonics of the Mediterranean Region, Royal Astronomic Society Geophysics Journal 30, 109-185.

Medialdea, T.; Vegas, R.; Somoza, L.; Vázquez, J. T.; Maldonado, A.; Díaz-del-Río, V.; Maestro, A.; Córdoba, D.; Fernández-Puga, M. C. 2004. Structure and evolution of the Olistostrome complex of the Gibraltar Arc in the Gulf of Cadiz eastern Central Atlantic evidence from two long seismic cross sections. Mar. Geol., 209, p. 173-198.

Medialdea, T., Somoza, L., Pinheiro, L.M., Fernández-Puga, M.C., Vázquez, J.T., León, R., Ivanov, M.K., Magalhaes, V., Díaz-del-Río, V., Vegas, R. (2009). Tectonics and mud volcano development in the Gulf of Cádiz. Mar Geol 261:48 – 63.

Mezcua J., 1982. Catalogo General de Isosistas de la Peninsula Iberica. IGN, Madrid, 320 pp.

Miall, A. D. 1986. Eustatic sea-level change interpreted from seismic stratigraphy: a critique of the methodologie with particular reference to the North Sea Jurassic record. Am. Ass. Petrol. Geol. Bull., 70, p. 131-137.

Mitchum, R. M. Jr.; Vail, P. R. 1977. Seismic stratigraphy and global changes of sea level, part 7: Seismic stratigraphic interpretation procedure. In: Seismic Stratigraphy-Applications to Hydrocarbon Exploration. Payton, C. E. (Ed.). Am. Ass. Petrol. Geol., Mem. 26, p. 135-143.

Mitchum, R. M. Jr.; Vail, P. R.; Thompson, III, S.; 1977a. Seismic stratigraphy and global changes of sea level, part 2: The depositional sequence as a basic unit for stratigraphic analysis. In: Seismic Stratigraphy-Applications to Hydrocarbon Exploration. Payton, C. E. (Ed.). Am. Ass. Petrol. Geol., Mem. 26, p. 53-62.

Mitchum, R. M. Jr.; Vail, P. R.; Sangree, J. B.; 1977b. Seismic stratigraphy and global changes of sea level, part 6: Stratigraphic interpretation of seismic reflection patterns in depositional sequences. In: Seismic Stratigraphy-Applications to Hydrocarbon Exploration. Payton, C. E. (Ed.). Am. Ass. Petrol. Geol., Mem. 26, p. 117-133.

Morales, J. A., Borrego, J., San Miguel, E. G., López-González, N., Carro, B. 2008. Sedimentary record of recent tsunamis in the Huelva Estuary (southwestern Spain), Quaternary Sci. Rev., 27, 734–746.

Morel., J.L., Megrhraoui, M., 1996. Gorringe-Alboran-Tell tectonic zone: A transpressive system along the Africa-Eurasia plate boundary. Geology, 24, (8), 755-758.

Mougenot, D. 1989. Geologie de la Marge Portugaise. Thése 3^{éme} cicle, Univ. Pierre et Marie Curie, Paris,VI, 259 p.

Mulder, T.; Voisset, M.; Lecroart, p.; Le Drezen, E.; Gonthier, E.; Hanquiez, V.; Faugères, J-C.; Habgood, E.; Hernández-Molina, F. J.; Estrada, F.; Llave-Barranco, E.; Poirier, D.; Gorini, C.; Fuchey, Y.; Voelker, A.; Freitas, P.; Lobo Sanchez, F.; Fernandez, L. M.; Kenyon, N. H.; Morel, J. 2003. The Gulf of Cadiz: an unstable giant contouritic levee. Geo-Mar. Lett., 23, p. 7-18.

Olivet, J. L.; Bonnin, J.; Beuzart, P.; Auzenda, J. M. 1984. Cinématique de l'Atlantique nord et central. Brest, Centre Nationale pour l'Explotation des Océans, Rapports Scientifiques et Techniques, v. 54, 108 p.

Payton, C. E. 1977. Seismic Stratigraphy-Applications to Hydrocarbon Exploration. Am. Ass. Petrol. Geol., Mem. 26, 516 p.

Pinheiro, L. M.;. Wilson, R. C. L; Pena dos Reis, R.; Whitmarsh, R. B. & Ribeiro, A. (1996) - The Western Iberia Margin: a geophysical and geological overview, Proceedings of the Ocean Drilling Program, Scientifics Results, 149, pp. 3-23.

Pinheiro, L.M., Ivanov, M.K., Sautkin, A., Akhmanov, G., Magalhaes, V.H., Volkonskaya, A., Monteiro, J.H., Somoza, L., Gardner, J., Hamouni, N., Cunha, M.R., 2003. Mud volcanism in the Gulf of Cadiz: results from the TTR-10 cruise. Marine Geology 195, 131–151.

Purdy, G.M., 1975. The eastern end of the Azores–Gibraltar plate boundary. Geophys. J. R. Astr. Soc., 43, 973–1000.

Reid, J.L., 1979. On the contribution of the Mediterranean Sea outflow to the Norwegian-Greenland Sea. Deep Sea Res., 44: 1199-1223.

Ribeiro, A., Cabral, J., Baptista, R., Matias, L., 1996. Stress pattern in Portugal mainland and the adjacent Atlantic region, West Iberia. Tectonophysics 15 (2), 641–659.

Riley, S. J., S. D. DeGloria and R. Elliot (1999). A terrain ruggedness index that quantifies topographic heterogeneity, Intermountain Journal of Sciences, vol. 5, No. 1-4.

Roque, C., 2007. Tectonostratigrafia do Cenozóico das margens continentais Sul e Sudoeste Portuguesas: um modelo de correlação sismostratigráfica. PhD Thesis, Universidade de Lisboa. Departamento de Geologia.

Roque,C., H. Duarte, P. Terrinha, V. Valadares, J. Noiva, M. Cachão, J. Ferreira, P. Legoinha, N. Zitellini (2012) - Pliocene and Quaternary depositional model of the Algarve margin contourite drifts (Gulf of Cadiz, SW Iberia): Seismic architecture, tectonic control and paleoceanographic insights. Marine Geology, Volumes 303-306, pages 42-62.

Rosas, F., Duarte, J., Terrinha, P., Silva, S., Neves, M., Gràcia, E., Matias, L. (2008). Analogue modelling of major thrust and strike-slip fault interference at the Iberia – Nubia plate boundary, gulf of cadiz. Geomod, Firenze.

Rosas, F.M., Duarte, J.C., Terrinha, P., Valadares, V., Matias, L., 2009. Morphotectonic characterization of major bathymetric lineaments in NW Gulf of Cadiz (Africa-Iberia plate boundary): insights from analogue modelling experiments. Marine Geology 261, 33–47.

Rosas, F.M., Duarte, J.C., Neves, M.C., Terrinha, P., Silva, S., Matias, L., 2012. Thrust-wrench interference between major active faults in the Gulf of Cadiz (Africa-Eurasia plate boundary, offshore SW Iberia): tectonic implications from analogue and numerical modeling. Tectonophysics, 548-549, 1 – 21.

Rosenbaum, G.; Lister, G. S.; Duboz, C.; 2002. Reconstruction of the tectonic evolution of the western Mediterranean since the Oligocene. J. Virtual Explorer, 8, p. 107-126.

Rosenbaum, G.; Lister, G. S. 2004. Formation of arcuate orogenic belts in the western Mediterranean region. In: Sussman, A. J.; Weil, A. B. (Eds.). Orogenic curvature: Integrating paleomagnetic and structural analysis. Geol. Soc. Am. Spec. Paper, 383, p. 41-56.

Royden, L. H. 1993. Evolution of retreating subduction boundaries formed during continental collision. Tectonics, 12 (3), p. 629-638.

Ryan, W. B. F.; Hsü, K. J.; Cita, M. B.; Dumitrica, P.; Lort, J. M.; Maync, W.; Nesteroff, W. D.; Pautot, G.; Stradner, H.; Wezel, F. C.; 1973. Site DSDP 120. Initial Reports of the Deep Sea Drilling Project, 13, p. 19-41.

Sallarès,V.; Gailler,A.; Gutscher, M-A.; Graindorge,D.; Bartolomé, R.; Gràcia, E.; Díaz, J.; Dañobeitia, J.J.; Zitellini, N.; 2011. Seismic evidence for the presence of Jurassic oceanic crust in the central Gulf of Cadiz (SW Iberian margin). EPSL, 311, 112-123.

Sangree, J. B.; Widmer, J. M. 1977. Seismic stratigraphy and global changes of sea level, part 9: Seismic interpretation of clastic depositional facies. In: Seismic Styratigraphy-Applications to Hydrocarbon Exploration. Payton, C. E. (Ed.). Am. Ass. Petrol. Geol., Mem. 26, p. 165-184.

Sappington, J.M., K.M. Longshore, and D.B. Thomson. 2007. Quantifiying Landscape Ruggedness for Animal Habitat Anaysis: A case Study Using Bighorn Sheep in the Mojave Desert. Journal of Wildlife Management. 71(5): 1419 -1426.

Sartori, R.; Torelli, L.; Zitellini, N.; Peis, D.; Lodolo, E. 1994. Eastern segment of the Azores-Gibraltar line (central-eastern Atlantic): An oceanic plate boundary with diffuse compressional deformation. Geology, 22, p. 555-558.

Sibuet, J.-C., S. P. Srivastava, and W. Spakman (2004), Pyrenean orogeny and plate kinematics, J. Geophys. Res., 109, B08104.

Sibuet, J.-C., Srivastava, S. P., & Manatschal, G. 2007. Exhumed mantle-forming transitional crust in the Newfoundland-Iberia and associated magnetic anomalies. Journal of Geophysical Research, 112, B06105 (23pp), Storetvedt et al., 1987

Silva, S., Matias, L., Romsdorf, M., Geissler, W., Terrinha, P., Nearest working group, 2010. Instrumental seismicity in the Gulf of Cadiz: Results from the NEAREST Project acquisition campaign. e –Terra 10, 6.

Sloss, L. L. 1963. Sequence in cratonic interior of North America. Geol. Soc. Am. Bull., 74, p. 93-114.

Sloss, L. L. 1988. Forty years of sequence stratigraphy. Geol. Soc. Am. Bull., 100, p. 1661-1665.

Solares, J. M. M. and López Arroyo, A. 2004. The great historical 1755 earthquake. Effects and damage in Spain, J. Seismol., 8, 275–294.

Somoza, L.; Díaz-del-Río, V.; Leon, R.; Ivanov, M.; Fernández-Puga, M. C.; Gardner, J. M; Hernández-Molina, F. J.; Pinheiro, L. M.; Rodero, J.; Lobato, A.; Maestro, A.; Vázquez, J. T.; Medialdea, T.; Fernández-Salas, L. M. 2003. Seabed morphology and hydrocarbon seepage in the Gulf of Cadiz mud volcano area. Acoustic imagery multibeam and ultra high resolution seismic data. Mar. Geol., 195, p. 153-176.

Souriau A. , 1984. Geoid anomalies over Gorringe Ridge, North Atlantic Ocean: Earth and Planetary Science Letters , v. 68, p. 101–114.

Srivastava, S.P., Roest, W.R., Kovacs, L.C., Oakey, G., Lévesque, S., Verhoef, J., Macnab, R. 1990. Motion of Iberia since the Late Jurassic: results from detailed aeromagnetic measurements in the Newfoundland Basin. Tectonophysics 184, 229–260.

Stampfli, G. M.; Borel, G. 2004. The Transmed Transects in Space and Time: Constraints on the Plaeotectonic Evolution of the Mediterranean Domain. In: Cavazza, W.; Roure, F. M.; Spakman, W.; Stampfli, G. M.; Ziegler, P. A. (Eds.). The Transmed Atlas – The Mediterranean Region from Crust to Mantle. Springer, p. 53-80.

Stich, D.; Serpelloni, E.; Mancilla, F-L.; Morales, J. 2006. Kinematics of the Iberia-Maghreb plate contact from seismic moment tensors and GPS observations. Tectonophysics, 426, p. 295-317.

Stich, D., Mancilla, F. de L., Pondrelli, S., Morales, J., 2007. Source analysis of the February 12th 2007, M_w 6.0 Horseshoe earthquake: Implications for the 1755 Lisbon earthquake. Geophysical Research Letters 34, 12.

Terrinha, P., 1998. Structural Geology and Tectonic Evolution of the Algarve Basin, South Portugal. Department of Geology. London, University of London.

Terrinha, P., Dias, R.P., Ribeiro, A., Cabral, J., 1999. The Portimão Fault, Algarve Basin, South Portugal. Comunicacões do Instituto Geológico e Mineiro 86, 107–120.

Terrinha, P.; Ribeiro, C.; Kullberg,J. C.; Lopes, C.; Rocha, R. & Ribeiro, A. (2002) - Compressive Episodes and Faunal Isolation during Rifting, Southwest Iberia. The Journal of Geology, 110, pp. 101–113.

Terrinha, P., Pinheiro, L.M., Henriet, J.-P., Matias, L., Ivanov, M.K., Monteiro, J.H., Akhmetzhanov, A., Volkonskaya, A., Cunha, T., Shaskin, P., Rovere, M., 2003. Tsunamigenic–seismogenic structures, neotectonics, sedimentary processes and slope instability on the southwest Portuguese Margin. Marine Geology 195 (1–4), 55–73.

Terrinha, P., Matias, L., Vicente, J.C., Duarte, J., Luís, J., Pinheiro, L., Lourenço, N., Diez, S., Rosas, F.M., Magalhães, V., Valadares, V., Zitellini, N., Mendes-Víctor, L., MATESPRO Team, 2009. Morphotectonics and Strain Partitioning at the Iberia–Africa plate boundary from multibeam and seismic reflection data. Marine Geology 267, 156-174.

Teves Costa, P., 2005. Terramotos e Tsunamis, (Coord.). Livro Aberto, Editores Livreiros Lda., Lisboa.

Thiebot, E., Gutscher, M.A., 2006. The Gibraltar Arc seismogenic zone (part1): constraints on a shallow east dipping fault plane source for the 1755 Lisbon earthquake provided by seismic data, gravity and thermal modeling. Tectonophysics 427, 135–152.

Thompson, J.A., Bell, J.C., Butler, C.A., 2001. Digital elevation model resolution, effects on terrain attribute calculation and quantitative soil-landscape modeling. Geoderma 100, 67-89.

Torelli, L., R. Sartori and N. Zitellini, 1997. The giant chaotic body in the Atlantic Ocean off Gibraltar: new results from a deep seismic reflection survey. Marine and Petroleum Geology 14(2): 125-134.

Tortella, D.; Torne, M.; Pérez-Estaún, A. 1997. Geodynamic Evolution of the Eastern Segment of the Azores-Gibraltar Zone: The Gorringe Bank and the Gulf of Cadiz. Mar. Geophy. Res., 19, p. 211-230.

Tucholke, B.E., Sawyer, D.S., Sibuet, J.-C., 2007. Breakup of the Newfoundland–Iberia rift. In: Karner, G.D., Manatschal, G., Pinheiro, L.M. (Eds.), Imaging, Mapping and Modelling Continental Lithosphere Extension and Breakup, vol. 282. Geological Society, London, Special Publication, pp. 9–46.

Udías, A. 1988. Focal mechanisms and seismotectonics of the Iberian Península. In: European geotransverse (EGT) project- the IberiAN Peninsula. Banda, E.; Mendes-Victor, L. A. (Eds.), p. 137-143.

Vail, P. R.; Mitchum, R. M. Jr.; Thompson, M. S.; 1977. Seismic stratigraphy and global changes of sea level, part 4: Global cycles of relative changes of sea level. In: Seismic Styratigraphy-Applications to Hydrocarbon Exploration. Payton, C. E. (Ed.). Am. Ass. Petrol. Geol., Mem. 26, p. 83-97.

Verati, C., Rapaille, C., Féraud, G., Marzoli, A., Bertrand, H., Youbi, H., 2007. 40Ar/39Ar ages and duration of the Central Atlantic Magmatic Province volcanism in Morocco and Portugal and its relation to the Triassic–Jurassic boundary. Palaeogeography Palaeoclimatology Palaeoecology 244, 308–325.

Vilanova, S.P., Nunes, C.F. and Fonseca, J.F.B.D., 2003. Lisbon 1755: A Case of Triggered Onshore Rupture? Bulletin of the Seismological Society of America 93 (5), 2056-2068.

Walker, R. G. 1990. Facies modeling and sequence stratigraphy. Journ. Sed. Petrol., 60 (5), p. 77-786.

Weaver, P.P.E., and Thomson, J. (Eds.), 1987. Geology and Geochemistry of Abyssal Plains. Geol. Soc. Spec. Publ. London, 31.

Westaway, R., 1990. Present-day kinematics of the plate boundary zone between Africa and Europe, from the Azores to the Aegean. Earth Planet. Sci. Lett. 96, 393–406.

Winter, H. de la R. 1984. Tectonostratigraphy, as applied to the analysis of the South African Phanerozoic basins. Trans. Geol. Soc. South . Afr., 87, p. 169-179.

Ziegler, P. A. 1988. Post-Hercynian plate reorganization in the Tethys and Arctic-North Atlantic domains. In: Triassic-Jurassic rifting continental breackup and the origin of the Atlantic Ocean and passive margins. Manspeizer, W. (Ed.). Developments in Geotectonics, 22, p. 711-754

Zitellini, N.; Chierici, F.; Sartori, R.; Torelli, L. 1999. The tectonic source of the 1755 Lisbon Earthquake. Ann. Geof., 42, (1), p. 49-55.

Zitellini, N., Ligi, M., Matias, L., Rovere, M., the Shipboard Scientific Parties, 2002. Voltaire 2002 Cruise Report. IGM-CNR Technical Report.

Zitellini, N. & SWIM 2005 Shipboard Party. 2005 – SWIM 2005 Cruise Report. Unpublished.

Zitellini, N., Mendes, L. A., Cordoba, D., Danobeitia, J., Nicolich, R., Pellis, G., Ribeiro, A., Sartori, R., Torelli, L., Bartolomé, R., Bortoluzzi, G., Calafato, A., Carrilho, F., Casoni, L., Chierici, F., Corela, C., Correggiari, A., Della Vedova, B., Gràcia, E., Jornet, P., Landuzzi, M., Ligi, M., Magagnoli, A., Marozzi, G., Matias, L., Penitenti, D., Rodriguez, P., Rovere, M., Terrinha, P., Vigliotti, L., Zahinos Ruiz, A., 2001. Source of 1755 Lisbon Earthquake and Tsunami Investigated. Eos Trans. AGU, 82, (26), 285, 290–291.

Zitellini, N., Rovere,M., Terrinha, P., Chierici, F.,Matias, L., Team, B., 2004. Neogene through quaternary tectonic reactivation of SW iberian passive margin. Pure and Applied Geophysics 161, 565–587.

Zitellini, N., Gracia, E., Matias, L., Terrinha, P., Abreu, M.A., DeAlteriis, G., Henriet, J.P., Dañobeitia, J.J., Masson, D.G., Mulder, T., Ramella, R., Somoza, L., Diez, S., 2009. The quest for the Africa-Eurasia plate boundary west of the Strait of Gibraltar. Earth and Planetary Science Letters, 280, 1-4, pp: 13-50.

8 - Appendixes

Rosas, F.M.; J. Duarte, P. Terrinha, V. Valadares, L. Matias, (2009) Morphotectonic characterization of major bathymetric lineaments in Gulf of Cadiz (Africa-Iberia plate boundary): Insights from analogue modelling experiments. Marine Geology, Volume 261, Issues 1-4, pages 33-47.

Terrinha, P., Matias, L., Vicente, J., Duarte, J., Luís, J., Pinheiro, L., Lourenço, N., Diez, S., Rosas, F, Magalhães, V., Valadares, V. ,Zitellini, N., Mendes Víctor, L., MATESPRO Team (2009) - Morphotectonics and Strain Partitioning at the Iberia-Africa plate boundary from multibeam and seismic reflection data. Marine Geology, Volume 267, Issues 3-4, pages 156-174.

Duarte, J.C., Valadares, V., Terrinha, P., Rosas, F., Zitellini, N., Gràcia, E. (2009). Anatomy and tectonic significance of WNW-ESE and NE-SW lineaments at a transpressive plate boundary (Nubia-Iberia). Trabajos de Geología 29, 237-241.

Duarte, J.C., P. Terrinha, F.M. Rosas, V. Valadares, L.M. Pinheiro, L. Matias, V. Magalhaes, C. Roque (2010) - Crescent-shaped morphotectonic features in the Gulf of Cadiz (offshore SW Iberia). Marine Geology, Volume 271, Issues 3-4, 15, pages 236-249.

C. Roque, H. Duarte, P. Terrinha, V. Valadares, J. Noiva, M. Cachão, J. Ferreira, P. Legoinha, N. Zitellini (2012) - Pliocene and Quaternary depositional model of the Algarve margin contourite drifts (Gulf of Cadiz, SW Iberia): Seismic architecture, tectonic control and paleoceanographic insights. Marine Geology, Volumes 303-306, pages 42-62.

8 - Appendixes

Marine Geology 261 (2009) 33–47

Contents lists available at ScienceDirect

Marine Geology

journal homepage: www.elsevier.com/locate/margeo

Morphotectonic characterization of major bathymetric lineaments in Gulf of Cadiz (Africa–Iberia plate boundary): Insights from analogue modelling experiments

F.M. Rosas [a,*], J.C. Duarte [a,b], P. Terrinha [b], V. Valadares [b], L. Matias [c]

[a] LATTEX, IDL, Universidade de Lisboa, Departamento de Geologia da Faculdade de Ciências, Edifício C6, Piso 4, 1749-016 Lisboa, Portugal
[b] LATTEX, IDL, INETI, Departamento de Geologia Marinha do INETI, Estrada da Portela Zambujal-Alfragide Apartado 7586, 2720-866 Amadora, Portugal
[c] CGUL, IDL, Universidade de Lisboa, Departamento de Física da Faculdade de Ciências, Edifício C8, Piso 6, 1749-016 Lisboa, Portugal

ARTICLE INFO

Article history:
Received 22 October 2007
Received in revised form 1 July 2008
Accepted 6 August 2008

Keywords:
Gulf of Cadiz
morphotectonic lineaments
seismotectonic interpretation
analogue modelling
dextral wrenching
low-angle transpression

ABSTRACT

New high-resolution multi-beam bathymetry data allowed the recognition of several bathymetric lineaments (ca. 100 km long, trending WNW–ESE) in seafloor sediments of the Gulf of Cadiz, offshore SW Iberia. The interpretation of multi-channel (MCS) profiles crosscutting these lineaments showed that they are controlled by underlying deep seated faults, which have endured a polyphase reactivation history. To get insights on the Recent tectonic evolution of these structures, we performed two sets of analogue modelling experiments, assuming: 1) right-lateral strike-slip basement faulting and coupled passive shearing affecting an overlying soft cover; and 2) low-angle transpressive deformation along a narrow shear band overlying the fault. Our results show a good correlation between the experimentally obtained structural patterns and the natural morphotectonic lineaments, allowing the use of some of the observed natural features as strain gauges. Based on this, we conclude that the study lineaments correspond to the bathymetric expression of ongoing dextral wrenching reactivation of WNW–ESE pre-existing faults, and we estimate the age of this tectonic reactivation as being ca. 1.8 Ma (i.e. form late Pliocene to Present day). These characteristics agree with the most recent kinematic models derived from geodetic observations, indicating that Present day convergence between Nubia and Iberia is subparallel to the newly identified lineaments and occurs at a 4 mm/yr rate.

1. Introduction

The Gulf of Cadiz area, located West of the Gibraltar Strait, offshore SW Iberia and NW Morocco (Fig. 1), has been increasingly recognized as a critical site for the understanding of the tectonics related with the Africa (Nubia)–Iberia plate boundary (e.g. Sartori et al., 1994; Zitellini et al., 1999; Maldonado et al., 1999; Gutscher et al., 2002; Gracia et al., 2003; Terrinha et al., 2003; Gutscher, 2004; Zitellini et al., 2001, 2004; Medialdea et al., 2004; Thiebot and Gutscher, 2006; Terrinha et al., under review). This boundary extends along the WNW–ESE Azores–Gibraltar line, comprising to the West the Azores triple junction and the Gloria fault, and to the East the Gulf of Cadiz domain (Fig. 1A). In this domain, the average direction of the Maximum Horizontal Compressive Stresses (S_{Hmax}), deduced from earthquake focal mechanisms, is ~N45W (Ribeiro et al., 1996; Borges et al., 2001), meanwhile recently reported geodetic models show the existence of WNW–ESE oblique convergence between Nubia and Iberia, at a Present day rate of approximately 4 mm/yr (e.g. Nocquet and Calais, 2004; Stich et al., 2006; Fernandes et al., 2007, inset of Fig. 1B). Recent mapping of the main tectonic structures in the area (Fig. 1B) suggests that compression is presently being dissipated in a complex manner, essentially through inter-plate brittle deformation, characterized by the development of different structures with different orientations and kinematics. Previously reported earthquake recurrence data, epicentre location data, and focal mechanisms (Buforn et al., 1995, 2004; Borges et al., 2001; Stich et al., 2005, 2006) point to a general scenario of moderate magnitude seismicity, mostly related to thrusting and strike-slip movement, along numerous faults at shallow to intermediate depths (above 60 km). This area is also prone to high magnitude earthquakes and destructive tsunami like the 1/11/1755 Great Lisbon Earthquake (estimated magnitude between 8.5 and 8.8, e.g. Abe, 1979; Johnston, 1996; Martínez-Solares and López Arroyo, 2004). Other large magnitude events, such as the 28/02/1969 earthquake (Ms = 7.9) occurring in the Gulf of Cadiz illustrate the practical need to improve our knowledge regarding the Present day tectonic evolution of this key region.

In this work we present new results concerning the study of several major bathymetric lineaments, recorded in recent seafloor sediments of the NW Gulf of Cadiz area. These features were firstly recognized using the high-resolution multi-beam bathymetry recently acquired during the MATESPRO campaign (MAjor TEctonic and Sedimentary PROcesses in the Portuguese Margins, Terrinha et al.,

* Corresponding author. Tel.: +351 21 7500375; fax: +351 21 7500064.
E-mail address: frosas@fc.ul.pt (F.M. Rosas).

0025-3227/$ – see front matter © 2008 Elsevier B.V. All rights reserved.
doi:10.1016/j.margeo.2008.08.002

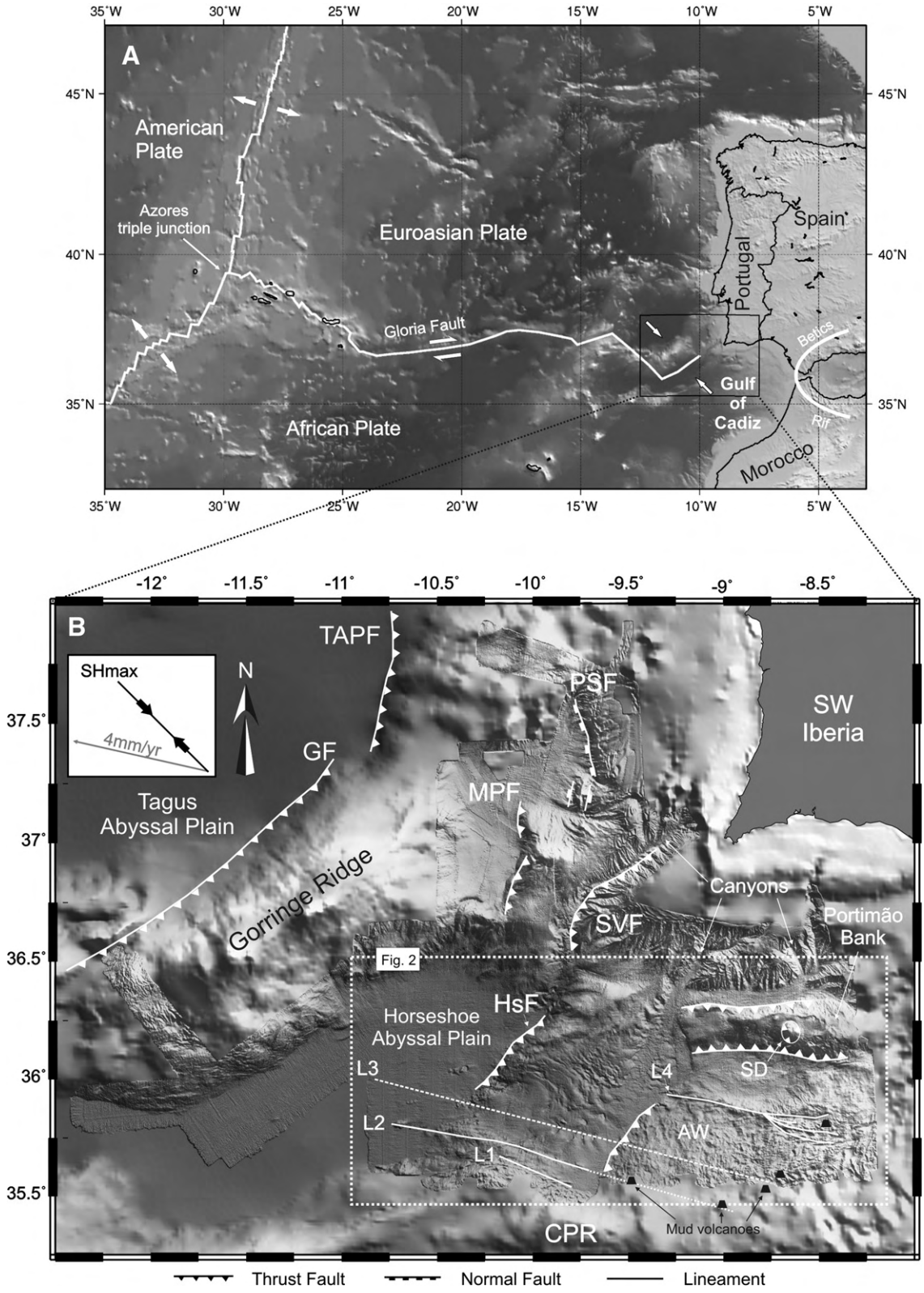

Fig. 1. (A) Location of the Gulf of Cadiz area in the general tectonic setting of the Euroasia (Iberia)–Africa (Nubia) plate boundary (Bathymetry GEBCO 2000; Plate boundaries according to model PB2002 of Bird, 2003); (B) Simplified tectonic map of the NW Gulf of Cadiz area (bathymetry corresponds to the PARSIFAL 2000, HITS 2001, and MATESPRO 2004 surveys, completed by GEBCO 2000). Inset in the upper left showing (in black) the average direction of the Maximum Horizontal Stresses—S_{Hmax}, and (in grey) the direction of the 4 mm/yr convergence rate between Nubia and Iberia (Nocquet and Calais, 2004; Stich et al., 2006; Fernandes et al., 2007). TAPF—Tagus Abyssal Plain Fault; GF—Gorringe Fault; PSF—Pereira de Sousa Fault; MPF—Marques de Pombal Fault; SVF—Sao Vicente Fault; HsF—Horseshoe Fault; SD—D. Carlos Salt Diapir; AW—Accretionary wedge; CPR—Coral Patch Ridge; L1–L4—Bathymetric lineaments.

under review), and were subsequently studied using several multi-channel seismic (MCS) profiles. In addition, several analogue modelling experiments were carried out to get new insight on their origin, kinematic evolution and tectonic meaning. This was done through comparison of the obtained experimental results with the correspondent natural examples, which showed that some morphotectonic patterns associated to the lineaments could be used in a quantitative manner, as natural strain gauges, allowing a better understanding of the main tectonic processes at stake.

2. Morphotectonic characterization of the study objects

2.1. Morphologic description

The new MATESPRO bathymetry dataset obtained in NW Gulf of Cadiz revealed a complex geomorphology, interpreted as the result of the combined action of different processes such as tectonics, sedimentation, gravity, and submarine erosion (Terrinha et al., under review). These data allowed, for the first time, the identification of several major bathymetric lineaments (L1 to L4 in Fig. 2). These linear features strike approximately WNW–ESE, exhibiting widths of a few kilometres (typically 1.5 km to 3 km), and maximum bathymetric lengths of ca. 100 km. L1 is best characterized by sets of discontinuous oblique (W–E) morphologic undulations, consisting in alternating crest and troughs up to 6 km long, displaying a general en-échelon geometrical disposition (Fig. 3A,B and C); L2 exhibits an overall more continuous morphology, characterized by two main wide elevated areas, elongated along strike, and located on opposite sides of a central linear trough (Fig. 3D).

Unlike the previous described lineaments, L3 is barely seen in the high-resolution bathymetry. The L4 lineament, although clearly observable in the bathymetry, does not show any consistently interpretable morphologic patterns, probably due to the incoherent rheology response to stress of the tectonic mélange of the Gulf of Cadiz accretionary wedge (see AW in Fig. 1B). For much of its length, L4 coincides with the northern border of this disturbed seafloor domain, suggesting that it may be controlled by a deep structure. Because of these features in the present work we will concentrate on L1 and L2 as the main targets for our analogue modelling.

2.2. Structural characterization

The MCS reflection profiles which crosscut the lineaments L1 to L3 show that these coincide with deep seated faults (Figs. 2 and 4). Taking into account the previously established seismostratigraphy in the area (e.g. Sartori et al., 1994; Torelli et al., 1997; Tortella et al., 1997), the interpretation of different segments of the IAM line (Fig. 4) shows that these faults cut through Mesozoic units (Jurassic to Cretaceous age), and through a late Miocene (Tortonian) body with a typical chaotic seismic signature. They also often seem to coincide with possible paths of abundant upwards fluid migration, seemingly originated at the base of the Mesozoic (Fig. 4A), and previously recognized by several authors in this area (e.g. Somoza et al., 2003; Pinheiro et al., 2003; Hensen et al., 2007).The upper units of the seismostratigraphic sequence correspond to hemipelagic sediments of Plio-Quaternary age, with thickness varying between 0.3 and 0.6 s TWT. In the IAM3 line, the fault corresponding to the L1 lineament, bordering the north-eastern flank of the Coral Patch Ridge (CPR, Fig. 4), is interpreted has having behaved as a reverse fault, since the Mesozoic reflectors in the hanging wall reveal a folding geometry congruent with shortening (Fig. 5). Based only on these profiles it was not possible to ascribe a definite kinematic evolution to the other (L2 and L3) faults. The Plio-Quaternary hemipelagic sediments, although some times locally folded, are generally not cut by the described faults (Fig. 4B). This suggests that the reverse fault kinematics mentioned above, does not correspond to the Present day active kinematics on these structures.

Both the morphological and structural description of the study objects points to the conclusion that these lineaments correspond to the bathymetric expression of major WNW–ESE trending faults. The examined MCS lines show the Plio-Quaternary hemipelagic sediments sealing the faults (Fig. 4), suggesting that the bulk movement along these structures does not correspond to active thrusting. Furthermore, the en-échelon crests and troughs associated to L1 seem compatible with a Present day dextral wrenching reactivation (Fig. 3A, B and C).

The same MCS lines also show that the fault associated to L2 extends along ca. 200 km, from the accretionary wedge in the East, coinciding with several previously described mud volcanoes (e.g. Pinheiro et al., 2003), to the Horseshoe abyssal plain in the West, where it looses its morphologic expression (Figs. 1B and 2). It should

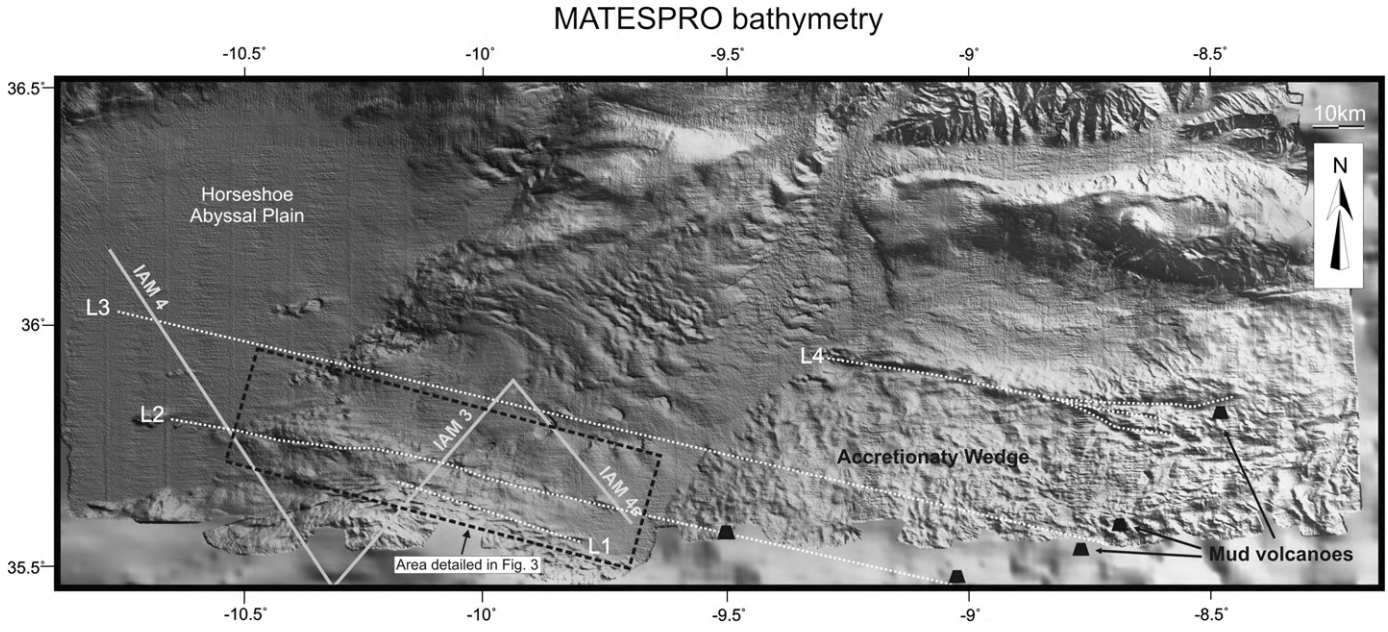

Fig. 2. Bathymetry of NW Gulf of Cadiz MATESPRO campaign, Terrinha et al. (under review). Location of the IAM multi-channel seismic reflection profiles intersecting the (L1 to L3) lineaments, interpreted in Fig. 4.

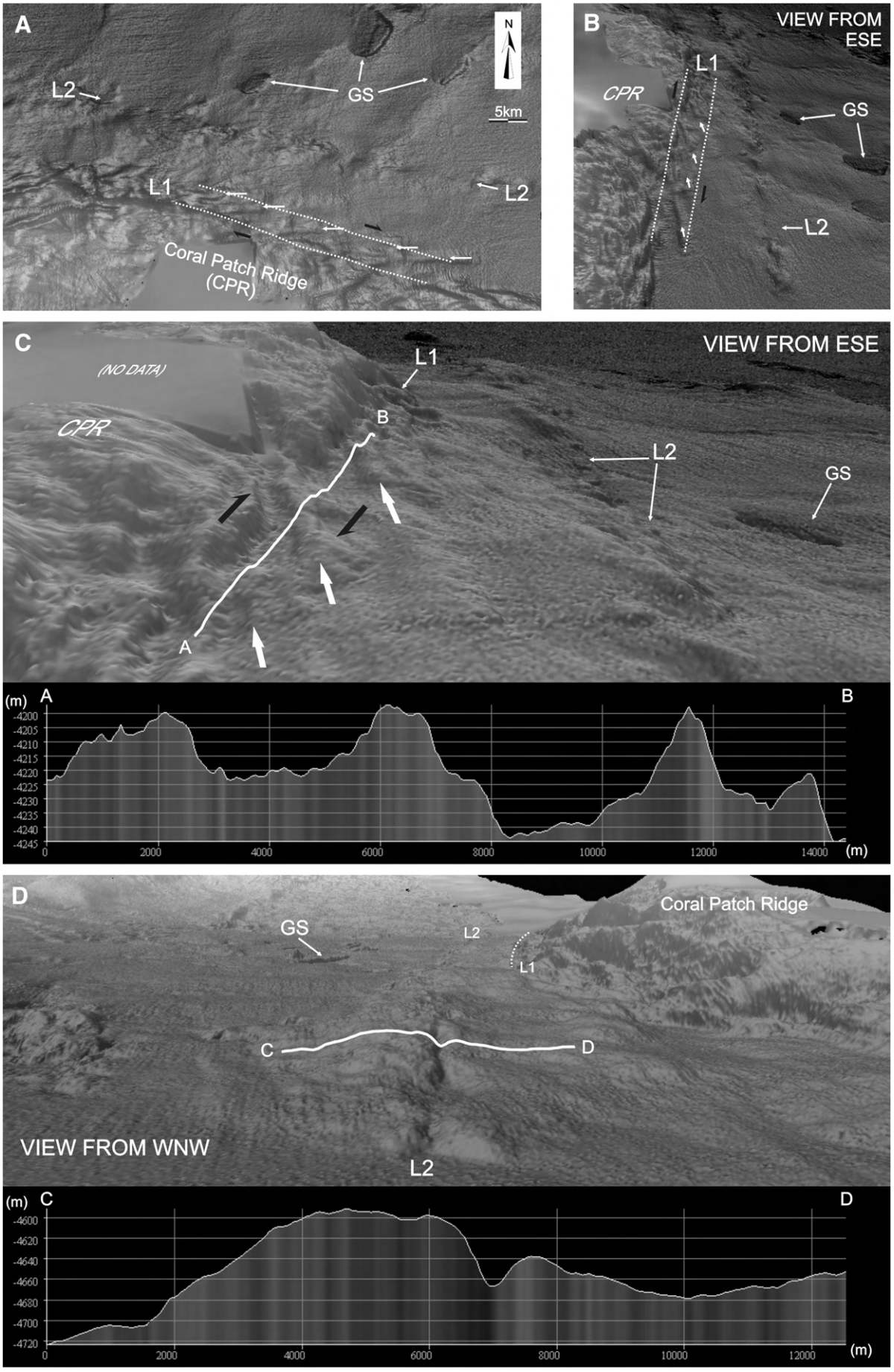
A
N
L2
GS
5km
L1
L2
Coral Patch Ridge
(CPR)
B
VIEW FROM
ESE
L1
CPR
GS
L2
C
VIEW FROM ESE
(NO DATA)
L1
CPR
B
L2
GS
A
(m)
A
B
-4200
-4205
-4210
-4215
-4220
-4225
-4230
-4235
-4240
-4245
0
2000
4000
6000
8000
10000
12000
14000
(m)
D
Coral Patch Ridge
GS
L2
L1
C
D
VIEW FROM WNW
L2
(m)
C
D
-4600
-4620
-4640
-4660
-4680
-4700
-4720
0
2000
4000
6000
8000
10000
12000
(m)

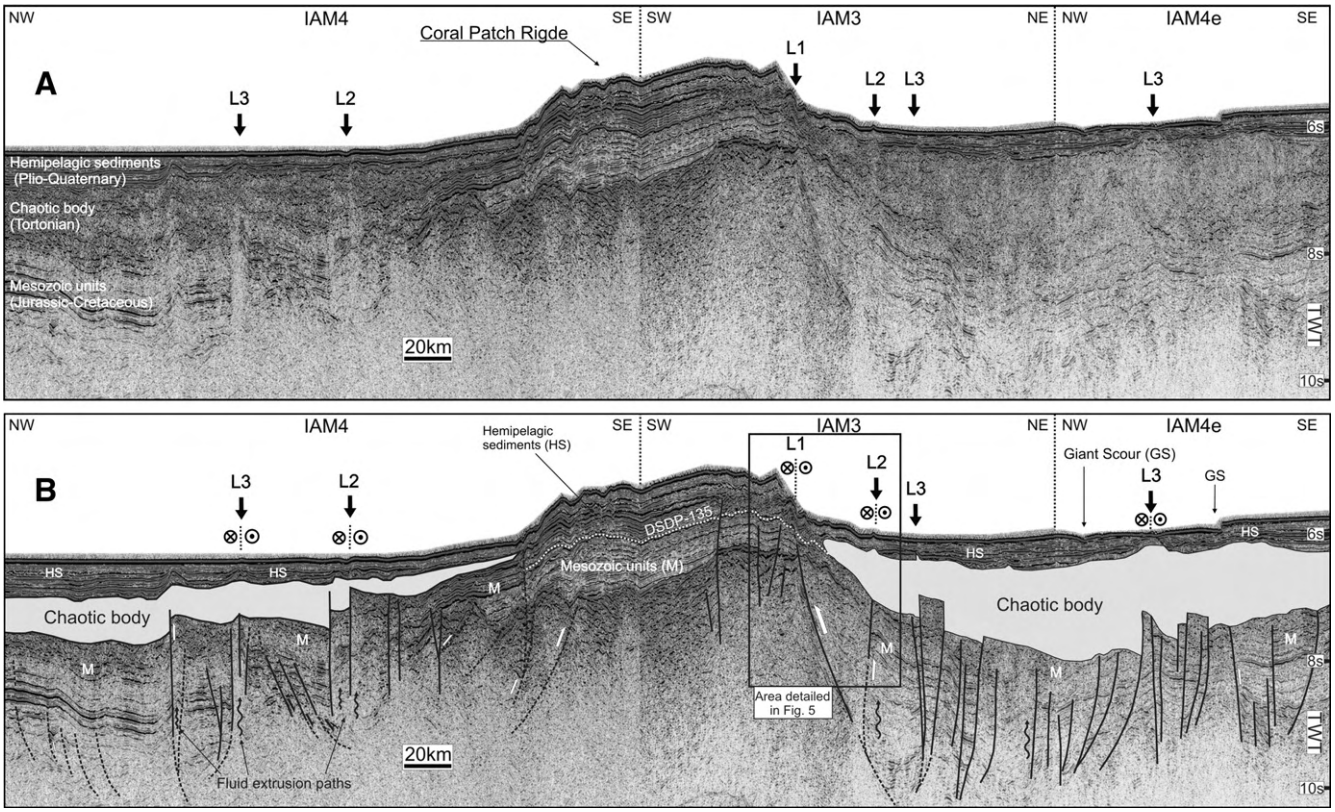

Fig. 4. (A) Uninterpreted multi-channel seismic profiles IAM4, IAM3 and IAM4e migrated with the water velocity (location in Fig. 2). (B) Simplified seismostratigraphic and tectonic interpretation of the same profiles. L1, L2 and L3 mark the intersection with the lineaments identified in the high-resolution bathymetry. Near the fault planes white arrows represent interpreted kinematics. HS—Hemipelagic sediments; M—Mesozoic units; GS—Giant Scours; (DSDP-135 marks the seismostratigraphic top of the Mesozoic units).

be noted that with the available MCS dataset the deep seated fault associated to L2 is perfectible traceable in the Horseshoe abyssal plain, and further to the West until the base of the Gorringe Ridge. The mentioned fact that its bathymetric expression is practically non-existent in this area is probably due to an average greater thickness of the post Mesozoic sediment pile, particularly in the area close to the footwall of the Horseshoe fault.

3. Analogue modelling

In the study area recently reported kinematic models derived from geodetic data (Nocquet and Calais, 2004; Stich et al., 2006; Fernandes et al., 2007) show a Present day 4 mm/yr convergence rate, along a direction subparallel to the trend of the study morphotectonic lineaments (see inset of Fig. 1B). This agrees with the general possibility of the prevailing compression being presently dissipated through bulk dextral wrenching along the major faults associated to these lineaments, which was the main focus of our analogue modelling.

In the NW Gulf of Cadiz area, the detailed vertical rheology profile of the lithosphere, and of the uppermost crust, is unknown. However, a non-negligible rheology contrast must exist between the lithified, harder, Mesozoic units, and the uppermost soft sedimentary cover, corresponding in part to the unconsolidated hemipelagic sediments of Plio-Quaternary age. If so, bulk dissipation of the compressive stress must preferably occur in the Mesozoic rigid basement, through dextral strike-slip faulting, deforming the overlying soft cover mostly in a passive manner. Therefore, our first set of experiments consisted on the simulation of basement, right-lateral, strike-slip faulting, and coupled passive shearing in an overlying soft cover.

Nonetheless, given the uncertainty of the upper crust rheology profile in the area, we also preformed a second set of experiments assuming that the study faults could nucleate low-angle transpressive shearing along an narrow band in the overlying sediments. This possibility implies the assumption of a different rheology structure for the upper crust, comprising a less abrupt rheology contrast between a somewhat less viscous basement and the softer sedimentary cover. Accordingly, the previously faulted Mesozoic basement must be able to deform, at least to some degree, in a ductile way to allow low-angle transpressive shearing in the soft cover sediments along a narrow band overlying the fault. It should be noted that in the case of this second set of experiments, our objective was simply to look at the kind of morphotectonic pattern that is expected to form in the soft cover alone, under the mentioned transpressional conditions. In all situations, we focused mainly on the ductile experimental output, comparing both results with the various natural examples. For the basement strike-slip deformation experiments, we further use this comparison to quantify the amount of shear strain (γ), the along strike displacement (Δx), and the age of the corresponding shearing deformation affecting the soft cover sediments.

The present simulation of wrench fault systems and associated passive shearing follows, with some modifications, the work

Fig. 3. (A and B) Different views of the L1 and L2 bathymetric lineaments and associated morphologic features. (C) View of L1 from ESE. AB bathymetric profile just north of L1. White arrows point the en-échelon morphologic crests and troughs; (D) View of L2 from WNW. CD bathymetric profile perpendicular to the L2 lineament. CPR—Coral Patch Ridge; GS—Giant scours. Black arrows always indicate the interpreted sense of shear.

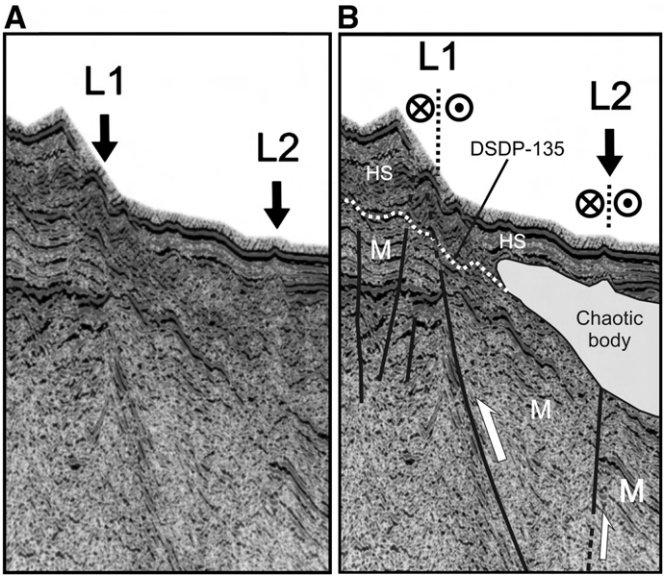

Fig. 5. (A) Zoomed segment of the IAM3 seismic profile of Fig. 4. (B) Illustration of the interpreted kinematics along L1 fault (white arrows); HS—hemipelagic sediments (Plio-Quaternary); M—Mesozoic units (DSDP-135 marks the seismostratigraphic top of the Mesozoic units).

previously put forward by other authors (e.g. Wilcox et al., 1973; Richard et al., 1991; Richard and Krantz, 1991; Casas et al., 2001). The main difference is that the prime motivation of our analogue modelling was not to theoretical address the study of the implicated deformation regimes (e.g. simple shear, transpression), but instead, to use the obtained experimental results instrumentally, i.e., to compare them with the natural structures to try to quantify the strain involved in their formation. Another important difference is that we focused in the formation of ductile structures, rather than brittle ones, to try to understand the way through which a soft sedimentary cover, comprising poorly or even unconsolidated sediments, endures deformation under the referred conditions.

3.1. First set of experiments: basement strike-slip faulting and coupled shear deformation

3.1.1. Experimental procedure

In the first set of experiments we used a Perspex strike-slip deformation rig (Fig. 6) with dimensions of $50 \times 25 \times 5$ cm, comprising two confining vertical walls and two basal, laterally juxtaposed, rigid plates, moving relatively to each other in opposite directions, driven at constant velocity (~0.028 mm s^{-1}) by an electric motor.

The materials used as analogues of the soft cover seafloor sediments include: (1) Dry quartz sand (grain size<0.25 mm) with negligible cohesion and a friction angle of about 30° to simulate brittle sedimentary layers (e.g. Hubbert, 1951; Horsfield, 1977); (2) Transparent silicone putty (PDMS, a polydimethyl-siloxane, manufactured by Dow Corning of Great Britain under the trade name SGM 36) as an analogue of weak layers within the upper crust (see Weijermars 1986a,b,c for PDMS properties), simulating the deformation behaviour of natural sedimentary rocks such as shales, clays or salt (e.g. Ballard et al., 1987; Vendeville et al., 1987; Richard et al., 1989, 1991; Marques and Coelho, 2001; Rosas et al., 2001, 2002). In some experiments a mixture of dry sand and a fraction of mortar (~40%) was also used to increase the cohesiveness of the material (measured internal friction angle around 35°), and thus improve the simulated reproduction of brittle structures in the model (e.g. Hampel et al., 2004).

To simulate passive deformation of a sedimentary cover above a basement strike-slip fault system, we constructed an initial model (see Fig. 6) in which the rigid basement is represented by the basal Perspex plates. These are overlain by a 1 cm thick silicone layer, corresponding to the approximately 1 km thickness of the Plio-Quaternary sedimentary cover (scale ≈ 1/100.000). In most experiments a two-layered silicone-sand cake with the same total thickness was used instead, with the intention of monitoring the generation of brittle structures in the sand layers, as well as the ones expected to form in the silicone. The surface between the silicone layer and the basal rigid plates is non-lubricated, promoting total adherence between them. The relative opposite movement of the plates simulates dextral strike-slip along a pre-existent basement fault plane, transmitting this movement to the overlying silicone and sand layers. Square grids, straight lines and circles were drawn on top of the model surface to be used as passive strain markers. The dimensions of the deformation rig are sufficiently large to guarantee that the bulk of the model is not affected by boundary effects. The experiments were repeated several times to ensure the consistency of the obtained results, and top view photographs were taken at regular time intervals.

3.1.2. Experimental results

In the cover silicone-sand layers of our model, the strike-slip basement faulting was mostly accommodated through the development of different types of brittle and ductile structures (Figs. 7A, B and 8).

The obtained brittle structures are dominant in the sand (sand-mortar) layers and comprise mainly (inset of Fig. 8): a) Oblique synthetic Riedel shears (*R*), orientated at low angles to the bulk shear direction (15°–20° for the first increments of deformation); b) Synthetic *P* shears which originate at the tips of *R* shears also at low angles to the shear direction (10°–15°); c) Few antithetic Riedel shears (*R'*) at high angles (70°–75°) with the bulk shear direction; and d) Few tension gashes or extension fractures (*T*) at original 45° to the shear direction.

Ductile structures also developed in the sand layers, but were clearly dominant in the silicone cover layers of our models (lower right photos of Fig. 7A and B), consisting in sets of en-échelon folds, originally formed at 45° to the shear direction, and progressively rotating towards it as shear strain (γ) increased. In the sand layers, the en-échelon folds are also pervasively cut by an anastomosing grid of synthetic Riedels (*R*) and *P* shears (Figs. 7A and 8).

3.2. Second set of experiments: low-angle transpression

3.2.1. Experimental procedure

As mentioned above, we carried out this second set of experiments essentially to be able to monitor the type of morphotectonic patterns that are expected to form under dextral, low-angle, transpression, affecting soft cover sediments along a narrow shear band. To do so we used a transpressive deformation rig (Fig. 9) comprising two lateral (vertical) walls, moving relatively to each other in opposite directions on top of a fixed (horizontal) basal rigid plate. The walls are driven by a motor connected to a pair of long screws, pushing them along a direction making a horizontal angle of 15° with the shear direction, at the constant velocity of approximately 0.028 mm s^{-1}.

We employed the same materials with the same properties described for the first set of experiments: dry sand as an analogue of upper crust brittle behaviour, and transparent silicone putty (PDMS) to simulate week layers of the upper crust soft sedimentary cover. Similarly to what was described for the first set of experiments, a sand-mortar mixture was also some times used to favour the reproduction of brittle structures.

The constructed initial model consisted in a 1 cm-thick layered silicone-sand cake (Fig. 9) corresponding to the scaled estimated thickness of the Plio-Quaternary sedimentary cover (≈1:100,000). It should be noted that in this case the basal Perspex plate does not represent an analogue of the Mesozoic basement rocks, since we

focused exclusively on the low-angle transpressive shearing affecting the cover.

Total free slip was achieved along the contact surface of the basal Perspex plate with the silicone layer, by lubricating it with neutral soap. Conversely, the contact surface between the silicone layer and the vertical moving walls was non-lubricated, promoting a total adherence of the silicone to these walls. Straight lines and circles were drawn on top of the model surface to be used as passive strain markers. Experiments were repeated several times, and top view photographs were obtain at regular intervals.

3.2.2. Experimental results

In these experiments (Fig. 10A and B) synthetic Riedels (*R*) also formed at a low angle to the bulk shear direction, but neither in the silicone layer, nor in the sand-mortar one, did any set of en-échelon folds developed. Instead, in early stages (Fig. 10A), a central elongated bulge formed, consisting in two aligned asymmetric fold segments, trending parallel to the bulk shear direction, and bounded at both sides by incipient, opposite directed, early thrusts. For higher amounts of shortening and lateral displacement (Fig. 10B), synthetic *R* shears continued to form, and the folded bulged band narrowed as folds got tighter and thrusts developed.

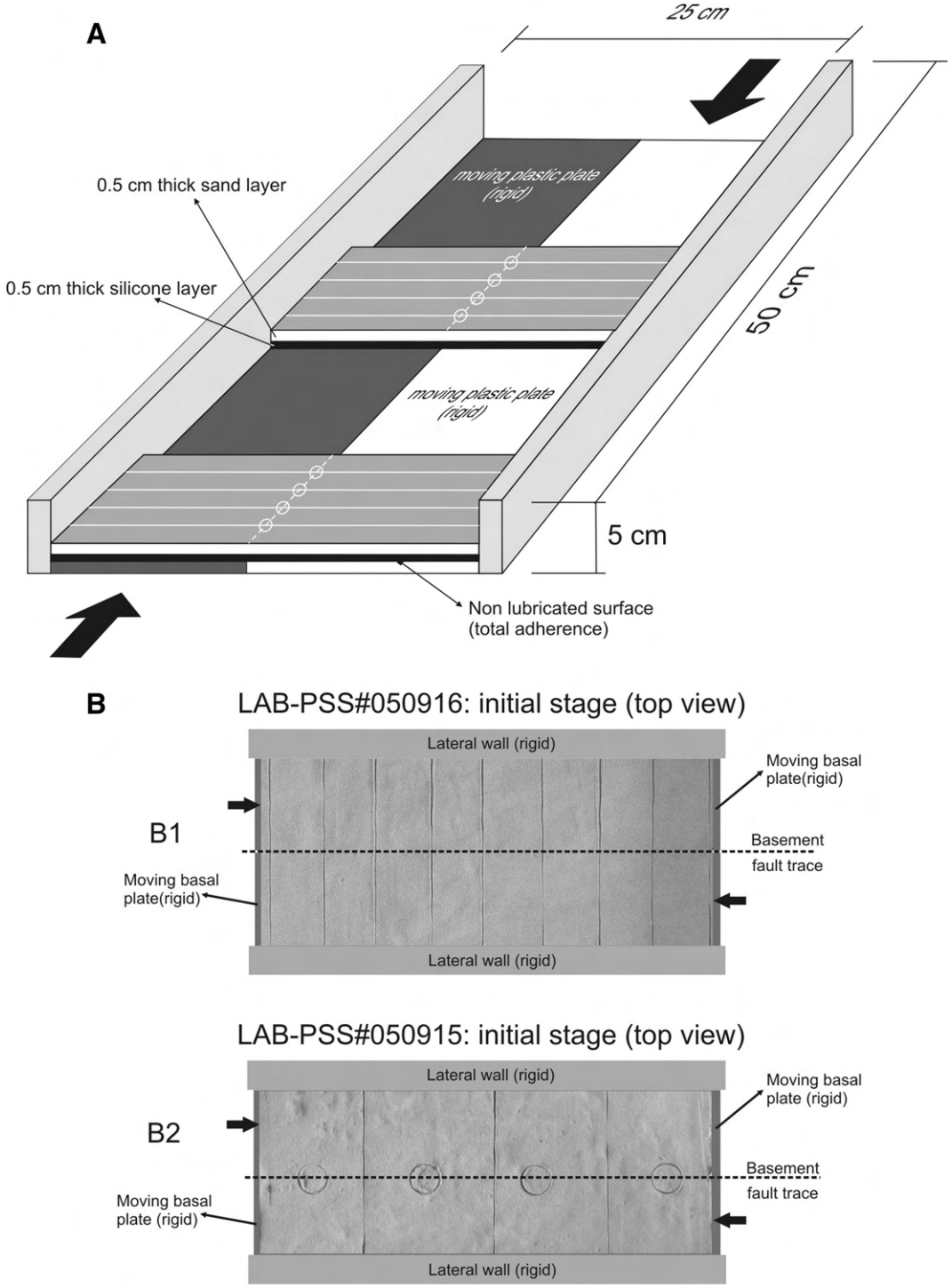

Fig. 6. (A) Experimental apparatus and model setting used in the first set of experiments to simulate basement strike-slip faulting and coupled shear deformation (modified after Casas et al., 2001); (B) Top views of the initial state for two of the preformed experiences (LAB-PSS#050915 and LAB-PSS#050916).

4. Comparison of the experimental results with the natural examples

For both sets of experiments the obtained brittle structural patterns recorded in the sand cover layers are similar, consisting essentially in the more or less pervasive development of synthetic *R* and *P* shears (see Figs. 7 and 10). Conversely, the ductile patterns, comprising the development of folds both in sand and silicone layers, are clearly different, depending on which set of experiments is considered: for strike-slip basement faulting and coupled passive shearing, an en-échelon fold pattern was obtained (see Fig. 7A and B), whereas for low-angle transpression a totally different pattern of folds formed (see Fig. 10).

In the first case, the experimentally obtained structural pattern correlates well with the en-échelon spatial distribution of bathymetric crests associated with L1 (Fig. 11A and B), which suggests that this corresponds to a morphotectonic pattern formed passively in the seafloor soft sediments, as the result of dominant right-lateral strike-slip reactivation of the underlying basement fault.

For the second set of experiments the obtained structural pattern resembles more the morphology characterizing L2 (Fig. 11C), suggesting an origin preferably related with low-angle dextral transpressive shearing along a narrow band nucleated by the reactivation of the underlying fault.

For both sets of experiments, the obtained structural patterns correlate with the natural examples, only when the ductile deformation output is considered. Both L1 and L2 lack any kind of associated brittle structures, such as the R or P shears that formed in the analogue models. This shows that the deformation which originated the natural morphotectonic patterns was essentially ductile, affecting poorly lithified soft sediments of Recent age.

Note that it was not possible to compare the obtained experimental results with L3 and L4 lineaments, because L3 is hardly recognizable in the bathymetry, and deformation associated with L4 is probably masked by the local wrinkled seafloor morphology (corresponding to the accretionary wedge domain, AW in Figs. 1B and 2).

4.1. Structural analysis

In our first set of experiments the en-échelon folds were observed to form and rotate closely to what is theoretically predicted for passive strain markers in simple shear progressive deformation. In this deformation regime, shear strain (γ) is defined as the ratio between the displacement parallel to the shear direction (Δx) and the width of

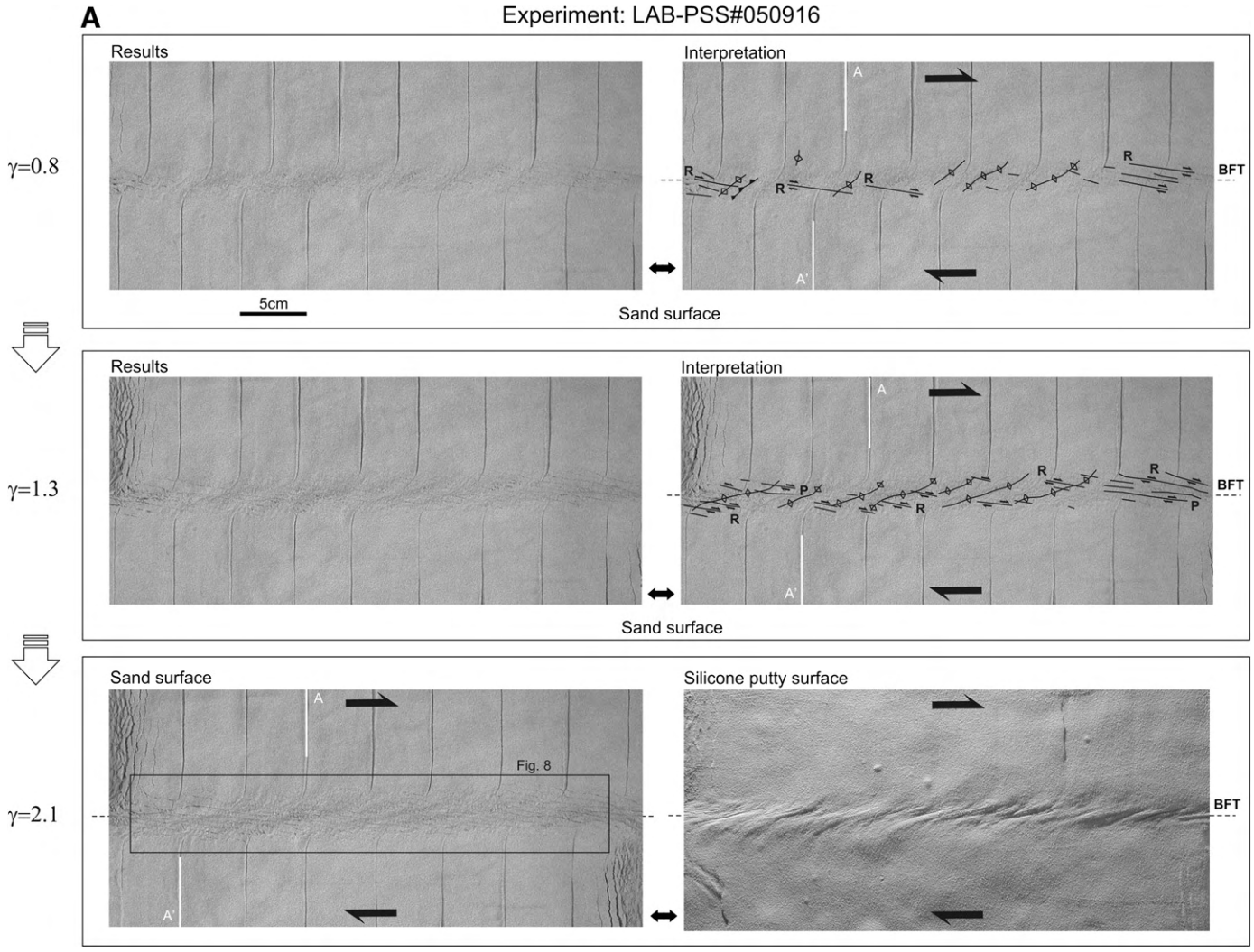

Fig. 7. Example of the results obtained in the first set of experiments to simulate basement strike-slip faulting and coupled shear deformation, (A) using a silicone-sand layered cake (experiment LAB-PSS#050916, see corresponding initial state in Fig. 6B1), and (B) using a top layer corresponding to a sand-mortar mixture (LAB-PSS#050915, initial state in Fig. 6B2). Top views of the sand/sand-mortar surface are shown for successive increments of γ shear strain. Lower right photos in A and B correspond to the silicone surface top view after removal of the previous overlying sand/sand-mortar layer. *R*—synthetic Riedel shears; *R'*—antithetic Riedel shears; *P*—synthetic *P* shears; *T*—tension gashes or extension fractures; BFT—Basement fault trace.

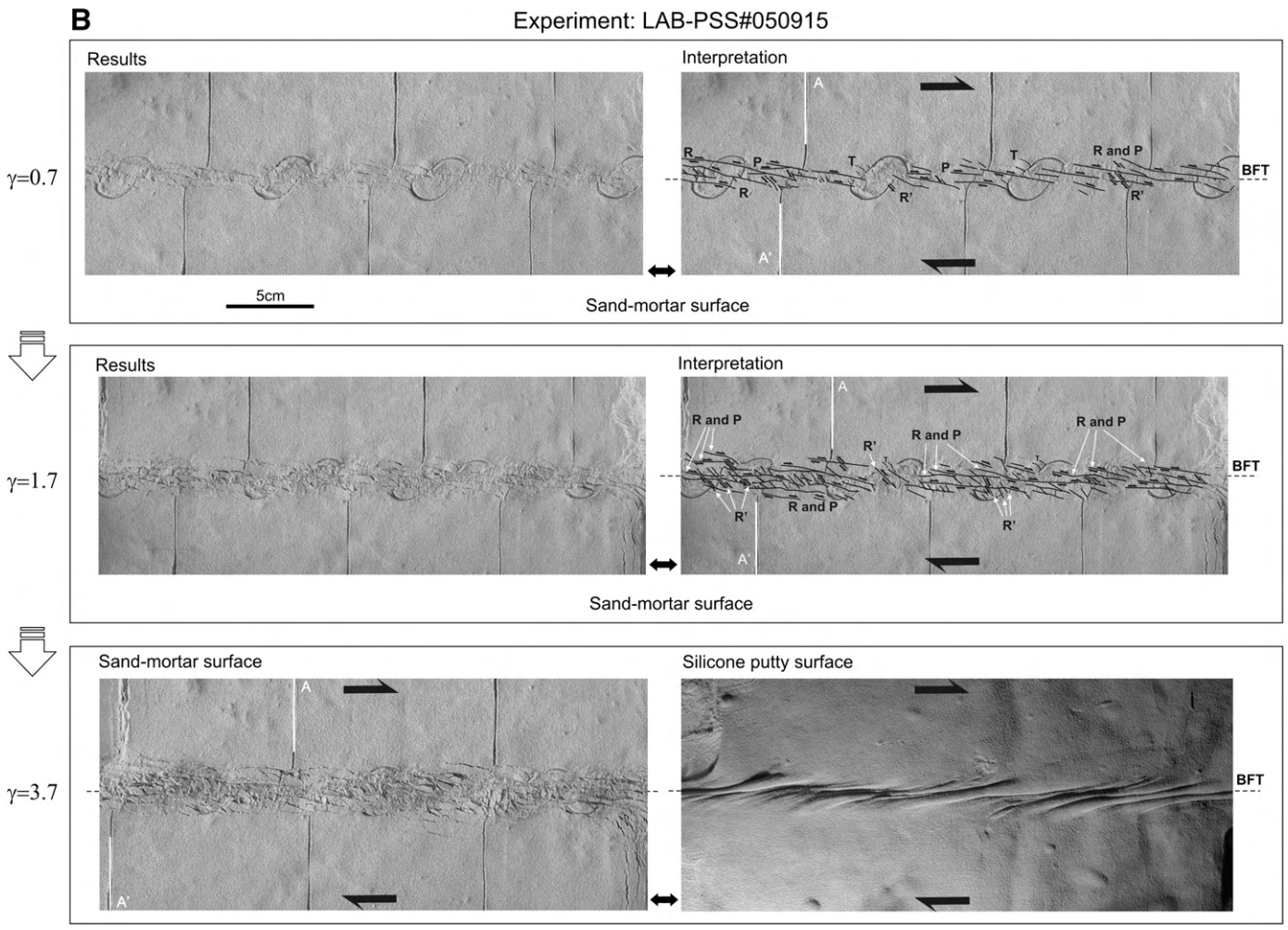

Fig. 7 (*continued*).

the shear zone (Y) (Fig. 12A). A classical strain maker corresponds to the strain ellipse of Ramsay and Huber (1983), which in simple shear forms instantaneously, for infinitesimal increments of shear strain, with its longest axis at an angle (θ) at 45° to the shear plane (Fig. 12B). As γ shear strain accumulates, the axial ratio of the strain ellipse increases and its longest axis rotates towards the shear plane, with consequent reduction of the angular θ value (Fig. 12B). This behaviour can be simply described in terms of the relation between γ and θ, as in the equation presented by Ramsay and Graham (1970) (see Eq. (1) below, and Fig. 12B). Accordingly, our experimental results show that, for infinitesimal deformation increments, the en-échelon folds formed with their hinges approximately parallel to the e_1 principal axis of the instantaneous strain ellipse, at an angle of $\theta \approx 45°$ to the shear plane (Fig. 12C), and rotated towards it during the progressive non-coaxial deformation, as γ shear strain increased. This similarity between the observed experimental behaviour of the en-échelon folds and the theoretical prediction for simple shear deformation, is shown by the good correlation that exists between the points corresponding to the measurements made for θ and γ in the succeeding progressive deformation stages of the several experiments done, and the equation curve of Ramsay and Graham (1970) (Fig. 12D). This correlation shows that the en-échelon folds obtained in our first set of experiments formed under deformation conditions similar to bulk simple shear, and hence, given the comparison with the natural examples presented above, that the same would also apply to the L1 bathymetric lineament and associated natural en-échelon folds.

Based on this deduction, measuring the mean value of θ (= 24.20°) in the natural en-échelon folds of L1 lineament (see Fig. 11B) made it possible to determine the approximate amount of shear strain (γ) that originated these structures in their present orientation. This was done using equation

$$\gamma = \frac{2}{\tan 2\theta}, \tag{1}$$

(Ramsay and Graham, 1970) in which $\theta = 24.20°$ gives $\gamma = 1.78$.

Furthermore, using this γ value and the mean width of the L1 shear zone Y (~4000 m), which was estimated based on the observed spatial distribution of the en-échelon folds (see Fig. 11B), it was also possible to determine the along strike displacement (Δx) implied in the shear deformation responsible for the present orientation of the en-échelon folds. This was done using equation

$$\gamma = tg(\Psi) = \frac{\Delta x}{Y}, \tag{2}$$

of Ramsay and Huber (1983), in which for $\gamma = 1.78$ and $Y = 4000$ m, we obtain $\Delta x \approx 7000$ m.

In our second set of experiments, concerning the L2 lineament and associated deformation pattern, the absence of natural structures useful as reliable (i.e. measurable) strain markers, did not allow a more quantitative insight, regarding strain quantification of the transpressive shearing, through comparison between the observations and the experimental results.

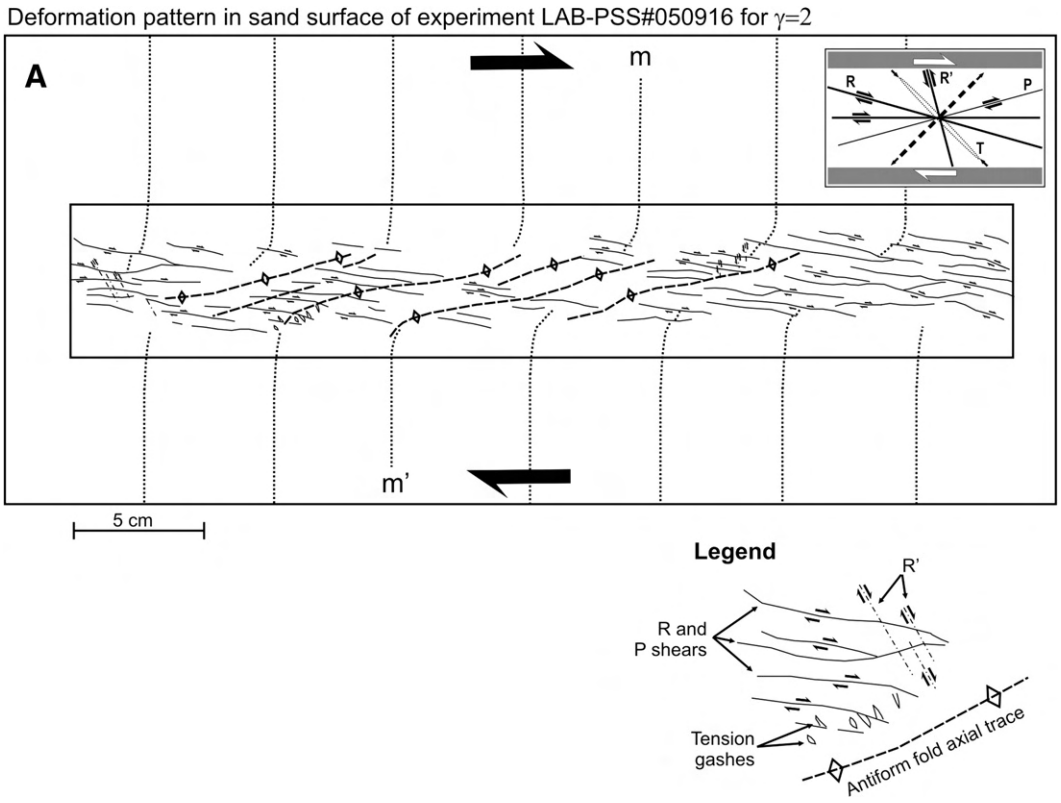

Fig. 8. Deformation pattern obtained in the sand layer of experiment LAB-PSS#050916 for $\gamma \approx 2$ (see Fig. 7A for location).

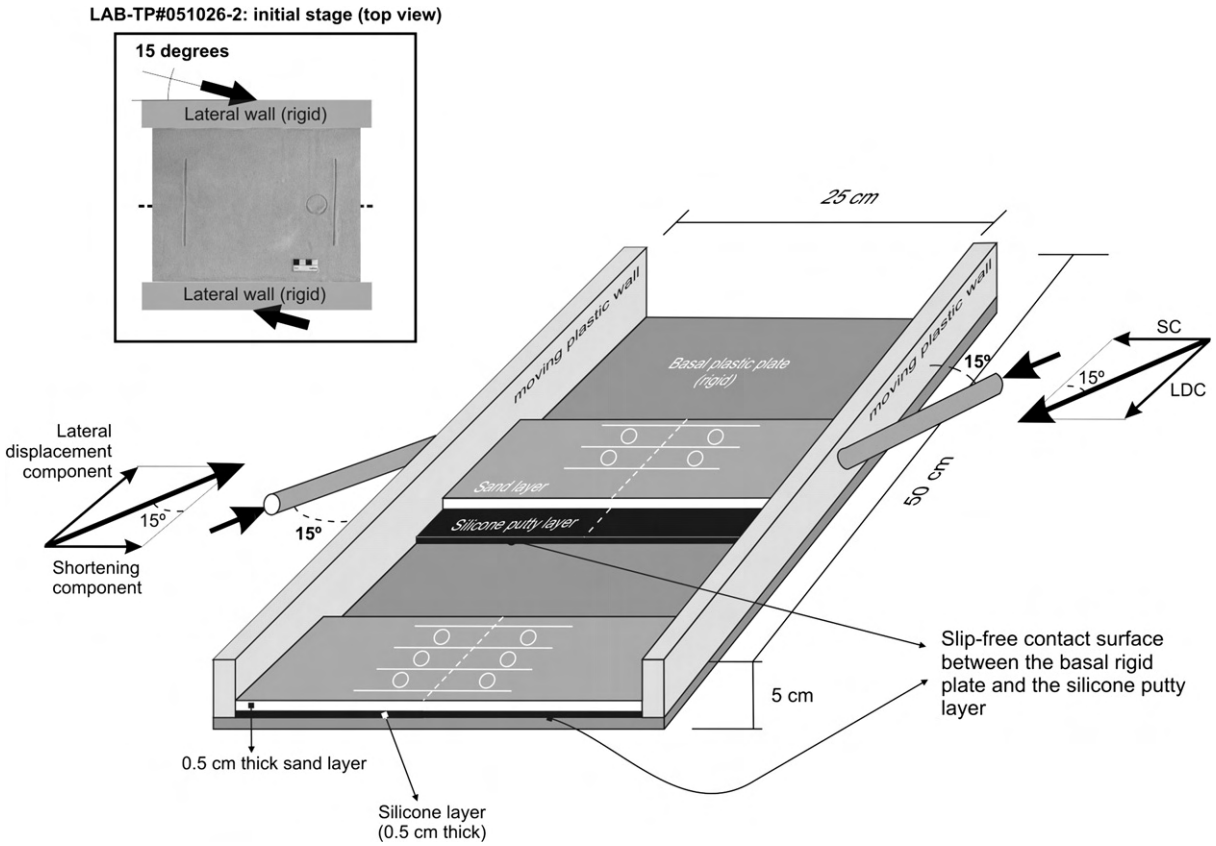

Fig. 9. Experimental apparatus and model setting used in the second set of experiments to simulate low-angle transpression (modified after Casas et al., 2001). Upper left inset showing top view initial state of one of the preformed experiences (LAB-TP#051026-2).

4.2. Age of the deformation associated to the L1 morphotectonic pattern

According to the recently reported kinematic models for the Gulf of Cadiz computed from geodetic data (e.g. Nocquet and Calais, 2004; Stich et al., 2006; Fernandes et al., 2007), the ongoing convergence between Nubia and Iberia occurs along a WNW–ESE direction, subparallel to the shear direction associated to L1, at a rate of approximately 4 mm/yr (see inset in Fig. 1B). Thus, by considering the value of the along strike

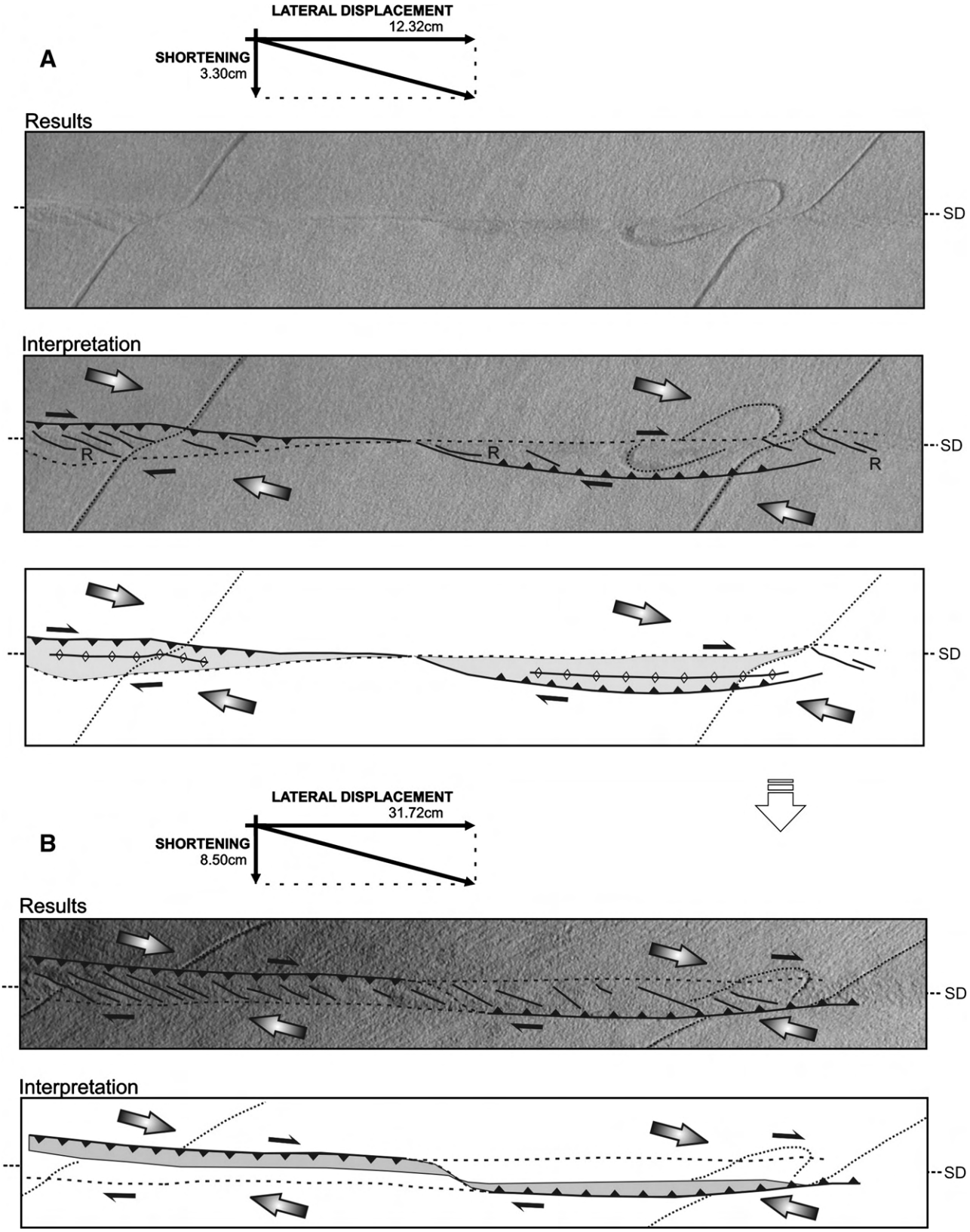

Fig. 10. Example of the results obtained in the second set of experiments to simulate low-angle transpression (exp: LAB-TP#051026-2, initial state in the inset of Fig. 9). *R*—synthetic Riedel shears. SD—Shear direction.

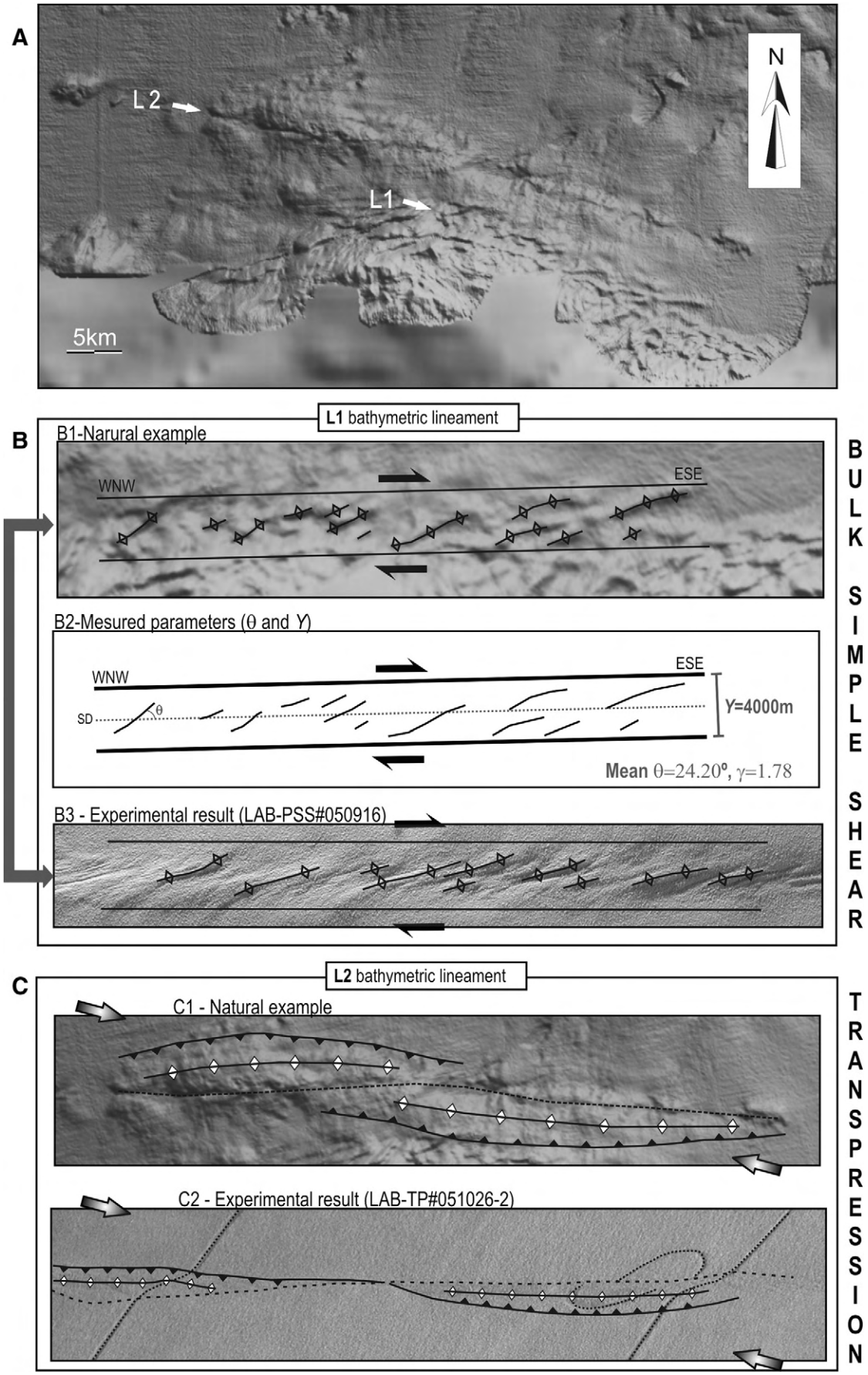

Fig. 11. Comparison of the natural examples (A—study bathymetric lineaments L1 and L2) with the obtained first (B) and second (C) set experiments. θ—angle between the en-échelon folds and the shear direction (SD); γ—corresponding shear strain; Y—shear zone width.

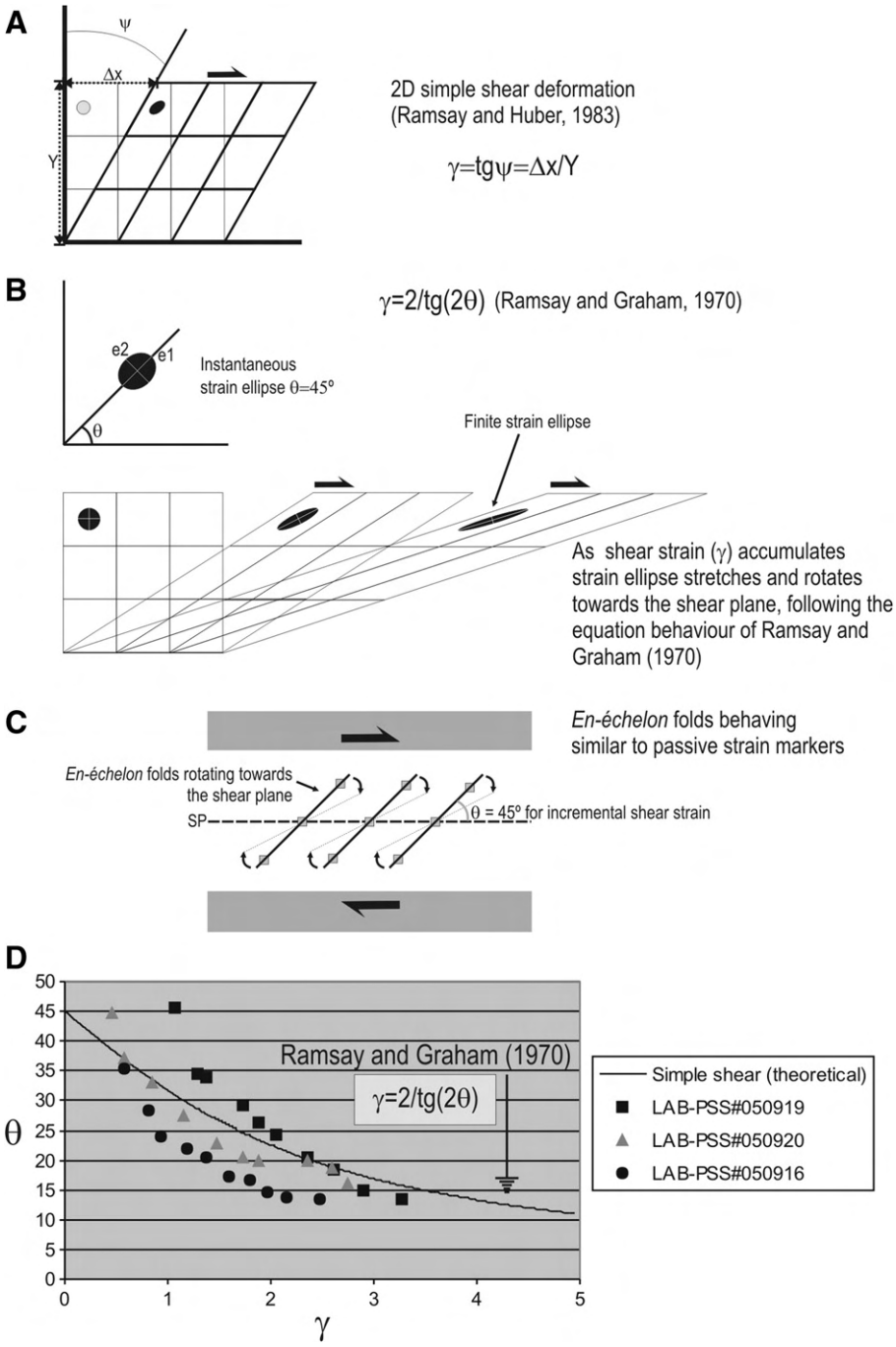

Fig. 12. (A and B) Schematic representation of the theoretical behaviour of passive strain markers under simple shear deformation (adapted from Ramsay and Huber, 1983). (C) Schematic representation of en-échelon folds behaving as passive strain markers under simple shear deformation. (D) Plot of θ and γ values, measured for succeeding deformation stages of several experiments, against the equation curve of Ramsay and Graham (1970).

displacement ($\Delta x \approx 7000$ m) obtained above, and the reported 4 mm/yr convergence rate, it was possible to estimate the maximum age of 1.8 Ma for the deformation responsible for the L1 morphotectonic pattern. This estimate is based on the assumption that the cover sediments recording this pattern are soft (poorly lithified), deforming mostly in a ductile manner, which suggests a simultaneous character of sedimentation and strain. In accordance, the syntectonic sedimentation rate would be of critical influence on the nucleation and development of the L1 structures, since relatively larger sedimentation rates would tend to attenuate the morphologic expression of the developing structures. Therefore, the well preserved L1 morphotectonic patterns seemingly suggest low syntectonic sedimentation rates, which agrees with the average 30 cm/Ky (0.3 mm/y) reported by Lebreiro et al. (1997) for the horseshoe abyssal plain.

5. Summary and conclusions

Based on our experimental results, and on the bathymetry and seismic reflection data presented above, we conclude that: (1) In the Gulf of Cadiz, the WNW-ESE lineaments correspond to the bathymetric expression of active deep seated faults; (2) These faults show a Present day kinematics consisting in bulk dextral wrenching; (3) The deformation which originated the study morphotectonic lineaments started at a maximum age of ca. 1.8 Ma. (4) These lineaments formed

in soft, most probably, poorly consolidated sediments, deposited at relatively low rates of syntectonic sedimentation.

Our results show that the morphotectonic pattern associated to L1 was formed as a consequence of dextral strike-slip reactivation of a basement fault, coupled with passive simple shear deformation of the overlying soft sedimentary cover. On other hand, the seafloor bathymetry pattern associated to L2 must have formed preferably as a consequence of low-angle dextral transpression. However, in this case, the uncertainty concerning the local upper crust vertical rheology profile, did not allow a better comprehension of the process governing the nucleation of a transpressive shear band in the soft sedimentary cover overlying the correspondent fault. Moreover, since no natural structural features useful as strain gauges were found in this case, a more quantitative insight was also impossible to achieve. It should be noted that L1 borders the northern–eastern flank of the CPR (Figs. 1B, 2 and 3), which could correspond to a rigid body resisting shortening and favouring lateral slip, instead of transpressive shearing, along this limit.

5.1. Tectonic implications

In the Gulf of Cadiz, the faults associated to the studied lineaments were previously reported to have endured a complex tectonic evolution from Early Mesozoic through Cenozoic (Terrinha et al., under review). Based on the inspected seismic profiles (see Figs. 4 and 5), it was in some cases possible to recognize a kinematic behaviour characterized by reverse faulting. These faults cut through the Mesozoic and the base of the Tortonian chaotic body, but do not affect the top of this unit, neither the overlying sediments which are generally sealing these structures (see Figs. 4 and 5). This shows that the reverse fault kinematics is not presently active.

Our conclusions fit the whole-scale strain partitioning scenario, recently proposed by Terrinha et al. (under review), according to which the Nubia–Iberia collision in the Gulf of Cadiz area is Presently being accommodated through oblique westwards thrusting along NNE–SSW faults, such as the Horseshoe fault and Marques de Pombal active faults (see Fig. 1B), and simultaneously through bulk dextral strike-slip reactivation of pre-existent WNW–ESE faults, corresponding to the studied bathymetric lineaments. According to our experimental results, the age of this deformation recorded by Recent bottom floor soft sediments in the Gulf of Cadiz is ca. 1.8 Ma (late Pliocene). Furthermore, given the WNW–ESE trend of the faults their interpreted kinematic behaviour is in good agreement with the kinematic models derived from geodetic data yielding a 4 mm/yr convergence rate, subparallel that same direction.

Acknowledgements

Experiments were performed in the Experimental Tectonics Laboratory of LATTEX-IDL, a research unit funded by PLURIANUAL (125/N/92). MATESPRO (PDCTM/P/MAR/15264/1999), EUROMARGINS SWIM (01-LEC-EMA09F). V. Valadares acknowledges a Ph.D. scholarship (SFRH/BD/17603/2004) of FCT. Dr. Rui Dias (Évora University) is acknowledged for constructive discussions, which helped to improve the present work. We also thank to two anonymous reviewers and the editor-in-chief of Marine Geology, Gert J. De Lange, for their constructive and thorough reviews of the manuscript.

References

Abe, K., 1979. Size of great earthquakes of 1837–1974 inferred from tsunami data. J. Geophys. Res. 84, 1561–1568.
Ballard, J.F., Brun, J.P., Van den Driessche, J., Allemand, P., 1987. Propagation des chevauchements au-dessus des zones de décollement: modèles experimentaux. Comptes Rendus de l'Académie des Sciences de Paris 305, 1249–1253.
Bird, P., 2003. An updated digital model of plate boundaries. Geochem. Geophys. Geosyst 4 (3), 1027. doi:10.1029/2001GC000252.
Borges, J.F., Fitas, A.J., Bezzeghoud, M., Costa, P.T., 2001. Seismotectonics of Portugal and its adjacent Atlantic Area. Tectonophysics 331, 373–387.
Buforn, E., Sanz de Galdenao, C., Udías, A., 1995. Seismotectonics of the Ibero–Maghrebian region. Tectonophysics 248, 247–261.
Buforn, E., Bezzeghoud, M., Udías, A., Pro, C., 2004. Seismic sources on the Iberia–African plate boundary and their tectonic implications. Pure Appl. Geophys. 161, 623–646.
Casas, A.M., Gapais, D., Nalpas, T., Besnard, K., Román-Berdiel, K., 2001. Analogue models of transpressive systems. J. Struct. Geol. 23, 733–743.
Fernandes, R.M.S., Miranda, J.M., Meijninger, B.M.L., Bos, M.S., Noomen, R., Bastos, L., Ambrosius, B.A.C., Riva, R.E.M., 2007. Surface velocity field of the Ibero-Maghrebian segment of the Eurasia–Nubia plate boundary. Geophys. J. Int. 169 (1), 315–324.
Gracia, E., Dañobeitia, J., Vergés, J., PARSIFAL Team, 2003. Mapping active faults offshore Portugal (36°N–38°N): implications seismic hazard assessment along the south-west Iberian margin. Geology 31 (1), 83–86.
Gutscher, M-A., 2004. What caused the Great Lisbon earthquake? Science 305, 1247–1248.
Gutscher, M.-A., Malod, J., Rehault, J.-P., Contrucci, I., Klingelhoefer, F., Spakman, W., Mendes-Victor, L., 2002. Evidence for active subduction beneath Gibraltar. Geology 30 (12), 1071–1074.
Hampel, A., Adam, J., Kukowski, N., 2004. Response of the tectonically erosive south Peruvian forearc to subduction of the Nazca Ridge: analysis of three-dimensional analogue experiments. Tectonics 23, TC5003. doi:10.1029/2003TC001585.
Hensen, C., Nuzzo, M., Hornibrook, E., Pinheiro, L.M., Bock, B., Magalhães, V.H., Bruckmann, W., 2007. Sources of mud volcano fluids in the Gulf of Cadiz—indications for hydrothermal imprint. Geochim Cosmochim Ac. 71, 1232–1248.
Horsfield, W.T., 1977. An experimental approach to basement-controlled faulting. Geol. Mijnbouw 56 (4), 363–370.
Hubbert, M.K., 1951. Mechanical basis for certain familiar geologic structures. Geol. Soc. Am. Bull. 62 (4), 355–372.
Johnston, A., 1996. Seismic moment assessment of earthquakes in stable continental regions—III. New Madrid, 1811–1812, Charleston 1886 and Lisbon 1755. Geophys. J. Int. 126, 314–344.
Lebreiro, S.M., McCave, N.I., Weaver, P.E., 1997. Late Quaternary turbidite emplacement on the Horseshoe abyssal plain (Iberian margin). J. Sediment. Res. 67 (5), 856–870.
Maldonado, A., Somoza, L., Pallarés, L., 1999. The Betic orogen and the Iberian–African boundary in the Gulf of Cadiz: geological evolution (central North Atlantic). Mar. Geol. 155, 9–43.
Marques, F.O., Coelho, S., 2001. Rotation of rigid elliptical cylinders in viscous simple shear flow: analogue experiments. J. Struct. Geol. 23, 609–617.
Martínez-Solares, J.M., López-Arroyo, A., 2004. The great historical 1755 earthquake. Effects and damage in Spain. J. Seismology 8, 275–294.
Medialdea, T., Vegas, R., Somoza, L., Vázquez, J.T., Maldonado, A., Díaz-del-Río, V., Maestro, A., Córdoba, D., Fernández-Puga, M.C., 2004. Structure and evolution of the "Olistostrome" complex of the Gibraltar Arc in the Gulf of Cádiz (eastern Central Atlantic): evidence from two long seismic cross-sections. Mar. Geol 209, 173–198.
Nocquet, J.-M., Calais, E., 2004. Geodetic measurements of crustal deformation in the Western Mediterranean and Europe. Pure Appl. Geophys. 161, 661–681.
Pinheiro, L., Ivanov, M.K., Sautkin, A., Akhmanov, G., Magalhães, V., Volkonskaya, A., Monteiro, J.H., Somoza, L., Gardner, J., Hamouni, N., Cunha, M.R., 2003. Mud volcanism in the Gulf of Cadiz: results from the TTR-10 cruise. Mar. Geol. 195, 131–151.
Ramsay, J.G., Graham, M.I., 1970. Strain variation in shear belts. Can. J. Earth Sci. 7, 786–813.
Ramsay, J.G., Huber, M.I., 1983. Modern Structural Geology: Volume 1: Strain Analysis. Academic Press, Londres. 307 pp.
Ribeiro, A., Cabral, J., Baptista, R., Matias, L., 1996. Stress pattern in Portugal mainland and the adjacent Atlantic region, West Iberia. Tectonophysics 15 (2), 641–659.
Richard, P., Ballard, J.F., Colletta, B., Cobbold, P., 1989. Naissance et evolution de failles audessus d'un décrochement de socle: modélisation analogique et tomographie. Cr. Acad. Sci. Paris 309, 2111–2118.
Richard, P., Krantz, R.W., 1991. Experiments on fault reactivation in strike-slip mode. Tectonophysics 188, 117–131.
Richard, P., Mocquet, B., Cobbold, P.R., 1991. Experiments on simultaneous faulting and folding above a basement wrench fault. Tectonophysics 188, 133–141.
Rosas, F.M., Marques, F.O., Coelho, S., Fonseca, P.E., 2001. Sheath fold development in bulk simple shear: analougue modeling of natural examples from the Southern Iberian Variscan Fold Belt. In: Koyi, H.A., Mancktelow, N.S. (Eds.), Tectonic Modeling: A Volume in Honor of Hans Ramberg. Geol. Soc. Am. Mem., 193, pp. 101–110.
Rosas, F.M., Marques, F.O., Luz, A., Coelho, S., 2002. Sheath folds formed by drag induced by rotation of rigid inclusions in viscous simple shear flow: nature and experiment. J. of Struct. Geol. 24, 45–55.
Sartori, R., Torelli, L., Zitellini, N., Peis, D., Lodolo, E., 1994. Eastern segment of the Azores–Gibraltar line (central-eastern Atlantic): an oceanic plate boundary with diffuse compressional deformation. Geology 22, 555–558.
Somoza, L., Díaz-del-Río, V., León, R., Ivanov, M., Fernandez-Puga, M.C., Gardner, J.M., Hernández-Molina, F.J., Pinheiro, L.M., Rodero, J., Lobato, A., Maestro, A., Vázquez, J.T., Medialdea, T., Fernández-Salas, L.M., 2003. Seabed morphology and hydrocarbon seepage in the Gulf of Cádiz mud volcano area: acoustic imagery, multibeam and ultra-high resolution seismic data. Mar. Geol. 195, 153–176.
Stich, D., Mancilla, F.-L., Morales, J., 2005. Crust–mantle coupling in the Gulf of Cadiz (SW-Iberia). Geophys. Res. Lett. 32, L13306. doi:10.1029/2005GL023098.
Stich, D., Serpelloni, E., Mancilla, F.-L., Morales, J., 2006. Kinematics of the Iberia–Maghreb plate contact from seismic moment tensors and GPS observations. Tectonophysics 426, 295–317.
Terrinha, P., Matias, L., Vicente, J.C., Duarte, J., Luís, J., Pinheiro, L., Lourenço, N., Diez, S., Rosas, F.M., Magalhães, V., Valadares, V., Zitellini, N., Mendes-Víctor, L., MATESPRO

Team, under review. Morphotectonics and Strain Partitioning at the Iberia–Africa plate boundary from multibeam and seismic reflection data. Marine Geology.
Terrinha, P., Pinheiro, L., Henriet, J.-P., Matias, L., Ivanov, M.K., Monteiro, J.H., Azhmetzhanov, A., Volkonskaya, A., Cunha, T., Shaskin, P., Rovere, M., 2003. Tsunamigenic–seismogenic structures, neotectonics, sedimentary process and slope instability on the southwest Portuguese margin. Mar. Geol. 195, 55–73.
Thiebot, E., Gutscher, M.-A., 2006. The Gibraltar Arc seismogenic zone (part 1): constraints on a shallow east dipping fault plane source for the 1755 Lisbon earthquake provided by seismic data, gravity and thermal modelling. Tectonophysics 426 (1–2), 135–152.
Torelli, L., Sartori, R., Zitellini, N., 1997. The giant chaotic body in the Atlantic Ocean off Gibraltar: new results from a deep seismic reflection survey. Mar. Petrol. Geol. 14 (2), 125–138.
Tortella, D., Torne, M., Pérez-Estaún, A., 1997. Geodynamic evolution of the eastern segment of the Azores–Gibraltar Zone: the Gorringe bank and the Gulf of Cadiz Region. Mar. Geophys. Res. 19, 211–230.
Vendeville, B., Cobbold, P.R., Davy, P., Brun, J.P., Choukroune, P., 1987. Physical models of extensional tectonics at various scales. In: Coward, M.P., Dewey, J.F., Hancock, P.L. (Eds.), Continental Extensional Tectonics. Special Publications, vol 28. Geological Society, London, pp. 95–107.
Weijermars, R., 1986a. Flow behaviour and physical chemistry of bouncing putties and related polymers in view of tectonic laboratory applications. Tectonophysics 124, 325–358.
Weijermars, R., 1986b. Polydimethyloxane flow defined for experiments in fluid dynamics. Appl. Phys. Lett. 48, 109–111.
Weijermars, R., 1986c. Finite strain of laminar flows can be visualized in SGM 36-polymer. Naturwissenschaften 73, 33.
Wilcox, R.E., Harding, T.P., Seely, D.R., 1973. Basic wrench tectonics. Am. Assoc. Petr. Geol. B. 57 (1), 74–96.
Zitellini, N., Chierici, F., Sartori, R., Torelli, L., 1999. The tectonic source of the 1755 Lisbon earthquake and tsunami. Ann. Geofis 42 (1), 49–55.
Zitellini, N., Mendes, L.A., Córdoba, D., Dañobeitia, J., Nicolich, R., Pellis, G., Ribeiro, A., Sartori, R., Torelli, L., Bartolomé, R., Bortoluzzi, G., Calafato, A., Carrilho, F., Casoni, L., Chierici, F., Corela, C., Correggiari, A., Della Vedova, B., Gràcia, E., Jornet, P., Landuzzi, M., Ligi, M., Magagnoli, A., Marozzi, G., Matias, L., Penitenti, D., Rodríguez, P., Rovere, M., Terrinha, L., Vigliotti, L., Zahinos-Ruiz, A., 2001. Source of the 1755 Lisbon earthquake and tsunami investigated. Eos Trans. AGU 82 (26), 290–291 285.
Zitellini, N., Rovere, M., Terrinha, P., Chierici, F., Matias, L., BIGSETS Team, 2004. Neogene through Quaternary tectonic reactivation of SW Iberian Passive Margin. Pure Appl. Geophys 161, 565–587.

Marine Geology 267 (2009) 156–174

Contents lists available at ScienceDirect

Marine Geology

journal homepage: www.elsevier.com/locate/margeo

Morphotectonics and strain partitioning at the Iberia–Africa plate boundary from multibeam and seismic reflection data

P. Terrinha [a,d,*], L. Matias [b], J. Vicente [c], J. Duarte [a,d], J. Luís [e], L. Pinheiro [f], N. Lourenço [e,g], S. Diez [h], F. Rosas [d], V. Magalhães [f], V. Valadares [a,d], N. Zitellini [i], C. Roque [a,g], L. Mendes Víctor [b], MATESPRO Team [1]

[a] *Laboratório Nacional de Energia e Geologia (LNEG), Unidade de Geologia Marinha, Portugal*
[b] *Fac. Science Univ. Lisbon (CGUL, IDL), Portugal*
[c] *Câmara Municipal de Lisboa, Portugal*
[d] *Fac. Science Univ. Lisbon (LATTEX, IDL), Portugal*
[e] *Univ. Algarve, CIMA, Portugal*
[f] *Universidade de Aveiro, CESAM, Portugal*
[g] *EMEPC, Portugal*
[h] *Unidad de Tecnología Marina (UTM-CSIC), Barcelona, Spain*
[i] *Istituto di Scienze Marine, (ISMAR), Bologna, Italy*

ARTICLE INFO

Article history:
Received 2 March 2009
Received in revised form 23 September 2009
Accepted 29 September 2009
Available online 13 October 2009

Communicated by D.J.W. Piper

Keywords:
Gulf of Cadiz
Southwest Iberia Margin
multibeam bathymetry
morphotectonics
seismotectonics
wrench tectonics
strain partitioning
migration of deformation

ABSTRACT

The Gulf of Cadiz, off SW Iberia and the NW Moroccan margin, straddles the cryptic plate boundary between Africa and Eurasia, a region where the orogenic Alpine compressive deformation in the continental collision zone passes laterally to the west to strike-slip deformation. A set of new multibeam bathymetry, multi-channel and single-channel seismic data presented here image the main morphological features of tectonic origin of a significant part of the Gulf of Cadiz from the continental shelf to the abyssal plain. These morphotectonic features are shown to result from the reactivation of deeply rooted faults that changed their kinematics from the early Mesozoic rifting, through the Late Cretaceous–Paleogene collision, to the Pliocene–Quaternary thrusting and wrenching. The old faults control deep incised, more than 100 km long canyons and valleys. Several effects of neotectonics on deep water seabed are shown. These include: i) the complex morphology caused by wrenching on the 230 km long WNW–ESE faults that produced en echelon folds on the sediments; ii) the formation of up to 5 km wide crescent shaped scours at roughly 4 km water depth by reactivation of thrusts; iii) 10 km long creep folds on the continental slope; and iv) the formation of landslides on active fault escarpments. The present day deformation is partitioned on NE–SW thrusts and WNW–ESE to W–E strike-slip faults and is propagating northwards on N–S trending thrusts along the West Iberia Margin from 35.5°N to 38°N, which should be considered for seismic hazard.

1. Introduction

1.1. Scope and objectives

In recent years the Gulf of Cadiz (Fig. 1) has been recognized as a key site to understand a broad spectrum of geological issues, such as: i) the tectonic evolution of the Africa–Iberia plate boundary, the formation of the Gibraltar orogenic arc, the earthquake and tsunamigenic structures, the origin of the catastrophic 1755 Lisbon earthquake and tsunami (Argus et al., 1989; DeMets et al., 1994; Sillard et al., 1998; Maldonado et al., 1999; Kreemer and Holt, 2001; Zitellini et al., 2001; Gutscher et al., 2002; Sella et al., 2002; Calais et al., 2002; Calais et al., 2003; Terrinha et al., 2003; Fernandes et al., 2003; Gràcia et al., 2003a; Gràcia et al., 2003a,b; Nocquet and Calais, 2004; Medialdea et al., 2004; Stich et al., 2006), ii) the Mediterranean Outflow Water (MOW) and its relation to sedimentation and climate changes (Ambar et al., 2002; Somoza et al., 2003; Mulder et al., 2003; Hernandez-Molina et al., 2003; Voelker et al., 2006), iii) fluid escape and mud volcanism (Somoza et al., 2003; Pinheiro et al., 2003; Van Rensbergen et al., 2005; Pinheiro et al., 2006), and iv) chemosynthetic ecosystems associated to cold seeps (Niemann et al., 2006).

Behind this diversity of processes affecting the geosphere, the biosphere and the hydrosphere, is a complex geological evolution of the area throughout the Neogene. It is now well established, after various studies based on seismic reflection profiles, sidescan sonar and ground truthing, that the whole area is under compressive deformation. A number of active tectonic structures with high tsunamigenic potential were mapped (Terrinha et al., 2003; Gràcia et al., 2003a,b; Zitellini et al., 2004) and various multilayered complexes of

* Corresponding author. Marine Geology Unit, LNEG, Estrada da Portela, 2721-866 Amadora, Portugal. Tel.: +351 21 470 55 41; fax: +351 214 719 018.
E-mail address: pedro.terrinha@ineti.pt (P. Terrinha).
[1] MATESPRO Team: Teresa Medialdea, Marzia Rovere, Caterina Basile, Toni Bermudez.

0025-3227/$ – see front matter © 2009 Elsevier B.V. All rights reserved.
doi:10.1016/j.margeo.2009.09.012

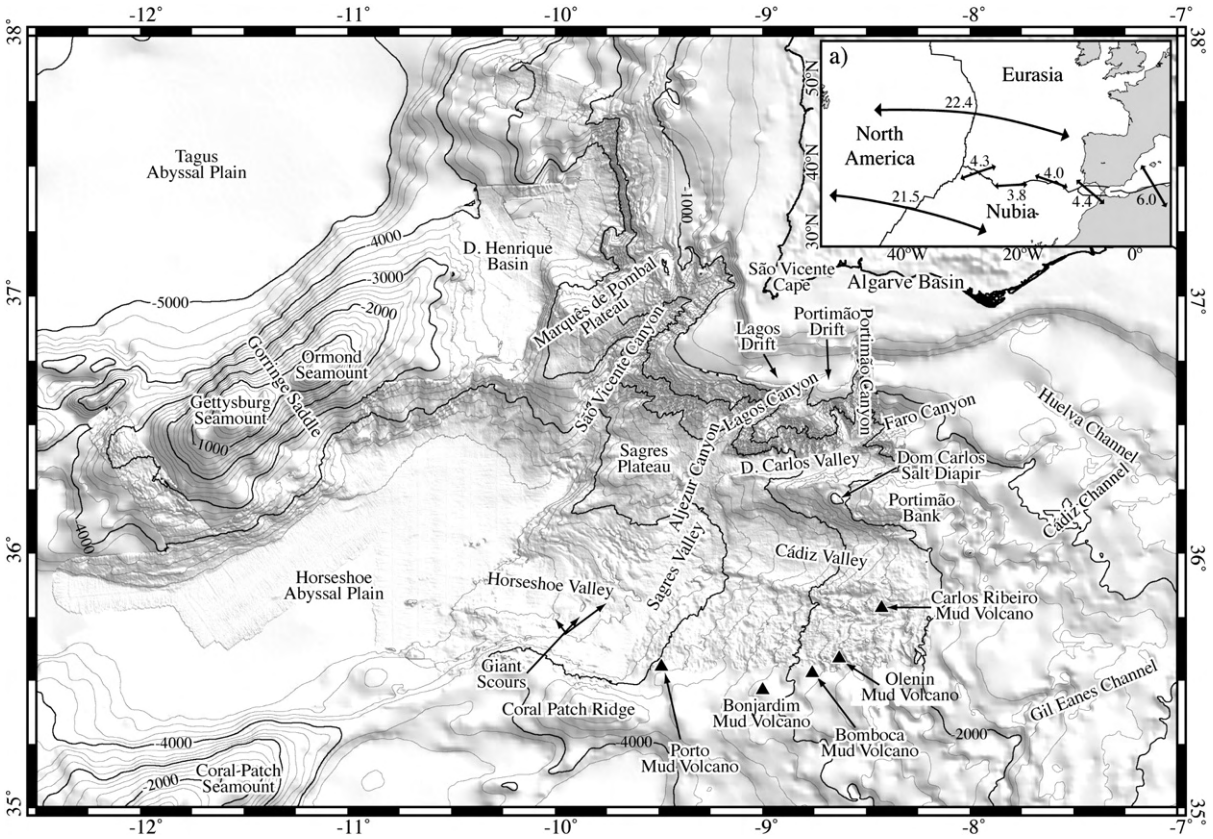

Fig. 1. Location and main morphological features of the study area. Inset shows the geotectonic location of the area and the relative motions of the Eurasia, Nubia and North America lithospheric plates in mm/yr. Triangles show the locations of mud volcanoes.

hemipelagic-mass wasting deposits of Holocene and Pleistocene age were imaged and dated (Vizcaino et al., 2006).

The morphology of the northeastern part of the Gulf of Cadiz was described by Hernandez-Molina et al. (2003), Mulder et al. (2003) and Somoza et al. (2003). The morphology of the southern part of this sector is clearly influenced by the tectonomorphic processes associated with the deformation of the Gulf of Cadiz accretionary wedge (Maldonado et al., 1999; Gutscher et al., 2002), as well as gravitational processes (Gutscher et al., 2008), while in the northern part the shaping processes are sedimentary, erosive and tectonic, associated with the MOW and to diapiric ridges.

The objective of this work is to describe the morphology of the northwestern part of the Gulf of Cadiz and discuss the morphogenetic processes in relation to the tectonic deformation of the Alpine collision front and the Gloria transform fault. This is done based on the interpretation of an original multibeam bathymetry data and seismic reflection profiles.

1.2. Geological setting

During Triassic through Early Cretaceous times the southern and western Iberian margins underwent tectonic rifting, which led to oceanic break-up of the West Iberian Margin from Barremian to Aptian times (Pinheiro et al., 1996). Although the existence of oceanic lithosphere in the Gulf of Cadiz is still a matter of debate (Srivastava et al., 1990; Gràcia et al., 2003a,b; Rovere et al., 2004), some authors postulated the existence of a south Iberia subduction zone that accommodated the Africa–Iberia convergence, from Late Cretaceous–Paleogene through Miocene times (e.g. Srivastava et al., 1990). Accordingly, this process led to the formation of back arc basins and associated tectonic terranes in the western Mediterranean, the formation of the Betic orogen, as well as to the tectonic inversion of the rifted autochthonous south Portuguese and south Spanish margins (e.g. Terrinha, 1998; Maldonado et al., 1999; Rosenbaum et al., 2002; Lopes et al., 2006). Westward directed thrusting of the Internal Betics domains and orogenic collapse, possibly associated with roll back of the Africa subducted slab, formed the Gibraltar orogenic arc, the Gulf of Cadiz accretionary wedge and lithospheric thinning in the Alboran Sea (Rosenbaum et al., 2002; Faccenna et al., 2004). These tectonic processes led to the formation of an accretionary wedge westward of the Gibraltar arc (Gutscher et al., 2002) or imbricate wedge with a westward directed tectonic transport, and an associated distal olistostrome complex (e.g., Horseshoe Gravitational Unit in Iribarren et al., 2007; Giant Chaotic Body in Torelli et al., 1997) that extends across the Horseshoe Abyssal Plain (Fig. 2). The MCS lines reveal a basal decollement horizon of the stacked thrusts of the accretionary wedge near the top of the Cretaceous. Both the accretionary prism and the olistostrome are sealed by sediments of Late Miocene to Lower Pliocene age (Tortella et al., 1997; Torelli et al., 1997; Roque, 2007). The segment of the Azores–Gibraltar Fracture Zone to the east of the Gloria Fault (inset in Fig. 1) was described by Sartori et al. (1994) as a diffuse plate tectonic boundary and various plate kinematic models indicate a 4 mm/yr rate of NW–SE to WNW–ESE convergence between Nubia and Iberia along this fault (insets in Figs. 1 and 8), (Argus et al., 1989; DeMets et al., 1994; Sillard et al., 1998; Kreemer and Holt, 2001; Sella et al., 2002; Calais et al., 2002; Calais et al., 2003; Fernandes et al., 2003; Nocquet and Calais, 2004; Stich et al., 2006). Ribeiro et al. (1996) postulated the formation of an incipient West Iberia subduction zone during Pliocene–Quaternary times, based on the computed NW–SE present day main compression direction.

N–S to NE–SW faults formed in the Permian during the late Variscan fracturing event (Arthaud and Matte, 1977; Ribeiro, 2002) and they were subsequently reactivated during the Mesozoic rifting, the Mesozoic transient compressive episodes (Terrinha et al., 2002)

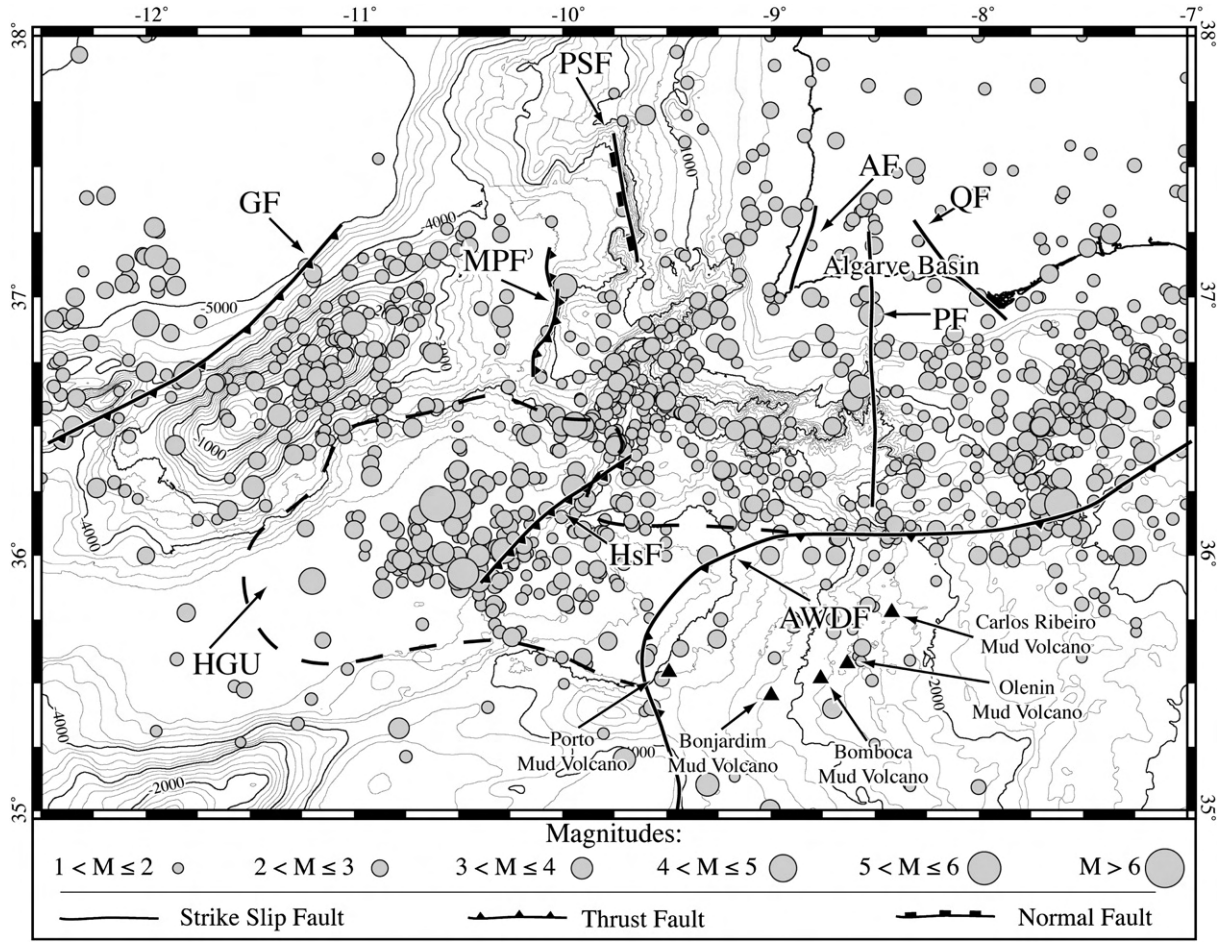

Fig. 2. Seismicity of the study area, the main faults and boundaries of the Accretionary Wedge of the Gulf of Cadiz and Horseshoe Gravitational Unit as mapped in previous works (Sartori et al., 1994; Torelli et al., 1997; Gutscher et al., 2002; Gràcia et al., 2003a; Terrinha et al., 2003; Iribarren et al., 2007). AF — Aljezur Fault; AWDF — Accretionary Wedge Deformation Front; GF — Gorringe Fault; HGU — Horseshoe Gravitational Unit; HsF — Horseshoe Fault; MPF — Marquês de Pombal Fault; PF — Portimão Fault; PSF — Pereira de Sousa Fault; QF — Quarteira Fault; triangles show the locations of mud volcanoes.

and the Cenozoic through Present compression (Fig. 2, Dias, 2001; Carrilho et al., 2004).

Offshore, the N–S trending Marquês de Pombal and Pereira de Sousa faults lie on the north to south trending southernmost segment of the West Iberian Margin. These faults were described as active in the Quaternary by Zitellini et al. (1999), Zitellini et al. (2001), Gràcia et al. (2003a,b) and Terrinha et al. (2003). The uneven surface of the Marquês de Pombal fault scarp is due to widespread slumping and landslides with mass transport distances that exceed 20 km. The Pereira de Sousa fault scarp is also heavily incised and the D. Henrique basin shows a series of radial ridges that consist of turbidite levees transported downslope from the highs that surround it (Terrinha et al., 2003; Gràcia et al., 2003a,b).

WSW–ENE to W–E trending Mesozoic rifting faults were inverted during the latest Cretaceous through early Miocene times (Terrinha, 1998; Lopes et al., 2006).

Duarte et al. (2005) showed the existence of presently active WNW–ESE trending faults in the Gulf of Cadiz and Medialdea (2007) proposed that these faults acted as transfer faults between the Gorringe Bank and the Marquês de Pombal fault across the Horseshoe fault. Onshore southwest Portugal, WNW–ESE trending Lower Jurassic extensional faults were described by Ribeiro and Terrinha (2007). Zitellini et al. (2009) proposed the existence of a Nubia–Eurasia plate boundary based on a set of 600 km long WNW–ESE trending set of strike-slip faults that cut across the Horseshoe Abyssal Plain and Gulf of Cadiz connecting the Gloria Fault and the Tell tectonic zone onshore north-west Morocco.

Earthquake frequency and epicentre location (Fig. 2) show that SW Iberia is an area of moderate seismicity which accommodates the brittle deformation associated with the Nubia–Iberia collision west of Gibraltar, by means of thrusting and strike-slip events of shallow and intermediate depth. However, the existence of historical and instrumental high magnitude earthquakes such as the 1/11/1755 Lisbon earthquake ($M = 8.5$ to 8.9) and the 28/2/1969 ($Ms = 7.9$) event require clarification of the present tectonic setting of the SW Iberia–NW Africa region, and identification of the structures that generate large magnitude earthquakes and tsunami in this area. The Gorringe Bank Fault is a north westwards directed thrust that sits at the northern base of this morphologic feature. This thrust uplifted the seafloor from approximately −5000 m to −24 m, it reached its paroxysmal activity in Miocene times and has accommodated negligible shortening since then (Sartori et al., 1994; Tortella et al., 1997). Although the Gorringe Bank is by far the most conspicuous morphotectonic structure in the study area (Fig. 1), the distribution of seismicity (Fig. 2), numerical models for tsunami wave propagation (Baptista et al., 1998) and the interpretation of MCS lines (Sartori et al., 1994), led various researchers to abandon it as the source of the 1755 Lisbon earthquake.

Recent models proposed the existence of two faults, the Marquês de Pombal Fault and the Horseshoe fault (Terrinha et al., 2003; Gràcia et al., 2003a,b) (Fig. 2) or the Marquês de Pombal Fault and the Guadalquivir Bank fault (Baptista et al., 2003), acting together simultaneously to generate the 1755 event by adding up their rupture areas (Terrinha et al., 2003; Baptista et al., 2003; Gràcia et al., 2003a,b). Alternatively, Gutscher et al. (2002) proposed that the 1755 Lisbon

earthquake was generated in the Gibraltar subduction zone imaged on seismic tomography, arguing that this was also the source of the deep 1954 Granada earthquake.

1.3. Data and methods

38,000 km^2 of multibeam swath bathymetry data were acquired in the MATESPRO Survey with a hull-mounted Simrad EM 120 echosounder aboard the research vessel *NRP D. Carlos I* in 3 legs from 14 June to 7 July 2004 (Figs. 3 and 4). The survey was carried out in order to comply with a level 3 hydrographic survey as established by the International Hydrographic Organization. The EM 120 operates at a main frequency of 12 kHz (from 11.25 to 12.6 kHz) with 191 beams covering a 150° fan with a width of 1°. In order to increase data quality the angular value was reduced to 120° and the ping width was of 2°. One sound velocity profile (SVP) was performed every 24 h and at locations chosen to spatially cover the entire area in order to compensate the effect of the Mediterranean Outflow Water on the sound velocity in the water column regionally. SVP data were acquired down to 2000 m of water depth. From −2000 to −4000 m sound velocity was taken from climatologic profiles provided by the Instituto Hidrográfico of Portugal in this area. Quality control lines were also performed totalizing about 10% of the area; the depth errors found were below 0.3% of the water depth. Bathymetric data filtering and processing was carried using CARIS HIPS software and a 100 m grid was generated.

The positioning of the vessel was done with both GPS and DGPS mounted on different parts of the vessel in order to better determinate the position and make the yaw corrections; the errors associated with the navigation positioning were around 5 m.

The seismic data presented here are of two types: multi-channel seismic (MCS) profiles from three previous surveys, ARRIFANO (acronym of Arco Rifano; Sartori et al., 1994), IAM (acronym of Iberian Atlantic Margin; Banda et al., 1995) and VOLTAIRE (acronym of Valuation Of Large Tsunamis And Iberian Risk for Earthquakes) and one single-channel profile acquired during the TTR-14 survey (Training Through Research; Kenyon et al., 2006).

The IAM and ARRIFANO deep MCS have a similar central peak frequency of approximately 30 Hz and the VOLTAIRE MCS has a central peak frequency of approximately 50 Hz. As a result, the vertical resolution in the sedimentary section is of around 20 m for the IAM and ARRIFANO profiles and of about 15 m for the VOLTAIRE data, assuming a mean seismic velocity of 2500 ms^{-1} in the sedimentary section (data from bore-holes in Fig. 3 and González et al., 1998). The central peak frequency of the single-channel TTR profile is around 100 Hz with a corresponding vertical resolution of about 6 m. Information on acquisition and processing of these profiles is summarized in Table 1.

The presented seismostratigraphic interpretation was based on the stratigraphy of five industry wells offshore the Algarve Basin (stars in Fig. 1, Lopes et al., 2006), as well as published data from the offshore Guadalquivir Basin (Maldonado et al., 1999).

2. Morphology of the NW part of the Gulf of Cadiz

The MATESPRO multibeam dataset (Fig. 4) shows a variety of seafloor major morphological features within which smaller scale features indicative of genetic processes discussed elsewhere in this paper are found.

2.1. The submarine sediment drainage system

The drainage system of the study area is subdivided in two groups: a northern one that drains the Portuguese continental margin from north to south, and a southern one that drains the western continental shelf of Spain.

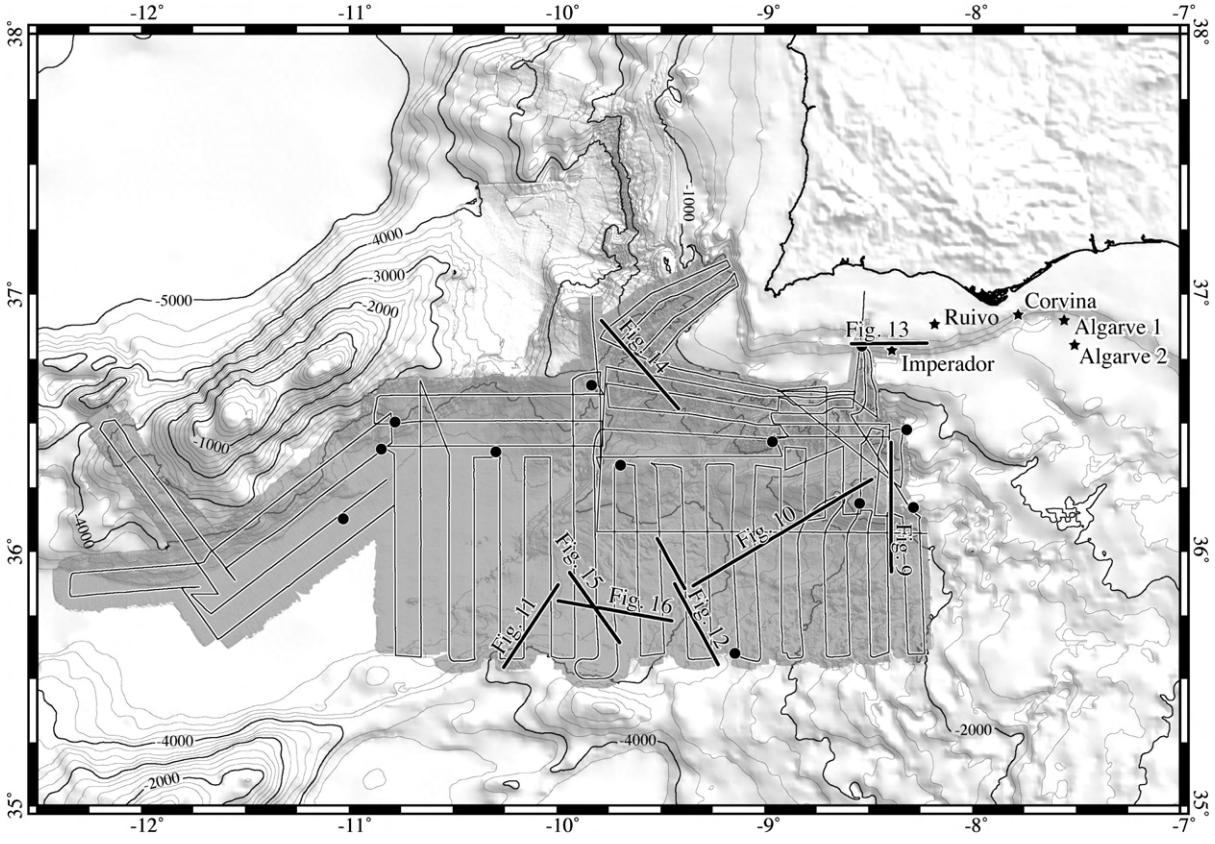

Fig. 3. Map showing the acquisition track lines of the MATESPRO multibeam bathymetry and the position of the seismic reflection lines shown in this work. Circles indicate locations of the sound velocity profiles performed. Location of oil prospection wells (stars) is also shown. Altimetry data derived from SRTM (USGS, 2004).

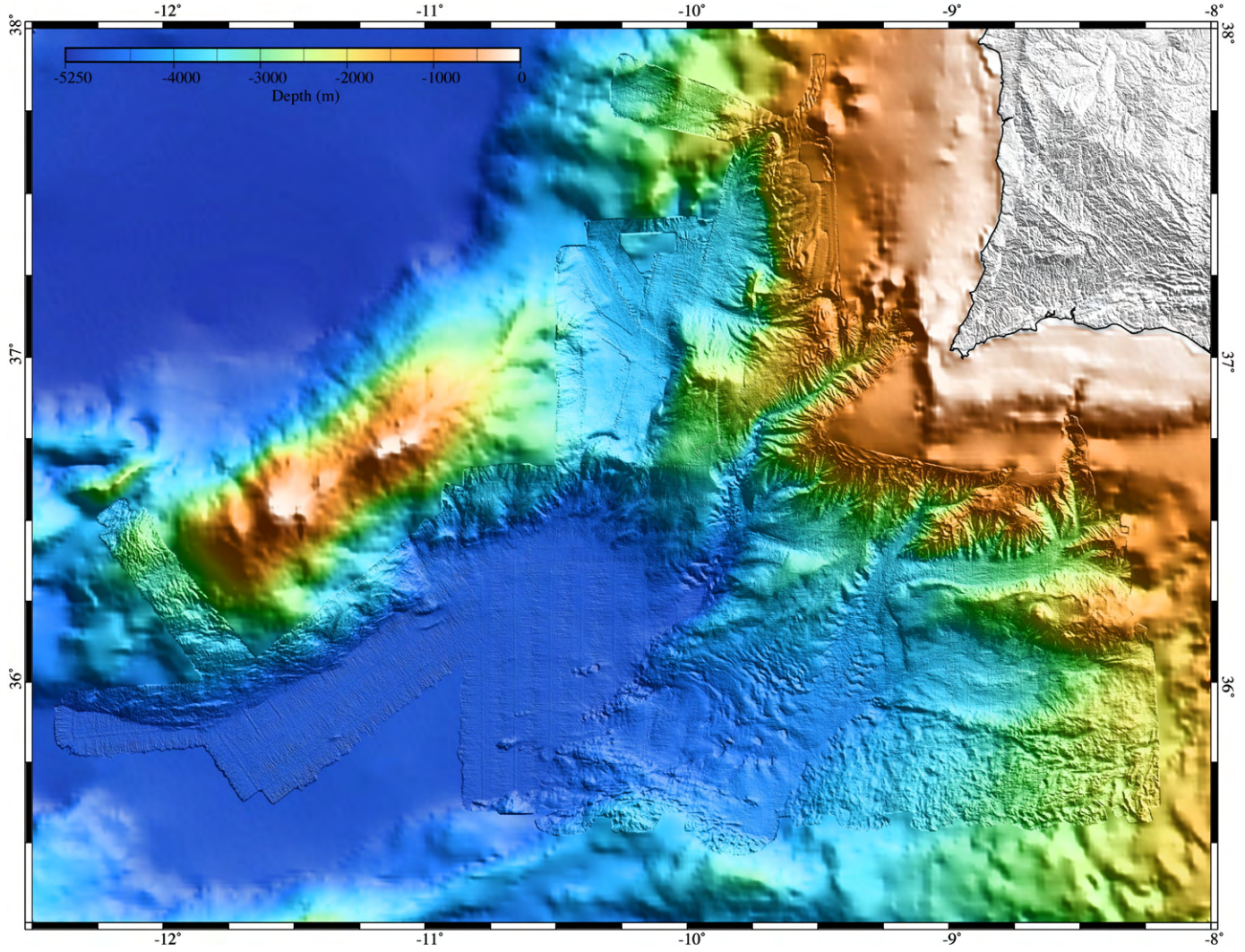

Fig. 4. Multibeam bathymetry map of the MATESPRO study area, offshore SW Iberia. Topography of onshore area also shown as shaded relief with a maximum of 902 m. Mercator projection, datum WGS84. PARSIFAL bathymetry of the Marquês de Pombal area and Pereira de Sousa escarpment published by Gràcia et al. (2003a,b). Bathymetry for other offshore areas and onshore altimetry is taken from Gebco (data from IOC et al., 2003).

2.1.1. The north to south sediment drainage system

The north to south oriented drainage system consists of a poorly organized network of gullies and canyons. The deeply incised 120 km long São Vicente canyon (Fig. 1) has its head scarp at 70 m below sea level (mbsl), cuts across the shelf and slope and ends in the Horseshoe Abyssal Plain. The maximum incision into the sedimentary substratum

Table 1
Aquisition parameters, geometry and processing for the seismic reflection profiles shown in this work.

	ARRIFANO	IAM	VOLTAIRE	TTR-14
Year	1992	1993	2002	2004
Vessel	*R/V OGS Explora*	*Geco Sigma*	*R/V Urania*	*R/V Prof Logachev*
Reference	Sartori et al. (1994)	Banda et al. (1995)	Zitellini et al. (2002)	Kenyon et al. (2006)
Seismic source	32 airguns (80 l max.)	30 airguns (125 l max.)	2 GI guns	1 airgun (120 bar)
Shooting interval	50 m	74 m	50 m	10 s (aprox. 30 m)
Sample interval recorded	1 ms	4 ms	1 ms	1 ms
Number of channels	120	192	48	1
Resampling	4 ms	8 ms	2 ms	1 ms (no resampling)
Signal processing			Trace editing	
			Shot delay removal	
	Spiking deconvolution	NMO correction	Amplitude recovery	Static correction
	Spherical divergence correction	Kirchoff migration	Predictive deconvolution	Spiking deconvolution
	NMO correction	(constant velocity 1700 m/s)	Velocity analysis every 200 CMPs	Spherical divergence correction
	Finite-difference wave-equation migration	AGC, 500 ms time gate	NMO correction	Butterworth bandpass filtering (20–60–180–240 Hz)
	Time variant bandpass frequency filter		Stack	
			Bandpass-frequency filtering	
			Time migration using stacking velocities	

on the continental slope is of 2 km. This canyon is made up of two segments oriented NE–SW and N–S that collect the sediment from the gullies that incise the shelf and slope (Figs. 4 and 5). Also note that the flanks of the NE–SW trending segment and the eastern flank of the N–S trending segment display higher degree of incision, while the western flank of the N–S trending segment and both flanks of the deepest part of the canyon are smoother. The close up in Fig. 6A shows a submarine landslide near the termination of the canyon. The lack of the mass transport deposit within the canyon is an indication of the activity of the canyon in terms of sediment erosion and transport.

The 70 km long Portimão canyon also has its head scarp in the shelf at roughly 70 mbsl. The canyon cuts across the shelf and slope sedimentary sequence with a maximum incision of 1 km. The canyon terminates abruptly at the meeting point with the Faro canyon and D. Carlos valley that drain east to west. These features have a different physiography, with a flat and broad bottom capable of accommodating larger sediment influx. The Portimão canyon is fairly rectilinear and sits along the Portimão Fault (Terrinha et al., 1999).

The Aljezur and Lagos canyons only incise the continental slope. The NNE–SSW trending Aljezur canyon is short, rectilinear and drains into the Sagres valley. The western flank of the Aljezur canyon displays a series of anastomosed submarine slide scars at approximately 1300 mbsl, at a main morphologic break of the continental slope near the base of the Lagos contourite drift (Fig. 6B).

The Sagres valley collects the east to west draining D. Carlos and Cadiz valleys and the Aljezur and Lagos canyons. The Aljezur canyon and Sagres valley lie on the southern prolongation of an important slope break that can be observed in the low resolution bathymetry (see Figs. 2, 4 and 5) and also on the southern continuation of the Aljezur Fault that cuts across the Meso–Cenozoic Algarve Basin and Paleozoic basement (Fig. 2).

The Lagos canyon has its head scarp roughly at 800 mbsl, where it incises the Pliocene through Holocene Lagos contourite drift.

2.1.2. East to west oriented sediment drainage system

The seafloor of the inner part of the Gulf of Cadiz dips to the west towards the Atlantic Ocean. The seafloor is shaped by a variety of morphological features of various scales, many of which have been described by Mulder et al. (2003), Somoza et al. (2003), Hernandez-Molina et al. (2006), and Gutscher et al. (2008).

The most important E–W trending valleys of the study area lie in the prolongation of the sinuous and broader E–W channels that initiate on the Gibraltar Arc owing to erosion and sedimentation by the MOW and to downslope gravity processes (Hernandez-Molina et al., 2003). In the study area these valleys are broad, with flat gently dipping bottom. The Faro canyon and D. Carlos valley collect the sediment transport from the South Portuguese margins, a large number of gullies, valleys and the Portimão canyon. The D. Carlos valley changes from narrow channel to broad valley downslope from the merge of the Portimão Canyon.

The Cadiz valley lies between the Portimão Bank and the wrinkled surface of the Gulf of Cadiz accretionary wedge. The Sagres valley that lies in the prolongation of the Aljezur canyon establishes the connection between the drainage system located to the east of the Horseshoe Fault scarp and the Horseshoe Abyssal Plain. The Sagres valley displays a corrugate bottom north of the confluence with the Cadiz valley; from this point to the south it has a smooth surface and less dip. The flanks of the Sagres valley display various evidences of gravity slumping (Fig. 6B).

The Horseshoe valley is a roughly rectangular area, 80 km × 50 km, dipping to the west (mean dip of ~0.5°), connecting the Gulf of Cadiz seafloor and the Horseshoe Abyssal Plain across the Horseshoe Fault scarp (Fig. 1). The valley is limited by the Sagres plateau in the north, the Coral Patch Ridge in the south and the Gulf of Cadiz accretionary wedge in the east. It is cross cut by WNW–ESE trending morphological lineaments

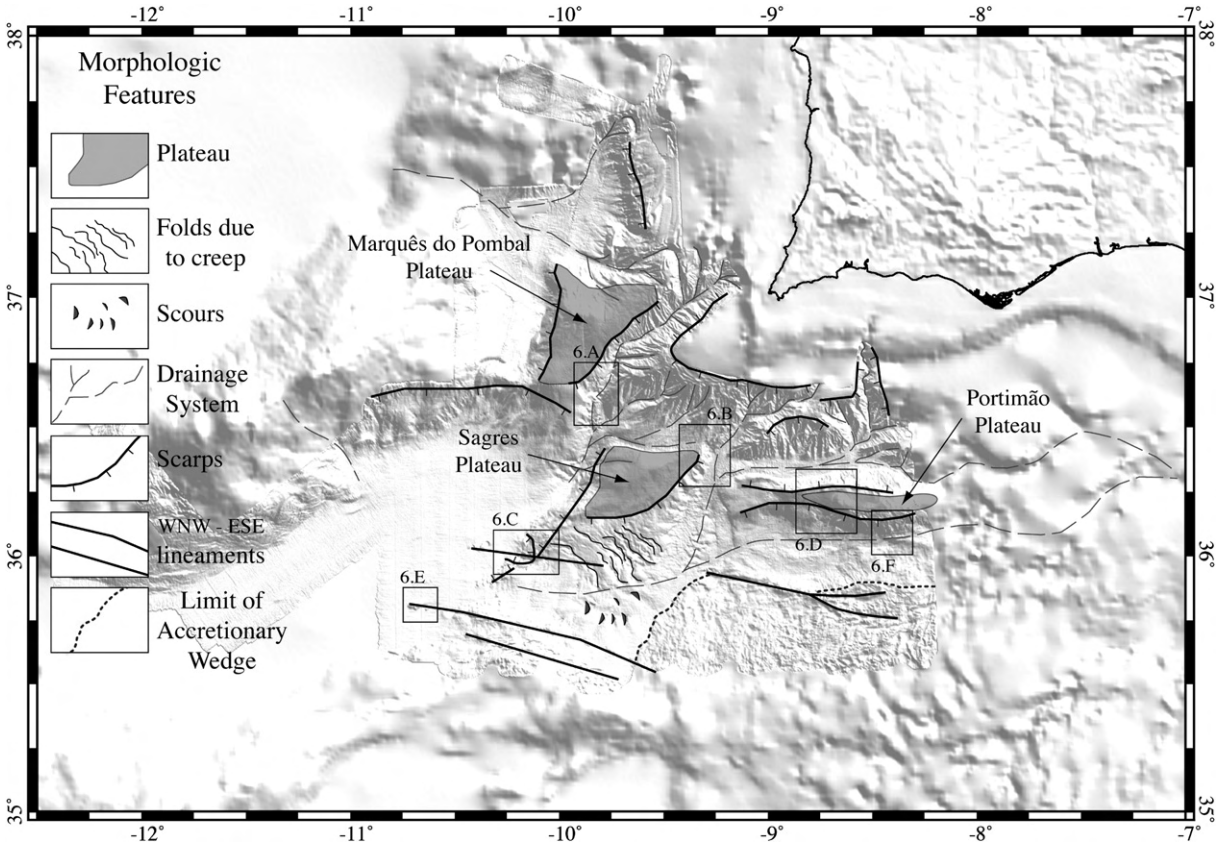

Fig. 5. Interpretative sketch of the morphology of the study area. 6.A to 6.F, locations of the features imaged in 3D in Fig. 6.

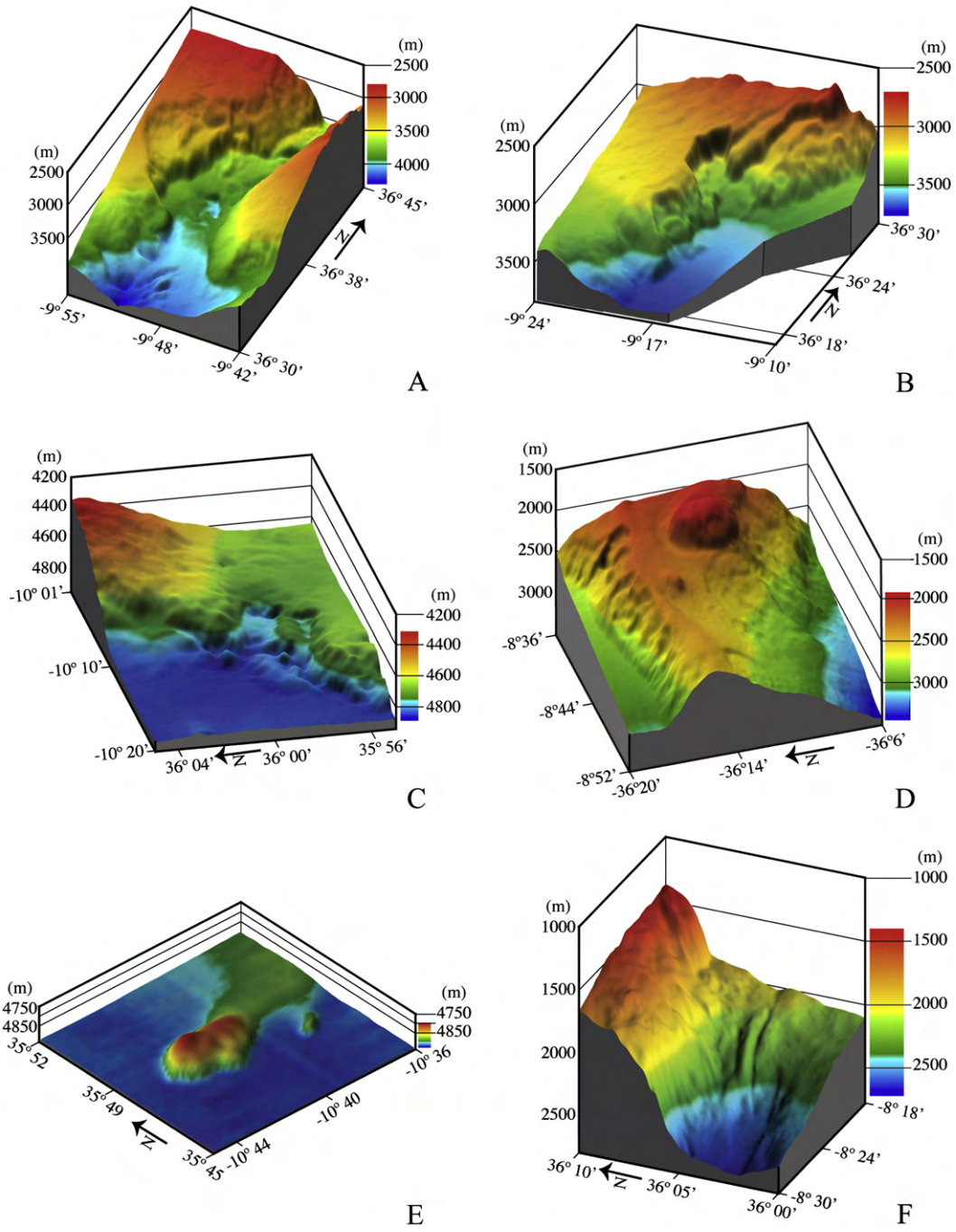

Fig. 6. 3D block diagrams of selected morphologic features of the study area. Images made from MATESPRO multibeam data presented in this work. A) Slide scar on the western flank of the S. Vicente canyon. B) Slide scar on the western flank of the Sagres valley. C) Slide scar on the Horseshoe fault scarp at the intersection with the WNW–ESE trending lineaments. D) D. Carlos salt diapir protruding through the top of the Portimão Bank (cf. with Fig. 10 for internal structure). Note the incisions on both flanks of the plateau, mainly on the northern side. E) E–W oriented hill in the Horseshoe Abyssal Plain sitting on top of one of the WNW–ESE trending lineaments. F) E–W trending channel at the foot of the Portimão Bank, whose structure in depth is imaged in MCS profile in Fig. 9. See text for detailed description.

described elsewhere in this paper. This wide valley collects the mouths of well developed canyons and valleys that drain the sediments from the north and eastern shelves. The drainage to the Horseshoe Abyssal Plain is poorly developed (Fig. 5) and the Horseshoe fault scarp is being eroded in various segments showing evidences of landsliding (Fig. 6C). These different styles and degrees of maturation of the sediment drainage pattern suggest that this area acts simultaneously as a by-pass and receptacle region for the sediments that are carried from the continental shelves to the Horseshoe Abyssal Plain.

Despite the general low slope of this area, there are NE–SW trending scarps with a maximum height of approximately 150 m (Fig. 7). The flat areas have maximum dips of 3° and slope breaks in which formed convex upwards crescent shaped escarpments. The crescent shaped three-dimensional features measure up to 5 km across, are shown in detail in Fig. 7 to occur between 3900 and 4700 mbsl, have an internal escarpment up to ~100 m high with an internal slope varying from 6° to 27°.

2.2. Plateaus and escarpments

The plateaus in the study area are the Marquês de Pombal, Sagres and Portimão plateaus (Figs. 1, 4 and 5). The Marquês de Pombal

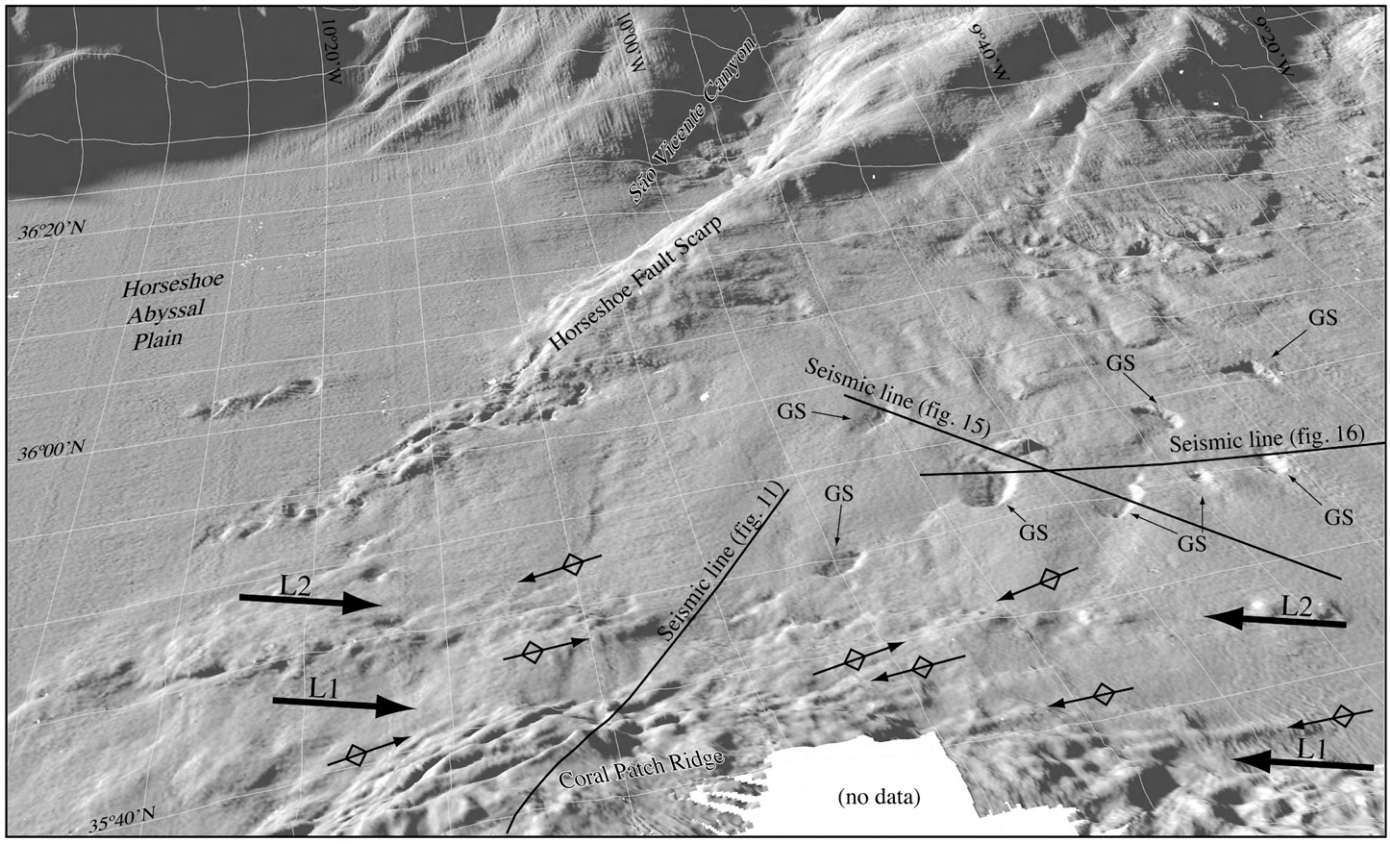

Fig. 7. Shaded relief image (perspective view) of the Giant Scours (GS), L1 and L2 WNW–ESE trending lineaments (interpreted as strike-slip faults, max. total length 250 km, see Fig. 11) and associated en echelon folds on sea floor recent sediments indicating dextral strike-slip movement component on the faults. Approximate depth 4000 m, confer with Figs. 1 and 4. Position of seismic lines in Figs. 11, 15 and 16 is also shown. Detail of the en echelon folds on L1 in the Horseshoe Abyssal Plain is shown in Fig. 6E.

plateau is a roughly rectangular surface bound by the NNE–SSW trending Marquês de Pombal reverse fault scarp in the west and by the São Vicente canyon in the east, as described by Gràcia et al. (2003a,b).

The Sagres plateau has an approximately rectangular shape divided by a diagonal NE–SW trending crest. To the west, the Sagres plateau is bound by the Horseshoe reverse fault scarp and the São Vicente canyon and by the Aljezur canyon and the Sagres Valley in the east. In the north this plateau is separated from the mid and upper continental slope and shelf by a rectilinear E–W trending valley that lies in the prolongation of the D. Carlos valley.

The Horseshoe fault scarp is only well developed on its northern segment. The southern part is being eroded (Fig. 6C) by the sediment drainage system described previously.

The southern part of the Sagres plateau dips gently towards the Horseshoe valley. This surface dips approximately 1.5°, is very uneven, and has a wavy appearance comprising undulations that vary from hundreds of meters to more than 10 km in length, and 0.5 km to 5 km across (Figs. 4 and 5).

The Portimão plateau is an E–W elongated surface limited by the two prominent escarpments which constitute flanks of the D. Carlos and Cadiz valleys. The northern escarpment is sinuous, while the southern one, is fairly rectilinear, trending WNW–ESE, draped by recent sediments carried by the local drainage. The top of this plateau shows circular positive reliefs, the larger one of which has been labeled here as the D. Carlos salt diapir (Figs. 1, 4 and 6D), whose origin is discussed elsewhere in this paper.

2.3. The Horseshoe Abyssal Plain

The extremely flat HAP has general slopes of less than 0.1° sharply contrasting with the slopes of the foot of its boundaries, between 5° and 10° in general.

The foot of the slope of the Gorringe Bank presents a remarkable offset of about 14 km at roughly 11°W (Fig. 4). This offset lies at the end of a valley that originates at the Gorringe saddle (see Fig. 1 for location). It is also clear that the southern flanks of the Gettysburg and Ormonde seamounts display fairly different topographic roughness. The Ormonde southern flank smooth topography resembles the morphological types of the continental slope or of the Sagres plateau, while the edges of the Gettysburg and Coral Patch Ridge display a similar wrinkled surface. It is possible that this offset and valley coincide with the ocean–continent boundary proposed by Rovere et al. (2004) at the Gorringe Bank.

The interior of the HAP is only locally perturbed by four elongated groups of hills that rise between 40 m and 200 m above seafloor (Fig. 4 and 6E). The largest of these groups is 16 km in length and the largest individual hill is 6 km long. The hills in each group are aligned along approximately E–W directions and each one of the hills has their crest parallel to NE–SW, approximately. These hills are aligned along the WNW–ESE oriented tectonic morphological lineaments described and discussed elsewhere in this paper.

2.4. Lineaments

Long WNW–ESE trending discrete lineaments of tectonic origin were for the first time revealed in the Gulf of Cadiz sea floor by the MATESPRO multibeam survey (Duarte et al., 2005 and Rosas et al., 2009). These lineaments consist of an aligned series of elongate WNW–ESE trending crests and troughs, more or less continuous, with a typical width of a few hundreds of meters (Figs. 4 and 7). Pervasive sets of E–W linear undulations, up to 8 km long, accompany these lineaments (Fig. 7). To the east of the Horseshoe escarpment these lineaments present uninterrupted segments as large as 100 km of length, approximately, while in the Horseshoe Abyssal Plain these

lineaments are discontinuous. Altogether, from the Gorringe Bank flank across the Horseshoe Abyssal Plain and lower continental slope of the Gulf of Cadiz, lineaments of 250 km can be identified, from approximately 4870 to 2000 mbsl (Fig. 4). It is worthwhile to note that various mud volcanoes sit on top of the lineaments (Figs. 2 and 4).

3. Structure of the NW part of the Gulf of Cadiz

A structural map of the study area based on the interpretation of the MATESPRO bathymetry and available MCS profiles is presented in Fig. 8. The main faults are here described based on MCS profiles that are quoted from published works or presented here. Fig. 8 also shows a compilation of focal mechanisms and main horizontal compression taken from Ribeiro et al. (1996).

3.1. WNW–ESE to E–W Faults

One of the most prominent features in the north-western part of the Gulf of Cadiz is the above described WNW–ESE to E–W trending set of valleys, escarpments and lineaments (Figs. 4 and 7). The seismic lines that are shown in Figs. 9–11 and hereafter described show that all these features are associated with faults, whose geometry and kinematic history are different.

The D. Carlos and Cadiz valleys that bound the Portimão plateau sit on top on two faults, as shown in Fig. 9. According to this the Portimão plateau can be interpreted as a pop-up structure. The D. Carlos valley lies at the south-western edge of the Guadalquivir acoustic basement high that, at the precise location of this seismic profile, bears a WNW–ESE strike as can be seen on the bathymetry (Fig. 4). The drag evident in the sediments of the uppermost sequence and the superficial gravity extensional faults indicate that the northernmost valley flank fault is undergoing extensional deformation at Present. The folds in the Mesozoic through Miocene–Lower Pliocene of the central and northern parts of the Portimão pop-up depict an asymmetry that indicates northwards tectonic transport on top of the acoustic basement fault.

Since it has been known for long that the Guadalquivir Bank is made up of Variscan basement metamorphosed flysch of Carboniferous age (e.g. Ribeiro et al., 1979; Gràcia et al., 2003a,b) the stratigraphy across the northern fault of the Faro valley implies that it played an extensional role during the Mesozoic followed by northwards directed thrusting during the Paleogene through Miocene and resumed extensional movement during Pliocene–Quaternary times.

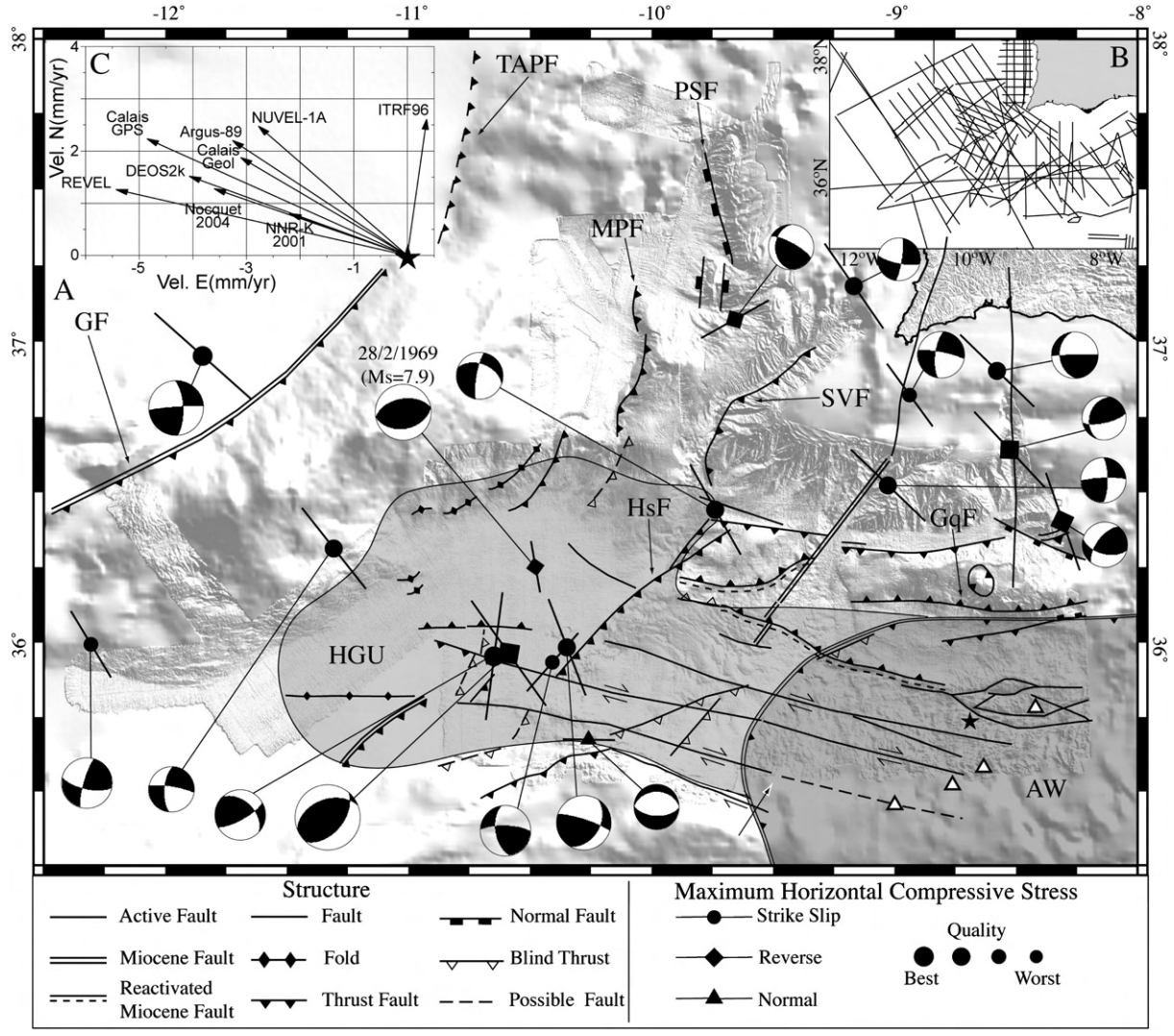

Fig. 8. A) Structural map of the study area with a compilation of stress indicators and focal mechanisms. Stress indicators computed from earthquake focal mechanisms and faults from interpretation of MCS profiles dataset shown in inset B). The size of the stress indicators is proportional to their quality. Note that the positions of mud volcanoes (white triangles) are in close spatial association with interpreted WNW–ESE dextral strike-slip faults. Fault names from published work as in Fig. 2. PbF — Portimão Bank fault; SVF — S. Vicente Fault; TAPF — Tagus Abyssal Plain Fault. B) Location of the MCS profiles used in this work. C) Plate kinematic data taken from various indicated sources indicated in the text. Black star shows position of computed movements of Nubia with respect to Iberia.

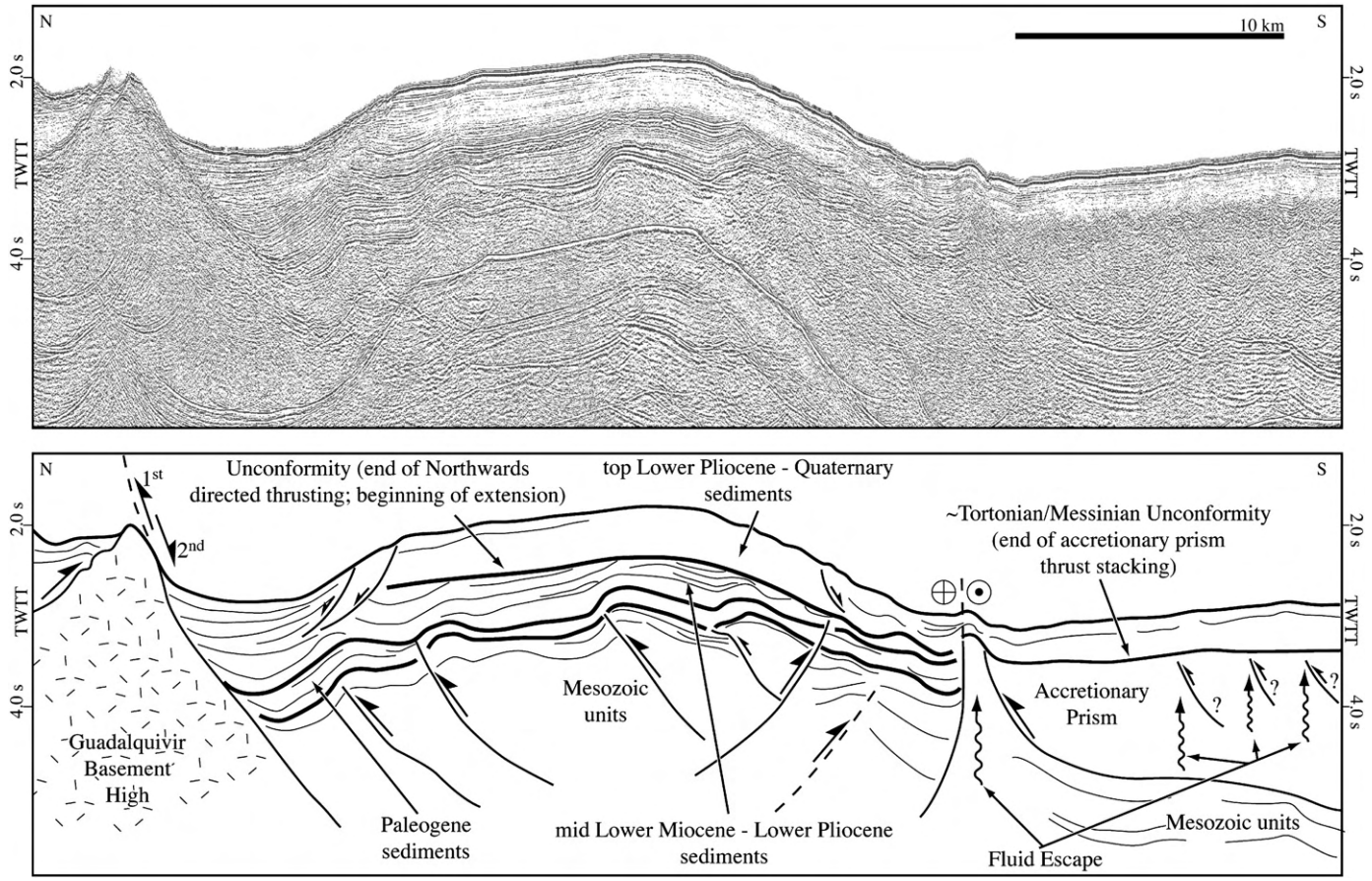

Fig. 9. Multi-channel seismic line VOLTAIRE 3 and line drawing interpretation. The Guadalquivir basement high of Carboniferous age is bound by a NW–SE trending Mesozoic extensional fault, reactivated as a reverse fault (1st movement) that resumed its extensional movement in late Miocene through Present times (see text for discussion, for location of line see Fig. 1). The topographic bulge on top of the strike-slip fault is imaged in 3D in Fig. 6F.

The southern boundary of the Portimão pop-up block shows both the topography and the Mesozoic through Quaternary sedimentary packages dipping to the south (Fig. 9). The following features are also evident in the seismic line across the southern part of Portimão plateau (Fig. 9), as follows: i) tectonic deformation affects the topmost sediments (Fig. 6F), ii) the pre-Pliocene folds asymmetry is southwards verging, iii) there is no correspondence on the seismic stratigraphy between the pre-Pliocene sediments of the Portimão pop-up and the southern counterpart and iv) the Mesozoic units show a wedge geometry. From these observations it is inferred that, firstly, this boundary of the Portimão plateau is an old fault with opposite dip with respect to the north boundary of the plateau, secondly, this was a northerly dipping extensional fault during the Mesozoic, thirdly, it was inverted with a southwards directed tectonic transport during the Paleogene through Miocene times and, fourthly it is going tectonic deformation at Present.

The southernmost segment of the seismic profile in Fig. 9 cuts across the Cadiz valley and up slope the gently dipping north western part of the Gulf of Cadiz accretionary wedge. The profile shows a sub-horizontal, mildly deformed sequence of sediments covering the chaotic seismic facies of the accretionary wedge or imbricate thrust wedge, as described by Gutscher et al. (2002) and Iribarren et al. (2007), respectively. The base of the chaotic seismic facies unit is made up by coherent high amplitude reflectors here interpreted as Jurassic through Cretaceous syn-rift sediments on top of which detached the thrust wedge. It is worthwhile to note that these sediments are disrupted by vertical discontinuities, with small vertical displacement, that can be followed up into the chaotic body and overlying topmost sequence.

The sub-vertical discontinuity that separates the Portimão plateau from the southern plain is neither compatible with thrusting nor with extensional tectonics (Fig. 9). Alternatively, it is interpreted as a transpressive E–W trending strike-slip fault at Present based on the fact that it displays evidence of shortening structures, folds and north wards and south wards directed thrusts on both sides of the fault. These observations imply that the main compression direction rotated from high angle to low angle with respect to the E–W strike of the faults, which is compatible with the counter-clockwise rotation of the movement of Africa with respect to Iberia in the Cenozoic, from approximately south to north in the Paleogene, to south east to north west in the Miocene to ESE to WNW in the Present (Dewey et al., 1989).

The circular dome protruding the top of the Portimão plateau depicted in the bathymetry is interpreted as D. Carlos salt diapir (Figs. 1, 4 and 10). The salt does not outcrop at the surface but is popping-up underneath the sedimentary cover. The two reverse faults that bound this structure were interpreted as smaller scale structures accommodating internal shortening across the Guadalquivir Bank by Zitellini et al. (2004). This is a clear example where the map view image clarifies specific not fully understood superficial structures in reflection seismics.

The deep structure of the WNW–ESE trending lineaments (Fig. 8) is imaged in the seismic profiles shown in Figs. 9, 10 and 11 in the work of Rosas et al. (2009). It can be seen in these seismic profiles that the rectilinear morphologic lineaments overlie vertical discontinuities that are rooted far below the accretionary wedge detachment, i.e. into the Jurassic sediments. These discontinuities cut the Mesozoic into blocks of 3–5 km of width, with small vertical offset and stratigraphic mismatch. The symmetry of the upward drag of the seismic horizons with respect to these discontinuities from the deepest stratigraphic levels across the chaotic facies, the disturbance observed in the cover

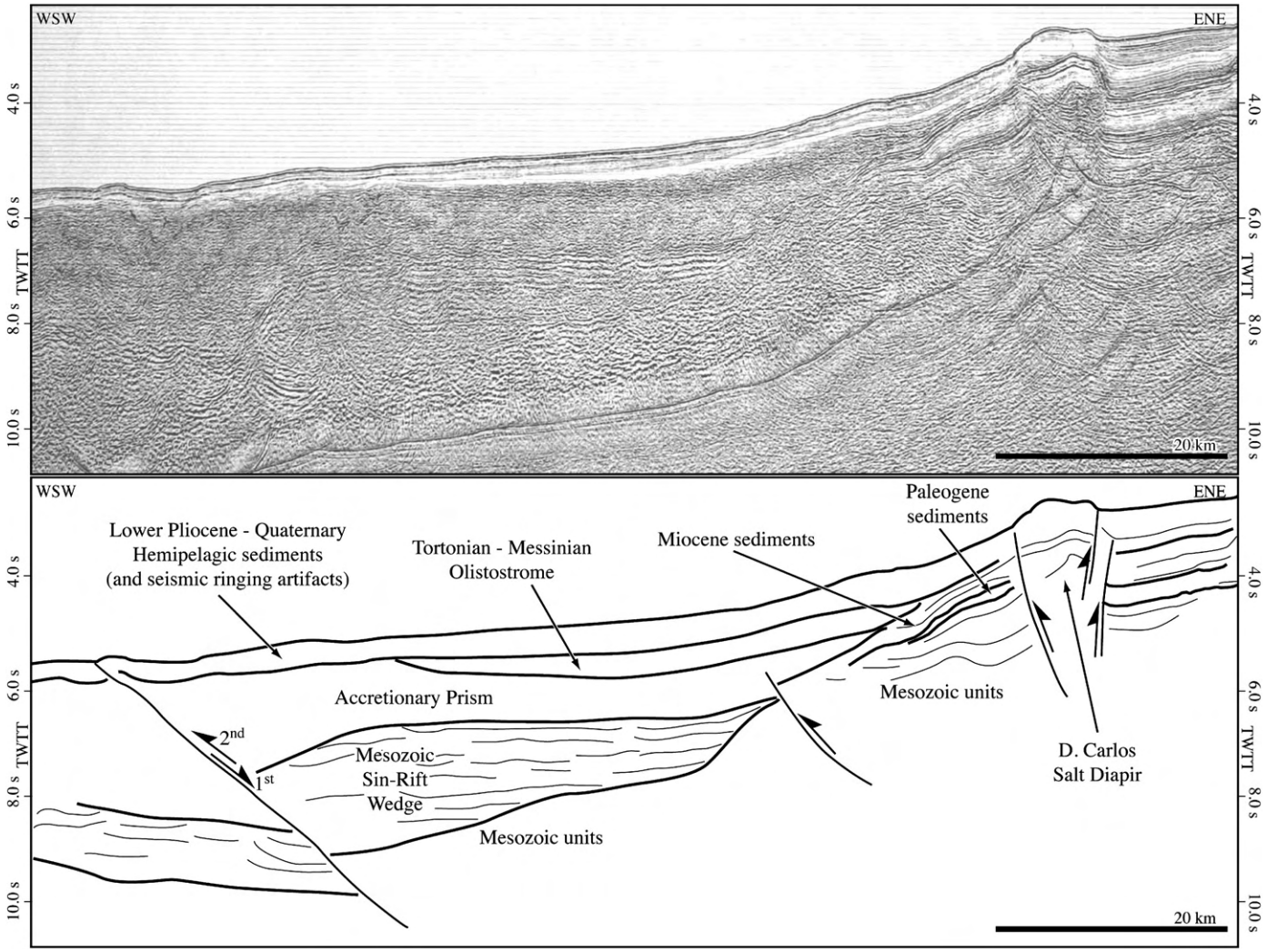

Fig. 10. Segment of multi-channel seismic line ARRIFANO 92-04 and line drawing interpretation. 1st and 2nd movements on main faults are of Jurassic–Cretaceous age and latest Miocene through Present, respectively. For location of seismic line see Fig. 3. The D. Carlos salt diapir 3D topography is shown in Fig. 6D.

sediments and the existence of mud volcanoes sitting on top of these lineaments (Figs. 8 and 12), strongly argues in favour of upward injection of fluids along these faults (cf. with Figs. 9 and 11). These characteristics strongly suggest that these discontinuities can correspond to tensile fractures with a strike-slip movement component.

The pervasive set of E–W trending undulations that accompany the E–W to WNW–ESE trending faults are en echelon folds (Figs. 7 and 11), i.e. kinematic indicators that show a dextral strike-slip lateral movement on these faults.

The growth wedge of Mesozoic sediments clearly associated to some of these WNW–ESE trending faults (Fig. 10) is another indication for the deep root of these faults.

3.2. N–S to NE–SW faults

The Aljezur canyon–Sagres valley and the Portimão canyon sit on top of the offshore prolongation of the Aljezur and Portimão faults, respectively (Figs. 2 and 8). Inspection of the seismic profiles confirms the Pliocene–Quaternary activity of these faults that show an important decrease in tectonic deformation after Miocene times (Figs. 12 and 13). The offshore mapping of these faults shows they have continuous segments larger than 100 km in length that, when added together with the onshore segments, they constitute discontinuous steep faults of approximately 200 km long, as happens with the left-lateral strike-slip late Variscan faults in the central and northern parts of the Iberian peninsula (Arthaud and Matte, 1977; Ribeiro, 2002), which are also active in the Quaternary (Cabral, 1989).

The Tagus Abyssal Plain Fault is proposed on the basis of the N–S trending sharp morphological scarp that lies to the north of the Gorringe Bank thrust. However, recent unpublished work by Cunha (2008) confirms the existence of this reverse fault that cross cuts Pliocene–Quaternary sediments.

The São Vicente Fault strikes NE–SW (Fig. 14) outcrops along the southeast flank of the São Vicente canyon. It is a southeastwards dipping steep fault, possibly part of the Odemira–Ávila fault (also known as the Messejana dyke), an approximately 600 km long vertical left-lateral late Variscan fault intruded by a basic dyke of Early Jurassic age (Dunn et al., 1998). Pliocene–Quaternary vertical displacement along this fault onshore was described by Cabral (1995).

The NE–SW trending Horseshoe fault was described as an active fault in the Present by Gràcia et al. (2003a,b) and Zitellini et al. (2004), and has a cluster of seismicity associated to it (Figs. 1 and 2). Its fault scarp is very well depicted in the MATESPRO bathymetry, from the Coral Patch Ridge well into the South Portuguese continental slope bordering the Sagres plateau. It can be seen that the height of the scarp increases northwards and it is intercepted by WNW–ESE trending faults. At these interceptions the Horseshoe fault scarp is either deflected or offset across the WNW–ESE dextral strike-slip faults and landslides formed (Figs. 4, 5, 6C and 8).

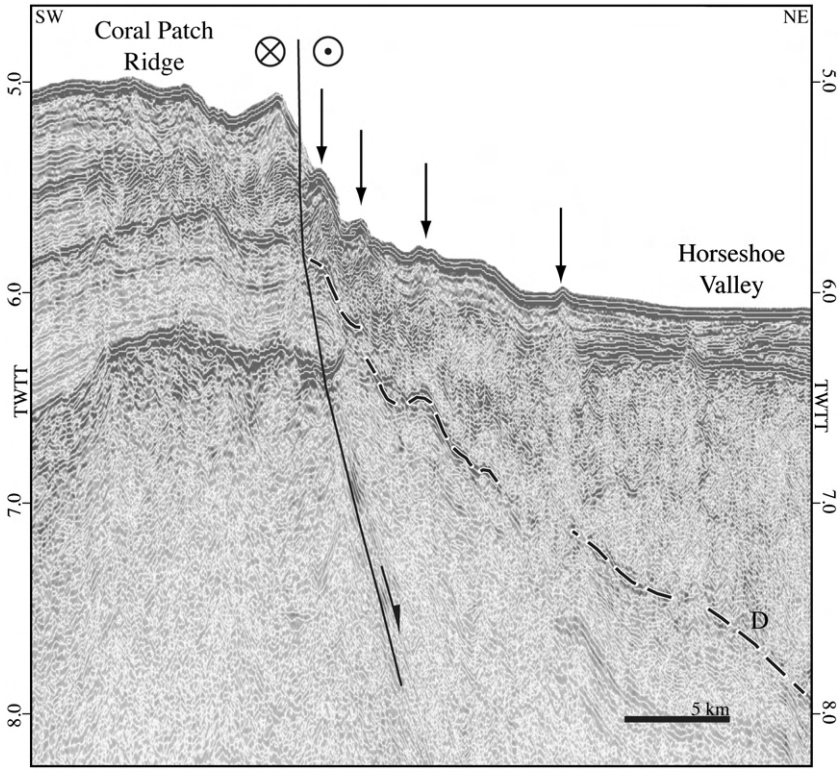

Fig. 11. Segment of multi-channel seismic profile IAM-3 at the contact between the Coral Patch Ridge (CPR) and the Horseshoe valley. Arrows point to folds in recent sediments on the seafloor as imaged on the MATESPRO bathymetry (see Figs. 3 and 7). Note that these faults cut across seismic discontinuity D that outlines the decollement of the seismic chaotic facies.

The NE–SW escarpments at the back of the Horseshoe fault host some of the crescent shaped Giant Scours described elsewhere in this work. These scarps sit on top of blind thrusts, as shown in Fig. 15 that appear to be recent reactivation of individual faults from within the Gulf of Cadiz Accretionary Wedge or Gulf of Cadiz Imbricate Unit, after Gutscher et al. (2002) or Iribarren et al. (2007), respectively. Single-channel seismic line across two of the Giant Scours show that the internal parts of the crescents consist of depressions filled in with upslope prograding sedimentary units. These units develop towards the Giant Scour crescent shaped scarp, which sharply truncates sediments behind it (Fig. 16).

3.3. Chaotic seismic units

The MATESPRO bathymetry clearly shows the divide between the wrinkled topography that overlies the Gulf of Cadiz Accretionary Wedge, after Gutscher et al. (2002) and the surrounding smoother areas (Figs. 2 and 4). The MCS profiles shown in Figs. 12 and 15 show the existence of a complex of stacked thrusts underneath the wrinkled surface of the so-called accretionary wedge and also under the smoother topography of the Sagres and Cadiz valleys.

In all seismic profiles it is evident that the complex of stacked thrusts is overlain by a package of sediments that is not involved in

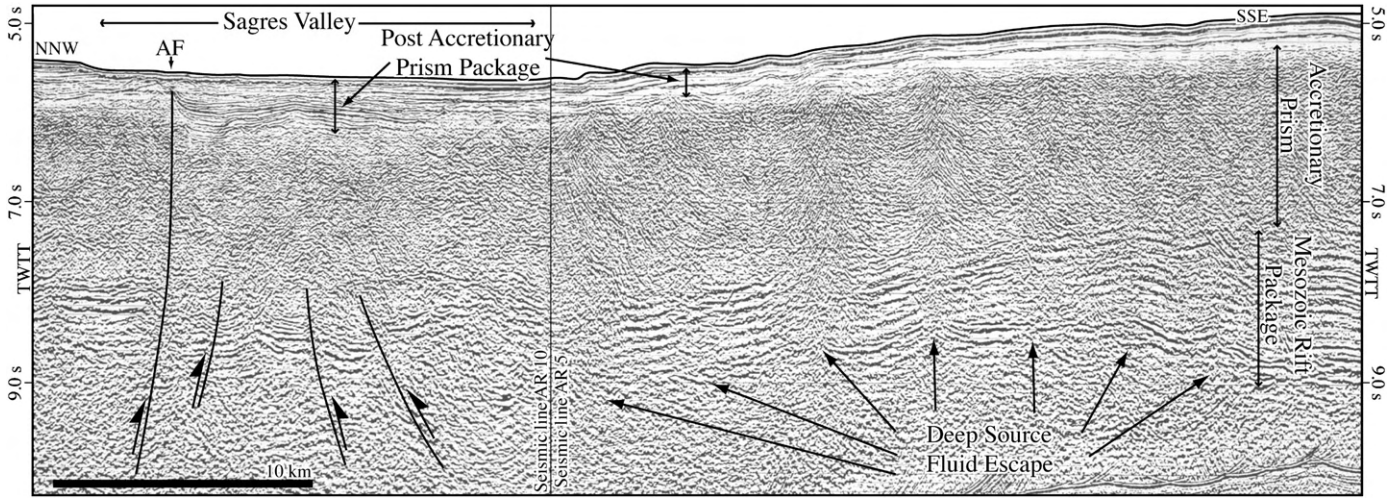

Fig. 12. Segment of multi-channel seismic line ARRIFANO 92-10 showing the deep origin of fluidized sediments breaching through the Mesozoic rift units and accretionary prism. Also note that the most recent unit is not involved in the thrust stacking tectonics of the accretionary wedge (see text for discussion, for location of line see Fig. 3). The steeply dipping north westernmost fault is the Aljezur fault bounding the deposits of the Sagres valley. Note that the chaotic body under the Sagres valley also has imbricated horizons but has no influence on the seafloor morphology (see text for discussion).

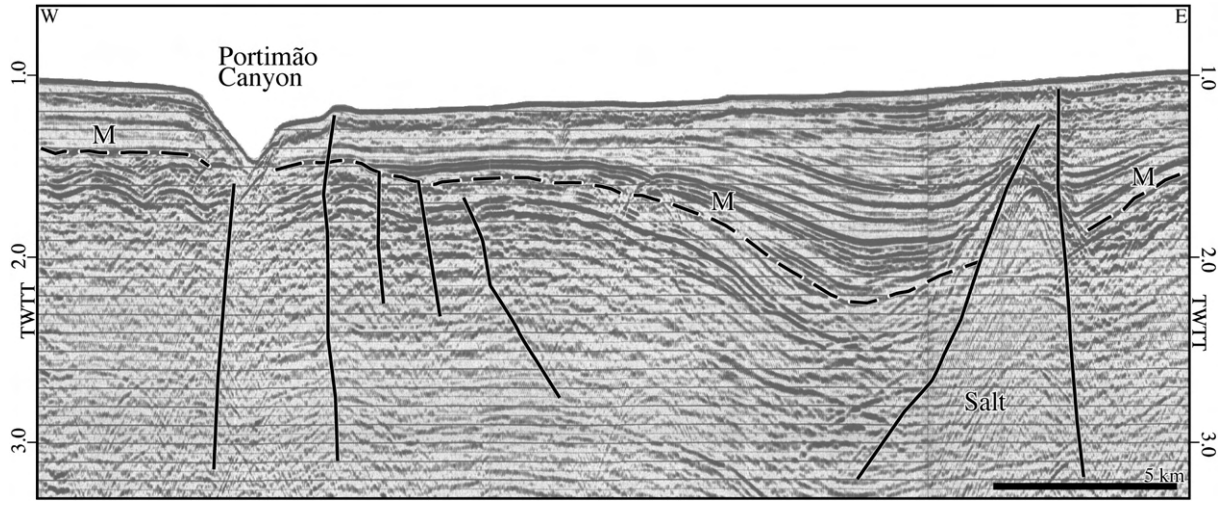

Fig. 13. Segment of multi-channel seismic line perpendicular to the Portimão canyon. Note that the Lower Miocene unconformity (M) truncates the folds that resulted from tectonic inversion on both sides of the Portimão canyon fault. However, mild deformation associated with this fault is visible on the eastern side of the fault and canyon. The salt-wall shown in the east of the profile also affects the recent sediments.

the thrust stacking. The thickness of this sedimentary cover is generally around 0.3–05 sec. TWT and the earliest age of these sediments is Early Pliocene after Roque (2007). However, this sedimentary cover is deformed by the E–W to WNW–ESE dextral strike-slip faults and by discrete reactivation of individual thrusts of the stacked thrusts units, as described elsewhere in this work, as well as, by widespread extrusion of mud volcanism, gravitational faulting described by various authors as mentioned before.

A unit of chaotic facies that has neither coherent internal layering nor imbricate fabrics, probably an olistostrome, is shown in Fig. 10. This unit is not involved in the thrust stacking of the accretionary wedge and is overlain by the well layered Pliocene–Quaternary sediments. This olistostrome lies between the Portimão Bank and the wrinkled surface of the Gulf of Cadiz Accretionary Wedge, in the Cadiz valley. It is worthwhile to note that the olistostrome pinches out on top of the Portimão Bank, suggesting that it could have been fed from the uplifted area of the Portimão Bank during the Tortonian phase of compression, i.e. the pop-up of the bank.

4. Discussion

4.1. Morphology and tectonics

4.1.1. The escarpments and seamounts

It was shown in this paper that the E–W trending Portimão Bank formed initially as a graben during Mesozoic times, was subsequently inverted during the Paleogene and Miocene compression and is now, probably since Early Pliocene times, undergoing dextral transpressive strike-slip deformation along its southern boundary, while the northern boundary experiences local extension due to a releasing bend formed by the basement fault. Seismicity and focal mechanisms (Fig. 2) attest for the compression at the southern edge of this seamount, preferentially concentrated to the east of the study area where the fault becomes NE–SW trending, i.e. at a higher angle to the main NW–SE oriented compression direction.

The Sagres plateau is bound by the NE–SW trending Horseshoe thrust of Miocene age in the west (Gràcia et al., 2003a,b, Zitellini et al., 2004) and the steeply dipping Aljezur fault in the east. The height of

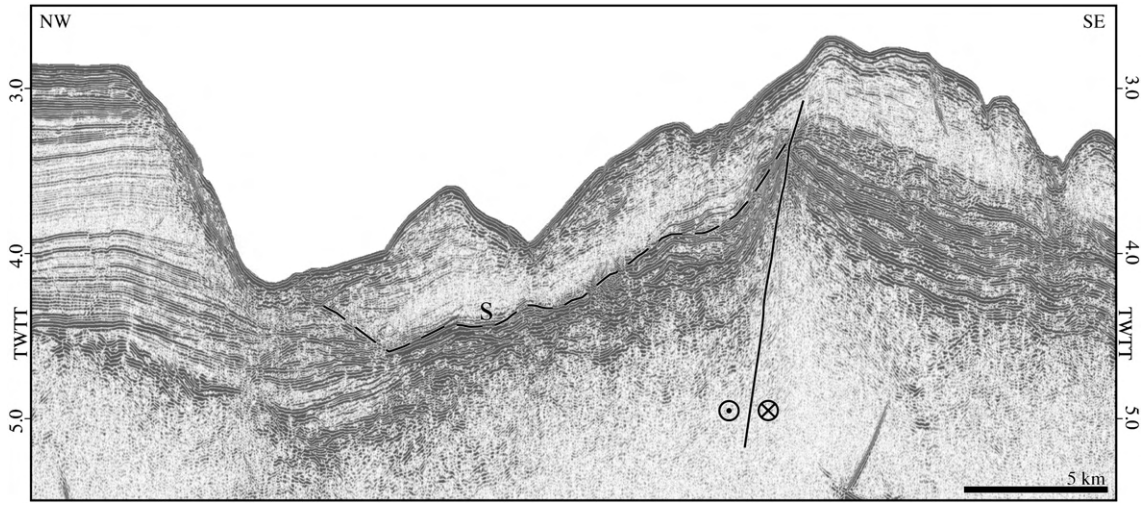

Fig. 14. Segment of multi-channel seismic line perpendicular to the S. Vicente canyon. Note the main fault controlling the position of the eastern flank of the canyon. This is a steep fault, possibly en echelon with the Messejana dyke fault (see text for description). Sediments on both sides of the fault are tilted and deformed including seismic reflector S, which is interpreted as a paleo-canyon bottom.

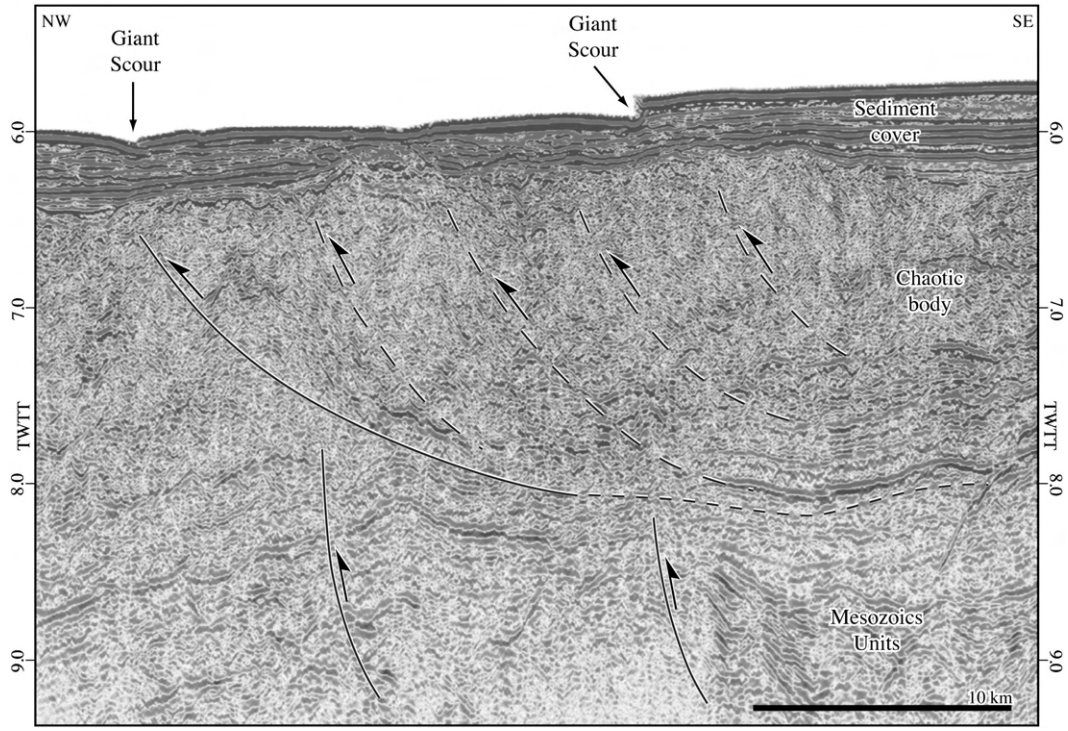

Fig. 15. Multi-channel seismic reflection profile across the Giant Scours. For location of the lines see Figs. 3 and 7. Seismic line IAM-4E shows the existence of stacked blind thrusts with present activity underneath the Giant Scours in the Sagres valley.

the plateau diminishes towards the south and its morphological expression disappears at the contact with one of the WNW–ESE strike-slip faults. The cluster of instrumental seismicity in Fig. 2 attests for its present day activity (Stich et al., 2007).

The Marquês de Pombal plateau also resulted from tectonic inversion of an N–S trending continent-wards directed extensional fault. The Pereira de Sousa fault is a N–S trending steep Mesozoic rift fault still in activity at Present (Terrinha et al., 2003; Gràcia et al., 2003a,b).

The north westwards directed Gorringe Bank thrust with a paroxysmal activity in the Tortonian (after Tortella et al., 1997; Sartori et al., 1994) is still an active structure as attested by the instrumental seismicity cluster (Fig. 2).

It can be concluded that the escarpments, seamounts and uplifted plateaus of the study area, all formed in association with compressive tectonic events and resulted from polyphase tectonics. The Pereira de Sousa fault escarpment is the only one that owes its morphology mostly to the Mesozoic rifting.

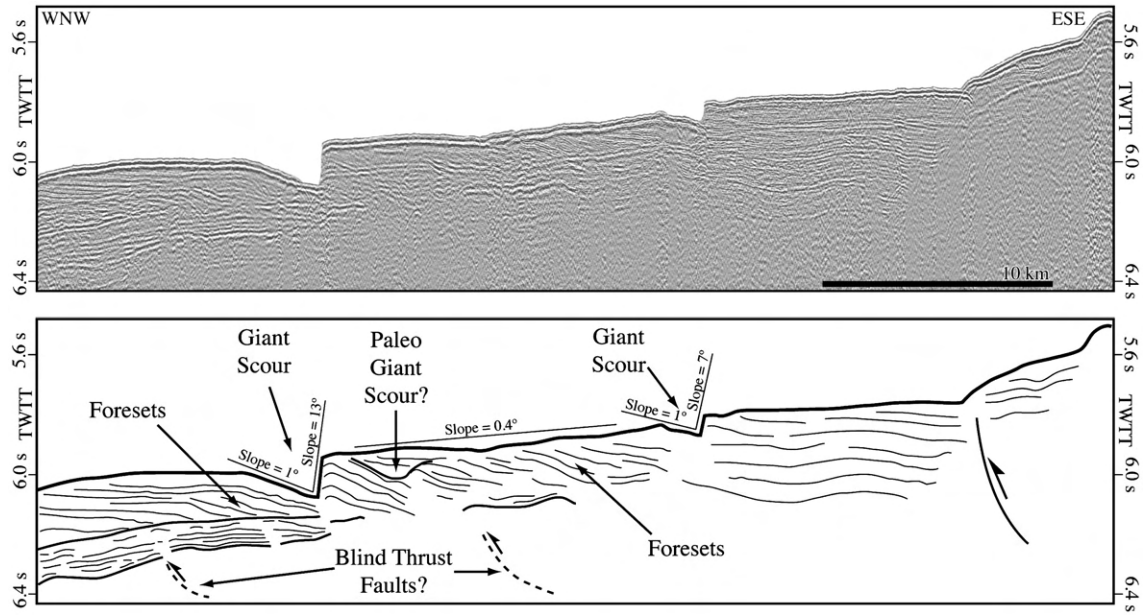

Fig. 16. Single-channel seismic line PSAT246 across two scours and line drawing interpretation. Note the erosive character of the escarpments and the sediments prograding towards the escarpment. For location see Figs. 3 and 7.

The tectonic shaping processes are still active in the Present, as shown by the on-going formation of very recent features that are indicative of uplift and tectonic instability, such as the popping-up of the D. Carlos salt diapir (Fig. 10), the mass wasting processes, such as submarine slides and various manifestations of soft sediment deformation and mass wasting processes in the Sagres plateau–Aljezur canyon, the São Vicente canyon and the Portimão plateau, Horseshoe Faul scarp, as well as, on the Marquês de Pombal, Gorringe and Pereira de Sousa escarpments as described by Gràcia et al. (2003a,b), Terrinha et al. (2003) and Vizcaino et al. (2006).

4.1.2. The Giant Scours

The Giant Scours are crescent shaped depressions with scarps that can reach more than 100 m high and slopes up to 27° located in a relative flat area of the Horseshoe Valley that collects the sediments from the Northern and North-eastern parts of the Gulf of Cadiz (Figs. 4, 5 and 7). The scours sit on the edge of folds draping Pliocene to Quaternary thrusting and the frontal depressions are filed up with upslope progradational bodies (Figs. 15 and 16). These bodies can be interpreted as been fed by material withdrawn from the retreating scarps (Fig. 17; Duarte et al., 2007). This scenario requires the existence of continuous scouring and sedimentation at unusual depths by means of bottom currents, possibly of turbidite origin as documented offshore the Shetland Islands and Monterrey East Channel (Kenyon et al., 2000; Kenyon et al., 2006; Fildani et al., 2006). The interaction of bottom and turbidity currents with seafloor morphological features formed by Recent tectonic activity can lead to flux separation and formation of vortexes that cause seafloor erosion and the formation of scours. These processes were proposed for the formation of similar structures in other places and different geological settings between 600 m and 3500 m water depth (Faugères et al., 1997; Bulat and Long, 2001; Verdicchio and Trincardi, 2006; Fildani et al., 2006). This process could account simultaneously for the formation of the scarp of the scour, the progradational bodies and the maintenance of the scarp, at least as long as the bottom current lasted and the retreating escarpment does not meet an obstacle.

An alternative model is that the Giant Scours could form due to the interaction of along slope bottom currents with the sea floor, such as the North Atlantic Deep Water. This interaction could lead to the formation of giant eddies that could locally erode and amplify pre-existing tectonic escarpments. However, the existence of along slope currents at these depths has not been documented in this area.

Evidences for alternative mechanisms for the formation of these features, such as slide–slump processes caused by slope instabilities or collapse processes associated with fluid escape along major tectonic structures (similar to those of pockmark formation), were not observed on the present dataset despite the evidences for mass wasting processes, and the existence of widespread mud volcanism and fluid migration activity in other areas of the Gulf of Cadiz.

4.1.3. The canyons

The São Vicente and Portimão canyons are by far the deepest incisions on the northern margin of the Gulf of Cadiz and they are underlain and controlled by important steep faults. The Aljezur canyon–Sagres valley system is also controlled by a steep fault. These offshore faults connect with others that were inherited from the late Variscan fracturing, subsequently reactivated during the Mesozoic rifting and Cenozoic tectonic inversion (see Fig. 2).

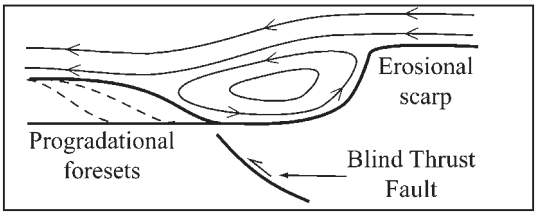

Fig. 17. Sketch of the effect of bottom currents on the retreat of the scarp and simultaneous progressive sedimentation of the progradation foresets. Scarp initially formed by uplift of hanging-wall on top of a blind thrust (see text for discussion).

The MCS profiles shown in this work attest for the Quaternary activity of these faults but also show that the deformation after Miocene times has severely diminished in the case of the Portimão and Aljezur faults.

Gràcia et al. (2003a,b) and Zitellini et al. (2004) showed the important activity of the northern segment of the Horseshoe fault that constitutes the eastern flank of the terminal part of the São Vicente canyon.

The São Vicente and Portimão canyons show important gravity slides on their western flanks. This can be interpreted as caused by the increase of the tilting associated with the west wards directed thrusting of the Marquês de Pombal and Horseshoe faults. Alternatively, in the Sagres valley the sliding can be caused by excavation at the meeting point of this valley with the Cadiz valley.

The minor present day tectonic deformation on the faults that control the localization of the canyons together with the important incision and land sliding close to the active Marquês de Pombal and Horseshoe thrusts can be interpreted as an indication of passive uplift of the continental slope carried on top of these thrusts.

4.1.4. The chaotic bodies

Three bodies of chaotic facies were distinguished in this work, all covered by unit hemipelagic sediments usually of 0.3–0.5 sec TWT. One is referred to as the Gulf of Cadiz Accretionary Wedge (GCAW) by Gutscher et al. (2002) or alternatively as the Gulf of Cadiz Imbricate Wedge by Iribarren et al. (2007). This body has a strong morphologic imprint on the seafloor morphology (Fig. 12).

A second one, that extends across the Horseshoe Abyssal Plain and Horseshoe Valley, has been considered as a gravitational unit, an olistostrome (e.g. Torelli et al., 1997; Iribarren et al., 2007). It is shown in this paper that this unit (Figs. 12 and 15) has imbricate seismic reflections that are interpreted as stacked thrusts, some of which have been recently reactivated forming blind thrusts morphologic scarps where the Giant Scours nucleated. These recent scarps are, however, the only morphologic manifestation on the seafloor surface of this body.

A third body with internal non-organized chaotic facies overlies the first described one, as shown in Fig. 10.

It is shown in this work that the two first described bodies consist of complexes of stacked thrusts and that the GCAW overthrusts the second one to the west (Fig. 10). Considering that these are tectono-stratigraphic units we speculate that only one accretionary wedge (or imbricate wedge) formed during the latest Cretaceous and Paleogene (perhaps through the Early Miocene). This event occurred before the Gibraltar arc formed (when the Internal Betic terranes were still a long way farther east, Fig. 18B). Then, from Early Miocene to earliest Pliocene (or Messinian?) times, when the Gibraltar orogenic arc formed, a part of this accretionary wedge was tectonically reworked forming the present day GCAW and its wrinkled topography (Fig. 18C). From the Pliocene to Present the thrust stacking within the GCAW severely diminished and the WNW–ESE dextral strike-slip faults formed (Fig. 18 D).

From a genetic point of view we consider the first two chaotic bodies as tectonic melanges made up of tectonised olistostromes and tectonosomes (see Camerlenghi and Pini, 2009 for discussion). The third chaotic body is a non tectonised olistostrome.

4.1.5. The WNW–ESE lineaments, strike-slip faults and recent folding

The WNW–ESE lineaments shown by the MATESPRO bathymetry in this paper (Fig. 7) display a series of en echelon folds materialized on the most recent seafloor soft sediments that indicate strain accumulation by means of dextral strike-slip (Figs. 3 and 6). Rosas et al. (2009) using quantitative strain analysis, analogue modelling and MCS data

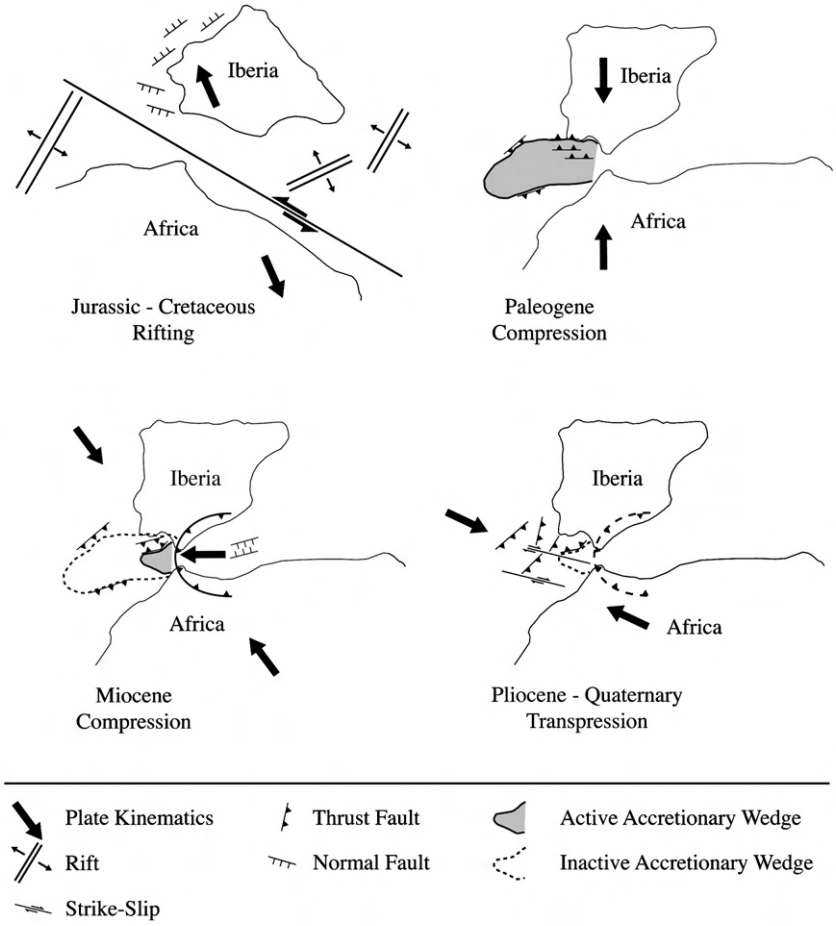

Fig. 18. Schematic tectonic evolution of the structure of the Gulf of Cadiz. In this simplified interpretation it is proposed the formation of an accretionary wedge (or thrust belt) that extended from Gibraltar across the Horseshoe Abyssal Plain during the latest Cretaceous–Paleogene compression. A second accretionary wedge formed (after Gutscher et al., 2002, or imbricate unit after Iribarren et al., 2007) during the Gibraltar orogenic arc westward overthrusting in Miocene times. In Pliocene–Quaternary times this accretionary wedge severely diminished its activity, the WNW–ESE dextral strike-slip faults formed and westward directed thrust increased along faults on the southern part of the West Portuguese Margin. See text for detailed discussion.

showed that these en echelon folds result from Quaternary reactivation of basement faults.

Inspection of MCS profiles in this paper show that these WNW–ESE faults are deeply rooted into the Jurassic–Cretaceous rift sequences, which is compatible to observations made onshore in the Algarve Basin at the Lower Jurassic of the S. Vicente cape (Ribeiro and Terrinha, 2007).

These faults also serve as conduits for the exhalation of fluidized sediments that form some of the Gulf of Cadiz mud volcanoes (Fig. 2), which is another evidence of the recent activity of the faults and also that they cut through the Gulf of Cadiz accretionary prism. Moreover, as shown on the MCS profile in Figs. 11 and 12, these strike-slip faults allow the escape of fluids from within deep in the Mesozoic sequences, probably at the Hettangian stratigraphic level that hosts the salt in south Portugal and northwest Morocco (Terrinha, 1998).

The strike-slip faults and folding are also active in the Horseshoe Abyssal Plain. However, the scarce morphotectonic features associated to these faults in the Horseshoe Abyssal Plain when compared to the continental slope to the east, suggests a westwards propagation of the recent deformation on the WNW–ESE faults, away from the Gibraltar Arc.

Because i) these faults have only recently been reactivated as strike-slip faults, ii) they strike at only a small angle to the present day trajectory of Africa with respect to Iberia, according to recently reported geodetic models (Fig. 8), iii) their minimum length exceeds 230 km as shown in the presented bathymetry and iv) they cut across the Horseshoe Abyssal Plain and the Gulf of Cadiz accretionary wedge; it is here suggested that they will play an important tectonic role in the new tectonic framework that is presently under development between Iberia and Nubia. As a matter of fact, some of the WNW–ESE faults described here are located within a 600 km × 40 km shear zone proposed by Zitellini et al. (2009) as a segment of the Eurasia–Nubia plate boundary that spans from the eastern tip of the Gloria Fault to the Rif–Tell plate boundary in north-western Morocco (Morel and Megrhraoui, 1996).

4.2. Strain partitioning, deformation migration and seismicity

The studied dataset shows that the E–W trending faults were inherited from the Jurassic–Lower Cretaceous rifting and subsequently inverted as reverse faults during the Cenozoic (Fig. 8); the same applies to the NE–SW to N–S trending faults as shown in previous works (Terrinha, 1998; Terrinha et al., 2002; Terrinha et al., 2003; Gràcia et al., 2003a; Rovere et al., 2004; Ribeiro and Terrinha, 2007). It was also shown that the Gulf of Cadiz accretionary wedge has diminished significantly its activity since latest Miocene times, possibly Early Pliocene, although disperse thrusts that still remain blind underneath the Messinian–Recent sediments are presently reactivated (Figs. 12 and 15).

Based on the presented dataset, we propose that the present day WNW–ESE convergent movement of Africa with respect to Iberia generates deformation in the study area, which is accommodated through partitioning on two approximately orthogonal fault sets, as follows. An N–S to NE–SW striking set of faults that accommodate shortening mainly by thrusting and an E–W to WNW–ESE striking, generally sub-vertical, set of faults that accommodate dextral strike-slip faulting.

The first set comprehends the main thrust faults of the area, Horseshoe Fault, Marquês de Pombal fault and Tagus Abyssal Plain

fault (see map of Fig. 2) that extend the Present east to west shortening for approximately 300 km from the South, near the contact with the Coral Patch Ridge (35.5°N), towards the north, along the West Portuguese Margin until a latitude of 38°N, as recently shown by Neves et al. (2009).

The second fault set is deeply rooted in Jurassic through Cretaceous rifting faults and were reactivated mainly in the Pliocene–Quaternary as dextral strike-slip faults, which is compatible with the present day movement of Nubia with respect to Iberia. These faults show considerably higher degree of deformation in the east than in the west, which argues in favour of propagation of deformation from east to west.

The thrusting on the N–S Marquês de Pombal fault is recent, as well as, on the Gorringe Bank fault (that had a quiescence period after the Tortonian), on the Tagus Abyssal Plain Fault (Cunha, 2008) and at the N–S trending faults at 38°N (Neves et al., 2009). Altogether, these observations lead us to argue that the deformation is migrating from the realm of Gibraltar to the west and along the Portuguese West Margin to the north.

Considering the sub-parallel strike of the N–S to NE–SW faults, their common origin in the Permian and reactivation during the Mesozoic rifting and Cenozoic inversion, it is here suggested that this 300 km en echelon fault zone can have a common detachment, underneath SW Iberia. Since the tomography data presented in Gutscher et al. (2002) suggest that the Horseshoe may penetrate at least till 100 km in the lithosphere, the 300 km long N–S trending fault system should be considered as *firstly,* a possible source candidate for the Lisbon 1/11/1755 earthquake and *secondly,* the propagation of a new front of compressive deformation towards the north along the West Portuguese Margin, which will eventually lead to the nucleation of a West Iberia incipient subduction zone, as proposed by Ribeiro et al. (1996).

Alternatively, even if these faults do not have a common detachment, a complex rupture scenario can be envisaged to explain the large energy released during the 1755 event. Complex seismic ruptures have been documented in other locations, such as, for instance the 1958 Gobi-Altay event which produced 260 km of surface rupture from the segmented main fault with a strike-slip movement and simultaneous rupture of nearby thrust faults (Kurushin et al., 1997), or the Tangshan earthquake of 1976, which was a combination of several ruptures, strike-slip and thrust faults, following each other only a few tens of seconds (Butler et al., 1979). The hypothesis of complex ruptures involving triggering or "domino-effect" is consistent with the majority of the historical documents that report a very long vibration (up to 20–30 min) and various sub-events for the 1st November 1755 earthquake (e.g. Martinez-Solares, 2001).

We also speculate that the location of recent epicentres in front of the Horseshoe fault in the Horseshoe Abyssal Plain, such as the 1969 event (Ms = 7.9) (Fukao, 1973), as well as the Mw = 6.0 12/02/2007 and the ML = 4.5 21/06/2006 events (Stich et al., 2007), all with a major dip-slip component can be interpreted as an indication of nucleation of new thrusts to the west of the main Horseshoe fault.

The NW–SE S_{Hmax} direction calculated from earthquake focal mechanism is in very good agreement with the Eurasia–Africa convergence direction estimated by the NUVEL-1 model (DeMets et al., 1994). However, recent estimates of this velocity using space geodetic techniques, and considering the Africa plate split into Nubia and Somalia, give for the Nubia–Eurasia collision a WNW–ESE direction, in the middle of the Gulf of Cadiz (Fig. 8). This discrepancy is interpreted as the coupled result of strain partitioning on E–W and NNE–SSW trending faults and aseismic deformation along the plate boundary.

5. Conclusions

The following conclusions are drawn.

1. The escarpments, seamounts and uplifted plateaus of the study area, all formed in association with polyphase compressive tectonic events from the late Cretaceous through Present, with the exception of the Pereira de Sousa fault escarpment that owes most of its morphology to the Mesozoic rifting. The Quaternary uplift has generated mass transport deposits (also reported by Gràcia et al. (2003a,b), Terrinha et al. (2003) and Vizcaino et al. (2006)), kilometric scale soft sediment unstable folds on the continental slope and incision of the canyons.
2. The Giant Scours display erosive and depositional structures that result from vortexes of high-density bottom currents at the edge of scarps formed at the crest of blind thrusts anticlines of Recent age.
3. The chaotic bodies buried under uppermost Miocene–lower Pliocene sediments in the Horseshoe Abyssal Plain and Horseshoe Valley together with the GCAW formed as stacked thrusts (possibly an accretionary wedge) in the Late Cretaceous–Earliest Miocene times before the emplacement of the Gibraltar orogenic Arc. Miocene reactivation of the eastern part of this body originated the GCAW and thrusting of this tectono-stratigraphic unit to the west. The third chaotic body corresponds to a non tectonised olistostrome that seals the most important thrust stacking in early Pliocene times.
4. The WNW–ESE trending lineaments are the superficial expression of steep faults deeply rooted in the Mesozoic substratum and underlying acoustic basement or Paleozoic basement onshore. Segments of these faults acted as rift faults during the Mesozoic and were reactivated in Quaternary times as strike-slip faults that cross cut the NE–SW trending thrusts.
5. The present day NW-wards movement of Nubia with respect to Iberia generates strain partitioning by means of dextral wrenching on WNW–ESE trending steep faults and thrusting on the NE–SW trending fault in the Gulf of Cadiz and Horseshoe Abyssal Plain. Further north, at the base of the continental slope of the southernmost part of the West Iberia Margin, NNE–SSW to N–S westerly dipping thrusts accommodate shortening in an area where wrenching has not been observed, which indicates that westward directed thrusting propagated from the Gibraltar Arc to the west (Horseshoe Fault) and to the north along the Portuguese margin (Marquês de Pombal Fault and Tagus Abyssal Plain Fault).

Acknowledgments

The work was sponsored by MATESPRO (PDCTM/P/MAR/15264/1999), EUROMARGINS SWIM (01-LEC-EMA09F), MVSEIS (01-LEC_EMA24F; PDCTM 72003/DIV/40018) and TOPOMED (TOPOEUROPE/0001/2007) projects and Instituto Scienze Marine (CNR) Bologna contribution 1630. JD and VV benefited from PhD grants from Fundação para a Ciência e a Tecnologia (SFRH/BD/31188/2006, SFRH/BD/17603/2004). We acknowledge the PARSIFAL Project MAR1998-1837-CE for the use of bathymetry data. We also wish to thank to the captain Cte. Paulo Marreiros and his crew of the *NRP D. Carlos I*. We acknowledge the financial support from the ESF EuroMargins Program, contract n. 01-LEC-EMA09F and from EU Specific Programme "Integrating and Strengthening the European Research Area", Sub-Priority 1.1.6.3, "Global Change and Ecosystems", contract n. 037110 (NEAREST). We acknowledge the support by Landmark Graphics Corporation via the Landmark University Grant Program.

References

Ambar, I., Serra, N., Brogueira, M.J., Cabecadas, G., Abrantes, F., Freitas, P., Gonçalves, C., Gonzalez, N., 2002. Physical, chemical and sedimentological aspects of the Mediterranean outflow off Iberia. Deep-Sea Research Part 2. Topical Studies in Oceanography 49, 4163–4177.

Argus, D.F., Gordon, R.G., DeMets, C., Stein, S., 1989. Closure of the Africa–Eurasia–North America plate motion circuit and tectonics of the Gloria fault. Journal of Geophysical Research 94 (B5), 5585–5602.

Arthaud, F., Matte, P., 1977. Late Paleozoic strike-slip faulting in Southern Europe and Northern Africa: result of a right-lateral shear zone between the Appalachians and the Urals. Geological Society of America Bulletin 88, 1305–1320.

Banda, E., Torné, M., IAM group, 1995. IAM group investigates deep structure of ocean margins: EOS (transaction of Am. Gephys. Union), 76, pp. 25–29.

Baptista, M.A., Miranda, P.M.A., Miranda, J.M., Victor, L.M., 1998. Constrains on the source of the 1755 Lisbon tsunami inferred from numerical modelling of historical data on the source of the 1755 Lisbon tsunami. Journal of Geodynamics 25 (1–2), 159–174.

Baptista, M.A., Miranda, J.M., Chierici, F., Zitellin, N., 2003. New study of the 1755 earthquake source based on multi-channel seismic survey data and tsunami modeling. Natural Hazards and Earth System Sciences 3, 333–340.

Bulat, J., Long, D., 2001. Images of the seabed in the Faroe–Shetland Channel from commercial 3D seismic data. Marine Geophysical Researches 22, 345–367.

Butler, R., Stewart, G.S., Kanamori, H., 1979. The July 27, 1976 Tangshan, China earthquake—a complex sequence of intraplate events. Bulletin of the Seismological Society of America 69 (1), 207–220.

Cabral, J., 1989. Na example of intraplate neotectonic activity, Vilariça Basin, Northeast Portugal. Tectonics 8 (2), 285–303.

Cabral, J., 1995. Neotectónica em Portugal Continental. Memórias do Instituto Geológico e Mineiro, Meméria 31, Lisboa, pp. 241.

Calais, E., Nocquet, J.-M., Jouanne, F., Tardy, M., 2002. Current strain regime in the Western Alps from continuous Global Positioning System measurements, 1996–2001. Geology 30 (7), 651–654.

Calais, E., DeMets, C., Nocquet, J.-M., 2003. Evidence for a post-3.16-Ma change in Nubia–Eurasia–North America plate motions? Earth and Planetary Science Letters 216, 81–92.

Camerlenghi, A., Pini, G.A., 2009. Mud volcanoes, olistostromes and Argille scagliose in the Mediterranean region. Sedimentology 56 (1), 319–365.

Carrilho, F., Teves-Costa, P., Morais, I., Pagarete, J., Dias, R., 2004. GEOALGAR Project: first results on seismicity and fault-plane solutions. Pure and Applied Geophysics 161 (3), 589–606.

Cunha, T., 2008. Gravity Anomalies, Flexure and the Thermo-Mechanical Evolution of the West Iberia Margin and its Conjugate of Newfoundland.; PhD Thesis, Department of Earth Sciences, University of Oxford.

DeMets, C., Gordon, R.G., Argus, D.F., Stein, S., 1994. Effect of recent revisions to the geomagnetic reversal time scale on estimates of current plate motions. Geophysical Research Letters 21 (20), 2191–2194.

Dewey, J.F., Helman, M.L., Turco, E., Hutton, D.H., Knott, S.D., 1989. Kinematics of the Western Mediterranean. In: Coward, M.P., Dietrich, D., Park, R.G. (Eds.), Alpine Tectonics: Geol. Soc. Spec. Publ., vol. No. 45, pp. 265–283.

Dias, R.P., 2001. Neotectónica da região do Algarve. Dissertação de doutoramento, Universidade de Lisboa, 369 pp.

Duarte, J.C., Rosas, F., Pinheiro, L.M., Matias, L.M., Carvalho, A.M., Terrinha, P., Ivanov, M., 2005. Interpretation of recent sedimentary and tectonic structures off SW Iberia from multibeam bathymetry, seismic reflection and experimental modeling. Geophysical Research Abstracts 7, 07867.

Duarte, J.C., Rosas, F., Terrinha, P., Valadares, V., Taborda, R., Matias, L., Roque, C., Magalhães, V., Henriet, J.P., Pinheiro, L., 2007. Deep Submarine Giant Scours in northern Gulf of Cadiz (offshore SW Iberia): a singular case of sedimentary and tectonic coupling. Geophysical Research Abstracts 9, 03940.

Dunn, A.M., Reynolds, P.H., Clarke, D.B., Ugidos, J.M., 1998. A comparison of the age and composition of the Shelburne dyke, Nova Scotia, and the Messejana Dyke, Spain. Canadian Journal of Earth Sciences 35 (10), 1110–1115.

Faccenna, C., Piromallo, C., Crespo-Blanc, A., Jolivet, L., Rossetti, F., 2004. Lateral slab deformation and the origin of the western Mediterranean arcs. Tectonics 23 (TC1012).

Faugères, J.C., Gonthier, È., Bobier, C., Griboulard, R., 1997. Tectonic control on sedimentary processes in the southern termination of the Barbados Prism. Marine Geology 140, 117–140.

Fernandes, R.M.S., Ambrosius, B.A.C., Noomen, R., Bastos, L., Wortel, M.J.R., Spakman, W., Govers, R., 2003. The relative motion between Africa and Eurasia as derived from ITRF2000 and GPS data. Geophysical Research Letters 30 (16).

Fildani, A., Normark, W.R., Kostic, S., Parker, G., 2006. Channel formation by flow stripping: large-scale scour features along the Monterey East Channel and their relation to sediment waves. Sedimentology 53, 1265–1287.

Fukao, Y., 1973. Thrust faulting at a lithospheric plate boundary, the Portugal earthquake of 1969. Earth and Planetary Science Letters 18, 205–216.

González, A., Córdoba, D., Vegas, R., Matias, L.M., 1998. Seismic crustal structure in the southwest of the Iberian Peninsula and the Gulf of Cadiz. Tectonophysics 296, 317–331.

Gràcia, E., Dañobeitia, J., Vergés, J., Bartolomé, R., 2003a. Crustal architecture and tectonic evolution of the Gulf of Cadiz (SW Iberian margin) at the convergence of the Eurasian and African plates. Tectonics 22 (4).

Gràcia, E., Danobeitia, J., Vergés, J., Cordoba, D., PARSIFAL Team, 2003b. Mapping active faults offshore Portugal (36°N–38°N): implications seismic hazard assessment along the southwest Iberian margin. Geology 31 (1), 83–86.

Gutscher, M.A., Malod, J., Rehault, J.-P., Contrucci, I., Klingelhoefer, F., Mendes-Victor, L., Spakman, W., 2002. Evidence for active subduction beneath Gibraltar. Geology 30 (12), 1071–1074.

Gutscher, M.-A., Dominguez, S., Westbrook, G.K., Gente, P., Babonneau, N., Mulder, T., Gonthier, E., Bartolome, R., Luis, J., Rosas, F., Terrinha, P., The Delila DelSis Scientific Teams, 2008. Tectonic shortening and gravitational spreading in the Gulf of Cadiz accretionary wedge: observations from multi-beam bathymetry and seismic profiling. Marine and Petroleum Geology 26, 647–659.

Hernandez-Molina, J., Llave, E., Somoza, L., Fernandez-Puga, M.C., Maestro, A., Leon, R., Medialdea, T., Barnolas, A., Garcia, M., del Rio, V.D., Fernandez-Salas, L.M., Vazquez, J.T., Lobo, F., Dias, J.M.A., Rodero, J., Gardner, J., 2003. Looking for clues to paleoceanographic imprints: a diagnosis of the Gulf of Cadiz contourite depositional systems. Geology 31 (1), 19–22.

Hernández-Molina, F.J., Llave, E., Stow, D.A.V., García, M., Somoza, L., Vázquez, J.T., Lobo, F.J., Maestro, A., Díaz del Río, V., León, R., Medialdea, T., Gardner, J., 2006. The contourite depositional system of the Gulf of Cádiz: a sedimentary model related to the bottom current activity of the Mediterranean outflow water and its interaction with the continental margin. Deep-Sea Research II 53, 1420–1463.

IOC, IHO and BODC, 2003. "Centenary edition of the GEBCO Digital Atlas", published on CDROM on behalf of the Intergovernmental Oceanographic Commission and the International Hydrographic Organization as part of the General Bathymetric Chart of the Oceans; British Oceanographic Data Centre, Liverpool.

Iribarren, L., Vergés, J., Camurri, F., Fullea, J., Fernàndez, M., 2007. The structure of the Atlantic–Mediterranean transition zone from the Alboran Sea to the Horseshoe Abyssal Plain (Iberia–Africa plate boundary). Marine Geology 243, 97–119.

Kenyon, N.H., Ivanov, M.K., Akhmetzanov, A., Akhmanov, G.G., 2000. Multidisciplinary study of geological processes on the North East Atlantic and Western Mediterranean Margins. IOC Technical Series, 56. UNESCO. 119 pp.

Kenyon, N.H., Ivanov, M., Akhmetzhanov, A., Koslova, E.V., 2006. Interdisciplinary geoscience studies of the Gulf of Cadiz and Western Mediterranean basins. : Intergovernmental Oceanographic Commission, Technical Series, 70. UNESCO. 115 pp.

Kreemer, C., Holt, W.E., 2001. A no-net-rotation model of present-day surface motions. Geophysical Research Letters 28 (23), 4407–4410.

Kurushin, R.A., Bayasgalan, A., Olziybat, M., Enhtuvshin, B., Molnar, P., Bayarsayhan, C., Hudnut, K.W., Lin, J., 1997. The surface rupture of the 1957 Gobi-Altay, Mongolia, Earthquake. Geological Society of America, Boulder.

Lopes, F.-C., Cunha, P.P., Le Gall, B., 2006. Cenozoic seismic stratigraphy and tectonic evolution of the Algarve Margin (offshore Portugal, southwestern Iberian Peninsula). Marine Geology 231, 1–36.

Maldonado, A., Somoza, L., Pallares, L., 1999. The Betic orogen and the Iberian–African boundary in the Gulf of Cadiz: geological evolution (central North Atlantic). Marine Geology 155 (1–2), 9–43.

Martinez-Solares, J.M., 2001. Los effectos en España del terremoto de Lisboa. Instituto Geografico Nacional, Madrid. 756 pp.

Medialdea, T., 2007. Estructura y evolucion tectonica del Golfo de Cadiz. Publicaciones del Instituto Geologico y Minero de España —Serie Tesis Doctorales N°8. ISBN 978-84-7840-728-2.

Medialdea, T., Vegas, R., Somoza, L., Vazquez, J.T., Maldonado, A., Diaz-del Rio, V., Maestro, A., Cordoba, D., Fernandes-Puga, M.C., 2004. Structure and evolution of the "Olistostrome" complex of the Gibraltar Arc in the Gulf of Cádiz (eastern Central Atlantic): evidence from two long seismic cross-sections. Marine Geology 209 (1 –4), 173–198.

Morel, J.L., Megrhraoui, M., 1996. Gorringe–Alboran–Tell tectonic zone: a transpression system along the Africa–Eurasia plate boundary. Geology 24 (8), 755–758.

Mulder, T., Voisset, M., Lecroart, P., Drezen, E.L., Gonthier, E., Hanquiez, V., Faugères, J.-C., Habgood, E., Hernandez -Molina, F.J., Estrada, F., Llave -Barranco, E., Poirier, D., Gorini, C., Fuchey, Y., Voelker, A., Freitas, P., Sanchez, F.L., Fernandez, L.M., Kenyon, N.H., Morel, J., 2003. The Gulf of Cadiz: an unstable giant contouritic levee. Geo -Marine Letters V23 (1), 7–18.

Neves, M.C., Terrinha, P., Afilhado, A., Moulin, M., Matias, L., Rosas, F., 2009. Response of a multi-domain continental margin to compression: study from seismic reflection–refraction and numerical modelling in the Tagus Abyssal Plain. Tectonophysics 468, 113–130.

Niemann, H., Duarte, J., Hensen, C., Omoregie, E., Magalhaes, V.H., Elvert, M., Pinheiro, L.M., Kopf, A., Boetius, A., 2006. Microbial methane turnover at mud volcanoes of the Gulf of Cadiz. Geochimica et Cosmochimica Acta 70 (21), 5336–5355.

Nocquet, J.M., Calais, E., 2004. Geodetic measurements of crustal deformation in the Western Mediterranean and Europe. Pure and Applied Geophysics 161, 661–681.

Pinheiro, L.M., Wilson, R., Pena dos Reis, R., Whitmarsh, R.B., Ribeiro, A., 1996. In: Whitmarsh, R.B., Sawyer, D.S., Klaus, A., Masson, D.G. (Eds.), The Western Iberia Margin: a Geophysical and Geological Overview. : Proceedings of the Ocean Drilling Program, Scientific Results, 149. Ocean Drilling Program, College Station, TX, pp. 3–23.

Pinheiro, L.M., Ivanov, M.K., Sautkin, A., Akhmanov, G., Magalhaes, V.H., Volkonskaya, A., Monteiro, J.H., Somoza, L., Gardner, J., Hamouni, N., Cunha, M.R., 2003. Mud volcanism in the Gulf of Cadiz: results from the TTR-10 cruise. Marine Geology 195, 131–151.

Pinheiro, L.M., Ivanov, M., Kenyon, N., Magalhães, V., Somoza, L., Gardner, J., Kopf, A., Van Rensbergen, P., Monteiro, J.H., Team, Euromargins MVSEIS, 2006. Structural control of mud volcanism and hydrocarbon-rich gas seepage: results from the TTR-15 and other previous cruises. Fluid seepages/mud volcanism in the Mediterranean and Adjacent Domains. CIESM Workshop Monographs 29, 53–58.

Ribeiro, A., 2002. Soft Plate and Impact Tectonics. Springer-Verlag. 324 pp.

Ribeiro, C., Terrinha, P., 2007. Formation, deformation and chertification of systematic clastic dykes in a differentially lithified carbonate multilayer. SW Iberia, Algarve Basin, Lower Jurassic. Sedimentary Geology 196 (1–4), 2001–2015.

Ribeiro, A., Antunes, M.T., Ferreira, M.P., Rocha, R., Soares, A., Zbyszewski, G., Moitinho de Almeida, F., 1979. Introduction à la géologie générale du Portugal. Serv. Geol. Portugal. 114 pp.

Ribeiro, A., Cabral, J., Baptista, R., Matias, L., 1996. Stress pattern in Portugal mainland and the adjacent Atlantic region, West Iberia. Tectonophysics 15 (2), 641–659.

Roque, C., 2007. Tectonostratigrafia do Cenozóico das margens continentais Sul e Sudoeste portuguesas: um modelo de correlação sismostratigráfica. Universidade de Lisboa, Departamento de Geologia.

Rosas, F.M., Duarte, J.C., Terrinha, P., Valadares, V., Matias, L., 2009. Morphotectonic characterization of major bathymetric lineaments in NW Gulf of Cadiz (Africa–Iberia plate boundary): insights from analogue modelling experiments. Marine Geology 261, 33–47.

Rosenbaum, G., Lister, G.S., Duboz, C., 2002. Reconstruction of the tectonic evolution of the western Mediterranean since the Oligocene. In: Rosenbaum, G., Lister, G.S. (Eds.), Reconstruction of the evolution of the Alpine-Himalayan Orogen. Journal of the Virtual Explorer, 8, 107–126.

Rovere, M., Ranero, C.R., Sartori, R., Torelli, L., Zitellini, N., 2004. Seismic images and magnetic signature of the Late Jurassic to Early Cretaceous Africa–Eurasia plate boundary off SW Iberia. Geophysical Journal International 158 (2), 554–568.

Sartori, R., Torelli, L., Zitellini, N., Peis, D., Lodolo, E., 1994. Eastern segment of the Azores–Gibraltar line (central–eastern Atlantic): an oceanic plate boundary with diffuse compressional deformation. Geology 22, 555–558.
Sella, G., Dixom, T., Mao, A., 2002. REVEL: a model for Recent plate velocities from space geodesy. Journal of Geophysical Research 107.
Sillard, P., Altamimi, Z., Boucher, C., 1998. The ITRF96 realization and its associated velocity field. Geophysical Research Letters 25 (17), 3223–3226.
Somoza, L., Díaz-del-Río, V., León, R., Ivanov, M.K., Fernández-Puga, M.C., Gardner, J.M., Hernández-Molina, F.J., Pinheiro, L.M., Rodero, J., Lobato, A., Maestro, A., Vázquez, J.T., Medialdea, T., Fernández-Salas, L.M., 2003. Seabed morphology and hydrocarbon seepage in the Gulf of Cádiz mud volcano area: acoustic imagery, multibeam and ultra-high resolution seismic data. Marine Geology 195, 153–156.
Srivastava, S.P., Roest, W.R., Kovacs, L.C., Oakey, G., Levesque, S., Verhoef, J., Macnab, R., 1990. Motion of Iberia since the Late Jurassic: results from detailed aeromagnetic measurements in the Newfoundland Basin. Tectonophysics 184 (3–4), 229–260.
Stich, D., Serpelloni, E., Mancilla, F.-L., Morales, J., 2006. Kinematics of the Iberia–Maghreb plate contact from seismic moment tensors and GPS observations. Tectonophysics 426, 295–317.
Stich, D., Mancilla, F.de L., Pondrelli, S., Morales, J., 2007. Source analysis of the February 12th 2007, M_w 6.0 Horseshoe earthquake: implications for the 1755 Lisbon earthquake. Geophysical Research Letters 34, 12.
Terrinha, P., 1998. Structural Geology and Tectonic Evolution of the Algarve Basin, South Portugal. Department of Geology, University of London, London.
Terrinha, P., Dias, R.P., Ribeiro, A., Cabral, J., 1999. The Portimão Fault, Algarve Basin, South Portugal. Comunicacões do Instituto Geológico e Mineiro 86, 107–120.
Terrinha, P., Ribeiro, C., Kullberg, J.C., Rocha, R., Ribeiro, A., 2002. Compression episodes during rifting and faunal isolation in the Algarve Basins, SW Iberia. Journal of Geology 110, 101.113.
Terrinha, P., Pinheiro, L.M., Henriet, J.-P., Matias, L., Ivanov, M.K., Monteiro, J.H., Akhmetzhanov, A., Volkonskaya, A., Cunha, T., Shaskin, P., Rovere, M., 2003. Tsunamigenic–seismogenic structures, neotectonics, sedimentary processes and slope instability on the southwest Portuguese Margin. Marine Geology 195 (1–4), 55–73.
Torelli, L., Sartori, R., Zitellini, N., 1997. The giant chaotic body in the Atlantic Ocean off Gibraltar: new results from a deep seismic reflection survey. Marine and Petroleum Geology 14 (2), 125–134.
Tortella, D., Torné, M., Pérez-Estáun, A., 1997. Geodynamic Evolution of the Eastern Segment of the Azores–Gibraltar Zone: the Gorringe Bank and the Gulf of Cadiz Region. Marine Geophysical Researches 19 (3), 211–230.
USGS, 2004. Shuttle Radar Topography Mission, 1 Arc Second scene SRTM_u03_n008e004, Unfilled Unfinished 2.0, Global Land Cover Facility. University of Maryland, College Park, Maryland. February 2000.
Van Rensbergen, P., Depreiter, D., Pannemans, B., Moerkerke, G., Van Rooij, D., Marsset, B., Akhmanov, G., Blinova, V., Ivanov, M., Rachidi, M., Magalhaes, V.H., Pinheiro, L.M., Cunha, M.R., Henriet, J.-P., 2005. The El Arraiche mud volcano field at the Moroccan Atlantic slope, Gulf of Cadiz. Marine Geology 219 (1), 1–17.
Verdicchio, G., Trincardi, F., 2006. Short-distance variability in slope bed-forms along the Southwestern Adriatic Margin (Central Mediterranean). Marine Geology 234, 271–292.
Vizcaino, A., Gracia, E., Pallas, R., Garcia-Orellana, J., Escutia, C., Casas, D., Willmott, V., Diez, S., Asioli, A., Danobeitia, J., 2006. Sedimentology, physical properties and age of mass transport deposits associated with the Marques de Pombal Fault, Southwest Portuguese Margin. Norwegian Journal of Geology 86 (3), 177–186.
Voelker, A., Lebreiro, S., Schonfeld, J., Cacho, I., Erlenkeuser, H., Abrantes, F., 2006. Mediterranean outflow strengthening during northern hemisphere coolings: a salt source for the glacial Atlantic? Earth and Planetary Science Letters 245, 39–55.
Zitellini, N., Chierici, F., Sartori, R., Torelli, L., 1999. The tectonic source of the 1755 Lisbon earthquake and tsunami. Annali di Geofisica 42 (1).
Zitellini, N., Mendes, L. A., Cordoba, D., Danobeitia, J., Nicolich, R., Pellis, G., Ribeiro, A., Sartori, R., Torelli, L., Bartolomé, R., Bortoluzzi, G., Calafato, A., Carrilho, F., Casoni, L., Chierici, F., Corela, C., Correggiari, A., Della Vedova, B., Gràcia, E., Jornet, P., Landuzzi, M., Ligi, M., Magagnoli, A., Marozzi, G., Matias, L., Penitenti, D., Rodriguez, P., Rovere, M., Terrinha, P., Vigliotti, L., Zahinos Ruiz, A., 2001. Source of 1755 Lisbon Earthquake and Tsunami Investigated. Eos Trans. AGU, 82, (26), 285, 290–291.
Zitellini, N., Ligi, M., Matias, L., Rovere, M., the Shipboard Scientific Parties, 2002. Voltaire 2002 Cruise Report. IGM-CNR Technical Report.
Zitellini, N., Rovere, M., Terrinha, P., Chierici, F., Matias, L., Team, B., 2004. Neogene through quaternary tectonic reactivation of SW iberian passive margin. Pure and Applied Geophysics 161, 565–587.
Zitellini, N., Gracia, E., Matias, L., Terrinha, P., Abreu, M.A., DeAlteriis, G., Henriet, J.P., Dañobeitia, J.J., Masson, D.G., Mulder, T., Ramella, R., Somoza, L., Diez, S., 2009. The quest for the Africa–Eurasia plate boundary west of the Strait of Gibraltar. Earth and Planetary Science Letters 280 (1–4), 13–50.

Trabajos de Geología, Universidad de Oviedo, 29 : 237-241 (2009)

Anatomy and tectonic significance of WNW-ESE and NE-SW lineaments at a transpressive plate boundary (Nubia-Iberia)

J. C. DUARTE[1, 2*], V. VALADARES[1, 2], P. TERRINHA[1, 2], F. ROSAS[1], N. ZITELLINI[3] AND E. GRÀCIA[4]

[1]*LATTEX, IDL, UL, Faculdade de Ciências da Universidade de Lisboa, Edificio C6, Piso 3, Campo Grande, 1749-016 Lisboa, Portugal.*

[2]*UGM-LNEG, Estrada da Portela Zambujal, Alfragide, Apartado 7586, 2720-866 Amadora, Portugal.*

[3]*Istituto di Scienze Marine, (ISMAR, Área della ricerca di Bologna, Via Pierro Gobetti,101-40129, Bologna, Italy.*

[4]*Unidad de Tecnología Marina, CSIC, Passeig Maritim de la Barceloneta, 37-49, 08003 Barcelona, Spain.*

[*]*e-mail: joao.duarte@lneg.pt*

Abstract: Recent mapping of the Gulf of Cadiz seafloor permitted to identify major tectonic lineaments: the SWIM lineaments (Zitellini *et al.*, 2009) and Cadiz lineament, striking WNW-ESE and NE-SW, respectively. Multibeam swath bathymetry and interpretation of multi-channel seismic data indicate that these features can be interpreted to correspond to the seafloor morphological expression of active dextral strike-slip faults. Based on the interpreted data and recently published GPS plate kinematic velocity vectors of Nubia with respect to Iberia and the Alboran block (e.g. Fernandes *et al.*; 2003 Stich *et al.*, 2006) we propose that the SWIM Faults are related to the general NW-SE convergence of Nubia with respect to Iberia, and the Cadiz fault is related to the westward movement of the Gibraltar orogenic arc.

Keywords: Gulf of Cadiz, seafloor mapping, SWIM lineaments, Cadiz lineament, active tectonics, Alboran block, Gibraltar orogenic arc.

The Gulf of Cadiz is located in a complex tectonic area, encompassing the controversial SW Eurasia-NW Africa plate boundary (see figure 1). Some authors believe that this is a diffuse plate boundary (Sartori *et al.*, 1994; Medialdea *et al.*, 2004), other describe an active subduction with roll-back of a subducted slab (Gutscher *et al.*, 2002), while others postulate a prolongation of a transpressive deformation belt from the Rif-Tell (Morel and Meghraouie, 1996; Zitellini *et al.*, 2009). This region experiences a general NW-SE to WNW-ESE convergence between Nubia and Eurasia at a rate of 5-6 mm a^{-1} (Calais *et al.*, 2003). Stich *et al.* (2006) proposed that the SW Iberian Margin is also accommodating a 3.5 mm a^{-1} of westward motion of the Gibraltar arc relative to intraplate Iberia. Seismicity is distributed over a more than 400 km wide zone between the Gibraltar arc and the Horseshoe fault (Fig. 1) and earthquakes are characterized by magnitudes usually smaller than 5.5. In the western part of the Gulf of Cadiz, in the area that encompasses the Horseshoe fault until the eastern part of the Gloria fault, seismicity is distributed over a narrower area and instrumental seismicity is higher, with recent events of M=6

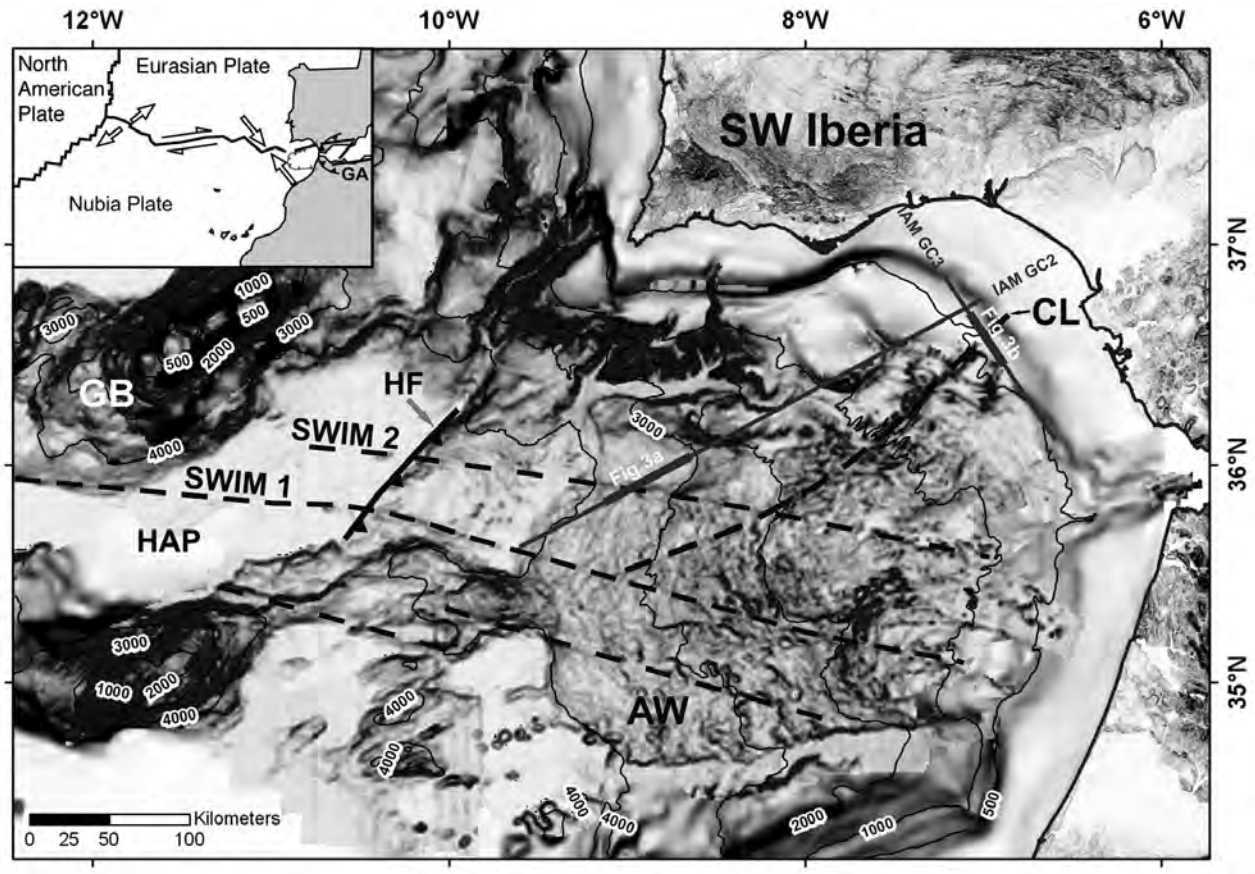

Figure 1. Bathymetric map of the Gulf of Cadiz (low resolution multibeam compilation of the SWIM dataset and GEBCO bathymetry). Topography of onshore area is also shown as shaded relief. Dashed lines represent the main tectonic lineaments studied in this work. The inset shows the tectonic context of the area (adapted from Gutscher *et al.*, 2002). The location of two seismic profiles, IAM GC2 and IAM GC3, are also shown. AW: Accretionary Wedge; CL: Cadiz Lineament; GA: Gibraltar Arc; GB: Gorringe Bank; HF: Horseshoe Fault; HAP: Horseshoe Abyssal Plain.

and the 1969 event of M=7.9 (Fukao, 1973; Stich *et al.*, 2006). Zitellini *et al.* (2004) described a number of active structures scattered along the Gulf of Cadiz and SW Portugal showing that tectonic strain is presently accommodated between 35.5º N and 38º N (approximately 250 km), which suggests a diffuse strain distribution of the plate convergence.

Over the last two decades a large amount of geological and geophysical data have been collected aiming at identifying the main tectonic features present in the Gulf of Cadiz and to clarify how deformation has been accommodated during Alpine to present times (Zitellini *et al.*, 2009). In this work we describe the morphology and structure of WNW-ESE and one NE-SW trending lineaments recently mapped in the Gulf of Cadiz region and discuss their tectonic significance.

This work is extracted from a much larger study based on the analysis and interpretation of 180,000 km^2 of multibeam swath bathymetry and reflectivity (backscatter) data of the Gulf of Cadiz area and more than 20,700 km multi-channel seismic profiles. This dataset was collected throughout several surveys carried out by international teams of several countries and compiled for the ESF Eurocores EuroMargins SWIM project (Earthquake and Tsunami hazards of active faults at the South-West Iberian Margin: deep structure, high-resolution imaging and paleo-seismic signature, REN2002-11234-EMAR, 01-LEC-EMA09 F) (http://www.swim.ul.pt/index_topo.htm) and NEAREST project (Integrated observations from NEAR shore sourcES of Tsunamis: towards an early warning system, GOCE Contract n. 037119) (http://nearest.bo.ismar.cnr.it/).

The SWIM lineaments

Morphology

The SWIM lineaments are linear features that strike approximately WNW-ESE and extend from the east-

ernmost part of the Gulf of Cadiz accretionary wedge until the Horseshoe abyssal plain, south of the Gorringe submarine mountain (Fig. 1). They cut across various morphological domains, contain various active mud volcanoes along their path and offset the NE-SW Horseshoe fault scarp (Fig.2), an active reverse fault (Gràcia *et al.*, 2003; Zitellini *et al.*, 2004). These linear features correspond to the alignment of elongated crests and troughs on the sea floor with wavelengths of the order of tens of kilometers. According to Zitellini *et al.* (2009), the longest of the SWIM lineaments, SWIM 1, exceeds 600 km, and it can be followed from the Gorringe bank southern flank to the Morocco shelf and corresponds to a strike-slip fault. In some segments of this lineament it is possible to identify E-W-striking undulations with maximum lengths of about 8 km (Fig. 2). These features show an en echelon pattern that corresponds to oriented folds of the recent sedimentary cover, allowing us to establish a dextral strike-slip movement. The width of each individual SWIM lineament is only of a few hundreds of meters.

ment because the wedge (Unit B) is over-thrusted towards the SW. This reactivation probably occurred during Paleogene to Miocene times (Rosas *et al.*, *in press*; Terrinha *et al.*, 2009). This movement seems to be coeval with the installation of the Accretionary wedge (Unit D) since it clearly tapers towards the eastern part of the profile. The SWIM fault also deforms and folds the Plio-Quaternary unit (Unit E) and cuts through the seafloor.

The Cadiz lineament

Morphology

The morphology of the Cadiz lineament is more complex than that of the SWIM 2 lineament. It is relatively diffuse and occupies a broader area, with widths varying from several hundreds of meters to a few kilometers. It strikes approximately NE-SW and extends for about 200 km from the northeastern Gulf of Cadiz continental shelf to the westernmost

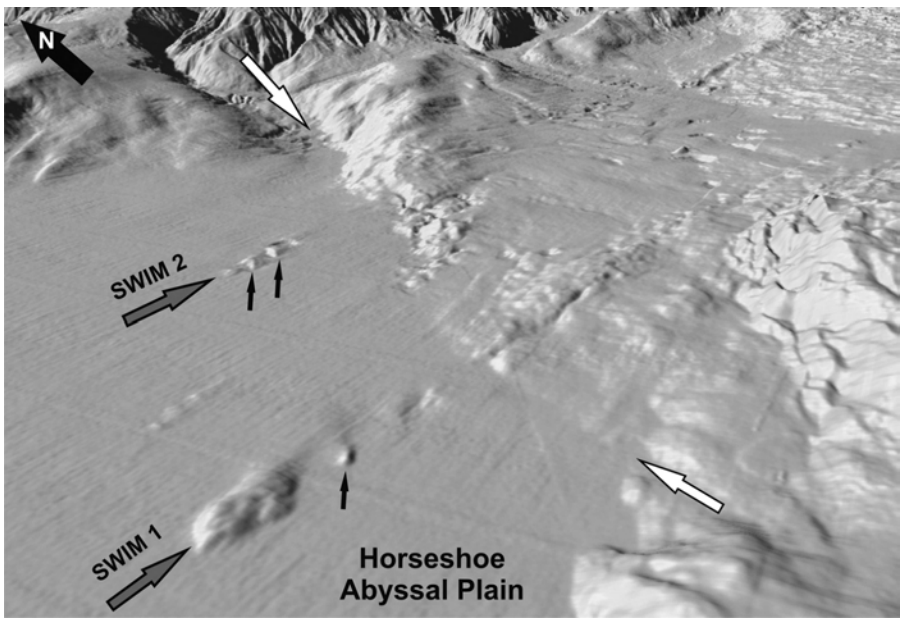

Figure 2. Shaded relief 3D image of the Horseshoe Abyssal Plain and continental rise to the east; view from SW, showing the SWIM tectonic lineaments 1 and 2, indicated by grey arrows; MATESPRO bathymetric data Terrinha *et al.* (2009) and Rosas *et al.* (2009). The small black arrows show seafloor deformation corresponding to NE-SW-oriented en echelon folds. The white arrows indicate the slope break that corresponds to the morphological expression of the Horseshoe Fault.

Structure

The interpretation of a segment of a profile across SWIM 2 lineament (Fig. 3a) shows that it corresponds to a fault that cuts through Mesozoic sediments (Unit A) (Tortella *et al.*, 1997). This fault formed during the Mesozoic rifting as a normal fault. This assumption is corroborated by the presence of a syn-rift growth wedge (Unit B). The SWIM 2 fault was later reactivated with a southwards reverse move-

part of the accretionary wedge (Fig.1). The lineament is slightly curved towards the west at the south-western part where it meets the SWIM 1 fault (Fig. 1). It is materialized on the seafloor by the alignment of several different features such as crests, scarps, channels and diapiric ridges (Somoza *et al.*, 2003). The Cadiz lineament is more prominent in its northeastern segment, where it is adjacent to the Guadalquivir bank (a basement high with active seismicity) and it loses morphological expression progressively towards

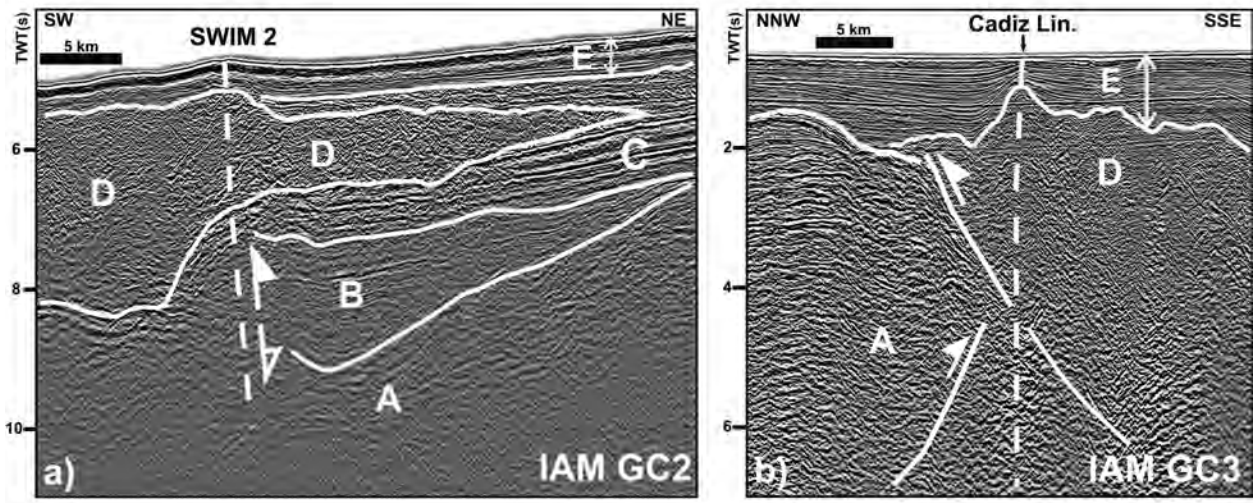

Figure 3. (a) Multi-channel seismic reflection profiles IAM GC2, and (b) IAM GC3. The white dashed lines mark the fault zones corresponding to the lineaments (SWIM 2 on the left and the Cadiz Lineament on the right). The profile a) shows two previous vertical movements of the SWIM fault (white arrows). On profile b) the following features are pointed out, reverse fault of the Guadalquivir basement to the SSE; and a thin-skinned fault of accommodating the over-thrusting movement of the Accretionary wedge over the Guadalquivir basement. A: Basement; B: Sin-rift wedge (Mesozoic age); C: Post-rift unit; D: Accretionary Wedge unit (Miocene age); E: Cover unit (Plio-Quaternary age).

the SW, where it intercepts the SWIM 2 lineament and is almost untraceable in the surroundings of the SWIM 1 lineament.

Structure

A segment of IAM GC3 seismic profile (Fig. 3b) across the Cadiz lineament shows that it seats on top of a fault zone. This fault is parallel to the deep blind thrust of the Guadalquivir bank towards the SE, as interpreted in figure 3 (Unit A). This movement is corroborated by the gentle folding of the reflectors of Unit A. It is also possible to observe a thin-skinned fault accommodating the over-thrusting of the accretionary wedge described by Gutscher *et al.* (2002) towards NE over the Guadalquivir basement (Unit D). This unit corresponds to imbrications of NNW-verging thrusts, as shown by the planar fabric of the acoustic facies. Near the surface the more continuous cover sediments are clearly folded; however, they do not show evidences of major vertical displacement (Unit E).

Discussion

Based on bathymetric and structural observations we interpret the SWIM lineaments as the morphological expression of dextral WNW-ESE trending strike-slip faults rooted in the Mesozoic rift basin. This interpretation is derived from both observed coherent en echelon folding pattern on the seafloor associated with the faults and the minor vertical displacement of the post-Miocene cover. This assumption is in agreement with recent work by Zitellini *et al.* (2009) and Terrinha *et al.* (2009) that describes in detail the kinematic indicators and the age of these faults. Rosas *et al.* (2009), using analogue models and the en echelon folds has markers for a quantitative strain analysis, suggested that the SWIM lineaments initiated their strike-slip movement 1.8 Ma ago, at least. This interpretation is also in agreement with the general NW-SE to WNW-ESE convergence between Africa and Eurasia at a rate of 5-6 mm a^{-1} and the fact that the SWIM faults offset the Late Miocene movement of the Horseshoe Fault. In this way, the SWIM lineaments can be accommodating a strike-slip component of this convergence, while the main shortening is being accommodated in the northwestwards directed thrusts of the SW Iberian Margin, for example the Horseshoe fault.

The Cadiz lineament has a strong morphological expression, mainly in its northeastern part where salt diapirs have extruded (Somoza *et al.*, 2003). However, no kinematic indicators could clearly be detected in our analysis. It corresponds to an almost vertical fault that deforms the sedimentary cover with no major vertical displacement. Based on recent data published by Stich *et al.* (2006), that reported a 3.5 mm a^{-1} of westward motion of the Gibraltar arc relative to intra-plate Iberia, we propose that the Cadiz lineament is a major dextral strike-slip fault zone that is accommodating this

relative motion in the Gulf of Cadiz area. The lack of good strike-slip kinematic indicators in this part of the study area is probably due to the higher rate of recent sedimentation associated with the proximal parts of the Mediterranean Outflow Water and discharge of the Guadalquivir river as well as the extrusion of fluidized material along diapiric ridges (Somoza *et al.* 2003), as well as to the pure shortening at the front of the Guadalquivir bank thrust, as argued in this work.

Conclusions

In this work we studied various major tectonic lineaments localized in the Gulf of Cadiz area. We showed that they correspond to major transpressive dextral strike-slip faults with two different orientations: the WNW-ESE SWIM faults and the NE-SW Cadiz fault. Both faults are active and are probably related with two different driving mechanisms. The SWIM faults are related to the general WNW-ESE convergence between Nubia and Eurasia and the Cadiz fault is related to the westward expulsion of the Gibraltar Arc relative to Iberia, possibly associated with the convergence between the two lithospheric plates.

Acknowledgements

It is acknowledged the FCT PhD grant provided to support the work of J. Duarte (SFRH/BD/31188/2006) and V. Valadares (SFRH/BD/17603/2004). We acknowledge the support by Landmark Graphics Corporation via the Landmark University Grant Program.

References

Calais, E., DeMets, C. and Nocquet, J. M. (2003): Evidence for a post-3.16 Ma change in Nubia-Eurasia-North America plate motions? *Earth Planet. Sc. Lett.*, 216: 81-92.

Fernandes, R. M. S., Ambrosius, B. A. C., Noomen, R., Bastos, L., Wortel, M. J. R., Spakman, W. and Govers, R. (2003): The relative motion between Africa and Eurasia as derived from ITRF2000 and GPS data. *Geophys. Res. Lett.*, 30, 16.

Fukao, Y. (1973): Thrust faulting at a lithospheric plate boundary Portugal earthquake of 1969. *Earth Planet. Sc. Lett.*, 18: 205-216.

Gràcia, E., Dañobeitia, J., Vergés, J. and R. Bartolomé, R. (2003a): Crustal architecture and tectonic evolution of the Gulf of Cadiz (SW Iberian margin) at the convergence of the Eurasian and African plates. *Tectonics*, 22, 4: 1-19

Gutscher, M. A., Malod, J., Rehault, J. P., Contrucci, I., Klingelhoefer, F., Mendes-Victor, L. and Spakmanc, W. (2002): Evidence for active subduction beneath Gibraltar. *Geology*, 30, 12: 1071-1074.

Medialdea, T., Vegas, R., Somoza, L., Vazquez, J. T., Maldonado, A., Diaz-del Rio, V., Maestro, A., Cordoba, D. and Fernandes-Puga, M. C. (2004): Structure and evolution of the "Olistostrome" complex of the Gibraltar Arc in the Gulf of Cadiz (eastern Central Atlantic): evidence from two long seismic cross-sections. *Mar. Geol.*, 209, 1-4: 173-198.

Morel, J. L. and Megrhraoui, M. (1996): Gorringe-Alboran-Tell tectonic zone: A transpressiva system along the Africa-Eurasia plate boundary. *Geology*, 24, 8: 755-758.

Rosas, F., Duarte, J., Terrinha, P., Valadares, V., Matias, L. and Gutscher, M. A. (2009): Major bathymetric lineaments and soft sediment deformation in NW Gulf of Cadiz (Africa-Iberia plate boundary): new insights from high resolution multibeam bathymetry data and analogue modelling experiments. *Mar. Geol.,* 261: 33-47.

Sartori, R., Torelli, L., Zitellini, N., Peis, D. and Lodolo, E. (1994): Eastern segment of the Azores-Gibraltar line (central-eastern Atlantic): an oceanic plate boundary with diffuse compressional deformation. *Geology*, 22: 555-558.

Somoza, L., Díaz-del-Río, V., León, R., Ivanov, M. K., Fernández-Puga, M. C., Gardner, J. M., Hernández-Molina, F. J., Pinheiro, L. M., Rodero, J., Lobato, A., Maestro, A., Vázquez, J. T., Medialdea, T. and Fernández-Salas, L. M. (2003): Seabed morphology and hydrocarbon seepage in the Gulf of Cadiz mud volcano area: Acoustic imagery, multibeam and ultra-high resolution seismic data. *Mar. Geol.*, 195: 153-156.

Stich, D., Serpelloni, E., Mancilla, F. and Morales, J. (2006): Kinematics of the Iberia-Maghreb plate contact from seismic moment tensors and GPS observations. *Tectonophysics*, 426: 295-317.

Terrinha, P., Matias, L., Vicente, J. C., Duarte, J., Luís, J., Pinheiro, L., Lourenço, N., Diez, S., Rosas, F. M., Magalhães, V., Valadares, V., Zitellini, N., Mendes-Víctor, L., and MATESPRO Team (2009): Morphotectonics and Strain Partitioning at the Iberia-Africa plate boundary from multibeam and seismic reflection data. *Mar. Geol.,* 267: 156-174.

Tortella, D., Torne, M., and Pérez-Estaún, A. (1997): Geodynamic Evolution of the Eastern Segment of the Azores-Gibraltar Zone: The Gorringe Bank and the Gulf of Cadiz Region. *Mar. Geophys. Res.*, 19: 211–230.

Zitellini, N., Rovere, M., Terrinha, P., Chierici, F. and Matias, L. (2004): Neogene through quaternary tectonic reactivation of SW Iberian passive margin. *Pure Appl. Geophys.*, 161: 565-587.

Zitellini, N., Gràcia, E., Gutscher, M. A., Matias, L., Masson, D., Mulder, T., Terrinha, P., Somoza, L., de Alteriis, G., Henriet, J. P., Dañobeitia, J. J., Ramella, R., Pinto de Abreu, M. A. and Diez, S. (2009): The quest for the Iberia-Africa Plate boundary west of Gibraltar. *Earth Planet Sc. Lett.*, 280, 1-4: 13-50.

Marine Geology 271 (2010) 236–249

Contents lists available at ScienceDirect

Marine Geology

journal homepage: www.elsevier.com/locate/margeo

Crescent-shaped morphotectonic features in the Gulf of Cadiz (offshore SW Iberia)

J.C. Duarte [a,b,*], P. Terrinha [b], F.M. Rosas [a], V. Valadares [b], L.M. Pinheiro [c], L. Matias [d], V. Magalhães [c], C. Roque [b,e]

[a] LATTEX/IDL, Universidade de Lisboa, Departamento de Geologia da Faculdade de Ciências, Edifício C6, Piso 4, 1749-016 Lisboa, Portugal
[b] LNEG, Unidade de Geologia Marinha, Estrada da Portela Zambujal-Alfragide Apartado 7586, 2720-866 Amadora, Portugal
[c] Departamento de Geociências e CESAM, Universidade de Aveiro, Campus de Santiago, 3810-193, Aveiro, Portugal
[d] CGUL/IDL, Instituto D. Luíz, Campo Grande, Ed. C8, piso 3, 1749-016 Lisboa, Portugal
[e] EMEPC - Estrutura de Missão para a Extensão da Plataforma Continental. R. Costa Pinto, 165, 2770-047 Paço de Arcos, Portugal

ARTICLE INFO

Article history:
Received 31 July 2009
Received in revised form 11 February 2010
Accepted 15 February 2010
Available online 25 February 2010

Communicated by D.J.W. Piper

Keywords:
Gulf of Cadiz morphotectonics
deep sea crescent-shaped features
deep-water sedimentary processes
deep sea scouring

ABSTRACT

Multibeam swath bathymetry data from the Northwestern part of the Gulf of Cadiz revealed the existence of several intriguing kilometric crescentic depressions lying between −4300 m and −4700 m, never before reported to occur at such great depths. Morphological parameterization of these features, coupled with a detailed analysis of multi-channel and middle resolution seismic profiles, showed that these crescent-shaped features were formed due to the existence of specific time-recurrent interaction between: a) regional active thrusts, which portray the overall tectonic scenario in the area, and on top of which most crescentic depressions are carved; and b) tectonically induced scouring comprising localized erosion and simultaneous progradational sedimentation, produced by downslope currents of probable turbiditic origin. The obtained results also suggest a possible contribution of fluid migration and extrusion processes, such as mud volcanism and associated pockmark formation, besides gravity driven landslides and slumping, in the development of the studied crescentic depressions.

1. Introduction

1.1. Previous work

Crescent-shaped morphologies in association with escarpments are common in submarine and sub-aerial slope surfaces (e.g. sand dunes). They are frequently associated with gravitational mass transport (e.g. landslides and slumps) fluid escape and erosive processes. Landslides are typically bounded by arcuate concave-downhill head scarps and concave uphill toes (Locat and Lee, 2000; McAdoo et al., 2000; Wilson et al., 2004; Martel, 2004). Features caused by collapse processes associated with fluid escape and mud volcanism can also exhibit crescent-shaped morphologies (Dimitrov and Woodside, 2003; Somoza et al., 2003; León et al., 2006), as in the case of asymmetrical pockmarks when occurring on slopes (Hovland and Judd, 1988). Submarine crescent-shaped morphologies related to erosional processes, such as scouring, are also documented in various geological settings, and usually associated with turbidity, downslope and bottom currents: Faugères et al. (1997) reported the existence of erosion scours in the termination of the Barbados Prism, at depths of about 3000 m; Bulat and Long (2001) described a group of crescent-shaped scours in the Faroe–Shetland Channel with escarpments up to 200 m high, lying at depths of 200 m; Bonnel et al. (2005) described features in the Gulf of Lions formed by erosion-deposition processes associated with turbidity currents; Verdicchio and Trincardi (2006) reported a set of crescent-shaped features at depths of about 600 m with escarpments up to 50 m in the Southwest Adriactic Margin, formed by bottom currents; Fildani et al. (2006) recognized a group of crescent-shaped giant scours with escarpments up to 100 m height at depths of about 3500 m near Monterey East Channel.

In the North-eastern part of the Gulf of Cadiz, sub-circular seafloor features interpreted as asymmetrical pockmarks, slide scars and erosion scours, associated with mud volcanism, hydrocarbon seepage, mass wasting processes and bottom currents activity have also been described (e.g. Somoza et al., 2003; León et al., 2006; Hernández-Molina et al., 2006; Mulder et al., 2006; Hanquiez et al., 2007). However, unlike the ones discussed in this work, most of these features are located at relatively shallow depths, ranging from the outer continental shelf to the middle continental slope.

In the present paper we report the existence of submarine kilometric crescentic depressions at depths of more than 4000 m (between −4300 m and −4700 m). Based on recently acquired multibeam swath bathymetry data (Zitellini et al., 2009; Terrinha et al., 2009), coupled with the analysis of available multi-channel seismics (MCS) and middle

* Corresponding author. LATTEX/IDL, Universidade de Lisboa, Departamento de Geologia da Faculdade de Ciências, Edifício C6, Piso 4, 1749-016 Lisboa, Portugal. Tel.: +351 965543644.
E-mail address: joao_moedas@yahoo.com (J.C. Duarte).

0025-3227/$ – see front matter © 2010 Elsevier B.V. All rights reserved.
doi:10.1016/j.margeo.2010.02.017

resolution seismic profiles, we supply a detailed morphological description of these features, their internal sedimentary structure and their structural setting and discuss different processes that could have led to their formation.

1.2. General tectonic setting and geomorphology

The Gulf of Cadiz is located in the Atlantic Ocean offshore SW Iberia and NW Morocco (Fig. 1A and inset), comprising the easternmost segment of the Azores–Gibraltar Fracture Zone, which is interpreted as the Atlantic Africa–Eurasia main plate boundary (e.g. Purdy, 1975; Zitellini et al., 2009). The most important tectonic features presently observed in the Gulf of Cadiz (Fig. 1B) result from the Early Cenozoic to Late Miocene Alpine orogenesis overprinted onto pre-existent extensional basins of Triassic–Cretaceous age (Terrinha, 1998). This evolution is associated with the collision between Iberia and northwest Africa (Nubia) tectonic plates, which ultimately led to the formation of the Betic–Rif orogenic arc in Miocene times and the submarine accretionary wedge of the Gulf of Cadiz (e.g. Srivastava et al., 1990; Lonergan and White, 1997; Maldonado et al., 1999; Rosenbaum et al., 2002a, 2002b; Gutscher et al., 2002; Iribarren et al., 2007). Late Miocene to present tectonics is mainly determined by: a) oblique convergence between Nubia and Eurasia (Iberia) plates (Calais et al., 2003); and b) Eastward dipping subduction of an oceanic slab with development of the Gulf of Cadiz accretionary prism (Gutscher et al., 2002).

The overall morphological shaping of the Gulf of Cadiz results from the interaction between regional active tectonics, sedimentation and erosional processes, fluid migration and escape and oceanographic dynamics (Gutscher et al., 2002; Gutscher et al., 2009; Pinheiro et al., 2003; Somoza et al., 2003; Hernández-Molina et al., 2006; Terrinha et al., 2009). The form and geographic location of this region, enclosing in its easternmost domain the gateway to the Mediterranean Sea across the Straits of Gibraltar (Fig. 1), locally determines the behaviour of various major water masses, such as the North Atlantic Deep Water and particularly the Mediterranean Outflow Water — MOW (e.g. Ambar and Howe, 1979a,b; Llave et al., 2001; ; Johnson et al., 2002; Llave et al., 2006; Mulder et al., 2006; Hernández-Molina et al., 2006, 2008). A more detailed characterization of the Gulf of Cadiz allowed the recognition of the several main geomorphologic features depicted in Fig. 1A. The kilometric crescentic depressions targeted in this work are located in the so called Horseshoe Valley, offshore the SW Iberian margin (see Figs. 1A, 2, 3). This area displays a network of well developed submarine, canyons, gulleys and wide valleys, which are related to the channelling of downslope and turbidity currents, driving the sediments from the continental shelf and slope to the abyssal plain (Fig. 2B). Here, the impact of downslope processes on the shaping of the seafloor is clearly dominant. Moreover, this area is subjected to tectonic uplift (Terrinha et al., 2003, Gràcia et al., 2003), related to general north-westward thrusting in the Gulf of Cadiz, which favours erosion by valley inception as a response to higher slope and more abrupt morphology building (Zitellini et al., 2004, Terrinha et al., 2009).

2. Methodology and data

The discovery of the seafloor crescentic depressions described in this paper resulted from the analysis of two main sets of data: multibeam swath bathymetry and seismic reflection. The bathymetry data were used to characterize the geomorphology of the area where the crescentic depressions are situated and also to accomplish a detailed morphological parameterization of these features. The seismic reflection dataset comprises multi-channel and middle resolution seismics. The multi-channel seismics were used to unravel the general deep structure of the area where the crescentic depressions are located, whereas the analysis of higher resolution profiles aimed at a detailed characterization of the shallow structure and sedimentary architecture of these features.

2.1. Multibeam swath bathymetry data

The multibeam swath bathymetry dataset was acquired during the MATESPRO (Major TEctonic and Sedimentary PROcesses in the Portuguese Margins — see Figs. 2, 4) cruise, onboard the Portuguese vessel *NRP D. Carlos I* in June/July 2004 (Terrinha et al., 2009). The cruise covered a total area of approximately 38 000 km^2 in the northwestern part of the Gulf of Cadiz region. The bathymetric data were acquired using a hull-mounted Simrad EM120 multibeam echosounder, fulfilling the rules established by the International Hydrographic Organization for an order 3 hydrographic survey (see Terrinha et al., 2009). Interpretation was made using terrain analysis techniques and image analysis of the bathymetry using commercial software, ArcGIS and Fledermaus.

2.2. Seismic reflection data

Multi-channel seismic profiles of the Iberian Atlantic Margin campaign (Banda, E., M. Torné and I. A. M. Group, 1995; Tortella et al., 1997) were used for the inspection of the deep structure. Two single-channel seismic profiles were acquired (PSAT-244 and 246) during the 14th Training-Through-Research cruise of UNESCO –IOC, Leg 1, onboard of the Russian vessel *RV Professor Logachev* in July/August 2004 (Fig. 3; Kenyon et al., 2006), in the scope of the MVSEIS Euromargins Project. The MCS has a vertical resolution between 20 and 50 m and the single channel have a vertical resolution of about 2 to 5 m.

3. Morphotectonic characterization of the crescentic depressions

3.1. Morphotectonic setting: the Horseshoe Valley

The Horseshoe Valley, together with the S. Vincent canyon, is one of the two collectors of the shelf and slope erosive system of southwest Iberia that converge into the Horseshoe Abyssal Plain. The studied crescentic depressions are located in the Horseshoe Valley (HV) (Figs. 2, 3) that collects the Aljezur, Portimão, Lagos and Faro Canyons, the Portimão and the Cadiz Valley. The HV has a trapezoidal shape with depths varying between −4200 m to −4800 m and a mean slope of 0.5º to the west.

The HV is delimited by the Sagres Plateau in the North, by the Coral Patch Ridge in the South, and by the deformation front of the Gulf of Cadiz accretionary wedge in the East (Figs. 2A,C, 3). To the West, the HV is bounded by the NE–SW trending Horseshoe Fault, which corresponds to a westward directed active thrust (Gràcia et al., 2003, Zitellini et al., 2004), whose morphologic expression is marked by a hundred meter high scarp separating this domain from the westward adjacent Horseshoe Abyssal Plain (see Figs. 1B, 2C). The drainage system finds its way across the Horseshoe Fault scarp along narrows gullies that are the loci of retreating erosion showing evidences of landslide occurrence (Fig. 2).

The flat area of the Horseshoe Valley is thus interpreted as being uplifted on the hanging wall of the deep seated Horseshoe Fault (e.g. Tortella et al., 1997; Zitellini et al., 2004; Terrinha et al., 2009). This area is also affected by several major WNW–ESE trending lineaments, the SWIM lineaments (Figs. 1B, 3B), which were recently interpreted as aligned arrays of also deep seated, sub-vertical, dextral strike–slip faults (Terrinha et al., 2009; Rosas et al., 2009; Zitellini et al., 2009). The transitional area from the Sagres Valley to the Horseshoe Valley displays an undulated seafloor surface comprising waves varying from hundreds of meters to more than 10 km in length, and up to 5 km across (white arrows in Fig. 3). These features are generally straight to slightly sinuous, and their undulated surfaces have also been previously interpreted as the bathymetric expression of mass

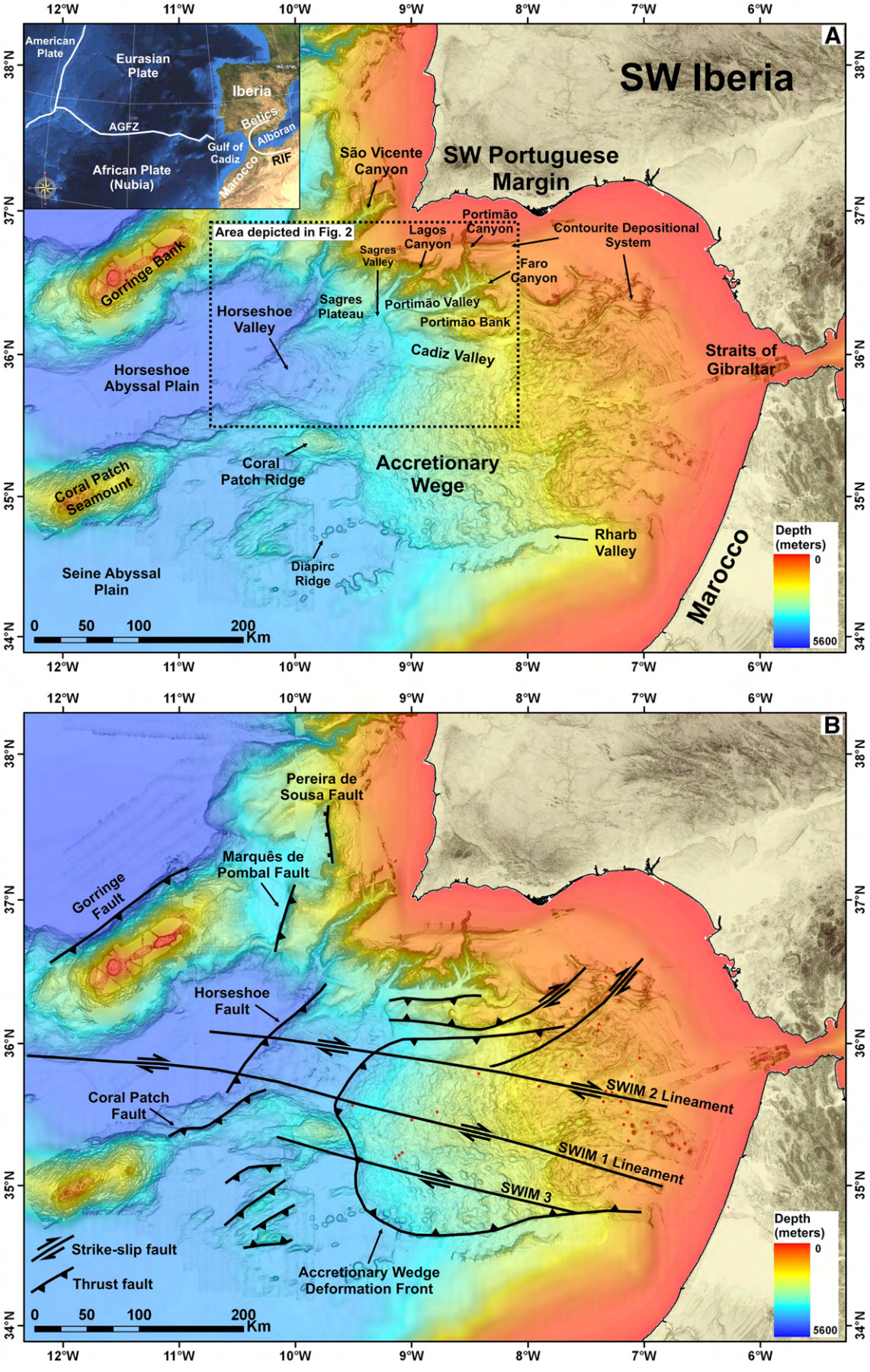
A
SW Iberia
American Plate
Eurasian Plate
Iberia
Betics
Alboran
AGFZ
Gulf of Cadiz
RIF
Marocco
African Plate (Nubia)
São Vicente Canyon
SW Portuguese Margin
Portimão Canyon
Lagos Canyon
Contourite Depositional System
Area depicted in Fig. 2
Sagres Valley
Faro Canyon
Gorringe Bank
Sagres Plateau
Portimão Valley
Portimão Bank
Horseshoe Valley
Cadiz Valley
Straits of Gibraltar
Horseshoe Abyssal Plain
Coral Patch Seamount
Coral Patch Ridge
Accretionary Wege
Rharb Valley
Diapirc Ridge
Seine Abyssal Plain
Marocco
Depth (meters)
0
5600
0 50 100 200 Km
12°W 11°W 10°W 9°W 8°W 7°W 6°W
38°N 37°N 36°N 35°N 34°N
B
Pereira de Sousa Fault
Marquês de Pombal Fault
Gorringe Fault
Horseshoe Fault
Coral Patch Fault
SWIM 2 Lineament
SWIM 1 Lineament
SWIM 3
Strike-slip fault
Thrust fault
Accretionary Wedge Deformation Front
Depth (meters)
0
5600
0 50 100 200 Km
12°W 11°W 10°W 9°W 8°W 7°W 6°W
38°N 37°N 36°N 35°N 34°N

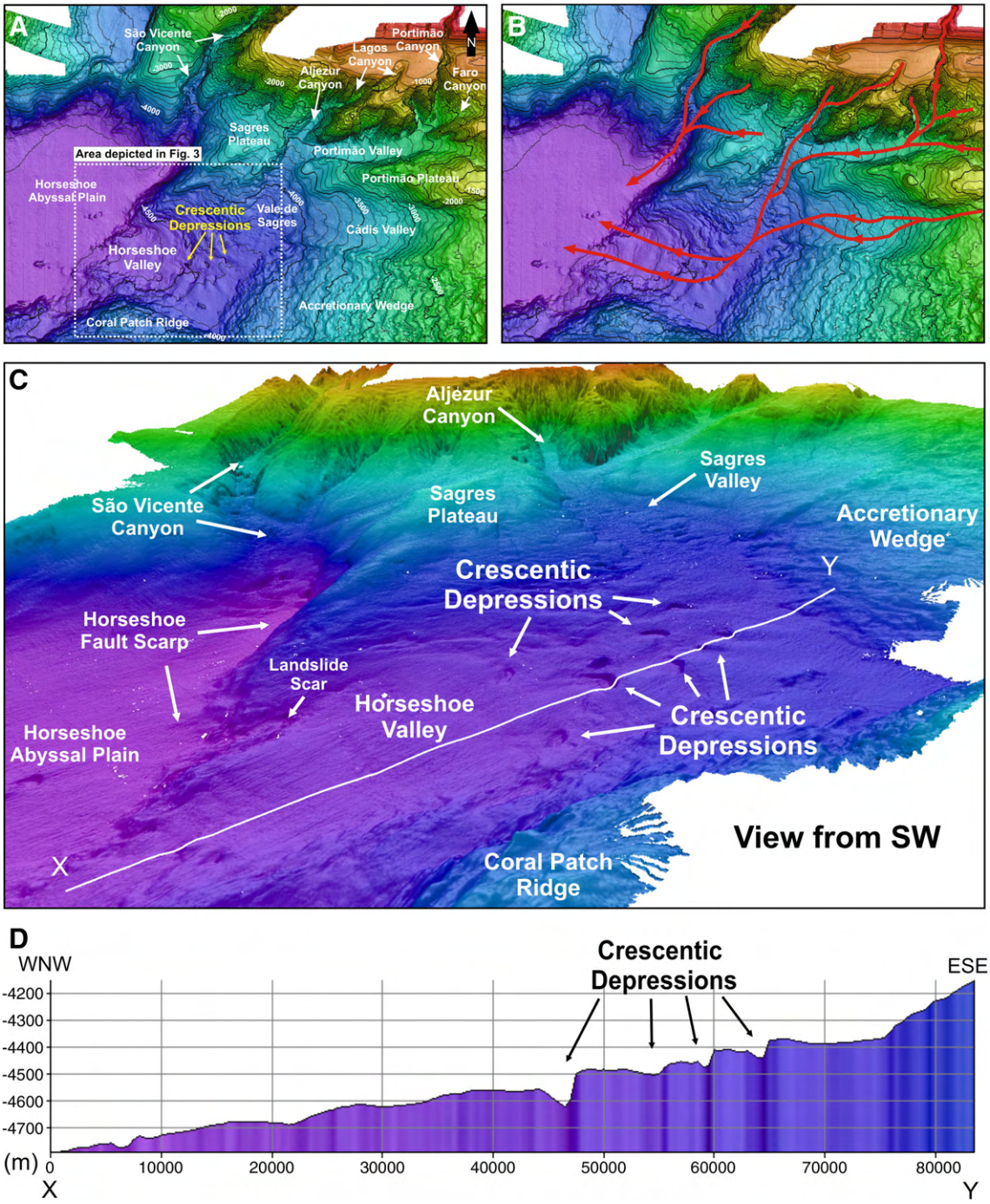

Fig. 2. (A) Location of the studied crescentic depressions offshore SW Iberian Margin (3D digital bathymetry model from MATESPRO dataset, Terrinha et al., 2009); (B) general drainage system of the local continental shelf and slope (after Duarte, 2007); (C) perspective view (from SW) of the Horseshoe Valley and surrounding main morphotectonic features; (D) WNW–ESE bathymetric profile along the Horseshoe Valley intersecting the crescentic depressions (vertical exaggeration factor of 8).

transport processes and soft sediment deformation, including gravity driven folds, small scale slumps and turbiditic erosional/deposition features (Terrinha et al., 2009).

Despite the shallow dip of the Horseshoe Valley, a thorough analysis of its bathymetry allowed the identification of slope breaks, separating a staircase-like series of flats, descending in the direction of the Horseshoe Abyssal Plain (Fig. 3). Some of these scarps correspond to NE–SW trending folds sitting on top of westwards directed blind thrusts as described elsewhere in this work. The crescentic depressions reported in this work are located on these slope breaks (Figs. 3, 4).

3.2. Geometry of the Horseshoe Valley crescentic depressions

The study objects of this work are the crescentic depressions that are located strictly within the HV only. This is because, *firstly*, they bear no obvious association with gravity or mass transport

Fig. 1. (A) Gulf of Cadiz main geomorphologic features. Inset: location of the Gulf of Cadiz area in the general tectonic setting of the Eurasia (Iberia)–Africa (Nubia) plate boundary (AGFZ — Azores-Gibraltar Fracture Zone); (B) simplified tectonic map of the Gulf of Cadiz area. Offshore bathymetry from SWIM Compilation (Zitellini et al., 2009) completed with GEBCO (2003). SWIM lineaments correspond to aligned arrays of deep seated, sub-vertical, dextral strike–slip faults (op. cit.). Red dots correspond to mud volcanoes (Hensen et al., 2007).

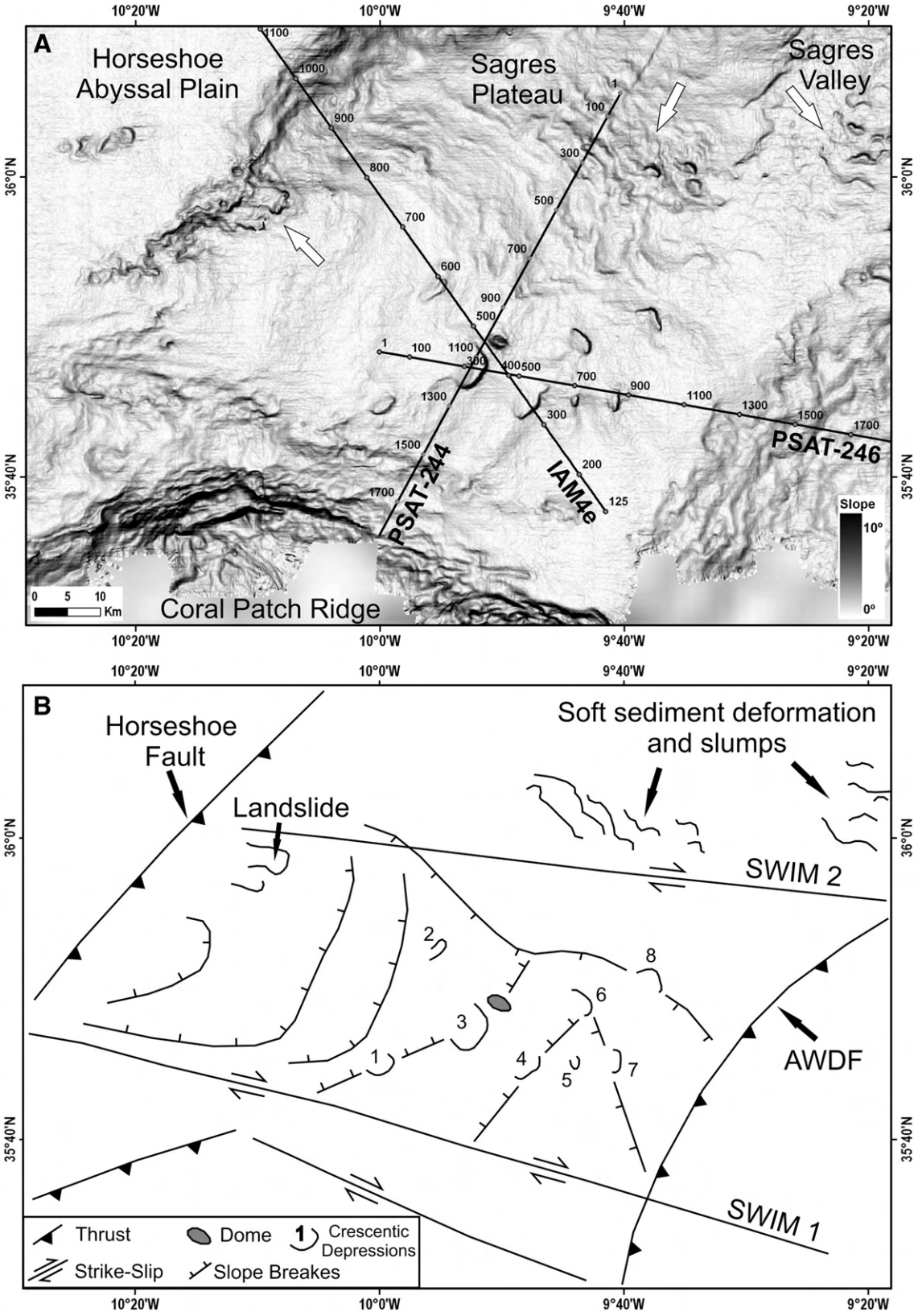

Fig. 3. (A) Bathymetry and slope map of the Horseshoe Valley. Location of the seismic profiles IAM-4e, PSAT-244 and PSAT-246; white arrows refer to the location of undulated seafloor features, e.g. slumps and landslides. (B) Line drawing depicting the interpretation of the main morphotectonic features observed and the numbering of the study crescentic depressions.

processes as others in the Gulf of Cadiz, like the ones located further north on the slope of the Sagres plateau (see Fig. 3), *secondly*, they cluster within the shallow dipping channel (HV mean dip is 0.5° and the maximum local dip is 3°) that collects the drainage system already mentioned, *thirdly*, they are located between two main tectonic structures, the Horseshoe Fault and the accretionary

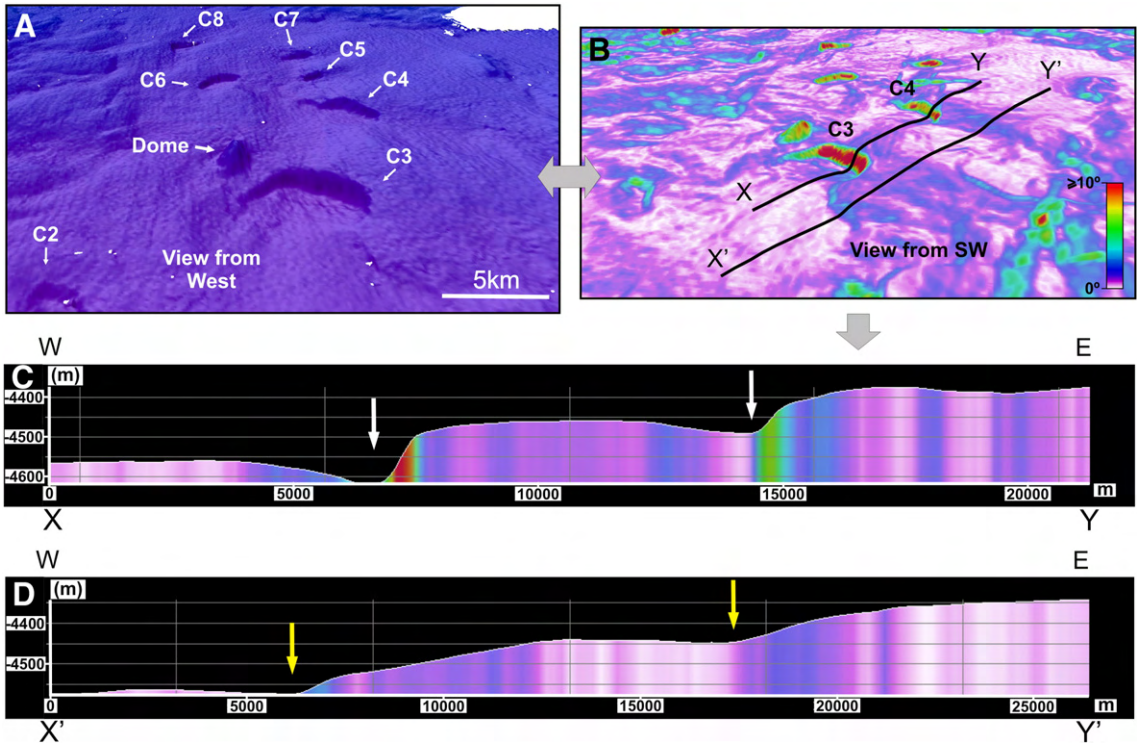

Fig. 4. 3D imaging of the Horseshoe Valley domain comprising the study crescentic depressions (digital bathymetry model from MATESPRO dataset, vertical exaggeration factor of 8): (A) general view from West of crescentic depressions C2 to C8; (B) depiction of slope value distribution in the study area (SW view); (C) bathymetric profile *X*–*Y* intersecting two slope breaks corresponding to the depressions 3 and 4 (white arrows), illustrating the striking contrast between the smooth dip of the Horseshoe Valley seafloor and the abruptness of the crescentic escarpments; (D) parallel bathymetric profile *X*′–*Y*′ that does not cut across the crescentic depressions, depicting the existence of smoother slope breaks in the Horseshoe Valley seafloor (yellow arrows).

wedge and, *fourthly*, they are probably the deepest crescent shapes described in the scientific literature, between −4300 m and −4700 m.

The crescentic depressions exhibit a morphology consisting of downslope concave crescent-shaped escarpments surrounding an internal depression with kilometric lengths (Figs. 4, 5A). Morphological parameters were used to describe eight crescentic depressions in the HV, as depicted in Fig. 5B and in Table 1.

3.2.1. Height and slope of the crescentic depression scarps

The height and slope of the crescent-shaped escarpments can be seen as expressing the degree of abruptness (or steepness) of these features. The measured data (Table 1) show a mean slope value of approximately 0.2 (~11° dip), with the exception of crescentic depression 5 in which the escarpment exhibits a higher slope of 0.51 (~27° dip). The escarpment heights vary mostly between 80 m and 120 m, with the exceptions of depressions 1 and 2, which show heights of 50 m and 30 m respectively. Based on these data (slope and height) no consistent relationship can be drawn between the variation of the abruptness of the individual crescentic depressions and their location in the HV. In fact, the data shows that some constancy exists in the steepness of the escarpment crescents regardless of their different locations, shapes and sizes. The roughly linear relationship between height and width suggests that the steepness might depend on material properties, such as cohesion or plastic yield point, for the cases of loose materials like sand or clays, respectively.

3.2.2. Crescentic depression axial ratio — a

The internal depressions of the studied features exhibit widths and lengths (parameters CW and CL as defined in Fig. 5A — inset, and B) that vary from 500 m to 2500 m, and between 750 and 5000 m, respectively (Table 1). The axial ratio of the crescentic depressions is here defined as:

$$a = \frac{CL/2}{CW}$$

Parameter *a* equals 1 when the general overall shape of the depression approximates a semi-circumference. If depressions show semi-elliptical shapes, *a* is either > 1, when CL/2 > CW as is generally the case, or *a* < 1, when CL/2 < CW.

Similarly to what was referred above for height and slope, no coherent/linear relationship exists between *a* and the individual location of the crescentic depressions in the Horseshoe Valley. Moreover, it is also clear from the graphic in Fig. 5D that with the exception of feature 2, all samples plot at values of $a \geq 1$, meaning that crescentic depressions tend to develop similar shapes in spite of their different locations.

In Fig. 5E, the relationship between the slope and the axial ratio is graphically illustrated. Because the slope values are constant (between ~0.1 and ~0.25, see Fig. 5C), all samples but feature 5 cluster under constant slope of ~0.25 and it is clear that the crescentic depressions cluster in three groups as a function of their different values of *a*. The first group (Group 1 in Fig. 5E) consists of feature 2 only, which exhibits a singular low *a* value, implying an extreme concavity, and a highly elongated geometry parallel to the direction of its longest CW axis (see Figs. 3B, 4, 5A). Group 2 includes 5 of the 8 crescentic depressions with *a* values comprised between 1.0 and 1.5 (mean *a* value of ~1.23). Finally, the third group comprises crescentic depressions 4 and 7 with relatively high *a* values of 2.5, implying highly elongated semi-elliptical shapes.

It should be noted that with the exception of crescentic depressions 2 and 5, which show anomalous values of axial ratio and slope, all the crescentic escarpments are oriented parallel to the direction of the large scale slope breaks that disrupt the Horseshoe Valley seafloor (see Figs. 3, 4).

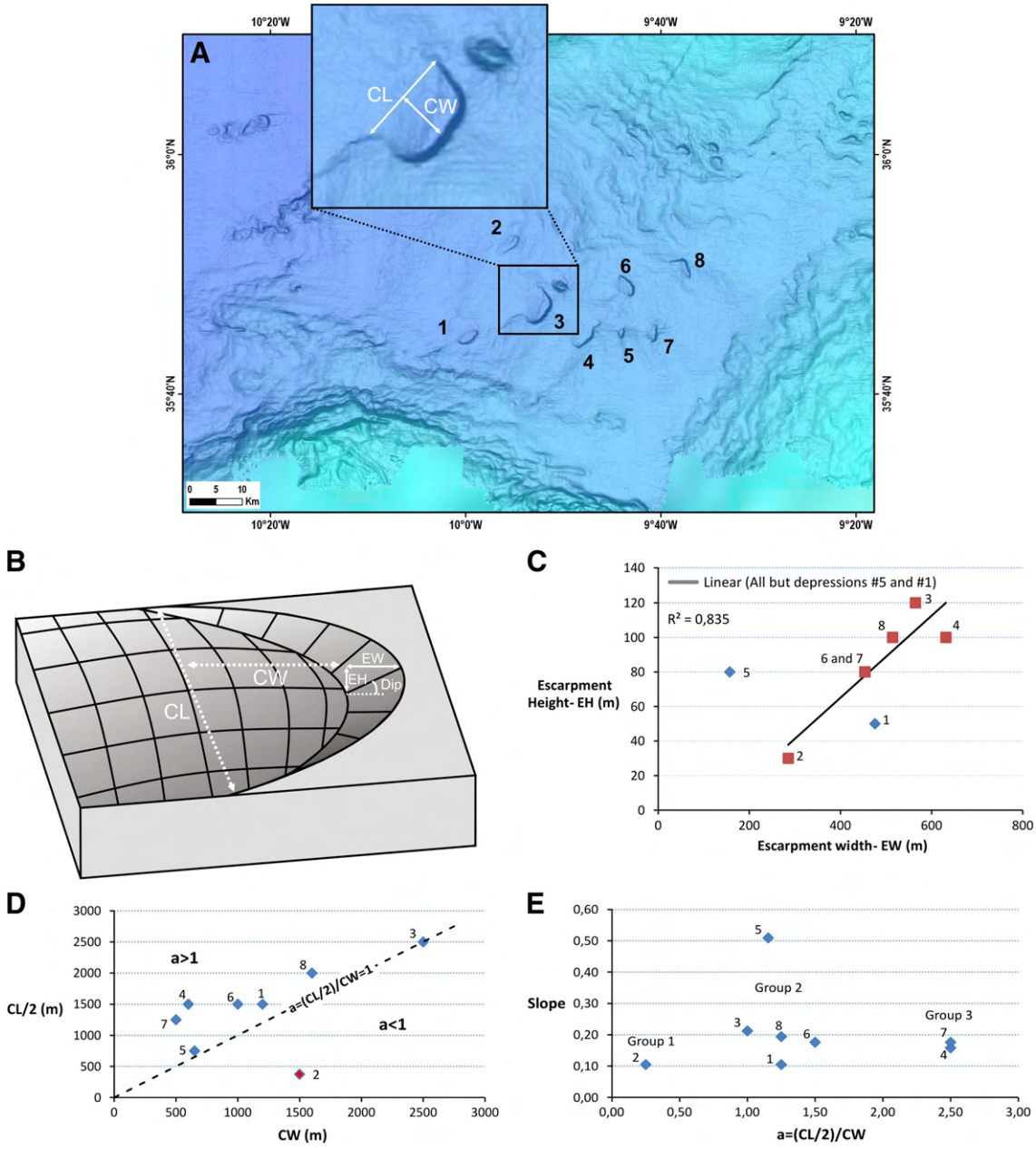

Fig. 5. Morphological parameterization of the studied crescentic depressions. (A) Location of the crescentic depressions in the Horseshoe Valley (1 to 8), and zoom of depressions 3; (B) — 3D sketch of a crescentic depressions illustrating the used morphological parameters: CL — crescentic depression length; CW — crescentic depression width; EW — escarpment width; EH — escarpment height; (C) graphic display of measured values of EH versus EW (escarpment slope) for all the studied features; (D) graphic display of CL/2 versus CW (parameter *a*) for the studied features (dashed line corresponds to CL/2 = CW); and (E) graphic display of obtained values of slope versus *a* parameter for all crescentic depressions. See further explanation in the text. R^2 — squared linear correlation coefficient.

3.3. Sedimentary and tectonic structure of the crescentic depressions

The description of the detailed structural architecture of the crescentic depressions was based on the interpretation of multi-channel (IAM4e, Fig. 6) and middle resolution seismic profiles (PSAT246 and PSAT 244, Figs. 7, 8).

3.3.1. Multi-channel seismic profile IAM4e

The IAM4e profile strikes NW–SE along the Horseshoe Valley intersecting crescentic depressions 2 and 4 and passing close to number 3 (see Figs. 6, 3 for the location of the profile). It comprises the following seismostratigraphic units and sub-units:

a) A basal unit (A) of coherent high amplitude, continuous and parallel reflections, with a thickness of about 2 s (twt), corresponding to Mesozoic through Eocene rocks (Tortella et al., 1997). This unit is cut by several reverse faults that also affect the overlying units, but do not breach out at the seafloor surface. The exception to this is the Horseshoe Fault, which cuts through all the cover units offsetting them by approximately 1 s (twt).

b) Unit B is approximately ~1.5 s (twt) thick, has a semi-chaotic seismic signature, characterized by high amplitude shallow dipping discontinuous seismic reflections with continuous eastwards dipping reflections. The latter can be continuously followed for more than 10 km and have been interpreted by various authors as thrust imbricate of middle Miocene age, and olistostromes deposits (Torelli et al., 1997; Tortella et al., 1997), that detach at the sole of Unit B (Fig. 6). Some of these thrusts were reactivated as blind thrusts in Pliocene–Quaternary times because they deform the sediments of this age that are included in Unit C. The deformation caused by the blind thrusts is accommodated by the

Table 1
Measured morphological parameters.

Crescentic depressions (see Fig. 5)	Escarpment height — EH (m)	Escarpment width — EW (m)	Dip (°)	Slope	Crescentic depressions length — CL (m)	CL/2 (m)	Crescentic depressions width — CW (m)	Axial ratio $a = (CL/2)/CW$
1	50	476	6	0.11	3000	1500	1200	1.25
2	30	285	6	0.11	750	375	1500	0.25
3	120	565	12	0.21	5000	2500	2500	1.00
4	100	631	9	0.16	3000	1500	600	2.50
5	80	157	27	0.51	1500	750	650	1.15
6	80	454	10	0.18	3000	1500	1000	1.50
7	80	454	10	0.18	2500	1250	500	2.50
8	100	514	11	0.19	4000	2000	1600	1.25
Mean values	80	442	11.38	0.20	2843.75	1421.88	1193.75	1.43

top Unit C by folds that account for the stepped morphology of the HV. The majority of the crescentic depressions are located along these folds, carved in their slope breaks that disrupt the Horseshoe Valley seafloor (see Figs. 3, 4, 6).

c) A top Unit C of ~0.5 s (twt) of thickness, generally characterized by very well imaged parallel reflections, corresponding to a hemipelagic sedimentary cover that accordingly with Tortella et al. (1997) comprises two seismostratigraphic sub-units of different age (SU1 and SU2 in Fig. 6):
   — A Late Miocene sub-unit (SU1) that exhibits a thickness varying between 0.1 s to 0.3 s (twt), consisting of high amplitude, high frequency, coherent reflections with onlap and downlap terminations on top of a folded and faulted basal discontinuity, which separates SU1 from the underlying lower to middle Miocene unit;
   — An Pliocene–Quaternary sub-unit (SU2) with a fairly constant thickness of about 0.2 s (twt), consisting of a sequence of high amplitude reflections, although less coherent than those of SU1, showing a parallel to prograding geometry, with downlap and onlap terminations.

In the IAM4e profile a dome-like structure at the top of Unit B can be seen around shot point 460 (Fig. 6). This dome is seemingly impinging the uppermost cover unit, reaching the seafloor surface and producing a bathymetric ellipsoidal ridge in the vicinity of crescentic

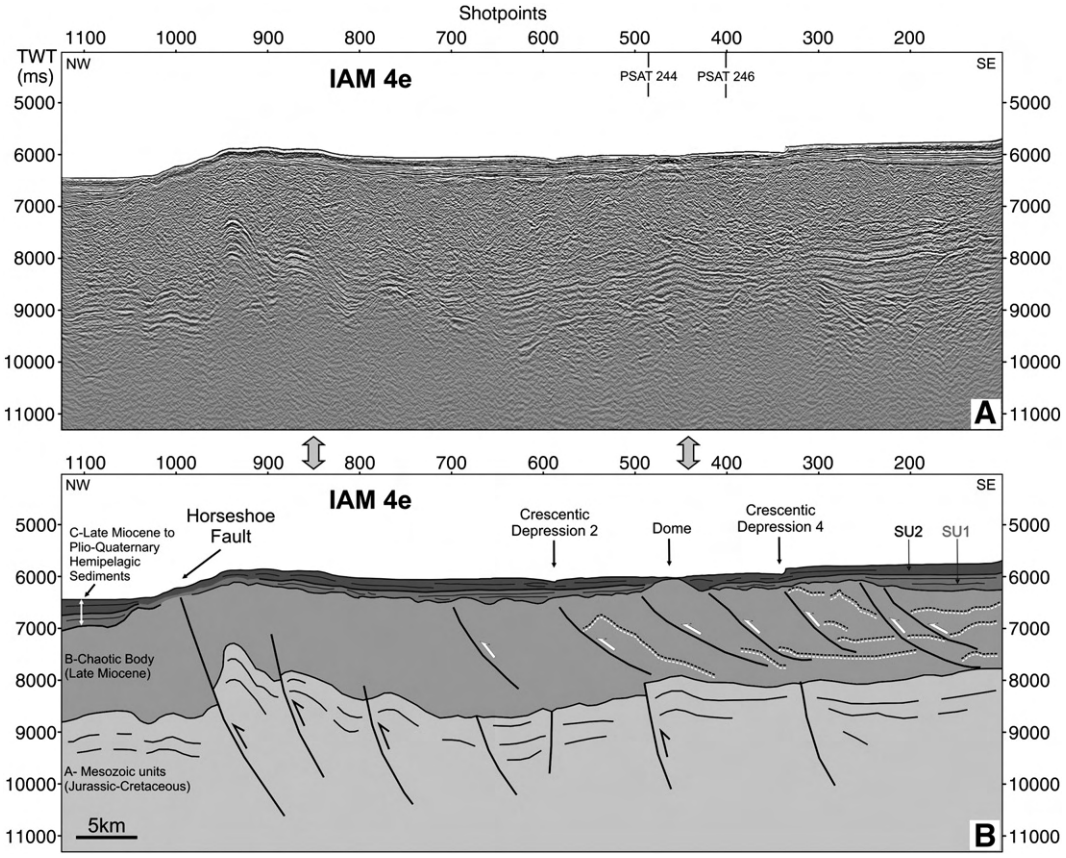

Fig. 6. (A) Multi-channel seismic profile IAM-4e intersecting crescenting depressions 2 and 4 (see Fig. 3 for location); and (B) correspondent seismostratigraphic and tectonic interpretation. Thin black lines — seismic reflectors interpreted as stratigraphic horizons; double-dashed black and white lines — intra-chaotic body reflections interpreted as decollement horizons and folded layered sediments. Note that crescentic depressions 2 and 4 are located on top of blind thrusts rooted in the sole of the chaotic body. SU1 and SU2 — Late Miocene to Plio-Quaternary sub-units.

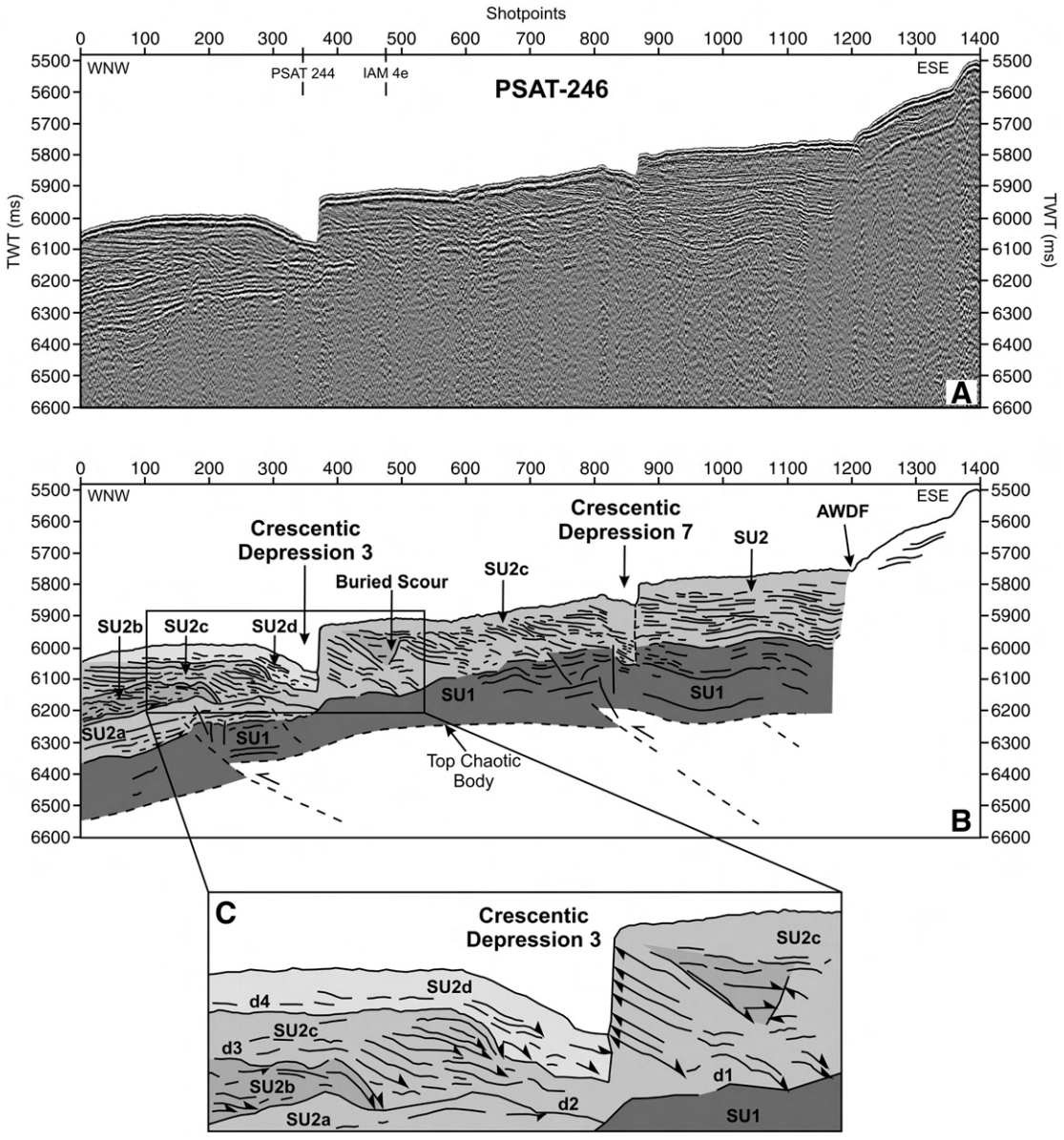

Fig. 7. (A) PSAT-246 seismic profile, intersecting the Accretionary Wedge Deformation Front (AWDF), and crescentic depressions 3 and 7 (see Fig. 3 for location); and (B) simplified seismostratigraphic/structural interpretation. SU1 and SU2 — Late Miocene to Plio-Quaternary sub-units; SU2a–d — Progradational bodies (lobes); d1-4 — stratigraphic discontinuities.

depression 3, clearly seen in the bathymetry (see Figs. 3, 4). This dome shows a WNW–ESE elongation and a maximum high of 100 m.

Crescentic depressions 2 and 4 incise the sub-unit SU2 as imaged at shot points 587 and 340 in the IAM4e profile (Fig. 6). These crescentic depressions are located on top of hanging wall anticlines of upward propagating blind thrusts that are well recognized in Unit B. Despite the low resolution of this multi-channel seismic reflection profile it is clear that the escarpment of depression 4 corresponds to an erosional surface, since it truncates the uppermost seismic horizons. An upward convex geometry of the internal part of the depression is also detectable at this resolution and is imaged at a higher resolution in Fig. 7.

3.3.2. Middle resolution seismic profiles (PSAT-246 and PSAT-244)

The detailed structure of the crescentic depression could only be comprehensively addressed through the examination of the higher resolution seismic profiles PSAT-246 and PSAT-244 specifically acquired for this purpose. The attenuation of acoustic energy by the water column of 4 km and sediments did not allow imaging below stratigraphic Unit C, to a maximum of circa 0.5 s (twt). The base of Unit C was cross checked with IAM4e seismic profile.

The WNW–ESE oriented PSAT-246 profile cuts across crescentic depressions 3 and 7 (Figs. 7, 3 for location). In its eastern part, between the Accretionary Wedge Deformation Front (AWDF) and depression 7, the lower SU1 sub-unit shows a succession of coherent reflectors with parallel, gently folded configuration (Fig. 7). The continuation of this unit to the West of depression 7 is not clear, and it was only interpretatively assumed by correlation with the slightly oblique (NW–SE) IAM4e profile (see Fig. 3). The sub-unit SU2 is recognizable along the whole of the WNW–ESE profile length. Between the AWDF and crescentic depression 7, the reflectors in this sub-unit also exhibit a slightly folded configuration, but this is attenuated towards the surface, where the reflections are almost horizontal (Fig. 7). Close to crescentic depressions 7 and 3, to the West of each of their escarpments, sub-unit SU2 consists of several individual uphill progradation bodies. This, together with the truncation of sub-unit SU2 horizons behind the crescent-shaped scarps suggests uphill progradation of the sedimentary infill simultaneous with escarpment retreat (Fig. 7B). In the internal part of depression 3 several progradation bodies are buried (SU2a, SU2b

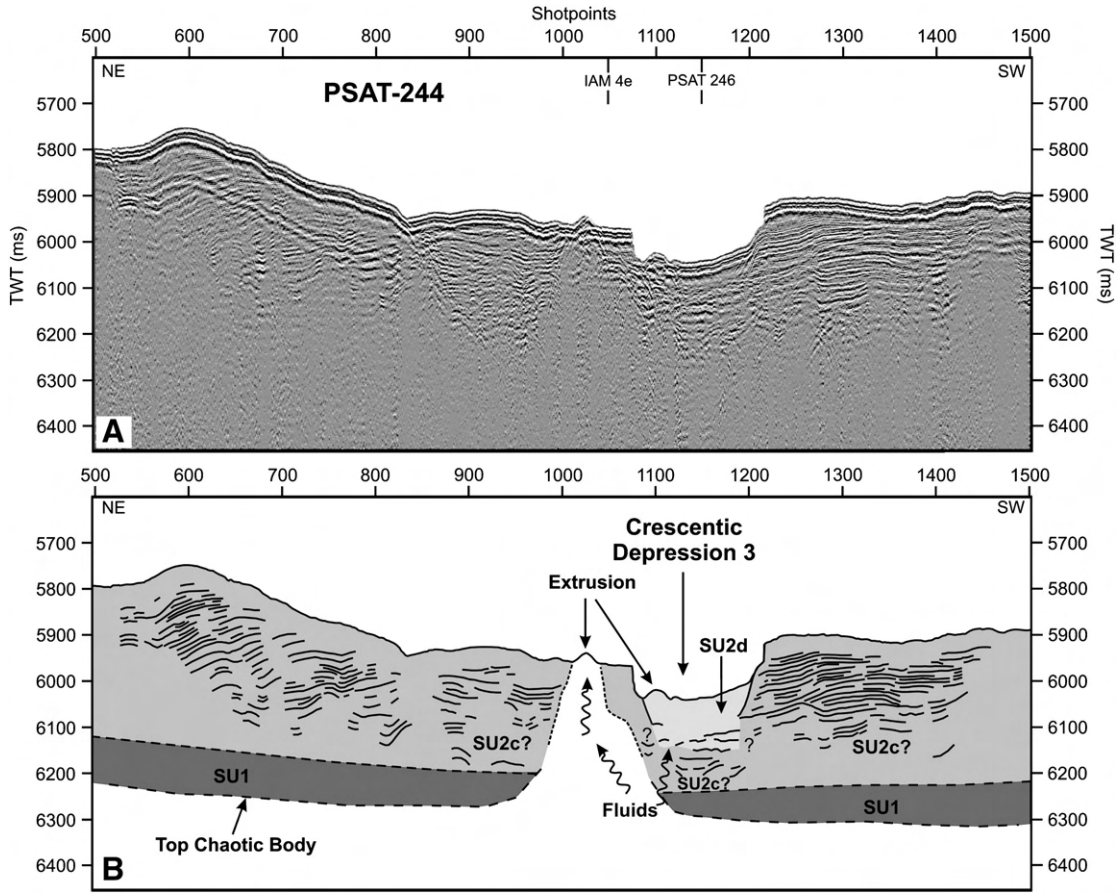

Fig. 8. (A) PSAT-244 seismic profile intersecting crescentic depression 3 (see Fig. 3 for location); and (B) simplified seismostratigraphic interpretation. Note the dome-like structure related with fluid migration and extrusion processes in the vicinity of the crescentic depression.

and SU2c — Fig. 7C), separated by planar discontinuities (d2, d3 and d4, respectively) matching erosive truncations, against which the reflectors often exhibit onlap and downlap terminations.

The NE–SW oriented PSAT-244 profile intersects the internal part of crescentic depression 3, thus providing a strike-section of the prograding internal bodies and sections across the tip points of the depressions scarp (Figs. 3, 8). It is also possible to observe the dome-like structure (shot points 1026 in PSAT-244 and 460 in IAM4e, Figs. 6, 8, respectively) underlain by a seismically transparent zone, the origin of which is unknown. Considering the widespread existence of mud volcanoes and salt diapirs with morphological expression on the seafloor in the Gulf of Cadiz, it is hypothesized that this dome could correspond to a fluid escape structure as well.

4. Discussion

The morphologic parameters of the studied crescentic depressions determined above (Section 3.2), specifically slope and axial ratio (a), show that both their general shape and the steepness of their escarpments are independent of their location along the westwards smoothly dipping Horseshoe Valley, whose general morphology is most probably essentially related with the collection and transport of sediments from the shallower northern and northeastern domains of the Gulf of Cadiz (continental shelf and slope, see Figs. 1A, 2B). This suggests a similar fundamental origin for these features, associated with natural processes other than only, or predominantly, the varying smooth slope of the Horseshoe Valley as a whole.

4.1. Active tectonics

The studied features consist of crescent-shaped erosional depressions carved in seafloor slope breaks (see Figs. 3, 4) that correspond to the morphologic expression of blind thrusts, as shown in Fig. 6. The interpretation of the middle resolution seismic profiles (Fig. 7) also showed that the sedimentary units deposited within the crescentic depressions, and the external ones eroded by the retreating scarp (SU2 in Fig. 7C), are of the same age at the considered timescale. This scenario is compellingly indicative of the control exerted by present day active thrusting in the formation and localization of the crescentic depressions.

4.2. Hypothetic hydrodynamic models

In the present situation, hydrodynamic models can only be discussed hypothetically, given the fact that the detailed deep-water circulation in the Gulf of Cadiz, and particular in the Horseshoe Valley, is still fundamentally unknown. The progradational architecture of the sedimentary lobes (Section 3.3.2) is indicative of upslope deposition towards the internal part of the crescentic depressions, coeval with upslope erosion of their scarps. This requires the existence of deep water currents, which would be responsible for simultaneous localized erosion and sedimentation. Such specific dynamics of interaction between a flow current and a pre-existent morphology has previously been described worldwide by several authors, although at shallower depths (Stow et al., 2002a,b; Verdicchio and Trincardi, 2006; Bulat and Long, 2001; Fildani et al., 2006; Normark et al., 2009).

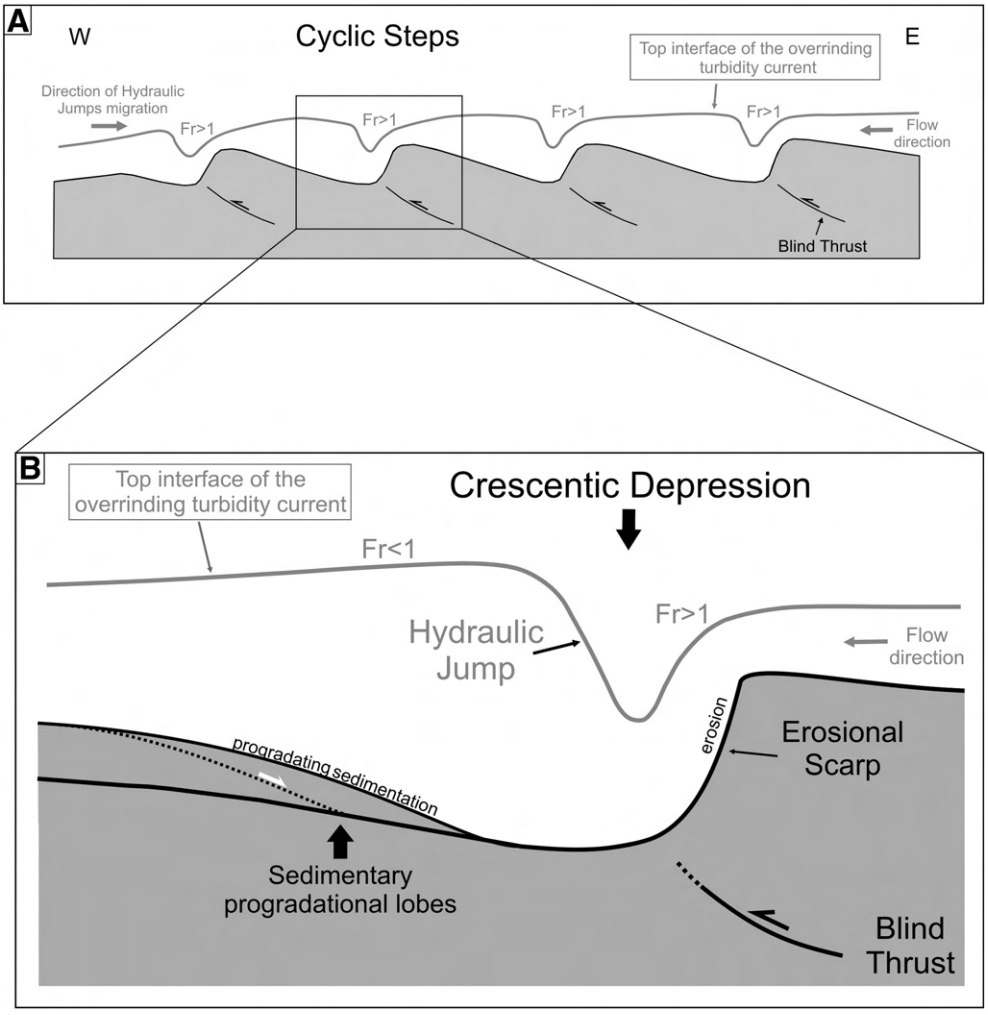

Fig. 9. Hypothetical adaptation of the conceptual model of cyclic steps (as proposed by Fildani et al., 2006) to the studied crescentic depressions in the Horseshoe Valley. (A) Schematic illustration of the formation of cyclic steps by a net-erosional turbidity current (adapted from op. cit.). Fr — Froude number; and (B) zoomed individual crescentic depression: sketch illustration of a hydraulic jump depicting progradational sedimentation downstream (Fr<1) and simultaneous erosion upstream (Fr>1).

4.2.1. Bottom currents

In this case, the observed erosional scarps and upslope progradational bodies could hypothetically be both generated by the lateral movement of a bottom current, such as the North Atlantic Deep Water, parallel to the tectonically originated slope breaks. However, this interaction would preferably cause the formation of more linear erosive and depositional features, similarly to mounded, elongated and separated drifts (Faugères et al., 1999; Rebesco and Stow, 2001; García et al., 2009), rather than confined crescentic depressions.

Alternatively, the crescentic depressions could also be generated by the action of vertical eddies associated to this same type of current, at least by two different mechanisms (e.g. Hernández-Molina et al., 2008): i) the influence of energetic Meddies in the base of the Mediterranean Outflow Water, which could propagate to the seafloor; and ii) due to the local interaction of different water masses with similar densities. Accordingly, vertical eddy movement could generate erosional/depositional seafloor features, characterized by less linear, i.e. more equidimensional, morphologies (Hernández-Molina et al., 2008). An objection to this, is the fact that even the more equidimensional features generated by vertical eddies would probably tend to display a random localization in the HV and have a subcircular (or semi-circular) geometry, rather than corresponding to sets of crescentic depressions with scarps systematically orientated downslope located on morphologic steps of the seafloor, as observed in the present case. In addition, this mechanism also does not provide a clear explanation for the formation of the observed upslope sedimentary bodies.

Another possibility corresponds to admit that the crescentic scarps could represent the scars of major landslides triggered by tectonic events, which would later be reworked and filled in with sediments by the action of bottom currents, in a similar manner to the formation of the "infill drifts" (Rebesco and Stow, 2001).

4.2.2. Turbidity currents

The existence of erosive crescentic scarps consistently oriented downslope along the Horseshoe Valley main drainage axis (see

Fig. 10. Schematic representation of the main succeeding events envisaged as leading to the formation of the crescentic depressions in the Horseshoe Valley seafloor. (A) Initial stage representing an original smooth surface in the Horseshoe Valley and an underlying inactive (inherited) blind thrust; (B) first blind thrust reactivation event creates an abrupt slope break and triggers coeval scouring and sedimentation associated to an hydraulic jump; inset: crescent-shaped landslide scar could be responsible for channelling and localization of turbidity currents; (C) evolution of a retreating escarpment and simultaneous sedimentation with the formation of the progradational body SU_n; and (D) eventual complete smoothing of the surface stepping morphology, as a consequence of simultaneous sedimentation and erosion. Note preservation of a buried (paleo) slope break marked by surface d_n, underlying SU_n. (E) Second blind thrust reactivation and resetting of the cycle, with retriggering of scouring implying erosion of the previously formed SU_n sub-unit, and simultaneous aggradation leading to Su_{n+1} formation. Comparison with the geometric configuration deduced from the PSAT246 seismic profile.

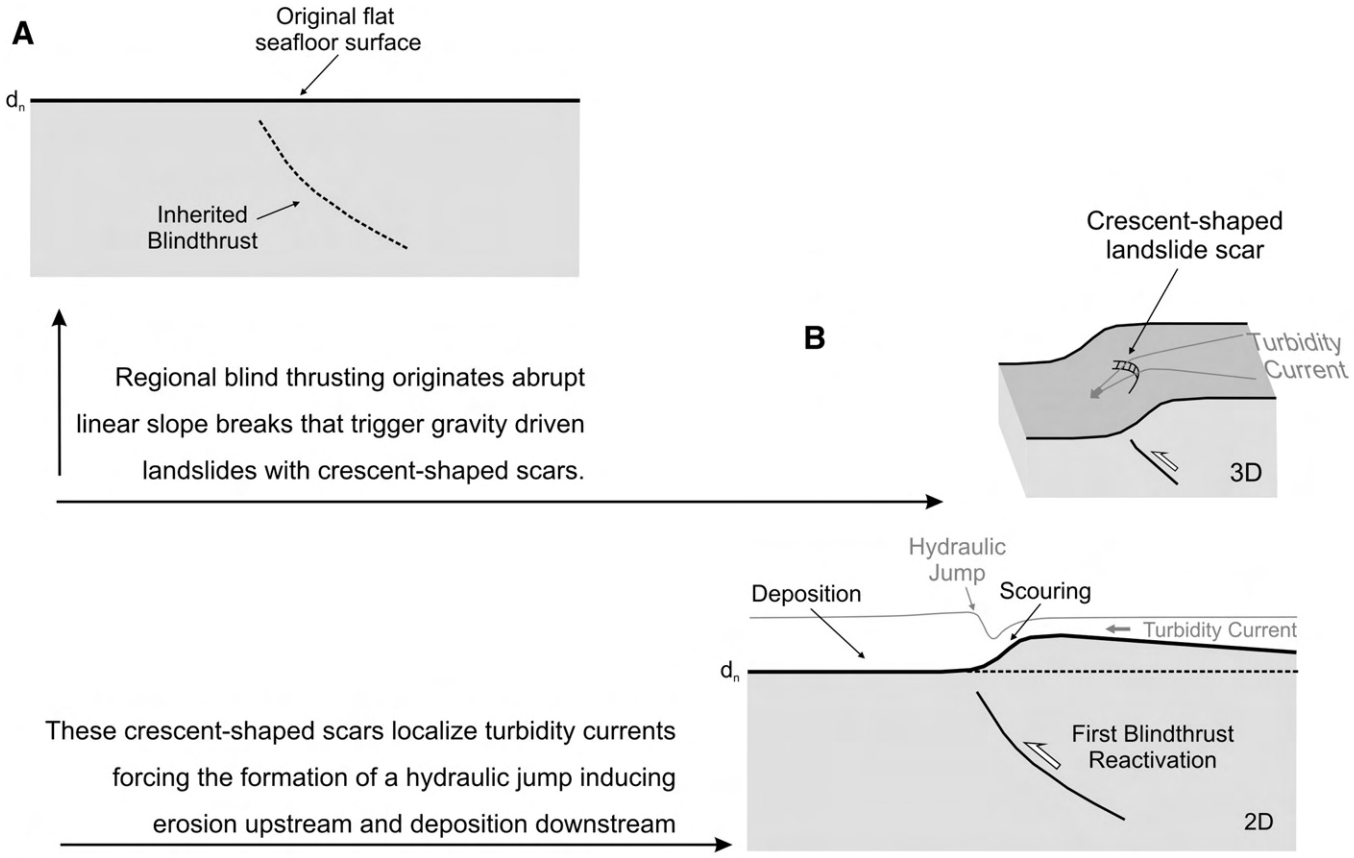

Simultaneous erosion of the newly formed ecarpments and progadating sedimentation of the eroded material towards these same escarpments, ultimately leading to the eventually complete smoothing of the stepping morphology

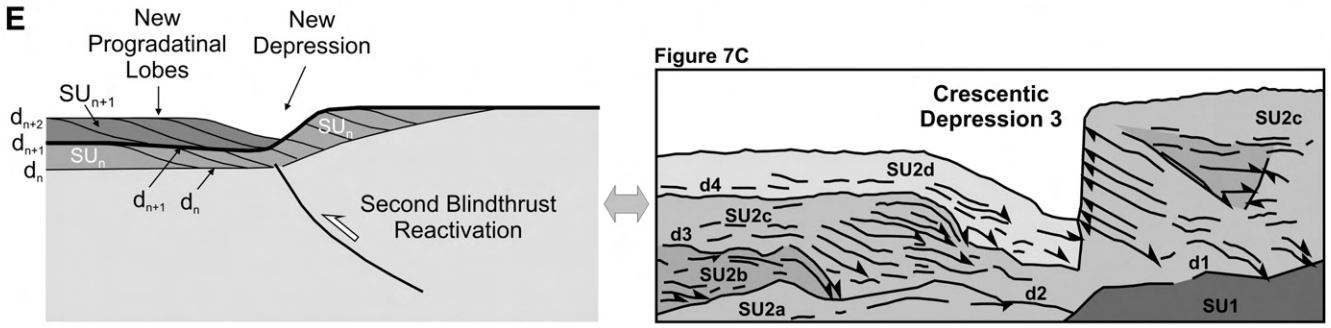

Resetting of the whole process by tectonic reactivation of the main (blind)thrusts, and consequent retriggering of scouring and progradating sedimentation. Comparison with the overall geometric configuration deduce from the PSAT246 sesmic profile (Fig. 7C)

Fig. 2B), strongly suggests the contribution of downslope turbity currents to the formation of these features. Such currents have previously been reported to interact with seafloor localized morphologies causing simultaneous erosion (scouring) and (re)deposition (Fildani et al., 2006; Alexander, 2008; Lamb et al., 2008; Heinio and Davies, 2009; Normark et al., 2009).

In the Monterey East system Fildani et al. (2006) studied several features that originated in a field of sandwaves, geometrically similar to the ones described here. Following previous theoretical (Parker and Izumi, 2000; Sun and Parker, 2005) and laboratory (Koyama and Ikeda, 1998; Taki and Parker, 2005) work, the cited authors modelled the formation of linear sets of crescentic giant scours based on the idea of cyclic steps. The formation of cyclic steps (Fig. 9A) is determined by the occurrence of hydraulic jumps (Fig. 9B), in which a flow makes a rapid change from thin, rapid supercritical flow (Froude number>1) to thick, tranquil sub-critical flow (Froude number <1, Fildani et al., 2006; Normark et al., 2009). According to these ideas, in the Horseshoe Valley, the flow of an overriding turbidity current could be forced to accelerate to supercritical velocities (i.e. with a Froude number>1) as a consequence of straightening caused by the seafloor uplift on the hanging wall of the blind thrusts underlying the studied crescentic depressions (see Fig. 9). When passing one of these obstacles the flow would be abruptly slowed, increasing in height and dissipating some of its own kinematic energy through turbulence (hydraulic jump; see Fig. 9B). Upstream of the hydraulic jump the occurrence of high bed shear stress would locally favour erosion, while downstream of the jump, very rapid deposition would be favoured (see Fig. 9B). These two areas would move in tandem upstream, forcing the hydraulic jump in the same direction (see Fig. 9A, Fildani et al., 2006; Alexander, 2008; Lamb et al., 2008; Heinio and Davies, 2009; Normark et al., 2009).

It should be noted that unlike the features studied by Fildani et al. (2006), the crescentic depressions described in the present paper are not aligned in one single linear train, but rather scattered along a broad area (see Fig. 3). These different spatial configurations are probably due to the broad and curved geometry of the thalweg in the upper part of the Horseshoe Valley (see Fig. 2B), which forces the flow to spread and sub-divide. On the other hand, some degree of lateral alignment (Fig. 3B) concurs with the tectonic control determined by the existent underlying blind thrusts (see above section 4.1.).

4.3. Interplay between active tectonics and turbidity currents

The above discussion of the possible hydrodynamic models, shows that the contribution of bottom currents for the formation of the study crescentic features should not be discarded, namely in view of previously reported interpretations for similar features in somewhat different contexts (e.g. Bulat and Long, 2001; Stow et al., 2002a,b; Verdicchio and Trincardi, 2006; Hernández-Molina et al., 2008). However, in the present case, the observed crescentic shape of the studied depressions, as well as their particular architecture resulting from simultaneous erosion and deposition, are still difficult to explain exclusively as the result of these processes. Because of this, the contribution of downslope turbidity currents should also be considered, and in the face of the presently available dataset, the formation and upstream migration of a tectonically controlled hydraulic jump seemingly provides a simpler explanation for the particular crescentic shape of the observed erosional scarps and associated upslope sedimentary bodies. In accordance, the following events must be considered to explain the origin of the crescentic depressions (Fig. 10):

a) Active blind thrusting was responsible for the formation of several morphological steps in the smooth seafloor of the Horseshoe Valley (Fig. 10A–B).
b) These abrupt linear slope breaks can originate gravity instabilities that exhibit crescent-shaped scarps. These scarps localize the downslope turbidity currents (Fig. 10B, inset), triggering the formation of a hydraulic jump, inducing scouring upstream of the jump and simultaneous prograding sedimentation of the eroded material downstream (Fig. 10B–C).
c) The fact that some of the progradational sedimentary lobes are buried and incised by shallower ones, strongly suggests a tectonic reactivation of the main blind thrusts, thus resetting the whole process, steepening the eroded retreated escarpments, or forming new ones, retriggering scouring and prograding sedimentation (Fig. 10D–E).

4.4. The possible role of fluid escape processes

Besides tectonics and scouring associated with the downslope currents, the middle resolution seismic data also reveals the possible importance of fluid escape processes, in the formation of the crescentic depressions as discussed elsewhere in the text and shown in Figs. 6, 8 and in the bathymetry (see Figs. 3, 4). The assumption that the dome localized close to crescentic depression 3 can be related to fluid escape processes is based not only on the transparent character of a shallow stratigraphic unit, but also by the fact that in the Gulf of Cadiz, particularly in the shallow sediments of the accretionary wedge domain, several tectonically controlled mud volcanoes and pockmarks of similar dimensions (Fig. 1A) have also been reported by other authors (e.g. Pinheiro et al., 2003; Somoza et al., 2003). These are described to be associated with widespread occurrence of fluid flow, and more recently were also reported to exist at greater depths, close to the Accretionary Wedge Deformation Front (e.g. Hensen et al., 2007). Moreover, some asymmetrical pockmarks also exhibit ground collapse geometries remarkably similar to the presently studied crescentic depressions (Schroot and Schfittenhelm, 2003; Somoza et al., 2003; Dimitrov and Woodside, 2003). However, because there is only one of these structures nearby one of the studied features, this mechanism alone could not account for the generalized origin of these features, and should preferably be seen as one possible contribution amid the dominant cause related to the tectonic/turbidity currents interplay.

Acknowledgments

This work was sponsored by MATESPRO (Major Tectonic and Sedimentary Processes in the Portuguese Margins, FCT/PDCTM/P/MAR/15264/199), TOPOEUROPE/0001/2007-TOPOMED (Plate re-organization in the western Mediterranean: lithospheric causes and topographic consequences), EUROMARGINS MVSEIS (Tectonic Control, Deep Crustal Structure and Fluid Escape Pathways in the Gulf of Cadiz Mud Volcano Field, 01-LEC_EMA24F; PDCTM 72003/DIV/40018) and ALMOND (multiscale modelling of deformation in the Gulf of Cadiz, PTDC/CTE-GIN/71862/2006) projects and NEAREST (Integrated observations from NEAR shore sourcES of Tsunamis: towards an early warning system, ESF EuroMargins Program, contract n. 01-LEC-EMA09F and from EU Specific Programme “Integrating and Strengthening the European Research Area”, Sub-Priority 1.1.6.3, “Global Change and Ecosystems”, contract n. 037110). João Duarte and Vasco Valadares thank FCT for the PhD grants, SFRH/BD/31188/2006 and SFRH/BD/17603/2004, respectively. Cristina Roque benefits a FCT PostDoc grant (Ref: SFRH/BPD/42534/2007). The support by Landmark Graphics Corporation via the Landmark University Grant Program and NASA WorldWind are also acknowledged. We thank the MATESPRO and TTR-14 teams, Jean-Pierre Henriet, David Van Rooij, Anneleen Foubert (RCMG, Ghent University), Rui Taborda (Lisbon University), Susana Lebreiro (IGME) and Nicholas Mouchot for insightful discussions. We also thank David Piper, Javier Hernández Molina and an anonymous reviewer for editorial work and constructive reviews.

References

Alexander, J., 2008. Bedforms in Froude-supercritical flow. Marine and River Dune Dynamics Proceedings. Leeds, U.K. April 2008.

Ambar, I., Howe, M.R., 1979a. Observations of the Mediterranean outflow-I. Mixing in the Mediterranean outflow. Deep-Sea Res. 26A, 555–568.

Ambar, I., Howe, M.R., 1979b. Observations of the Mediterranean outflow-II. The deep circulation in the vicinity of the Gulf of Cadiz. Deep-Sea Res. 26A, 555–568.

Banda, E., M. Torné and I. A. M. Group, 1995. Iberia Atlantic Margin Group investigates deep structure of ocean margins. Eos Trans. 76, 25–29 AGU.

Bonnel, C., Dennielou, B., Droz, L., Mulder, T., Berné, S., 2005. Architecture and depositional pattern of the Rhône Neofan and recent gravity activity in the Gulf of Lions (western Mediterranean). Mar. Petrol. Geol. 22, 827–843.

Bulat, J., Long, D., 2001. Images of the seabed in the Faroe–Shetland Channel from commercial 3D seismic data. Mar. Geophys. Res. 22, 345–367.

Calais, E., DeMets, C., Nocquet, J., M., 2003. Evidence for a post-3.16-Ma change in Nubia–Eurasia–North America plate motions? Earth Planet. Sci. Lett. 216, 81–92.

Dimitrov, L., Woodside, J., 2003. Deep sea pockmark environments in the eastern Mediterranean. Mar. Geol. 195, 263–276.

Duarte, J.C., 2007. Morfoestruturas quilométricas em forma de crescente nas águas profundas do Golfo de Cádis, MSc thesis, 118 pp., Univ. Évora, Évora, Portugal.

Faugères, J.C., Gonthier, È., Bobier, C., Griboulard, R., 1997. Tectonic control on sedimentary processes in the southern termination of the Barbados Prism. Mar. Geol. 140, 117–140.

Faugères, J.C., Stow, D.A.V., Imbert, P., Viana, A., 1999. Seismic features diagnostic of contourite drifts. Mar. Geol. 162, 1–38.

Fildani, A., Normark, W.R., Kostic, S., Parker, G., 2006. Channel formation by flow stripping: large-scale scour features along the Monterey East Channel and their relation to sediment waves. Sedimentology 53, 1265–1287.

Gebco, 2003. British Oceanographic Data Centre on behalf of IOC and IHO. GEBCO Digital Atlas.

Gràcia, E., Dañobeitia, J., Vergés, J., Bartolomé, R., 2003. Crustal architecture and tectonic evolution of the Gulf of Cadiz (SW Iberian margin) at the convergence of the Eurasian and African plates. Tectonics 22 (4).

García, M., Hernández-Molina, F.J., Llave, E., Stow, D.A.V., León, R., Fernández-Puga, M.C., Díaz del Río, V., Somoza, L., 2009. Contourite erosive features caused by the Mediterranean Outflow Water in the Gulf of Cadiz: Quaternary tectonic and oceanographic implications. Mar. Geol. 257, 24–40.

Gutscher, M.A., Malod, J., Rehault, J.P., Contrucci, I., Klingelhoefer, F., Mendes-Victor, L., Spakman, W., 2002. Evidence for active subduction beneath Gibraltar. Geology 30, 1071–1074.

Gutscher, M.A., Dominguez, S., Westbrook, G.K., Gente, P., Babonneau, N., Mulder, T., Gonthier, E., Bartolome, R., Luis, J., Rosas, F., Pedro, T., the Delila and DelSis Scientific Teams, 2009. Tectonic shortening and gravitational spreading in the Gulf of Cadiz accretionary wedge: observations from multi-beam bathymetry and seismic profiling. Mar. Petrol. Geol. 26, 647–659.

Hanquiez, V., Mulder, T., Lecroat, P., Gonthier, E., Marchès, E., Voisset, M., 2007. High resolution seafloor images in the Gulf of Cadiz, Iberian Margin. Mar. Geol. 246, 42–59.

Heinio, P., Davies, R.J., 2009. Trails of depressions and sediment waves along submarine channels on the continental margin of Espirito Santo Basin, 121. GSA Bulletin, Brazil, pp. 698–711.

Hensen, C., Nuzzo, M., Hornibrook, E., Pinheiro, L.M., Bock, B., Magalhaes, V.H., Bruckmann, W., 2007. Sources of mud volcano fluids in the Gulf of Cadiz — indications for hydrothermally alteres fluids. Geochim. Cosmochim. Acta 71, 1232–1248.

Hernández-Molina, F.J., Llave, E., Stow, D.A.V., García, M., Somoza, L., Vázquez, J.T., Lobo, F.J., Maestro, A., Díaz del Río, V., León, R., Medialdea, T., Gardner, J., 2006. The contourite depositional system of the Gulf of Cádiz: a sedimentary model related to the bottom current activity of the Mediterranean outflow water and its interaction with the continental margin. Deep-Sea Res. II 53, 1420–1463.

Hernández Molina, F.J., Maldonado, A., Stow, D.A.V., 2008. Abyssal plain contourites. In: Contourites, Rebesco, M., Camerlenghi, A. (Eds.), Developments in Sedimentology, 60. Elsevier, pp. 347–377.

Hovland, M., Judd, A.G., 1988. Seabed Pockmarks and Seepages. Impact on Geology, Biology and the Marine Environment. Graham and Trotman Inc, Norwell, USA, p. 302.

Iribarren, L., Vergés, J., Camurri, F., Fullea, J., Fernàndez, M., 2007. The structure of the Atlantic–Mediterranean transition zone from the Alboran Sea to the Horseshoe Abyssal Plain (Iberia–Africa plate boundary). Mar. Geol. 243, 97–119.

Johnson, I., Ambar, I., Serra, N., Stevens, I., 2002. Comparative studies of the spreading of Mediterranean water through the Gulf of Cadiz. Deep-Sea Res. II 49, 4179–4193.

Kenyon, N.H., Ivanov, M.K., Akhmetzhanov, A.M., Kozlova, E.V., 2006. Interdisciplinary geoscience studies of the Gulf of Cadiz and Western Mediterranean basins: preliminary results of investigations during the TTR-14 cruise of *RV Professor Logachev*, July–September, 2004, IOC, 70.

Koyama, T., Ikeda, H., 1998. Effect of riverbed gradient on bedrock channel configuration: a flume experiment. Proceedings of the Environmental Research Center, 23. Tsukuba University, Japan, pp. 25–34.

León, R., Somoza, L., Medialdea, T., Maestro, A., Díaz-del-Río, V., Fernández-Puga, M.C., 2006. Classification of sea-floor features associated with methane seeps along the Gulf of Cádiz continental margin. Deep-Sea Res. Part II 53, 1464–1481.

Llave, E., Hernández-Molina, F.J., Somoza, L., Díaz-del-Río, V., Stow, D.A.V., Maestro, A., Alveirinho Dias, J.M., 2001. Seismic stacking pattern of the Faro–Albufeira contourite system (Gulf of Cadiz): a Quaternary record of paleoceanographic and tectonic influences. Mar. Geophys. Res. 22, 487–508.

Lamb, M.P., Parsons, J.D., Mullenbach, B.L., Finlayson, D.P., Orange, D.L., Nittrouer, C.A., 2008. Evidence for superelevation, channel incision, and formation of cyclic steps by turbidity currents in Eel Canyon, California. GSA Bull. 20, 463–475.

Llave, E., Schonfeld, J., Hernández-Molina, F.J., Mulder, T., Somoza, L., Díaz del Río, V., Sánchez-Almazo, I., 2006. High-resolution stratigraphy of the Mediterranean outflow contourite system in the Gulf of Cadiz during the late Pleistocene: the impact of Heinrich events. Mar. Geol. 227, 241–262.

Locat, J., Lee, H.J., 2000. Submarine landslides: advances and challenges. Proceedings of the 8th International Symposium on Landslides, Cardiff, U.K, p. 30.

Lonergan, L., White, N., 1997. Origin of the Betic–Rif mountain belt. Tectonics 16, 504–522.

Maldonado, A., Somoza, L., Pallarés, L., 1999. The Betic orogen and the Iberian–African boundary in the Gulf of Cádiz: geological evolution (central North Atlantic). Mar. Geol. 155, 9–43.

Martel, S.J., 2004. Mechanics of landslide initiation as a shear fracture phenomenon. Mar. Geol. 203, 319–339.

McAdoo, B.G., Pratson, L.F., Orange, D.L., 2000. Submarine landslide geomorphology, US continental slope. Mar. Geol. 169, 103–136.

Mulder, T., Voisset, M., Lecroart, P., Le Drezen, E., Gonthier, E., et l'equipe embarqué e Cadisar 2, 2006. The western part Gulf of Cádiz: interaction between contour and turbidity currents. Geo-Mar. Lett. 26, 31–41.

Normark, W.R., Paull, C.K., Caress, D.W., Ussler III, W., Sliter, R., 2009. Fine-scale relief related to Late Holocene channel shifting within the floor of the upper Redondo Fan, offshore Southern California. Sedimentology 56, 1690–1704.

Parker, G., Izumi, N., 2000. Purely erosional cyclic and solitary steps created by flow over a cohesive bed. J. Fluid Mech. 419, 203–238.

Pinheiro, L., Ivanov, M.K., Sautkin, A., Akhmanov, G., Magalhães, V., Volkonskaya, A., Monteiro, J.H., Somoza, L., Gardner, J., Hamouni, N., Cunha, M.R., 2003. Mud volcanism in the Gulf of Cadiz: results from the TTR-10 cruise. Mar. Geol. 195, 131–151.

Purdy, G.M., 1975. The eastern end of the Azores–Gibraltar plate boundary. Geophys. J. R. Astr. Soc. 43, 973–1000.

Rebesco, M., Stow, D., 2001. Seismic expression of contourites and related deposits: a preface. Mar. Geophys. Res. 22, 303–308.

Rosas, F., Duarte, J., Terrinha, P., Valadares, V., Matias, L., 2009. Morphotectonic characterization of major bathymetric lineaments in Gulf of Cadiz (Africa–Iberia plate boundary): insights from analogue modelling experiments. Mar. Geol. 261, 33–47. doi:10.1016/j.margeo.2008.08.002.

Rosenbaum, G., Lister, G.S., Duboz, C., 2002a. Relative motions of Africa, Iberia and Europe during Alpine orogeny. Tectonophysics 359, 117–129.

Rosenbaum, G., Lister, G.S., Duboz, C., 2002b. Reconstruction of the tectonic evolution of the western Mediterranean since the Oligocene. In: Rosenbaum, G., Lister, G.S. (Eds.), Reconstruction of the evolution of the Alpine–Himalayan Orogen: Journal of the Virtual Explorer, 8, pp. 107–126. 2002.

Schroot, B.M., Schfittenhelm, R.T.E., 2003. Shallow gas and gas seepage: expressions on seismic and other acoustic data from the Netherlands North Sea. J. Geochem. Explor. 78–79, 305–309.

Somoza, L., Díaz-del-Río, V., León, R., Ivanov, M., Fernandez-Puga, M.C., Gardner, J.M., Hernández-Molina, F.J., Pinheiro, L.M., Rodero, J., Lobato, A., Maestro, A., Vázquez, J.T., Medialdea, T., Fernández-Salas, L.M., 2003. Seabed morphology and hydrocarbon seepage in the Gulf of Cádiz mud volcano area: acoustic imagery, multibeam and ultra-high resolution seismic data. Mar. Geol. 195, 153–176.

Srivastava, S.P., Roest, W.R., Kovacs, L.C., Oakey, G., Levesque, S., Verhoef, J., Macnab, R., 1990. Motion of Iberia since the Late Jurassic: results from detailed aeromagnetic measurements in the Newfoundland Basin. Tectonophysics 184 (3–4), 229–260.

Stow, D.A.V., Pudsey, C.J., Howe, J.A., Faugères, J.C., Viana, A.R., 2002a. Deep water Contourite Systems: Modern Drifts and Ancient Series, Seismic and Sedimentary Characteristics, Memoirs, vol. 22. Geological Society of London, London. 464pp.

Stow, D.A.V., Faugères, J.C., Howe, J.A., Pudsey, C.J., Viana, A.R., 2002b. Bottom currents, contourites and deep-sea sediment drifts: current state-of-the-art. In: Stow, D.A.V., Pudsey, C.J., Howe, J.A., Faugères, J.C., Viana, A.R. (Eds.), Deep-water Contourite Systems: Modern Drifts and Ancient Series, Seismic and Sedimentary Characteristics. : Memoirs, vol. 22. Geological Society of London, London. 7–20pp.

Sun, T., Parker, G., 2005. Transportational cyclic steps created by flow over an erodible bed. Part 2. Theory and numerical simulation. J. Hydraul. Res. 43, 502–514.

Taki, K., Parker, G., 2005. Transportational cyclic steps created by flow over an erodible bed. Part 1. Experiments. J. Hydraul. Res. 43, 488–501.

Terrinha, P., 1998. Structural geology and tectonic evolution of the Algarve Basin, South Portugal, Ph.D. Thesis, Imperial College, London.

Terrinha, P., Pinheiro, L.M., Henriet, J.-P., Matias, L., Ivanov, M.K., Monteiro, J.H., Akhmetzhanov, A., Volkonskaya, A., Cunha, T., Shaskin, P., Rovere, M., the TTR10 Shipboard Scientific Party, 2003. Tsunamigenic–seismogenic structures, neotectonics, sedimentary processes and slope instability on the southwest Portuguese Margin. Mar. Geol. 195, 55–73.

Terrinha, P., Matias, L., Vicente, J., Duarte, J., Luís, J., Pinheiro, L., Lourenço, N., Diez, S., Rosas, F., Magalhães, V., Valadares, V., Zitellini, N., Mendes Víctor, L., MATESPRO Team, 2009. Morphotectonics and strain partitioning at the Iberia–Africa plate boundary from multibeam and seismic reflection data. Mar. Geol. 267, 156–174.

Torelli, L., Sartori, R., Zitellini, N., 1997. The giant chaotic body in the Atlantic Ocean off Gibraltar: new results from a deep seismic reflection survey. Mar. Petrol. Geol. 14 (2), 125–134.

Tortella, D., Torné, M., Pérez-Estáun, A., 1997. Geodynamic evolution of the eastern segment of the Azores–Gibraltar Zone: the Gorringe Bank and the Gulf of Cadiz Region. Mar. Geophys. Res. 19, 211–230.

Verdicchio, G., Trincardi, F., 2006. Short-distance variability in slope bed-forms along the Southwestern Adriatic Margin (Central Mediterranean). Mar. Geol. 234, 271–292.

Wilson, C.K., Long, D., Bulat, J., 2004. The morphology, setting and processes of the Afen Slide. Mar. Geol. 213, 149–167.

Zitellini, N., Rovere, M., Terrinha, P., Chierici, F., Matias, L., Team, Bigsets, 2004. Neogene through Quaternary tectonic reactivation of SW Iberian passive margin. Pure Appl. Geophys. 161, 565–587.

Zitellini, N., Gràcia, E., Matias, L., Terrinha, P., Abreu, M.A., DeAlteriis, G., et al., 2009. The quest for the Africa–Eurasia plate boundary west of the Strait of Gibraltar. Earth Planet. Sci. Lett. 280, 13–50.

Marine Geology 303–306 (2012) 42–62

Contents lists available at SciVerse ScienceDirect

Marine Geology

journal homepage: www.elsevier.com/locate/margeo

Pliocene and Quaternary depositional model of the Algarve margin contourite drifts (Gulf of Cadiz, SW Iberia): Seismic architecture, tectonic control and paleoceanographic insights

C. Roque [a,b,c,*], H. Duarte [a], P. Terrinha [a,c], V. Valadares [a,c], J. Noiva [a], M. Cachão [d], J. Ferreira [d], P. Legoinha [e], N. Zitellini [f]

[a] LNEG, Laboratório Nacional de Energia e Geologia, Unidade de Geologia Marinha. Apartado 7586, 2720-866 Amadora, Portugal
[b] EMAM, Estrutura de Missão para os Assuntos do Mar, Portugal
[c] IDL, Instituto D. Luíz, Portugal
[d] Universidade de Lisboa, Centro e Dep. Geologia Fac. Ciências, Portugal
[e] CICEGe, DCT, Faculdade de Ciências e Tecnologia, Universidade Nova de Lisboa, Portugal
[f] ISMAR, Istituto di Scienze Marine, Bologna, Italy

ARTICLE INFO

Article history:
Received 1 July 2011
Received in revised form 2 November 2011
Accepted 3 November 2011
Available online 12 November 2011

Communicated by D.J.W. Piper

Keywords:
contourite drifts
Algarve margin
Mediterranean Outflow Water
Pliocene–Quaternary
seismostratigraphy
tectonics

ABSTRACT

The contourite drifts off southwest Iberia that formed as a result of the interaction of the Mediterranean Outflow Water (MOW) with the continental middle slope were studied in the Algarve margin using multichannel reflection seismic lines, oil-wells, piston cores, and a bathymetric compilation of four datasets. The seismostratigraphic interpretation of a dense array of oil industry seismic and stratigraphic correlation allowed the identification of five seismic units of Early Pliocene through Holocene in the Faro and Albufeira drifts and four correlative seismic units in the Lagos and Sagres drifts and three in the Portimão drift. A three-phased evolutionary model for the contourite formation is proposed. Firstly, a precursory phase of Pliocene age made up of sheeted drifts represents an initial phase of deposition under bottom-current activity that is correlated with the first stages of an enhanced MOW at about 3.5 Ma. Secondly, the building up phase of Early Pleistocene age is related to a strengthening of the MOW close to the onset of the Northern Hemisphere glaciations at about 2.6 Ma during which were deposited low-mounded drifts. Thirdly, the growing phase from Middle-Pleistocene through Holocene suggests the presence of a stronger MOW since the beginning of the Middle-Pleistocene Transition at about 1.3–1.0 Ma, accounting for the deposition of mounded drifts and formation of the Álvares Cabral moat. Seismostratigraphic interpretation and isochron maps allowed for the establishment of the main oceanographic, climatic, morphologic and tectonic factors that controlled the drifts deposition: i) the Pliocene and Quaternary MOW circulation forced by climate changes; ii) the sea bottom topography inherited from the Late Miocene, mainly shaped by the Portimão, Lagos and Bartolomeu Dias canyons system; iii) the interaction between along-slope and down-slope processes since the Pliocene; and iv) Pliocene–Quaternary fault-activity and diapirism.

1. Introduction

The contourite drifts of the Algarve margin are located on the northern Gulf of Cadiz, between 500 and 700 m water depth and are formed as a consequence of the interaction of the Mediterranean Outflow Water (MOW) with the middle continental slope of southwest Iberia. The existence of the contourite drifts in the Algarve margin was firstly described by Siedler (1968) followed by several works, most of them dedicated to the Faro and Albufeira drifts (e.g. Vanney and Mougenot, 1981; Faugères et al., 1985a, 1985b; Stow et al., 1986; Nelson et al., 1993; Sierro et al., 1999; Llave et al., 2001; Hernández-Molina et al., 2003, 2006; Llave et al., 2006, 2007, 2011). Conversely, a small number of works investigated the Lagos and Portimão drifts (Marchès et al., 2007, 2010) and the Sagres drift (Llave et al., 2007). These works rely on the interpretation of gravity cores, high-resolution seismic lines, multibeam bathymetry and backscatter, focusing on the relationships between the depositional architecture and morphology of the drifts, the Quaternary climatic/eustatic changes and consequent modifications in the MOW circulation pattern (e.g. Faugères et al., 1985b; Llave et al., 2001; Hernández-Molina et al., 2006; Llave et al., 2006; Hanquiez et al., 2007; Toucanne et al., 2007).

* Corresponding author at: LNEG, Laboratório Nacional de Energia e Geologia, Unidade de Geologia Marinha. Apartado 7586, 2720-866 Amadora, Portugal. Tel.: +351 210 924 600; fax: +351 2147919018.
E-mail address: cristina.roque@lneg.pt (C. Roque).

0025-3227/$ – see front matter © 2011 Elsevier B.V. All rights reserved.
doi:10.1016/j.margeo.2011.11.001

An integrated vision of the contourite drifts formation as part of a broader and more complex depositional system controlled by changes in the MOW circulation pattern was firstly proposed by Kenyon and Belderson (1973), and reappraised by Hernández-Molina et al. (2003, 2006).

This work presents an attempt to reconstruct the temporal and spatial evolution of a contourite depositional system (CDS) during global climate changes from Early Pliocene through Quaternary. The detail of this study allows the understanding of the influence of external factors, such as tectonics, paleogeography and climate changes on a CDS from its very beginning, confirming the degree of responsiveness of this system to environmental changes and how it can be assessed using seismic reflection methods.

The forthcoming IODP 339 Expedition (November, 2011, Mediterranean Outflow http://publications.iodp.org/scientific_prospectus/339/339sp_5.htm) will allow: i) accurate timing of the events described in this paper, ii) their sedimentological and climatic characterization and iii) depth conversion of two way time maps and quantitative sedimentary and erosive modeling associated with the MOW.

The novelty of this work is threefold, consisting of: i) the use of a full multichannel reflection seismic dataset that images the sedimentary record of the Algarve basin from the Mesozoic through the Holocene; ii) the re-appraisal of the Pliocene faunal data of the oil-industry reports of the offshore wells and iii) the dating of recently acquired seafloor samples. The interpretation of these data allowed to: 1) better constrain the age of the contourite drift formation; 2) determine the development of the depositional architecture of the drifts through space and time since their formation through present; 3) identify and characterize the main build-up phases; and 4) propose a model for the evolution of the contourite drifts that aims to understand the relationships between the seismostratigraphic architecture and the general depositional, tectonic and oceanographic processes of the study area from Early Pliocene to the present.

2. Geological and oceanographic settings

2.1. Geological setting

The continental slope of the Algarve margin (SW Iberia) is located in the northern part the Gulf of Cadiz near the northwest Africa (Nubia)–Eurasia plate boundary (Zitellini et al., 2009). The kinematics and relative trajectory changes between these two major plates since early Mesozoic times until the present governed the geodynamic evolution of this margin. During the Mesozoic a rift basin formed in a sinistral transtensive regime, and is related to the opening of the Neo-Tethys and the North Atlantic from Triassic through Cenomanian times (Terrinha et al., 2002). Tectonic inversion of the Algarve rift basin occurred from the Late Cretaceous through the Paleogene (Terrinha, 1998; Roque, 2007), related to the Alpine compression as a consequence of the Eurasia–Africa collision and subduction of the Tethyan oceanic crust between Iberia and Africa. As a consequence of this, a series of southwards directed imbricate thrusts formed (Terrinha, 1998; Lopes et al., 2006; Terrinha et al., 2006, 2009), some of which were reactivated in the Miocene.

In Miocene times, the subduction of the Tethyan oceanic crust in the westernmost Mediterranean and the collision between Iberia and Africa led to the formation of the Betic–Rif orogenic arc, the submarine accretionary wedge of the Gulf of Cadiz (Maldonado et al., 1999; Gutscher et al., 2002; Gràcia et al., 2003; Medialdea et al., 2004) and the closure of the oceanic communication between the Tethys and the Atlantic. At the same time the Algarve basin went through flexural subsidence that lasted until the Quaternary (Terrinha, 1998; Lopes et al., 2006; Roque, 2007).

2.2. Oceanographic setting

The oceanic circulation dynamics in the Gulf of Cadiz is driven by density contrast between the water masses of Atlantic and Mediterranean origin that flow on either side of the Gibraltar Straits (Fig. 1a) (Armi and Farmer, 1988; Bryden and Kinder, 1991; Baringer and Price, 1999). This water exchange defines an inverse estuarine circulation pattern that involves an eastwards upper layer of Atlantic water into the Mediterranean Sea and a westwards bottom layer of outflowing Mediterranean water, the MOW (Ambar et al., 2002; Serra et al., 2005).

The Atlantic Inflow Water (AIW) is a 0–500 m layer formed by the North Atlantic Surface Water (NASW) and North Atlantic Central Water (NACW) (Criado-Aldeanueva et al., 2006). The NASW originates from shallow NACW that has been modified by the sea–atmosphere interactions and flows at depths shallower than 100 m, with temperatures above 16 °C and salinity around 36.40‰. The NACW flows between 100 and 700 m, has temperature of 11 °C to 17 °C and salinity of 35.6–36.5‰ (Criado-Aldeanueva et al., 2006).

The Mediterranean Water originates in the Mediterranean Sea as a consequence of excess of evaporation over precipitation and runoff and consists mainly of the mixture of two types of water masses, the Levantine Intermediate Water and the Western Mediterranean Deep Water (Pinardi and Masetti, 2000).

The MOW exits the Gibraltar Straits (Fig. 1a) as a warm (13 °C) and dense (37.00‰) water mass that sinks and flows westwards into the Gulf of Cadiz as a bottom current, with eroding capability of bottom structures such as mud volcanoes (Ferreira et al., 2008), being deflected northwards due to the Coriolis force (Madelain, 1970; Zenk, 1970; Ambar and Howe, 1979a, 1979b; Baringer and Price, 1997; Ambar et al., 2002; Serra et al., 2005). The MOW shows a westwards velocity decrease from 250 to 180 cm s^{-1} near the Gibraltar Straits gateway to values between 80 and 40 cm s^{-1} along the northern continental slope of the Gulf of Cadiz where it is constrained to flow along valleys bounded by diapiric ridges (Nelson et al., 1993). The lowest velocity (about 10 cm s^{-1}) is reached along the South Portuguese continental slope although locally it can reach values up to 50 cm s^{-1} as in the Diogo Cão Deep (Ambar and Howe, 1979b). As the MOW spreads westwards its density progressively decreases by turbulent entrainment of overlying less-salty NACW at depths between 500 and 1500 m, until it approaches neutral buoyancy near 8° W at about 1000 m depth (Ambar and Howe, 1979a; Ambar et al., 2002; Bower et al., 2002; Serra et al., 2005; Ambar et al., 2008).

Westwards of 6°20′–7° W, the main core of the MOW separates into two major cores and two minor ones with distinct densities and flowing at different depths (Fig. 1a) (Zenk, 1970; Ambar and Howe, 1979a, 1979b; Ambar et al., 2002, 2008). The two major cores are the Mediterranean Upper Water (MU) and the Mediterranean Lower Water (ML) and the minor cores are the Shallow Core (SC) and Deep Core (DC) (Madelain, 1970; Zenk, 1970; Ambar and Howe, 1979a; Ambar et al., 2002; 2008). The MU is warmer and less saline (13–14 °C and 35.7–37‰) and flows at depths between 600 and 1000 m depth, centered at 700–800 m depth close to the continental slope of southwest Iberia. The ML is colder and more saline (10.5–11.5 °C and 36.5–37.5‰) and flows at depths between 1000 and 1300 m depth, stabilizing at around 1200–1300 m depth. After turning the Cape St. Vincent, the ML splits into a major branch flowing westwards and northwestwards and a minor branch that progresses northwards along the continental slope of the West Portuguese margin, reaching the North Atlantic (Bower et al., 2002). The SC is found at around 400–600 m depth along the continental slope off southwest Iberia, being characterized by comparatively higher temperatures (Ambar et al., 2002, 2008). The DC is traceable from the Portimão Canyon to the Cape St. Vincent at depths between 1300 and 1600 m (Ambar et al., 2002; Bower et al., 2002;

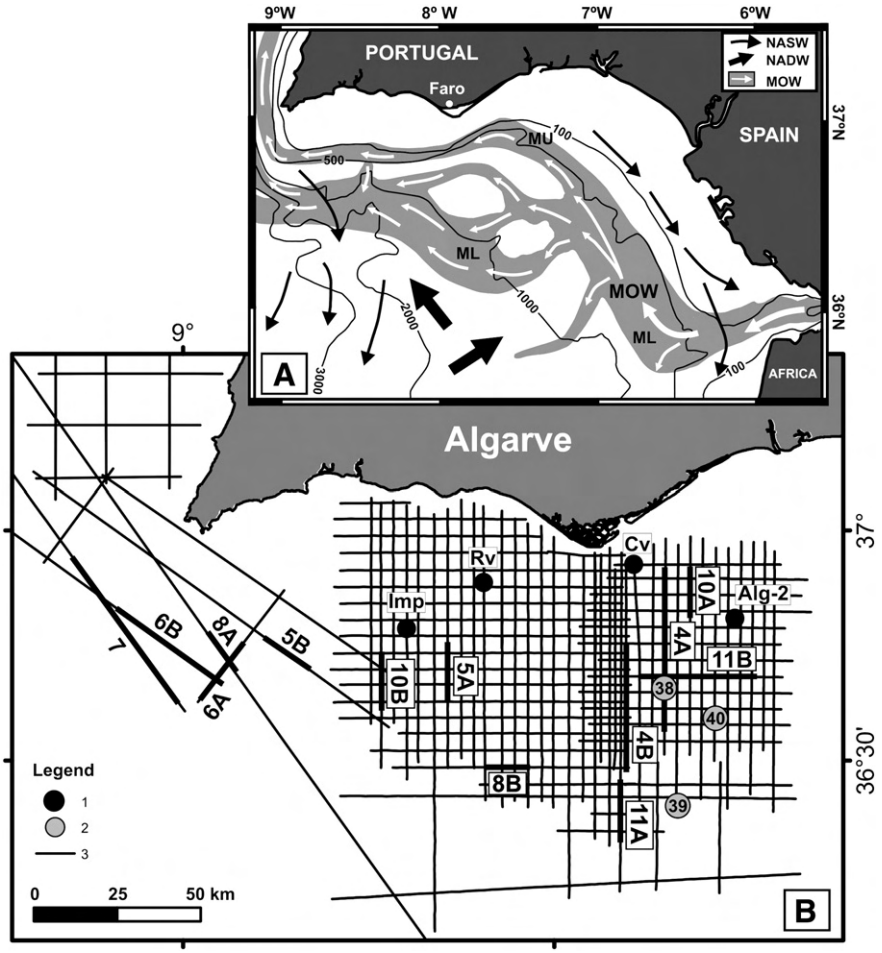

Fig. 1. (A) General oceanographic circulation pattern in the Gulf of Cadiz (modified from García et al., 2009) involving the main water masses, the Mediterranean Outflow Water (MOW), the North Atlantic Superficial Water (NASW) and the North Atlantic Deep Water (NADW). MU, Mediterranean Upper Water; ML, Mediterranean Lower Water. (B) Location of datasets used in this work: (1) — oil-wells (I, Imperador; R, Ruivo; C, Corvina; A, Algarve-2); (2) — SWIM04 piston cores (38, 39, 40); (3) — multichannel reflection seismic lines (Chevron74, Esso81, GSI84, BIGSETS). Thick lines indicate the location of the seismic line segments shown in Figs. 5, 6, 7, 8, 9, 11 and 12.

Ambar et al., 2008) and it is characterized by salinities of 36.42–36.53‰. This core seems to be a structure detached from the ML associated with pulses of denser water forced to descent to greater depths by interaction with the canyon topography (Bower et al., 2002; Ambar et al., 2008).

The Portimão Canyon acts also as a source of meddies detached from the DC, which are found farther downstream from the canyon (Ambar et al., 2002; Serra et al., 2005; Ambar et al., 2008). The Cape St. Vincent is another area for meddies formation detached from the ML (Ambar et al., 2008).

The North Atlantic Deep Water (NADW) that originates in the Nordic and Labrador Seas flows southwards underneath the MOW is a cold (3°–8 °C) and low salinity (34.95–35.20‰) water (Reid, 1979; Via and Thomas, 2006).

2.3. The Pliocene–Quaternary paleoceanography of the MOW

The knowledge of the Quaternary MOW oceanographic variability improved over the past decades due to the use of multiple proxies analyses applied to the last 90–15 ka sedimentary record: measurement of molecular biomarkers (Cacho et al., 2000, 2006); planktonic and benthic foraminifers $\delta^{13}C$ and $\delta^{18}O$ records (e.g. Schönfeld and Zahn, 2000; Rogerson et al., 2005, 2006; Cacho et al., 2006; Voelker et al., 2006; Schmiedl et al., 2010); measurement of Mg/Ca ratios in benthic foraminifera (Cacho et al., 2006); total organic carbon (Cacho et al., 2000); magnetic susceptibility (Llave et al., 2006; Voelker et al., 2006); high-resolution grain-size analysis (e.g. Faugères et al., 1985b; Nelson et al., 1993; Rogerson et al., 2005; Llave et al., 2006; Toucanne et al., 2007; Hanquiez et al., 2010); radiocarbon dating (Schönfeld and Zahn, 2000; Llave et al., 2006; Voelker et al., 2006); Nd and Pb isotope record of past ambient seawater from authigenic ferromanganese coatings of sediments (Stumpf et al., 2010).

Reconstruction models based on such proxies and on modeling studies (e.g. Myers, 2002; Xu et al., 2007) indicate a distinct behavior of the MOW under different climatic conditions. During the glacials, a saltier, denser and enhanced MOW sank to depth levels about 700 m deeper than today, impinging the continental slope at 1600–2200 m water depths (Schönfeld and Zahn, 2000; Rogerson et al., 2005; Llave et al., 2006; Voelker et al., 2006; García et al., 2009). This enhancement of the MOW occurred during Heinrich events, Dansgaard-Oeschger stadials and Younger Dryas (Sierro et al., 2005; Llave et al., 2006; Voelker et al., 2006). During the interglacials, the MOW was weaker and sub-divided into several branches, with the upper branch flowing between 600 and 1000 m water depths, along the Álvares Cabral moat. The present-day circulation pattern was established after the Younger Dryas, between 7.5 and 5.5 ka (Schönfeld and Zahn, 2000; Rogerson et al., 2005, 2006; García et al., 2009).

Conversely, little is known about the circulation regime of the MOW during the Pliocene and what kind of modifications it underwent in response to climatic changes. There is general agreement that the re-establishment of water mass exchanges between the Mediterranean Sea and Atlantic Ocean through the Gibraltar Straits

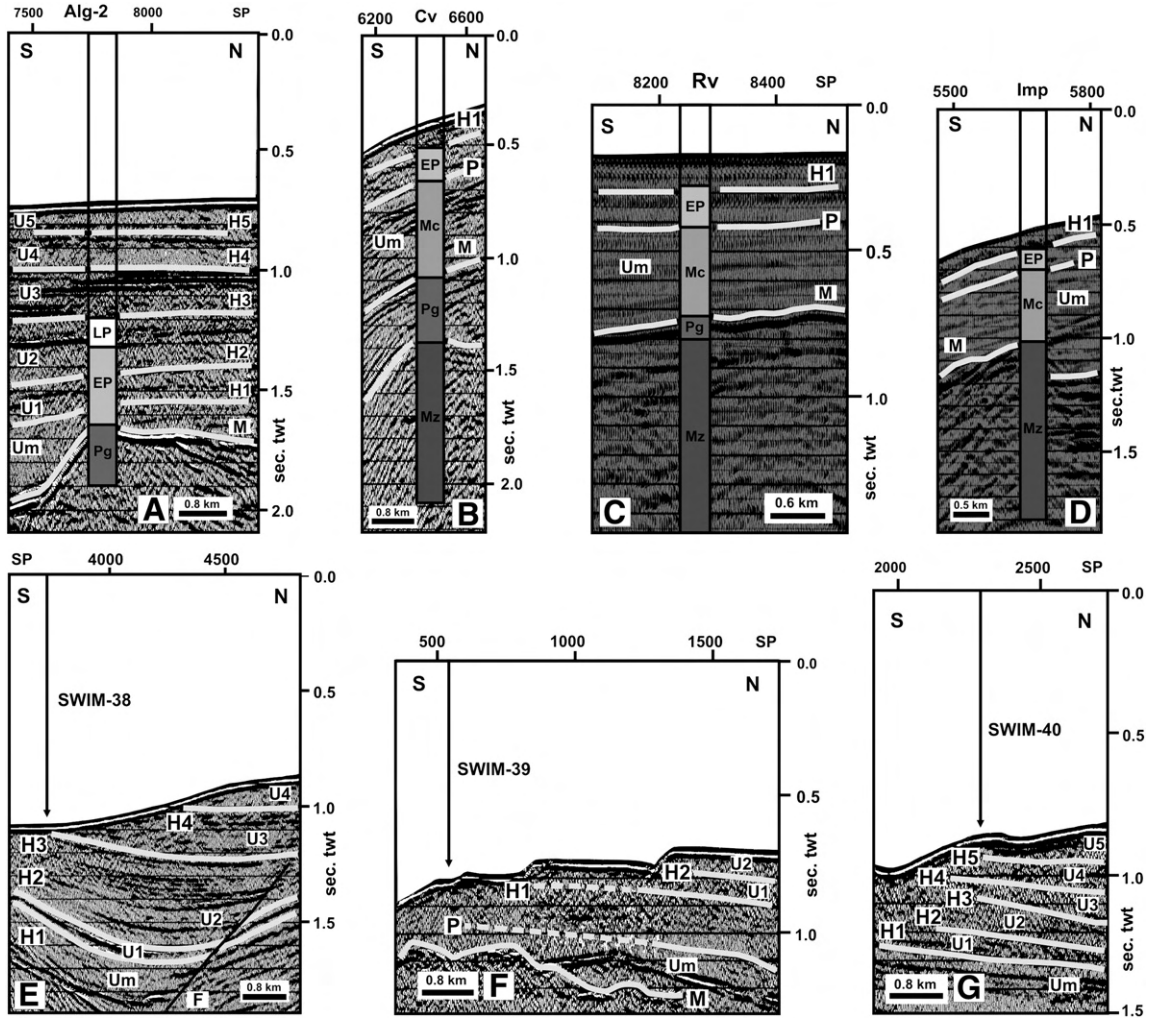

Fig. 2. Stratigraphic correlation of oil-wells (Alg-2, Algarve-2; Cv, Corvina; Rv, Ruivo; Imp, Imperador) and SWIM piston cores (arrows show location of piston cores 38, 39, 40) with site survey-multichannel seismic lines. See Fig. 1b for location. Indication of chronostratigraphic units interpreted in the wells: Mz, Mesozoic; Pg, Paleogene; Mc, Miocene; EP, Early Pliocene; LP, Late Pliocene. The following discontinuities and seismic units indicated on the figures are highlighted in light gray: M, unconformity at the base of Early Miocene; P, base of Pliocene; F, fault, as well as reflectors H1 to H5 and units Um and U1 to U5.

began after the end of the Messinian Salinity Crisis, which affected the Mediterranean region between 5.96 and 5.33 Ma (Cita, 2001). The following works focused on the hydrography of the MOW and on its circulation into the North Atlantic during the Pliocene used different proxies: i) sapropel events (Béthoux and Pierre, 1999); ii) planktonic and benthic foraminiferal $\delta^{18}O$ records in the Mediterranean Sea (Rio et al., 1990; Becker et al., 2006); iii) the decline and extinction of some deep-water benthic foraminifers species belonging to families *Pleurostomellidae*, *Stilostomellidae*, *Nodosariidae* in the Mediterranean Sea and outside this region (Hayward et al., 2009); iv) comparison of neodymium isotopes, $\delta^{18}O$, Mg/Ca-based temperature, and bottom water salinity results from ODP and DSDP sites on the Alboran Sea and Northeast Atlantic margin (Khélifi et al., 2009); and v) onset of cold-water coral mounds development at 2.7 Ma (Kano et al., 2007).

These works show that warm and humid climate prevailed in the Mediterranean region until 3.4 Ma (Béthoux and Pierre, 1999), when changed to cold and arid (Fauquette et al., 1998). Such climate conditions triggered two periods of enhanced production of cooler, saltier and more oxygenated Mediterranean deep-water and invigorated circulation regime. The first period occurred at 3.4–3.0 Ma, i.e. roughly at the onset of the Northern Hemisphere glaciations (3.1–2.7 Ma) (Rio et al., 1990; Hayward et al., 2009; Khélifi et al., 2009). The second period at 1.3–1.0 Ma coincided with the Mid-Pleistocene Transition (1.2–0.55 Ma) (Hayward et al., 2009). The re-introduction of the MOW in the North Atlantic could be recorded by an unconformity at the base of cold-water coral mounds in the Ireland margin, which represents a 6 Ma hiatus spanning from 8.96 Ma to 2.7 Ma (e.g. Van Rooij et al., 2003; De Mol et al., 2007; Kano et al., 2007).

3. Data and methods

The data used in this work consists of multichannel reflection seismic lines (MCS), bathymetric compilation, oil-industry wells and piston cores.

Table 1
Metadata of the oil-wells Algarve-2 (Alg-2), Corvina (Cv), Ruivo (Rv), Imperador (Imp) and piston cores SWIM04 (38, 39, 40) made in the Algarve margin.

Oil-well/core	Latitude N	Longitude W	Water depth (m)	Total penetration (m)
Alg-2	36.8096	7.5156	540	2227
Cv	36.9249	7.7863	189	3073
Rv	36.8862	8.1913	91	2224
Imp	36.7863	8.3983	370	2633
SWIM 38	36.65860	7.76371	797	3.21
SWIM 39	36.40525	7.67304	798	0.70
SWIM 40	36.59131	7.56957	635	4.15

3.1. Multichannel seismic lines

The MCS interpreted in this work were obtained during the 1970s and 1980s Chevron74, Esso81, GSI84 oil-industry surveys in the Algarve Basin and during the BIGSETS survey (Zitellini et al., 2001) (Fig. 1b). The Chevron74 seismic lines were acquired using 22 airguns, 48 channels, a streamer length of 2350 m and a 50 m shooting interval. The Esso81 seismic lines were acquired using 36 airguns, 224 channels, a streamer length of 3250 m and a 22 m shooting interval. The GSI84 seismic lines were acquired using 2775 in^3 airgun array, 120 channels, a streamer length of 3000 m and a 25 m shooting interval. Finally, the BIGSETS seismic lines were acquired using 4 airguns, 48 channels, a streamer length of 1350 m and a 37.5 m shooting interval.

The paper variable fill wiggle plots available for interpretation (Chevron74, Esso81, GSI84) were time migrated stacked sections with a trace separation of 25 m and a typical vertical resolution varying between 15 and 30 m (for frequency bandwidths of approximately 5–75 Hz). These paper plots were rasterized and converted to SEG-Y format with the *tif2segy* UNIX C-shell script by MacRae (2001). After conversion to SEG-Y, all the lines were imported to an OpenWorks (from Landmark Graphics Corporation) database, and interpreted with other Landmark software (SeisWorks, PowerView, AssetView) in order to better correlate the profiles with core logs and to map out horizons and interpolate the geological surfaces. These surfaces were exported to ArcGis 9.3 and isobaths and isopach maps (milliseconds TWT), respectively of basal discontinuity and seismic units, were produced using a grid of 500 m cell size.

3.2. Oil-industry wells and SWIM piston cores

The seismic lines were calibrated with four oil-wells made in the Algarve basin (Algarve-2, Corvina, Ruivo, Imperador) and three piston cores acquired during the SWIM04 survey (SWIM-38, SWIM-39, SWIM-40) (Figs. 1b, 2, Table 1).

3.3. Bathymetry data

The bathymetry presented in this paper was obtained from a compilation of different datasets: SWIM, INGMAR, SeaSEISMIC and GEBCO (Fig. 3a). The SWIM dataset results from a compilation of nineteen high-resolution multibeam swath bathymetry surveys performed in the southwest Iberia and northwest Morocco covering more than 180,000 km^2 from water depths ranging from −30 m to more than −5200 m (Zitellini et al., 2009). All the surveys were calibrated with sound velocity profiles in order to control the effect of the MOW currents and their different sound velocity properties on the data collected (Zitellini et al., 2009).

The INGMAR dataset is a bathymetric model produced in the Marine Geology Unit of the Laboratório Nacional de Energia e Geologia (LNEG) from 1971 to 1999 consisting of bathymetric contours spaced every 10 m from the shoreline to 200 m water depth. It results from the merging of data from several oceanographic cruises, depths of sampling surveys and ship track depth data.

The SeaSEISMIC dataset consists of a surface resulting from the picking of the seafloor from Chevron74 and Esso81 seismic lines. For most of the study area this dataset fills in the gap between the first two datasets and due to its better quality in areas of overlap, it was used instead of the INGMAR data.

The global GEBCO dataset (grid cell size of ~1852 m) was added in order to fill the small gaps between the other datasets and provide a better bathymetric map of the Gulf of Cadiz and SW Iberia. These data were imported as points spaced every 30 arcsec (~926 m) and merged onto the grid with other data. The SeaSEISMIC dataset (grid cell size of 300 m) was imported as points, the INGMAR contour lines were scanned from the original maps and both were merged with the 100 m cell size of the SWIM grid. After a quality control, a final seafloor surface was obtained using the Inverse Distance Weight, power 2, interpolation method in order to produce a grid of 200 m cell size (Fig. 3a). These actions described were carried in ESRI's ArcGis 9.3.

Bathymetric profiles (Fig. 3b) were made using the Fledermaus software.

4. Morphology of the contourite system

A general overview of the morphological features associated with the Gulf of Cadiz contourite system was presented by Hernández-Molina et al. (2003), while the detailed description of smaller scale features was presented on other works (e.g. Mulder et al., 2003, 2006; Hanquiez et al., 2007; García et al., 2009; Mulder et al., 2009). The deep down-slope system located west of 8°W and its tectonic control was presented by Terrinha et al. (2009) and Duarte et al. (2010). This section of the paper addresses only the main morphological features associated with the CDS on the Algarve continental margin based on the interpretation of the bathymetric data (Fig. 3a) and seismic lines (Fig. 1b). The main morphostructural features identified can be grouped in: i) contourite drifts and moat, ii) submarine canyons, valleys and channels, and iii) structural highs.

4.1. Contourite drifts and moat

Along the Algarve margin five contourite drifts are identified that were built by the action of the upper core of the MOW at water depths of 500 to 700, the Faro, Albufeira, Lagos, Portimão and Sagres drifts (Figs. 3, 4, 5, 6, 7, 8). They spread for approximately 150 km, display a smooth morphology and are separated by the Diogo Cão Deep (DCD), Bartolomeu Dias Deep (BDD), Portimão (PC) and Lagos canyons (LC) (Fig. 3).

The Faro and Albufeira elongated and separated mounded drifts display an asymmetric shape with a steeper northern slope (respectively, about 5.4° and 4°) bounded to the north by the Álvares Cabral Moat (ACM) (Figs. 3, 5a, 6a). The Faro and Albufeira drifts rise above the moat axis, respectively about 200 m and 150 m and evolve southwards into the Faro and the Bartolomeu Dias sheeted drifts, respectively, giving the seafloor a smooth and almost flat morphology with gradients of about 1° (Figs. 3b, 5b). Near the PC, the surface of the Albufeira drift is deformed by the piercing of a small salt diapir

Fig. 3. (A) Bathymetric map and main morphological features of the Algarve contourite system. Inset shows the dataset used in the bathymetric compilation (a — SWIM; b — SeaSEISMIC; c — INGMAR; d — GEBCO). Legend of symbols: 1 — shelf edge; 2 — progradational front of contourite drifts; 3 — mounded to sheeted drift transition; 4 — bathymetric contours in meters; 5 — Bartolomeu Dias paleocanyon; 6 — upper core of the MOW; 7 — lower core of the MOW; 8 — downslope drainage pathway; 9 — past MOW pathway; 10 — thrust-fault; 11 — normal fault; 12 — fault. Legend of features in alphabetical order: ACM, Álvares Cabral Moat; AD, Albufeira drift; AF, Albufeira fault; AH, Albufeira High; BDD, Bartolomeu Dias Deep; BDSD, Bartolomeu Dias sheeted drift; C1–C3, channels; CV, Cadiz Valley; d, salt diapir; DCD, Diogo Cão Deep; FMD, Faro mounded drift; FSD, Faro sheeted drift; g, gullies; GB, Guadalquivir Bank; GC, Guadalquivir Channel; HC, Huelva Channel; LC, Lagos canyon; LD, Lagos drift; LH, Lagos High; LV, Lagos Valley; PB, Portimão Bank; PC, Portimão canyon; PD, Portimão drift; PF, Portimão fault; PV, Portimão Valley; SD, Sagres drift; SMQF, São Marcos–Quarteira fault; SP, Sagres plateau; SVC: St. Vincent canyon; SVH: St. Vincent High; sls, slide scars. (B) Bathymetric profiles across the main morphological features in the area: Faro drift (I); Albufeira and Bartolomeu Dias drifts, and Guadalquivir Bank (II); Diogo Cão Deep (III); Lagos Canyon (IV); Bartolomeu Dias Deep (V); Portimão Canyon (VI).

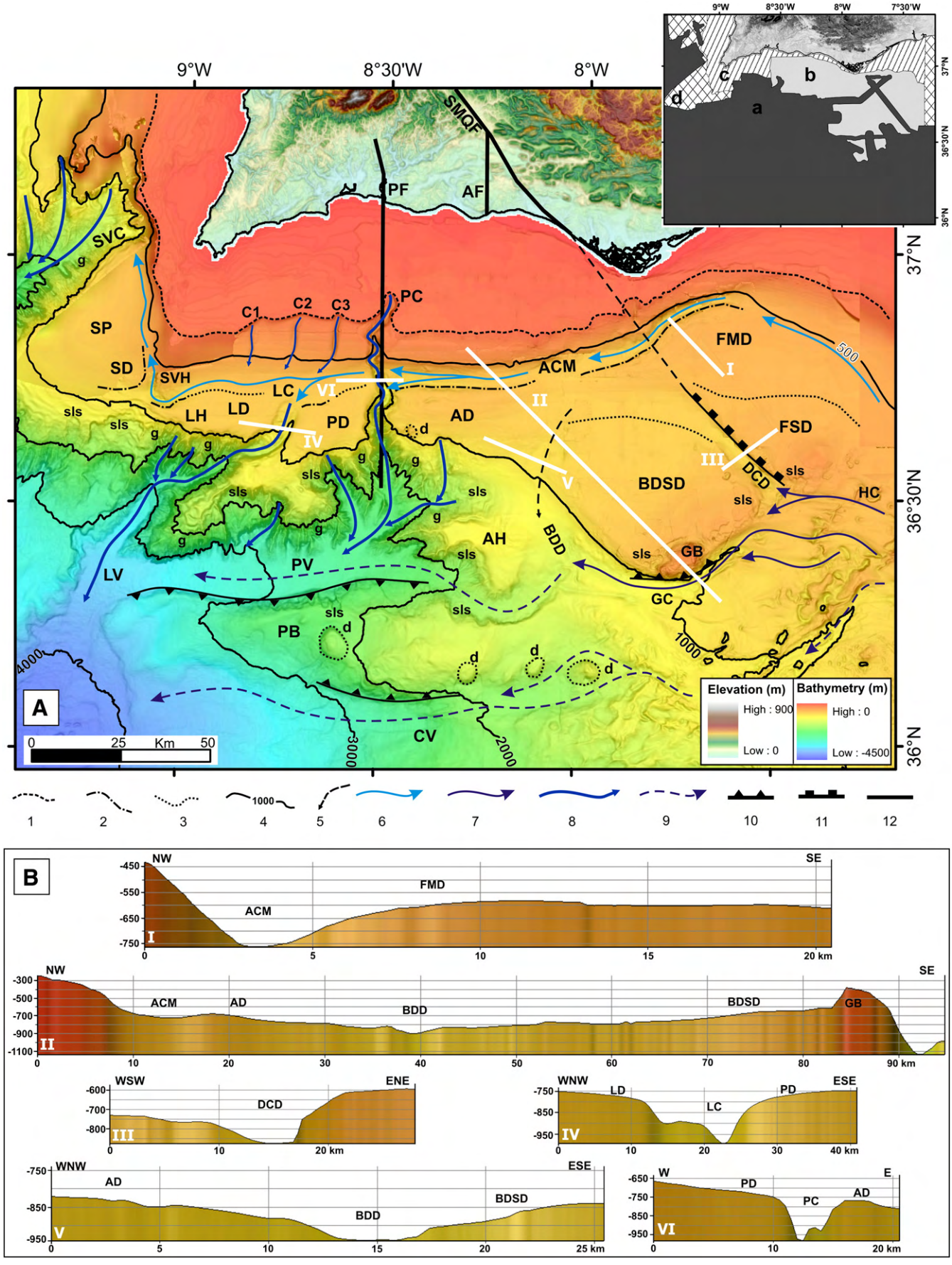
9°W
8°30'W
8°W
7°30'W
37°N
36°30'N
36°N
SMQF
PF
AF
PC
C1
C2
C3
SVC
SP
SD
SVH
LC
VI
LH
LD
PD
AD
ACM
FMD
FSD
DCD
BDSD
HC
GB
GC
BDD
AH
PV
LV
PB
CV
sls
g
d
500
1000
2000
3000
4000
I
II
III
IV
V
a
b
c
d
A
0 25 Km 50
Elevation (m)
High : 900
Low : 0
Bathymetry (m)
High : 0
Low : -4500
1 2 3 4 1000 5 6 7 8 9 10 11 12
B
NW
SE
FMD
ACM
I
-450
-550
-650
-750
0 5 10 15 20 km
NW
SE
ACM
AD
BDD
BDSD
GB
II
-300
-500
-700
-900
-1100
0 10 20 30 40 50 60 70 80 90 km
WSW
ENE
DCD
III
-600
-700
-800
0 10 20 km
WNW
ESE
LD
LC
PD
IV
-750
-850
-950
0 10 20 30 40 km
WNW
ESE
AD
BDD
BDSD
V
-750
-850
-950
0 5 10 15 20 25 km
W
E
PD
PC
AD
VI
-650
-750
-850
-950
0 10 20 km

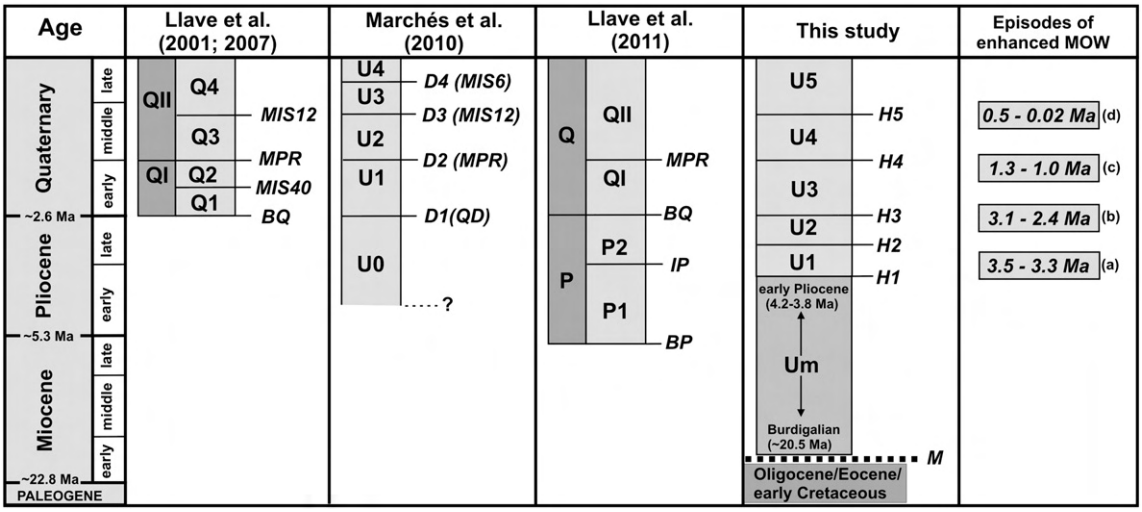

Fig. 4. Chronostratigraphic chart showing the correlation between seismic units and discontinuities identified in this work and published seismostratigraphic models by Llave et al. (2001, 2006, 2011) and Marchès et al. (2010) The main episodes of enhanced MOW production and circulation proposed by (a) Khélifi et al. (2009), (b) Fauquette et al. (1998), (c) Hayward et al. (2009) and (d) Llave et al. (2006) are also indicated.

and landslide scars are identified where the drift meets with the canyon (Fig. 3a).

The ACM is an 82 km long, ENE–WSW to E–W trending moat incised by the westwards flowing upper core of the MOW, bounding the northwards progradational front of Faro and Albufeira drifts. The ACM is wider and deeper towards west (3.5 km width and 754 m depth off Faro; 7 km width, 900 m depth near the PC) (Figs. 3b, 5a, 6a). The Portimão and Lagos drifts extend from the PC to the St. Vincent High (SVH) over approximately 50 km and are separate by the LC (Figs. 3a, 6b, 7, 8a, b). They display a smooth seafloor morphology with gradients less than 0.5° (Fig. 3b) and were classified both as sheeted drifts (Hernández-Molina et al., 2003; Marchès et al., 2007, 2010). However, the inspection of Fig. 3a and seismic lines (Figs. 7, 8a,b, 9) shows that the shape of the Lagos drift evolves from a sheeted drift near the LC to a mounded drift separated from the SVH by a moat. The smooth seafloor morphology of the drift is disturbed in some areas of the southern flank by landslides suggesting that erosion and deposition processes are competing at present (Figs. 3a, 8b).

The Sagres drift lies between the SVH and the St. Vincent canyon (SVC), on the transition of the south Portuguese margin to the west Portuguese margin (Figs. 3a, 8a, c). The lack of extensive multibeam bathymetry coverage of the Sagres drift does not allow for a detailed description of its surface. However, a small coverage of the multibeam bathymetry shows a well developed moat also seen in seismic lines (Figs. 3a, 8a, c). The inspected GEBCO bathymetry depicts a fairly flat and smooth seafloor (Fig. 3a).

4.2. Submarine canyons, valleys and channels

The Algarve margin is incised by four types of erosional features (Fig. 3a): i) submarine canyons shaped by down-slope processes, as the PC, LC and St. Vincent (SVC) canyons; ii) E–W submarine valleys carved by the MOW, such as the Cadiz and Huelva channels and the Portimão valley; iii) NW–SE linear submarine valleys, such as DCD and BDD that cut across the Faro and Albufeira contourite drifts; and iv) three N–S channels (C1–C3) on the upper slope parallel to PC.

Considering that the E–W submarine valleys and channels C1–C3 have been extensively described by various authors (e.g. Hernández-Molina et al., 2003; Mulder et al., 2003, 2006; Hanquiez et al., 2007; García et al., 2009; Terrinha et al., 2009; Duarte et al., 2010; Marchès et al., 2010), the main features described in this paper are the PC, LC, SVC, DCD and BDD.

The submarine canyons system, including a network of tributaries and gullies, is developed to the west of the Guadalquivir Bank (GB) and cuts across the continental slope of the Algarve margin. The PC separates the Faro–Albufeira drifts in the east from the Portimão–Lagos drifts to the west, extending over 50 km, from 110 m to 2500 m water depth, where it connects to the Portimão Valley (PV) (Fig. 3a). The canyon displays a linear N–S trend, asymmetrical in cross-section, with steep flanks (gradients >20°) up to 1 km high (Fig. 3b). The PC seems to be controlled by the N–S striking Portimão fault (Fig. 3a), a tardi-Variscan structure reactivated during the Early Jurassic as an extensional-fault and as a transfer and strike-slip fault during the Alpine tectonic inversion and during the Pliocene–Quaternary tectonic reactivation (Terrinha et al., 2009).

The LC trends NNE–SSW in the upper part and NE–SW in the lower part and runs from the continental slope at about 760 m depth down to the Lagos Valley at 3500 m depth (Fig. 3a). In the upper part the canyon is about 6 km wide and asymmetrical with a steeper eastern flank (about 4°) and a gentle and smooth western flank (about 2°) with elongated terraces probably a consequence of slope failure scars (Fig. 3a, b-IV). In the lower part of the canyon, this asymmetry is enhanced by a higher western flank that reaches about 1700 m high and slope of about 8° whereas the eastern flank is steeper (about 13°) and 770 m high. In this area the canyon is around 14 km wide and both flanks are cut by several erosive gullies and failure scars (Fig. 3a).

The upper part of the SVC is only partially imaged in the Fig. 3a, as a NE–SW trending wide valley incised by two N–S tributaries and numerous gullies.

The NW–SE rectilinear valleys DCD and BDD intercept the Faro and Albufeira drifts and deeply incise into the GB structural high (Fig. 3a). The DCD separates the Faro and Bartolomeu Dias sheeted drifts and extends for over 30 km, deepening towards the SE from 780 m to 895 m water depth and is incised by the northwards diverted branch of the MOW that flows along the Huelva channel (Fig. 3a). The SE part of the DCD shows an asymmetrical cross-section with a steep (~9°) eastern flank, which rises about 270 m above the sea bottom, whereas the western flank is gentler (~3°) and about 110 m high (Fig. 3b). The onshore–offshore digital terrain model together with the geological map shows that the DCD is aligned with the onshore São Marcos–Quarteira Fault (SMQF), which has been described onshore as a Paleozoic thrust reactivated as a syn-rift fault and later during the Paleogene inversion as a transpressive fault (Fig. 3a) (Terrinha et al., 2002, 2009).

The BDD is parallel to the DCD and separates the Bartolomeu Dias sheeted drift from the Albufeira High (AH) and connects with the Portimão Valley to the west (Fig. 3a). The BDD is asymmetrical, has a 650 m high eastern flank and a 250 m high west flank. The eastern flank is steeper reaching about 2.9° while the western flank slope gradient is less than 0.8° (Fig. 3b). Localized landslide scars are identified on the flanks of both the DCD and BDD (Fig. 3a).

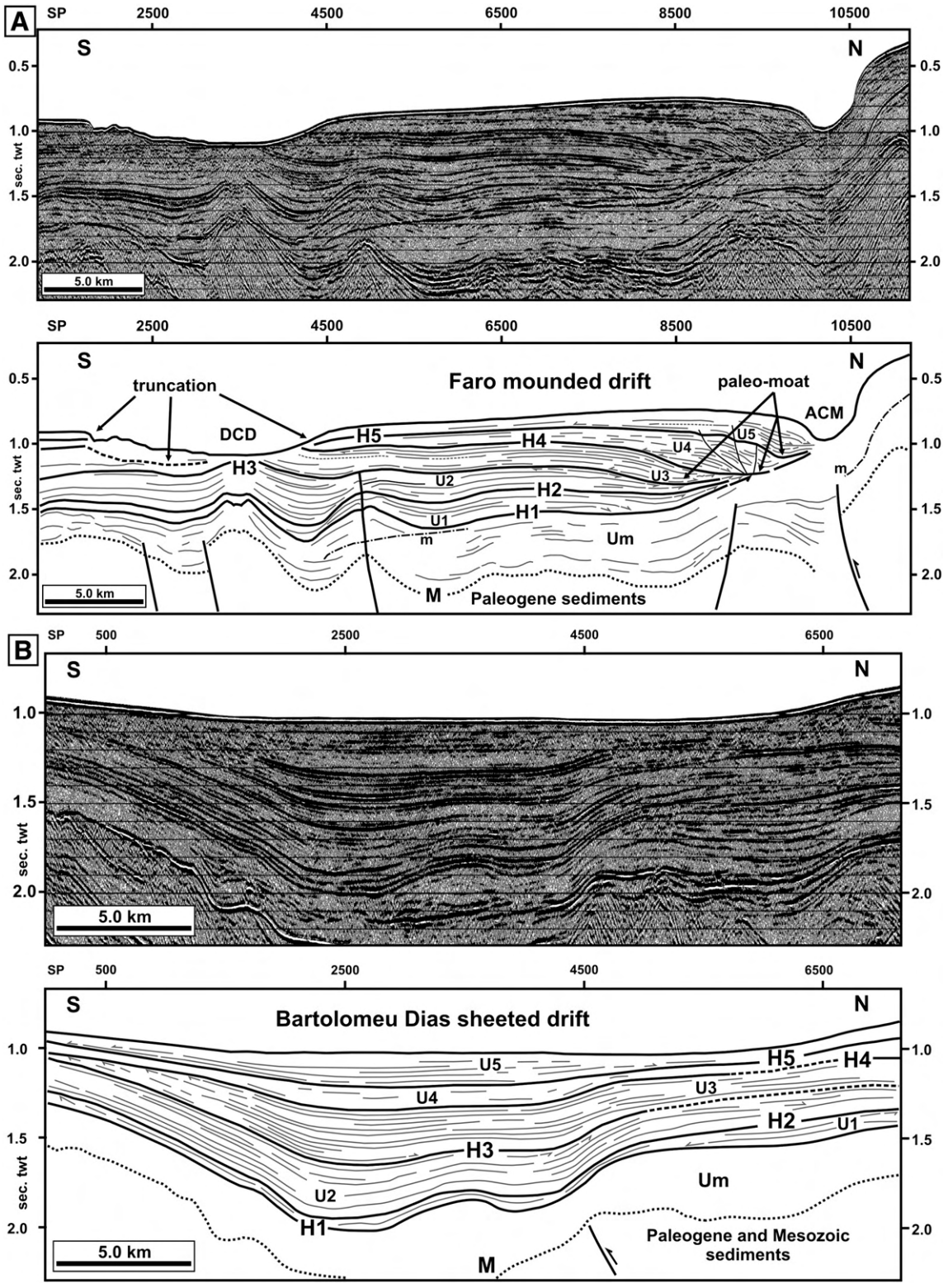

Fig. 5. (A) Multichannel seismic line P81-19 across the Faro mounded drift and line drawing interpretation. This drift is bounded by the Álvares Cabral Moat (ACM) and by the Diogo Cão Deep (DCD) that truncates seismic units U3 to U5. Seismic units U1 and U2 display an aggradational configuration while the mounded configuration and paleomoats are displayed in seismic units U3 through U5. Sediment failure affects seismic units U4 and U5. (B) Multichannel seismic line P81-25 across the Bartolomeu Dias sheeted drift and line drawing interpretation. Note the sagging of this sector of the Algarve basin after M unconformity (M) and its attenuation after discontinuity H5. The major thickening of the sheeted drift occurred since discontinuity H2 mainly during deposition of seismic units U2 and U3. M, base of Early Miocene unconformity; m, multiple.

4.3. Structural highs

The structural highs shown in Fig. 3a are the Guadalquivir Bank (GB), Portimão Bank (PB), Sagres plateau (SP), Albufeira High (AH) and St. Vincent High (SVH). The first three have been described by several authors as tectonically uplifted blocks related to thrust faults, which resulted from tectonic inversion of Mesozoic rift faults (Ribeiro et al., 1979; Mougenot, 1988; Gràcia et al., 2003; Terrinha et al., 2003; Zitellini et al., 2004; Terrinha et al., 2009). The NW–SE trending scarp of the AH corresponds to an extensional fault associated with present-day dextral strike-slip motion on the W–E Portimão Bank fault (Terrinha et al., 2009). This paper addresses only the SVH. This feature separates the Sagres and Lagos mounded drifts and is a morphologic extension of two important reliefs, the offshore prolongation of the onshore Paleozoic basement high (Terrinha, 1998; Terrinha et al., 2002) that separated the south and west Portuguese passive margins and the northern prolongation of the Horseshoe fault scarp. The intersection of this plateau with the strong erosion of the canyons and gullies at roughly 1000 m below sea level narrows to almost nil the horizontal surface on top of which the mound drifts accumulate. This is a zone where deposition and downslope mass transport processes compete (Figs. 3a, 8c).

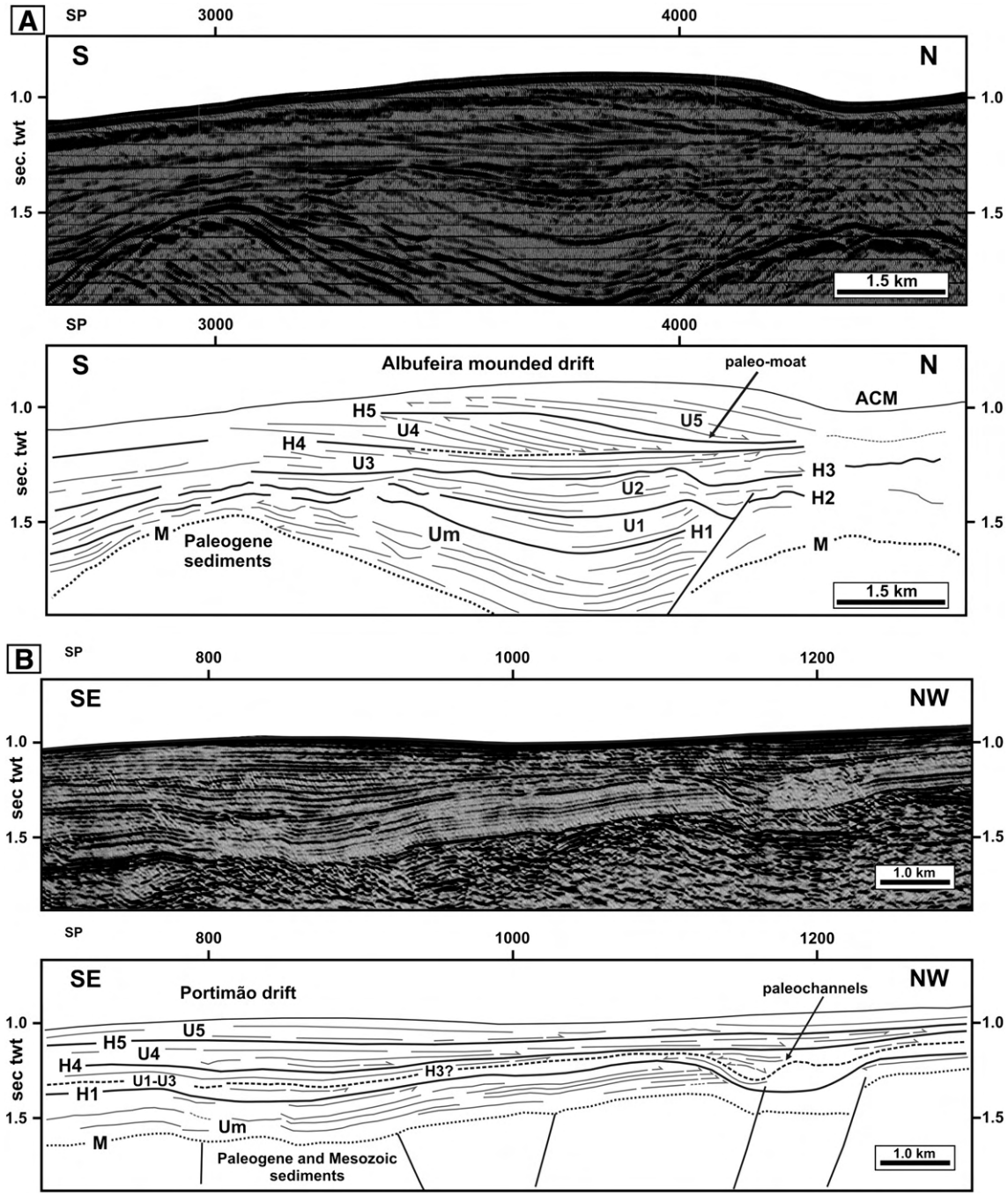

Fig. 6. (A) Multichannel seismic line P74-13 across the Albufeira mounded drift and line drawing interpretation. The progradation of the drift towards the north and its major growing occurred during deposition of seismic units U4 and U5, showing respectively, oblique and sigmoidal–oblique configuration. Seismic unit U3 is aggradational. (B) Multichannel seismic line S84-76 across the Portimão drift and line drawing interpretation. Note the presence of paleochannels topped by discontinuity H4. The growth of this drift began since deposition of seismic units U4 and U5, defining a sheeted drift. ACM, Álvares Cabral Moat. M, base of Early Miocene unconformity.

5. Seismic architecture and chronostratigraphic constraints

Seismostratigraphic interpretation made in this work allowed the identification of five seismic units (U1 to U5) bounded by major discontinuities (H1 to H5) within the Pliocene and Quaternary sedimentary record of Faro, Albufeira, Portimão, Lagos and Sagres drifts. These drifts are underlined by pre-contourite sediments of Miocene and Early Pliocene age (seismic unit Um). Seismostratigraphic model proposed in this work was correlated with published models by Llave et al. (2001, 2006, 2011) and Marchès et al. (2010) as shown in Fig. 4.

The chronostratigraphic constraints for each seismic unit relay on the stratigraphic calibration of the MCS lines using reviewed biostratigraphic data from the oil-wells (Roque, 2007) and the SWIM04 piston cores acquired from the Algarve Basin (Fig. 2).

The oil-wells penetrated rocks and sediments from the Upper Triassic through the Pliocene (Figs. 1b, 2a–d), but for the purpose of this work, only the recovered Pliocene sediments are described. The Early Pliocene was deposited in a bathyal environment and consists of claystones (Corvina and Imperador wells), sandstones and conglomerates (Ruivo well). A hiatus that separates the Eocene neritic limestones from the Early Pliocene bathyal claystones is found in the Algarve-2 well, because it was made on top of a structural high. This well is the only one where the Upper Pliocene claystones were retrieved.

Core-catchers of piston cores SWIM04-38 and SWIM04-39 (Figs. 1b, 2e, f) were respectively, filled with fossil-rich silty mud and semi-consolidated marls. Core SWIM04-40 (Fig. 2g) recovered fossil-rich sand. Samples taken from the core-catcher SWIM04-39 (Fig. 2f) indicate an age of 4.2–3.8 Ma based on the nannofossil and planktonic foraminifera assemblages: *Amaurolithus delicatus*, *Discoaster asymmetricus*, *D. brouweri*, *D. pentaradiatus*, *D. quinqueramus*, *D. surculus*, *D. variabilis*, *D. triradiatus*, *Helicosphaera selli*, *Pseudoemiliania lacunosa*, *Scyphosphaera intermedia*, *Sphenolithus abies*, *Globigerina (Zg.) nepenthes*, *Globigerinoides obliquus*, *Globorotalia limbata*,

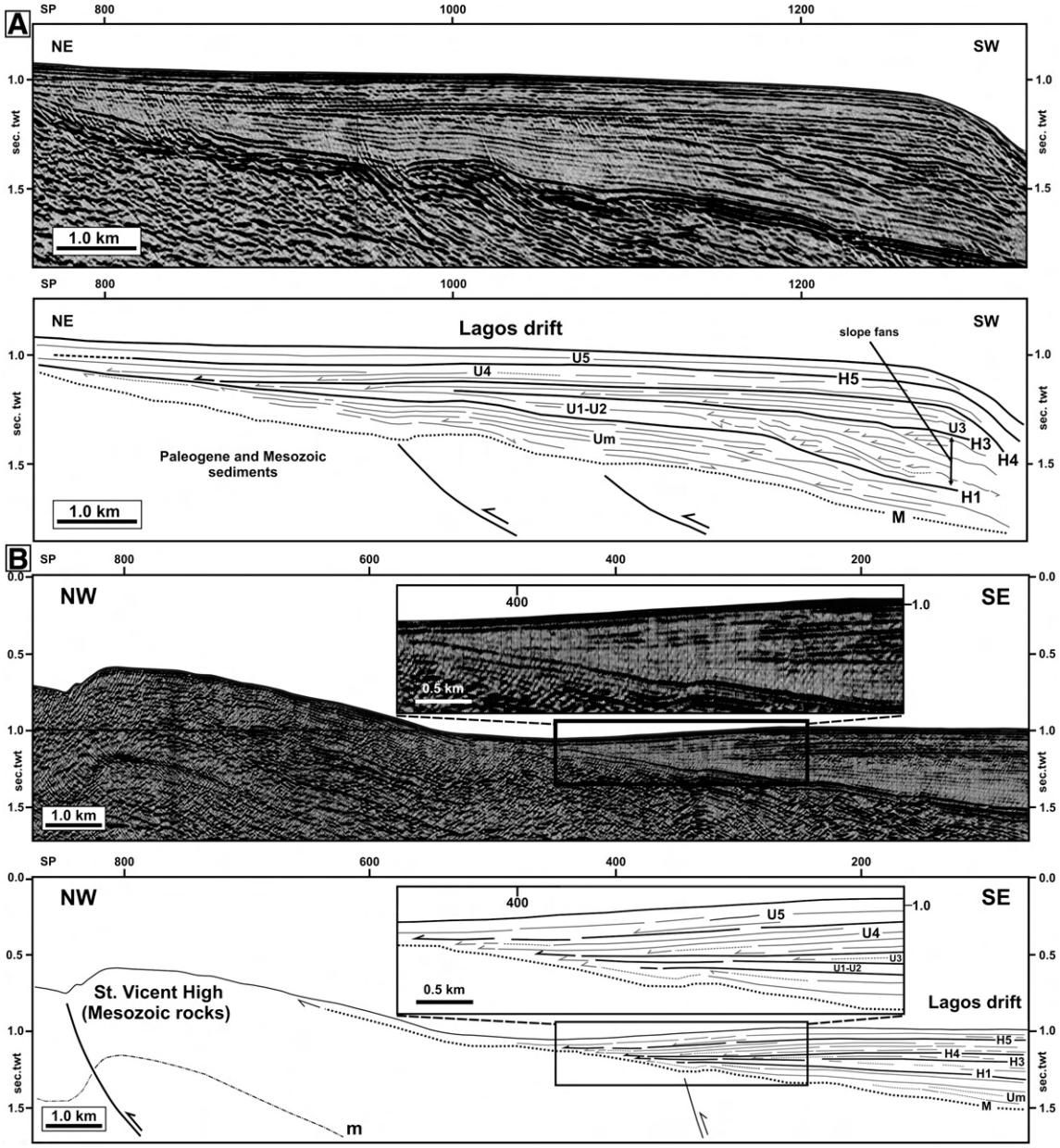

Fig. 7. (A) Multichannel seismic line S84-77 across the eastern sector of the Lagos drift and line drawing interpretation. Seismic unit U1–U2 displays facies of slope fans (SF) possibly related to past activity of channels C1–C3 seen in Fig. 3a. (B) Multichannel seismic line S84-78 across the central sector of the Lagos drift and line drawing interpretation. Note the aggradational configuration and onlap terminations of reflections against the M unconformity (M) towards the St. Vincent High. m, multiple reflection.

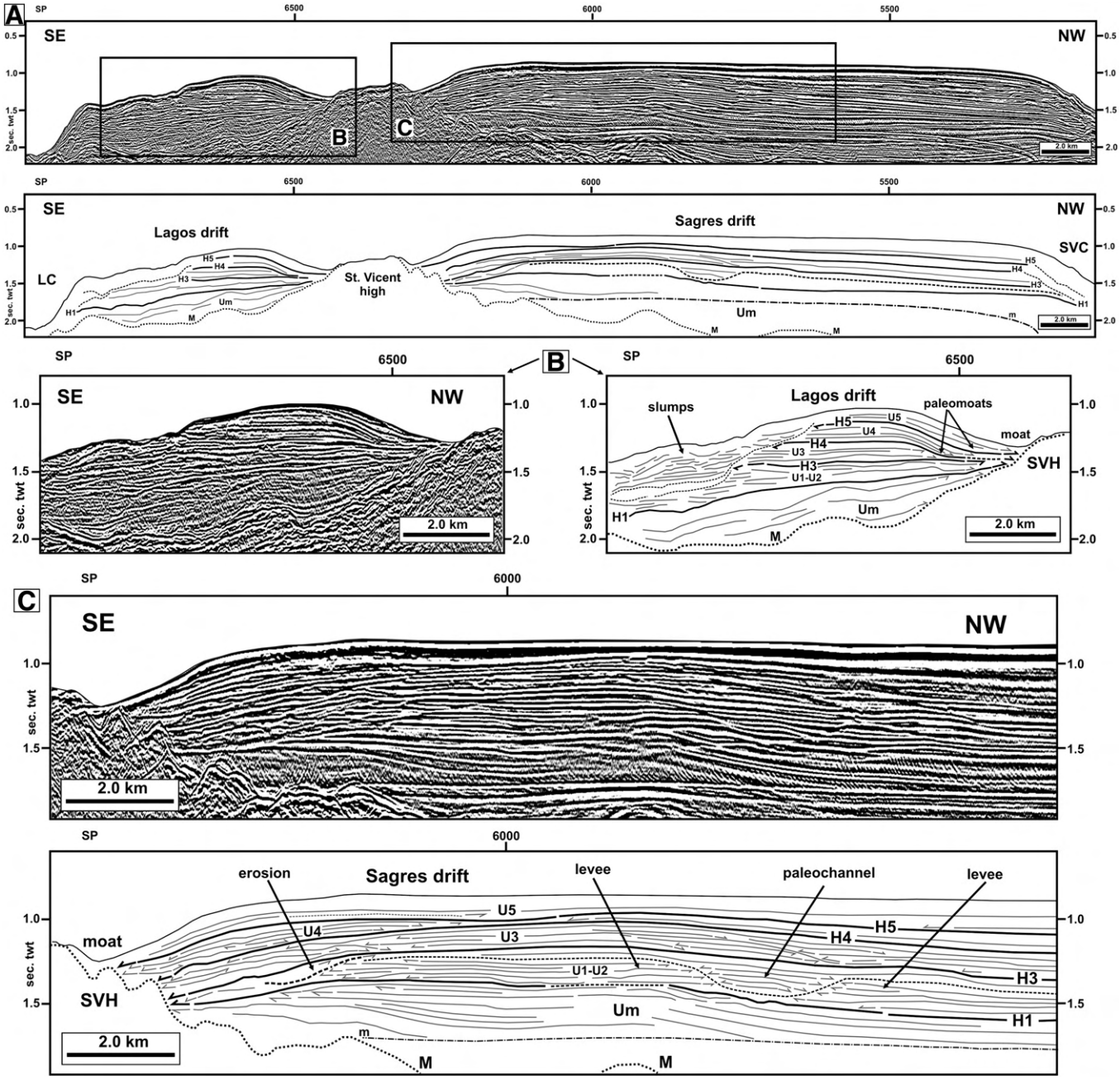

Fig. 8. (A) Multichannel seismic line BS-08 across the Lagos and Sagres drifts and line drawing interpretation. Both drifts are separated from the St. Vincent High by moats and are bounded by the Lagos canyon (LC) and St. Vincent canyon (SVC), respectively. (B) Inset from (A) showing a section across the Lagos drift. The mounded geometry and paleomoats of the Lagos drift began to develop during deposition of seismic units U4 and U5. The southeastern end of the drift is affected by sediment failure, slumps that truncate seismic units towards the Lagos canyon. (C) Inset from (A) showing a section across the Sagres drift. As in the Lagos drift the mounded geometry of this drift began to develop since deposition of seismic units U4 and U5. Paleochannels are topped by discontinuity H3. M, base of Early Miocene unconformity; m, multiple.

Sphaeroidinellopsis kochi, *Sphaeroidinellopsis* sp. Samples taken from core SWIM-38 core-catcher and the base of the first section of the core SWIM-40 (Fig. 2e, g) contained *Globorotalia (T.) truncatulinoides*, *Globigerinoides extremus*, *Neoquadrina humerosa*, *Globorotalia (T.) crassaformis* indicating an age of 2.0 to 1.8 Ma (see Supplementary data).

5.1. The Faro and Bartolomeu Dias drifts

The Faro and Bartolomeu Dias drifts (Figs. 4, 5, 10, 11a, 12) are the best developed contourite drifts in the Gulf of Cadiz CDS and thus their seismic architecture, seismic facies and bounding discontinuities will be considered as reference for the subsequent description of the

Fig. 9. (A) Multichannel seismic line BS-07 across a channel–levee system and line drawing interpretation. The paleochannel is top bounded by discontinuity H4. (B) Multichannel seismic line P74-34 across the Bartolomeu Dias paleocanyon and line drawing interpretation. Note the infill pattern made up of a succession of infilling packages top-bounded by high-amplitude horizons that truncate the underlying reflections. Seismic units U1 to U4 facies suggest contourite deposits possibly interbedded with turbidites. Truncations by discontinuities H2 to H5 represent major erosion events by down-slope currents. Since discontinuity H5, the along-slope processes dominate and the canyon was filled-up by deposition of the Bartolomeu Dias sheeted drift (seismic unit U5). M, base of Early Miocene unconformity; F, fault.

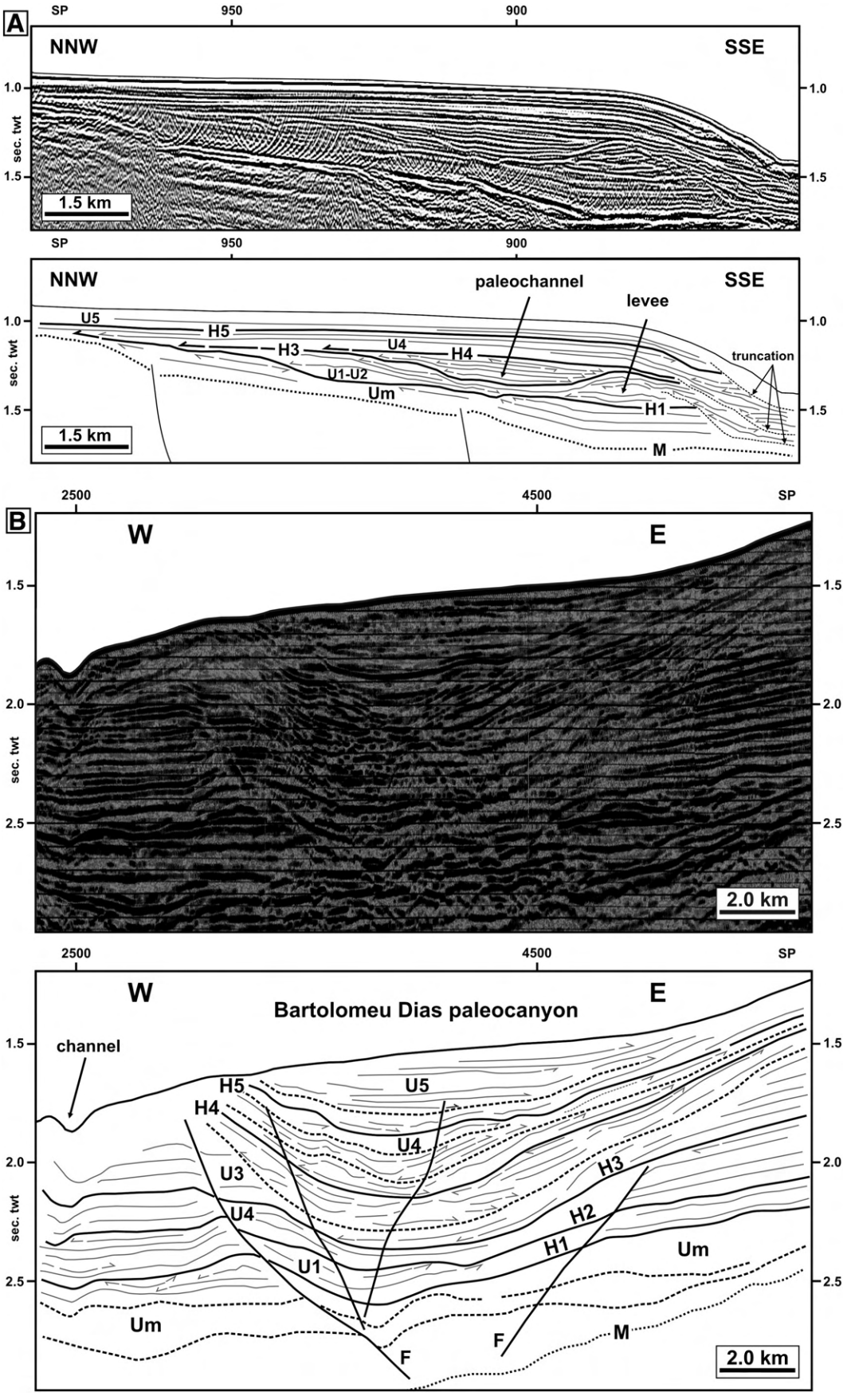
A
SP
950
900
NNW
SSE
1.0
1.5
sec. twt
1.5 km
SP
950
900
NNW
paleochannel
levee
SSE
U5
H5
H3
U4
H4
U1-U2
Um
H1
M
truncation
1.5 km
B
2500
4500
SP
W
E
1.5
2.0
2.5
sec. twt
2.0 km
2500
4500
SP
W
Bartolomeu Dias paleocanyon
E
channel
H5
U5
H4
U4
U3
H3
U4
H2
H1
U1
Um
Um
F
F
M
2.0 km

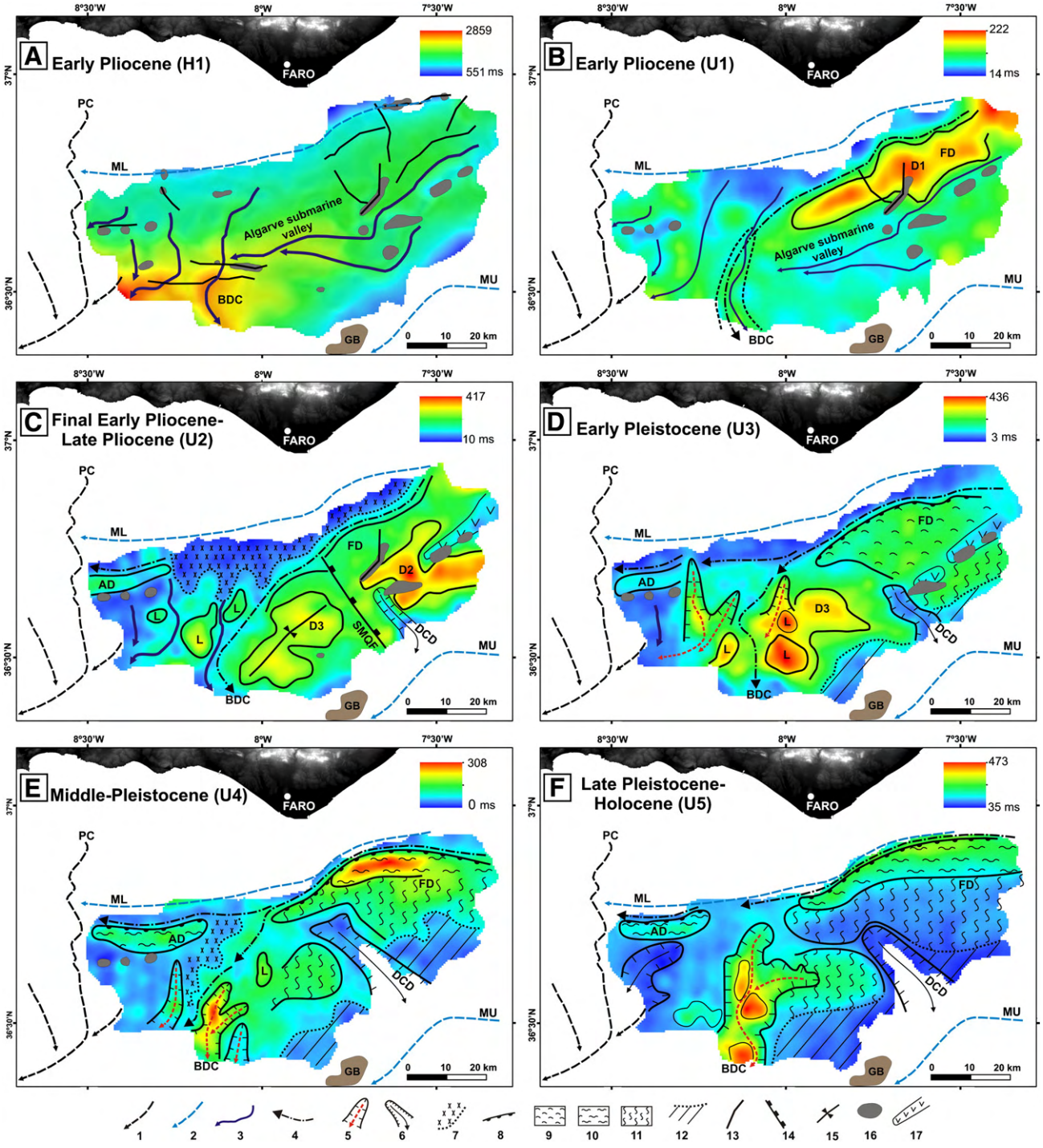

Fig. 10. Geological interpretation of seismic mapping (ms TWT). (A) Isobath map of discontinuity H1 (Early Pliocene). (B) Isopach map of seismic unit U1 (Early Pliocene). (C) Isopach map of seismic unit U2 (Final Early Pliocene–Late Pliocene). (D) Isopach map of seismic unit U3 (Early Pleistocene). (E) Isopach map of seismic unit U4 (Middle Pleistocene). (F) Isopach map of seismic unit U5 (Late Pleistocene–Holocene). Symbol legend: 1 — present-day downslope drainage pathway; 2 — present-day MOW circulation path; 3 — ancient drainage path; 4 — paleo-MOW circulation path; 5 — filled-up paleochannel; 6 — channel; 7 — truncation; 8 — progradational front of the drift; 9 — aggradational or plastered drift; 10 — mounded drift; 11 — sheeted drift; 12 — uplifted area; 13 — fault; 14 — normal fault; 15 — syncline; 16 — salt dome; 17 — diapiric ridge. Legend of features in alphabetical order: AD, Albufeira drift; BDC, Bartolomeu Dias paleocanyon; D1–D3, depocenters; DCD, Diogo Cão Deep; FD, Faro drift; GB, Guadalquivir Bank; L, levees; ML, lower core of the MOW; MU, upper core of the MOW; PC, Portimão canyon; SMQF, São Marcos–Quarteira fault.

Albufeira, Portimão, Lagos and Sagres drifts. The Faro drift seats above a basal discontinuity H1 that top-bounds a pre-contourite seismic unit Um that corresponds to a succession of slope prograding wedges (Figs. 5a, 11a). The basal boundary of Um is the M unconformity (Figs. 4, 5, 11, 12), a basin-scale erosive surface that separates the underlying folded Early Cretaceous and Paleogene rocks from the overlying Miocene rocks (Terrinha et al., 2006; Roque, 2007). The age assigned to the seismic unit Um by correlation with biostratigraphic data from oil-wells Corvina, Ruivo and Imperador and core SWIM04-39 (Figs. 1, 2f), spans from the Burdigalian (~20.5 Ma) to the Early Pliocene (4.2–3.8 Ma).

The Faro and Bartolomeu Dias drifts consist of seismic units U1 to U5 separated by discontinuities H1 to H5 (Figs. 4, 5, 10, 11a, 12) and reach, respectively, about 0.75 s TWT and 1.0 s

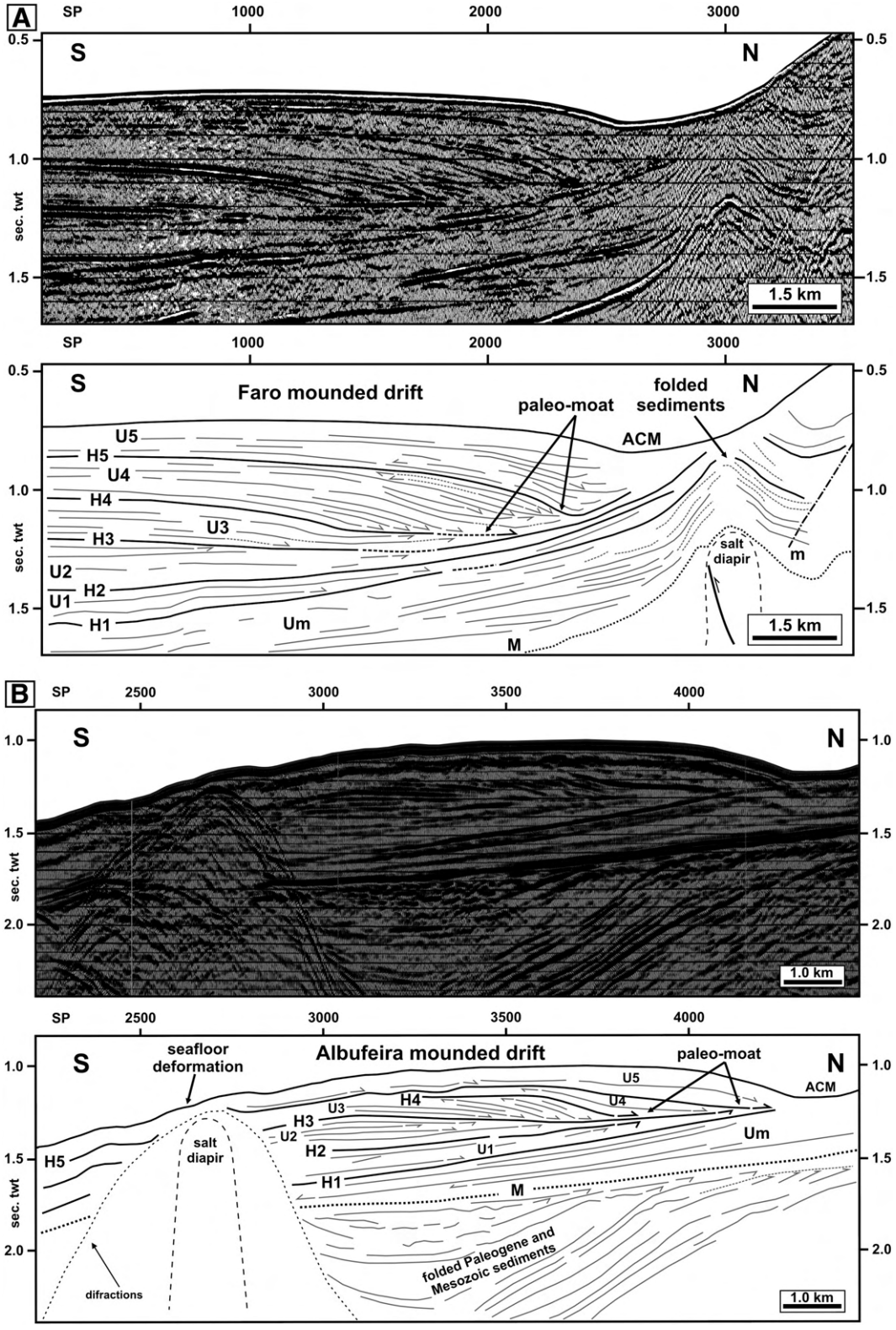

Fig. 11. (A) Multichannel seismic line P81-15 across the Faro drift and its relationship with tectonics and salt diapir deformation underneath the Álvares Cabral Moat (ACM) and line drawing interpretation. The diapir deformed the above sediments since the Miocene. Note the folding of discontinuities H1 to H3. (B) Multichannel seismic line P74-03 across the salt dome at the end of the Albufeira drift and line drawing interpretation. Note that this diapir is piercing through seismic units U1 until U5 and discontinuity H5 is folded at top of this structure. In this site the seafloor is deformed and a circular feature is seen in bathymetry shown in Fig. 3A. M, base of Early Miocene unconformity; m, multiple.

TWT thickness. The Faro drift architecture changed through time from slope sheet to mounded drift with a well developed moat (Figs. 5a, 10, 11a), while its southwards continuation developed simultaneously overtime as the Bartolomeu Dias sheeted drift (Figs. 5b, 10, 12).

Seismic unit U1 is bounded by discontinuity H1, an erosional surface deepening southwestwards, and is truncated by discontinuity H2 towards north (Figs. 5a, 10b, 11a). Unit U1 displays semi-transparent to stratified seismic facies with medium amplitude and low continuity reflections and aggradational configuration onlapping

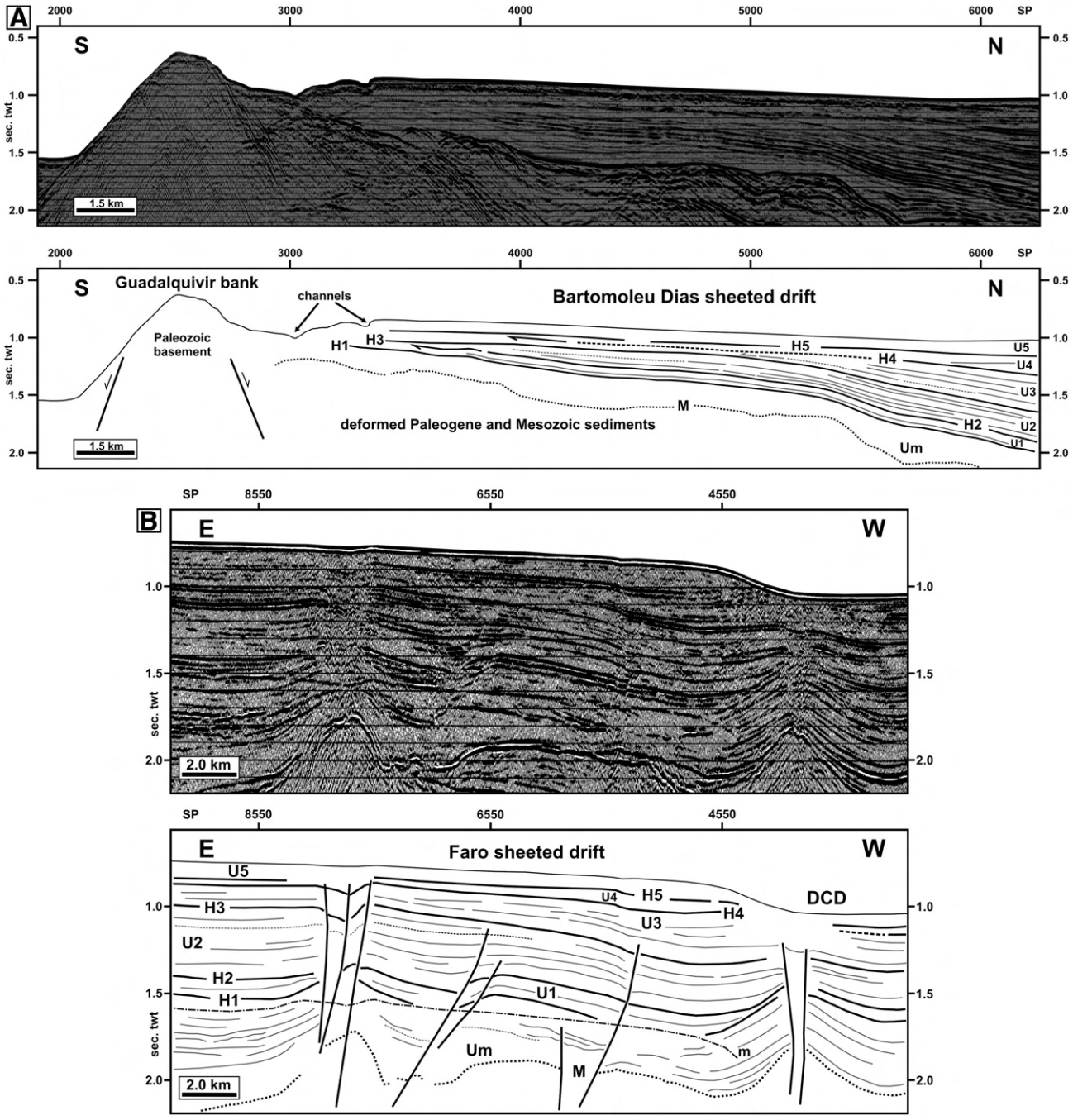

Fig. 12. (A) Multichannel seismic line P74-39 across the Guadalquivir Bank, the Bartolomeu Dias sheeted drift and line drawing interpretation. (B) Multichannel seismic line P81-12 across the Diogo Cão Deep (DCD), and Faro sheeted drift and line drawing interpretation. M, base of Early Miocene unconformity; m, multiple.

northwards the slope of basal discontinuity H1 (Figs. 5, 11a). This geometry point to a slope sheet drift developed against H1 (Figs. 5a, 11a) that evolves southwards to a sheeted drift (Fig. 5b). Seismic unit U1 should be younger than the underneath sediments of seismic unit Um (4.2–3.8 Ma) (Fig. 2f), possibly final-Early Pliocene. Seismic unit U1 is correlated with the upper part of seismic unit P1 identified by Llave et al. (2011) (Fig. 4).

Seismic unit U2 displays a similar seismic facies and configuration compared to seismic unit U1and is truncated towards the north by discontinuity H3, a high-amplitude and high continuity reflection that marks a major erosional phase in the northern area (Figs. 5, 10c, 11a). Geometry of this drift changes from slightly low-mounded at north (Figs. 5a, 11a) to sheeted at south (Figs. 5b, 12). An age of final Early Pliocene–Late Pliocene is proposed considering its stratigraphic calibration using Algarve-2 well (Fig. 2a). Seismic unit U2 can be correlated with part of seismic units P1 and P2 of Llave et al. (2011) (Fig. 4).

Seismic unit U3 is topped by discontinuity H4, which has high amplitude and high continuity with erosional character towards the north (Figs. 5a, 11a). Unit U3 presents a sigmoidal configuration with a marked aggradational component that evolves to a slight progradational geometry towards north, and can be classified as an elongated low-mounded drift (Figs. 5a, 10 d, 11a), suggesting a low intensity current (Faugères et al., 1999). The southern part of U3

shows aggradational configuration indicating a sheeted drift (Figs. 5b, 10 d, 12). An Early Pleistocene age for U3 is proposed based on its stratigraphic constrains, according biostratigraphic data from samples taken from cores SWIM04 (Fig. 2e, f, g). The basal discontinuity H3 can be correlated with horizons BD and D1 assigned to the base of Quaternary and described, respectively by Llave et al. (2001, 2007, 2011) and Marchès et al. (2010) (Fig. 4).

Seismic unit U4 is topped by discontinuity H5, a high amplitude and medium lateral continuity reflection or is truncated southwards in the DCD (Figs. 5a, 11a, 12b). Towards the ACM, unit U4 shows a general mounded geometry and progradational sigmoidal configuration and downlap terminations defining a mounded drift (Figs. 5a, 10e, 11a). Locally unit U4 is offset by syn-depositional faults related to slope instability (Fig. 5a). Towards the south, aggradational configuration dominates (Figs. 5b, 12). Considering the biostratigraphic age from the SWIM cores, the basal discontinuity H4 should be younger than 2.0–1.8 Ma and thus a middle Pleistocene age is proposed for U4 (Fig. 2). This discontinuity is correlated with discontinuity MPR (Mid-Pleistocene Revolution) identified by Llave et al. (2001, 2007, 2011) and Marchès et al. (2010) (Fig. 4).

Seismic unit U5 is topped by the seafloor and presents progradational geometry with sigmoidal to oblique configuration and downlap terminations towards the ACM (Figs. 5a, 10f, 11a). The mounded drift geometry is best developed in this direction, whereas the sheeted morphology developed southwards (Figs. 5b, 10f, 12). An upper Pleistocene–Holocene age is tentatively assigned to this seismic unit considering its stratigraphic position (Fig. 2). The basal discontinuity H5 can be correlated with horizons ID12 and D3 identified respectively by Llave et al. (2001, 2007, 2011) and Marchès et al. (2010), both correlated with MIS 12 (~0.55 ka) (Fig. 4).

5.2. The Albufeira drift

The Albufeira drift (Figs. 6a, 10, 11b) consists of seismic units U1 to U5 bounded by discontinuities H1 to H5 as in the Faro drift. Seismic unit U1 onlaps H1 northwards and shows semi-transparent facies and geometry of a slope sheet drift onlaping H1(Fig. 11b). Seismic unit U2 presents a succession of reflections with high-amplitude and continuity and low-mounded drift geometry (Fig. 11b). It is top-bounded by discontinuity H3, a high-amplitude, irregular reflection that marks the end of deformation and the beginning of channeling associated with the erosion of a paleo-moat (Figs. 10c, 11b). Seismic unit U3 lies on top of H3 and is topped by H4, which is a sharp, continuous and sub-horizontal reflection. The facies of this unit are stratified with sub-horizontal and parallel high-amplitude and continuity reflections defining an aggradational pattern (Fig. 6a) that changes to progradational oblique towards north defining a mounded drift (Fig. 11b). Seismic unit U4 marks the beginning of the build-up of a thicker mounded drift with progadational oblique configuration. Seismic unit U5 shows a progradational sigmoidal–oblique configuration with alternating transparent and high amplitude facies. All seismic units are deformed by salt diapirs (Figs. 10, 11b).

5.3. The Portimão drift

The Portimão drift is composed of three seismic units (U1–U3 combined, U4 and U5), respectively bounded by horizons H1, H4, and H5 (Fig. 6b). Seismic unit U1–U3 corresponds to a condensed section of seismic units U1, U2 and U3 found in the Faro and Albufeira drifts. It shows a set of very high-amplitude parallel reflections at the bottom that become low and high-amplitude reflections through the top, fills-up a paleochannel that incised the Miocene and Early Pliocene deposits (Fig. 6b) aligned with one of the present-day channels (possibly C3 in Fig. 3a). Seismic unit U4 seals this paleochannel, has low amplitude reflections at the bottom and high-amplitude and continuous reflections near the top (Fig. 6b). The configuration is aggradational defining a sheeted drift. Seismic unit U5 shows semi-transparent facies that change to a succession of high-amplitude reflections near the top. Although the configuration is aggradational defining a sheeted drift, a slightly mounded geometry in the upper part suggests a small progradational component.

5.4. The Lagos drift

The seismic architecture and morphology shown by the Lagos drift evolve from a sheeted drift in the eastern sector (Fig. 7a–b) to a mounded and separated drift in the western sector (Fig. 8a–b). The Lagos drift consists of seismic units U1–U2, U3, U4 and U5 bounded by discontinuities H1, H3, H4 and H5. Seismic unit U1–U2 corresponds to a condensed section of seismic units U1 and U2 well developed in the Faro drift (Figs. 7, 8b). This unit shows a succession of slope fans of Miocene through Early Pliocene age (Fig. 7a), possibly related to past activity of channels C1–C3 (Fig. 3a).

The sheeted drift (Fig. 7a) has a flat morphology and seismic units present aggradational configuration, with facies characterized by a succession of high-amplitude sub-horizontal and parallel reflections. This configuration is generally interpreted as an indicator of deposition under a weak bottom current.

On the slope of the SVH, drift sediments onlap the M unconformity (Fig. 7b). Seismic units U1–U2 and U3 show internal discontinuous and high amplitude reflections. Units U4 and U5 show a slight mounded geometry and consist of high-amplitude parallel reflections. No moat is observed and the seafloor surface is almost sub-horizontal and flat (Fig. 7b). This configuration suggests a slight enhancement of the bottom-current in this site as it flows towards the SVH.

The mounded drift (Fig. 8a, b) has a well marked moat and displays an overall progradational configuration associated to the growth of seismic units U3 to U5. Seismic unit U1–U2 rests above discontinuity H1, which truncates the underlying deposits, and shows channel–levee facies that changes to aggradational pattern towards SVH onlaping this feature (Fig. 8a, b). Discontinuity H3 is high amplitude, truncates seismic unit U1–U2 and marks a change in the stacking pattern, with the overlying seismic unit U3 displaying aggradational pattern and units U4 and U5 showing mounded geometry prograding towards the SVH (Fig. 8a, b). The geometry of the discontinuity H4 shows the development of a paleo-moat at this stage. The observed change from sheeted to mounded geometry is indicative of a strong bottom-current (Faugères et al., 1999), which is probably the consequence of a local increase of the MOW strength as a result of abutting against the hard rock relief of the SVH, surrounding it and diverting northwards along the West Portuguese margin.

Channels incised during seismic unit U1–U2 times were filled-up by unit U3 and are top-bounded by horizon H4 (Fig. 9a). These paleochannels could be related to channels C1, C2 and C3 that incise the present-day continental slope of the Algarve margin (Fig. 3a).

5.5. The Sagres drift

The Sagres drift (Figs. 3a, 8a, c) has a similar geometry and seismic architecture to the westernmost part of the Lagos drift and consists of four seismic units U1–U2, U3, U4 and U5. The basal discontinuity H1 is sharp with a strong erosional character close to the SVH. Seismic unit U1–U2 is truncated by discontinuity H3 and its configuration shows a clear aggradational component. Seismic unit U3 and the overlying units U4 and U5 are mounded drifts with a poorly developed moat. Therefore, the Sagres drift major growing phase, as a thicker mounded drift, occurred since Middle-Pleistocene times (seismic units U4 and U5), suggesting the presence of a permanent or semi-permanent bottom current contouring the SVH since that time. Towards the SVC seismic units U1–U2 and U3 show the

development of channel–levee facies (Fig. 8c) and evidence of slide scars filled-up by sediments near the flank of the canyon (Fig. 8a).

6. Discussion

6.1. Depositional and age model

The knowledge of how the different depositional and erosional processes acted in the northern margin of the Gulf of Cadiz since the Early Pliocene, especially the interaction between down-slope and along-slope processes, is crucial for the reconstitution of the contourite drifts evolution through time. Considering the seismostratigraphic architecture of the drifts and the mapping of seismic units, a three phased depositional model is proposed: i) a precursor phase since Early through Late Pliocene; ii) a building phase during Early Pleistocene; and iii) a growing phase from Middle-Pleistocene to Holocene.

6.1.1. Precursor phase (Pliocene)

The inherited morphology of the Algarve margin eastwards of the PC in the Early Pliocene is shown by the isobaths map of discontinuity H1 (Fig. 10a), which displays a NE–SW elongated central depression deepening towards the SW, the Algarve submarine valley, bounded to the north by the paleo-continental slope and to the south by the GB uplifted area. Two submarine drainage trends are recognized: i) a central NE–SW valley; and ii) a N–S down-slope drainage system parallel to the PC.

This paleotopography was also shaped by diapirism shown by the elongated NE–SW diapiric ridge separating two valleys in the eastern sector and by an E–W alignment of salt domes in the western sector (Fig. 10a). Some of these domes have been active until the present deforming the above Pliocene through Holocene sediments (Fig. 11) and are depicted in the present-day bathymetry (Fig. 3a).

The precursor phase of contourite drift deposition during the Pliocene is represented by seismic units U1 and U2 in the Faro and Albufeira drifts and the correlative condensed sections in the Portimão (seismic unit U1–U3), Lagos (seismic unit U1–U2) and Sagres drifts (seismic unit U1–U2) (Figs. 4, 5, 6 and 7). The earlier stage of this depositional phase, represented by seismic unit U1, marks the beginning of the contourite drifts development off Faro (Fig. 4). Inspection of the isopach map of this unit (Fig. 10b) reveals the existence in the eastern sector of a NE–SW trending depocenter (D1) that corresponds to the earliest development of the Faro drift, a slope sheet drift onlaping H1 (Fig. 5a) indicating a weak bottom-current flowing from NE to SW.

The joint inspection of Figs. 9b and 10b suggests the existence of a MOW pathway towards the SW probably being captured by the Bartolomeu Dias paleocanyon (BDC) in a similar way to the present-day interaction between the MOW and the PC (Serra et al., 2005; Ambar et al., 2008). The isopach map of seismic unit U2 (Fig. 9c) is strikingly different with respect to U1, which indicates important sedimentation changes at the final early Pliocene and during Late Pliocene. Firstly, in the eastern sector, the Faro drift migrated northwards. Secondly, two main depocenters (D2 and D3) along the NE–SW direction, separated by the NW–SE striking SMQF, are observed in the deeper part of the basin. Both depocenters indicate that the subsidence associated with the basin sagging initiated during the deposition of this unit and the activity of the SMQF also resumed in this time as well as the activity of the NE–SW striking diapiric ridge whose impingement into this unit reduced its thickness to nil. Thirdly, in the western sector, the Albufeira drift appears as an E–W minor depocenter, indicating an incipient development of this drift during the Pliocene (Fig. 6a) and levees associated with the BDC and PC systems are observed (Fig. 9b). Fourthly, in the northern sector, the truncation of seismic unit U2 indicates a regional erosional event by the end of the Late Pliocene linked to the channeling of the MOW and formation of a moat during subsequent H3 times (Fig. 5a).

In the Portimão, Lagos and Sagres drifts the down-slope processes dominate, as shown by the presence of slope fans and channel–levee (Figs. 6b, 7a, 8, 9a).

6.1.2. Building phase (Early Pleistocene)

The isopach map of seismic unit U3 (Fig. 10d), which marks the onset of the building up of the drifts during the Early Pleistocene shows the following main features: firstly, that the progradation of the Faro drift continued northwards; secondly, a precursory moat of the present-day ACM started to be perceptible and, thirdly, that the NE–SW striking diapiric ridge was still active during this phase, acting as a barrier to sedimentation and dividing the Faro drift in two areas with different stacking patterns: a progradational mounded drift in the north and a sheeted drift in the south (Fig. 4). A NNW–SSE trending channel is recognized in the present-day position of the DCD, draining towards the SW joining up with the Guadalquivir channel (Fig. 3a). The area of D3 was the main depocenter at this phase (Fig. 10d).

The MOW followed two main pathways during the building phase. The previous pathway along the BDC remained active (Fig. 9b), but the westwards flow parallel to the continental slope increases its importance, as shown by the growing of the depocenter associated with the Albufeira drift (Fig. 6a).

In the Lagos and Sagres drifts the building phase is comparatively insignificant, however, a change in the configuration of seismic units is observed from slope fan facies (Fig. 7a), towards a bottom current shaped architecture (Fig. 8).

6.1.3. Growing phase (middle Pleistocene–Holocene)

The growing phase started in Middle Pleistocene times and is still active at the present and can be divided in two stages represented by seismic units U4 and U5 separated by discontinuity H5 (Figs. 5, 6, 7, 8). It is characterized by the thickening of the Faro and Albufeira mounded drifts and major development of the Portimão, Lagos and Sagres drifts. In this phase the MOW flowed westwards along a moat precursory of the ACM, following a circulation pattern that resembles the present-day one (Fig. 10e, f). As the mounded drifts grew prograding northwards, they filled-up a succession of paleo-moats suggesting an enhanced MOW circulation (Figs. 5a, 6a).

The isopach map of seismic unit U4 (Fig. 10e) shows a well-developed Faro mounded drift separated from the continental slope by a distinctly paleo-ACM (Fig. 5a) and a thick-sheeted drift towards the SE (Fig. 5b). The subsidence of the depocenter D3 ceased and the deposition of a sheeted drift in this area filled-up most of the BDC and the channels located in its western flank (Fig. 9b). An uplift episode of the GB area occurred during the deposition of seismic unit U4 (Figs. 10e, 12a).

The Albufeira mounded drift experienced its most important growth as it prograded to the north accompanying the development of the paleo-ACM and to the south filling up the shallower part of the BDC (Figs. 6a, 9b, 10e–f).

The N–S paleo-channels related to C1 to C3 were sealed by this seismic unit (Figs. 5b, 8a).

The isopach map of seismic unit U5 (Fig. 10f), from near Late Pleistocene through Holocene, shows a well developed Faro and Albufeira mounded drifts and the ACM. Northwards progradation of the Faro and Albufeira drifts is clear in this depositional stage (Figs. 5a, 6a, 10f). The BDC was finally filled-up by this seismic unit (Fig. 9b), indicating a preferential circulation of the MOW along the paleo-ACM.

6.2. Controlling factors of the contourite drifts development

The spatial and temporal evolution of the contourite system of the Algarve margin results from a complex interplay between the

following factors that can act locally or regionally: i) the circulation of the MOW forced by the Pliocene–Quaternary climate changes; ii) the influence of seafloor topography; iii) the interaction between down-slope and along-slope processes and iv) tectonics.

6.2.1. The circulation of the MOW forced by the Pliocene–Quaternary climate changes

The association between deposition of the CDS and variability of the MOW driven by the Late Quaternary climate changes has been investigated by several authors (e.g. Hernández-Molina et al., 2006; Llave et al., 2006; García et al., 2009; Marchès et al., 2010). Considering this association and assuming an analog behavior of the MOW during older glacials and interglacials, this section of the paper presents a discussion of the relationships between the contourite drifts development phases and the major climate and MOW circulation changes since Pliocene.

The global warmer climate that prevailed since the beginning of the Pliocene favored an increase of freshwater input in the Mediterranean Sea leading to surface waters stratification and decrease of the MOW intensity (Béthoux and Pierre, 1999). Climate started to cool at about 3.6 Ma (MIS Gi2) (Lisiecki and Raymo, 2005) and increasing arid and cold conditions in the Mediterranean region triggered the formation of a saltier and intense MOW at about 3.5–3.0 Ma (Béthoux and Pierre, 1999; Becker et al., 2006; Hayward et al., 2009; Khélifi et al., 2009). The observed sudden change of the sedimentary architecture from the Miocene to the Pliocene, i.e. the beginning of the Faro drift deposition (seismic units U1 and U2), together with the onset of erosion on the continental slope (Figs. 4, 5, 10a, b) is possibly the first evidence of the early MOW circulation along the paleo-continental slope of the Algarve margin. The aggradational component of this precursory phase indicates a weak bottom current, yet persistent and stable.

The second major change in MOW circulation, with a well established anti-estuarine regime (e. g. Rio et al., 1990; Béthoux and Pierre, 1999; Hayward et al., 2009), coincided with the onset of Northern Hemisphere glaciations at 2.7 Ma (MIS 104) (e.g. Jansen et al., 2000; Lisiecki and Raymo, 2007). At that time the growth and southwards advance of ice-sheets caused arid and cold conditions in the Mediterranean and North Atlantic regions that inhibited or even suppressed the formation of NADW reducing the thermohaline circulation in the North Atlantic and conversely favored the stronger formation of saltier MOW (Becker et al., 2006). It is speculated here that this enhancement of the MOW is recorded by the seismic unit U3 (Fig. 4), the earliest clear progradational unit of the CDS indicating sedimentation under a stronger bottom-current. The building and growth of thick contourite drifts increased since that time onwards.

A third intensification of the MOW happened at about 1.3–1.0 Ma (e.g. Rio et al., 1990; Hayward et al., 2009) around the Mid-Pleistocene Transition (MPT) (Fig. 4), which started at 1.5–1.25 Ma with increasing climate deterioration towards major growth and advance of the Northern Hemisphere ice-sheets at 0.9–0.8 Ma (MIS 22) (Lisiecki and Raymo, 2007). Since the MPT, the climate variability became asymmetrical with long glaciations and short deglaciations for each cycle modulated by orbital eccentricity forcing (100 ky periodicity) (Lisiecki and Raymo, 2005; Crowley and Hyde, 2008). The onset of these climate changes and MOW circulation variability should be recorded by deposition of seismic unit U4 (Fig. 4).

At about 550 ka a fourth strengthening of the MOW occurred (e.g. Hayward et al., 2009), which coincided roughly with the coldest Pleistocene time interval recorded in the Mediterranean region at 474–427 ka (MIS 12) (Hughes et al., 2007), characterized by rapid advance and growth of ice-sheets towards lower latitudes (Toucanne et al., 2009) and weakening of thermohaline circulation (Wang et al., 2002). These climate conditions were more severe when compared to the ones of the LGM, thus suggesting the existence of an even stronger MOW flowing at greater depths than at present, probably without an upper core circulating along the ACM during MIS 12, following the analogy with the model of García et al. (2009). This period could be recorded by discontinuity H5 as a no-deposition surface.

The subsequent interglacial, from 420 to 360 ka (MIS 11), was the longest and warmest of the past 500 ka (Jouzel et al., 2006), marking a change in the amplitude of the following glacial/interglacials, with strong and longer interglacials in opposition to colder and rapid glacials (Jouzel et al., 2006). Following the same analogy used before, these warmer conditions during MIS 11 could have restarted the MOW circulation at shallower levels, and with it, the onset of the last growing stage of contourite deposition (seismic unit U5). The prevalence of longer and warmer interglacials since MIS 11 (such as MIS 9 and MIS 5) possibly favored the circulation of a persistent and stable enough upper core of MOW during these periods, in order to allow the building-up of a thicker drift (Figs. 4, 5, 6, 7, 8). The progradational mounded geometry of the drifts (e.g. Fig. 5a) possibly reflects the maintenance for longer time of a strong current at shallower levels during interglacials, longer than the time left without current circulation during short glacials. During these periods the general morphology of the drift and moat was preserved, but either no sedimentation occurred or it consisted mainly of turbidites or hemipelagites. At each new interglacial, as the circulation of MOW upper core restarted at these depths, the previous moat was filled-up with sediments as progradation of the drift progress landwards and a new moat was formed (Figs. 5a, 6a, 11).

6.2.2. The seafloor topography, down-slope and along-slope processes and tectonics

The basin topography controls the intensity and pathway of the current, as well as the geometry of the contourite deposits, and plays an important role in the competition between down-slope and along-slope sedimentation. This is well seen in the Algarve margin as the contourite deposits evolved, as a whole, from sheeted to mounded drifts, from Early Pliocene through the present, as the Algarve submarine valley progressively filled up with time (Fig. 10). An example of the topographic control on drift morphology is shown by the Lagos drift that changes from sheeted to mounded (seismic units U4 and U5) from east towards the SVH (Figs. 7, 8). This geometry change reflects the acceleration of the MOW as it swings around the St. Vincent cape, flowing northwards.

At the basin scale the contourite thicknesses mapping (Fig. 10b–f) showed how the flow of the MOW presumably changed from Early Pliocene times through present. According to the evolution of the contourite depocenters (Fig. 10) it is proposed that the MOW was captured and driven to deeper levels by the BDC, the PC and the LC. The progressive filling up of BDC (Fig. 9b) interrupted the capture process in Quaternary times and forced the MOW to flow westwards along the slope, thus contributing to the greater development of the Albufeira, Portimão, Lagos and Sagres drifts onwards (Figs. 6, 7, 8).

The interplay between drift development by bottom-current activity and its destruction by gravity-processes is shown by the Lagos drift (Fig. 8a, b) where several sediment failures affected the drift sediments towards the LC. In the Sagres drift, the down-slope processes related to SVC dynamics are prevalent towards the canyon and a succession of infill-channels and levees are seen within the drift sedimentary record (Fig. 8a, c).

In the western sector, down-slope processes have been dominant since the Miocene–Early Pliocene (Figs. 3a, 6b, 7a, 8, 9a, 10), as testified by: i) the presence of slope fans of Miocene and Early Pliocene age (seismic unit U1–U2); ii) the presence of channel–levee formed during the early to Late Pliocene (seismic unit U1–U2); iii) paleovalleys and paleochannels filled-up by Early Pleistocene bottom-current deposits (seismic unit U3); iv) the small development of the Portimão, Lagos and Sagres drifts (seismic units U3, U4 and U5); and v) the present-day morphology, which is mainly shaped by canyon incision and mass-wasting.

The influence of tectonics in the edification of the Algarve margin contourites since the Early Pliocene results from i) basin sagging, ii) activity of SMQF, GBF, PF, and iii) diapirism, that segmented the contourite bodies since the Early Pliocene (Fig. 10b–f). However, through time sedimentation rate overcame tectonics and the contourite grew smoothing the morphology (Fig. 3a).

Sagging of the Algarve basin, active since the Early Miocene (Terrinha et al., 2006; Roque, 2007), intensified throughout the Pliocene and Quaternary, as recorded by H1 to H5 episodes (Fig. 5b). Activity of SMQF also accounts for subsidence of the eastern sector during the Pliocene (Fig. 10c). Sagging favored contourite deposition by deepening of the seafloor, exposing it to the MOW circulation, and by creation of accommodation space. Recent displacement of SMQF is masked both by the high sedimentation of Faro–Bartolomeu Dias drift (Figs. 4, 9) and erosion at DCD (Fig. 10, 12b).

Uplift of the GB (Figs. 10, 12a) is shown by i) the progressive steepening of H1–H5; ii) successive truncation of units U1 to U5 towards this feature; iii) landward sloping of the seafloor; and iv) truncation of U5 reflections. This uplift allowed the deposition of the sheeted drifts (Figs. 10b–f) that covered the ancient Algarve submarine valley, the BDC and PC (Fig. 10a), shaping the present-day smooth morphology (Fig. 3a).

Also the fill-up of the BDC, controlled by NW–SE trending faults as the DCD (Figs. 9b, 12b), diminished the importance of the capture of the MOW into depth, favoring the development of the along-slope sedimentation.

The Portimão fault (PF) that controls the PC favored its incision through time until the present by capturing the MOW and preventing it being filled-up like the BDC.

Salt diapir activity influenced the Faro and Albufeira drifts deposition since Early Pliocene until present-day (Fig. 3a), by confining these bodies and deforming the sediments (Fig. 11).

7. Conclusions

The following conclusions can be drawn:

1. The overall architecture of the Algarve contourites is diachronic from east to west and dependent on the paleogeography of the seafloor and paleoceanography of the MOW, both of which are related with tectonics and climate changes.
2. Three sequential phases of development were established in the development of the Algarve margin contourites, the precursor, building up and growing phases. These phases developed diachronically, i.e. the first phase developed in the Early Pliocene in the east while in the west, near St. Vincent High, the last phases developed only in Quaternary times. The most expanded seismic units are observed in the Faro and Albufeira drifts allowing the dating of these three phases of development: firstly, the precursor phase from Early Pliocene to the end of Late Pliocene; secondly, the building up phase of Early Pleistocene age and; thirdly, the growing phase from mid-Pleistocene through Holocene.
3. The precursor phase is associated with the initial stages of the enhanced MOW along the Algarve margin at about 3.5–3.0 Ma; the building up phase is probably related to the major change in the MOW circulation at the onset of Northern Hemisphere glaciations at 2.6–2.4 Ma; and the growing phase is related to the changes in the MOW circulation after the Middle Pleistocene Transition (1.3–1.0 Ma).
4. The distribution of the main drift depocenters east of the Portimão canyon strongly suggests that the MOW was initially captured and driven to deeper levels along the Bartolomeu Dias paleo-canyon (BDC). The filling up of this canyon and general diminishment of the accommodation space in the middle slope enhanced the circulation of the MOW to the west increasing the sedimentation rate (growing phase) of the mounded contourites and the eroding capacity of the MOW onto the Algarve slope.
5. The growth of the NE–SW trending diapiric ridge and the activity of the NW–SE striking São Marcos–Quarteira fault (SMQF) as an extensional fault mainly in Pliocene times played an important role in the localization of depocenters. This diapiric ridge conditioned the flow of the MOW and controlled the trend of the Faro drift in the Pliocene.

Supplementary materials related to this article can be found online at doi:10.1016/j.margeo.2011.11.001.

Acknowledgments

We thank the support of Fundação para a Ciência e a Tecnologia (FCT) through the projects TOPOMED- "Plate re-organization in the western Mediterranean: lithospheric causes and topographic consequences" (ref. TOPOEUROPE/0001/2007), PEST-OE/CTE/LA0019/2011-12 and Cd-ToxCoN (FCT PTDC/MAR/102800/2008). C. Roque benefits a FCT Post-Doc grant (SFRH/BPD/42534/2007) and V. Valadares a FCT Ph.D. scholarship (SFRH/BD/17603/2004). This is an ISMAR contribution n.1741. We wish to thank to the crew of the *R/V Urania* during SWIM2004 cruise. We also thank the support by Landmark Graphics Corporation via the Landmark University Grant Program. D. Van Rooij, an anonymous reviewer and editor D. J. W. Piper are thanked for their valuable comments, which greatly improved the manuscript.

References

Ambar, I., Howe, M.R., 1979a. Observations of the Mediterranean outflow — I. Mixing in the Mediterranean outflow. Deep Sea Research 26A, 535–554.
Ambar, I., Howe, M.R., 1979b. Observations of the Mediterranean outflow — II. The deep circulation in the vicinity of the Gulf of Cadiz. Deep Sea Research 26A, 555–568.
Ambar, I., Serra, N., Brogueira, M.J., Cabeçadas, G., Abrantes, F., Freitas, P., Gonçalves, C., Gonzalez, N., 2002. Physical, chemical and sedimentological aspects of the Mediterranean outflow off Iberia. Deep Sea Research 49, 4163–4177.
Ambar, I., Serra, N., Neves, F., Ferreira, T., 2008. Observations of the Mediterranean Undercurrent and eddies in the Gulf of Cadiz during 2001. Journal of Marine Systems 71, 195–220.
Armi, L., Farmer, D.M., 1988. The flow of Mediterranean water through the Strait of Gibraltar. Progress in Oceanography 21, 1–106.
Baringer, M.O., Price, J.F., 1997. Mixing and spreading of the Mediterranean Outflow. Journal of Physical Oceanography 27, 1654–1677.
Baringer, M.O., Price, J.F., 1999. A review of the physical oceanography of the Mediterranean outflow. Marine Geology 155, 63–82.
Becker, J., Lourens, L.J., Raymo, M.E., 2006. High-frequency climate linkages between the North Atlantic and the Mediterranean during marine oxygen isotope stage 100 (MIS100). Paleoceanography 21, PA3002. doi:10.1029/2004PA001168.
Béthoux, J.-P., Pierre, C., 1999. Mediterranean functioning and sapropel formation: respective influences of climate and hydrological changes in the Atlantic and the Mediterranean. Marine Geology 153, 29–39.
Bower, A., Serra, N., Ambar, I., 2002. Structure of the Mediterranean undercurrent and Mediterranean water spreading around the southwestern Iberian Peninsula. Journal of Geophysical Research 107 (C10), 3161. doi:10.1029/2001JC001007.
Bryden, H.L., Kinder, T.L., 1991. Steady, two-layer exchange through the Strait of Gibraltar. Deep Sea Research 38, 445–463.
Cacho, I., Grimalt, J.O., Sierro, F.J., Shackleton, N.J., Canals, M., 2000. Evidence of enhanced Mediterranean thermohaline circulation during rapid climatic coolings. Earth and Planetary Science Letters 183, 417–429.
Cacho, I., Shackleton, N., Elderfield, H., Sierro, F.J., Grimaltd, J.O., 2006. Glacial rapid variability in deep-water temperature and $\delta^{18}O$ from the Western Mediterranean Sea. Quaternary Science Reviews 25, 3294–3311.
Cita, M.B., 2001. The Messinian salinity crisis in the Mediterranean. In: Briegel, U., Xiao, W. (Eds.), Paradoxes in Geology. Elsevier Science, pp. 353–360.
Criado-Aldeanueva, F., García-Lafuentea, J., Vargas, J.M., Del Río, J., Vázquez, A., Reul, A., Sánchez, A., 2006. Distribution and circulation of water masses in the Gulf of Cadiz from in situ observations. Deep-Sea Research II 53, 1144–1160.
Crowley, T.J., Hyde, W.T., 2008. Transient nature of late Pleistocene climate variability. Nature 456, 226–230.
De Mol, B., Kozachenko, M., Wheeler, A., Alvares, H., Henriet, J.-P., Olu-Le Roy, K., 2007. Thérèse Mound: a case study of coral bank development in the Belgica Mound Province, Porcupine Seabight. International Journal of Earth Sciences 96, 103–120.
Duarte, J.C., Terrinha, P., Rosas, F.M., Valadares, V., Pinheiro, L.M., Matias, L., Magalhães, V., Roque, C., 2010. Crescent-shaped morphotectonic features in the Gulf of Cadiz (offshore SW Iberia). Marine Geology 27, 236–249.
Faugères, J.-C., Cremer, M., Monteiro, H., Gaspar, L., 1985a. Essai de reconstitution des processus d'edification de la ride sedimentaire de Faro (marge sud-portugaise). Bulletin de l'Institut de Géologie du Bassin d'Aquitaine 37, 229–258.

Faugères, J.-C., Frappa, M., Gonthier, E., Grousset, F., 1985b. Impact de la veine d'eau méditerranéenne sur la sedimentation de la marge sud et ouest Iberique au Quaternaire recent. Bulletin de l'Institut de Géologie du Bassin d'Aquitaine 37, 259–287.
Faugères, J.-C., Stow, D.A.V., Imbert, P., Viana, A.R., 1999. Seismic features diagnostic of contourite drifts. Marine Geology 162, 1–38.
Fauquette, S., Guiot, J., Suc, J.-P., 1998. A method for climatic reconstruction of the Mediterranean Pliocene using pollen data. Palaeogeography, Palaeoclimatology, Palaeoecology 144, 183–201. doi:10.1016/S0031-0182(98)00083-2.
Ferreira, J., Cachão, M., González, R., 2008. Reworked calcareous nannofossils as oceanic dynamic tracers: the Guadiana shelf case study (SW Iberia). Estuarine, Shelf and Coastal Science 79, 59–70.
García, M., Hernández-Molina, F.J., Llave, E., Stow, D.A.V., León, R., Fernández-Puga, M.C., Diaz del Río, V., Somoza, L., 2009. Contourite erosive features caused by the Mediterranean OutflowWater in the Gulf of Cadiz: Quaternary tectonic and oceanographic implications. Marine Geology 257, 24–40.
Gràcia, E., Dañobeitia, J., Verges, J., Bartolome, R., 2003. Crustal architecture and tectonic evolution of the Gulf of Cadiz SW Iberian margin at the convergence of the Eurasian and African plates. Tectonics 22, 1033. doi:10.1029/2001TC901045.
Gutscher, M.-A., Malod, J., Rechault, J.-P., Contrucci, I., Klingelhoefer, F., Mendes-Victor, L., Spakman, W., 2002. Evidence for active subduction beneath Gibraltar. Geology 30, 1071–1074.
Hanquiez, V., Mulder, T., Lecroart, P., Gonthier, E., Marchès, E., Voisset, M., 2007. High resolution seafloor images in the Gulf of Cadiz, Iberian margin. Marine Geology 246, 42–59.
Hanquiez, V., Mulder, T., Toucanne, S., Lecroart, P., Bonnel, C., Marchès, E., Gonthier, E., 2010. The sandy channel–lobe depositional systems in the Gulf of Cadiz: gravity processes forced by contour current processes. Sedimentary Geology 229, 110–123.
Hayward, B.W., Sabaa, A.T., Kawagata, S., Grenfell, H.R., 2009. The Early Pliocene recolonisation of the deep Mediterranean Sea by benthic foraminifera and their pulsed Late Pliocene–Middle Pleistocene decline. Marine Micropaleontology 71, 97–112.
Hernández-Molina, F.J., Llave, E., Somoza, L., Fernández-Puga, M.C., Maestro, A., Léon, R., Medialdea, T., Barnolas, A., García, M., Díaz del Río, V., Fernández-Salas, L.M., Vázquez, J.T., Lobo, F., Alveirinho Dias, J.M., Rodero, J., Gardner, J., 2003. Looking for clues to paleoceanographic imprints: a diagnosis of the Gulf of Cadiz contourite depositional system. Geology 31, 19–22.
Hernández-Molina, F.J., Llave, E., Stow, D.A.V., García, M., Somoza, L., Vázquez, J.T., Lobo, F.J., Maestro, A., Díaz del Río, V., León, R., Medialdea, T., Gardner, J., 2006. The contourite depositional system of the Gulf of Cadiz: a sedimentary model related to the bottom current activity of the Mediterranean outflow water and its interaction with the continental margin. Deep-Sea Research II 53, 1420–1463.
Hughes, P.D., Woodward, J.C., Gibbard, P.L., 2007. Middle Pleistocene cold stage climates in the Mediterranean: new evidence from the glacial record. Earth and Planetary Science Letters 253, 50–56.
Jansen, E., Fronval, T., Ranck, F., Channell, J.E.T., 2000. Pliocene–Pleistocene ice rafting history and cyclicity in the Nordic Seas during the last 3.5 Myr. Paleoceanography 15, 707–721.
Jouzel, J., Lorius, C., Raynaud, D., 2006. Climat et atmosphère au Quaternaire: de nouveaux carottages glaciaires. Comptes Rendus Palevol 5, 45–55.
Kano, A., Ferdelman, T.G., Williams, T., Henriet, J.-P., Ishikawa, T., Kawagoe, N., Takashima, C., Kakizaki, Y., Abe, K., Sakai, S., Browning, E.L., Li, X., IODP Exp. 307 Scientists, 2007. Age constraints on the origin and growth history of a deep-water coral mound in the northeast Atlantic drilled during Integrated Ocean Drilling Program Expedition 307. Geology 35, 1051–1054.
Kenyon, N.H., Belderson, R.H., 1973. Bedforms of the Mediterranean undercurrent observed with side-scan sonar. Sedimentary Geology 9, 77–99.
Khélifi, N., Sarnthein, M., Andersen, N., Blanz, T., Frank, M., Garbe-Schönberg, D., Haley, B.A., Stumpf, R., Weinelt, M., 2009. A major and long-term Pliocene intensification of the Mediterranean outflow, 3.5–3.3 Ma ago. Geology 37, 811–814. doi:10.1130/G30058A.
Lisiecki, L.E., Raymo, M.E., 2005. A Plio-Pleistocene stack of 57 globally distributed benthic $\delta^{18}O$ records. Paleoceanography 20, PA1003. doi:10.1029/2004PA001071.
Lisiecki, L.E., Raymo, M.E., 2007. Plio-Pleistocene climate evolution: trends and transitions in glacial cycle dynamics. Quaternary Science Reviews 26, 56–69.
Llave, E., Hernández-Molina, F.J., Somoza, L., Díaz del Río, V., Stow, D.A.V., Maestro, A., Alveirinho Dias, J.M., 2001. Seismic stacking pattern of the Faro–Albufeira contourite system (Gulf of Cadiz): a Quaternary record of paleoceanographic and tectonic influences. Marine Geophysical Research 22, 487–508.
Llave, E., Schönfeld, J., Hernández-Molina, F.J., Mulder, T., Somoza, L., Díaz del Río, V., Sanchez-Almazo, I., 2006. High-resolution stratigraphy of the Mediterranean outflow contourite system in the Gulf of Cadiz during the late Pleistocene: the impact of Heinrich events. Marine Geology 227, 241–262.
Llave, E., Hernández-Molina, F.J., Somoza, L., Stow, D.A.V., Díaz del Río, V., 2007. Quaternary evolution of the contourite depositional system in the Gulf of Cadiz. In: Viana, A.R., Rebesco, M. (Eds.), Geological Society, London, Special publications, 276, pp. 49–79.
Llave, E., Matias, H., Hernández-Molina, F.J., Ercilla, G., Stow, D.A.V., Medialdea, T., 2011. Pliocene–Quaternary contourites along the northern Gulf of Cadiz margin: sedimentary stacking pattern and regional distribution. Geo-Marine Letters. doi:10.1007/s00367-011-02441-3.
Lopes, F.C., Cunha, P.P., Le Gall, B., 2006. Cenozoic seismic stratigraphy and tectonic evolution of the Algarve margin (offshore Portugal, southwestern Iberian Peninsula). Marine Geology 231, 1–36.
MacRae, A., 2001. The Unixshell script Tif2segy. http://seismic.ocean.dal.ca/pwpwiki/static/Tif2segy.html2001consulted the 3rd March 2008.
Madelain, F., 1970. Influence de la topographie du fond sur l'écoulement Méditerranée entre de Detroit de Gibraltar et le Cap St. Vicent. Cahiers Oceanographiques 22, 43–61.
Maldonado, A., Somoza, L., Pallarés, L., 1999. The Betic orogen and the Iberian–African boundary in the Gulf of Cadiz: geological evolution (central North Atlantic). Marine Geology 155, 9–43.
Marchès, E., Mulder, T., Cremer, M., Bonnel, C., Hanquiez, V., Gonthier, E., Lecroart, P., 2007. Contourite drift construction influenced by capture of Mediterranean Outflow Water deep-sea current by the Portimão submarine canyon (Gulf of Cadiz, South Portugal). Marine Geology 242, 247–260.
Marchès, E., Mulder, T., Gonthier, E., Cremer, M., Hanquiez, V., Garlan, T., Lecroart, P., 2010. Perched lobe formation in the Gulf of Cadiz: interactions between gravity processes and contour currents (Algarve Margin, Southern Portugal). Sedimentary Geology 229, 81–94.
Medialdea, T., Vegas, R., Somoza, L., Vázquez, J.T., Maldonado, A., Díaz del Río, V., Maestro, A., Córdoba, D., Fernández-Puga, M.C., 2004. Structure and evolution of the Olistostrome complex of the Gibraltar Arc in the Gulf of Cadiz eastern Central Atlantic evidence from two long seismic cross sections. Marine Geology 209, 173–198.
Mougenot, D., 1988. Geologie de la Marge Portugaise. Thése 3éme cicle, Univ. Pierre et Marie Curie, Paris, VI, 259 p.
Mulder, T., Voisset, M., Lecroart, P., Le Drezen, E., Gonthier, E., Hanquiez, V., Faugèrés, J.-C., Habgood, E., Hernandez-Molina, F.J., Estrada, F., Llave-Barranco, E., Poirier, D., Gorini, C., Fuchey, Y., Voelker, A., Freitas, P., Lobo Sanchez, F., Fernandez, L.M., Kenyon, N.H., Morel, J., 2003. The Gulf of Cadiz: an unstable giant contouritic levee. Geo-Marine Letters 23, 7–18. doi:10.1007/s00367-003-0119-0.
Mulder, T., Lecroart, P., Hanquiez, V., Marches, E., Gonthier, E., Guedes, J.-C., Thiébot, E., Jaaidi, B., Kenyon, N., Voisset, M., Perez, C., Sayago, M., Fuchey, Y., Bujan, S., 2006. The western part of the Gulf of Cadiz: contour currents and turbidity currents interactions. Geo-Marine Letters 26, 31–41. doi:10.1007/s00367-005-0013-z.
Mulder, T., Gonthier, E., Lecroart, P., Hanquiez, V., Marches, E., Voisset, M., 2009. Sediment failures and flows in the Gulf of Cadiz (eastern Atlantic). Marine and Petroleum Geology 26, 660–672.
Myers, P.G., 2002. Flux-forced simulations of the paleocirculation of the Mediterranean. Paleoceanography 17 (1), 1009. doi:10.1029/2000PA000613.
Nelson, C.H., Baraza, J., Maldonado, A., 1993. Mediterranean undercurrent sandy contourites Gulf of Cadiz, Spain. Sedimentary Geology 82, 103–131.
Pinardi, N., Masetti, E., 2000. Variability of the large scale general circulation of the Mediterranean Sea from observations and modelling: a review. Palaeogeography, Palaeoclimatology, Palaeoecology 158, 153–173.
Reid, J.L., 1979. On the contribution of the Mediterranean Sea out flow to the Norwegian–Greenland Sea. Deep Sea Research 26A, 1199–1223.
Ribeiro, A., Antunes, M.T., Ferreira, M.P., Rocha, R.B., Soares, A.F., Zbyszewski, G., Almeida, F.M., Carvalho, D., Monteiro, J.H., 1979. Introduction à la géologie générale du Portugal. Serviços Geológicos de Portugal.
Rio, D., Sprovieri, R., Thunell, R., Vergnaud, C., Claçon, G., 1990. Pliocene–Pleistocene paleoenvironmental history of the western Mediterranean: a synthesis of the ODP Site 652 results. In: Kadtens, K.A., Mascle, J. (Eds.), Proceedings of the Ocean Drilling Program, Scientific Results 107, Colege Station TX (Ocean Drilling Program), pp. 695–704.
Rogerson, M., Rohling, E.J., Weaver, P.P.E., Murray, J.W., 2005. Glacial to interglacial changes in the settling depth of the Mediterranean Outflow plume. Paleoceanography 20, PA3007. doi:10.1029/2004PA001106.
Rogerson, M., Rohling, E.J., Weaver, P.P.E., 2006. Promotion of meridional overturning by Mediterranean-derived salt during the last deglaciation. Paleoceanography 21, PA4101. doi:10.1029/2006PA001306.
Roque, C., 2007. Tectonostratigrafia do Cenozóico das margens continentais Sul e Sudoeste portuguesas: um modelo de correlação sismostratigráfica. Departamento de Geologia, Universidade de Lisboa.
Schmiedl, G., Kuhnt, T., Ehrmann, W., Emeis, K.-C., Hamann, Y., Kotthoff, U., Dulski, P., Pross, J., 2010. Climatic forcing of eastern Mediterranean deep-water formation and benthic ecosystems during the past 22 000 years. Quaternary Science Reviews 29, 3006–3020.
Schönfeld, J., Zahn, R., 2000. Late glacial to Holocene history of the Mediterranean Outflow: evidence from benthic foraminiferal assemblages and stable isotopes at the Portuguese margin. Palaeogeography, Palaeoclimatology, Palaeoecology 159, 85–111.
Serra, N., Ambar, I., Käse, R., 2005. Observations and numerical modelling of the Mediterranean outflow splitting and eddy generation. Deep-Sea Research II 52, 383–408.
Siedler, G., 1968. The frequency distribution of water types in the outflow region of Straits. Kieler Meeresforschungen 24, 59–65.
Sierro, F.J., Flores, J.A., Baraza, J., 1999. Late glacial to recent paleoenvironmental changes in the Gulf of Cadiz and formation of sandy coutourite layers. Marine Geology 155, 157–172.
Sierro, F.J., Hodell, D.A., Curtis, J.H., Flores, J.A., Reguera, I., Colmenero-Hidalgo, E., Bárcena, M.A., Grimalt, J.O., Cacho, I., Frigola, J., Canals, M., 2005. Impact of iceberg melting on Mediterranean thermohaline circulation during Heinrich events. Paleoceanography 20, PA2019. doi:10.1029/2004PA001051.
Stow, D.A.V., Faugères, J.-C., Gonthier, E., 1986. Facies distribution and textural variation in Faro Drift contourites: velocity fluctuations and drift growth. Marine Geology 72, 71–100.
Stumpf, R., Frank, M., Schönfeld, J., Haley, B.A., 2010. Late Quaternary variability of Mediterranean Outflow Water from radiogenic Nd and Pb isotopes. Quaternary Science Reviews 29, 2462–2472.
Terrinha, P., 1998. Structural Geology and Tectonic Evolution of the Algarve Basin, South Portugal. Department of Geology, University of London, London.

Terrinha, P., Ribeiro, C., Kullberg, J.C., Rocha, R., Ribeiro, A., 2002. Compression episodes during rifting and faunal isolation in the Algarve Basins, SW Iberia. Journal of Geology 110, 101–113.

Terrinha, P., Pinheiro, L.M., Henriet, J.-P., Matias, L., Ivanov, M.K., Monteiro, J.H., Akhmetzhanov, A., Volkonskaya, A., Cunha, T., Shaskin, P., Rovere, M., 2003. Tsunamigenic–seismogenic structures, neotectonics, sedimentary processes and slope instability on the southwest Portuguese margin. Marine Geology 195, 55–73.

Terrinha, P., Rocha, R., Rey, J., Cachão, M., Moura, D., Roque, C., Martins, L., Valadares, V., Cabral, J., Azevedo, M.R., Barbero, L., Clavijo, E., Dias, R.P., Gafeira, J., Matias, L., Madeira, J., Silva, C.M., Munhá, J., Rebelo, L., Ribeiro, C., Vicente, J., Youbi, N., 2006. A bacia do Algarve: estratigrafia, paleogeografia e tectónica. In: Dias, R., Araújo, A., Terrinha, P., Kullberg, J. (Eds.), Geologia de Portugal no contexto da Ibéria. Universidade de Évora, pp. 35–61.

Terrinha, P., Matias, L., Vicente, J., Duarte, J., Luís, J., Pinheiro, L., Lourenço, N., Diez, S., Rosas, F., Magalhães, V., Valadares, V., Zitellini, N., Roque, C., Mendes Víctor, L., Team, M.A.T.E.S.P.R.O., 2009. Morphotectonics and strain partitioning at the Iberia–Africa plate boundary from multibeam and seismic reflection data. Marine Geology 267, 156–174.

Toucanne, S., Mulder, T., Schönfeld, J., Hanquiez, V., Gonthier, E., Duprat, J., Cremer, M., Zaragosi, S., 2007. Contourites of the Gulf of Cadiz: a high-resolution record of the paleocirculation of the Mediterranean outflow water during the last 50,000 years. Palaeogeography, Palaeoclimatology, Palaeoecology 246, 354–366.

Toucanne, S., Zaragosi, S., Bourillet, J.F., Gibbard, P.L., Eynaud, F., Giraudeau, J., Turon, J.L., Cremer, M., Cortijo, E., Martinez, P., Rossignol, L., 2009. A 1.2 Ma record of glaciation and fluvial discharge from the West European Atlantic margin. Quaternary Science Reviews 28, 2974–2981.

Van Rooij, D., De Mol, B., Huvenne, V., Ivanov, M., Henriet, J.-P., 2003. Seismic evidence of current-controlled sedimentation in the Bélgica mound province, upper Porcupine slope, Southwest of Ireland. Marine Geology 195, 31–53.

Vanney, J.-R., Mougenot, D., 1981. La plate-forme continental du Portugal et les provinces adjacentes: analyse géomorphologique. Memória dos Serviços Geológicos de Portugal 28.

Via, R.K., Thomas, D.J., 2006. Evolution of Atlantic thermohaline circulation: Early Oligocene onset of deep-water production in the North Atlantic. Geology 34, 441–444. doi:10.1130/G22545.1.

Voelker, A.H.L., Lebreiro, S.M., Schönfeld, J., Cacho, I., Erlenkeuser, H., Abrantes, F., 2006. Mediterranean outflow strengthening during northern hemisphere coolings: a salt source for the glacial Atlantic? Earth and Planetary Science Letters 245, 39–55.

Wang, Z., Mysak, L.A., McManus, J.F., 2002. Response of the thermohaline circulation to cold climates. Paleoceanography 17, 1006. doi:10.1029/2000PA000587.

Xu, X., Chassignet, E.P., Price, J.F., Özgökmen, T.M., Peters, H., 2007. A regional modeling study of the entraining Mediterranean outflow. Journal of Geophysical Research 112, C12005. doi:10.1029/2007JC004145.

Zenk, W., 1970. On the temperature and salinity structure of the Mediterranean water in the Northeast Atlantic. Deep Sea Research 17, 627–631.

Zitellini, N., Mendes, L.A., Córdoba, D., Dañobeitia, J., Nicolich, R., Pellis, G., Ribeiro, A., Sartori, R., Torelli, L., Bartolomé, R., Bortoluzzi, G., Calafato, A., Carrilho, F., Casoni, L., Chierici, F., Corela, C., Correggiari, A., Della Vedova, B., Gràcia, E., Jornet, P., Landuzzi, M., Ligi, M., Magagnoli, A., Marozzi, G., Matias, L., Penitenti, D., Rodriguez, P., Rovere, M., Terrinha, P., Vigliotti, L., Ruíz-Zahinos, A., 2001. Source of 1755 Lisbon earthquake and tsunami investigated. Eos 28 (285), 290–291.

Zitellini, N., Rovere, M., Terrinha, P., Chierici, F., Matias, L., Team, Bigsets, 2004. Neogene through Quaternary tectonic reactivation of SW Iberian Passive Margin. Pure and Applied Geophysics 161, 565–587.

Zitellini, N., Gràcia, E., Matias, L., Terrinha, P., Abreu, M.A., DeAlteriis, G., Henriet, J.P., Dañobeitia, J.J., Masson, D.G., Mulder, T., Ramella, R., Somoza, L., Diez, S., 2009. The quest for the Africa–Eurasia plate boundary west of the Strait of Gibraltar. Earth and Planetary Science Letters 280, 13–50.